

X-RAY BINARY SYSTEMS IN GLOBULAR CLUSTERS

D. Pooley

Astronomy Department, University of California, Berkeley, USA

Chandra Fellow

ABSTRACT

The extreme stellar densities in the cores of globular clusters are expected to result in a number of interesting dynamical effects because of the relatively high frequency of close encounters (and even mergers) between cluster members. It has been known for decades that globular clusters are a favored environment for X-ray binaries, with formation rates per unit mass exceeding those in the Galactic disk by orders of magnitude. These X-ray binaries, as well as other close binaries, play a pivotal role in a cluster's evolution. Even a modest population of binaries contains a potential reservoir of binding energy that easily exceeds the kinetic energy of all single stars in the cluster.

The interplay between stellar dynamics and stellar evolution, as external and internal factors modifying the binary properties, is highly complex, and many details of these processes are not well understood. However, in recent years, we have made much progress, due in large part to X-ray observations from *Chandra* and *XMM-Newton*, which are extremely efficient at finding large numbers of close binary systems. Identifying the nature of these systems allows us to assess the effects of the parent cluster's physical properties on its different binary subpopulations. I will discuss this ongoing effort and some of the highlights of this new era.

Key words: globular clusters; binaries; X-rays.

1. INTRODUCTION

An excellent recent review of the state of globular cluster X-ray research was given by Verbunt & Lewin (2005), and the reader is encouraged to peruse that article for a comprehensive overview. I highlight only a few areas in this talk.

The X-ray sources in globular clusters have historically been divided into two phenomenological classes: the

high luminosity sources (with $L_X \gtrsim 10^{35.5}$ erg s⁻¹) and the low luminosity sources (with $L_X \lesssim 10^{34}$ erg s⁻¹). In each of these classes, I have selected a few topics to illustrate that unusual objects are found in large numbers in globular clusters, indicating that the dense stellar environment is responsible, at least in part, for their production.

2. HIGH LUMINOSITY X-RAY SOURCES

It has long been known that globular clusters are a favored environment for X-ray binaries, with formation rates per unit mass exceeding those in the Galactic disk by orders of magnitude (Clark, 1975; Katz, 1975). There are currently 13 high luminosity X-ray sources known in a total of 12 GCs (Deutsch et al., 2000; White & Angelini, 2001). Twelve of them are known to be neutron star low-mass X-ray binaries (NS-LMXBs) because they exhibit Type I X-ray bursts (Kuulkers et al., 2003), which are known to be thermonuclear runaways on the surface of a neutron star (see Lewin et al. 1993 for a review), and the thirteenth one is probably a NS-LMXB as well, based on the properties of its X-ray spectrum (in't Zand et al., 1999; White & Angelini, 2001).

One particularly interesting aspect of this population is that many of these NS-LMXBs show good evidence of having "ultrashort" binary periods of less than 80 min. Such a binary is so compact that the Roche-lobe filling donor star cannot be a lower main-sequence hydrogen burning star; it must be partially degenerate and partially depleted in hydrogen. Following Verbunt & Lewin (2005), I review the evidence for such ultracompact systems in globular clusters.

The source X1820–30 in NGC 6624 and the source X1850–087 in NGC 6712 have known orbital periods. Stella et al. (1987) first found the 11.47 min period of X1820–30 using *EXOSAT* data, and Anderson et al. (1997) found it in *HST* UV observations. Fig. 1 shows the X-ray and UV power spectra. Homer et al. (1996) discovered the 20.6 min period of X1850–087 with *HST*.

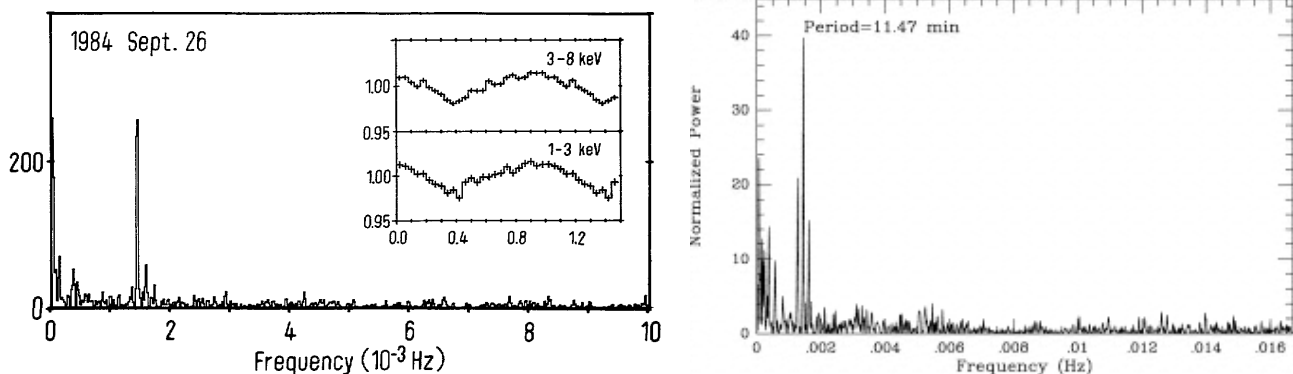


Figure 1. Left: The X-ray power spectrum of X1820–30 found by Stella et al. (1987). Right: The UV power spectrum of X1820–30 found by Anderson et al. (1997).

In addition to this direct evidence of an ultracompact nature, there are three lines of indirect evidence which indicate that a number of other globular cluster LMXBs are ultracompact. These come from considering the X-ray burst properties, the optical luminosities, and the broadband spectra of these sources.

Many of the globular cluster LMXBs have exhibited radius-expansion bursts, in which the maximum luminosity achieved in the burst is closely related to the Eddington limit. Kuulkers et al. (2003) have shown that in a number of these radius-expansion bursts the maximum luminosity is higher than is possible for hydrogen rich accretion, implying that the donor stars are at least partly depleted. This suggests that these sources — the high luminosity LMXBs in NGC 1851, NGC 6652, NGC 7078 (X-2), and Terzan 2 — are likely ultracompact systems.

Based on the relationship between the optical luminosity, X-ray luminosity, and orbital period of an X-ray binary found by van Paradijs & McClintock (1994), the LMXBs in NGC 6652 and NGC 1851 are likely to have ultrashort periods. Because the optical flux of a bright LMXB is dominated by light from the accretion disk, a small disk (or a low L_X) will give a low optical luminosity. Therefore, the X-ray to optical flux ratio can give some idea of the orbital period. Based on *HST* observations of NGC 1851 (Deutsch et al., 2000) and NGC 6652 (Heinke et al., 2001), the high luminosity LMXBs in these clusters likely have very short periods.

In a comprehensive analysis of the broadband X-ray spectra of all of the high-luminosity globular cluster LMXBs, Sidoli et al. (2001) found that the best-fit parameters of a multicolor disk blackbody plus comptonized spectrum separated the known ultracompact systems from the known normal period systems. Based on their similarity in best-fit spectral parameters to the known ultracompact systems, the LMXBs in NGC 1851, NGC 6652, and Terzan 5, are suggestive of also being ultracompact.

In summary, there are definitely two, probably four, and as many as seven ultracompact LMXBs in globular clusters. This is a remarkably high fraction (~ 15 – 50%) of

the high luminosity X-ray sources. The formation of ultracompacts is not well understood. See the Verbunt & Lewin review for an overview of the theories and their associated shortcomings, as well as recent work by Ivanova et al. (2005); Lombardi et al. (2005); van der Sluys et al. (2005a,b). One thing does seem clear, however, and it is that cluster dynamics has a large role in producing the observed population. The role of dynamics in producing unusual populations can be further explored by investigating the low luminosity sources.

3. LOW LUMINOSITY X-RAY SOURCES

An additional population of X-ray sources (those with low X-ray luminosity) was discovered in globular clusters with the *Einstein* satellite (Hertz & Grindlay, 1983a,b) and further explored with *ROSAT* (Verbunt, 2000). The nature of this population remained elusive for nearly two decades. Of the 57 low luminosity sources discovered by *ROSAT*, only two were securely classified: a cataclysmic variable (CV) in NGC 5904 (Hakala et al., 1997; Margon et al., 1981) and a millisecond pulsar (MSP) in NGC 6626 (Lyne et al., 1987; Saito et al., 1997).

The earliest *Chandra* observations of globular clusters — 47 Tuc (Grindlay et al., 2001a), NGC 6397 (Grindlay et al., 2001b), NGC 6440 (Pooley et al., 2002b), and NGC 6752 (Pooley et al., 2002a) — revealed not only a much larger population, but also allowed for the identification of optical and radio counterparts due to the subarcsecond angular resolution. This is clearly shown in Fig. 2 (from Verbunt 2004), which displays the *ROSAT* grayscale images of NGC 6752 and NGC 6440 with the *Chandra*-detected point sources overlaid as filled circles.

To date, *Chandra* has observed about two dozen globular clusters to a luminosity limit of a few $\times 10^{30}$ erg s^{-1} and a few even lower than this. Over 800 sources are detected within the half-light radii (Harris, 1996) of these clusters, with about 150 of them expected to be background sources based on the number-flux relation of Giacomini et al. (2001). One way to represent these sources

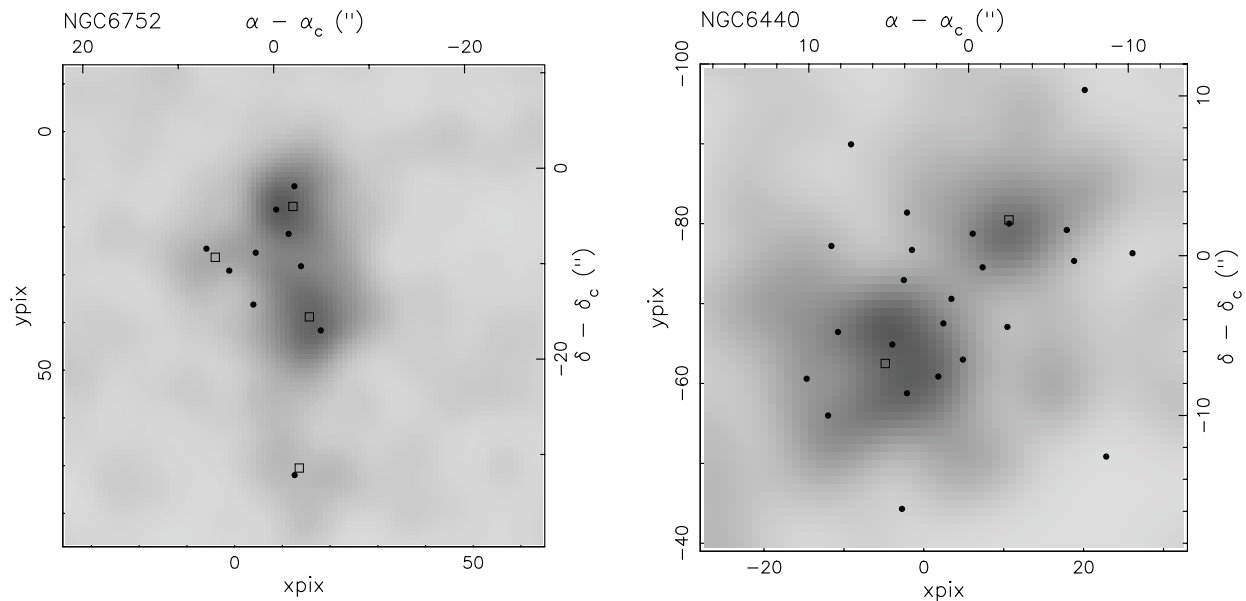


Figure 2. ROSAT grayscale images of NGC 6752 (top) and NGC 6440 (bottom) with Chandra sources overlaid as filled circles. The ROSAT identified point sources are indicated with open squares. From Verbunt (2004).

is on an X-ray color-magnitude diagram (Fig. 3), with the X-ray color defined as the logarithm of the ratio of flux in the 0.5–2 keV band to that in the 2–6 keV band, and the magnitude defined as the logarithm of the 0.5–6 keV luminosity.

Based on half the current sample, Pooley et al. (2003) found evidence that the number of X-ray sources in a globular scales with the encounter frequency (Γ) of the cluster. The encounter frequency is a measure of the dynamical activity of the cluster (see Pooley et al. 2003 for specifics of the calculation). This result suggests that the majority of these systems were formed dynamically.

Using the current sample, I have performed a similar analysis. I now use “specific” units, i.e., the number of X-ray sources per mass and the encounter frequency per mass. This is plotted in Fig. 4; the mass unit is $10^6 M_\odot$, with values obtained from Gnedin & Ostriker (1997). Using specific units mitigates the complication that arises from the natural correlation between encounter frequency and mass: on average, more massive clusters have higher encounter frequencies. The previous finding is seen to hold, namely, that over many orders of magnitude the number of X-ray sources (per mass) associated with a globular cluster scales with the encounter frequency (per mass).

This relationship deals with a hodge podge of close binaries, and there is no *a priori* reason to believe that the relationship should be same for each subpopulation (LMXBs, CVs, main-sequence binaries, and MSPs). It is therefore important to separate the subpopulations and deal with them on their own.

In general, classifying these low luminosity sources re-

quires a radio or optical counterpart identification, but it is becoming clear that we can make a rough classification of source type at the upper end of this luminosity regime based solely on the X-ray data. Above a few times 10^{31} erg s^{-1} , the observed X-ray sources are largely LMXBs and CVs, and the LMXBs are much softer spectrally than the CVs. This is best illustrated by *XMM-Newton* observations of two sources in ω Cen (Fig. 5).

We can therefore construct a fairly complete picture of the LMXBs in these clusters, and it appears that the number of LMXBs follows almost a linear relationship with the encounter frequency, in agreement with the conclusion from the 1970s. This result has been found by a number of authors (Pooley et al., 2003; Heinke et al., 2003; Gendre et al., 2003b)

As for the CVs, if we assume that the upper end of the CV luminosity distribution can act as a tracer for the whole CV population, we can then begin to explore whether the CVs also exhibit evidence of dynamical formation. We also need to assume that the number of bright, hard sources in the X-ray color magnitude diagram is dominated by CVs, and the results on the few clusters that have been analyzed in detail appears to support this. Therefore, we can use this bright hard region of the X-ray color-magnitude diagram as some kind of measure of the CV population. Fig. 6 shows the relationship of these sources versus the encounter frequency. Although there is a large dispersion, it does appear that a general trend exists. This is therefore the first evidence that CV formation in globular clusters is also influenced by the internal dynamics. Note that for any population that is strictly primordial, the number of sources per mass should be constant, plotted against *any* parameter. This is clearly not the case for these bright hard sources, which show a factor of ~ 40

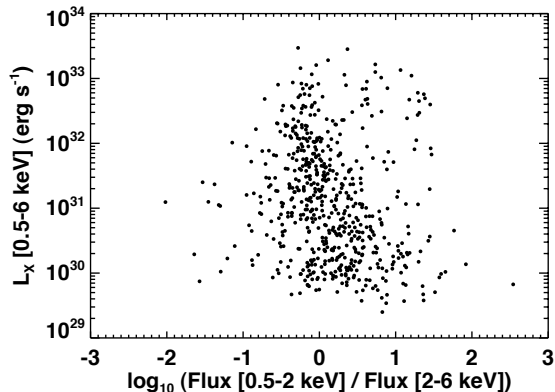


Figure 3. X-ray color-magnitude diagram of all Chandra detected low-luminosity globular cluster sources. An absorption correction (described in Pooley et al. 2002a) has been applied to all sources, based on the column density to the cluster, to bring all sources onto a common scale.

variation in the number per mass. Although perhaps not the entire story, dynamics is definitely playing a role.

4. SUMMARY

We know from observations that globular clusters are very efficient catalysts in forming unusual binary systems, such as LMXBs (and the even more unusual ultra-compact LMXBs), CVs, and MSPs, with formation rates per unit mass exceeding those in the Galactic disk by orders of magnitude. The high stellar densities in globular clusters trigger various dynamical interactions: exchange encounters, direct collisions, destruction of binaries, and tidal capture. This binary population is, in turn, critical to the stabilization of a cluster against gravitational collapse (Goodman & Hut, 1989); the long-term stability of a globular cluster is thought to depend on tapping into the gravitational binding energy of such close binaries (Hut et al., 1992). The various interactions that tap this energy (exchanges in encounters with binaries, direct collisions, destruction of binaries, and tidal capture) can change the state of the core dramatically and can kick stars and binaries out of the core or even out of the cluster altogether.

The details of these processes are not well understood, primarily because of the complex feedback between stellar evolution and cluster dynamics and the strong dependence on the globular cluster's physical properties. For example, the relative importance of tidal capture and exchange encounters for the formation of binaries with neutron stars or white dwarfs is still uncertain and cannot, due to the complexity of the physics involved, be answered by theory alone. These dynamical issues can best be addressed by studying the empirically confirmed close binary populations of globular clusters, which is efficiently accomplished with *Chandra* and *XMM-Newton* observations.

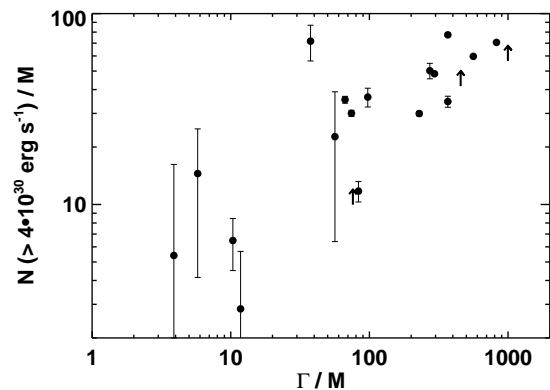


Figure 4. The number of X-ray sources above $4 \times 10^{30} \text{ erg s}^{-1}$ (per $10^6 M_{\odot}$) within the half-light radius of a cluster (minus the expected number of background sources) versus the encounter frequency Γ (per $10^6 M_{\odot}$) of the cluster. An arrow indicates a cluster that was not observed long enough to reach $4 \times 10^{30} \text{ erg s}^{-1}$.

ACKNOWLEDGMENTS

DP gratefully acknowledges support provided by NASA through Chandra Postdoctoral Fellowship grant number PF4-50035 awarded by the Chandra X-ray Center, which is operated by the Smithsonian Astrophysical Observatory for NASA under contract NAS8-03060.

REFERENCES

- Anderson, S.F., Margon, B., Deutsch, E.W., Downes, R.A., & Allen, R.G. 1997, *ApJ*, 482, L69
- Clark, G. W. 1975, *ApJ*, 199, L143
- Deutsch, E.W., Margon, B., & Anderson, S.F. 2000, *ApJ*, 530, L21
- Gendre, B., Barret, D., & Webb, N.A. 2003a, *A&A*, 400, 521
- Gendre, B., Barret, D., & Webb, N.A. 2003b, *A&A*, 403, L11
- Giacconi, R. et al. 2001, *ApJ*, 551, 624
- Gnedin, O.Y., & Ostriker, J.P. 1997, *ApJ*, 474, 223
- Goodman, J. & Hut, P. 1989, *Nature*, 339, 40
- Grindlay, J.E., Heinke, C., Edmonds, P.D., & Murray, S.S. 2001a, *Science*, 292, 2290
- Grindlay, J.E., Heinke, C.O., Edmonds, P.D., Murray, S.S., & Cool, A.M. 2001b, *ApJ*, 563, L53
- Hakala, P.J., Charles, P.A., Johnston, H.M., & Verbunt, F. 1997, *MNRAS*, 285, 693.

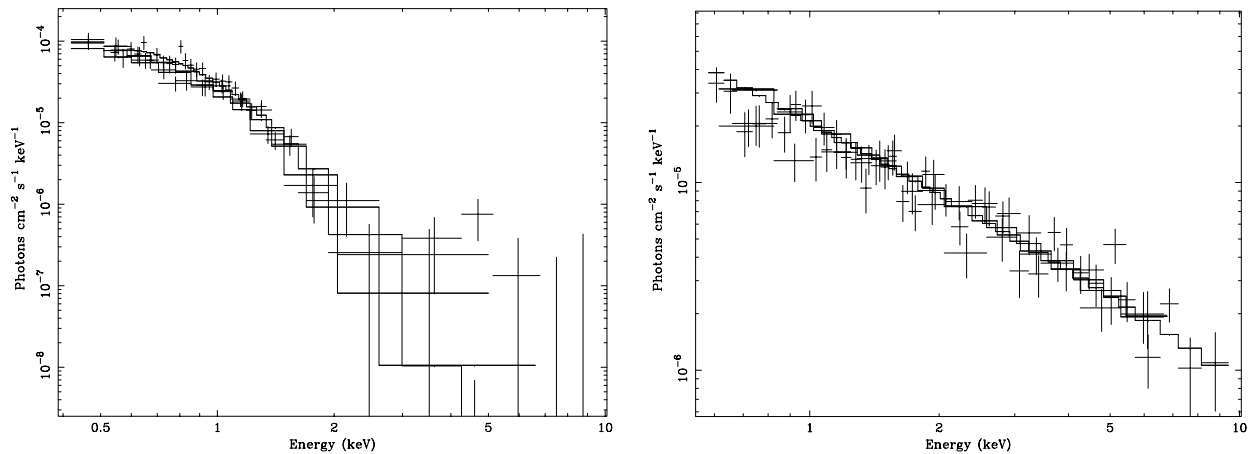


Figure 5. XMM-Newton spectra of two sources in ω Cen (from Webb & Barret 2005, originally in Gendre et al. 2003a). The quiescent LMXB (left) is much softer than the CV (right).

Harris, W. E. 1996, AJ, 112, 1487

Heinke, C.O., Edmonds, P.D., & Grindlay, J.E. 2001, ApJ, 562, 363

Heinke, C.O., Grindlay, J.E., Lugger, P.M., Cohn, H.N., Edmonds, P.D., Lloyd, D.A., & Cool, A.M. 2003, ApJ, 598, 501

Hertz, P. & Grindlay, J., 1983a, ApJ, 267, L83.

Hertz, P. & Grindlay, J., 1983b, ApJ, 275, L105.

Homer, L., Charles, P.A., Naylor, T., van Paradijs, J., Auriere, M., & Koch-Miramond, L. 1996, MNRAS, 282, L37

Hut, P. et al. 1992, PASP, 104, 981

in 't Zand, J.J.M., Verbunt, F., Strohmayer, T.E., Bazzano, A., Cocchi, M., Heise, J., van Kerkwijk, M.H., Muller, J.M., Natalucci, L., Smith, M.J.S., & Ubertaini, P. 1999, A&A, 345, 100

Ivanova, N., Rasio, F.A., Lombardi, J.C., Jr., Dooley, K.L., & Proulx, Z.F. 2005, ApJ, 621, L109

Katz, J. I. 1975, Nature, 253, 698

Kuulkers, E., den Hartog, P.R., in't Zand, J.J.M., Verbunt, F.W.M., Harris, W.E., & Cocchi, M. 2003, A&A, 399, 663

Lewin, W.H.G., van Paradijs, J., & Taam, R.E. 1993, Space Sci. Rev., 340, 367

Lombardi, J.C., Jr., Proulx, Z.F., Dooley, K.L., Theriault, E.M., Ivanova, N., & Rasio, F.A. 2005, ApJ, submitted, astro-ph/0509511

Lyne, A.G., Brinklow, A., Middleditch, J., Kulkarni, S.R., & Backer, D.C. 1987, Nature, 328, 399.

Margon, B., Downes, R.A., & Gunn, J.E. 1981, ApJ, 247, L89.

Pooley, David; Lewin, Walter H. G.; Homer, Lee; Verbunt, Frank; Anderson, Scott F.; Gaensler, Bryan M.; Margon, Bruce; Miller, Jon M.; Fox, Derek W.; Kaspi, Victoria M.; van der Klis, Michiel 2002a, ApJ, 569, 405

Pooley, David; Lewin, Walter H. G.; Verbunt, Frank; Homer, Lee; Margon, Bruce; Gaensler, Bryan M.; Kaspi, Victoria M.; Miller, Jon M.; Fox, Derek W.; van der Klis, Michiel 2002b, ApJ, 573, 184

Pooley, D., Lewin, W.H.G., Anderson, S.F., Baumgardt, H., Filippenko, A.V., Gaensler, B.M., Homer, L., Hut, P., Kaspi, V.M., Makino, J., Margon, B., McMillan, S., Portegies Zwart, S., van der Klis, M., & Verbunt, F. 2003, ApJ, 591, L131

Saito, Y., Kawai, N., Kamae, T., Shibata, S., Dotani, T., & Kulkarni, S.R. 1997, ApJ, 477, L37.

Sidoli, L., Parmar, A.N., Oosterbroek, T., Stella, L., Verbunt, F., Masetti, N., & Dal Fiume, D. 2001, A&A, 368, 451

Stella, L., Priedhorsky, W., & White, N.E. 1987, ApJ, 312, L17

van der Sluys, M.V., Verbunt, F., & Pols, O.R. 2005a, A&A, 431, 647

van der Sluys, M.V., Verbunt, F., & Pols, O.R. 2005b, A&A, 440, 973

van Paradijs, J., & McClintock, J.E. 1994, A&A, 290, 133

Verbunt, F. 2000, A&A, 368, 137

Verbunt, F. 2004, to appear in *Interacting Binaries*, eds. Antonelli et al., American Institute of Physics, astro-ph/0412524

Verbunt, F., & Lewin, W.H.G. 2005, to appear as Chapter 8 in *Compact Stellar X-ray Sources*, eds. W.H.G. Lewin and M. van der Klis, Cambridge University Press, astro-ph/0404136

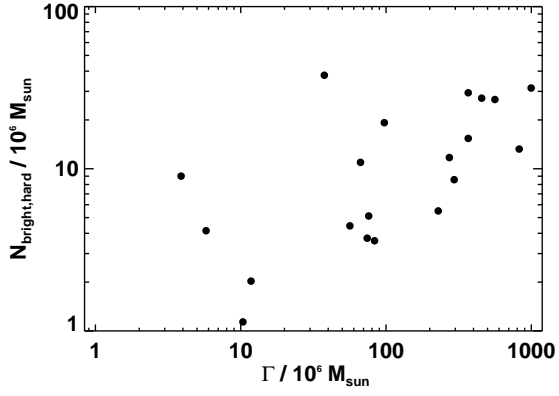


Figure 6. The number (per $10^6 M_{\odot}$) of hard X-ray sources at the bright end of the low luminosity regime versus the encounter frequency Γ (per $10^6 M_{\odot}$) of the cluster. This number is expected to be a tracer of the entire CV population.

Webb, N.A., & Barret, D. 2005, in *The Astrophysics of Cataclysmic Variables and Related Objects*, eds. J.-M. Hameury and J.-P. Lasota., Astronomical Society of the Pacific, astro-ph/0411506

White, N. E. & Angelini, L. 2001, *ApJ*, 561, L101

AN END-TO-END TEST OF NEUTRON STARS AS PARTICLE ACCELERATORS

Patrizia A. Caraveo

INAF IASF-Milano, Via Bassini, 15; 20133 Milano; Italy

ABSTRACT

Combining resolved spectroscopy with deep imaging, XMM-Newton is providing new insights on the particle acceleration processes long known to be at work in the magnetospheres of isolated neutron stars. According to a standard theoretical interpretation, in neutron stars' magnetospheres particles are accelerated along the B field lines and, depending on their charge, they can either move outward, to propagate in space, or be funnelled back, towards the star surface. While particles impinging on the neutron star surface should heat it at well defined spots, outgoing ones could radiate extended features in the neutron star surroundings.

By detecting hot spots, seen to come in and out of sight as the star rotates, as well as extended features trailing neutron stars as they move in the interstellar medium, XMM-Newton provides the first end-to-end test to the particle acceleration process.

Key words: Neutron stars; pulsars; Geminga; ESA; X-rays.

1. INTRODUCTION

Isolated neutron stars (INSs) are natural particle accelerators. Their, presumably dipolar, rapidly rotating magnetic fields, naturally inclined with respect to the star rotation axis, induce electric fields ideally suited to accelerate particles already present in the stars' magnetospheres or extracted from the crusts. Following the seminal paper of Goldreich and Julian (1969) and Sturrock (1971), a lot has been done to work out the details of such an acceleration, focusing on its most likely location(s) inside the INS magnetosphere and on its efficiency. Traditionally, two classes of models have been developed: on one side the polar cap ones (Ruderman & Sutherland, 1975, Harding & Daugherty, 1998, Rudak & Dyck, 1999), where the acceleration takes place near the star surface, just above the magnetic pole; on the other side, the outer gap ones (Romani, 1996), where the acceleration is taking place in the outer magnetosphere, not far from the light cylinder. Recently, the slot gap model, extending

from the polar cap to the light cylinder, has been added as a third alternative (Muslinov & Harding, 2003, Dyck & Rudak, 2003, Harding, 2005). Notwithstanding important differences between models, the interaction between accelerated particles (typically electrons) and the star magnetic field results in the production of high energy gamma-rays which, in turn, are not able to escape the highly magnetic environment and are converted into electron positron pairs. This initiates a cascade rapidly filling the magnetosphere with energetic particles which, interacting with the magnetic field, are responsible for the vast majority of the INSs' multiwavelength phenomenology.

2. ACCELERATION BY-PRODUCTS

INSs are mainly studied through their non thermal radio emission. Radio searches have been highly successful and the current radio catalogues list more than 1500 pulsars (Manchester et al. 2005).

In spite of the sheer number of objects and their very diverse phenomenology, INS radio emission accounts for a negligible fraction of the star rotational energy loss. A far more important fraction of the star energy reservoir goes into high-energy radiation, mainly in high-energy gamma-rays. While the number of objects shrinks to less than 1% of the radio ones (Thompson et al., 2001), in gamma rays the INSs' luminosity can reach a sizable fraction of the total rotational energy loss, with an increase in efficiency for the older objects.

The rich INSs' phenomenology encompasses now also X and optical emissions. While the numbers are slightly higher than the gamma-ray ones (a dozen in the optical (Caraveo, 2000, Mignani et al. 2004) and two scores in X-rays (Becker & Aschenbach, 2002) the nature of the radiation is not as clear cut as in the radio or gamma-ray domains. In the optical, as well as in X-rays, aged neutron stars exhibit both thermal and non-thermal emissions. Indeed, when non-thermal emission somewhat weakens with age, the thermal one begins to emerge to tell the story of the cooling crust of the neutron star. INS thermal emission, however, is not totally unrelated to the magnetospheric particle acceleration. Depending

on their electric charge, particles move in different directions along the magnetic field lines. While those moving outward try to escape the INS magnetosphere, those moving inward hit the star and heat its crust at well defined spots, that, under the assumption of a dipolar magnetic field, should coincide with its polar caps (return currents, see e.g. Ruderman & Sutherland 1975; Arons & Scharlemann 1979). Thus, thermal emission could be of use to trace non-thermal phenomena.

The escaping particles, on the other side, are part of the neutron stars' relativistic wind which is supposed to account for the bulk of their observed rotational energy loss. Such relativistic wind can be traced through its interaction with the interstellar medium (ISM), both in the immediate surroundings of the stars, where the INS magnetic field is still important, or farther away, where the wind radiation pressure is counterbalanced by the shocked ISM. An important player to determine the shape and the phenomenology of the resulting Pulsar Wind Nebula (PWN) is the actual neutron star speed. INSs are known to be high velocity objects and, plunging supersonically through the ISM, they can give rise to a rich bow shocks phenomenology seen in the radio, optical and X-ray domains (e.g. Chattarjee & Cordes, 2002).

Fig.1 summarizes the neutron star *acceleration tree*: starting from the synoptic view (Harding, 2005) of the mechanisms responsible the gamma ray emission (the aspect most intimately related to the actual particle acceleration) and following the destiny of the particle moving inward (left) and outward (right). Using past and present space observatories operating at X and gamma-ray domain, we can construct such a tree with the aim to improve our understanding of the neutron star physics.

3. THE OBSERVATIONAL PANORAMA

Our task is now to briefly review the data related to the three steps highlighted in Fig.1 in order to find INSs observed throughout the *acceleration tree*.

3.1. High-energy gamma-rays

Waiting for the next generation of gamma-ray instruments such as Agile (Tavani et al., 2003) and Glast (Michelson et al., 2003), we try to make the best use of the EGRET results. INSs (be they radio loud or radio quiet) are the only class of galactic sources firmly identified as high-energy gamma-rays emitters. Indeed, pulsars are especially appealing to gamma-ray astronomers since their timing signature allows to overcome the identification problem due to the relatively large gamma-ray error boxes. However, in spite of more than a decade of relentless efforts based on the EGRET data, only Crab, Vela, PSR 1706-44, PSR1951+32, PSR1055-52 and the radio quiet Geminga are confirmed gamma-ray sources (Thompson et al., 2001). A few more pulsars have been

proposed as sources of pulsed gamma-radiation, but the claims are still awaiting confirmations. Several positional coincidences between newly discovered pulsars and old Egret sources (Hartman et al. 1999) have been reported, but, again, such suggestions cannot be confirmed without an operating gamma-ray telescope. Thus, for the moment being, our gamma-ray sample encompasses a very young (and energetic) object such as the Crab, two slightly older pulsars (Vela, PSR 1706-44) and three middle-aged INSs (PSR1055-57, Geminga and the fast spinning PSR1951+32). It is worth noting that the efficiency for conversion of rotational energy loss into gamma-rays changes as a function of pulsar age. It goes from the value of $\sim 0.009\%$, for the Crab, to several %, for Geminga and PSR 1055-57.

3.2. Hot spots

The presence of hot spots on the surface of INSs has been long suspected on the basis of their overall X-ray spectral shape requiring more than a simple black-body to describe the data. Usually two black-body curves, characterized by different temperatures and emitting areas, are needed to fit the X-ray spectra for all but the very youngest INSs. A slightly colder black-body, covering the majority of the INS surface, provides the bulk of the X-ray luminosity while a hotter one, covering a smaller surface, is needed to obtain a satisfactory spectral fit.

Long XMM-Newton observations of Geminga, PSR0656+14 and PSR 1055-57, three middle-aged, rather similar INSs, have added an important piece of information. Taking advantage of their exceptional photon harvest, De Luca et al (2005a) were able to perform space resolved spectroscopy of the three INSs. For all objects they have shown that

- the spectra are varying significantly throughout the rotational phase
- the hot blackbody contribution is the most dramatically variable spectral component.

This is shown in Fig.2 where the emitting radii, computed on the basis of the phase-resolved spectral fits, are shown as a function of the pulsar rotational phase. While for PSR B0656+14 the modulation in the emitting radius wrt. the average value is $<10\%$, similar to the value found for the cool blackbody component, in the case of PSR B1055-52 we see a 100% modulation, since the hot blackbody component is not seen in 4 out of 10 phase intervals. A similar, 100% modulation is observed also for Geminga, although in this case the hot blackbody component is seen to disappear in just one phase interval, and the profile of its phase evolution is markedly broader. It is natural to interpret such marked variations as an effect of the star rotation, which alternatively brings into view or hides one or more hot spots on the star surface. As outlined above, such hot spots arise when charged particles, accelerated in the magnetosphere, fall back to the polar caps along magnetic field lines. Straight estimates of neutron star polar cap sizes, based on a simple "centered" dipole magnetic field geometry (polar

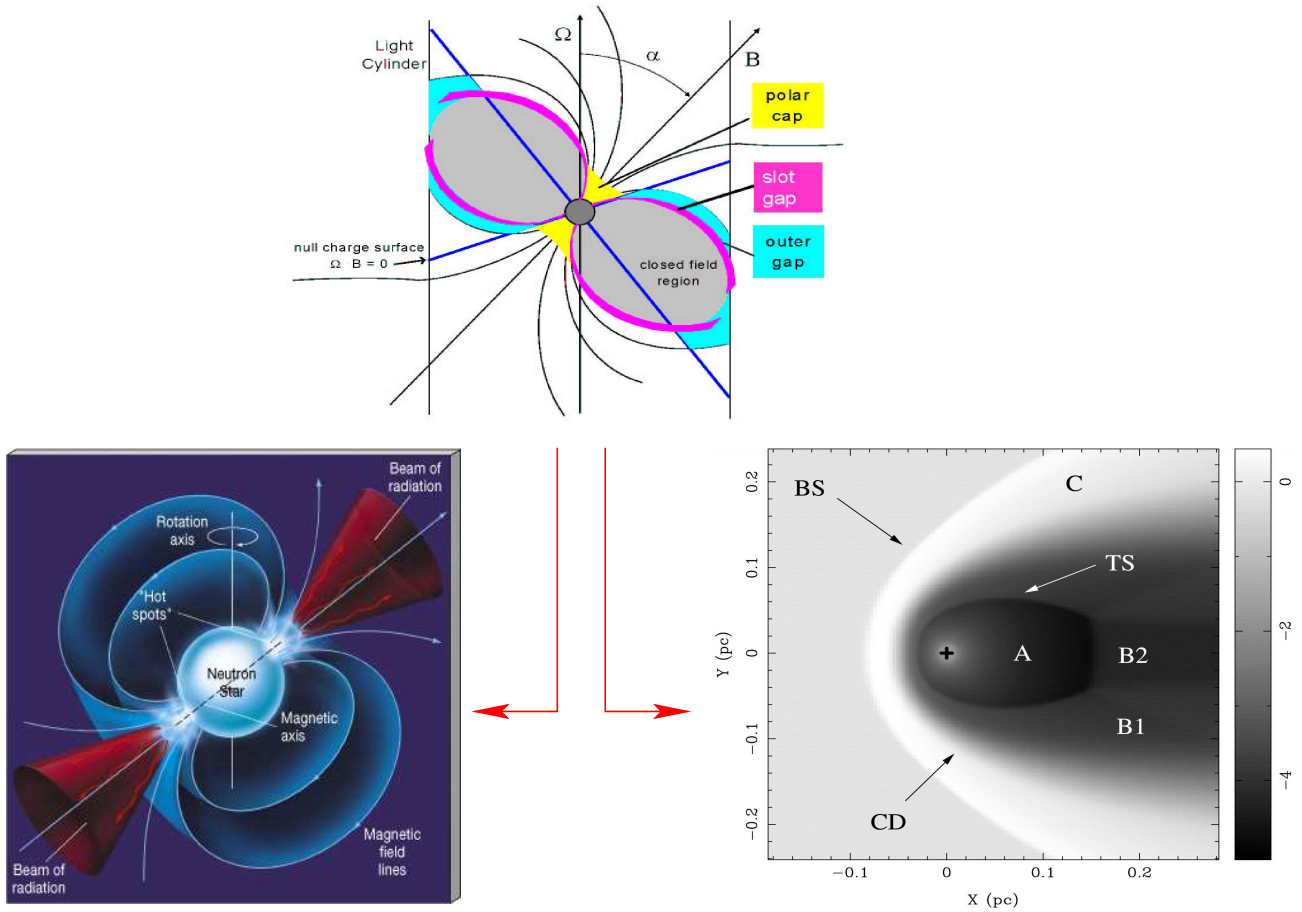


Figure 1. Neutron star acceleration tree. Top panel : schematic view of a pulsar magnetosphere showing the gamma-ray emitting regions, according to the various classes of models (from Harding, 2005). Bottom left: a similar view of a pulsar magnetosphere showing the hot spots on the pulsar polar caps. Bottom right: hydrodynamic simulation of a bow shock (BS) generated by the interaction of the isotropic relativist wind of a neutron star (marked with a cross), moving horizontally from right to left, with the ISM (Gaensler et al, 2004). A indicates the pulsar wind cavity, where the electrons propagate freely, B is used for the shocked pulsar wind material, while C represents the shocked ISM. The termination shock, TS, is where the energy density of the pulsar wind is balanced by the external pressure, while CD is the contact discontinuity bounding the shocked pulsar wind material.

cap radius $R_{PC} = R\sqrt{\frac{R\Omega}{c}}$, where R is the neutron star radius, Ω is the angular frequency and c is the speed of light), predict very similar radii for the three neutron stars, characterized by similar periods (233 m for PSR B0656+14, 326 m for PSR B1055-52 and 297 m for Geminga, assuming a standard neutron star radius of 10 km). The observed radii are instead markedly different, with values ranging from ~ 60 m for Geminga to ~ 2 km for PSR B0656+14 (see De Luca et al, 2005a for a detailed discussion).

While waiting to enlarge the sample of deeply scrutinized X-ray pulsars, it does not come as a surprise that two of the three objects showing direct evidence for the presence of rotating hot spots are highly efficient gamma-ray sources.

3.3. Pulsar Wind Nebulae

When the particle wind from a fast moving INS interacts with the surrounding ISM, it gives rise to complex structures, globally named ‘‘Pulsar Wind Nebulae’’ (PWNe) where $\sim 10^{-5} - 10^{-3}$ of the NS \dot{E}_{rot} is converted into electromagnetic radiation (for recent reviews see Gaensler et al 2004, and Gaensler 2005). The study of PWNe may therefore give insights into aspects of the neutron star physics which would be otherwise very difficult to access, such as the geometry and energetics of the particle wind and, ultimately, the configuration of the INS magnetosphere and the mechanisms of particle acceleration. Moreover, PWNe may probe the surrounding medium, allowing one to measure its density and its ionisation state.

A basic classification of PWNe rests on the nature of the external pressure confining the neutron star wind (e.g. Pellizzoni et al. 2005). For young NSs ($< \text{few } 10^4$ y) the pressure of the surrounding supernova ejecta is effective and a ‘‘static PWN’’ is formed. For older systems ($> 10^5$ y) the neutron star, after escaping the eventually faded supernova remnant, moves through the unperturbed ISM and the wind is confined by ram pressure to form a ‘‘Bow-shock’’ PWN.

Static PWNe (Slane, 2005, for a review) usually show complex morphologies. Striking features such as tori and/or jets (as in the Crab and Vela cases), typically seen in X-rays, reflect anisotropies of the particle wind emitted by the energetic, central INS and provide important constraints on the geometry of the system. A remarkable axial symmetry, observed in several cases, is assumed to trace the rotational axis of the central INS. For the Crab and Vela PWNe, such an axis of symmetry was found to be coincident with the accurately measured direction of the INS proper motion (Caraveo & Mignani 1999, Caraveo et al. 2001). This provided evidence for an alignment between the rotational axis and the proper motion of the two neutron stars, with possible important implications for the understanding of supernova explosion mechanisms (Lai et al. 2001). The alignment between spin axis and space

velocity, directly observed only for Crab and Vela, is now assumed as a standard property of NSs (Ng & Roman, 2004).

Bow-shocks (for a review see Pellizzoni et al. 2005, Gaensler et al 2004) have a remarkably simpler, ‘‘velocity-driven’’ morphology. They are seen frequently in H_α as arc-shaped structures tracing the forward shock, where the neutral ISM is suddenly excited. In other cases, X-ray emission (and/or radio emission on larger scales) is seen, with a cometary shape elongated behind the neutron star, due to synchrotron radiation from the shocked NS particles downstream (only in the case of PSR B1957+20 both the H_α and the X-ray structures have been observed, Stappers et al., 2003). According to the lower energetics of the central, older INS, bow shocks are typically fainter than static PWNe and proximity is a key parameter for their observation.

Since we aim at tracing the high energy particle escaping the INS magnetosphere, we concentrate on the X-ray PWNe. Inspecting the list of Gaensler et al (2004), we find only PSR B1951+32 in common with the gamma-ray database, leaving little hope to find an object displaying all the aspects of the *acceleration tree*.

However, recent observations of Geminga, combined with previous ones by XMM-Newton, have unveiled the presence of a bona fide PWN with complex diffuse features trailing the pulsar perfectly aligned with its well known proper motion (De Luca et al., 2005b; Caraveo et al. 2003).

Thus, the combined EGRET, XMM-Newton and Chandra results on Geminga make this source the most suitable example for our end-to-end test of particle acceleration. For a review on the multiwavelength phenomenology of Geminga, see Bignami & Caraveo (1996).

4. GEMINGA AS A TEST CASE

Fig.3 summarizes all the observational evidence collected so far on the presence of high energy electrons/positrons in the magnetosphere of Geminga. First, the EGRET light-curve whose > 100 MeV photons could not have been produced without high energy particles and magnetic fields.

Next, the contribution of a 100 ksec XMM-Newton observation which yielded both

a) the evidence for the presence of minute hot spot(s) varying throughout the pulsar phase (Caraveo et al., 2004)

b) the detection of two elongated tails, trailing the pulsar in its supersonic motion through the ISM and perfectly aligned with the proper motion direction. The flat spectral shape of the tails’ X-ray photons suggests a synchrotron origin which, combined with the typical magnetic field present in a shocked ISM, implies the presence of $\sim 10^{14}$ eV electrons/positrons, i.e. of particle at the upper limit of the energy range achievable for an INS like Geminga. Moreover, the lifetime of such electrons (or, more precisely, the time it takes for them to lose half of their en-

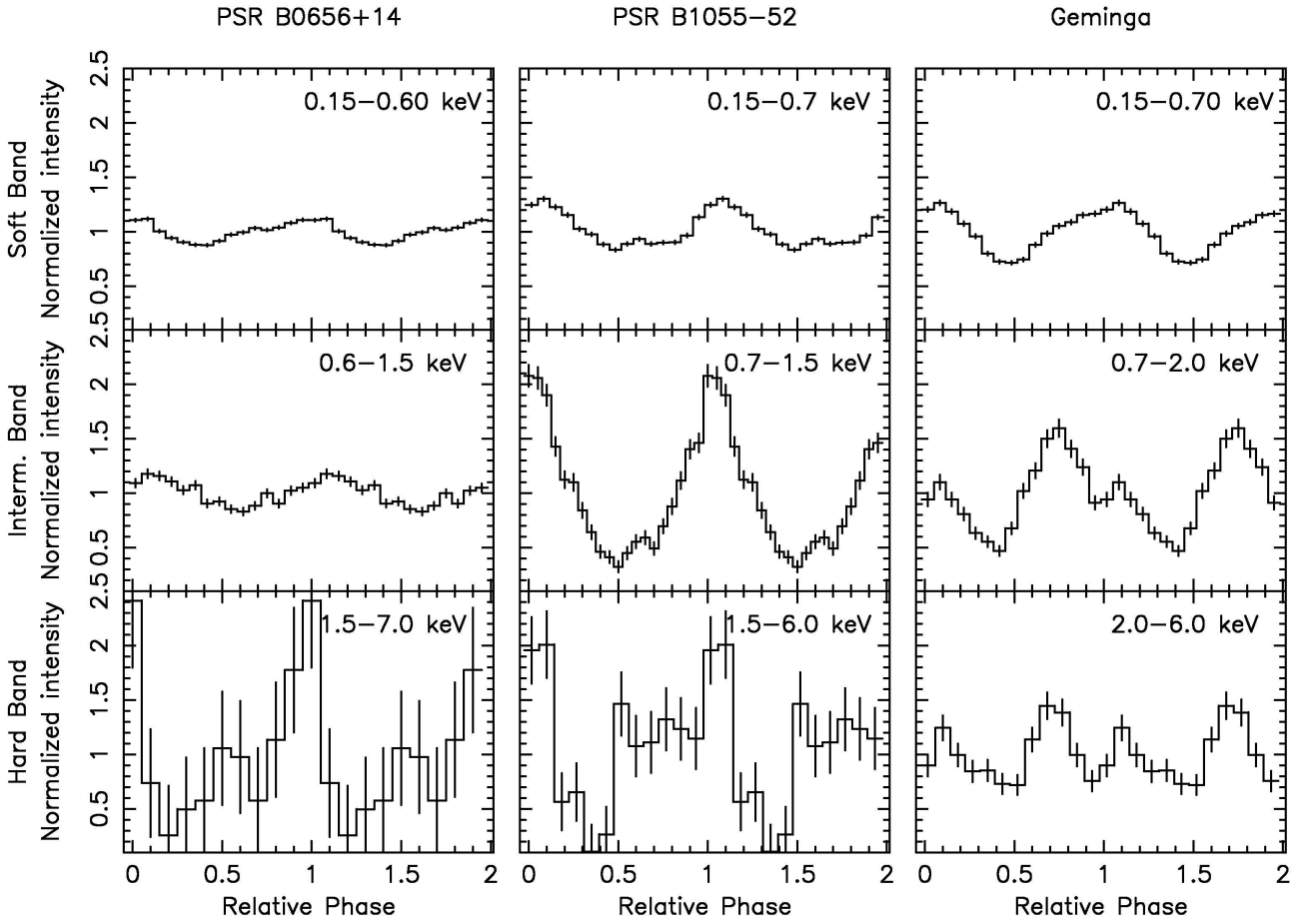


Figure 2. Energy-resolved light curves of PSR B0656+14, PSR B1055-52 and Geminga in different energy ranges. To ease the comparison of the behaviour of the three INSs, all light curves have been plotted setting phase 0 to the X-ray maximum. Pulsed fractions (computed as the ratio between the counts above the minimum and the total number of counts) are as follows: PSR B0656+14 $12.3 \pm 0.4\%$ in 0.15-0.6 keV, $16.9 \pm 2.3\%$ in 0.6-1.5 keV, $75 \pm 20\%$ in 1.5-7.0 keV; PSR B1055-52 $16.7 \pm 0.6\%$ in 0.15-0.7 keV, $67 \pm 3\%$ in 0.7-1.5 keV, $90 \pm 10\%$ in 1.5-6.0 keV; Geminga $28.4 \pm 0.6\%$ in 0.15-0.7 keV, $54.5 \pm 2.4\%$ in 0.7-2.0 keV, $33 \pm 5\%$ in 2.0-6.0 keV.

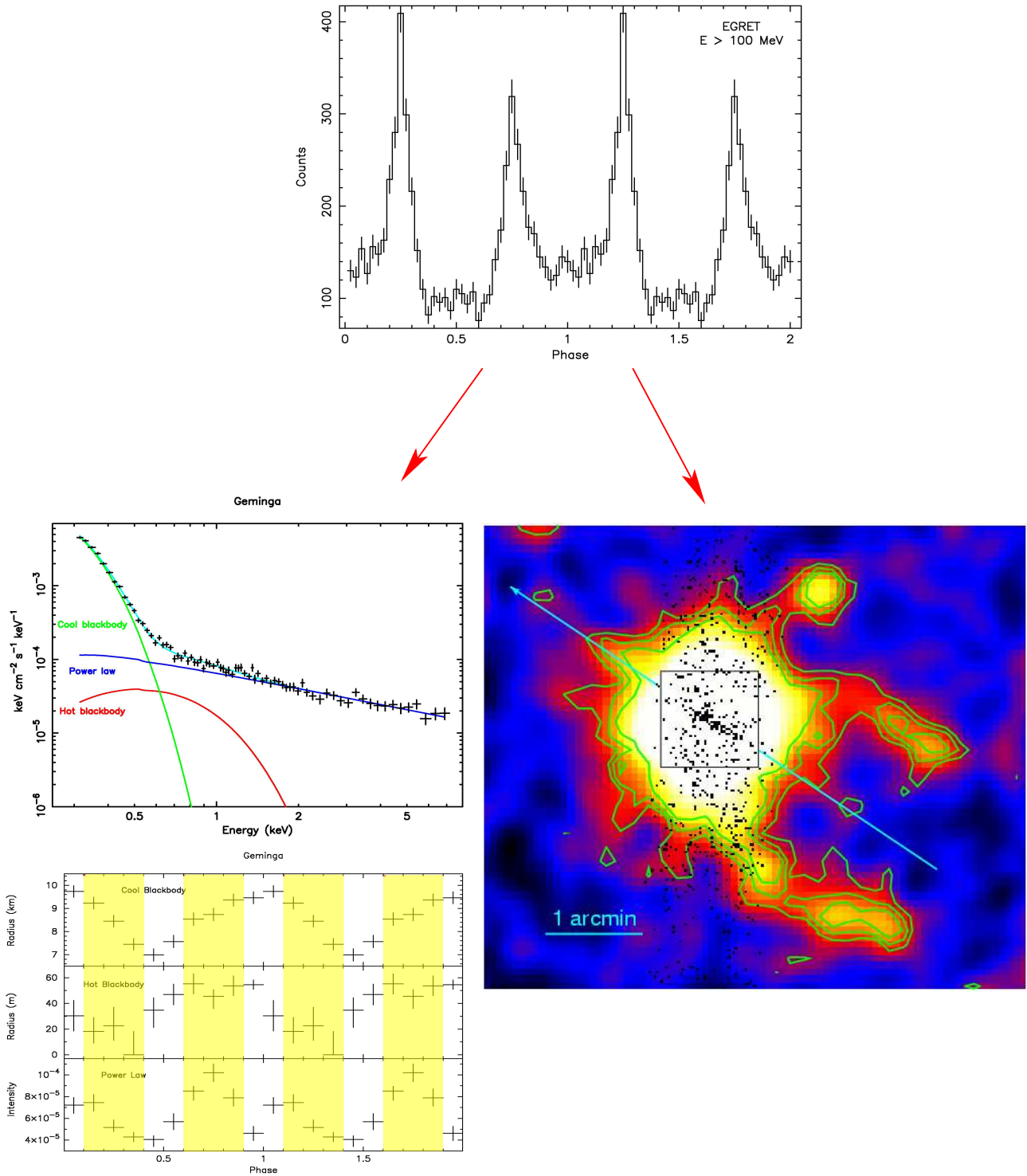


Figure 3. The acceleration tree as observed for Geminga. Top: the gamma-ray light curve. Left: the XMM-Newton average spectrum as well as the results of phase-resolved spectroscopy, showing the evolution of the black-body emitting regions as a function of the INS rotational phase. The shaded area mark the phase intervals corresponding to the γ -ray peaks observed by EGRET. The highest γ -ray peak occurs at phase 0.25 ± 0.15 , the second one at phase 0.75 ± 0.15 (the uncertainty is due to the extrapolation of the EGRET ephemeris to the epoch of the XMM-Newton observation). Right: Geminga as seen by Chandra and XMM-Newton (from De Luca et al., 2005b). The Chandra image, rebinned to a pixel size of $2''$ has been superposed on the XMM-Newton/MOS image obtained by Caraveo et al.(2003). Surface brightness contours for the XMM image have been also plotted. The ACIS field of view is limited to a rectangular region 1 arcmin wide. The pulsar proper motion direction is marked by an arrow.

ergy) in the bow-shock magnetic field is ~ 800 years. On the other hand, Geminga's proper motion (170 mas/year) allows one to compute the time taken by the pulsar and its bow shock to transit over the apparent length of the x-ray structures in the sky ($3'$ from the central source). Such a time is close to 1,000 years. Thus, Geminga's tails remain visible for a time comparable to the electron synchrotron X-ray emission life time after the pulsar passage. The comet-like structure seen by Chandra is as luminous as the larger and fainter tails and its spectrum is equally hard.

Hot spot(s), elongated, faint tails and short, brighter trail have roughly the same luminosity, corresponding to $\sim 10^{-6}$ of its \dot{E}_{rot} .

We note that the morphology and hard spectrum of the Trail is reminiscent of the jet-like collimated outflows structures seen in the cases of Crab and Vela (Helfand et al., 2001, Pavlov et al. 2003, Willingale et al., 2001, Mori et al. 2004) and associated to the neutron stars spin axis direction. In particular, the small Geminga's Trail can be compared to the "inner counterjet" of the Vela PSR (Pavlov et al., 2003), characterized by a similar spectrum (photon index ~ 1.2) and efficiency ($L_X \sim 10^{-6} \dot{E}$). The projected angle between Geminga proper motion and its backward jet is virtually null, which implies that also the pulsar spin axis should be nearly aligned with them. Geminga would thus be the third observed neutron star having its rotational axis aligned with its space velocity, after the cases of the Crab and Vela.

The whole scenario, encompassing both the large Tails and the small Trail, could therefore fit in the frame of an anisotropic wind geometry. It includes jet structures along the spin axis and relativistic shocks in the direction of the magnetic axis where most of the wind pressure is concentrated due to the near radial outflow from magnetosphere open zones.

The coupling of the jet-like Trail seen by Chandra with the larger, arc-shaped Tails seen by XMM has no similarity with other pulsars.

5. CONCLUSION

The particle acceleration going on in an INS magnetosphere can now be traced from end-to-end. While gamma ray emission probes directly the particle population in the magnetosphere, using the current generation of X-ray observatories we are now able to follow the destiny of the particles traveling up and down the magnetic field lines through the study of hot spots on the star surface and of PWNe. The same process responsible for the copious gamma-ray emission of Geminga would thus also be responsible for the appearance of the hot spots on its surface (Halpern & Ruderman, 1993). Such a strong link between the X-and gamma-ray behaviour of the source could be exploited to map the relative positions of the regions responsible for the different emissions. A precise comparison of the source X and gamma-ray light curves

is crucial at this point, but the lack of operating high energy gamma ray telescope makes it impossible. Simultaneous observations performed by XMM-Newton and by Agile and/or GLAST (foreseen to be operational in the coming years) will add important pieces of information to test INSs' capability to accelerate particles.

ACKNOWLEDGMENTS

The analysis of XMM-Newton as well as Chandra data is supported by the Italian Space Agency (ASI).

REFERENCES

- Arons, J. & Scharlemann, E.T., 1979, ApJ 231, 854
- Becker, W.; Aschenbach, B., 2002, MPE Report 278. Edited by W. Becker, H. Lesch, and J. Trmper. Garching bei Munchen: Max-Planck-Institut fr extraterrestrische Physik, 64
- Bignami, G.F. & Caraveo, P.A. 1996, Ann.Rev. Astron. Astrophys. 34,331
- Caraveo, P.A. 2000 in "Pulsar Astronomy - 2000 and Beyond", ASP Conference Series, Ed.s M. Kramer, N. Wex, and N. Wielebinski, 202,289
- Caraveo, P.A., De Luca, A., Mereghetti, S., Pellizzoni, A., Bignami, G.F., 2004, Science 305, 376
- Caraveo, P.A., Bignami, G.F., De Luca, A., et al., 2003, Science 301, 1345
- Caraveo, P.A., De Luca, A., Mignani, R.P., Bignami, G.F., 2001, ApJ 561, 930
- Caraveo, P.A., Mignani, R.P., 1999, A&A 344, 367
- Chatterjee, S. & Cordes, J. M., 2002, Ap.J. 575, 407
- De Luca, A. et al. 2005a Ap.J, 623, 1051
- De Luca, A. et al. 2005b A&A in press (astro-ph/0511185)
- Dyks, J. and B. Rudak, 2003, Ap.J., 598, 1201
- Gaensler, B.M., van der Swaluw, E., Camilo, F., et al., 2004, ApJ 616, 383
- Gaensler, B.M., 2005, "Young Neutron Stars and Their Environment", ASP Conf.Proc., eds F.Camilo and B.M.Gaensler, p.151 7)
- Goldreich, P. Julian, W.H., 1969, Ap.J.,157, 869
- Halpern J.P. and M. Ruderman, 1993, Ap.J., 415,286
- Harding, A. K. and J. K. Daugherty, 1998, Adv. Space Res. 21, 251
- Harding, A. K. 2005, Proceedings of the 22nd Texas Symposium on Relativistic Astrophysics at Stanford University, Stanford, 2004, edited by P. Chen et al., eConf C041213
- Hartman, R.C. et al., 1999, Ap.J.S.,123,79
- Helfand, D.J., Gotthelf, E.V., Halpern, J.P., 2001, ApJ 556, 380
- Lai, D., Chernoff, D.F., Cordes, J.M., 2001, ApJ 549, 1111
- Manchester, R.N. et al.,2005, A.J., 129,1993

- P.F. Michelson SPIE, 2003, 4851,1144 <http://www-glast.stanford.edu/>
- Mignani, R. P., de Luca, A., Caraveo, P. A., 2004, IAU Symposium no. 218 Ed.s Fernando Camilo and Bryan M. Gaensler. Astronomical Society of the Pacific, 2004,391
- Mori et al., 2004, ApJ, 609, 186
- Muslimov, A. G. and A. K. Harding, 2003, Ap. J 588, 430
- Ng, C.-Y., Romani, R.W., 2004, ApJ 601, 479
- Pavlov, G.G., Teter, M.A., Kargaltsev, O., Sanwal, D., 2003, ApJ 591, 1157
- Pellizzoni, A., Mattana, F., De Luca, A., et al., 2005, "High Energy Gamma-Ray Astronomy", eds. F.A. Aharonian, H.J.Vlk, D.Horns, AIP Conference Proceedings, 745, p.371
- Romani, R. W.,1996, Ap. J 470, 469
- Rudak, B. and J. Dyks, 1999, Mon. Not. R. Astron. Soc. 303, 477.
- Ruderman, M. A. & P. G. Sutherland 1975 Ap. J 196, 51
- Slane, P., 2005, Adv.Sp.Res. 35, 1092
- Stappers, B.W., Gaensler, B.M., Kaspi, V.M., van der Klis, M., Lewin, W.H.G., 2003, Science 299, 1372
- Sturrock, P. A., 1971 Ap. J 164, 529
- Tavani, M. et al., 2003, SPIE, 4851, 1151 <http://agile.mi.iasf.cnr.it>
- Thompson, D. J., 2001 in High Energy Gamma-Ray Astronomy, eds. F. A. Aharonian, H. Volk, AIP Conf. Proc. 558, p. 103112, 2001.
- Zhang, B. and A. K. Harding, 2000, Ap. J 532, 1150
- Willingale et al., 2001, A&A, 365, L212

XMM OBSERVATIONS OF THE SUPERSOFT SOURCE RX J0513.9-6951

K. E. McGowan¹, P. A. Charles², A. J. Blustin¹, M. Livio³, D. O’Donoghue², and B. Heathcote⁴

¹Mullard Space Science Laboratory, Holmbury St. Mary, Dorking, Surrey, RH5 6NT, UK

²South African Astronomical Observatory, P.O. Box 9, Observatory, 7935, South Africa

³STScI, 3700 San Martin Drive, Baltimore, MD 21218, USA

⁴Barfold Observatory, Glenhope, Victoria, 3444, Australia

ABSTRACT

Supersoft X-ray sources (SSSs) are thought to be Eddington limited accreting white dwarfs undergoing surface hydrogen burning, powered by thermally unstable mass transfer from a 1-2 M_{\odot} companion. However, this model has lacked direct confirmation from observations. The key SSS is RX J0513.9-6951 which has recurrent X-ray outbursts every 100-150 d (lasting ~ 40 d) during which the optical flux declines by 1 mag. We present the first XMM observations of RX J0513.9-6951 through one of its optical low states. We find that as the low state progresses the temperature and X-ray flux decrease; anti-correlated with the optical/UV emission. As the optical intensity recovers the white dwarf radius increases. The high resolution spectra show evidence of deep absorption features which vary during the optical low state.

Key words: stars; binaries; X-rays.

1. INTRODUCTION

Supersoft sources (SSSs) are a class of X-ray objects with the defining characteristic of extremely luminous emission ($L_X \sim 10^{37} - 10^{38}$ erg s⁻¹) at very soft (< 0.5 keV) X-ray energies. The presence of strong emission lines of H, HeII and higher ionization species in the optical spectra of SSSs indicate that they are low mass X-ray binaries (LMXBs; e.g. van Paradijs & McClintock 1995). However, the nature of the compact object was unclear. “Normal” LMXBs containing neutron star or black hole accretors radiate in a wider energy range at the typical luminosities observed in the SSSs. Using the observed SSS temperatures and bolometric luminosities, van den Heuvel et al. (1992, hereafter vdH92) proposed that the SSSs contain white dwarfs. The near-Eddington luminosities are achieved because the white dwarf accretor is able to sustain steady nuclear burning at its surface. This requires high accretion rates of $> 10^{-7} M_{\odot} \text{ yr}^{-1}$. Such rates are attainable if the donor star is comparable to or

more massive than the white dwarf, so that thermally unstable mass transfer occurs (e.g. Paczyński 1971).

While several systems show SSS characteristics, the vdH92 model for the SSSs lacked convincing observational confirmation. Circumstantial evidence in its favour was presented by Southwell et al. (1996; hereafter S96) who showed that the observed bipolar outflow emission lines (Pakull et al. 1993; Cowley et al. 1996) in the transient SSS, RX J0513.9-6951 (hereafter RXJ0513), have velocities comparable to the escape velocity of a massive white dwarf.

MACHO (Alcock et al. 1995) observations of RXJ0513 provided a breakthrough in our understanding of the SSSs. S96 produced a 3.5 year lightcurve of the optical counterpart which revealed recurrent low states (dropping by ~ 1 mag) at quasi-regular intervals (every 100 – 200 d) and remaining low for $\sim 20 - 40$ d. More importantly, *ROSAT* X-ray detections of RXJ0513 (Schaeidt et al. 1993) are only reported during such optical low states, while no outbursts have been observed during the extensive optical high states i.e. the X-ray and optical states are anti-correlated.

The behaviour observed in RXJ0513 is difficult to reconcile with a regular thermonuclear flash model which is normally accompanied by radius expansion and an increased optical luminosity. Instead, S96 proposed that contraction of the white dwarf from an expanded, Eddington-limited state to a steady shell-burning phase could cause the X-ray outburst. S96 suggested that the contractions could be due to a decrease in the otherwise very high accretion rate, which would also account for the simultaneous optical low states. Of course, the shell luminosity will be even higher in the optically bright state, but the system is then close to the top of the steady burning strip in the $M - M_{WD}$ plane (Nomoto 1982) which means the white dwarf is inflated (Kovetz & Prialnik 1994). Hence most of the shell luminosity would then be emitted in the UV or EUV. This leads to the prediction that, if this model is correct, as the X-ray outburst evolves it will end with its peak emission shifting into the EUV

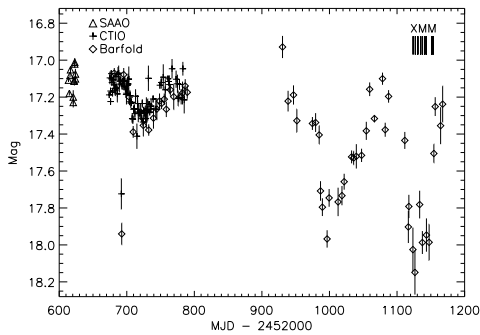


Figure 1. Optical lightcurve of RXJ0513. The observations were obtained at SAAO (triangles), CTIO (crosses) and Barfold Observatory (diamonds). The start times of the X-ray observations are marked.

and UV.

We present *XMM-Newton* observations of RXJ0513 through one of its optical low states. We use these data to examine the validity of the vdH92 paradigm for SSS via the prediction of S96 for the X-ray turn-on and turn-off. If we can confirm directly the vdH92 paradigm for SSS then this will also establish them as one of the strong candidates for the progenitors of type Ia supernovae (see e.g. Livio 1996).

2. OBSERVATIONS AND DATA REDUCTION

We monitored RXJ0513 using ground based optical instruments from 2002 December 5 to 2004 June 11. The optical light curve of RXJ0513 is shown in Figure 1. When RXJ0513 started its ~ 1 mag drop in the optical we triggered our *XMM-Newton* ToO observations. A set of nine X-ray measurements were taken from 2004 April 28 to 2004 May 28. The start of each *XMM-Newton* observation is marked in Figure 1.

We obtained *XMM-Newton* data using the Optical Monitor (OM; Mason et al. 2001), both EPIC instruments, MOS (Turner et al. 2001) and PN (Strüder et al. 2001), and the Resolution Grating Spectrometer (RGS; den Herder et al. 2001). The data were reduced using the *XMM-Newton* SCIENCE ANALYSIS SYSTEM (SAS).

The OM observations were taken using the *UVW2* filter. We performed the photometry using a $5''$ radius aperture, subtracting a background extracted from a $10''$ aperture offset from the source.

The EPIC observations were taken in timing mode, with the thin filter. The data were filtered to exclude times of high background and events that may have incorrect energies, to include only single photon events for MOS and only single and double photon events for PN, and to include only photons with energies in the range $0.3 - 10$ keV. EPIC spectra were extracted using a region centered

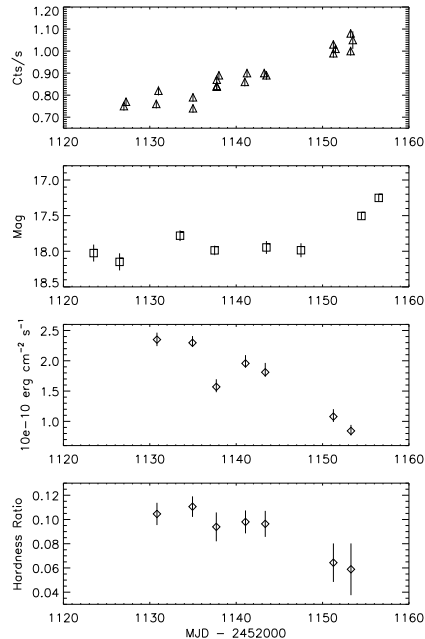


Figure 2. First panel: OM *UVW2* light curve of RXJ0513, second panel: contemporaneous optical data from Barfold Observatory, third panel: EPIC-PN lightcurve ($0.2-10$ keV), fourth panel: hardness ratio.

on RXJ0513, corresponding background spectra were extracted using a region of similar size offset from the source position. In each case we created a photon redistribution matrix (RMF) and ancillary region file (ARF). The spectra were regrouped by requiring at least 30 counts per spectral bin. The subsequent spectral fitting and analysis was performed using XSPEC. We extracted source and background light curves from the filtered event files, which had been barycentrically corrected, using the same regions.

We extracted RGS spectra for RXJ0513, subtracting the background using regions adjacent to that containing the source. We combined the RGS1 and RGS2 spectra, including both first and second order data, channel by channel for each observation using the method described by Page et al. (2003). We analysed the RGS spectra using SPEX v2.00 (Kaastra et al. 2002).

3. UV AND OPTICAL LIGHTCURVES

We show in Figure 2 the OM lightcurve of RXJ0513 with contemporaneous ground-based optical data points. The UV intensity is roughly constant at the start of the observations. By MJD 2453137 the UV flux had started to increase, this brightening continued during the remaining observations. By comparing the start of the rise in the UV intensity to the rise in the optical we can see that the UV leads the optical. The lightcurves indicate that the UV brightening is more gradual than in the optical.

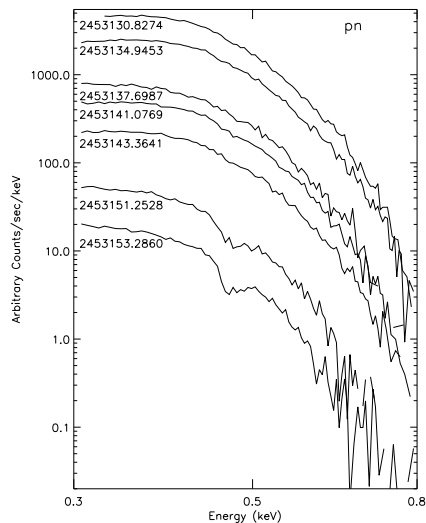


Figure 3. EPIC-PN spectra of RXJ0513 plotted in chronological order of descending time.

We have also plotted the EPIC PN flux in the 0.2 – 10 keV band. The overall trend for the X-rays during our observing period is a reduction in the X-ray flux. The fourth panel in Figure 2 shows the hardness ratio, which is seen to decrease as the UV and optical intensity increases. We define the hardness ratio for our data as $(0.5 - 0.8)/(0.3 - 0.5)$ keV.

4. LOW RESOLUTION X-RAY SPECTROSCOPY

For the spectral analysis we have only used the higher signal-to-noise PN data. Since no substantial emission is detected at energies > 0.8 keV we extracted the PN spectrum over 0.3 – 0.8 keV for each observation. In each case we fitted the PN spectra with a blackbody model modified by neutral photoelectric absorption. We modelled all the PN spectra simultaneously and found $N_H = (0.62^{+0.03}_{-0.01}) \times 10^{21} \text{ cm}^{-2}$ (consistent with the galactic value) and $kT = 43.95^{+0.55}_{-3.45} \text{ eV}$. We fit each individual PN spectra, fixing the column density at the value found from fitting all of the PN spectra simultaneously.

We find that the blackbody model does not fit the spectra well implying that a more sophisticated model is required to describe the X-ray emission from RXJ0513. We show in Figure 3 the PN spectra in chronological order. The last two spectra show apparent broad absorption features just below 0.5 keV. Adding one or more absorption edges to the fit (at the observed energy they could originate from C V and/or C VI) does not improve the fit.

While the blackbody model is a poor fit to the spectra, we can however investigate the evolution of the spectra by treating the values obtained as representative of the gross spectral properties. We find that the temperature varies between 38.7 – 47.5 eV, and the blackbody luminosity between $(1.1 - 2.0) \times 10^{38} \text{ erg s}^{-1}$. These values

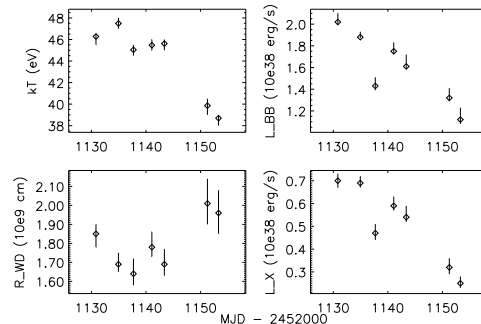


Figure 4. The evolution of kT , blackbody luminosity (L_{BB}), white dwarf radius (R_{WD}) and X-ray luminosity in the 0.2–10 keV band (L_X).

are consistent with those found by Schaeidt et al. (1993) from the ROSAT data, as is the value for N_H . We show in Figure 4 the evolution of kT , blackbody luminosity, white dwarf radius and X-ray luminosity in the 0.2 – 10 keV band, during our observations. As the source starts to emerge from the optical low state we see that the temperature and X-ray luminosity both decrease. This is anti-correlated with the optical and UV emission.

5. HIGH RESOLUTION X-RAY SPECTROSCOPY

The RGS spectra (Figure 5) show evidence of deep absorption features and probably some low significance narrow emission lines. The absorption lines can be identified with transitions from a range of high-ionization ions. Figure 6 shows three individual features plotted in velocity space: C VI Ly α at 33.736 Å, Ar XIII/Ar XIV at 27.463 Å (blended at the RGS spectral resolution), and S XIV at 30.441 Å. It is clear that the lines are blue-shifted and that there are two or more velocity components; the outflow velocity along our line of sight lies between zero and $\sim 3000 \text{ km s}^{-1}$.

Figure 6 also indicates that the optical depth of the absorbers increases over the course of the observations. This is seen most clearly in the case of C VI Ly α , which is barely present in the first spectrum, deepens significantly and becomes heavily saturated by the final observation. The velocity structure of the medium is best indicated by the S XIV and Ar XIII/Ar XIV features; although there are some apparent changes over the course of the observations, there appear to be two main velocity components at $\sim -1000 \text{ km s}^{-1}$ and $\sim -3000 \text{ km s}^{-1}$ respectively.

Figure 7 shows a comparison of the fifth RGS spectrum (MJD 2453141.5636) with a simple photoionized absorption model to highlight the positions of the major features. The model continuum was chosen to represent the overall shape of the first RGS spectrum (MJD 2453127.0784), which has the least amount of intrinsic ionized absorption and therefore the most continuum visible. The model continuum consists of a Compton-

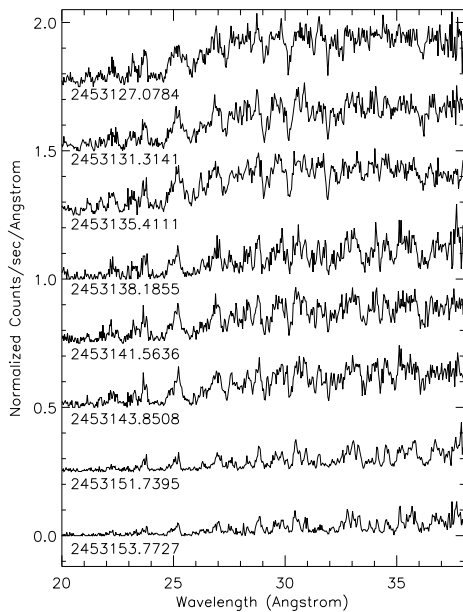


Figure 5. RGS spectra of RXJ0513 plotted in increasing time order from top to bottom.

scattered 70 eV blackbody, with Galactic neutral absorption at the average column derived from the fits to the PN data. The intrinsic ionized absorption is represented using the *xabs* photoionized absorption model in SPEX v2.00 (Kaastra et al. 2002). We find that the depths of the observed features require abundances that are greater than Solar. If the relative elemental abundances in the ionized outflows in RXJ0513 really are several factors above Solar values, this may imply that the outflows contain the products of hot CNO burning.

Comparing the models with the observed spectrum in Figure 7, it is clear that a simple photoionized absorption model is not an adequate representation of the data; this is unsurprising since the assumption of absorption from the ground state would not be valid in a high density medium such as a white dwarf atmosphere. It is also very likely that atomic data are missing or perhaps inaccurate in the current model for various features in the spectrum; identification of ionic species is further complicated by the likelihood that the observed features consist of complicated blends of many different transitions.

Approximating the underlying continuum as a blackbody spectrum is probably still too simplistic; the continuum and intrinsic absorption will need to be modelled self-consistently in order to reach a more accurate understanding of both. Lanz et al. (2005) have shown that a white dwarf atmosphere model is a good representation of the soft X-ray spectrum of the supersoft source CAL 83, although they found no evidence for a high-speed outflow in that source. A white dwarf atmosphere model with the addition of winds and outflows may indeed be required to reproduce the RGS spectra of RXJ0513. Nevertheless, the present model demonstrates clearly that much of the soft X-ray spectral complexity of RXJ0513 is consistent

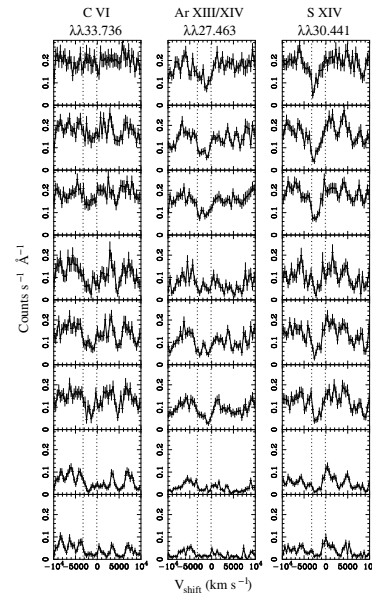


Figure 6. Absorption features from the RGS spectra plotted in velocity space; C VI Ly α , an Ar XIII/Ar XIV blend and a S XIV line at 33.736, 27.463 and 30.441 Å, respectively. The dotted lines at 0 and -3000 km s $^{-1}$ mark the approximate boundaries of the features.

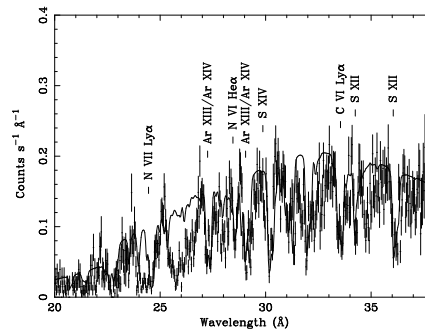


Figure 7. RGS spectrum 5 (MJD 2453141.5636) compared with a simple photoionized absorption model. The positions of various important features are labelled.

with the presence of highly ionized outflowing gas.

6. DISCUSSION

The white dwarf contraction model proposed by S96 is based on the prediction that the rise in the X-rays occurs after the drop in optical luminosity. From the vdH92 model, during the optical bright state the accretion rate is very high ($> 10^{-7} M_{\odot} \text{ yr}^{-1}$). Under these conditions, the white dwarf is slightly inflated, and a large majority of the shell luminosity is likely emitted in the UV. As the accretion rate drops, leading to a reduction in the optical flux, the photosphere contracts slightly (e.g. Kovetz & Prialnik 1994), this raises the effective temperature and hence produces an increase in the X-ray luminosity.

We do not have X-ray observations before the drop, however, previous observations have shown that X-rays are not detected when the source is in its optical high state. Our observations confirm that while RXJ0513 is in its optical low state we see the source in X-rays.

The behaviour of the UV and optical intensity is roughly correlated in the optical low state. However, the UV flux starts to rise before the optical luminosity increases. We find that as the optical low state progresses the X-ray flux decreases, this is anti-correlated with the optical and UV. This implies that as the X-ray outburst is evolving the peak of the emission has moved into the UV, confirming the prediction of the contraction model.

Although our blackbody fits to the PN spectra are poor, the values implied by the fits are indicative of the global evolution of the X-ray emission. We find that the temperature and luminosity decrease during the optical low state. The radius determined from the fits decreases during the first observations. As the optical (and UV) intensity recovers the radius increases. In the context of the contraction model (e.g. Hachisu & Kato 2003a,b), the enhanced X-ray flux will irradiate the companion star and, either by inflating material above the secondary's photosphere and causing it to be transferred (e.g. Ritter 1988) or by heating the magnetic spot region (see Parker 1979), will cause the mass transfer rate to increase again. This coincides with the white dwarf photosphere re-inflating, hence the radius gets larger, and the X-ray flux decreases again. Therefore, as RXJ0513 returns to its optical high state the source is once again not observable in X-rays.

Our spectral fits to the PN data indicate that a more complicated model is needed to describe the X-ray emission. The higher spectral resolution data from the RGS reveal the existence of highly ionized gas outflowing along our line of sight at speeds of up to 3000 km s^{-1} , with multiple velocity components that evolve over time. The optical depth of the ionized absorption appears to increase over the course of the RGS observations; this is borne out by the lower-resolution PN spectra, in which deep absorption features become apparent in the final two spectra. The presence of this absorption partly explains why the blackbody fits are so poor.

There are a variety of possible causes for the increase in optical depth of the intrinsic absorption. We could be viewing the system close to pole-on (i.e. low inclination) through the (presumably) bipolar outflow, and the intrinsic covering factor of the outflow is changing. Possible explanations for this include the effects of a magnetic cycle of the optical star, the expansion of the white dwarf or the system precessing with respect to our line of sight.

Alternatively, it might not be the bipolar outflow we are seeing, but actually the process of expansion of the white dwarf surface itself, as highly ionized nova by-products stream out from the white dwarf surface and gradually build into an optically-thick inflated surface, confined by the gravity of the white dwarf. The increase in optical/UV radiation would then occur as the 'intrinsic' X-rays are

down-scattered in the increasingly optically thick outer inflated layer of the white dwarf. The apparently anomalous abundances of Sulphur, Argon and Nitrogen in the ionized outflow may indeed imply that the gas originated in the nova nucleosynthesis. The abundances may be modified in the atmosphere of the steady nuclear burning white dwarf via hot CNO burning (cf. CNO abundances for CAL83 using NLTE model atmospheres, Lanz et al. 2005).

We find that the RGS spectra deviate from the blackbody approximation at $24 - 27 \text{ \AA}$ this may be due to effects of carbon transitions in this range due to a white dwarf atmosphere. A white dwarf atmosphere with an effective temperature as deduced from the blackbody fits to the PN data shows that with increasing gravity (white dwarf mass) above the C VI edge the atmospheric density increases. This shifts the ionization equilibrium toward a lower degree of ionization, causing the emission edges to turn to absorption (e.g. Hartmann & Heise 1997). For the same gravity the energy of the C absorption shifts to lower energies due to a change of the ionization state of C. Thus the C V-VI absorption due to the white dwarf stellar atmosphere may be at least partly responsible for the disagreement found from the blackbody approximation (see Paerels et al. 2001; Rauch et al. 2005).

The existence of an ionized absorber in the X-ray spectrum of RXJ0513 seems plausible as the absorption lines found in the RGS spectrum of the fifth (and other) observations of the source require a shift due to a velocity up to 3000 km s^{-1} which is consistent with the escape velocity of a massive white dwarf. In RXJ0513 the existence of absorption structures which cannot be explained by a photoionized absorber model (especially those between $24 - 27 \text{ \AA}$) indicates that the absorption takes place in a high-density medium. This would be consistent with an origin in a white dwarf atmosphere.

The spectral model we constructed for the fifth RGS spectrum in the series does reproduce many spectral features due to the ionized outflow in RXJ0513. The ionization structure for such an ionization parameter would be consistent with that of the outflowing version of model 8 in Kallman & McCray (1982), which models gas photoionized by a blackbody emitter. We can estimate the mass outflow rate assuming the accretion is slightly super-Eddington. The Eddington luminosity is $L_{Edd} \sim 1.2 \times 10^{38} M / M_{\odot} \text{ erg s}^{-1}$ (e.g. Grimm et al. 2002). As $\dot{M}_{out} \nu = L_{Edd} / c$ (see King & Pounds 2003), we determine with $M = 1 M_{\odot}$, $L_{Edd} = 1.2 \times 10^{38} \text{ erg s}^{-1}$, and $\nu = 3000 \text{ km s}^{-1}$, $\dot{M}_{out} = 2.1 \times 10^{-7} M_{\odot} \text{ yr}^{-1}$. This value for the mass outflow rate is consistent with the wind mass loss rate estimated by Hachisu & Kato (2003b) for RXJ0513.

We can also directly compare the physical parameters inferred from the observational data of the low-state egress of RXJ0513 with the parameters predicted by the model of Hachisu & Kato (2003b), for the high/low state transitions of RXJ0513. The evolution of the blackbody temperature inferred from the EPIC-PN data follows roughly

the evolution of the temperature as inferred by Hachisu & Kato (2003b), although the temperatures and the radii inferred from the observations are about 25% higher and a factor of 2 smaller, respectively. One prediction of the Hachisu & Kato (2003b) model are winds from the white dwarf with a wind mass-loss rate of $\sim 10^{-7} M_{\odot} \text{ yr}^{-1}$ during this part of the lightcurve. We can estimate the optical depth of such a highly ionized wind due to Thomson scattering opacity assuming an outflow velocity of 3000 km s^{-1} and a radius of 10^9 cm . For a wind mass-loss rate of $10^{-7} M_{\odot} \text{ yr}^{-1}$ we calculate an optical depth of 1 which is sufficient to obscure the soft X-ray source during the low-state egress.

7. SUMMARY

We have presented a series of *XMM-Newton* EPIC-PN and RGS observations during the late phase (onset of egress) of an optical low-state of the supersoft X-ray source RXJ0513. Simultaneous *XMM-Newton* OM and long-term ground based optical monitoring are also reported. We have derived the evolution of the fluxes in the observed bands and the evolution of the X-ray spectral parameters from a blackbody spectral fit to the EPIC-PN data. We find that the temperature and luminosity decrease, and an indication of an increase in the radius of the blackbody emitter with time. During the late phase of the optical low-state we find broad spectral dips in the EPIC-PN spectra just below 0.5 keV. The RGS spectra show deep absorption features (e.g. C VI, Ar XIII/XIV, S XIV) which deepen with time and in addition some weak emission lines. We model the RGS spectra with a Compton-scattered 70 eV blackbody with Galactic neutral absorption and additional intrinsic ionized absorption due to outflowing gas using a photoionized absorption model. Our spectral model for the fifth RGS spectrum, which was taken in the deepest part of the optical low state, requires velocities of the outflowing gas of up to 3000 km s^{-1} . We find that the spectral model lies above the observed spectrum in the $24 - 27 \text{ \AA}$ regime which is likely to be due to effects related to the white dwarf atmosphere.

ACKNOWLEDGMENTS

This work is based on observations obtained with *XMM-Newton*, an ESA science mission with instruments and contributions directly funded by ESA Member States and NASA.

REFERENCES

- Alcock C., et al. 1995, *Phys. Rev. Lett.*, 74, 2867
- Cowley A. P., Schmidtke P. C., Crampton D., Hutchings J. B. 1996, In: eds van den Heuvel E. P. J., van Paradijs J., Proc. IAU Symp. 165: Compact Stars in Binaries, Kluwer, Dordrecht, p. 439
- den Herder J. W., et al. 2001, *A&A*, 365, L7
- Grimm H. -J., Gilfanov M., Sunyaev R. 2002, *A&A*, 391, 923
- Hachisu I., Kato M. 2003a, *ApJ*, 590, 445
- Hachisu I., Kato M. 2003b, *ApJ*, 588, 1003
- Hartmann H. W., Heise J. 1997, *A&A*, 322, 591
- Kaastra J. S., Mewe R., Raassen A. J. J. 2002, in *ESA SP-488, New visions of the X-ray Universe in the XMM-Newton and Chandra Era*, ed. F. Jansen, electronic proceedings
- Kallman T. R., McCray R. 1982, *ApJS*, 50, 263
- King A. R., Pounds K. A. 2003, *MNRAS*, 345, 657
- Kovetz A., Prialnik D. 1994, *ApJ*, 424, 319
- Lanz T., Telis G. A., Audard M., et al. 2005, *ApJ*, 619, 517
- Livio M. 1996, in: ed Greiner J., *Lecture Notes in Physics 472: Supersoft X-ray Sources*, Springer-Verlag, p. 183
- Mason K. O., et al. 2001, *A&A*, 365, L36
- Nomoto K. 1982, *ApJ*, 253, 798
- Paerels F., Rasmussen A. P., Hartmann H. W., et al. 2001, *A&A*, 365, 308
- Paczyński B. 1971, *ARAA*, 9, 183
- Page M. J., Davis S. W., Salvi N. J. 2003, *MNRAS*, 343, 1241
- Pakull M. W., et al. 1993, *A&A*, 278, L39
- Parker E. N. 1979, *Cosmical Magnetic Fields* (Oxford: Clarendon)
- Rauch T., Werner K., Orio M. 2005, *Proceedings ITAMP Workshop: X-ray Diagnostics for Astrophysical Plasmas: Theory, Experiment, and Observation*. 2004 November 15-17 Cambridge, USA, (astro-ph/0501012)
- Ritter H. 1988, *A&A*, 202, 93
- Schaeidt S., Hasinger G., Trümper J. 1993, *A&A*, 270, L9
- Southwell K. A., Livio M., Charles P. A., et al. 1996, *ApJ*, 470, 1065
- Strüder L., et al. 2001, *A&A*, 365, L18
- Turner M. J. L., et al. 2001, *A&A*, 365, L27
- van den Heuvel E. P. J., Bhattacharya D., Nomoto K., Rappaport S. A. 1992, *A&A*, 262, 97
- van Paradijs J., McClintock J. E. 1995, In: eds Lewin W. H. G., van den Heuvel E. P. J., *X-ray Binaries*, Cambridge Univ. Press, Cambridge, p. 58

DENSITY DIAGNOSTICS OF THE HOT PLASMA IN AE AQUARII WITH XMM-NEWTON

Manabu Ishida

Department of Physics, Tokyo Metropolitan University, 1-1 Minami-Osawa, Hachioji, Tokyo 192-0397, JAPAN

ABSTRACT

We report on *XMM-Newton* observations of the magnetic cataclysmic variable (mCV) AE Aqr. High resolution spectroscopy of the He-like triplet of N and O with the RGS has enabled us to measure the electron number density of the plasma to be $\sim 10^{11} \text{ cm}^{-3}$. Incorporating this with the emission measure, we estimate the geometrical scale of the plasma responsible for the N and O line emission, with ionization temperature $kT_i = 0.2\text{--}0.3 \text{ keV}$, to be $\ell_p \simeq (2\text{--}3) \times 10^{10} \text{ cm}$. Since both the density and the scale are incompatible with a standard post-shock accretion column of a mCV, the hot plasma in AE Aqr cannot be a product of mass accretion onto the white dwarf. The widths of the H-like $K\alpha$ emission (= $\text{Ly}\alpha$) lines of N and O, on the other hand, are measured to be $1250\text{--}1600 \text{ km s}^{-1}$ with the RGS. This is significantly larger than the thermal velocity expected for the ionization temperature of N and O plasma, but is rather consistent with that of the maximum plasma temperature $kT_{\text{max}} = 4.6 \text{ keV}$ measured with the EPIC cameras. It is known that Balmer series and UV emission lines also show similar line widths. As the optical and UV lines, the X-ray emission lines also show dramatic flaring activity. These facts strongly suggest that all these broad emission lines from X-ray to optical wavebands are produced in the course of adiabatic cooling of the plasma once heated up to T_{max} in the deep gravitational potential of the white dwarf.

Key words: binaries: close — novae, cataclysmic variables — stars: individual (AE Aquarii) — plasmas — X-rays: stars.

1. INTRODUCTION

AE Aqr is a close binary system composed of a magnetized white dwarf rotating at a period of 33.08 s (Patterson, 1979) and a late type K3V-K5V star (Welsh, Horne, & Gomer, 1995) in a 9.88-h orbit (Welsh, Horne, & Gomer, 1993) whose inclination angle is $58^\circ \pm 6^\circ$ (Casares et al., 1996). The masses of the primary and

the secondary are evaluated to be $M_1 = 0.79 \pm 0.16 M_\odot$ and $M_2 = 0.50 \pm 0.10 M_\odot$ (Casares et al., 1996).

AE Aqr has been known as one of the most enigmatic magnetic Cataclysmic Variables (mCVs) showing large optical flares and flickering (Patterson, 1979), large radio flares (Bastian, Beasley, & Bookbinder, 1996), TeV γ -ray emissions (Meintjes et al., 1994). In addition to these, although the long orbital period leads us to expect an accretion disk, the spectral profile of an $\text{H}\alpha$ emission line is single-peaked and its centroid velocity is found to be inconsistent with the white dwarf orbit but lags behind the secondary orbit by some $70^\circ\text{--}80^\circ$ (Welsh, Horne, & Gomer, 1993). Spectral widths of Balmer emission lines are highly variable with a full width at zero intensity of $\sim 1000 \text{ km s}^{-1}$ to over 4000 km s^{-1} during flares for the $\text{H}\alpha$ line (Welsh, Horne, & Gomer, 1998). The widths of the same order are reported also for $\text{H}\beta$ and $\text{H}\gamma$ emission lines (Reinsch & Beuermann, 1994). Hard X-ray emission from mCVs originates from the post-shock plasma in an accretion column whose temperature is a few tens of keV in mCVs in general (Ezuka & Ishida, 1999; Ishida & Fujimoto, 1995). The maximum temperature of AE Aqr is, on the other hand, as low as $\sim 3 \text{ keV}$ (Eracleous, 1999; Choi, Dotani, & Agrawal, 1999). All of these results, along with the discovery of a steady spin-down of the white dwarf at a rate $\dot{P} = 5.64 \times 10^{-14} \text{ s s}^{-1}$ (de Jager et al., 1994), led Wynn, King, & Horne (1997) to introduce the magnetic propeller model in which “blobby” accreting matter originally following a ballistic trajectory from the inner Lagrangian point, experiences a drag from the magnetic field of the white dwarf, and is finally blown out of the binary due to so-called propeller action.

In this paper, we present results of density diagnostics of the plasma in AE Aqr by means of a well-resolved He-like triplet of N and O with the RGS. The results of this observation will be found in full detail in Itoh et al. (2006).

2. OBSERVATION

AE Aqr was observed with *XMM-Newton* on 2001 November 7–8. In total, 27 ks data are available for the

RGS and 17 ks for the EPIC pn/MOS. A detailed observation log can be found in Itoh et al. (2006). In Fig. 1 shown are the pn, MOS1, RGS1 and RGS2 light curves. As evident from the RGS2 light curve, the X-ray emis-

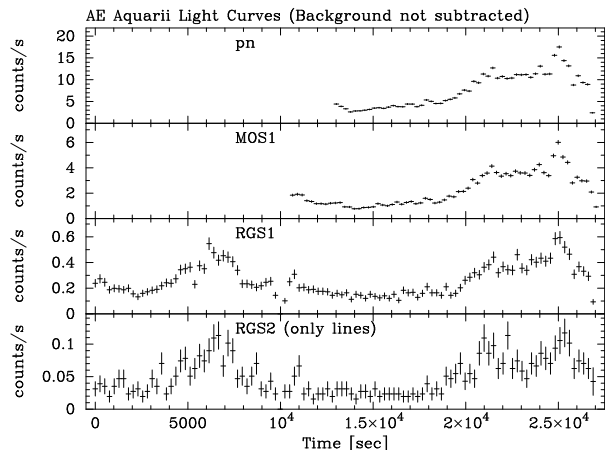


Figure 1. The light curves of EPIC pn and MOS1 in the band 0.2–15 keV, RGS1 in the band 5–35 Å, and RGS2 only with H-like and He-like $K\alpha$ photons from N, O and Ne, but excluding the He-like $K\alpha$ of O for which the corresponding CCD chip is dead. A common bin size of 256 sec is adopted. The source integration region is a circle with a radius of $57''.4$ and $50''.6$ for pn and MOS1, respectively. The RGS light curves are created with the 1st order photons.

sion lines show dramatic flaring activity as the optical and UV emission lines do (Eracleous & Horne, 1996), in correlation with the continuum emission that dominates the EPIC light curves and spectra.

We have searched for an X-ray pulsation in the EPIC pn light curve created in the band 0.2–10 keV, and have detected a sinusoidal pulse at a period of 33.08 ± 0.04 s by means of the epoch folding method both during quiescence and flare periods (time intervals of 13,000–18,700 s and 21,000–27,000 s in Fig. 1, respectively). The pulse period is consistent with the optical one (Patterson, 1979; de Jager et al., 1994).

3. DATA ANALYSIS

3.1. EPIC Spectra

The time-averaged energy spectrum extracted from the EPIC MOS2 is shown in Fig. 2. A number of H-like and/or He-like $K\alpha$ emission lines of abundant metals from N through Fe can be recognized. The coexistence of these lines indicates that the X-ray-emitting plasma is optically thin and thermal, and has a significant temperature distribution in the range $kT \simeq 0.1$ –10 keV. In fact, we need four optically thin thermal plasma emission components with different temperatures to fit the spectra of the EPIC pn, MOS1, and MOS2 simultaneously. The

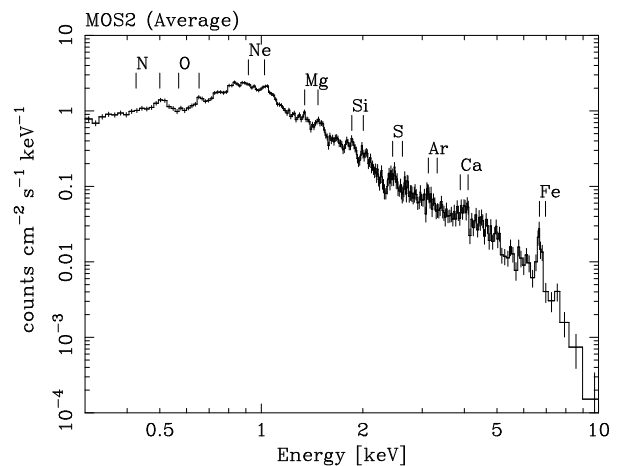


Figure 2. The time-averaged spectrum of AE Aqr taken with the EPIC MOS2. Energies of hydrogenic and He-like $K\alpha$ lines from N through Fe are indicated with short vertical lines.

parameters of the best-fit 4-temperature VMEKAL model are summarized in table 1. The resultant temperatures are 0.14, 0.59, 1.4, and 4.6 keV. Their emission measures are 1.3, 3.6, 2.7, and $5.3 \times 10^{53} \text{cm}^{-3}$, and in total $1.29 \times 10^{54} \text{cm}^{-3}$, for an assumed distance of 100 pc (Welsh, Horne, & Oke, 1993; Friedjung, 1997). A common hydrogen column density of $3.6 \times 10^{20} \text{cm}^{-2}$ is necessary to represent the photoelectric absorption. The metal abundances are subsolar and are in the range 0.4–0.8 Z_{\odot} in general, except for N, where $Z = 3.5 \pm 0.9Z_{\odot}$.

3.2. Spectra of He-like Triplets from the RGS

In Fig. 3 we have shown the RGS spectrum averaged throughout the observation. $K\alpha$ emission lines from N through Si in the H-like and/or He-like ionization states can easily be recognized. Figure 4 (a)–(c) are blow-ups of energy bands of the He-like triplets of N, O, and Ne. In the next column (d)–(f) shown are the spectra predicted by the best-fit 4-temperature VMEKAL model. The intercombination line (*i* in the figure) is stronger and the forbidden (*f* in the figure) is weaker in the observed spectra, compared to the model spectra for N and O. This behavior can be attributed to a high density effect. If the electron density exceeds a certain critical value inherent in each element, on the other hand, one of the two electrons excited to the upper level of the forbidden line (3S_1) is further pumped to the higher level $^3P_{2,1}$ by another impact of a free electron, and is then relaxed by radiating the intercombination line. The relative intensities of the intercombination and forbidden lines can therefore be utilized as a density diagnostic (Gabriel & Jordan, 1969; Pradhan & Shull, 1981; Porquet et al., 2001).

In order to obtain the electron number density n_e , we begin by evaluating intensities of the He-like triplets. For this, we utilize the 4-temperature VMEKAL model that provides the best-fit to the EPIC pn and MOS spectra

Table 1. The best-fit parameters of the 4 temperature vmekeal model being fit to EPIC pn and MOS spectra

Parameter	Value	Element	Abundance ^a
N_{H} (10^{20}cm^{-2})	$3.59^{+1.47}_{-1.20}$	N	$3.51^{+0.92}_{-0.81}$
kT_1 (keV)	$4.60^{+0.60}_{-0.47}$	O	$0.74^{+0.17}_{-0.23}$
kT_2 (keV)	$1.21^{+0.13}_{-0.08}$	Ne	$0.43^{+0.28}_{-0.25}$
kT_3 (keV)	$0.59^{+0.02}_{-0.02}$	Mg	$0.70^{+0.15}_{-0.14}$
kT_4 (keV)	$0.14^{+0.05}_{-0.02}$	Si	$0.81^{+0.15}_{-0.12}$
N_1^{b} (10^{-3})	$4.45^{+0.41}_{-0.44}$	S	$0.73^{+0.20}_{-0.18}$
N_2^{b} (10^{-3})	$2.25^{+0.52}_{-0.51}$	Ar	0.21 (< 0.89)
N_3^{b} (10^{-3})	$3.04^{+0.47}_{-0.41}$	Ca	0.19 (< 1.11)
N_4^{b} (10^{-3})	$1.07^{+0.64}_{-0.37}$	Fe	$0.47^{+0.07}_{-0.06}$
$N_{\text{pn}}/N_{\text{MOS}}^{\text{c}}$	$1.08^{+0.01}_{-0.01}$	Ni	$1.27^{+0.57}_{-0.50}$
χ^2_{ν} (d.o.f.)	1.22 (992)		

a: Solar Abundances (Anders & Grevesse, 1989)

b: Normalization of the VMEKAL component obtained with pn camera in a unit of $10^{-14}/4\pi D^2 \int n_e n_H dV$, where D [cm] is the distance to the target star.

c: Ratio of continuum normalizations.

(§ 3.1). The abundances are also fixed at the best-fit values, except for an element to be used as a density diagnostic, for which the abundance is set equal to zero, and instead, four Gaussians are added, representing the He-like triplet and the $\text{Ly}\alpha$ line. The best-fit model is displayed in Fig. 4 (a)-(c) as the histograms.

The ionization temperatures kT_i calculated from the intensity ratio between the $\text{Ly}\alpha$ and r are obtained to be 0.18, 0.30, and 0.34 keV for N, O, and Ne, respectively. The emission measures (EM s) of the plasma components with these temperatures can be calculated from the intensities of the $\text{Ly}\alpha$ and r lines with the aid of the EPIC abundances (see table 1), which result in $EM = 1.5$, 1.8, and $9.1 \times 10^{53} \text{cm}^{-3}$, respectively.

Given the line intensities of the triplets, we have carried out density diagnostics by means of the intensity ratio $f/(r+i)$. In Fig. 4 (g)-(i) shown are theoretical curves of the ratio $f/(r+i)$ versus the electron number density calculated with the plasma code SPEX (Kaastra, Mewe, & Nieuwenhuijzen, 1996) at kT_i of each element. In each panel we have also drawn a range of the intensity ratio allowed from the data and the resultant density range as a box. The electron number densities are found to be $(0.14\text{--}1.3) \times 10^{11} \text{cm}^{-3}$, $(0.40\text{--}6.8) \times 10^{11} \text{cm}^{-3}$, and $< 9.3 \times 10^{12} \text{cm}^{-3}$ for N, O, and Ne, respectively. As an approximation, we obtain $n_e \simeq 10^{11} \text{cm}^{-3}$. This density, together with the emission measure obtained above, results in the linear scale of the plasma components with $kT_i = 0.2\text{--}0.3$ keV of $\ell_p = (EM/n_e^2)^{1/3} \simeq (2\text{--}3) \times 10^{10} \text{cm}$.

3.3. Spectra of H-like $\text{K}\alpha$ Lines from the RGS

It is known that the wavelength of the $\text{H}\alpha$ line from AE Aqr shows a sinusoidal orbital Doppler modulation

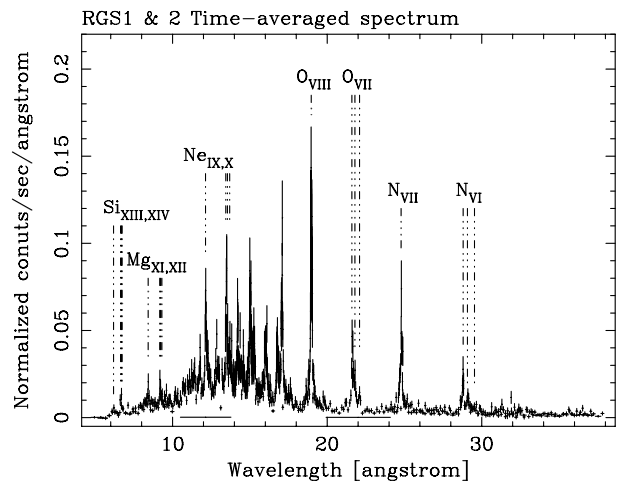


Figure 3. The averaged RGS spectra. Identifications of the H-line and He-like $\text{K}\alpha$ lines of N through Si are shown with dotted-dashed line. The other unidentified lines are mainly those associated with Fe-L transitions.

with an amplitude of $\sim 150 \text{km s}^{-1}$ (Robinson, Shafer, & Balachandran, 1991; Wynn, King, & Horne, 1997; Welsh, Horne, & Gomer, 1998). A similar behavior is found from a series of UV emission lines with a velocity amplitude of generally $110\text{--}220 \text{km s}^{-1}$ (Eracleous & Horne, 1996). In order to search the X-ray emission lines for a similar orbital modulation, we have made RGS spectra during the first and second flares separately. The spectra are accumulated during time intervals of 3,000–8,500 s and 19,000–26,000 s in Fig. 1 for the two flares. The corresponding orbital phases are $\phi = 0.81\text{--}0.93$ and $\phi = 0.29\text{--}0.46$, respectively. We have evaluated profiles of spectrally isolated H-like $\text{K}\alpha$ lines (= $\text{Ly}\alpha$ lines) from N and O by fitting a Gaussian to them. Unfortunately, the line central energies are consistent with those in the laboratory, and any systematic orbital motion of the line-emitting gas is not detected.

Note, however, that the 1σ line width $\Delta E_{\text{Ly}\alpha}$ is found to be $\simeq 1.2 \text{eV}$ and $\simeq 2 \text{eV}$ for the N and O $\text{Ly}\alpha$ lines on average, which corresponds to a line-of-sight velocity dispersion $\langle v_1 \rangle = (\Delta E_{\text{Ly}\alpha}/E_{\text{Ly}\alpha}) c$ of $\simeq 720 \text{km s}^{-1}$ and $\simeq 920 \text{km s}^{-1}$, respectively. These values are much larger than the thermal velocity, e.g., $\sim 0.16 \text{eV}$ or $\sim 70 \text{km s}^{-1}$ for oxygen, estimated from $kT_i = 0.3 \text{keV}$. Note also that the line-of-sight orbital velocity amplitude is $\simeq \frac{M_1}{M_1+M_2} \frac{2\pi}{P_{\text{orb}}} a \cos i \simeq 100 \text{km s}^{-1}$, which is also small enough.

4. DISCUSSION

4.1. Implication of the Low Plasma Density

The electron number density of the plasma measured from the He-like triplets of N and O ($\simeq 10^{11} \text{cm}^{-3}$) is smaller by several orders of magnitude than the con-

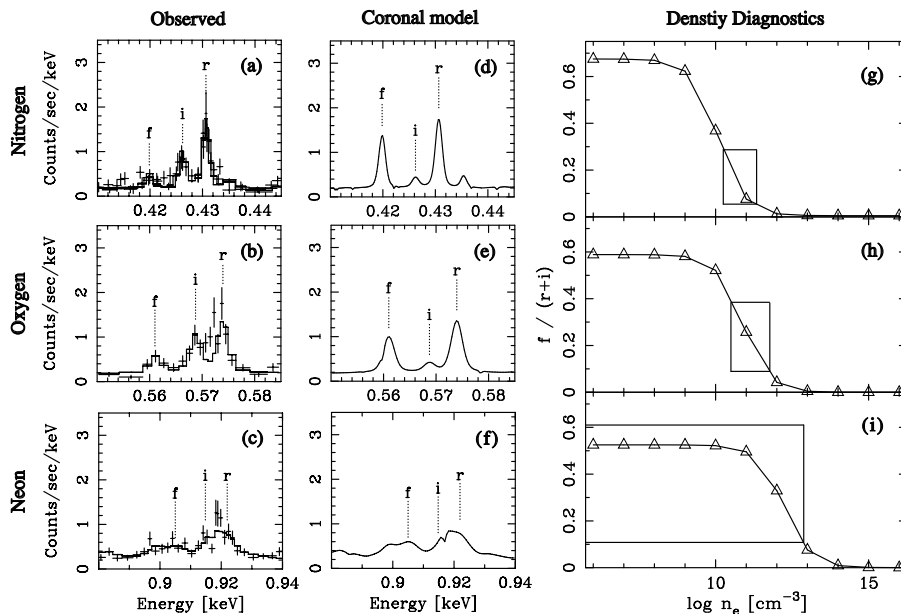


Figure 4. Density diagnostics by means of the He-like triplet. Panels of observed and coronal limit spectra around the He-like triplet, and the density diagnostics are arranged from left to right columns. The cases of Nitrogen, Oxygen, and Neon are arranged from upper to lower rows. The relative intensities of the intercombination (marked with ‘i’) and forbidden (marked with ‘f’) lines are undoubtedly inverted for N and O. Panels (g)-(i) compare theoretical curves of the intensity ratio $f/(r+i)$ as a function of n_e with the observed intensity ratio. In drawing the theoretical curves we have used the plasma code SPEX (Kaastra, Mewe, & Nieuwenhuijzen, 1996) at the ionization temperatures kT_i of 0.18, 0.30, and 0.34 keV for N, O, and Ne obtained from the intensity ratio between $\text{Ly}\alpha$ and r .

ventional estimate in the post-shock accretion column of mCVs, $n_e \simeq 10^{16} \text{ cm}^{-3}$ (Frank, King, & Raine, 2002). Moreover, the resultant scale ($\ell_p = (2-3) \times 10^{10} \text{ cm}$) is larger than the radius of the white dwarf (assumed to be $\sim 7 \times 10^8 \text{ cm}$ for a $0.79 M_\odot$ white dwarf) by more than an order of magnitude, and is rather a fraction of the size of the Roche lobe of the primary. We thus conclude that, unlike other mCVs, the X-ray-emitting plasma in AE Aqr is not a product of the mass accretion onto the white dwarf.

We would like to remark here that photo-excitation due to UV radiation can also pump a 3S_1 electron up into the $^3P_{2,1}$ level, thereby affecting the density diagnostics (Gabriel & Jordan, 1969; Pradhan & Shull, 1981; Porquet et al., 2001). Since there is no evidence of an accretion disk in AE Aqr (Welsh, Horne, & Gomer, 1993), and the secondary is a late type K3-K5 star, the hot polar cap region of the white dwarf, occupying 0.6 % of the surface area emitting with a 47,000 K blackbody spectrum (Ercleous & Horne, 1996), is the most efficient UV-radiation source. With this emission, however, the photo-excitation rate is only $\sim 0.2\%$ of the collisional-excitation rate, and hence, can be neglected (Itoh et al., 2006).

4.2. Plasma Heating and Propeller Condition

From the *XMM-Newton* observations, we have obtained the maximum temperature of the plasma kT_{max} to be 4.6 keV (table 1). This implies the matter transferred

from the secondary star is accelerated at least to the corresponding thermal velocity $v_{\text{th}} = (3kT_{\text{max}}/\mu m_{\text{H}})^{1/2} \simeq 1500 \text{ km s}^{-1}$. Such a high velocity can naturally be achieved by utilizing the gravitational potential of the white dwarf. Theoretical model calculations of the Doppler tomograms by Wynn, King, & Horne (1997) and Welsh, Horne, & Gomer (1998) also predict that the high velocity can be realized only within the Roche lobe of the white dwarf. We thus assume, as in Choi, Dotani, & Agrawal (1999), that the observed maximum temperature is attributed to the release of the gravitational energy. We can then make an order of magnitude estimate of the radius r_{th} where such thermalization takes place from

$$\frac{3}{2} kT_{\text{max}} \sim \frac{GM_1}{r_{\text{th}}} \mu m_{\text{H}}, \quad (1)$$

which results in $r_{\text{th}} \sim 1 \times 10^{10} \text{ cm}$. This number is roughly of the same order as the theoretical minimum distance estimates of blobs $r_{\text{min}} > 10^{10} \text{ cm}$ by Wynn, King, & Horne (1997). At r_{th} , the corotation velocity $v_{\text{co}} = 1.9 \times 10^9 \text{ cm s}^{-1}$ is much larger than the local Kepler velocity $v_{\text{K}} = 1.0 \times 10^8 \text{ cm s}^{-1}$. Hence, the plasma heated at $r \sim r_{\text{th}}$ is possible to be expelled due to the magnetic propeller action by the white dwarf.

4.3. Implications of the Broad H-like $K\alpha$ Lines

As presented in § 3.3, the observed spectral widths of the $\text{Ly}\alpha$ lines result in a line-of-sight velocity dispersion

$\langle v_1 \rangle$ of $\simeq 720 \text{ km s}^{-1}$ and $\simeq 920 \text{ km s}^{-1}$ for N and O, respectively. These values are much larger than that expected from the thermal broadening (§ 3.3). It is interesting to note that the three-dimensional velocity dispersion $\langle v_3 \rangle$ of $1250\text{--}1600 \text{ km s}^{-1}$ ($= \sqrt{3} \langle v_1 \rangle$) is comparable to the thermal velocity of the plasma $v_{\text{th}} = (3kT_{\text{max}}/\mu m_{\text{H}})^{1/2} = 1500 \text{ km s}^{-1}$ where $kT_{\text{max}} = 4.6 \text{ keV}$ (§ 3.1). The plasma of the N and O emission ($kT_i = 0.2\text{--}0.3 \text{ keV}$) can thus be regarded as having been cooled through adiabatic expansion of the seed blob which is once heated up to T_{max} in the deep gravitational potential of the white dwarf. This scenario is supported by the fact that the expansion timescale $t_{\text{exp}} = \frac{\ell_p}{v_{\text{th}}} \simeq 100 \text{ s}$ is much shorter than the radiative cooling time scale of the plasma $t_{\text{cool}} = \frac{3n_e kT_e V}{L_X} \simeq 4.8 \times 10^3 \text{ s}$ (Itoh et al., 2006). Theoretically, Wynn, King, & Horne (1997) estimated the density and the size of the original blob to be $10^{13}\text{--}10^{14} \text{ cm}^{-3}$ and 10^9 cm . By comparing these numbers with our estimates $n_e \sim 10^{11} \text{ cm}^{-3}$ and $\ell_p = (2\text{--}3) \times 10^{10} \text{ cm}$ (§ 3.2), we conclude that the plasma of the N and O emission can be interpreted as a result of the adiabatic expansion of the blob.

The observed N and O Ly α line width of $\langle v_1 \rangle = 720\text{--}920 \text{ km s}^{-1}$ is reminiscent of that of the Balmer series and UV emission lines. During optical flares, the spectral width of H β and H γ lines increases up to a full width at half maximum (FWHM) of $\sim 25\text{\AA}$ (Reinsch & Beuermann, 1994). Dividing the FWHM by a factor of 2.355, we obtain $\langle v_1 \rangle = 650\text{--}730 \text{ km s}^{-1}$ for the H β and H γ . Welsh, Horne, & Gomer (1998) have obtained a full width at zero intensity of H α emission line during optical flares to be $\sim 4000 \text{ km s}^{-1}$. Assuming the corresponding FWHM roughly to be $\sim 2000 \text{ km s}^{-1}$, we obtain $\langle v_1 \rangle \sim 850 \text{ km s}^{-1}$. Eracleous & Horne (1996) have estimated a FWHM of the He 2 line ($\lambda 1640$) to be 1700 km s^{-1} , equivalent to $\langle v_1 \rangle \simeq 720 \text{ km s}^{-1}$. The common observed spectral width of all these X-ray to optical emission lines strongly suggests that the plasmas responsible for these lines are all descendants of the blob once being heated up to T_{max} and then being cooled through adiabatic expansion. The observed X-ray to optical broad lines can be considered as being emitted in the course of this cooling process. As the optical and UV emission lines, the X-ray emission lines also show dramatic flaring activity, as shown in Fig. 1. This also supports the picture that all the emission lines have common origin.

The picture presented here can provide a solution to one of the problems (Welsh, 1999) in the original propeller model, the absence of the theoretically-predicted high velocity loop component (Wynn, King, & Horne, 1997) in the observed H α tomogram, which leads Welsh, Horne, & Gomer (1998) to introduce the colliding-blob model. This model intends to limit the H α emission location out of the Roche lobe of the primary by introducing distributions for the density and the size of the blobs. Our results, on the other hand, suppress the high velocity component of the H α emission line without any additional assumption in the way that the propelled plasma is still too hot

($kT_i = 0.2\text{--}0.3 \text{ keV}$) to emit H α lines within a radius of $\sim \ell_p$ (\simeq the Roche lobe size) from the white dwarf, where the high velocity component is expected to originate.

5. CONCLUSION

We have presented the results from *XMM-Newton* observations of AE Aqr carried out on 2001 November 7-8. Owing to the high energy-resolving power of the RGS, the intensity ratio of the intercombination to forbidden lines of the He-like triplet from nitrogen and oxygen is found to be larger than that expected for the plasma in the low-density limit, which has enabled us to measure the electron number density to be $\sim 10^{11} \text{ cm}^{-3}$. This, together with the emission measure ($\simeq 10^{53}\text{--}10^{54} \text{ cm}^{-3}$), results in a geometrical scale ℓ_p of the plasma of the N and O line emissions, with the ionization temperature kT_i of $0.2\text{--}0.3 \text{ keV}$, to be $\simeq (2\text{--}3) \times 10^{10} \text{ cm}$. The density is smaller than that of a standard post-shock plasma of mCVs by several orders of magnitude, and ℓ_p is much larger than the radius of a $0.79M_{\odot}$ white dwarf. We thus conclude that the X-ray-emitting plasma in AE Aqr cannot be a product of mass accretion onto the white dwarf.

Average spectra of the EPIC cameras can be reproduced by a four-temperature optically thin thermal plasma emission model with a maximum temperature kT_{max} of 4.6 keV . Assuming this temperature is achieved by converting gravitational potential energy into heat, we have made an order of magnitude estimate of the radius for the heating to occur as $r_{\text{th}} \sim 1 \times 10^{10} \text{ cm}$. As the corotation velocity with the white dwarf at r_{th} is much larger than the Keplerian velocity, the resultant hot plasma can be expelled due to the magnetic propeller action by the white dwarf.

RGS spectroscopy of H-like K α emission (= Ly α) lines of N and O has revealed that they show a significant broadening with a $1\text{-}\sigma$ width of $\sim 1.2 \text{ eV}$ and $\sim 2 \text{ eV}$, respectively, corresponding to a line-of-sight velocity dispersion $\langle v_1 \rangle$ of $720\text{--}920 \text{ km s}^{-1}$. Since the velocity dispersion $\langle v_3 \rangle = 1250\text{--}1600 \text{ km s}^{-1}$ ($= \sqrt{3} \langle v_1 \rangle$) is comparable to the thermal velocity of the plasma with $kT_{\text{max}} = 4.6 \text{ keV}$ ($v_{\text{th}} = (3kT_{\text{max}}/\mu m_{\text{H}})^{1/2} = 1500 \text{ km s}^{-1}$), the plasma producing the N and O emission lines ($kT_i = 0.2\text{--}0.3 \text{ keV}$) can be interpreted as having expanded adiabatically since it is heated up to T_{max} in the deep gravitational potential of the white dwarf. It is interesting to note that the Balmer series and UV emission lines also show a spectral width with a similar $\langle v_1 \rangle$ of $650\text{--}850 \text{ km s}^{-1}$. This strongly suggests that all these broad emission lines from X-ray to optical wavebands emanate from the plasma, which is once heated up to T_{max} at r_{th} , in the course of its adiabatic cooling. The dramatic flaring activity of the X-ray emission lines, along with the optical and UV lines, require a common origin for all these lines. The picture presented here can explain the absence of the high velocity component of the H α emission line in the way that the plasma expelled due to the propeller action is still too hot

($kT_i = 0.2-0.3$ keV) to emit the $H\alpha$ line within a region of $r < \ell_p$ (\simeq the Roche lobe size) from the white dwarf where the high velocity component is expected to originate.

REFERENCES

- Anders, E. & Grevesse, N. 1989, *Geochim. Cosmochim. Acta*, 53, 197
- Bastian, T. S., Beasley, A. J., & Bookbinder, J. A. 1996, *ApJ*, 461, 1016
- Casares, J., Mouchet, M., Martinez-Pais, I. G., & Harlaftis, E. T. 1996, *MNRAS*, 282, 182
- Choi, C., Dotani, T., & Agrawal, P. C. 1999, *ApJ*, 525, 399
- de Jager, O. C., Meintjes, P. J., O'Donoghue, D., & Robinson, E. L. 1994, *MNRAS*, 267, 577
- Eracleous, M. 1999, *ASP Conf. Ser. 157: Annapolis Workshop on Magnetic Cataclysmic Variables*, 343
- Eracleous, M., & Horne, K. 1996, *ApJ*, 471, 427
- Ezuka, H. & Ishida, M. 1999, *ApJS*, 120, 277
- Frank, J., King, A., & Raine, D. J. 2002, *Accretion Power in Astrophysics: Third Edition*, by Juhan Frank, Andrew King, and Derek J. Raine. Cambridge University Press, 2002, 398 pp., Chapter 6
- Friedjung, M. 1997, *New Astronomy*, 2, 319
- Gabriel, A. H. & Jordan, C. 1969, *MNRAS*, 145, 241
- Ishida, M. & Fujimoto, R. 1995, *ASSL Vol. 205: Cataclysmic Variables*, 93
- Itoh, K., Okada, S., Ishida, M., & Kunieda, H. 2006, *ApJ*, to appear in vol. 639 March 01 issue.
- Kaastra, J. S., Mewe, R., & Nieuwenhuijzen, H. 1996, *UV and X-ray Spectroscopy of Astrophysical and Laboratory Plasmas : Proceedings of the Eleventh Colloquium on UV and X-ray ... held on May 29-June 2, 1995, Nagoya, Japan*. Edited by K. Yamashita and T. Watanabe. Tokyo : Universal Academy Press, 1996. (Frontiers science series ; no. 15)., p.411
- Meintjes, P. J., de Jager, O. C., Raubenheimer, B. C., Nel, H. I., North, A. R., Buckley, D. A. H., & Koen, C. 1994, *ApJ*, 434, 292
- Patterson, J. 1979, *ApJ*, 234, 978
- Porquet, D., Mewe, R., Dubau, J., Raassen, A. J. J., & Kaastra, J. S. 2001, *A&A*, 376, 1113
- Pradhan, A. K. & Shull, J. M. 1981, *ApJ*, 249, 821
- Reinsch, K., & Beuermann, K. 1994, *A&A*, 282, 493
- Robinson, E. L., Shafter, A. W., & Balachandran, S. 1991, *ApJ*, 374, 298
- Welsh, W. F. 1999, *ASP Conf. Ser. 157: Annapolis Workshop on Magnetic Cataclysmic Variables*, 357
- Welsh, W. F., Horne, K., & Gomer, R. 1998, *MNRAS*, 298, 285
- Welsh, W. F., Horne, K., & Gomer, R. 1995, *MNRAS*, 275, 649
- Welsh, W. F., Horne, K., & Gomer, R. 1993, *ApJ*, 410, L39
- Welsh, W. F., Horne, K., & Oke, J. B. 1993, *ApJ*, 406, 229
- Wynn, G. A., King, A. R., & Horne, K. 1997, *MNRAS*, 286, 436

MRI-DRIVEN X-RAY DISC CORONAE IN CATAclySMIC VARIABLES

Peter J. Wheatley

Department of Physics, University of Warwick, Coventry CV4 7AL, UK

ABSTRACT

A prediction of the magneto-rotational instability (MRI) model for angular momentum transport in accretion discs is that high-state discs should have X-ray coronae. This is because magnetic flux is buoyant in the disc, and floats to high scale heights and low optical depths before depositing energy through reconnection. However, the best observed accretion discs, i.e. those in cataclysmic variables, have not supported the presence of a disc corona until now. I show that observations of high-state accretion discs with XMM-Newton and Chandra are now revealing a new X-ray emission component that may arise from an MRI-driven corona.

Key words: Eclipse, Accretion Disc Corona, X-rays.

1. INTRODUCTION

In order for accretion to proceed through an accretion disc, in-falling matter must lose energy and angular momentum. In general, energy can be lost quite easily, as it can be thermalised in shocks and then radiated. Angular momentum is more difficult to shed, and its transport in accretion discs tends to limit the rate of accretion by the central object.

Until relatively recently the mechanism of angular momentum transport in accretion discs remained a mystery. However, there is now a consensus that the most likely origin is the magneto-rotational instability (MRI; Balbus & Hawley, 1991). In this process, magnetic fields with radial components allow neighbouring disc annuli to communicate. A net drag is applied to the inner annulus, which causes material to fall in-wards, but also to orbit with a higher velocity. Since this stretches the magnetic field lines further, the drag is increased, and the process is unstable. The effect is to drive MHD turbulence that results in net angular momentum transport and amplification of the magnetic field.

The magnetic pressure associated with MRI-driven magnetic flux in the accretion disc causes the flux to be buoy-

ant in the accretion disc, and so it tends to float to higher scale heights in the disc. This effect has been reproduced in numerical simulations (Miller & Stone, 2000). The result is a highly magnetised corona above a weakly magnetised accretion disc. Reconnection of the magnetic field is likely to heat the corona, leading to an observable optically-thin X-ray corona, much like that of the Sun (Balbus & Hawley, 1998).

This hot disc corona is often invoked to explain the hard X-ray spectra of active galactic nuclei (AGN) and Galactic black-hole X-ray binaries (BHXRBS), but in practise it is difficult to test this association. This is partly because the X-ray emission in black hole system is dominated by the extreme luminosity of the very inner-most region, whereas the MRI is a global disc phenomenon. It is also because the accretion discs in BHXRBS and particularly AGN do not evolve on accessible timescales. Ideally we would like to observe the global disc corona switch on and off as the accretion disc switched between high and low states of angular momentum transport.

Fortunately, just such an opportunity it provided by the accretion discs in cataclysmic variables. Dwarf nova outbursts allow us to observe their accretion discs in both high and low states within a few days (e.g. Wheatley et al., 2003). The global disc is visible because it is not out-shined by the inner most regions (because white dwarfs are less compact than black holes and their gravitational potential wells are less deep). And the location of any X-ray emission can be pinned down through eclipse observations of highly-inclined systems (e.g. Wheatley & West, 2003).

In this paper I discuss the observational evidence for MRI-driven X-ray corona in cataclysmic variables. Unambiguous detection of such a corona in the high-state, and its absence in the low-state, would provide rare observational evidence for MRI model as the source of angular momentum transport in accretion discs.

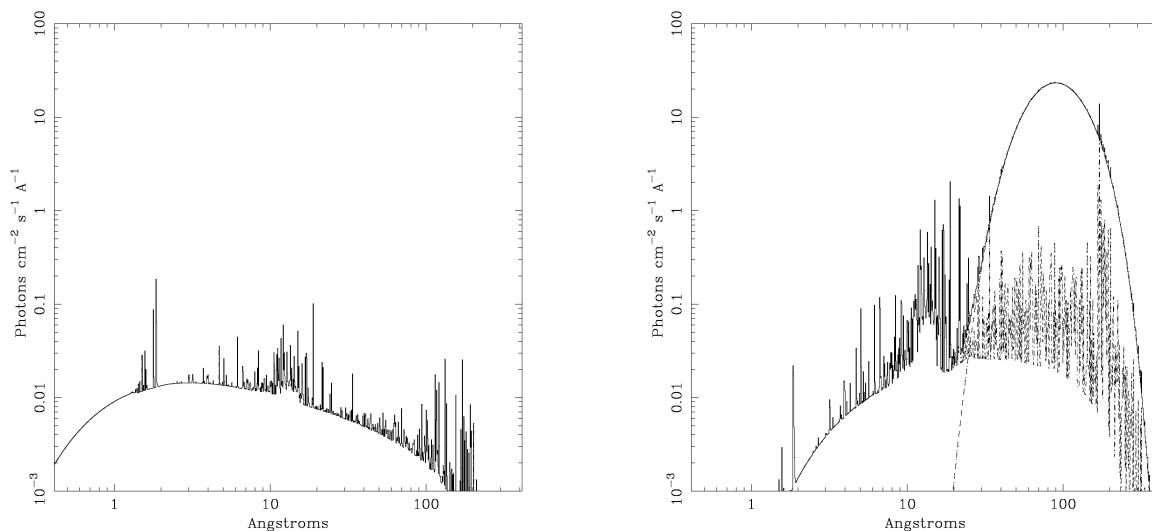


Figure 1. Schematic X-ray spectra of non-magnetic cataclysmic variables in the low state (left) and the high state (right).

2. THE X-RAY EMISSION OF CATAclysmic VARIABLES

The X-ray spectrum of non-magnetic cataclysmic variables changes dramatically between the low accretion rate state (or quiescence) and the high state (outburst). This is shown schematically in Fig. 1.

In quiescence the X-ray emission is hard, with characteristic temperatures around 10 keV. XMM-Newton observations of eclipsing systems show that this X-ray emission arises very close to the accretion object, in fact the X-ray emitting region as been constrained to be no larger than the white dwarf itself (Wheatley & West, 2003). This is usually interpreted as emission due to shock heating in the boundary layer between the accretion disc and white dwarf.

These observations essentially rule out significant X-ray emission from the accretion disc. Certainly there is no energetically important disc corona in the low state. This is expected, however, because the accretion rate is very low in the low state, angular momentum transport must be inefficient, and the MRI should not be operating.

In outburst the accretion rate rises dramatically, by about four orders of magnitude, and this must be due to increased angular momentum transport in the disc. It is in this state that the MRI should be operating and in which

we might expect to detect an accretion disc corona.

Observations in outburst show that the hard X-ray emission is suppressed, and that it is replaced by intense extreme-ultraviolet emission (e.g. Wheatley et al., 2003). This is usually interpreted as the boundary layer becoming optically-thick to its own emission and suffering a cooling catastrophe (due to the increased mass transfer rate through this region). The X-ray emission does not disappear entirely however, and the residual X-ray emission is seen to be softer than in quiescence (e.g. Baskill et al., 2005).

Eclipse observations in outburst have caused confusion because no eclipse is seen in the intense extreme-ultraviolet emission (e.g. Naylor et al., 1988). At first sight this seems inconsistent with the interpretation of this component arising from the boundary layer, which clearly is eclipsed in quiescence. The solution is that a significant fraction of the extreme-ultraviolet boundary layer emission is resonantly scattered in the outflowing accretion-disc wind, which is also a feature of high-state accretion discs. Observations with *EUVE* showed that the spectra of the low-inclination systems are dominated by optically-thick boundary-layer emission, whereas the spectra of highly inclined systems are dominated by strong and broad low-excitation resonance lines, i.e. boundary layer photons scattered by the wind (Mauche & Raymond, 2000).

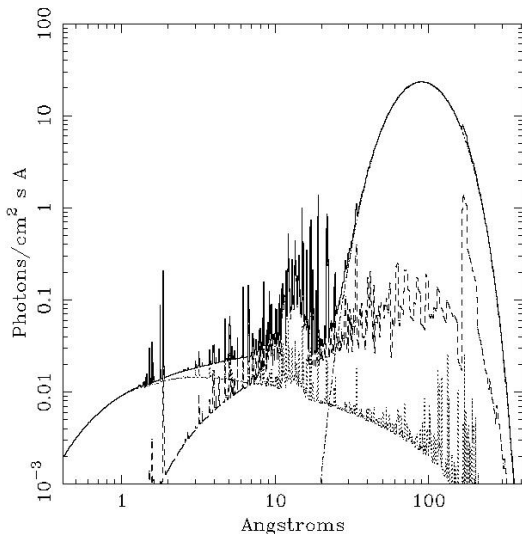


Figure 2. Revised schematic of the X-ray spectra of high-state cataclysmic variables showing the newly discovered two-component nature of the X-ray emission component. The hard emission is eclipsed in UX UMa, the soft emission is not.

3. EVIDENCE FOR A HIGH-STATE X-RAY CORONA

The standard picture of the X-ray emission of cataclysmic variables (above) leaves no room for a high-state MRI-driven accretion disc corona. All the high-energy emission is accounted for. However, this situation changed with the remarkable XMM-Newton observation of UX UMa (Pratt et al., 2004). UX UMa is a member of the *nova-like* class of cataclysmic variable, i.e. high-state cataclysmic variables that are commonly thought of as systems in permanent outburst. It is also an eclipsing system, and the XMM-Newton light curve revealed an X-ray eclipse for the first time in any high-state cataclysmic variable. The eclipsed emission is hard and must arise from the boundary layer, as in quiescence. Remarkably, this XMM-Newton observation also revealed the presence of a second, softer, X-ray component that is not eclipsed. This must be in addition to any extreme-ultraviolet component, which would lie softwards of the XMM-Newton bandpass. This new three-component picture of the high-energy emission of cataclysmic variables is illustrated by the schematic diagram in Fig. 2.

Pratt et al. (2004) interpret the uneclipsed soft X-ray emission of UX UMa as arising from resonant scattering, just like the extreme-ultraviolet emission. However, this interpretation is problematic because there is no evidence from low-inclination systems for intense continuum emission from the boundary layer in this wavelength range ($\sim 10 - 20 \text{ \AA}$). Consequently there are insufficient photons available to the wind to scatter into the line of sight of the observer.

Instead, I suggest that this newly discovered intermediate/soft energy emission component may arise in an MRI-driven accretion disc corona. If this can be confirmed it would provide evidence in support of the MRI model as the source of angular momentum transport in accretion discs. This is because this emission has all the characteristics of the reconnection-heated corona predicted by that model (i.e. its extent and temperature), and also because we know that this component is present only in the high state, just as expected for the MRI.

In search of additional supporting evidence for this interpretation I turn to the Chandra observations of WZ Sge in outburst presented by Wheatley & Mauche (2005). WZ Sge is not an eclipsing cataclysmic variable, but it is highly inclined and Wheatley & Mauche (2005) found that the extreme-ultraviolet emission is dominated by strong low-excitation resonance lines, just as is seen in the eclipsing systems. The X-ray spectrum of WZ Sge is clearly separated into distinct hard and soft components, just as in UX UMa, although the lack of eclipses means that we have to assume that the softer component arises from the extended emission region (by analogy with UX UMa).

The properties of the soft X-ray component of WZ Sge, described by Wheatley & Mauche (2005), are clearly inconsistent with the wind-scattering interpretation proposed by Pratt et al. (2004) for UX UMa. First, the emission lines are from highly excited species, and the line ratios are consistent with thermal emission (rather than resonant scattering). Second, the emission lines are relatively narrow: $\sim 800 \text{ km s}^{-1}$ compared with 3000 km s^{-1} for the resonantly-scattered extreme-ultraviolet lines. This velocity rules out not only resonant scattering, but also shock-heating in the wind, which should still carry the imprint of the high velocity outflow. In contrast, it is consistent with emission from material frozen to magnetic field lines that are rooted in the accretion disc. A velocity of 800 km s^{-1} corresponds to a Keplerian radius of $\sim 2 \times 10^{10} \text{ cm}$ which is characteristic of the accretion discs of cataclysmic variables.

4. CONCLUSIONS

I conclude that the properties of the soft-X-ray emission of UX UMa and WZ Sge, taken together, provide strong evidence in favour of the presence of an X-ray disc corona in these systems in their high state. This component is absent in WZ Sge in the low-state, as would be expected for a component driven by the MRI.

Further observations of eclipsing cataclysmic variables in the high state have the potential to prove the presence of global disc coronae, which would provide rare observational evidence in support of the MRI model of angular momentum transport in accretion discs.

ACKNOWLEDGMENTS

I thank Koji Mukai and Chris Mauche for many illuminating discussions.

REFERENCES

- Balbus, S. A. & Hawley, J. F. 1991, *ApJ*, 376, 214
- Balbus, S. A. & Hawley, J. F. 1998, *Reviews of Modern Physics*, 70, 1
- Baskill, D. S., Wheatley, P. J., & Osborne, J. P. 2005, *MNRAS*, 357, 626
- Mauche, C. W. & Raymond, J. C. 2000, *ApJ*, 541, 924
- Miller, K. A. & Stone, J. M. 2000, *ApJ*, 534, 398
- Naylor, T., Bath, G. T., Charles, P. A., et al. 1988, *MNRAS*, 231, 237
- Pratt, G. W., Mukai, K., Hassall, B. J. M., Naylor, T., & Wood, J. H. 2004, *MNRAS*, 348, L49
- Wheatley, P. J. & Mauche, C. W. 2005, in *ASP Conf. Ser. 330: The Astrophysics of Cataclysmic Variables and Related Objects*, 257–+
- Wheatley, P. J., Mauche, C. W., & Mattei, J. A. 2003, *MNRAS*, 345, 49
- Wheatley, P. J. & West, R. G. 2003, *MNRAS*, 345, 1009

A COMPREHENSIVE STUDY OF X-RAY EMISSION LINES FROM CATAclySMIC VARIABLES

K.P. Singh¹, V. R. Rana¹, E.M. Schlegel², V. Girish¹, and P.E. Barrett³

¹Tata Institute of Fundamental Research, Mumbai 400005, India

²University of Texas, San Antonio, U.S.A.

³Johns Hopkins University, Baltimore, MD 21218, U.S.A.

ABSTRACT

A comprehensive spectral study of a sample of 12 Cataclysmic Variables using high resolution X-ray data from the *Chandra* High Energy Transmission Grating is presented. The G-ratio value for the Fe XXV triplets suggests either coronal or photoionized conditions at 14 MK in U Gem, AO Psc, and one epoch of WX Hyi. For EX Hya it is either coronal plasma at temperatures <1 MK or photoionized plasma at 14 MK that dominates the spectrum. The G-ratio for Si XIII provides a lower limit of $\sim 10^6$ K for the electron temperature in all objects. SS Cyg and U Gem show significantly broadened emission lines during outburst compared to quiescence corresponding to a high velocity of ~ 2300 km s⁻¹. SS Cyg shows a flat-topped line profile for the Fe XXV line that is likely from outflowing wind. Significant broadening of fluorescent Fe line is observed in V603 Aql during its quiescent state. The phase resolved spectroscopy of AM Her shows that the centers of the emission lines of Fe XXVI, S XVI, and the resonance line of Fe XXV are shifted by a few hundred to 1000 km s⁻¹ from the theoretically expected values indicating bulk motion of ionized matter in the accretion column. Line intensities of H-like ions are modulated by the binary period in EX Hya.

Key words: Cataclysmic Variables; White dwarfs; X-rays:binaries; accretion.

1. INTRODUCTION

Cataclysmic Variables (CVs) are short period semi-detached binaries consisting of a white dwarf (WD) primary star accreting via L1 Lagrangian point from a Roche-lobe filling red dwarf main-sequence-like secondary star. CVs can be broadly divided into two main classes, non-magnetic and magnetic. Non-magnetic CVs are further divided into Classical Novae, Recurrent Novae, Dwarf Novae (DN) and Nova-like (NL) variables such as VY Scl and UX UMa. Magnetic CVs consist

of Intermediate Polars (IPs; including DQ Her stars) and Polars (AM Her stars). In non-magnetic CVs, the magnetic field of the WD < 10⁶ G (100 T) and accretion takes place through a disk via a boundary layer on the WD. X-ray emission is believed to arise from the boundary layer between the accretion disk and the white dwarf surface. In IPs the magnetic field of the WD is $\sim 10^6$ G and accretion takes place through a hollowed-out disk and then via accretion columns with the magnetic field controlling the flow in the final stages. Polars are observed to have large ($\sim 10\%$) circular polarization that varies with the orbital period implying a magnetic field > 10⁷ G (1000 T). The accretion takes place via a stream outside of the magnetosphere and one or more accretion columns inside the magnetosphere. The infalling material follows the magnetic field lines and approaches a velocity, $v_{ff} = (2GM/R)^{1/2} = 3600$ km s⁻¹ as it approaches the WD surface. A standing shock just above the surface converts the kinetic energy into thermal energy, decreasing the velocity by one quarter and increasing the density by four. The material radiates with a maximum temperature of ~ 50 keV in X-rays by cyclotron and bremsstrahlung radiation as it gradually settles on white dwarf surface.

We have analyzed data obtained from the *Chandra* archives for 18 observations of 12 CVs observed with the High Energy Transmission Grating (HETG) onboard the *Chandra* Observatory. There are five DN (SS Cyg, U Gem, WX Hyi, V426 Oph, & SU UMa), one NL (V603 Aql), four IPs (EX Hya, V1223 Sgr, AO Psc & GK Per) and two Polars (AM Her & V834 Cen).

Average spectra of five of the non-magnetic CVs in quiescence have been published previously by others (Mukai et al. (2003), Mauche et al. (2005), Mukai et al. (2005), Szkody et al. (2002), Homer et al. (2004), & Perna et al. (2003)). An early study by Mukai et al. (2003) fitted global models to 7 spectra categorising them into two groups: 'cooling flow' and 'photo-ionized'. Here, we have used line ratios as the diagnostics for the plasma conditions and plasma parameters. In addition, we have studied the line centers, line profiles and line fluxes in the quiescence and outburst states of the CVs and as a function of phase in AM Her and EX Hya. Details will appear

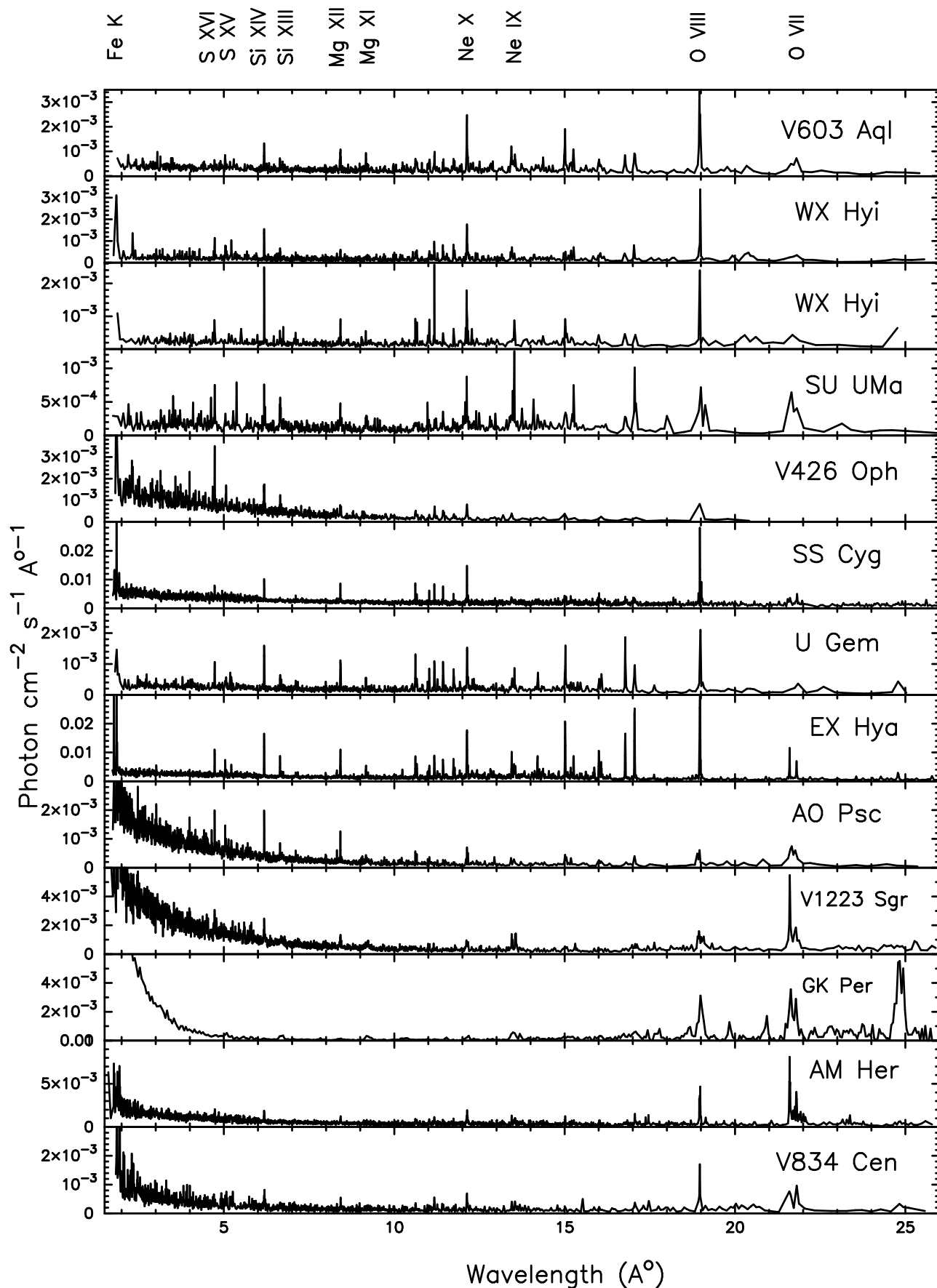


Figure 1. MEG spectra of all CVs in the quiescence state with +1 and -1 orders combined. The H-like and He-like emission lines from O, Ne, Mg, Si, S and Fe K emission lines are labeled.

in Rana et al. (2005), Schlegel et al. (2005) and Girish et al. (2005).

2. OBSERVATIONS

The observations were made with the HETG in combination with the Advanced CCD Imaging Spectrometer (ACIS; Garmire et al., 2003) in faint spectroscopy data mode. The HETG consists of the HEG (BW: 1.5–15 Å, $\Delta E = 0.012$ Å, accuracy of 0.006 Å (abs.), 0.001 Å (rel.)), and the MEG (BW: 2.5–31 Å, $\Delta E = 0.023$ Å, accuracy of 0.011 Å (abs.), 0.002 Å (rel.)). Most sources were observed during quiescence. SS Cyg and U Gem were also observed during outburst. SS Cyg was observed twice during a short outburst, near the peak of the outburst on 2000 September 12 and during an early decline of a narrow outburst on 2000 September 14. U Gem was observed at the peak of an outburst. AM Her was observed with the Chandra HETG when it was in an intermediate state ($V_m \sim 14$). Observation times ranged from 30–100 ksec.

3. ANALYSIS AND RESULTS

The spectra for these sources were extracted using the *Chandra Interactive Analysis of Observations* (CIAO v3.2) and CALDB v3.1. To improve the signal-to-noise ratio, the spectra for the +1 and -1 orders of the HEG and MEG arms were combined together. Several emission lines are seen in the spectra with the principal lines being the $K\alpha$ lines of Fe XXVI, S XVI, Si XIV, Mg XII, Ne X, and O VIII (all H-like), the triplets (r, i, f) of Fe XXV, S XV, Si XIII, Mg XI, Ne IX, and O VII (all He-like), the Fe XVII lines at 16.78, 17.05 and 17.10 Angstroms (Ne-like), and the Fe I $K\alpha$ fluorescence. The spectra of all CVs in quiescence along with their identified emission lines are shown in Figure 1. H-like and He-like lines dominate most of the spectra with H-like lines in lower Z ions being stronger. Among the He-like triplets that are resolved, the resonance lines are the most dominant. Strong resonance lines of Fe XXV indicate high temperature (> 30 MK) plasmas (Oelgoetz & Pradhan, 2001). And since no strong redward excess/shift is observed in the resonance lines, the contribution of the dielectronic satellites is probably insignificant.

The spectra are fitted for the continuum using a low order polynomial or a power-law, and Gaussians for the emission lines using XSPEC v11.3. While fitting these models, any broadening in the emission lines (other than instrumental) and possible shift in their positions from the expected values are tested by allowing the line width and center to vary for each line. The line widths are fixed to zero and the line centroids to their expected value, whenever they are found to be consistent with the instrumental resolution and the theoretically expected value. The line fluxes are determined with the 90% confidence. We

have used the C statistic (Nousek & Shue, 1989) to determine the confidence range for each parameter, since it gives better defined limits when using data having a small number of counts per bin. Line ratios R and G can be used for plasma diagnostics if the dielectronic satellites are assumed not to be important. However, density effects and photo-ionization need to be considered.

3.1. Plasma diagnostics

In Figure 2 we show the G ratio defined as $G=(f+i)/r$, where f, i, and r represent the forbidden, intercombination, and resonance line strengths of the He-like triplet. Given the errors of measurements, the data are not able to clearly indicate whether the coronal or the photoionization models dominate. Somewhat restrictive statements can be made in a few cases, however. For example, based on the G-ratios derived from Fe XXV in U Gem, one epoch of WX Hya, and AO Psc, we have either coronal conditions or photoionized conditions at temperatures >10 MK. In EX Hya it is either coronal plasma at low temperatures < 1 MK or photoionization at ~ 14 MK. From Si XIII, all objects have G values consistent with $T \geq 10^6$ K. However, the values with the smallest errors are consistent with $T \geq 10^{6.8}$ K: a temperature at which the coronal and photoionization conditions are inseparable. The errors for the G-values derived from S XV are too large to constrain. Similarly, the values of the R ratio ($=f/i$) indicate high densities. For data with the smallest error bars, we find that $N_e \geq 10^{16-17} \text{ cm}^{-3}$ for Fe, $\geq 10^{14} \text{ cm}^{-3}$ for S, $\geq 10^{13} \text{ cm}^{-3}$ for Si, $\geq 10^{12} \text{ cm}^{-3}$ for Mg, and $\geq 10^{11} \text{ cm}^{-3}$ for O.

3.2. Fe K line diagnostics for non-magnetic CVs

We have carried out a detailed study of the Fe K lines in the non-magnetic CVs. Hellier & Mukai (2004) have carried out a similar study of the available magnetic CVs. Figure 3 shows the Fe $K\alpha$ lines for non-magnetic CVs during quiescence along with the best fit model components. Various components of the Fe emission lines are marked. The resonance line is stronger as compared to the other two components of Fe XXV line for all the sources during quiescence, except for SU UMa. The relative strength of r line indicates that the temperature of the emitting plasma is above 3×10^7 K (Oelgoetz & Pradhan, 2001), where the principal lines dominate. Therefore, we can use these lines to infer the temperature and density of the emitting region. The G-ratio is very close to 1 (within 90% confidence limit) for all sources, indicating that the plasma is mainly in collisional ionization equilibrium (Oelgoetz & Pradhan, 2001) with electron temperatures $T_e \geq 10^7$ K for Fe XXV. Only SS Cyg during outburst shows a somewhat higher G-ratio value (~ 2.5) that might indicate the presence of hybrid plasma in the system. However, the lower limit of the 90% confidence interval on G-ratios for SS Cyg during outburst is again very close to unity.

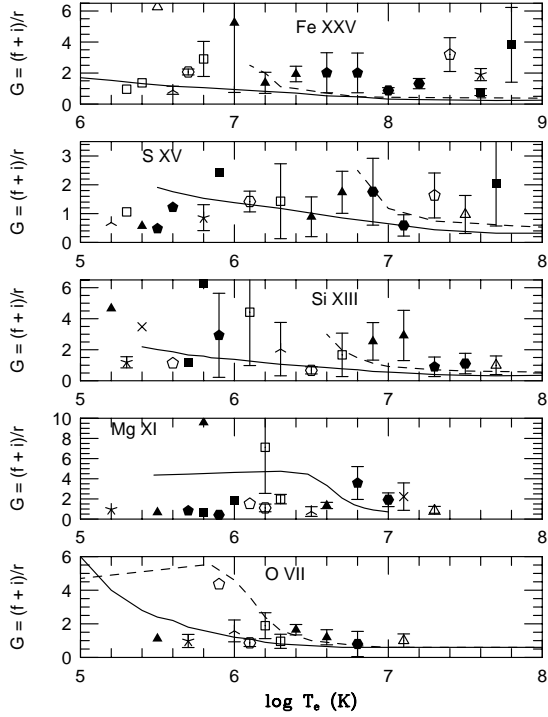


Figure 2. (Top to bottom) The G -ratios for Fe XXV, S XV, Si XIII, Mg XI and O VII. The curves define the loci of models for coronal (solid) and photoionized (dashed) conditions. The curves are from Bautista & Kallman (2000). Filled-in symbols are DN, star symbol is for AM Her, other starred symbols are for pure IPs, open symbols represent dual objects like DN+IP, Classical Novae+IP etc.

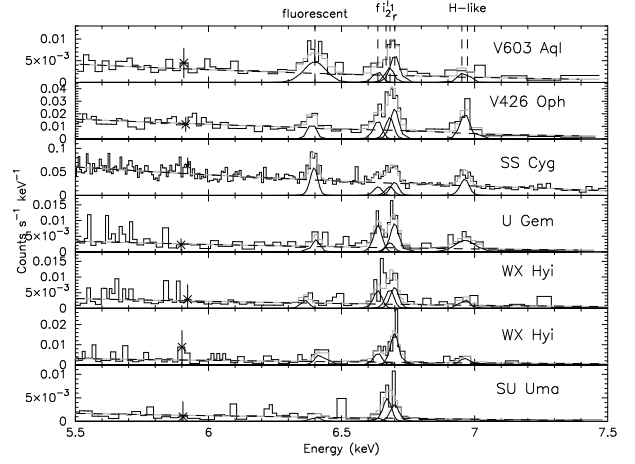


Figure 3. *Chandra* HEG spectra of non-magnetic CVs during the quiescence showing Fe $K\alpha$ emission lines. The Gaussian components used to model these lines are also shown.

The mean value of the R-ratio for SS Cyg, V603 Aql, V426 Oph, and WX Hyi (in 2002 July 28) varies between 0 and 2. For the two sources, U Gem and WX Hyi (in 2002 July 25), the R-ratios are essentially unconstrained at the lower limit and also the upper limits are very high. For these values the electron densities could be anywhere in the range of $10^{15-17} \text{ cm}^{-3}$, or more, thus not allowing us to constrain the range of plasma densities in the non-magnetic CVs studied here.

3.3. Center energies and profiles of Fe K lines

Most of the emission lines are observed to be consistent with the instrumental resolution during quiescence, but broadened during outbursts. In particular, the r , i and f components of Fe XXV are either broadened or shifted significantly from their expected values (see Fig. 4) during outbursts. The outburst (solid line) and the quiescence (dash-dotted line) spectra of U Gem are shown in the top panel of Fig. 4. The 90% confidence values for the widths (σ) of r and f lines are 51^{+17}_{-18} and 50^{+20}_{-19} eV, respectively, which corresponds to velocities of 2280^{+770}_{-800} and 2260^{+900}_{-860} km s^{-1} . SS Cyg shows a flat-top line profile and the broadened Gaussian line components do not reproduce the observed line profile (see Fig. 2). Such a profile has been reported for N VII line in O-type star, ζ Puppis using *Chandra* HETG data and attributed to small velocity gradient at the larger radii in the outflowing winds in the star (Cassinelli et al., 2001; Kahn et al., 2001). The broad emission lines in the outburst spectra of SS Cyg and U Gem have been previously reported by Mauche et al. (2005).

SS Cyg also shows redshifted Fe fluorescence lines during the two outburst observations. The best fit values of the line center show shifts that correspond to velocities of 2300^{+980}_{-900} and 2300^{+500}_{-440} km s^{-1} during 2000 Septem-

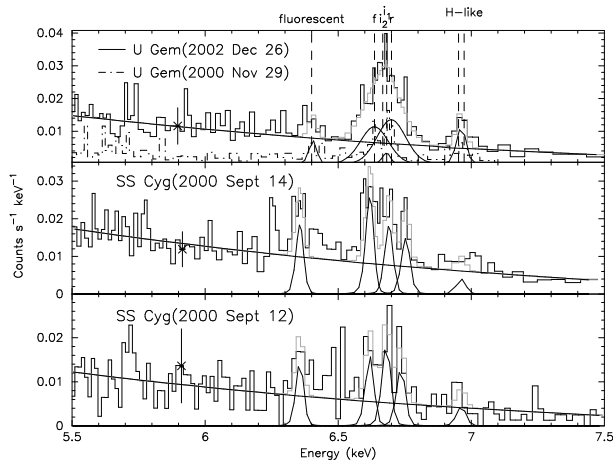


Figure 4. Chandra HEG spectra of U Gem and SS Cyg during the outburst. The dash-dotted curve in the top panel represents the spectrum of U Gem in quiescence. In contrast, the quiescent spectrum of SS Cyg is ~ 3 times brighter.

ber 12 and 14 observations for SS Cyg, respectively. This could be due to a wind flowing away from the system.

The old nova V603 Aql shows a strong fluorescent Fe I line with the highest EW of 162_{-65}^{+99} eV among all sources. The line is also found to be broadened by ~ 1700 km s $^{-1}$, that is probably due to Doppler broadening or Compton scattering of material in the accretion disk.

3.4. Phase resolved X-ray spectroscopy of AM Her

Phase resolved spectra are extracted for five non-overlapping phase bins, each of 0.2 width, by folding data using the well known ephemeris of AM Her. Except for the interval centered around the orbital phase minimum, other intervals had enough counts to estimate the energy and flux of the bright emission lines. The line energies of the Fe XXVI, Fe XXV (r), and S XVI are found to vary as a function of the phase. The most significant shifts are observed in Fe XXVI and are best explained as a sinusoid with semi-amplitude of 790 ± 190 km s $^{-1}$ plus a constant value of 220 ± 26 km s $^{-1}$. The line shifts in Fe XXV (r), S XVI and Mg XII are consistent with a constant velocity shifts of 770 ± 75 km s $^{-1}$, 500 ± 160 km s $^{-1}$, and 280 ± 195 km s $^{-1}$, respectively. The presence of a small sinusoid component in them cannot be ruled out, however, as shown in Fig. 5. These modulations indicate bulk motion of ionized matter in the accretion column of AM Her. Based on these velocity shifts and in the framework of the shock model of Aizu (1973) (see also Terada et al., 2001), we infer the temperature, density and height of the line emitting regions in the accretion column. The Fe XXVI ions show velocities that are close to the expected shock velocity for a 0.5 to 0.6 M_{\odot} white dwarf, and modulation due to a single pole accretion.

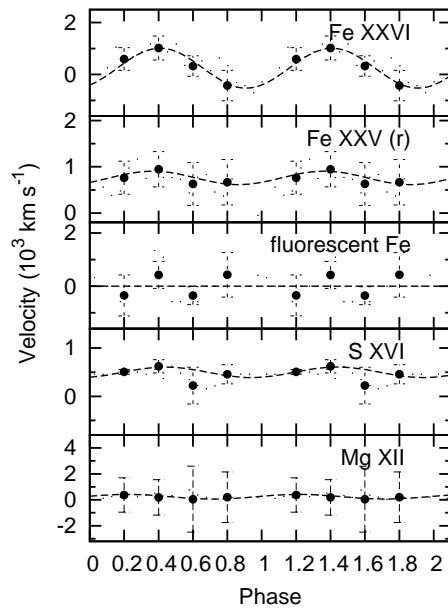


Figure 5. Velocity shifts as a function of orbital phase for the emission lines of Fe XXVI, Fe XXV(r), fluorescent Fe I, S XVI, and Mg XII. The curves show the best fit constant + sinusoidal variation observed.

3.5. Phase resolved X-ray spectroscopy of EX Hya

Data for EX Hya are folded using the ephemeris for the binary period as given by Hellier & Sproats (1992), and spectra are extracted for ten non-overlapping phase bins each of 0.1 width. A similar exercise was also done using the spin period of EX Hya. The line fluxes are derived for the principal emission lines observed. In Fig. 6, we show the orbital variation in the line fluxes of H-like emission lines from various ions. A clear phase dependent variation is seen for the O VIII line flux. The Ne X, Mg XII and Si XIV line fluxes show a marginal change over the binary cycle. However, the S XVI and Fe XXVI line fluxes are consistent with being constant over the binary period.

4. SUMMARY

Collisionally ionized plasmas appear to dominate the X-ray spectra of several CVs (magnetic as well as non-magnetic). Data are also consistent with photoionization at very high temperatures but present data are not sufficient to make a definitive statement. High densities are required in most CVs. Significant broadening of Fe XXV is seen in U Gem during outburst indicating high velocity gas. Broadening is also seen for fluorescent Fe in V603 Aql during its quiescence state. A broad Fe XXV line with a flat-top profile is seen in SS Cyg in outbursts: high velocity winds or outflows are indicated. Fluorescent Fe line is red-shifted by $\sim 2300 \pm 500$ km/s in SS Cyg indicating high velocity for fluorescent material during

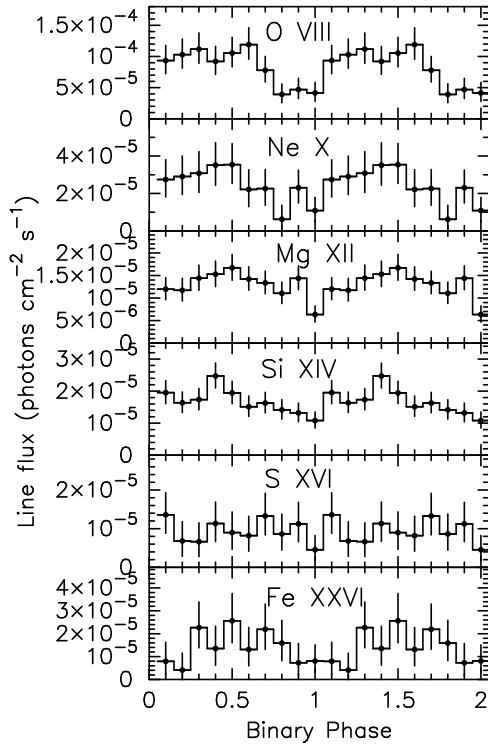


Figure 6. Variation of line fluxes of H-like emission lines from various ions in EX Hya as a function of its orbital phase.

outburst. In AM Her, Fe XXVI line is found to be shifted (~ 1000 km/s) and modulated at binary period, indicating possible detection of bulk motion in the accretion column. Phase resolved spectroscopy in EX Hya shows binary modulation of line intensity of low Z ions.

ACKNOWLEDGMENTS

REFERENCES

- Aizu, K., 1973, Prog. Theor. Phys., 49, 1184
- Bautista, M. A., & Kallman, T. R., 2000, ApJ, 544, 581
- Cassinelli, J. P., Miller, M. A., Waldron, W. L., MacFarlane, J. J., & Cohen, D. H., 2001, ApJ, 554, L55
- Garmire, G. P., Bautz, M. W., Ford, P. G., Nousek, J. A., & Ricker, G. R., Jr. 2003, SPIE, 4851, 28
- Girish, V., Rana, V. R., & Singh, K. P., 2005, ApJ(submitted)
- Hellier, C., & Sproats, L. N., 1992, Inf. Bulletin on Variable Stars, 3724, 1
- Hellier, C., & Mukai, K., 2004, MNRAS, 352, 1037
- Homer, L., et al., 2004, ApJ, 610, 991
- Kahn, S. M., et al., 2001, A&A, 365, L312

Mauche, C. W., Wheatley, P. J., Long, K. S., Raymond, J. C., & Szkody, P. 2005, ASP Conf. series, vol. 330, 355, Eds: J. M. Hameury & J. P. Lasota

Mukai, K., Kinkhabwala, A., Peterson, J. R., Kahn, S. M., & Pearels, F., 2003, ApJ, 586, L77

Mukai, K., & Orio, M., 2005, ApJ, 622, 602

Nousek, J. A., & Shue, D. R. 1989, ApJ, 342, 1207

Oelgoetz, J., & Pradhan, A. K., 2001, MNRAS, 327, L42

Perna, R., McDowell, J., Menou, K., Raymond, J., & Medvedev, M. V., 2003, ApJ, 598, 545

Rana, V. R., Singh, K. P., Schlegel, E. M., & Barrett, P. E., 2005, ApJ(submitted)

Schlegel, E. M., Rana, V. R., V. Girish, Singh, K. P., & Barrett, P. E., 2005 (in preparation)

Szkody, P., Nishikida, K., Raymond, J. C., Seth, A., Hoard, D. W., Long, K., & Sion, E. M., 2002, ApJ, 574, 942

Terada, Y., Ishida, M., Makishima, K., Imanari, T., Fujimoto, R., Matsuzaki, K., & Kaneda, H., 2001, MNRAS, 328, 112

OBSCURED HMXB UNVEILED BY INTEGRAL AND XMM-NEWTON

Roland Walter

INTEGRAL Science Data Centre, Chemin d'Ecogia 16, CH-1290 Versoix, Switzerland

On behalf of the INTEGRAL survey team

ABSTRACT

During the first year in operation, INTEGRAL, the European Space Agency's γ -ray observatory, detected more than 28 new bright sources which emit the bulk of their emission above 10 keV. Follow-up observations of a subset of these sources in the X-ray band with XMM-Newton indicate that 80% of them are very strongly absorbed. More than half of these absorbed sources show pulsations with long periods ranging from 139 to 1300s, i.e., they are slow X-ray pulsars. The infrared counterparts are not strongly absorbed demonstrating that the absorbing matter is local to the sources. Many of these new sources are super-giant high-mass X-ray binaries (HMXB) in which the stellar wind of the companion star is accreted onto the compact object. The large local absorption in these new sources can be understood if the compact objects are buried deep in dense stellar winds. These new objects represent half of the population of wind-fed supergiant HMXB.

1. INTRODUCTION

The second catalogue of soft γ -ray sources detected by INTEGRAL (Bird et al, 2005) lists 209 objects detected with high significance. In the Milky-Way it lists 104 accreting binaries, 4 supernova remnant, 4 pulsars, 2 molecular clouds. The accreting binaries include 78 neutron star systems (31 HMXB, 47 LMXB) plus 2 candidates, 4 black-hole systems plus 10 candidates and 7 cataclysmic variables. The catalogue also contains 55 unidentified sources discovered by INTEGRAL (counterparts/source types have now been proposed for about 20% of them). Many of them are of galactic origin and clustered within a few degrees of the galactic plane.

Here, we present the results of INTEGRAL, XMM-Newton and infrared observations of 9 newly-discovered sources. These were selected among the new sources detected by INTEGRAL in the galactic plane during the first year of the mission. We demonstrate that 8 out of the 9

sources are intrinsically absorbed and that 7 of them are persistent X-ray emitters. Many systems appear to have super-giant companions. Since the X-ray properties of the other unknown systems are similar, we propose that a significant number of the unknown sources are likely to be OB supergiant systems - doubling the number of such systems known in the Galaxy.

2. SOURCE SAMPLE AND COUNTERPARTS

Among the sources detected by INTEGRAL during the first six months of the mission, 6 sources were selected for follow-up observation with XMM-Newton. We added to this sample 4 sources (2 are transients) for which TOO observations had been obtained. Results could be found in Bodaghee et al, 2005; Hill et al, 2005; Walter et al, 2005 and Zurita et al, 2005.

In all cases, bright X-ray sources have been detected in the ISGRI error circles, with 2-10keV fluxes of the order of $1 - 10 \times 10^{-11}$ erg/s cm². One of them, IGR J17597-2201, is probably a LMXB system and will not be discussed any further.

Searching the 2MASS catalogue for near infrared counterparts in the XMM error circles provided a single candidate in most cases. Despite a K magnitude between 7 and 13, the counterparts are affected by interstellar extinction and are almost not detected in optical surveys. The analysis of the photometry provided upper limits to the source reddening that are comparable with the reddening derived from the galactic Hydrogen column densities in the direction of the sources. The spectral type could however not be determined from the photometry.

3. VARIABILITY

The INTEGRAL lightcurves of all sources do show variations. Excepting IGR J16465-4507, that was detected only once for a week, and IGR J17544-2619, that was

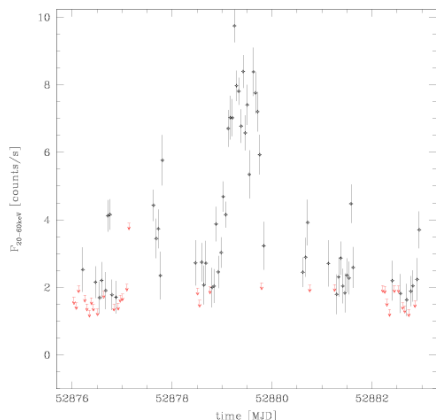


Figure 1. Short flare observed in IGR J17252-3616 by INTEGRAL.

detected flaring at three occasions separated by 165 ± 3 days, all sources could be detected in the different INTEGRAL visibility periods and could therefore be considered as persistent.

In all persistent sources, the X-ray fluxes detected by XMM-Newton matched the average hard X-ray fluxes accumulated by INTEGRAL over long time scales within a factor of two, excepting for IGR J16479-4514 for which the X-ray flux was found fainter by a factor of 20. As this source features strong flares (Sguera et al, 2005) XMM-Newton probably observed the source in quiescence.

Among the persistent sources, flaring activity has been observed on time scales of hours in six sources (IGR J16318-4848, IGR J16320-4751, IGR J16393-4641, IGR J16418-4532, IGR J16479-4514, IGR J17252-3616) with variability amplitude from 4 to 50. Such flares (figure 1 for an example) could be compared with the ones observed in fast transient (for a review see Negueruela, this volume) that typically varies by a factor of 100. In one persistent source, IGR J18027-2016 no flaring activity has been observed.

Long (139-1300s) pulse periods have been detected in all persistent sources excepting in IGR J16318-4848 (in which the pulse fraction cannot be higher than 10%) and in IGR J16479-4514 for which the XMM data were not of enough quality.

Estimates for the orbital period are available for two systems thanks to the detection of eclipses (figure 2):

- IGR J17252-3616: $P_{spin}=413.85s$; $P_{orb}=9.741d$; $f(M)=15M_{\odot}$; $a \times \sin(i) = 111$ lt-s; eclipse duration = 1.26d; flares by factor of 50; $N_H = 2 - 10 \times 10^{23} \text{cm}^{-2}$ (Zurita et al, 2005; Corbet et al, 2005)
- IGR J18027-2016: $P_{spin}=139.612$ s; $P_{orb}=4.5696d$; $f(M)=16M_{\odot}$; $a \times \sin(i) = 68$ lt-s; eclipse duration = 0.9d; absence of large scale variability (Hill et al, 2005; Auguello et al, 2003).

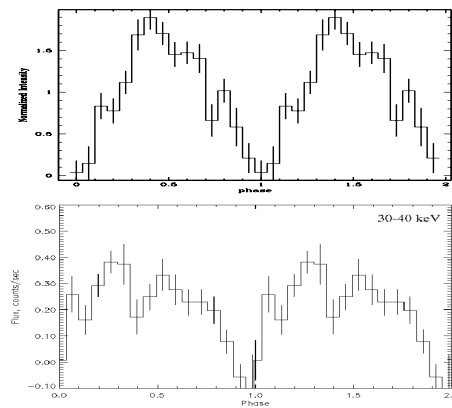


Figure 2. INTEGRAL orbital folded lightcurve of IGR J17252-3616 (top) and of IGR J18027-2016 (bottom).

Both sources appear to be located in the part of the supergiant wind accretors of the Corbet diagram. The large mass functions derived from the X-ray data and the optical/infrared spectra, with few lines, confirmed the early type stellar companions. The wide and probably asymmetric eclipse profiles are similar to ones observed in Vela X-1 (Feldmeier, 1996).

The two eclipsing systems, the identification of the counterpart of IGR J16318-4848 with an sgB[e] star (Fillard and Chaty, 2004) and the discovery of long spin periods in 3 persistent sources (that are therefore unlikely to be Be systems with short orbital period) suggest that all the persistent sources are supergiant HMXB systems and most of them wind-fed when they feature long spin periods.

The two transient sources of our sample (IGR J16465-4507 and IGR J17544-2619) have also been identified with supergiant systems (Smith, 2004; Negueruela, this volume).

The fraction of eclipsing systems among the observed sources is consistent with short orbital periods around supergiant stars.

4. SPECTRAL ANALYSIS

The detection of new bright persistent hard X-ray sources has been a surprise as they have remained almost unnoticed in previous X-ray galactic surveys. This suggested highly absorbed sources, which has been confirmed by the source spectra, obtained with XMM-Newton, featuring absorbing column densities, ranging from 10^{23} to $2 \times 10^{24} \text{cm}^{-2}$ (Walter et al, 2005 – see figure 3 for example spectra).

The weak detection of several sources at low energy by the X-ray monitor on board INTEGRAL or by ASCA/BeppoSAX indeed suggest that the absorption is persistent (Walter et al., 2004). So far this has been con-

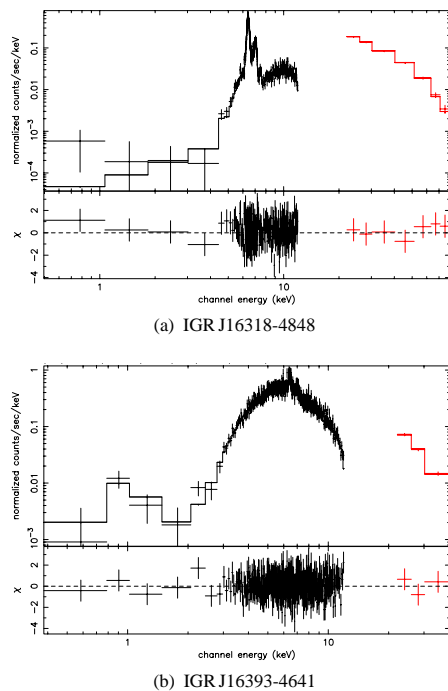


Figure 3. ISGRI (>20 keV) and EPIC (<15 keV) source count spectra with best fit model predictions and residuals.

firmed in the few sources observed several times in the X-ray band (Rodriguez, 2005; Kuulkers, pers comm.).

The continuum emission of all sources could be fitted with an absorbed power-law featuring a high energy cut-off or by a comptonization model that are typical for accreting pulsars.

When the absorbing column densities are large enough, a soft X-ray excess below 1 keV could be detected in all cases excepting in IGR J16318-4848. In supergiant HMXB systems, such excesses are expected to originate from the photoionized sphere surrounding the neutron star.

The strong fluorescence lines, together with the continuum spectral shape, point towards a transmission geometry in which the compact sources are embedded within a dense envelope of cold matter. The strength of the Fe $K\alpha$ lines, when compared to the unabsorbed continua are related to the absorbing column densities as expected for a spherical geometry (figure 4).

When detected well enough, the Fe $K\alpha$ line energy provided a lower limit on the distance separating the X-ray source and the matter in which fluorescence takes place. Depending on the object, this lower limit is as large as the expected or measured orbital radii.

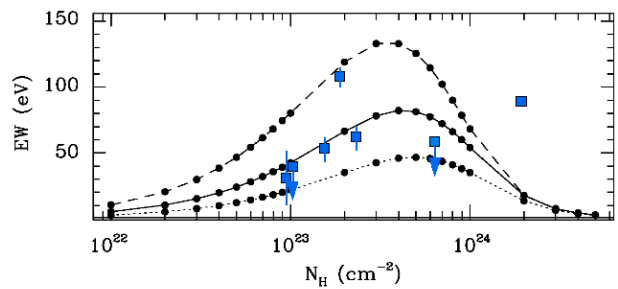


Figure 4. The observed Fe $K\alpha$ equivalent width calculated with reference to the unabsorbed continuum (and corrected for the peculiar Iron abundances when needed) plotted against the absorbing column density (squares). The curves show the prediction of a spherical distribution of matter around the X-ray source for different Iron abundances (from Matt, 2002). The square at the extreme right is IGR J16318-4848.

5. IGR J16318-4848

IGR J16318-4848 features an excess of absorption along the line of sight when compared with the strength of the Fe $K\alpha$ line (figure 4). This excess of absorption could explain the absence of a soft X-ray excess in that source if the excess of absorbing material is located at a distance larger than the orbital radius. This material could be the cold and dense equatorial wind that is often assumed to explain the numerous emission lines observed in B[e] stars. This scenario however requires that the thickness of that wind component is large as eclipses have not been observed in this system. An alternate possibility is that the accretion is Roche lobe dominated and that the excess absorption is related to an accretion disk.

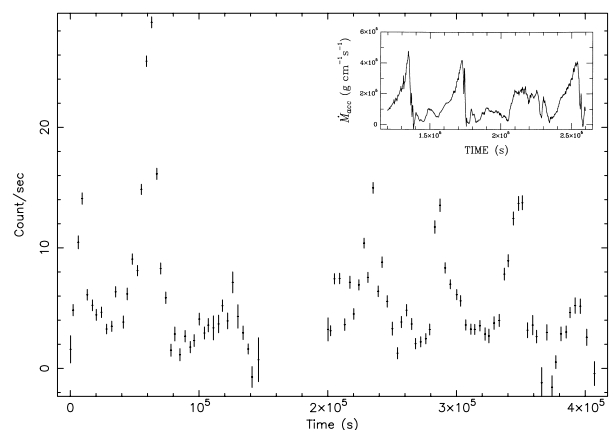


Figure 5. Flaring activity observed in IGR J16318-4848 by INTEGRAL (22-60keV ISGRI lightcurve). Inset: mass accretion rate variability driven by accretion wake oscillations (from Blondin et al, 1990).

As IGR J16318-4848 is the brightest of all the new persistent sources detected by INTEGRAL, its long term variability could be studied in more detail. The source shows constant variability on time scales of several hours. Dur-

ing peculiar periods it features sequences of flares with a characteristic time scale of 15-16 hours (figure 5), much too short to be an orbital period.

The observed sequences of flares do match very well the time-scale and variability amplitude predicted from accretion wake oscillations in the stellar wind of supergiant HMXB systems (Blondin et al, 1990). In that model the sign of the spin of the accreting flow changes regularly driving bursts of mass accretion (inset of figure 5). If this interpretation is correct, IGR J16318-4848 is a wind-fed system.

The possibility that accretion wakes or clumps in the stellar wind disruption zones around the compact sources are responsible for part of the flaring activity observed in the other sources and even possibly in the fast transient systems is worth considering.

6. GALACTIC DISTRIBUTION

INTEGRAL detected an overabundance of new HMXB candidates in the Norma arm tangent region (Walter, 2004). Figure 6 displays the distribution of all HMXB detected by INTEGRAL with galactic longitude, including the newly detected sources for which a strong indication for a high-mass system exists. The open histogram shows the same distribution including all unidentified sources that are within 2 degrees of the galactic plane. The two distributions are corrected for the effective exposure using a logN-logS slope of -0.7.

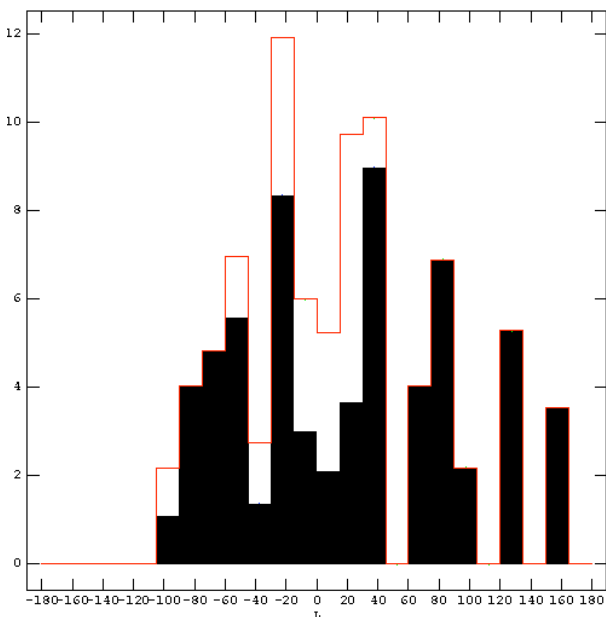


Figure 6. Distribution of HMXB (including candidates) detected by INTEGRAL. The open histogram includes all unidentified sources within 2 degrees from the galactic plane.

The galactic distribution of HMXB detected by INTEGRAL peaks within the inner arms of the galaxy and traces the region with the highest stellar formation rate of massive stars within the galaxy. This distribution is consistent with the identification of a good fraction of the unidentified INTEGRAL sources with HMXB systems.

7. CONCLUSIONS

A large fraction of the new obscured galactic sources detected by INTEGRAL share the properties of wind-fed supergiant HMXB. However the typical column densities that have been observed is of the order of $3 \times 10^{23} \text{cm}^{-2}$ which is significantly higher than what is expected in usual wind fed supergiant system outside of eclipses (Blondin, 1994). As the orbital radii, when available, are not peculiarly small, this points towards low luminosity systems, buried in rather dense stellar winds.

ACKNOWLEDGMENTS

Based on observations obtained with the ESA science missions INTEGRAL and XMM-Newton. The INTEGRAL and XMM-Newton instruments and data centers were directly funded by ESA member states and the USA (NASA).

REFERENCES

- G. Augello et al, 2003, ApJ 607, L63
- A. Bird et al., 2005, ApJ, in press
- J. Blondin et al., 1990, ApJ, 356, 591
- J. Blondin et al., 1994, ApJ, 435, 756
- A. Bodaghee et al., 2005, in press
- S. Corbet et al, 2005, ApJ in press
- P. Filliatre, S. Chaty, 2004, ApJ 616, 469
- A. Feldmeier et al., 1996, ApJ, 311, 793
- A. Hill et al., 2005, A&A, 439, 255
- G. Matt et al., 2005, A&A, 439, 255
- J. Rodriguez et al., 2005, MNRAS, submitted
- V. Sguera et al., 2005, A&A, in press
- D. Smith et al., 2004, ATel, 338
- R. Walter et al., 2004, ESA-SP 552, 417
- R. Walter et al., 2005, A&A, submitted
- J. Zurita et al., 2005, A&A, in press, see also this volume

SUPERGIANT FAST X-RAY TRANSIENTS: A NEW CLASS OF HIGH MASS X-RAY BINARIES UNVEILED BY *INTEGRAL*

I. Negueruela¹, D. M. Smith², P. Reig³, S. Chaty⁴, and J. M. Torrejón¹

¹Dpto. de Física, Ing. de Sistemas y Teoría de la Señal, Universidad de Alicante, Apdo. 99, E03080 Alicante, Spain

²Physics Dept & Santa Cruz Institute for Particle Physics, University of California Santa Cruz, 1156 High St., Santa Cruz, CA 95064

³IESL (FORTH) & Physics Dept., University of Crete, PO Box 2208, 71003 Heraklion, Crete, Greece

⁴AIM (UMR 7158 CEA/CNRS/Université Paris 7 Denis Diderot), CEA Saclay, DSM/DAPNIA/Service d'Astrophysique, Bât. 709, L'Orme des Merisiers, 91191 Gif-sur-Yvette, Cedex, France

ABSTRACT

INTEGRAL monitoring of the Galactic Plane is revealing a growing number of recurrent X-ray transients, characterised by short outbursts with very fast rise times (\sim tens of minutes) and typical durations of a few hours. Here we show that several of these transients are associated with OB supergiants and hence define a new class of massive X-ray binaries which we call Supergiant Fast X-ray Transients. Many other transient X-ray sources display similar X-ray characteristics, suggesting that they belong to the same class. Since they are difficult to detect and their number is growing fast and steadily, they could represent a major class of X-ray binaries.

Key words: binaries: close — stars: supergiants – X-rays: binaries.

1. INTRODUCTION

High Mass X-ray binaries (HMXBs) are X-ray sources composed of an early-type massive star and an accreting compact object. Most known HMXBs are Be/X-ray binaries, systems consisting of a neutron star accreting from the disc around a Be star. Even though a few Be/X-ray binaries are persistent weak X-ray sources (with $L_X \sim 10^{34}$ erg s⁻¹), the majority are transients, displaying bright outbursts with typical duration on the order of several weeks.

The second major class of HMXBs contains early-type supergiants. The compact object is fed by accretion from the strong radiative wind of the supergiant. These objects are persistent sources, with luminosities around $L_X \sim 10^{36}$ erg s⁻¹, very variable on short timescales, but rather stable in the long run. Because of their relative brightness and persistent nature, it has been generally assumed that

Supergiant X-ray Binaries (SGXBs) were easy to detect. About a dozen SGXBs were known before the launch of *INTEGRAL*, most of them having been discovered in the early days of X-ray astronomy. This low number was generally attributed to a real scarcity of such systems, as the short duration of the supergiant phase would result in very short lifetimes.

Since the launch of *INTEGRAL*, the situation is changing dramatically. Several new sources have been detected displaying the typical characteristics of SGXBs (Walter, these proceedings). In most cases, the sources had not been detected by previous missions due to high absorption, which renders their spectra very hard. Here we show that an even larger population of X-ray sources with OB supergiant companions may lie hidden in the Galaxy, undetected because of its transient nature.

2. X-RAY SOURCES WITH FAST OUTBURSTS

XTE J1739–302 = IGR J17391–3021

XTE J1739–302 was discovered during an outburst in August 1997 (Smith et al., 1998). Further observations, mostly with *RossiXTE*, but also with *ASCA* showed it to be a strange transient with very short outbursts, lasting only a few hours (Smith et al., 2006). Monitoring of the Galactic Centre region with *INTEGRAL* reveals that flares are rare, with typical intervals between outbursts of several months (Sguera et al., 2005).

The outbursts start with a very sharp rise (with a timescale < 1 h) and sometimes show complex structure, with several flare-like peaks (Lutovinov et al., 2005a; Sguera et al., 2005). The X-ray spectrum during the outbursts is generally very absorbed, though the absorption is variable. Good fits can be achieved with either a power law with a high-energy cut-off or a thermal bremsstrahlung

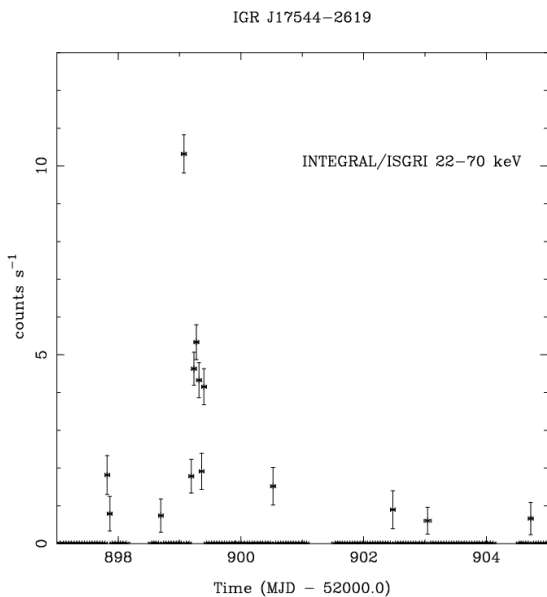


Figure 1. A typical outburst from a SFXE. *INTEGRAL* lightcurve for IGR J17544–2619 during the flare on 2003 September 17th. The data have been downloaded from the public data archive at the ISDC.

model with $kT \sim 20$ keV (Smith et al., 2006; Lutovinov et al., 2005a). Such spectra are typical of accreting neutron stars in a HMXB. The luminosity at the peak of the outbursts approaches $L_X \sim 10^{36}$ erg s $^{-1}$, also typical of HMXBs.

The source was not detected during most of an *ASCA* pointing in March 1999 (with an upper limit $L_X < 10^{33}$ erg s $^{-1}$), but went into outburst at the end of the same observation. *Chandra* detected the source at a moderate luminosity $L_X \sim 10^{34}$ erg s $^{-1}$, allowing the identification of the counterpart (Smith et al., 2006). VLT/FORS1 spectra taken in May 2004 show the counterpart to be an O8 Iab(f) star, placed at a distance ≈ 2.6 kpc (Negueruela et al., 2006). Interstellar absorption is much lower than the absorption implied by X-ray spectral fits.

IGR J17544–2619

IGR J17544–2619 was discovered by *INTEGRAL* during a short flare (~ 2 h; see Fig. 1) on 2003 September 17th (Sunyaev et al., 2003). Six hours later, it showed a longer (8 h) double-peaked outburst (Grebenev et al., 2003). On 2004 March 8th, it showed a complex outburst lasting more than 8 h (Grebenev et al., 2004).

The source was observed by *XMM-Newton* on 2003 September 11th and 17th and in both cases seen at $L_X \sim 10^{35}$ erg s $^{-1}$ (González-Riestra et al., 2004), though it was not detected during a serendipitous observation in March 2003 ($L_X \lesssim 2 \times 10^{32}$ erg s $^{-1}$). *Chandra* may have observed its quiescent state on 2004 July 3rd, as it was detected at only $L_X \sim 5 \times 10^{32}$ erg s $^{-1}$ and displaying a soft spectrum (In’t Zand, 2005). In outburst, the

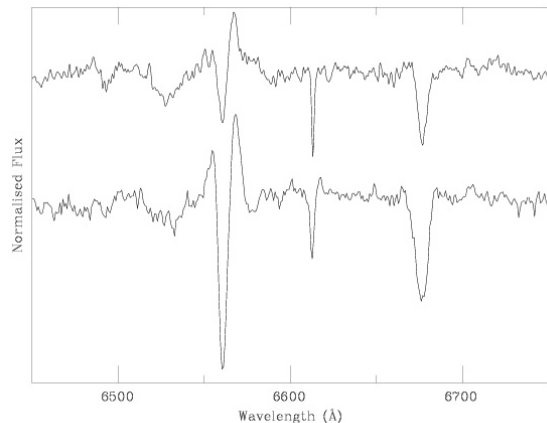


Figure 2. $H\alpha$ spectra of the counterparts to IGR J17544–2619 (top) and IGR J16465–4507 (bottom). Both display weak P-Cygni profiles, indicative of moderate mass loss.

spectrum is hard and moderately absorbed, with evidence for some variation in the amount of absorbing material.

The counterpart to the source has been unambiguously identified with the *XMM-Newton* and *Chandra* positions. Spectra taken with NTT/EMMI show it to be an O9 Ib supergiant, with a weak wind (see Fig. 2) at a distance of ~ 3 kpc (Pellizza et al., 2006).

IGR J16465–4507

IGR J16465–4507 was discovered by *INTEGRAL* during an X-ray flare on 2004 September 7th (Lutovinov et al., 2004). A subsequent *XMM-Newton* observation (Lutovinov et al., 2005b) revealed that the source is a pulsar with $P_{\text{spin}} = 228$ s and is extremely absorbed ($N_{\text{H}} \sim 7 \times 10^{23}$ cm $^{-2}$).

No further flares have been reported, but the *XMM-Newton* error circle contains only one star. NTT/EMMI spectra of this object were taken in February and March 2005. The blue spectrum, displayed in Fig. 3, is rather noisy, but allows an approximate classification. While the object is very obviously an early B-type star, the strength of all metallic lines indicates that it is a supergiant. Comparison to the spectrum of the B1 Ib supergiant ζ Per rebinned to the same dispersion clearly shows that the lines are very broad for a supergiant, suggesting a very high rotational velocity, a typical characteristic of HMXBs.

The presence of strong C III 4650Å and moderate Si III lines, while He II 4686Å is absent, is only compatible with a luminous star in the B0–B1 range. Unfortunately, the signal to noise of the spectrum falls below ~ 20 around $\lambda 4100$ Å and we cannot determine the strength of the Si IV lines that would allow an exact classification. The $H\alpha$ spectrum (see Fig. 2) shows evidence for a moderate mass loss.

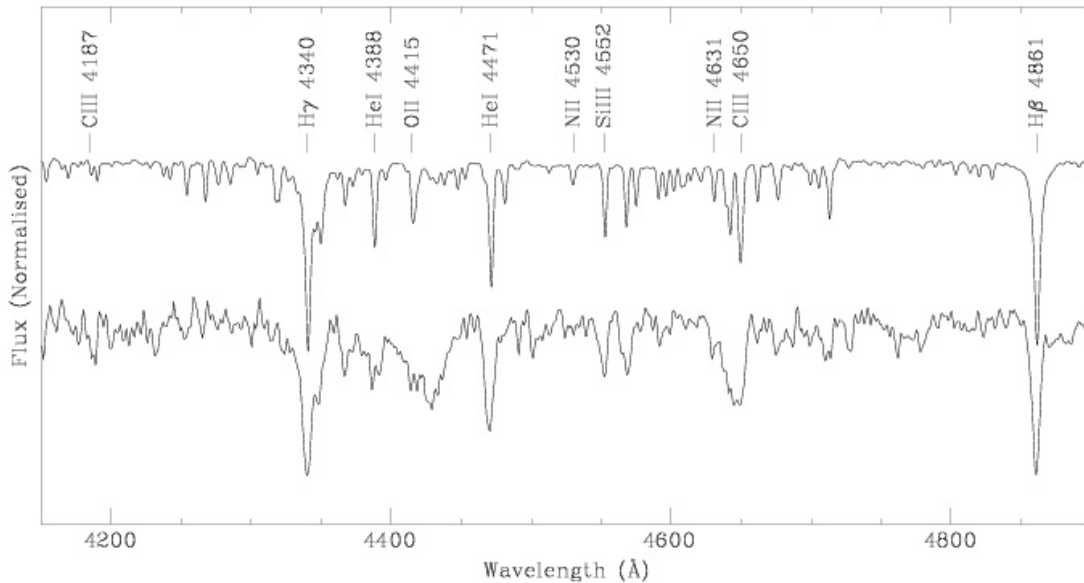


Figure 3. The spectrum of the optical counterpart to IGR J16465–4507 (bottom), compared to that of the B1 Ib supergiant ζ Per, rebinned to the same dispersion. The strength of the metallic lines indicates that the counterpart is a supergiant.

AX 1845.0–0433

AX 1845.0–0433 was discovered by *ASCA* during a strong flare in 1993. The outburst consisted of a very fast rise (on the order of a few minutes) followed by a number of peaks during the next few hours. The spectrum was well fit by an absorbed power law (Yamauchi et al., 1995). No further X-ray activity has been reported.

The *ASCA* error circle was studied by Coe et al. (1996), who found only one remarkable object, a late O-type supergiant. This star has been monitored with the 1.3-m telescope at Skinakas observatory. Some of the spectra are shown in Fig. 4. The star shows strong $H\alpha$ emission, typical of a luminous supergiant. Both the shape and strength of the line are variable, sometimes from night to night. Such variability is a typical signature of an interacting binary.

AX J1841.0–0536

AX J1841.0–0536 was observed as a violently variable transient by *ASCA* in April 1994 and then again in October 1999 (Bamba et al., 2001). The source showed multi-peaked flares with a sharp rise (tenfold increase in count-rate over ~ 1 h). Analysis of the *ASCA* data revealed that the source is a pulsar with $P_{\text{spin}} = 4.7$ s. The spectrum can be fit by an absorbed power law plus iron line (Bamba et al., 2001). Based on the detection of X-ray flares with a sharp rise, Bamba et al. (2001) suggested that AX 1845.0–0433, AX J1841.0–0536 and XTE J1739–302 could be members of a class with common physical features.

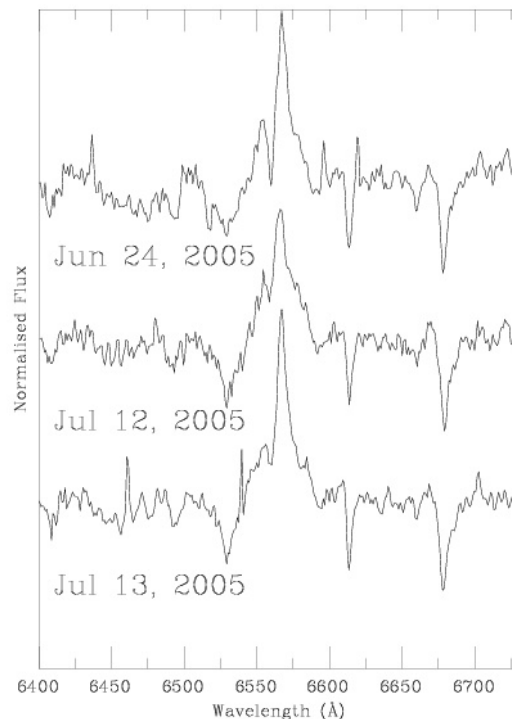


Figure 4. $H\alpha$ spectra of the proposed counterpart to AX 1845.0–0433, displaying strong variability, even between consecutive nights, a typical signature of an interacting binary.

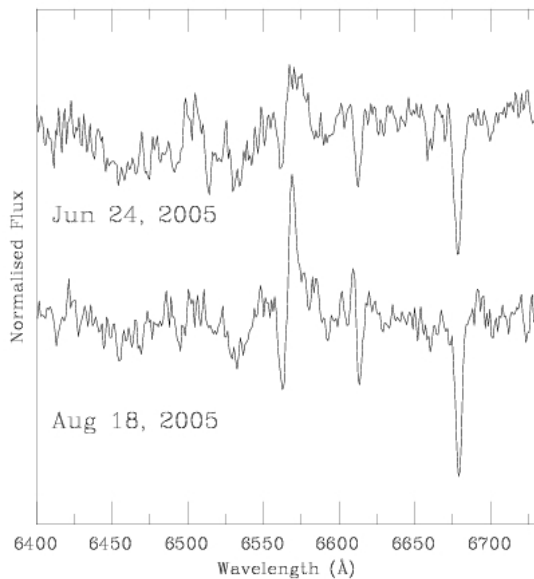


Figure 5. $H\alpha$ spectra of the counterpart to AX J1841.0–0536, showing P-Cygni profiles indicative of the stellar wind of a luminous star.

A *Chandra* observation of the field revealed the counterpart to AX J1841.0–0536, a reddened star with $H\alpha$ in emission (Halpern et al., 2004). We have taken spectra of this star with the 2.2-m at Calar Alto and the 1.9-m at SAAO. Though the spectra are very noisy, they strongly resemble that of the counterpart to IGR J16465–4507, displaying a very strong C III 4650Å line and no He II 4686Å. Therefore, it is also likely to be a luminous star in the B0–1 range.

Some red spectra have been taken with the 1.3-m telescope at Skinakas observatory (see Fig. 5). Again we find a shape reminiscent of a P-Cygni profile and strong variability, lending support to the idea that the object is a supergiant rather than a Be star. A fast outburst observed by *INTEGRAL* (IGR J18410–0535) has been attributed to this source (Halpern & Gotthelf, 2004).

3. SUPERGIANT FAST X-RAY TRANSIENTS: A NEW CLASS?

The five sources described in the previous section are characterised by the occurrence of X-ray outbursts of a very different nature from those seen in other X-ray binaries. These outbursts are very short (lasting from ~ 3 to ~ 8 hours) and present very sharp rises, reaching the peak of the flare in $\lesssim 1$ h. The decay is generally characterised by a complex structure, with two or three further flares. Three of the sources are associated with O-type supergiants. Though no pulsations have been detected, they display spectra typical of accreting neutron stars. The other two sources are X-ray pulsars and are asso-

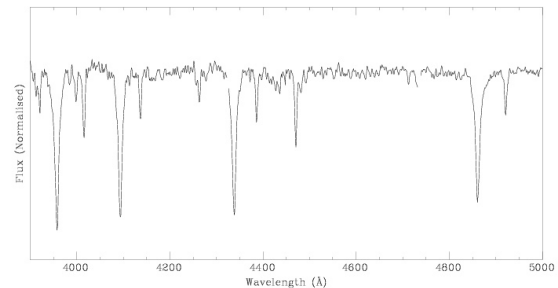


Figure 6. Optical spectrum of HD 168078.

ciated with luminous early B-type stars. In all cases, the spectra show moderate or high absorption. In the case of XTE J1739–302 and IGR J17544–2619, which are better studied, the amount of absorbing material is variable.

We therefore propose that all these objects form a class of HMXBs which we call Supergiant Fast X-ray Transients (SFXTs), because of the fast outbursts and supergiant companions. They differ from classical wind-fed SGXBs, whose X-ray luminosity is variable but always detectable around $L_X \sim 10^{36}$ erg s $^{-1}$. Quiescent fluxes of SFXTs have been near the sensitivity limit of focusing observatories, with values or upper limits in the range of $\sim 10^{32}$ to $\sim 10^{33}$ erg s $^{-1}$.

In spite of this difference, it must be noted that the commonalities between SFXTs and SGXBs are strong. As a matter of fact, at least three classical SGXBs have been observed to undergo bright flares on the same timescale: Vela X-1 (Laurent et al., 1995; Krivonos et al., 2003), 1E 1145.1–6141 (Bodaghee et al., 2004) and Cyg X-1 (Golenetskii et al., 2003, and references therein).

4. OTHER SOURCES DISPLAYING FAST OUTBURSTS

SAX J1818.6–1703

SAX J1818.6–1703 was discovered by *BeppoSAX* during a strong short outburst (with a rise time of ~ 1 h), in March 1998 (In’t Zand et al., 1998). *INTEGRAL* detected a double-peaked outburst in September 2003 (Grebenev & Sunyaev, 2005) and two more in October 2003 (Sguera et al., 2005). Other fast outbursts have been observed with the ASM on *RossixTE* (Sguera et al., 2005).

The X-ray lightcurve of SAX J1818.6–1703 is typical of a SFXT. The X-ray spectrum is very hard (Grebenev & Sunyaev, 2005). The optical counterpart to SAX J1818.6–1703 is not known. A bright early type star, HD 168078, is within both the *BeppoSAX* and *INTEGRAL* error circles. Spectra of this object, taken with the 1.3-m at Skinakas and the 1.9-m at SAAO show a normal B3 IV star, without indications of emission (see Fig. 6). As HD 168078 is not a convincing counterpart

to SAX J1818.6–1703, it might be worthwhile to search the error circle for a reddened supergiant.

IGR J16479–4514

IGR J16479–4514 was discovered by *INTEGRAL* during an outburst in August 2003 (Molkov et al., 2003). Several other short outbursts with very fast rise times were observed by *INTEGRAL* during 2003 (Sguera et al., 2005). The X-ray spectrum of IGR J16479–4514 is a power-law with high-energy cut-off, typical of a HMXB with a neutron star (Lutovinov et al., 2005b). All these characteristics are strongly suggestive of a SFXT.

XTE J1901+014

XTE J1901+014 was discovered by *RXTE* during a very bright outburst (reaching 0.9 Crab) that lasted less than 8 h, in 2002 (Remillard & Smith, 2002). Analysis of *RXTE*/ASM data revealed another fast outburst in 1997 (Remillard & Smith, 2002). Several outbursts have been observed by *INTEGRAL*. The *INTEGRAL* error circle contains two *ROSAT* sources and one *Einstein* source, one of which could represent the quiescent state of XTE J1901+014 (Stephen et al., 2005).

AX J1749.1–2733

AX J1749.1–2733 was observed by *ASCA* at a relatively low luminosity on several occasions (Sakano et al., 2002). It has recently been reported to show fast X-ray outbursts during *INTEGRAL* observations (Grebenev, quoted in In't Zand 2005).

5. DISCUSSION & CONCLUSIONS

Most X-ray transients, whether Be/X-ray binaries or low mass X-ray binaries (having either neutron star or black hole companions), display outbursts typically lasting from a few weeks to months. Such durations are compatible with viscous timescales in a typical accretion disc. Fast outbursts, with much shorter durations, must be due to a completely different physical mechanism. Here we have shown that at least a fraction of the recurrent fast X-ray transients are associated with luminous OB stars, suggesting that the mass transfer mechanism feeding the accreting compact object is a radiative wind, and therefore have identified the class of SFXTs.

We must note that not every source displaying short X-ray outbursts may be assigned to the class of SFXTs. Flare stars and RS CVn binaries display short X-ray flares and superbursts from low mass X-ray binaries have similar durations, though rather different luminosities and lightcurves (e.g. Grebenev & Sunyaev, 2005). The HMXB 1A 0535–668, in the LMC, has shown very bright X-ray outbursts lasting only a few days, but these outbursts are locked in phase with the orbital period of the system and may be related to periastron passage in a very eccentric orbit (cf. Charles et al., 1983).

IGR J00370+6122 could be a similar system (Reig et al., 2005). The black hole transient V4641 Sgr should not be grouped with SFXTs either. In this system, the mass donor is a B9 III giant (Orosz et al., 2001), which is not a massive star and cannot have a radiative wind. Moreover, its 1999 outburst was highly super-Eddington and accompanied by a huge optical brightening, properties that set it completely apart from SFXTs (Revnivtsev et al., 2002).

However, there are strong reasons to believe that the class of SFXTs comprises a much larger number of sources than the five objects described above. In Section 4, we list four reliable candidates, but other known sources might belong to this class. For example, the X-ray transient IGR J11215–5952 was observed by *INTEGRAL* during the decaying phase of an outburst. It is likely to be related to SFXTs if its association to the B1 Ia supergiant HD 306414 is confirmed (cf. Negueruela et al., 2005).

If only some of these candidates are confirmed, the number of SFXTs would already be comparable to that of classical SGXBs. We must consider, however, that classical SGXBs are persistent bright X-ray sources, while SFXTs are transient sources with very short duty cycles. Most of them are detectable, unless directly pointed at by *Chandra* or *XMM-Newton*, only for a few hours every several months. It is hence not surprising that most of the SFXTs so far found lie on the vicinity of the Galactic Centre, a region extensively monitored by *INTEGRAL* and other satellites.

But, if SFXTs are very difficult to detect, and we already know several of them in the region around the Galactic Centre, the implication is that the population of SFXTs in the Galaxy is much larger than the ten or so objects already known. As a matter of fact, it is difficult to avoid concluding that most binaries containing a supergiant and a compact object **must** be SFXTs or entirely quiescent. If we take into account the large number of obscured persistent HMXBs that *INTEGRAL* is discovering, it seems clear that the numbers of HMXBs must have been severely underestimated.

The physical reason for fast outbursts is still unknown. Golenetskii et al. (2003) speculated that the outbursts in Cyg X-1 could be due to some form of discrete mass ejection from the supergiant donor. In't Zand (2005) also suspects that wind variability is the cause of fast outbursts. As we have shown here, an important fraction of fast transients have supergiant companions and at least three classical SGXBs have shown fast outbursts. It seems then that the fast outbursts are related to the mass transfer mode, wind accretion. They cannot be related to the nature of the companion, as they are seen in black hole systems (Cyg X-1), slow X-ray pulsars (IGR J16465–4507) and faster X-ray pulsars (AX J1841.0–0536).

There is increasing evidence suggesting that the winds of B-type supergiants are highly structured and may have a fundamentally clumpy nature (Prinja et al., 2005, and references therein). If these clumps survive to the distance at which the compact object is orbiting, they could give

rise to sudden episodes of increased accretion rate. Alternatively, the outbursts could be related to the instability believed to be intrinsic to the wind accretion process (e.g. Foglizzo et al., 2005).

On the other hand, there is nothing in the optical properties of SFXTs setting them apart from classical SGXBs. It is therefore difficult to understand why their quiescent X-ray luminosities are rather lower. A possibility would be that SFXTs have wider orbits than SGXBs, and the compact object (in most cases, a neutron star) accretes from a less dense environment. This, however, would not explain why the sources spend some (still not quantified) fraction of time below detectability. If highly eccentric, wide orbits are invoked in order to explain the periods of very low X-ray luminosity, one would naïvely expect some (quasi-)periodicity in the recurrence of the outbursts, that has not been observed, as they would have to occur always relatively close to periastron.

Clearly, a more complete investigation of all the sources presented here is needed before common trends start to emerge and a characterisation of the group of SFXTs can be achieved. Understanding the reasons for their X-ray behaviour and the source of the difference with classical SGXBs will undoubtedly increase our knowledge of the accretion process and very likely provide valuable insights into the different paths leading to the formation of HMXBs and their subsequent evolution.

ACKNOWLEDGMENTS

IN is a researcher of the programme *Ramón y Cajal*, funded by the Spanish MCyT and the University of Alicante. This research is partially supported by the Spanish MCyT under grants AYA2002-00814 and ESP-2002-04124-C03-03.

Partly based on observations collected at the European Southern Observatory, La Silla, Chile (ESO 73.D-0081; 274.D-5010) and observations collected at the DSAZ, Calar Alto, operated by the MPI für Astronomie Heidelberg jointly with the Spanish CNA. We thank Calar Alto for allocation of director's discretionary time to this programme. Skinakas Observatory is a collaborative project of the University of Crete, the Foundation for Research and Technology-Hellas and the MPI für Extraterrestrische Physik. This research has made use of the Simbad data base, operated at CDS, Strasbourg, France.

We are very grateful to Jorge Casares for carrying out the observations at SAAO. We also thank Leonardo Pellizza for advancing results on IGR J17544–2619.

REFERENCES

- Bamba, A., et al. 2001, PASJ 52, 1179
- Bodaghe, A., Mowlavi, N., Ballet, J. 2004, ATel 290
- Charles, P.A., et al. 1983, MNRAS, 202, 657
- Coe, M.J., et al. 1996, MNRAS 281, 333
- Foglizzo, T., et al. 2005, A&A 435, 397
- Golenetskii, S., et al. 2003, ApJ 596, 1113
- González-Riestra, R., et al. 2004, A&A 420, 589
- Grebenev, S.A., Sunyaev, R.A. 2005, Ast. Lett. 31, 672
- Grebenev, S.A., et al. 2003 ATel 192
- Grebenev, S.A., et al. 2004 ATel 252
- Halpern, J.P., Gotthelf, E.V. 2004, ATel 341
- Halpern, J.P., et al. 2004, ATel 289
- In't Zand, J.J.M. 2005, A&A 441, L1
- In't Zand, J.J.M., et al. 1998, IAUC 6840
- Krivonos, S., et al. 2003, ATel 211
- Laurent, P., et al. 1995, A&A 300, 399
- Lutovinov, A., et al. 2004, ATel 329
- Lutovinov, A., et al. 2005a, A&A 430, 997
- Lutovinov, A., et al. 2005b, A&A, in press (astro-ph/0411550)
- Molkov, A., et al. 2003, ATel 176
- Negueruela, I., et al. 2005, ATel 469
- Negueruela, I., et al. 2006, ApJ, in press (astro-ph/0510675)
- Orosz, J.A., et al. 2001, ApJ 555, 489
- Pellizza, L.J., et al. 2006, A&A, submitted
- Prinja, R.K., et al. 2005, A&A 430, L41
- Reig, P., et al. 2005, A&A 440, 637
- Remillard, R.A., Smith, D.A. 2002, ATel 88
- Revnivtsev, M., et al. 2002, A&A 385, 904
- Rodríguez, J. et al. 2004, ATel 340
- Sakano, M., et al. 2002, ApJS 138, 19
- Sguera, V., et al. 2005, A&A, in press (astro-ph/0509018)
- Stephen, J.B., et al. 2005, A&A 432, L49
- Smith, D.M., et al. 1998, ApJ 501, L181
- Smith, D.M., et al. 2006, ApJ, in press (astro-ph/0510658)
- Sunyaev, R.A., et al. 2003 ATel 190
- Yamauchi, S., et al. 1995, PASJ 47, 189

ON PERIODIC X-RAY OUTBURSTS IN Be/X-RAY BINARIES

A.T. Okazaki¹ and K. Hayasaki^{2,3}

¹Faculty of Engineering, Hokkai-Gakuen University, Toyohira-ku, Sapporo 062-8605, Japan

²Department of Applied Physics, Graduate School of Engineering, Hokkaido University, Kita-ku, Sapporo 060-8628, Japan

³Centre for Astrophysics and Supercomputing, Swinburne University of Technology, PO Box 218, Hawthorn, Victoria 3122, Australia

ABSTRACT

We numerically study the accretion flow around the neutron star in Be/X-ray binaries, using a three dimensional Smoothed Particle Hydrodynamics code. We find that the viscous decretion disk around the Be star is tidally truncated at a radius smaller than the periastron distance for a wide range of orbital parameters. Due to the truncation of the Be disk and the eccentric orbit of the neutron star, the accretion rate is strongly phase dependent, and is sensitive to the orbital eccentricity and the inclination angle. In systems with low to moderate eccentricity, the accretion rate is too low to cause periodic X-ray outbursts. Such systems are likely to stay in quiescence normally and show only temporal X-ray outbursts when they have an enhanced mass-transfer from the Be star. In contrast, in highly eccentric systems, the peak accretion rate falls in a typical range of accretion rate for the periodic X-ray outbursts in Be/X-ray binaries unless the misaligned angle between the Be disk and the binary orbital plane is too large. This strongly suggests that, in the framework of the truncated Be disk model for Be/X-ray binaries, periodic X-ray outbursts are the phenomenon most frequently seen in highly-eccentric, coplanar systems.

Key words: accretion disks; Be/X-ray binaries; X-ray outbursts.

1. INTRODUCTION

The Be/X-ray binaries form the largest subclass of high mass X-ray binaries. They consist of a Be star and a neutron star. The orbit is wide ($10 \text{ d} \lesssim P_{\text{orb}} \lesssim 400 \text{ d}$) and mostly eccentric ($e \gtrsim 0.3$). Most of the Be/X-ray binaries show only transient X-ray activity due to transient accretion from the circumstellar disk of the Be star. Each Be/X-ray binary exhibits some or all of the following three types of X-ray activity:

1. periodic (Type I) X-ray outbursts, coinciding with periastron passage ($L_X \approx 10^{36-37} \text{ erg s}^{-1}$),
2. giant (Type II) X-ray outbursts ($L_X \gtrsim 10^{37} \text{ erg s}^{-1}$), which show no clear orbital modulation,
3. persistent low-luminosity X-ray emission ($L_X \lesssim 10^{34} \text{ erg s}^{-1}$)

(Stella et al. 1986; see also Negueruela et al. 1998). These features imply a complicated interaction between the Be-star envelope and the neutron star.

Be/X-ray binaries are also important as a laboratory for studying the physics of the tidal interaction, the mass transfer and the accretion process in eccentric binaries. They are unique in the sense that the neutron star is fed by the overflow from the circumstellar disk around the Be star, which is geometrically thin and nearly Keplerian. The radial velocity of the Be disk is smaller than a few km s^{-1} , at least within ~ 10 stellar radii (Hanuschik 1994; Hanuschik 2000; Waters & Marlborough 1994). These features are in good agreement with the viscous decretion disk model proposed by Lee et al. (1991) (Porter 1999; see also Okazaki 2001). In this model, the matter supplied from the equatorial surface of the star drifts outwards because of the viscous effect and forms the disk. Until recently, little work has been done on the interaction in these unique objects. See Fig. 1 for a schematic diagram of the interactions in Be/X-ray binaries.

Based on the viscous decretion disk model, Negueruela & Okazaki (2001) and Okazaki & Negueruela (2001) semi-analytically showed that the coplanar Be disk in Be/X-ray binaries is truncated at a radius smaller than the periastron distance, as long as $\alpha \ll 1$, where α is the Shakura-Sunyaev viscosity parameter. The result agrees with the observations by Reig et al. (1997) and Zamanov et al. (2001) that there is a positive correlation between the orbital size and the maximum equivalent width of H α ever observed in a system, a measure of the maximum disk

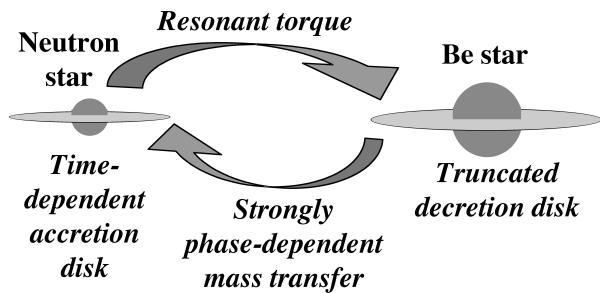


Figure 1. Schematic diagram of the interactions in Be/X-ray binaries.

size around the Be star in the system. It has also been confirmed by numerical simulations for a system with a short orbital period and a moderate orbital eccentricity (Okazaki et al., 2002).

In this paper, we study the origin of the periodic (Type I) X-ray outbursts in Be/X-ray binaries, performing three dimensional Smoothed Particle Hydrodynamics (SPH) simulations. Our results suggest that, in the framework of the truncated Be disk model for Be/X-ray binaries, the periodic X-ray outbursts are the phenomenon most frequently seen in highly-eccentric, coplanar systems.

2. NUMERICAL MODEL

We use a 3D SPH code, in which the Be disk and the accretion disk are modeled by an ensemble of gas particles of negligible masses and the Be star and the neutron star by two sink particles with corresponding masses (Okazaki et al. 2002; Hayasaki & Okazaki 2004; see also Bate et al. 1995). Gas particles which fall within a specified accretion radius are accreted by the sink particle. We assume that the Be star has the accretion radius of R_* , where R_* is the radius of the Be star. For the neutron star, we adopt the accretion radius of $r = 5 \times 10^{-3}a$, where a is the semi-major axis. For simplicity, we assume that both disks are isothermal at the temperature of half the effective temperature of the Be star and have the viscosity parameter $\alpha_{SS} = 0.1$. We set the binary orbit on the x - z plane with the major axis along the x -axis. At $t = 0$, the neutron star is at the apastron. The mass ejection mechanism from the Be star is modeled by constant injection of gas particles at a radius just outside the equatorial surface. As the Be star, we take a B0V star of $M_* = 18M_\odot$, $R_* = 8R_\odot$, and $T_{\text{eff}} = 26,000$ K. For the neutron star, we take $M_X = 1.4M_\odot$ and $R_X = 10^6$ cm.

3. TRUNCATION OF THE Be DISK

Until recently, models for periodic (Type I) X-ray outbursts in Be/X-ray binaries had assumed a large disk around the Be star so that the neutron star can accrete gas

when it passes through the disc near periastron. However, as mentioned above, Negueruela & Okazaki (2001) and Okazaki & Negueruela (2001) semi-analytically showed that the Be disk in Be/X-ray binaries is truncated at a radius smaller than the periastron distance. The truncation is due to the resonant torque exerted by the neutron star, which removes the angular momentum from the disk.

Fig. 2 shows the surface density evolution of the viscous decretion disk around the Be star. Panels (a) and (b) are for $e = 0.34$ and $e = 0.68$, respectively. In these simulations, the orbital period P_{orb} is 24.3 d and the Be disk is coplanar with the binary orbital plane. Each simulation finally had about 150,000 SPH particles. As shown in Fig. 2, the decretion disk around the Be star is tidally/resonantly truncated at a radius significantly smaller than the periastron distance. Since the resonant torque prevents disk material from drifting outwards, the disk density increases more rapidly than in disks around isolated Be stars. The wavy patterns seen in the surface density distribution in the left panel is due to the tightly wound spiral density wave excited in the disk. Note that the truncation is more efficient for a lower orbital eccentricity, as expected from the semi-analytical study. We have found that the tidal/resonant truncation works, except for systems with extremely high eccentricity ($e \gtrsim 0.8$).

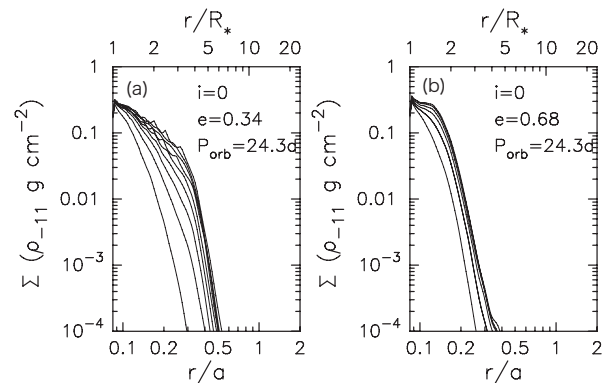


Figure 2. Surface density evolution of the Be decretion disk for (a) $i = 0^\circ$ and $e = 0.34$ and (b) $i = 0^\circ$ and $e = 0.68$, where i is the angle between the mid-plane of the Be disk and the orbital plane. The orbital period $P_{\text{orb}} = 24.3$ d. The time interval between adjacent contours is $5P_{\text{orb}}$. $\rho_{-11} = \rho_0/10^{-11} \text{ g cm}^{-3}$, where ρ_0 is the base density of the disk.

4. ACCRETION DISKS IN SYSTEMS WITH MODERATE ECCENTRICITY

Based on semi-analytical results for several Be/X-ray binaries with known orbital parameters, Okazaki & Negueruela (2001) discussed that the X-ray behavior of systems with moderate eccentricity depends on rather subtle details: Systems in which the disk is truncated in the vicinity of the critical lobe will regularly display

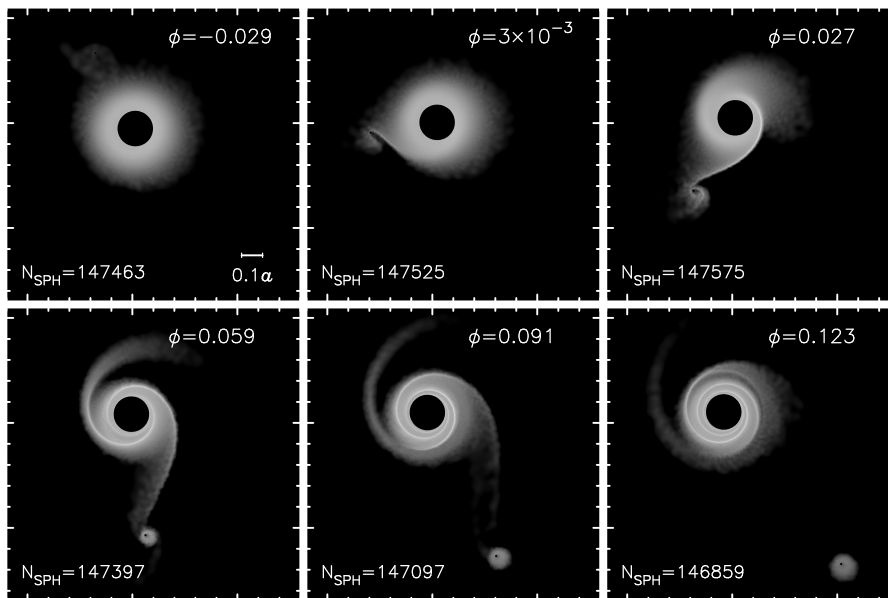


Figure 3. Snapshots of the accretion disk formation in a coplanar Be/X-ray binary with $P_{\text{orb}} = 24.3$ d and $e = 0.68$, which cover $\sim 0.15P_{\text{orb}}$ around the periastron passage. Each panel shows the surface density in a range of 5 orders of magnitude in the logarithmic scale. Annotated in each panel are the orbital phase and the number of SPH particles.

Type I outbursts, whereas those with the disk significantly smaller than the critical lobe will show Type I outbursts only when the disk is strongly disturbed.

Recently, Hayasaki & Okazaki (2004) and Hayasaki & Okazaki (2005) studied the accretion flow around the neutron star in a Be/X-ray binary with a short period ($P_{\text{orb}} = 24.3$ d) and a moderate eccentricity ($e = 0.34$), using a 3D SPH code and the simulation data by Okazaki et al. (2002) as the outer boundary condition. They found that the peak accretion rate on to the neutron star in their moderately eccentric system ($3 \times 10^{-11} M_{\odot} \text{ yr}^{-1}$) is much smaller than that corresponding to a typical luminosity range of Type I outbursts ($L_X \approx 10^{36-37} \text{ erg s}^{-1}$), which implies that this system is normally in quiescent state. They also found that a time-dependent accretion disk is formed and grows secularly, because the mass-accretion rate on to the neutron star is much smaller than the mass-transfer rate from the Be disk. Their results suggest that Be/X-ray binaries with moderate orbital eccentricities are likely to have persistent accretion disks around the neutron star, even if they exhibit no periodic (Type I) X-ray outbursts.

5. ACCRETION DISKS IN SYSTEMS WITH HIGH ECCENTRICITY

The mass-accretion rate on to the neutron star is expected to be higher in systems with a higher eccentricity. In order to study the effect of the orbital parameters on the accretion rate, we have run three simulations for highly eccentric systems with different orbital period P_{orb} and inclination angle i . In these simulations, the eccentricity

e was fixed at 0.68.

5.1. Coplanar System with a Short Orbital Period

Fig. 3 gives snapshots covering $\sim 0.15P_{\text{orb}}$ around the periastron passage, which occurs at phase $\phi = 0$, in a coplanar system ($i = 0$) with $P_{\text{orb}} = 24.3$ d and $e = 0.68$. Each panel shows the logarithm of the surface density. The dark spot near the center is the Be star. Annotated in each panel are the orbital phase and the number of SPH particles. As seen in Fig. 3, an accretion disk is formed around the neutron star at periastron, when the material is transferred from the Be disk for a short period of time. Most of the material transferred from the Be disk accretes on to the neutron star by the next periastron passage. Thus, the accretion disk in this highly eccentric system is transient, unlike the counterparts in moderately eccentric systems.

The orbital-phase dependence of the accretion rate on to the neutron star is shown in Fig. 5(a). To reduce the fluctuation noise, the data is folded on the orbital period over $5P_{\text{orb}}$. The periastron passage of the neutron star is denoted by the vertical dashed line. The right axis shows the X-ray luminosity L_X given by $L_X = GM_X \dot{M}_{\text{acc}} / R_X$. It is important to note that the X-ray luminosity ($\sim 5 \times 10^{36} \text{ erg s}^{-1}$) corresponding to the peak accretion rate of about $4 \times 10^{-10} M_{\odot} \text{ yr}^{-1}$ enters a typical luminosity range of the Type I X-ray outbursts in Be/X-ray binaries. Note also that the accretion rate profile has an initial spike followed by the major peak. This is because the specific angular momentum of the transferred mass from the Be disk rapidly increases with phase. Sim-

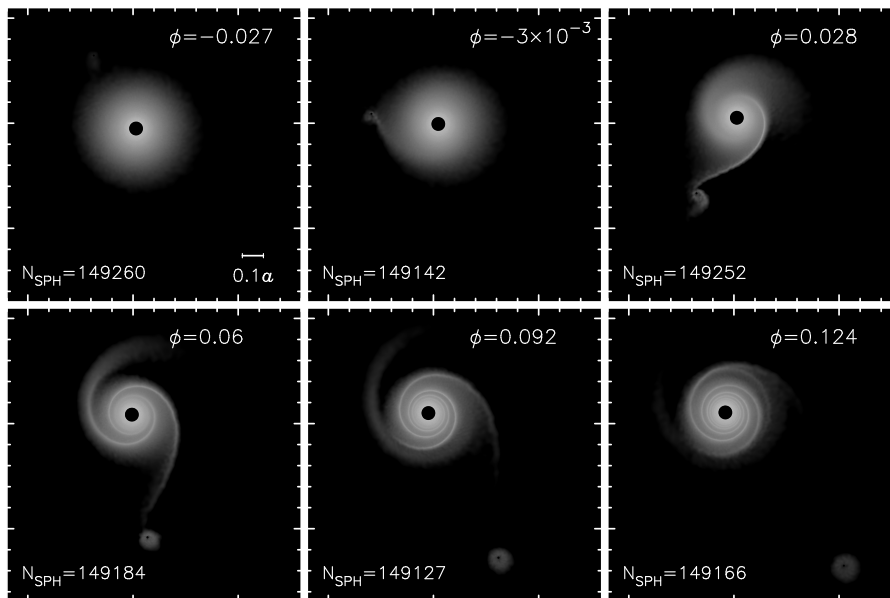


Figure 4. Same as Fig. 3, but for $P_{\text{orb}} = 100$ d.

ilar feature was recently found in EXO 2030+375 by Camero Arranz et al. (2005).

5.2. Coplanar System with a Long Orbital Period

Fig. 4 gives snapshots covering $\sim 0.15P_{\text{orb}}$ around the periastron passage in a coplanar system ($i = 0$) with $P_{\text{orb}} = 100$ d and $e = 0.68$. The format of the figure is the same as that of Fig. 3. In this simulation, a transient accretion disk is also formed around the neutron star at periastron.

The orbital-phase dependence of the accretion rate on to the neutron star is shown in Fig. 5(b). To reduce the fluctuation noise, the data is folded on the orbital period over $5P_{\text{orb}}$. In this simulation, the X-ray luminosity corresponding to the peak accretion rate of about $2 \times 10^{-10} M_{\odot} \text{ yr}^{-1}$ is about $2 \times 10^{36} \text{ erg s}^{-1}$, which also enters a typical luminosity range of the Type I X-ray outbursts. As in the short orbit case, the accretion rate profile has two peaks, although the dip between the two peaks is much inconspicuous.

5.3. Misaligned System with a Short Orbital Period

In order to study the effect of the inclination angle on the accretion on to the neutron star, we have run a simulation for $P_{\text{orb}} = 24.3$ d, $e = 0.68$ and $i = 30^{\circ}$ about y -axis, where i is the angle between the mid-plane of the Be disk and the orbital plane. We have found that the inclined Be disk is resonantly truncated as in coplanar systems. We have also found that the accretion disk formed around the neutron star is inclined from the orbital plane with an angle different from that of the Be disk.

Figure 5(c) shows the phase dependence of the accretion rate on to the neutron star. To reduce the fluctuation noise, the data is folded on the orbital period over $3P_{\text{orb}}$. In this simulation, the X-ray luminosity corresponding to the peak accretion rate of about $8 \times 10^{-11} M_{\odot} \text{ yr}^{-1}$ is about $10^{36} \text{ erg s}^{-1}$, which is roughly equal to the lower end of the luminosity range of Type I X-ray outbursts. Thus, the accretion rate is sensitive to the inclination angle i . Since the accretion rate decreases with increasing i , systems with large misalignment angles ($\gg 30^{\circ}$) are unlikely to exhibit Type I X-ray outbursts unless the Be disk is strongly disturbed. The accretion rate profile shows a two-peaked feature, but it is very modest compared with the profiles for coplanar systems.

6. CONCLUSIONS

We have performed three dimensional SPH simulations in order to study the accretion flow around the neutron star in Be/X-ray binaries. We have found that an accretion disk is formed around the neutron star whether or not the accretion rate is high enough to cause a Type I X-ray outburst. Due to the truncation of the Be disk and the eccentric orbit of the neutron star, the accretion rate on to the neutron star is strongly phase dependent, and is sensitive to the orbital eccentricity and the inclination angle. In systems with low to moderate eccentricity, the accretion rate is too small to cause periodic (Type I) X-ray outbursts. Such systems are likely to stay in quiescence normally. On the other hand, in highly eccentric systems, the peak accretion rate falls in a typical range of accretion rate for the Type I X-ray outbursts in Be/X-ray binaries. Since the accretion rate decreases with increase of orbital period and inclination angle, highly eccentric systems with small misaligned angles are most favorable

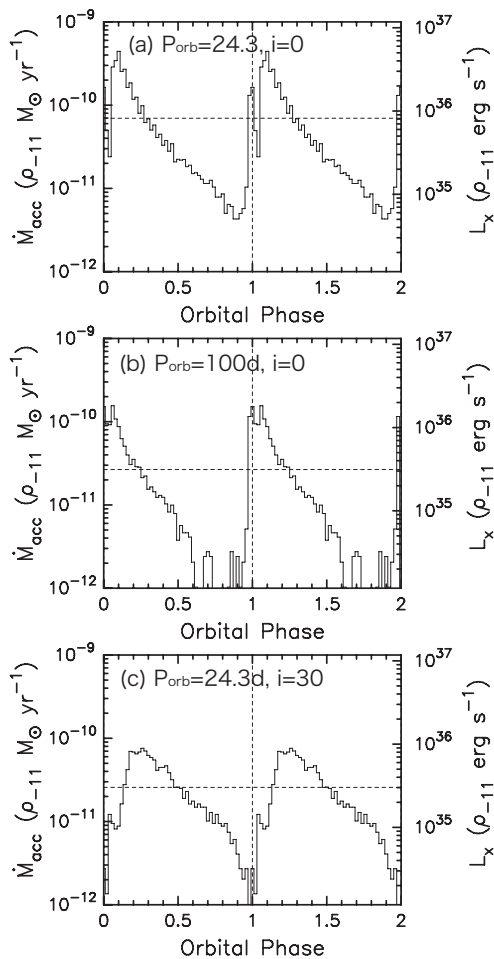


Figure 5. Orbital-phase dependence of the accretion rate on to the neutron star: (a) $P_{\text{orb}} = 24.3$ d and $i = 0^\circ$, (b) $P_{\text{orb}} = 100$ d and $i = 0^\circ$, and (c) $P_{\text{orb}} = 24.3$ d and $i = 30^\circ$ about y -axis. To reduce the fluctuation noise, the data is folded on the orbital period over $3 - 5P_{\text{orb}}$. The periastron passage of the neutron star, which occurs at phase 0, is denoted by the vertical dashed line. The right axis shows the X-ray luminosity corresponding to the mass-accretion rate.

for Type I X-ray outbursts.

REFERENCES

- Bate, M. R., Bonnell, I. A., & Price, N. M. 1995, MNRAS, 285, 33
- Camero Arranz, A., Wilson, C. A., Connell, P., Mart'nez N'úñez, S., Blay, P., Beckmann, V., & Reglero, V. 2005, A&A, 441, 261
- Hanuschik R.W., 1994, in Balona L.A., Henrichs H., Le Contel J.M., ed. Pulsation, Rotation and Mass Loss of Early-Type Stars, IAU Symp. 162, Kluwer Academic Publishers, Dordrecht, p.265

- Hanuschik R.W., 2000, in Smith M.A., Henrichs H.F., Fabregat J., ed. Be Phenomenon in Early-Type Stars, IAU Colloq. 185, ASP, San Francisco, p.518
- Hayasaki, K. & Okazaki, A. T. 2004, MNRAS, 350, 971
- Hayasaki, K. & Okazaki, A. T. 2005, MNRAS Letters, 360, L15
- Lee, U., Saio, H., & Osaki, Y. 1991, MNRAS, 250, 432
- Negueruela I., Reig P., Coe M.J., Fabregat J., 1998, A&A, 336, 251
- Negueruela, I. & Okazaki, A. T. 2001, A&A, 369, 108
- Okazaki A. T., 2001, PASJ, 53, 119
- Okazaki, A. T. & Negueruela, I. 2001, A&A, 377, 161
- Okazaki, A. T., Bate, M. R., Ogilvie, G. I., & Pringle, J. E. 2002, MNRAS, 337, 967
- Porter J.M., 1999, A&A, 348, 512
- Reig, P., Fabregat, J. & Coe, M. J. 1997, A&A, 322, 193
- Stella L., White N.E., Rosner R., 1986, ApJ, 208, 669
- Waters L.B.F.M., Marlborough J.M., 1994, in Balona L.A., Henrichs H., Le Contel J.M., ed. Pulsation, Rotation and Mass Loss of Early-Type Stars, IAU Symp. 162, Kluwer Academic Publishers, Dordrecht, p.399
- Zamanov, R. K., Reig, P., Mart, J., Coe, M. J., Fabregat, J., Tomov, N.A., & Valchev, T. 2001, A&A, 367, 884

USING XMM-NEWTON TO SEARCH OUT THE COMPACT BINARIES IN GLOBULAR CLUSTERS

N. A. Webb

Centre d'Etude Spatiale des Rayonnements, 9 avenue du Colonel Roche, 31028 Toulouse Cedex 04, France

ABSTRACT

Globular clusters are thought to harbour a large number of compact binaries that could be responsible for delaying the inevitable core collapse of these dense clusters. Compact binaries and their progeny were previously elusive in the optical domain because of the high stellar densities. Observing these clusters in X-rays, where in such a domain the compact binaries are bright, diminishes the over-crowding problem. We present observations of four of the eight Galactic globular clusters that we have made with XMM-Newton, along with follow-up optical photometry and spectroscopy made with the Very Large Telescope (VLT). We have identified neutron star low mass X-ray binaries and their descendants (millisecond pulsars), cataclysmic variables, active binaries as well as other exotic objects, such as subdwarf B stars and evidence for double degenerates. We discuss the characteristics of these systems, along with their formation and evolution in globular clusters and their use in tracing the dynamical history of these clusters.

Key words: globular clusters: individual:M 55 - NGC 3201 - M 22 - ω Centauri – X-rays: general – binaries: general – stars: variables: general.

1. INTRODUCTION

It is expected that globular clusters (GCs) should contain many binary systems, due to interactions occurring within the clusters (e.g. Di Stefano & Rappaport, 1994), and that these systems *could* play a critical role in the dynamical evolution of GCs, serving as an internal energy source which counters the tendency of GC cores to collapse (e.g. Hut et al., 1992, for a review). However, these binaries are extremely difficult to locate at long wavelengths, because of over-crowding. It is almost uniquely using X-ray observations that the binaries, which are also visible at such high energies, can be located. Indeed the small population of bright X-ray sources ($L_x > 10^{36}$ erg s $^{-1}$), known to be X-ray binaries (Hertz & Grindlay, 1983), were detected and identified primarily through

their X-ray emission. However, there is a large population of faint ($L_x \lesssim 10^{34.5}$ erg s $^{-1}$) X-ray sources, whose nature is only now beginning to be revealed. A variety of objects have been identified, including many binary systems and their progeny, i.e.: X-ray binaries (e.g. Gendre et al., 2003b; Rutledge et al., 2002); cataclysmic variables (e.g. Carson et al., 2000; Webb et al., 2005); millisecond pulsars (e.g. Grindlay et al., 2001; Camilo et al., 2000); active binaries (e.g. Kaluzny et al., 1996; Carson et al., 2000); as well as fore- and background objects, e.g. stars (e.g. Gendre et al., 2003a) or clusters of galaxies (Webb et al., 2004). The populations of these binaries, with the exception of neutron star X-ray binaries which appear to scale with the cluster encounter rate (Gendre et al., 2003a; Pooley et al., 2003; Heinke et al., 2003), are still unknown. It is important to determine the different populations in order to understand the evolution of the clusters as well as for studying the individual classes of objects.

Many types of field cataclysmic variables (CVs) show outbursts, primarily in the optical domain, every few weeks to months. Observers have therefore tried to exploit the large variations in the optical lightcurves of outbursting cataclysmic variables as a means to detect them in GCs (e.g. Bond et al., 2005; Kaluzny et al., 2005). Only very few GC outbursts have been observed (e.g. Paresce & de Marchi, 1994; Shara et al., 1996, 1987). Even when Ciardullo et al. (1990) searched for outbursts in 54 of M31's GCs over two years, they found no evidence for an outburst. The lack of outbursts observed in GC CVs remains one of the most striking and unexplained differences between GC cataclysmic variables and field CVs. Several theories have been proposed to explain the paucity of GC CV outbursts. Firstly, X-ray observations have shown themselves to be much more efficient in detecting the expected populations of cataclysmic variables (Webb et al., 2005, 2004; Heinke et al., 2005), which have X-ray luminosities of $\sim 10^{30}$ - $10^{32.7}$ ergs s $^{-1}$ (extrapolating from Verbunt et al. (1997) into the XMM-Newton 0.2-12 keV band). Thus it has been suggested that the X-ray detected GC CVs may be mainly magnetic CVs (polars and intermediate polars) c.f. the 5 magnetic CVs in Grindlay (1999), which could explain the lack of cataclysmic variable outbursts detected in GCs. Magnetic CVs have high L_x/L_{opt} values due to magnetically chan-

nelled accretion onto the white dwarf, making them more easily detected in X-rays (Patterson, 1994) and polars do not show outbursts because their accretion discs are disrupted by their magnetic fields. Edmonds et al. (2003b) has tentatively suggested that GC CVs may have low accretion rates, as first suggested by Shara et al. (1996), implied by their faint optical luminosities, which could explain the scarcity of GC CV outbursts, where some low mass transfer rate systems, such as SU UMa systems, can have quite long recurrence times between outbursts. However, more recently, Dobrotka et al. (2005) proposed that the lack of outbursts may be due to a combination of low mass transfer rates ($\lesssim 10^{14-15} \text{ g s}^{-1}$) and moderately strong white dwarf magnetic moments ($\lesssim 10^{30} \text{ G cm}^3$) which could stabilise the CV discs in GCs and thus prevent most of them from experiencing frequent outbursts.

Here we discuss four of the eight globular clusters (ω Centauri (NGC 5139), M 22 (NGC 6656), M 13 (NGC 6205), NGC 6366, M 55 (NGC 6809), NGC 3201, NGC 2808 and NGC 4372) that we have observed with *XMM-Newton* in which we have identified the nature of some of the sources through X-ray observations and determine their membership to the clusters. We also present optical observations of sources detected in the direction of M 22, which have allowed us to confirm the nature of the X-ray identified sources and to identify other objects.

2. OBSERVATIONS AND DATA REDUCTION

2.1. X-ray data

We have between 20 and 40 ks of *XMM-Newton* EPIC (MOS and *pn*) data for each of the GCs. This paper will focus on the GCs ω Centauri, M 22, M 55 and NGC 3201. Observations were made between September 2000 and May 2003 in the full frame mode (Turner et al., 2001), with the medium filter. The data were reduced with different versions of the *XMM-Newton* SAS (Science Analysis Software), see Webb et al. (2005, 2004) and Gendre et al. (2003a) for further details.

The MOS data were reduced using the ‘emchain’ with ‘embadpixfind’ to detect the bad pixels. The event lists were filtered, so that 0-12 of the predefined patterns (single, double, triple, and quadruple pixel events) were retained and the periods of high background counts were then flagged in the event list. We used the energy range 0.2-10.0 keV. The *pn* data were reduced using the ‘epchain’ of the SAS. Again the event lists were filtered, so that 0-4 of the predefined patterns (single and double events) were retained, as these have the best energy calibration. Here we used the energy range 0.5-10.0 keV and again removed high background periods.

The source detection is described in Webb et al. (2005, 2004); Gendre et al. (2003a,b). Many of our detected sources are background sources. We have used the statistical Log N-Log S relationship of extragalactic sources

derived from the Lockman Hole (Hasinger et al., 2001) to estimate the background population. We converted the source count rates to fluxes using a power law model ($\Gamma=2$), as Hasinger et al. (2001). We calculated the average limiting flux in the core, half mass radius and the whole field of view (radius=15’) with which we could estimate the number of sources expected.

2.2. Optical data

We have optical photometry and spectroscopy of the X-ray sources in M 22, see Webb et al. (2004; in prep.). Schott glass U-, B- and V-filter photometry was taken with the Wide Field Imager (WFI) mosaic at the 3.9m *Anglo Australian Telescope* (AAT) on September 15-16 2001. The camera has a field of view (FOV) of $33' \times 33'$, similar to the *XMM-Newton* FOV. Each image was bias-subtracted and then flat-fielded with twilight sky flats, using the *IRAF* software (Tody, 1986, 1993). The long U-band observations were also dark subtracted, as the dark-current was non-negligible in these longer exposures. The data were astrometrically calibrated using the *IRAF* package *MSCRED* (Valdes, 1998) and the package *Wide Field Padova REDuction* (WFPRED) developed at the Padova Astronomical Observatory (Held et al. in prep.) and the standard star fields. A refinement to the astrometry was then made using the UCAC (USNO CCD Astrograph Catalog) (Zacharias et al., 2000), so that the positions are good to less than $0.1''$. The data for each filter were then stacked to create a deep image and the photometry was carried out using DAOPHOT/ALLSTAR (Stetson, 1987). The instrumental magnitudes were corrected using the standard stars observed on 2001 September 13. We find 123 220 stars detected in the U-band and at least one of the other two bands, where the maximum matching distance was 3 pixels ($< 1.5''$). The magnitudes range from approximately 14.0-22.8 in each filter. The photometric errors range from 0.01-0.1 magnitudes.

Spectroscopic observations were made in service mode with the Visible Multi-Object Spectrograph (VIMOS) on the 8.2 m Melipal telescope of the European Southern Observatory Very Large Telescope (VLT), with an aim to identify the X-ray sources in Webb et al. (2004). The observations were carried out on three nights, June 9 and 22 and July 9 2004. The blue grism has a range of 3700-6700Å and a resolution of 180 for a $1''$ slit, with a dispersion of 5.3 \AA/pixel . The red grism has a range of 5500-9500Å, a resolution of 210 for a $1''$ slit and a dispersion of 7.1 \AA/pixel . The seeing was typically below $0.8''$, except for the last night when it exceeded $1''$. Flat-field and He-Ar arc lamps and flux standard stars were also observed during the night to calibrate the spectra.

The data were reduced using the latest public version of the VIMOS pipeline recipes (V1.0). The data were bias subtracted, but the dark current was negligible, so no dark correction was carried out. Due to flexures of the instrument, the flat-field corrections also made no improvement to the data and were thus disregarded. The spectral ex-

traction was carried out using the two step method in the pipeline, using either an optimal extraction method (Horne, 1986) or manually if the pipeline was unable to automatically distinguish between multiple sources, due to their close proximity. The wavelength correction was carried out in the standard manner using the pipeline. Using the flux standards we corrected for the instrument response and flux calibrated the spectra. We have both red and blue spectra for 8 of the 14 possible optical counterparts and blue spectra only for 3 further counterparts and a red spectrum for another. Some sources are without spectra due to a misalignment of the mask during the observations. We also have spectra of approximately 500 other stars in the line of sight of the cluster.

3. RESULTS AND DISCUSSION

The formation mechanism of neutron star low mass X-ray binaries in GCs has now been constrained, as described in Sect. 1. This result has also allowed Pooley et al. (2003) to predict the expected number of neutron star low mass X-ray binaries in Galactic GCs, thought to be approximately one hundred. However determining the CV formation mechanism is more difficult as we do not yet have a complete population of CVs. CVs are fainter than neutron star low mass X-ray binaries and with minimal X-ray data they can be confused with active binaries or even millisecond pulsars. Further, it is believed that there are two populations of GC CVs, those formed dynamically (as the neutron star low mass X-ray binaries), thought to be located in the dense cluster cores and those that have evolved without undergoing an encounter, formed as primordial binary. This latter population should reside outside the cluster core (Davies, 1997), where the stellar density is much lower than in the core. Davies (1997) states that the more concentrated GCs, which have higher core densities, have higher encounter rates, thus increasing the number of CVs formed through encounters. In addition, the time-scales of encounters between primordial binaries and single stars are shortened, thus decreasing the number of primordial CVs. The GCs that we have observed with *XMM-Newton* are particularly well adapted to searching for a primordial binary population, as we have chosen low core density clusters, to ensure that we can resolve all the X-ray sources, given that the angular resolution of the EPIC cameras is approximately 6'' Full Width at Half Maximum of the Point Spread Function. In addition, *XMM-Newton*'s large collecting area ensures that we have enough photons for a full spectral study of about 20% of the sources detected, advantageous for identifying CVs using X-ray data alone. Several CVs have already been detected in the cores of GCs e.g. AKO 9 in the GC 47 Tuc (Aurière et al., 1989) which Knigge et al. (2003) state was almost certainly formed dynamically, either via tidal capture or in a three-body encounter. Other such dynamically formed CVs exist in other GCs e.g. in ω Cen (e.g. Carson et al., 2000; Gendre et al., 2003a), M 22 (e.g. Webb et al., 2004), and in 47 Tuc (e.g. Edmonds et al., 2003a,b).

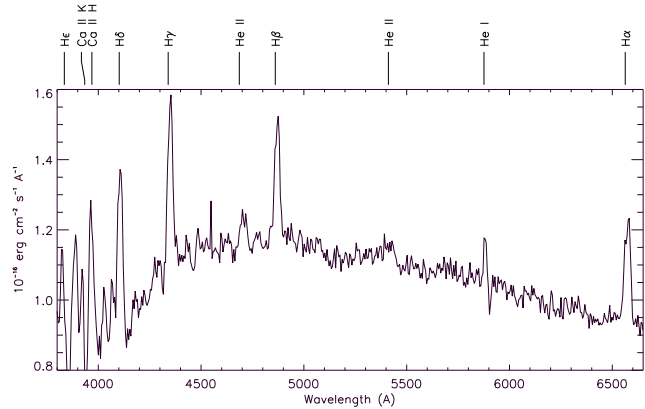


Figure 1. Spectrum of the optical counterpart to source 36. The Balmer lines are indicated as well as He I (5876Å) and He II (4686, 5411Å), which are all seen in emission. Also marked are the Ca H and K lines at 3968.49Å and 3933.68Å respectively.

We have found several X-ray sources in the GCs studied with *XMM-Newton* that lie outside of the half-mass radius and have X-ray luminosities, spectra/colours and lightcurves that infer that they may be CVs and may therefore be primordial. We find four such sources in the GC NGC 3201 (Webb et al., 2005). However, we also find possible millisecond pulsars (MSPs) in this region. Edmonds et al. (2003b) have shown that the distribution of millisecond pulsars and CVs is indistinguishable in the much more concentrated GC 47 Tuc, however all these sources fall within the half mass radius. As the possible CVs and MSPs in NGC 3201 appear to be similarly distributed outside of the half mass radius, we may be seeing evidence for disruption of NGC 3201. We have previously shown evidence for disruption of the GC ω Centauri. We found that many of the sources belonging to the cluster lie toward the exterior of the cluster. ω Cen is the most massive Galactic GC and an optical study by Pancino et al. (2000) showed that there are two stellar populations in this cluster, where we expect only one in a canonical GC. This could indicate that the cluster may have either been disrupted by the interaction with another body or that the cluster has accreted a stellar system during its past (see Gendre et al., 2003a, and references therein). NGC 3201 is also an unusual cluster as its orbit is retrograde with respect to the Galaxy and there is evidence for possible structure in the velocity field of the cluster stars (Côté et al., 1995). This could be due to several things including the stripping of stars of the cluster from prolonged interaction with the Galactic tidal field (see Webb et al., 2005, and references therein). This tidal interaction can disrupt the cluster, which could result in the perturbation of the mass segregation.

To confirm the nature of the sources found outside the half mass radius and to confirm their membership of the cluster, we require observations at longer wavelengths. We have thus managed to obtain time to take optical photometry of these clusters. Although we don't yet have these data, we do already have both optical photom-

Table 1. Equivalent widths and fluxes of CV1's principal spectral lines

Line	Eq. Width (Å)	Flux ($\times 10^{-16}$) ($\text{erg cm}^{-2} \text{s}^{-1} \text{Å}^{-1}$)
H α	-6.0	4.3
H β	-3.5	3.3
H γ	-3.7	3.9
H δ	-3.6	3.3
He I (5768Å)	-0.7	0.7
He II (4686Å)	-0.9	1.2
He II (5411Å)	-1.8	2.3

etry and spectroscopy of the X-ray sources in M 22. Our optical photometry has allowed us to identify the possible counterparts to eleven of the X-ray sources in M 22 (Webb et al., 2004). Using the good astrometry of these sources we were able to obtain the optical spectra described in Sect. 2.2 as well as a twelfth counterpart, identified by Anderson et al. (2003). The counterpart to this source was not detected in our AAT data as the core of the cluster was saturated. Anderson et al. (2003), using Hubble Space Telescope (HST) photometry, found a highly variable source, which showed H α emission and was coincident with the *Einstein/Rosat* source X4/B, which led them to conclude that this source is a cataclysmic variable and one of a very small number of confirmed or probable dwarf nova eruptions seen in globular clusters as well as being the first to be found in such a low-concentration cluster. Anderson et al. (2003) named this source CV1. Bond et al. (2005) confirmed the variable nature of CV1 using a four year light curve of this source, based on an analysis of accumulated data from the Microlensing Observations in Astrophysics (MOA) survey. From the regularity of the outbursts and their magnitude, Bond et al. (2005) also propose that this source is a CV.

CV1 is coincident with our *XMM-Newton* source 36 in Webb et al. (2004), where the *Einstein/Rosat* source X4/B has been resolved into two sources using the *XMM-Newton* data. We have extracted the optical spectrum of CV1 as described in Section 2.2, using the manual extraction as the source falls very close to its brighter neighbour. We estimate that the brighter neighbour in the optical data contributes approximately 5% to the spectrum of the optical counterpart of source 36. The neighbouring star's spectrum contains no emission lines and appears to be a mid K-type star. Our optical spectrum of CV1 (see Fig. 1) is typical of a cataclysmic variable, in support of the Anderson et al. (2003)/ Bond et al. (2005) identification. The spectrum shows Balmer line emission as well as some helium lines in emission, indicative of accretion. We give the equivalent widths and fluxes of the principal lines (Å) in Table 1. The Balmer lines show some evidence of a double peak that evolves with time, further support for an accretion disc. We have identified the Ca II H and K absorption lines at 3968.5 and 3933.7 Å which we assume are due to the late type secondary star.

Our observations were made with an aim to identify the

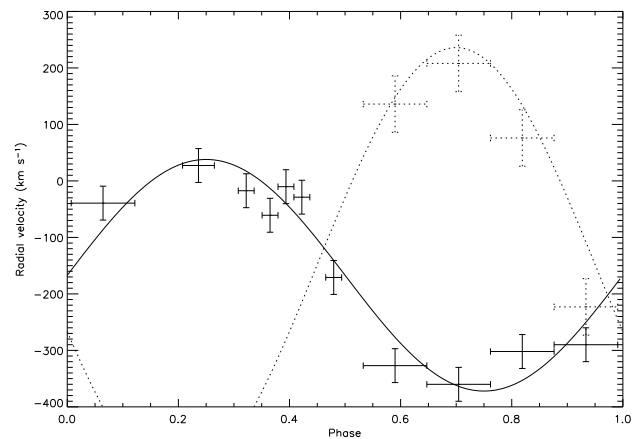


Figure 2. Radial velocities and errors of the disc H α lines (indicated by the solid crosses) and the best fit to these data folded on the ephemeris derived above (also solid line) and the radial velocities and errors of the calcium lines (dotted lines) and the best fit to these points.

X-ray sources through their optical counterparts. The observations made of the red and the blue end were split into four shorter observations (seven for the red end observations made on the 9th June) so as to not to saturate the brightest counterparts. We have taken advantage of the fact that the individual optical spectra of CV1 contain enough counts to carry out a radial velocity analysis. Initially we fitted a Gaussian line to the cleanest calcium line (the H-line), which we assume comes from the secondary star and measured the absolute velocity shifts. We also added all of the blue spectra together to create a template spectrum and cross-correlated the region between 3900 and 4000Å (containing the two calcium lines) with the same region in the four blue spectra, using the *IRAF* task *fxcor*. We find very similar results. As we have no means of measuring the radial velocity of the white dwarf, we cross correlated the H α line, because it is apparent in both the red and the blue spectra (6500-6600Å) with the template, even though it is unlikely that this line is emitted from the region closest to the white dwarf. The radial velocities obtained for the disc lines were plotted against time. This plot spans the 13 days between the red and the blue observations. We fitted the points assuming that CV1 is in a circular orbit and that it has the same velocity as the globular cluster M 22, $-148 \pm 0.8 \text{ km s}^{-1}$ (Peterson & Cudworth, 1994), where the escape velocity is 24.2 km s^{-1} . We found a period of 0.069866 ± 0.000012 days (~ 1.7 hours). Folding the data on this period we obtain the radial velocity curve given in Figure 2. The ephemeris is thus $\phi^{orb} = \text{MJD } 53166.1650(8) + 0.069866(12)\text{E}$, where $\phi^{orb} = 0$ indicates inferior conjunction of the white dwarf and the figures in brackets indicate the errors on the last decimal places. These errors are the formal 3σ errors to the fit. However, the true errors may be larger as the absolute wavelength calibration of the spectra is poor, although the calibration of consecutively taken spectra is reliable (errors of the order $\pm 1\text{Å}$). We have checked both the abso-

lute and relative calibration of the spectra using the spectra from other objects. We find shifts of $0 \pm 20 \text{ km s}^{-1}$ for consecutive spectra of stationary objects. However, it is for this reason we do not use the radial velocities to constrain the mass of the two stars. It is none the less encouraging that the radial velocities of the calcium lines, when folded on the above period are in almost anti-phase with the disc radial velocity, as one would expect if they are from the secondary.

Our X-ray spectrum of source 36 does not necessarily support the CV hypothesis. One would expect a high temperature bremsstrahlung model Richman (1996) or a single optically thin plasma model (i.e. the MEKAL model in XSPEC Baskill et al., 2005) to fit the X-ray spectrum. The X-ray spectrum to source 36 is best fitted using a power law plus a Gaussian absorption line, believed to be due to cyclotron resonance, as is found in several neutron star X-ray spectra (Webb et al., 2004). CV1, located at R.A.= $18^{\text{h}}36^{\text{m}}24^{\text{s}}74$ and dec.= $23^{\circ}54'35''8$ does indeed fall within the X-ray positional error circle of $5''$ (90% confidence). However, we have found a second serendipitous source in the slit placed on this proposed counterpart that shows $\text{H}\alpha$ emission. This source may be the optical counterpart to the X-ray source as it also falls within the X-ray positional error circle but on the other side of the X-ray source to CV1, at R.A.= $18^{\text{h}}36^{\text{m}}24^{\text{s}}75$ and dec.= $23^{\circ}54'43''03$. The two optical sources are separated by $7.2''$. It is possible that the latter is the optical counterpart to the X-ray source and is thus a neutron star. Alternatively the X-ray source that we detect is not a single source but two (or more) unresolved sources. Planned follow-up X-ray observations with the X-ray satellite Chandra, which has an angular resolution of $< 1''$ are necessary to determine whether the XMM-Newton X-ray source is indeed multiple X-ray sources or failing that, to improve the positional error, necessary to determine which of the two sources is the optical counterpart to the X-ray source.

Returning to the nature of CV1, it appears clear that it is indeed a CV. The presence of fairly strong (compared with the other emission lines) He II lines in emission, in particular the He II 4686Å line, see Table 1, could indicate that this CV is magnetic in nature, where the presence of strong He II emission lines usually indicates either a magnetic white dwarf or a nova-like system with a high level of mass transfer (Szkody et al., 2005). If the period determined is confirmed, this would rule out the nova-like possibility, as these objects have periods $\gtrsim 3$ hours. If CV1 is magnetic and as it has already been shown to undergo outbursts, it would seem likely that it is an intermediate polar (IP). IPs (which are thought to have lower magnetic fields than the polars) can undergo outbursts as an accretion disc can be present in the system. The magnetic field is powerful enough in these systems to influence the flow of the gas and disrupt the inner disc. If our derived period is confirmed, this would make it a very short period IP, in fact one of the shortest known, see Ritter & Kolb (2005). Further, many other CVs with periods $\lesssim 2$ hours have low mass transfer rates (Ritter & Kolb, 2005). This could support the mechanism proposed

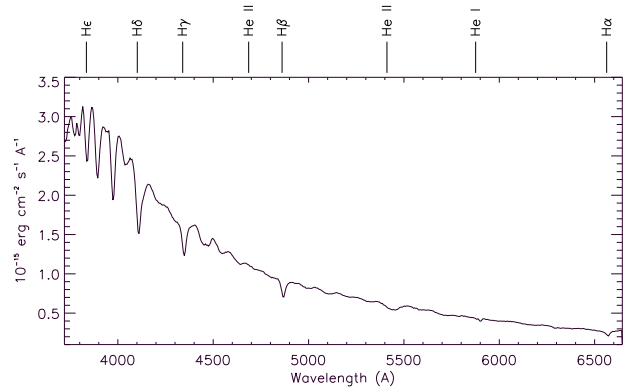


Figure 3. Spectrum of the optical counterpart to the X-ray source 20 (Webb et al., 2004).

by Dobrotka et al. (2005) to explain why GC CVs show so few outbursts is because they are *both* magnetic and have low mass transfer rates.

We have also started to identify other X-ray sources in M 22 through their optical counterparts. Fig. 3 shows the spectrum of the proposed optical counterpart to the X-ray source 20 (Webb et al., 2004). The photometric observations showed that this source falls in the blue-straggler region of the colour magnitude diagram and the spectroscopic observations support this (e.g. Shetrone & Sandquist, 2000). Blue stragglers appear brighter and bluer than the main-sequence turnoff and they are thought to be formed through stellar collisions or binary mass transfer and mergers. However, blue stragglers do not usually emit in the X-ray domain, although they are often binary systems (e.g. Kaluzny et al., 2004), where the other star in the binary could be the source of X-ray emission. We have searched for radial velocity variations in the same way as for CV1 and we find no evidence for binarity in these observations. This makes it unclear whether this is indeed the optical counterpart to our X-ray source 20.

Several of the other spectra may indicate that some of our X-ray sources are double degenerates. However, due to the faintness of these systems and the overcrowding in the optical, the spectra are contaminated by neighbouring star spectra. We are currently deconvolving these spectra and the results will be presented in Webb et al. (in prep.) along with the results of other spectral identifications of the M 22 X-ray sources and a number of serendipitously detected subdwarf stars.

Acknowledgements

I take this opportunity to thank my collaborators who worked with me on the papers presented here, without whom much of this work would not have been possible.

REFERENCES

- Anderson, J., Cool, A. M., & King, I. R. 2003, *ApJ*, 597, L137
- Aurière, M., Koch-Miramond, L., & Ortolani, S. 1989, *A&A*, 214, 113
- Baskill, D. S., Wheatley, P. J., & Osborne, J. P. 2005, *MNRAS*, 357, 626
- Bond, I. A., Abe, F., Eguchi, S., et al. 2005, *ApJ*, 620, L103
- Camilo, F., Lorimer, D. R., Freire, P., Lyne, A. G., & Manchester, R. N. 2000, *ApJ*, 535, 975
- Carson, J. E., Cool, A. M., & Grindlay, J. E. 2000, *ApJ*, 532, 461
- Ciardullo, R., Tamblyn, P., & Phillips, A. C. 1990, *PASP*, 102, 1113
- Côté, P., Welch, D. L., Fischer, P., & Gebhardt, K. 1995, *ApJ*, 454, 788
- Davies, M. B. 1997, *MNRAS*, 288, 117
- Di Stefano, R., & Rappaport, S. 1994, *ApJ*, 423, 274
- Dobrotka, A., Lasota, J.-P., & Menou, K. 2005, *ArXiv Astrophysics e-prints*
- Edmonds, P. D., Gilliland, R. L., Heinke, C. O., & Grindlay, J. E. 2003a, *ApJ*, 596, 1177
- . 2003b, *ApJ*, 596, 1197
- Gendre, B., Didier, B., & Webb, N. A. 2003a, *A&A*, 400, 521
- . 2003b, *A&A*, 403, L11
- Grindlay, J. E. 1999, in *ASP Conf. Ser. 157: Annapolis Workshop on Magnetic Cataclysmic Variables*, 377–+
- Grindlay, J. E., Heinke, C., Edmonds, P. D., & Murray, S. S. 2001, *Science*, 292, 2290
- Hasinger, G., Altieri, B., Arnaud, M., et al. 2001, *A&A*, 366, L45
- Heinke, C. O., Grindlay, J. E., Edmonds, P. D., et al. 2005, *ApJ*, 625, 796
- Heinke, C. O., Grindlay, J. E., Lugger, P. M., Cohn, H. N., Edmonds, P. D., Lloyd, D. A., & Cool, A. M. 2003, *ApJ*, 598, 501
- Hertz, P., & Grindlay, J. E. 1983, *ApJ*, 275, 105
- Horne, K. 1986, *PASP*, 98, 609
- Hut, P., McMillan, S., Goodman, J., et al. 1992, *PASP*, 104, 981
- Kaluzny, J., Kubiak, M., Szymanski, M., Udalski, A., Lrzeminski, W., & Mateo, M. 1996, *A&AS*, 120, 139
- Kaluzny, J., Olech, A., Thompson, I. B., Pych, W., Krzemiński, W., & Schwarzenberg-Czerny, A. 2004, *A&A*, 424, 1101
- Kaluzny, J., Pietrukowicz, P., Thompson, I. B., et al. 2005, *MNRAS*, 359, 677
- Knigge, C., Zurek, D. R., Shara, M. M., Long, K. S., & Gilliland, R. L. 2003, *ApJ*, 599, 1320
- Pancino, E., Ferraro, F. R., Bellazzini, M., Piotto, G., & Zoccali, M. 2000, *ApJ*, 534, L83
- Paresce, F., & de Marchi, G. 1994, *ApJ*, 427, L33
- Patterson, J. 1994, *PASP*, 106, 209
- Peterson, R. C., & Cudworth, K. M. 1994, *ApJ*, 420, 612
- Pooley, D., Lewin, W. H. G., Anderson, S. F., et al. 2003, *ApJ*, 591, L131
- Richman, H. R. 1996, *ApJ*, 462, 404
- Ritter, H., & Kolb, U. 2005, *VizieR Online Data Catalog*, 5113, 0
- Rutledge, R. E., Bildsten, L., Brown, E. F., Pavlov, G. G., & Zavlin, V. E. 2002, *ApJ*, 578, 405
- Shara, M. M., Bergeron, L. E., Gilliland, R. L., Saha, A., & Petro, L. 1996, *ApJ*, 471, 804
- Shara, M. M., Potter, M., & Moffat, A. F. J. 1987, *AJ*, 94, 357
- Shetrone, M. D., & Sandquist, E. L. 2000, *AJ*, 120, 1913
- Stetson, P. B. 1987, *PASP*, 99, 191
- Szkody, P., Henden, A., Fraser, O. J., et al. 2005, *AJ*, 129, 2386
- Tody, D. 1986, in *Instrumentation in astronomy VI: Proceedings of the Meeting, Tucson, AZ, Mar. 4–8, 1986. Part 2. Bellingham, WA, Society of Photo-Optical Instrumentation Engineers*, 733–+
- Tody, D. 1993, in *ASP Conf. Ser. 52: Astronomical Data Analysis Software and Systems II*, 173–+
- Turner, M. J. L., Abbey, A., Arnaud, M., et al. 2001, *A&A*, 365, L27
- Valdes, F. G. 1998, in *ASP Conf. Ser. 145: Astronomical Data Analysis Software and Systems VII*, 53–+
- Verbunt, F., Bunk, W. H., Ritter, H., & Pfeffermann, E. 1997, *A&A*, 327, 602
- Webb, N. A., Serre, D., Gendre, B., Barret, D., Lasota, J.-P., & Rizzi, L. 2004, *A&A*, 424, 133
- Webb, N. A., Wheatley, P. J., & Barret, D. 2005, *A&A*, 444, in press
- Zacharias, N., Urban, S. E., Zacharias, M. I., et al. 2000, *AJ*, 120, 2131

RESOLVING COMPONENTS OF THE MIRA AB INTERACTING BINARY SYSTEM

M. Karovska

Harvard-Smithsonian Center for Astrophysics, Cambridge, MA02138, USA

ABSTRACT

Mira AB is the the nearest symbiotic binary and the only interacting binary that has been resolved from X-ray to radio wavelengths. In this paper I describe results from multiwavelength observations of Mira AB carried over the past 20 years. These include recent Chandra observations that resolved this interacting system for the first time at X-ray wavelengths. A Chandra spectrum of Mira AB and follow-up HST and ground-based observations showed evidence for an unprecedented outburst from Mira A likely associated with magnetic flare followed by a mass ejection or jet-like activity. Chandra and HST images also detect a bridge between the components, showing that Mira B is also accreting *via* direct mass exchange. These results have major impact on our understanding of accretion processes in other currently unresolved “wind” interacting systems.

Key words: X-rays; binaries; symbiotic.

1. INTRODUCTION

Mira AB is one of the very few interacting binaries that has been resolved at wavelengths ranging from X-rays to radio (Karovska *et al.* 1991, Karovska *et al.* 1997, Karovska *et al.* 2005; Matthews & Karovska 2005). Mira AB is the nearest symbiotic system consisting of an evolved Asymptotic Giant Branch (AGB) star, Mira A, and an accreting compact object, likely a white dwarf, Mira B. Symbiotic systems are a very important class of interacting binaries since they are likely progenitors of Planetary Nebulae (PNs). In addition, they have been invoked as possible progenitors of SN type Ia, key distance indicators in the Universe (e.g., Munari & Renzini 1992; Corradi *et al.* 2000). In these systems, believed to be detached for most of their long orbital periods, the interaction between components is assumed to be via wind accretion. The cool component, a giant or a Mira-type star, loses its mass *via* a powerful wind; A fraction of the wind mass (\sim few %) is accreted by the compact hot accretor, often a white dwarf (e.g., Whitelock 1987; Livio 1988).

As in many other wind accreting systems, the accretion processes in symbiotics are currently not very well understood, and the theoretical models are limited by lack of knowledge of important input parameters such as wind mass and velocity, characteristics of the individual components (including radius and mass), orbital velocity and characteristics of the flow. These parameters can be accurately measured only when the system can be resolved and the components studied individually. Even in the case of the nearby symbiotic systems such as R Aqr and CH Cyg, neither the central region in the proximity of the binary, nor the binary itself have been resolved.

Mira AB is the only symbiotic systems that has been resolved so far. There are two reasons for this: first, the binary is nearby (\sim 130 pc, Perryman *et al.* 1997); second, the components are separated by at least 70AU. This angular separation is significantly greater than in other unresolved symbiotics (the nearest symbiotic systems are at a distance beyond \sim 250 pc) in which the components seem to be much closer than in Mira AB. Thus, Mira AB is an easier target for imaging with current high-angular resolution ground- and space-based telescopes.

Therefore, the Mira AB system provides a unique laboratory to study the individual components of an interacting binary, as well as accretion processes in detached systems with extended atmosphere donors.

In the following we highlight results from multiwavelength observations of Mira AB, and also present results from our recent Chandra observations that resolved the system for the first time at X-ray wavelengths.

2. RESOLVING MIRA AB

2.1. UV and Optical Observations

Mira AB was discovered by A.H. Joy in 1923 (Aitken 1923) at optical wavelengths. However, it took another 60 years before the components of the system were clearly separated for the first time using speckle interferometry observations in 1983 (Karovska *et al.* 1991). The “speckle” images obtained in the optical detected for the



Figure 1. 1995 HST observations of Mira AB resolved the components of this 0.6'' binary at optical and UV wavelengths (Karovska *et al.* 1997). North is up and East to the left.

first time an asymmetry in Mira A, the prototype of Mira-type variables.

Since 1983, observations of the system from X-ray to radio have provided unprecedented information about the characteristics of the components, Mira A and Mira B, and of the system as a whole. Specifically, they reveal a complex interacting system with tremendous changes in the components and the circumbinary environment.

For example, HST observations of Mira AB clearly resolved the components of the system at UV and optical wavelengths, and separated for the first time their spectra (Karovska *et al.* 1997). The HST images of Mira A (Fig. 1) confirmed the asymmetry in its extended atmosphere detected in the “speckle” images. Furthermore, the first UV image of Mira A showed a hook-like feature stretching toward Mira B, indicating possible mass flow toward the companion - an unexpected result given the large separation between the components (Karovska *et al.* 1997), see Fig.2.

Spectral observations carried out with the IUE in the early nineties, and HST observations carried out in 1995 and 1999, show tremendous changes in the UV luminosity of Mira AB (Fig. 3). Over an order of magnitude change in brightness was detected in the continuum and the line emission between 1999 and 1991. Furthermore, modeling of the Mg h&k line emission showed a decrease of Mira B mass loss of at least 2 magnitudes between 1991 and 1999, and a drop of the wind velocity by a factor of ~ 2 (Fig. 4). The 1999 HST observations and the followup FUSE observations in 2001 detected a forest of Ly α -fluoresced H₂ emission lines at wavelengths below 1600 Å which dominated the spectra, despite not being seen at all in the 1995 HST observations or by IUE (Wood, Karovska, & Hack 2001; Wood, Karovska, & Raymond, 2002, Wood and Karovska 2004)). These dramatic changes indicate that Mira B may have been approaching a low state in the late nineties, and/or that the accretion characteristics in the system have changed in a very significant way.

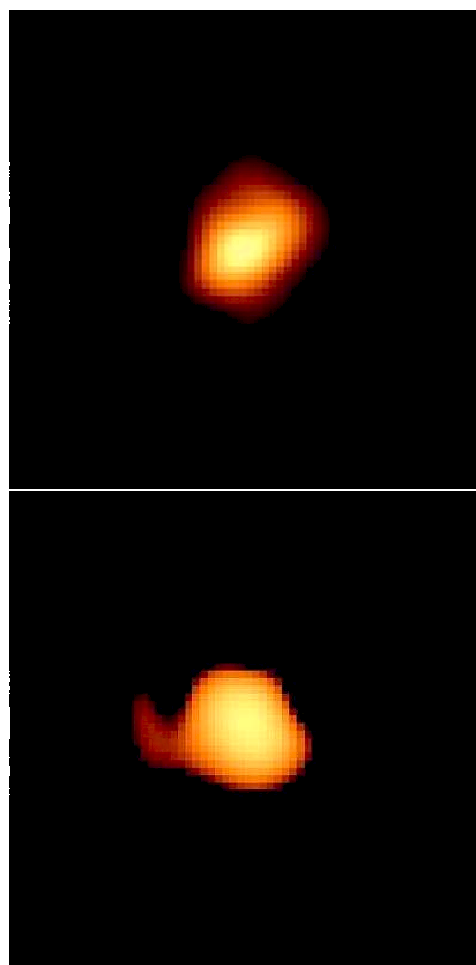


Figure 2. Deconvolved images of Mira A from the 1995 HST observations: (top panel) an optical image of Mira A showing a strong asymmetry in its envelope; (bottom panel) a UV image of Mira A showing an extension toward Mira B - an indication of a possible mass flow between the components (Karovska *et al.* 1997)

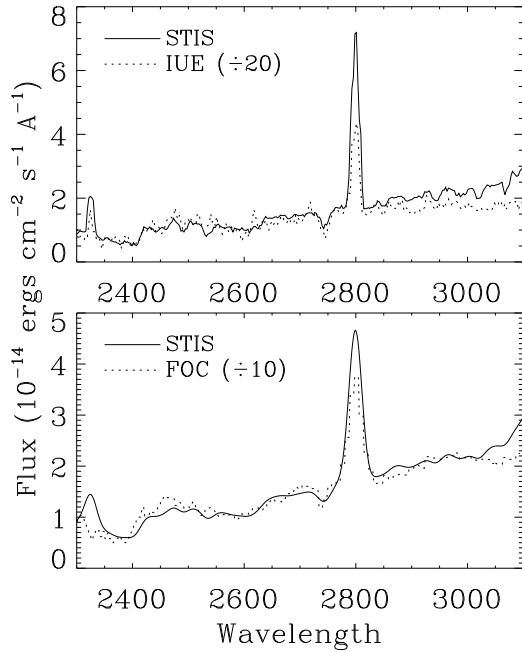


Figure 3. Comparison of the HST/STIS near-UV spectrum of Mira B with previous observations from IUE (top panel) and HST/FOC (bottom panel). In both panels, the STIS spectrum is rebinned and deresolved to match the resolution of the other observation. The peaks at 2325 Å and 2800 Å are C II] and Mg II lines, respectively. Note that the IUE and FOC fluxes had to be reduced by factors of 20 and 10, respectively, to match the STIS data (Wood *et al.* 2001).

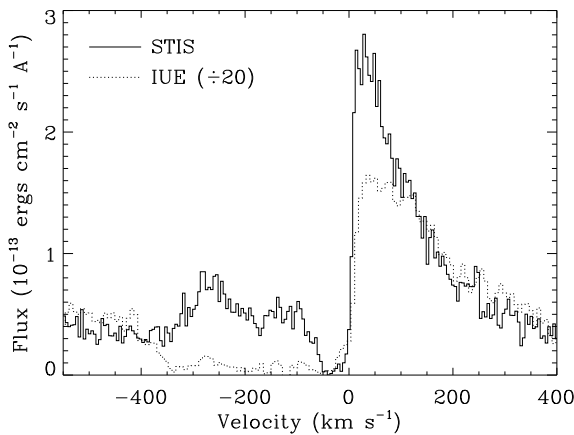


Figure 4. Comparison of the Mg II k line profile observed by HST/STIS (solid line) and one observed by IUE (dotted line), shown on a velocity scale centered on the rest frame of the star. The IUE fluxes are reduced by 20 to roughly match the STIS fluxes. Note the larger wind opacity between 0 and -400 km s^{-1} in the IUE spectrum (Wood, Karovska, & Hack 2001).

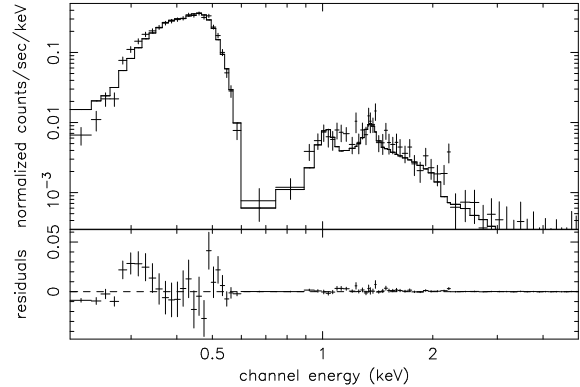


Figure 5. Chandra ACIS-S spectrum of Mira AB (plus signs) fit with a combination of Gaussians for the soft spectral component and a bremsstrahlung plus Gaussians for the hard component. Residuals fall mostly near the C edge at 0.3 keV where the response matrix is known to have errors (Karovska *et al.* 2005).

2.2. X-ray Observations

In 1993, a ROSAT observation resulted in the first unambiguous detection of X-ray emission from Mira AB (Karovska *et al.* 1996). This observation resolved the contradicting results from the analysis of the EINSTEIN observation; Jura & Helfand (1984) marginally detected an X-ray source, while Maggio *et al.* (1990) set an upper limit of $f_x < 1.4 \times 10^{-13}$ erg s^{-1} cm^{-2} . The ROSAT X-ray luminosity of the Mira AB system was estimated $\sim 10^{29}$ erg s^{-1} (Karovska *et al.* 1996) which is similar to the luminosity estimated from the XMM observations carried out about ten years later (Kastner & Soker 2004).

On 2003 December 6 we carried out a 70 Ksec pointed Chandra observation of Mira AB using the ACIS-S instrument (*vis* Karovska *et al.* 2005). We detected several thousand counts below 1 keV (see Fig. 5), associated with a new bright soft source in the system, which was not seen a few months before by XMM (Kastner & Soker, 2004), or by ROSAT in 1993 (Karovska *et al.* 1996).

The high-energy component (> 1 keV) is similar in appearance to the quiescent XMM and ROSAT spectra. However, a detailed comparison shows that a clear evolution has occurred in this portion of the spectrum (~ 1.2 – 1.8 keV) as well. Figure 6 shows the Chandra spectrum and the best spectral fit to the XMM data obtained on 2004 July 23 (Kastner & Soker, 2004).

The best-fit spectrum is most easily explained as blended emission of C + N lines. We fit the low-energy portion of the Chandra spectrum using an absorbed model spectrum consisting of a sum of Gaussians, each with a fixed center and zero width to represent an unresolved line. The best fit was obtained with lines at C VI 0.367 keV, N VI 0.426 keV, C VI 0.459 keV, and N VII 0.500 keV (line normalizations = 4.9, 6.2, 50.8, and 33.1, respectively, in units of 10^{-5} photons cm^{-2} s^{-1}). Fitting with a continuum component in the model resulted in a normalization

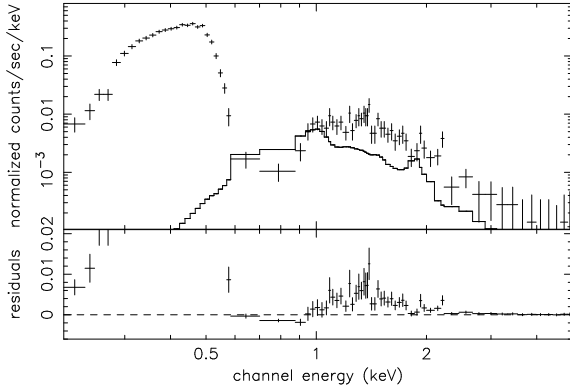


Figure 6. *Chandra ACIS-S spectrum of Mira AB (plus signs). Histogram shows the best fit XMM spectrum (Kastner & Soker 2004). Note the flux below 1 keV associated with the outburst, and the increased flux above ~ 1 keV*

consistent with zero.

The hard component was best-fit with a bremsstrahlung continuum of $kT \sim 0.78$ keV to mimic an optically thin thermal plasma, plus two zero-width gaussians representing emission lines at ~ 1 and ~ 1.35 keV, all absorbed by a column $N_{\text{H}} \sim 9.0 \times 10^{22} \text{ cm}^{-2}$. The gaussians have equivalent widths of ~ 240 and ~ 120 eV, respectively. We attribute these emission to Ne and Mg lines. The total X-ray luminosity of the Mira AB system was estimated $\sim 2 \times 10^{30} \text{ erg s}^{-1}$, and has increased by ~ 5 times since the XMM observations few months before.

A major further insight into the origin of the observed outburst came from the Chandra images. Given the Chandra high-angular resolution capabilities, and the fact that the data include information about the photon energies and positions, we were able to obtain images of each component by filtering according to the information derived from the spectrum. We obtained a “soft” image from 0.3 to 0.7 keV, and “hard” image from 0.7-2 keV. Figure 7 shows a comparison between the ACIS image of the system (0.3-2 keV) and the filtered images showing two separate components shifted by $\sim 0.5''$; The “hard” image is shifted to the East of the “soft” image.

We further explored the spatial extent of the X-ray sources using PSF models and a new multiscale deconvolution technique *EMC2* (Esch *et al.* 2004). This technique was specifically developed for low-count statistics data, and it provides error estimates in addition to the reconstructed images. This enabled us to search for additional sources of X-rays in the system at a resolution $0.1''$ (less than the $\sim 0.5''$ ACIS-S pixel size).

The deconvolved image (Fig. 8) shows two sources separated by $\sim 0.6''$. This is the first image of an interacting binary that has been spatially resolved at X-ray wavelengths. The location of the brighter source in the deconvolved image corresponds to the centroid position of the soft source as determined using filtered images.

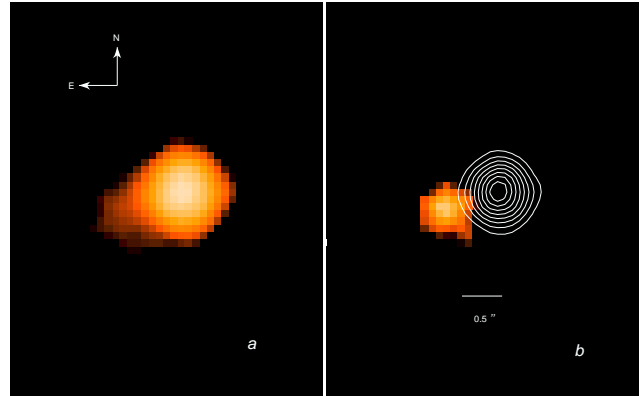


Figure 7. *Chandra images of Mira AB: (a) ACIS-S raw image of Mira AB filtered from 0.3 to 2 keV. Mira A is toward the West (see Fig. 10); (b) contours of the ACIS-S soft image (0.3-0.7 keV) (toward the West) overlaid on the image of the hard image (0.7-2 keV) (toward the East) (Karovska *et al.* 2005).*

We compared the X-ray images with the HST images of the Mira AB components (Fig. 9) obtained two months later in the near-UV (3729 \AA filter). The overlay of the HST and Chandra images obtained by shifting the HST image to match the X-ray components of the binary is shown in Fig. 10. The Chandra image of the soft X-ray source is in the vicinity of the 3729 \AA image of Mira A and therefore likely associated with the AGB star rather than with the accreting companion Mira B. Before these observations, it was assumed that all the X-rays came from the accretion disk surrounding the white dwarf, so the detection of an X-ray outburst from the giant star came as a surprise.

The soft X-ray outburst in Mira A could be caused by a magnetic flare followed by a large mass ejection. This outburst is possibly associated with jet-like activity, as evidenced by ground-based $H\alpha$ spectroscopy, and the changes in the Mgh&k lines in the 2004 HST spectra (Karovska *et al.* 2005). Furthermore, both HST and Chandra images show extended structures toward the North-West that could be associated with ejected material (e.g. Karovska *et al.* 2005; Karovska *et al.* 2006, in preparation).

In the case of mass ejection we could expect changes in the Spectral Energy Distribution (SED) of both components on a time scale of years. For example, we would expect increased dust formation in the system in the years following the outburst. Furthermore, assuming that the flow is propagating toward Mira B with speed of few hundred km/s, we would expect a dramatic response of the accretion disk on a time scale of few years.

The Chandra image also shows a faint “bridge-like” feature extending between the components. Similar structure can be seen in the HST image. This is consistent with the 1995 HST observations of Mira AB which showed extension from Mira A toward Mira B indicating possible

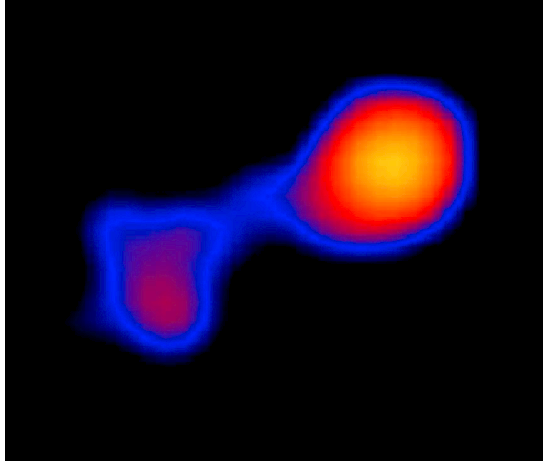


Figure 8. Chandra deconvolved image of Mira B (left) and Mira A (right), separated by $\sim 0.6''$, showing a bridge between the components. The Mira A image shows an elongation to the NW possibly associated with the outburst

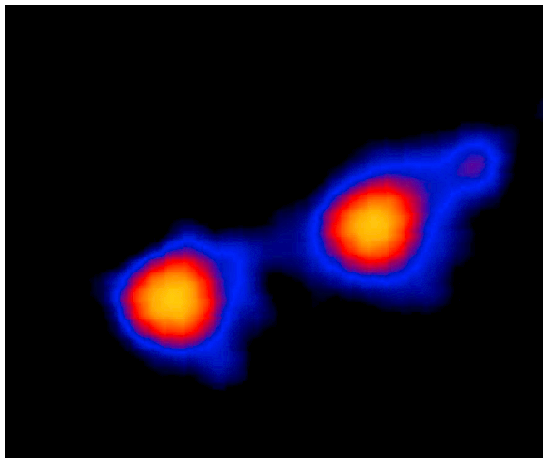


Figure 9. HST image of Mira AB obtained in February 2004 in the near-UV showing a possible extension in Mira A and a faint “bridge” between the components.

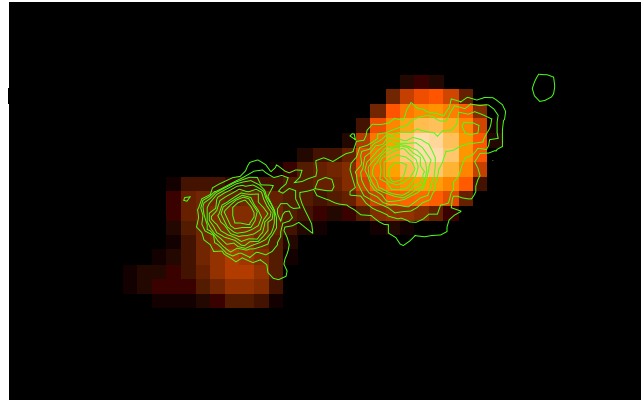


Figure 10. Chandra image of Mira B (left) and Mira A (right), separated by $\sim 0.6''$, with overlaid contours of the HST 3729 Å image of the system. North is up, East is to the left (Karovska *et al.* 2005).

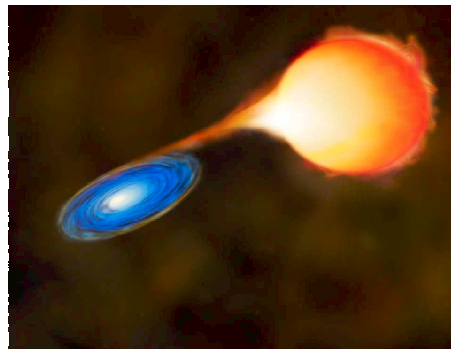


Figure 11. The mass exchange between the components of Mira AB: in addition to wind accretion there is evidence for Roche-lobe like overflow (CXC PRC 05-06 2005).

mass flow between the cool giant and the hot companion (Karovska *et al.* 1997; STScI-PRC1997-26). This was also an unexpected result, because the components are separated by at least ~ 70 AU, and it has been assumed in the past that the interaction between the components in such systems can be carried out *only via* wind accretion. The observations show that in addition to wind accretion this system interacts *via* direct mass exchange between the components as well (Fig. 11).

These results further challenge our understanding of accretion processes in detached systems and have important implications for understanding of accretion processes in other wind accreting systems in the Universe. This is very important since the flow of material from one component into the potential well of the other is a key in determining the future evolutionary histories of each component and the system itself, and particularly the production of degenerate companions and supernovae.

The key to further advances in accretion studies is resolving and directly imaging a wide range of interacting binaries, and studying their components and mass flows.

Increasing the resolution to *sub-milliarcsecond* level in the UV and X-rays will revolutionize the observational astrophysics of the 21st century and provide unprecedented opportunities for studies of many interacting binaries (Karovska *et al.* 2006).

For now it is very important to continue multi-wavelength studies of Mira AB and its dramatic transformations. Further monitoring of Mira AB at X-ray wavelengths is critical for understanding the accretion processes and the impact of the outburst on the surrounding circumstellar and circumbinary material and on the accreting companion and on the stability of the accretion disk.

ACKNOWLEDGMENTS

We are grateful to several colleagues that have participated in the long-term multi-wavelength study of Mira AB including Drs. E. Schlegel, B. Wood, J. Raymond, M. Marengo, W. Hack, E. Guinan, J. Mattei, L. Matthews, P. Nisenson, C. Papaliolios, R. Stefanik, and the AAVSO. This work was supported by NASA grants GO-5024A and GO-10091. MK is a member of the Chandra X-ray Center, which is operated by the Smithsonian Astrophysical Observatory under contract to NASA NAS8-39073.

REFERENCES

- Aitken, R. G. 1923, PASP, 35, 323.
- Corradi, R. L. M., Livio, M., Schwarz, H. E., & Munari, U. 2000, in *Asymmetrical Planetary Nebulae II: From Origins to Microstructures*, ASP Conference Series, Vol. 199, ed. J. H. Kastner, N. Soker, & S. Rappaport (ASP: San Francisco), 199
- Esch, D.N., Connors, A., Karovska, M., & van Dyk, D.A., 2004, ApJ, 610, 1213.
- Jura, M., & Helfand, D.J, 1984, ApJ, 287, 785.
- Karovska, M. 2006, in proceedings from conference “Close Binaries in the 21st century”, in press.
- Karovska, M., Nisenson, P., Papaliolios, C., & Boyle, R. 1991, ApJ, 374, L51.
- Karovska, M., Raymond, J., & Guinan, E. 1996, SAO Tech Report, Cambridge, SAO.
- Karovska, M., Hack, W., Raymond, J., & Guinan, E. 1997, ApJ, 482, L175.
- Karovska, M, Schlegel, E., Warren, H., Raymond, J., and Wood, B.E., 2005, ApJ, 623, L137.
- Karovska, M. *et al.* 2006, in prep.
- Kastner, J. H. & Soker, N. 2004, ApJ, 616, 1188.
- Livio, M. 1988, in *Symbiotic Phenomena*, Proceedings of IAU Coll. No. 103.
- Maggio, A. *et al.* 1990, ApJ, 348, 253.
- Matthews, L., & Karovska, M. 2005, submitted to ApJ.
- Munari, U. & Renzini, A. 1992, ApJ, 397, L87
- Perryman, M. A. C. *et al.* 1997, A&A, 323, L49
- Whitelock, P. A. 1987, PASP, 99, 573
- Wood, B. E., Karovska, M., & Hack, W. 2001, ApJ, 556, L51.
- Wood, B. E., Karovska, M., & Raymond, J., W. 2002, apj, 575, 1057.
- Wood, B.E., and Karovska, M. 2004, ApJ, 601, 502

ULTRALUMINOUS X-RAY SOURCES IN NEARBY GALAXIES: CLUES ON THEIR NATURE FROM X-RAY TIMING AND NEW OPTICAL DATA

L. Zampieri¹, P. Mucciarelli¹, R. Falomo¹, P. Casella², T. Belloni², R. Turolla³, A. Treves⁴, and P. Ranalli⁵

¹INAF-Osservatorio Astronomico di Padova, I-35122 Padova, Italy

²INAF-Osservatorio Astronomico di Brera, I-23807 Merate (LC), Italy

³Dipartimento di Fisica, Università di Padova, I-35131 Padova, Italy

⁴Dipartimento di Fisica e Matematica, Università dell'Insubria, I-22100 Como, Italy

⁵RIKEN Cosmic Ray Laboratory, 351-0106, Japan

ABSTRACT

We present results from new optical and X-ray data of two selected ULXs. A recent VLT observation of NGC 1313 X-2 shows that it is a high mass X-ray binary with a very massive donor, while a new *XMM* plus archival *XMM/RXTE* data of M 82 X-1 represent the most revealing timing data for a ULX to date.

Key words: galaxies: individual: M82, NGC 1313; X-rays: individual: M82 X-1, NGC 1313 X-2.

1. INTRODUCTION

First revealed by *Einstein*, the population of ultraluminous X-ray sources (ULXs) has increasingly grown up in the last decade mainly thanks to the observations of *ROSAT* (e.g. Colbert & Ptak 2002), *XMM-Newton* (e.g. Foschini et al. 2002a) and *Chandra* (e.g. Liu & Bregman 2005; Swartz et al. 2004). About 150 ULXs are included in the recent *Chandra* catalogue of Swartz et al. (2004). These point-like sources have X-ray luminosities $L_X \geq 10^{39}$ erg s⁻¹, in excess of that of a $\sim 10M_\odot$ compact object accreting at the Eddington limit. Variability in the X-ray flux on timescales of months is observed in about half of the *ROSAT* ULXs with multiple observations (Colbert & Ptak 2002), while about 5-15% of the *Chandra* ULXs show variability during a single observation (average exposure time ~ 40 ks, Swartz et al. 2004). For several sources with sufficiently good statistics, the best fit to the X-ray spectrum is obtained with a two-component model, a soft multicolor disk (MCD) blackbody plus a power law. Some ULXs show typical temperatures of the MCD component 5-10 times lower than those of Galactic X-ray binaries. The high luminosity, the very soft thermal component (if it represents the emission from a cool accretion disk) and the variability suggest that these sources may be powered by accretion

onto an Intermediate Mass Black Hole (IMBH) of 100-1000 M_\odot . Nevertheless, many of the ULX properties can be explained if they do not emit isotropically (King et al. 2001) or are dominated by emission from a relativistic jet (e.g. Kaaret et al. 2003). In this case, they may harbor stellar mass BHs and may be similar to Galactic black hole binaries.

Multiwavelength observations are definitely a powerful tool to investigate the nature of ULXs. Radio emission, when present, gives important clues on the geometry, energetics and lifetime of ULXs (Kaaret et al. 2003; Miller et al. 2005). Optical follow-ups are crucial to identify ULX counterparts and clean up the population from the significant contamination of background AGNs and interacting SNe (Foschini et al. 2002b; Masetti et al. 2003; Swartz et al. 2004). Up to now only a very small number of ULXs have been convincingly associated with stellar objects of known spectral type (e.g. Liu et al. 2002, 2004; Kaaret et al. 2004). All these ULXs are hosted in star-forming regions and their optical counterparts have properties consistent with those of early type O-B stars. Some ULXs are also associated with extended optical emission nebulae (Pakull & Mirioni 2002).

Another approach to study the nature of ULXs is through time variability. The analysis of the aperiodic variability in the X-ray flux of X-ray binaries is a powerful tool to study the properties of the inner regions of the accretion disk around compact objects (for a review see van der Klis 2005). In particular, Quasi-Periodic Oscillations (QPOs) provide well-defined frequencies, which can be linked to specific time scales in the disk. QPOs can be broadly divided into three classes: (a) QPOs at very low frequencies (< 0.02 Hz), probably associated to oscillations and instabilities in the accretion disk (see Morgan et al. 1997; Belloni et al. 1997, 2000); (b) Low-Frequency (LF) QPOs, with typical frequencies between 0.1 and 10 Hz, probably connected to similar oscillations in neutron star systems (see e.g. Belloni et al. 2002; Remillard et al. 2002a; van der Klis 2005; Casella, Belloni &

Stella 2005), over whose origin there is no consensus; in Black Hole Candidates (BHCs) 3 main different types of LF QPOs have been identified (Casella, Belloni & Stella 2005 and references therein); (c) “hecto-Hertz” QPOs, with a typical frequency of 100-300 Hz, in two cases observed to appear in pairs (Strohmayer 2001a,b). It is currently unclear whether these QPOs show a constant frequency for each source (see Homan et al. 2001; Remillard et al. 2002b), and whether they do appear in pairs obeying particular frequency ratios (see Remillard et al. 2002b). However, since they identify the highest frequencies observed in these systems, they are the best candidates for association with, e.g., the keplerian frequency at the innermost stable orbit, or relativistic precession frequencies. Whatever their physical nature, as they originate in the inner regions of accretion disks around black holes, these features are expected to be produced also in ULXs. However, if ULXs contain IMBHs of 100-1000 M_{\odot} , the frequencies involved are much smaller.

Here we present a follow-up study of the optical counterpart of NGC 1313 X-2 (based on photometric archive data obtained with the ESO VLT telescope) and a timing analysis of a new 105 ks *XMM-Newton* observation of M82 X-1 plus archival *RossixTE* observations of the same field.

2. NGC 1313 X-2

NGC 1313 X-2 is a prototypical ULX (see Miller et al. 2003; Zampieri et al. 2004 and references therein). With a luminosity $L_X \sim 10^{40} \text{ erg s}^{-1}$ in the 0.2-10.0 keV band, it is a good candidate for harboring an IMBH ($M \geq 100 M_{\odot}$). Such an option is corroborated by the presence of a very soft X-ray spectral component ($T \sim 200 \text{ eV}$) which points to a compact object of mass definitely larger than those of Galactic Black Hole candidates. Moreover, the object exhibits X-ray variability on a timescale of months. On the basis of a 19 ks *Chandra* exposure and accurate astrometry of field objects, Zampieri et al. (2004) (Z04 hereafter) derived the source position with an uncertainty of $0.7''$ (RA=03:18:22.34, DEC=-66:36:03.7; 1σ confidence level). Inside the *Chandra* error box a faint optical candidate was found on a R band image taken with the ESO 3.6 m telescope in January 2002.

We analyzed archive ESO VLT+FORS1 images (*BVR*) and spectra of NGC 1313 X-2 taken between December 2003 and January 2004 (Program ID 072.D0614). For details on the data reduction and analysis we refer to Mucciarelli et al. (2005a). Figure 1 shows the *R* and *B* images. Z04 give the *R* magnitude of a number of objects around NGC 1313 X-2 and of the proposed counterpart (object C in their paper). The latter was close to the limit of detectability on their image and appeared as a single object. Thanks to the higher resolution of the VLT image, in the *R* and *V* exposures we are able to resolve object C in two distinct point sources, C1 and C2. Both are inside the *Chandra* error box (see Figure 1). Object C2 is not

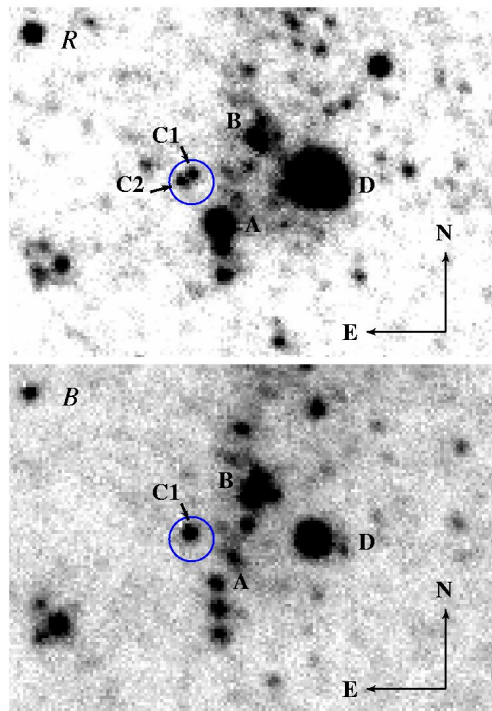


Figure 1. *R* (upper panel) and *B* (lower panel) VLT+FORS1 images of the field around NGC 1313 X-2 ($30'' \times 20''$). The circle is the 2σ *Chandra* error-box ($1.4''$). In the *R* frame, the counterpart is clearly resolved in two point sources, C1 and C2.

detected in the *B* band frame. Magnitudes, colors and astrometric positions of the two candidate counterparts, C1 and C2, and of objects A, B, and D (following Z04) are reported in Table 1. The photometric errors are the 2σ statistical errors on the measurements with the different Landolt standards. For object C2, we quote an upper limit to the *B* band magnitude using the plate limit ($B = 25.2$).

In addition to the images, we also analyzed four VLT+FORS1 spectra ($\lambda_c=5900 \text{ \AA}$, $\lambda/\Delta\lambda=440$ at λ_c) of objects C1+C2 taken in different nights. In these VLT+FORS1 spectra the two sources (C1 and C2) are not spatially resolved. The 2D spectrum taken on 15 January 2004 shows nebular emission lines of [OII] λ 3727 \AA , H_{γ} , H_{β} , [OIII] $\lambda\lambda$ 4959-5007 \AA , [OI] λ 6300 and 6364 \AA , H_{α} , [NII] λ 6583 \AA and [SII] $\lambda\lambda$ 6717-6731 \AA . Note that this is the first detection of a [OII] line from this nebula. A one dimensional spectrum was extracted over an aperture of $2.2''$ centered on object C1+C2 from each of the four combined spectra. After subtracting the nebular emission (see Mucciarelli et al. 2005a), the source spectra show no evident emission or absorption lines. Residuals are present in coincidence with some nebular lines (especially [OIII] and H_{α}), with an upper limit to the equivalent width of $\sim 30 \text{ \AA}$. In particular the residual flux in the [OIII] line is a non negligible fraction of the nebular flux. This appears to be caused by an increased emission of the nebular line around the position of object C1+C2.

Table 1. Astrometric positions, magnitudes and colors of the sources around NGC 1313 X-2 (see Figure 1).

Source	RA	DEC	B	V	R	B-V	V-R
A	03:18:21.97±0.05	-66:36:06.4±0.3	23.5±0.15	21.7±0.05	20.6±0.05	1.8±0.15	1.1±0.1
B	03:18:21.57±0.05	-66:36:00.8±0.3	22.4±0.15	22.7±0.05	22.5±0.05	-0.3±0.15	0.2±0.1
C1	03:18:22.26±0.05	-66:36:03.3±0.3	23.5±0.15	23.6±0.15	23.7±0.15	-0.1±0.2	-0.1±0.2
C2	03:18:22.36±0.05	-66:36:03.8±0.3	≥25.2	24.1±0.15	23.6±0.15	≥1.1	0.5±0.2
D	03:18:20.96±0.05	-66:36:03.6±0.3	20.3±0.15	18.9±0.05	18.1±0.05	1.4±0.15	0.8±0.1

It is not clear if this is simply induced by a change in the rather irregular spatial profile of the nebular line or by a variation of the physical conditions produced by the presence of the nearby ULX. Finally, marginal evidence of an excess in emission may be seen at 4686 Å, corresponding to HeII emission, but the line is not statistically significant.

3. M82 X-1

The first and, to date, only ULX where a QPO has been discovered is M82 X-1 (Strohmayer & Mushotzky 2003). The QPO has a frequency of 54.4 mHz and a FWHM of 11.4 mHz, leading to a quality value $Q = \nu/\Delta\nu \sim 5$. The total fractional rms of the QPO in the 2-10 keV band is 8.4%. Recently, Fiorito & Titarchuk (2004) reported the identification of another QPO at 106 mHz in the power spectrum of M82 X-1 from *RossixTE* data, arguing that it may be a harmonic of the QPO at 54 mHz.

Here we report the results from a timing analysis of a 105 ks *XMM-Newton* observation of M82 X-1 performed in April 2004 (Observation ID 0206080101, PI: P. Ranalli) and of archival *XMM* and *RossixTE* observations of the same field. For details on the X-ray data reduction of these observations we refer to Mucciarelli et al. (2005b). For the timing analysis of the *XMM* data we avoided intervals with high background radiation and limited the extraction to the longest (nearly) uninterrupted segment of data (66 ks) free from solar flares with count rate higher than 30 count s⁻¹. To minimize galactic contamination, source counts were extracted from a circular region of 8'' radius and at energies > 2 keV. We produced a light curve from pn+MOS data with a time binning of 0.5 s. A few gaps of typical duration of ~100 s were present in the light curve and were filled with a Poissonian realization around the mean value of counts before and after the gap. We produced a power spectrum (normalized after Leahy et al. 1983) from the resulting light curve and rebinned it by a factor of 256 reaching a frequency resolution of 3.9 mHz. A rather strong QPO peak is present in the power spectrum. We fitted the power spectrum with a model consisting of a constant (for the Poissonian level) plus two Lorentzian components (see Belloni et al. 2002): one zero-centered for the broad band-limited noise and one for the QPO peak. The characteristic frequency for the band-limited noise component (see Belloni et al. 2002 for a definition) is 39.4±8.6 mHz and its integrated fractional rms is ~22% (after subtracting the contribution of the host galaxy). The parameters of the QPO can be seen

in Table 2. The quality value Q , defined as the ratio of the centroid frequency over the FWHM of the QPO, is 4.3±0.5. We repeated the analysis in two separate energy bands, 2-4 keV and 4-10 keV. The fractional rms of the QPO in these bands resulted to be 13.8% and 23.9% respectively.

In order to investigate the possible variability of the QPO during the observation, we produced a spectrogram, by aligning power spectra obtained from consecutive stretches of data 2048 seconds long. A trend towards lower QPO frequencies is apparent, correlated with the source count rate. In order to quantify the decrease in centroid frequency, we divided the 66 ks interval in two segments of 33 ks each and repeated the power spectral analysis described above. A fit with the same model used for the total power spectrum confirms that the centroid frequency of the QPO decreased by 10.8±4.0% (see Table 2). In order to investigate the variability of the QPO frequency on longer time scales, we extracted from the *RXTE* public archive all 30 public observations of M82, spanning over the year 1997. For each observation, we accumulated PCA light curves in the channel range 0-35, corresponding to 2-13 keV, with a 0.5 s bin size and produced power spectra in the same way as for the *XMM* data. We detected a significant QPO in seven observations, including the three reported by Strohmayer & Mushotzky (2003) and Fiorito & Titarchuk (2004). The timing history of these detections is shown in Figure 2, where also the *XMM* detections are indicated. Although the frequencies are variable, they are roughly consistent with three groups in harmonic 1:2:3 ratio, as recently suggested by Fiorito & Titarchuk (2004). In order to calculate the significance of such an harmonic relation we did a numerical simulation and found the nine QPO frequencies (the seven from *RXTE* data plus the two from *XMM*) to be consistent at 2.8 σ with being harmonics of a fundamental frequency of 54.9 Hz. However, this is not sufficient to completely rule out that such a distributions occurs by chance. More detections are clearly needed in order to address this issue.

4. DISCUSSION

4.1. NGC 1313 X-2

The superb quality of the VLT images reveals that two distinct objects, C1 and C2, are visible inside the *Chandra* error box of NGC 1313 X-2 in the *R* and *V* bands.

Table 2. *M82 X-1. Parameters of the XMM QPO (1σ errors).*

Parameter	Total observation	First half	Second half
ν_0 (mHz)	113 ± 2	120 ± 3	107 ± 4
$FWHM$ (mHz)	26 ± 3	21 ± 4	19 ± 3
Frac % rms	18.3 ± 1.0	17.5 ± 1.1	17.3 ± 1.1
Signif. (σ)	8.9	8.3	8.2

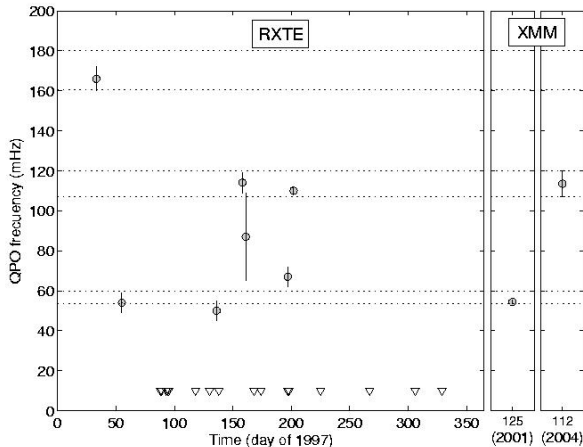


Figure 2. Time history of the centroid frequencies detected from *M82 X-1* in the XMM and RXTE data. The triangles indicate the times of RXTE observations when no significant QPO was detected. The pairs of dotted lines indicate the range of frequencies detected by XMM in 2004 and the corresponding intervals at half and 1.5 times the frequency.

From the astrometric positions reported in Table 1, we infer a separation of $0.75''$ and a position angle (C2 with respect to C1) of $\sim 131^\circ$.

The possibility that either C1 or C2 may be a background AGN appears very unlikely. In fact, no statistically significant emission line at wavelengths longer than H_α is observed in the optical spectrum nor any other feature that may be identified with a highly redshifted emission line (for a thorough discussion see Mucciarelli et al. 2005a). Within the photometric errors, the colors of object C1 appear to be consistent with those of a A3-O9 I or a A2-B0 V star, while those of C2 with a G8-G7 I star (see e.g. Cox 2000). Unfortunately, the optical continuum does not provide useful information for assessing the spectral type because the light from both objects contributes to it. Observationally, the slope of the continuum can be characterized by a power law, $\lambda^{-1.8}$. The absence or extreme weakness of the HeII λ 4686 Å emission line in the optical spectrum suggests that X-ray irradiation is not dominant. Taking Galactic absorption into account and assuming $A_V \simeq 0.3$ (Cardelli et al. 1989 extinction law with $R_V = A_V/E_{B-V} = 3.1$ has been used throughout), the unreddened colors of object C1 are $(V-R)_0 = -0.2\pm 0.2$ and $(B-V)_0 = -0.2\pm 0.2$, con-

sistent with those of a B8-O I or A0-O5 V star. For object C2 it is $(V-R)_0 = 0.4\pm 0.2$ and $(B-V)_0 \geq 1.0$, consistent only with a G4 I star. Recently, Liu et al. (2005) performed a 6.4 m Magellan/Baade observation of the field around NGC 1313 X-2 and found a $I = 23.3$ mag object in coincidence with the position of C1+C2 (that appear unresolved in their I frame). Assuming that the flux in the I band originates mainly from the redder object C2, we then obtain $(R-I) = 0.3 \pm 0.2$, consistent with our tentative spectral classification.

At the distance of NGC 1313 ($d = 3.7$ Mpc; Tully 1988) the V magnitudes of C1 and C2 (reported in Table 1) translate into the absolute magnitudes $M_V \sim -4.6$ and ~ -4.1 , respectively. Comparing these values with the absolute magnitudes of main sequence and supergiant stars (e.g. Cox 2000), we find that the observed value is consistent only with a B0-O9 main sequence star for C1, while it is consistent with a G4 supergiant of type Ib for C2. Therefore, we conclude that both C1 and C2 are stars in NGC 1313, with C1 an early type main sequence star and C2 a supergiant. The bolometric luminosities of the two objects are $\sim 3 \times 10^{38}$ erg s $^{-1}$ and $\sim 2 \times 10^{37}$ erg s $^{-1}$, respectively. Given the density of objects in the field of view ($\sim 50 - 100$ arcmin $^{-2}$), a significant fraction of which are supergiants in NGC 1313, the probability that C1 or C2 fall by chance inside the 2σ *Chandra* error box is not negligible (~ 0.1). However, the chance occurrence of two objects, separated by only $0.7''$, inside the X-ray error box is $\sim 5 \times 10^{-3}$, sufficiently small to be considered rather unlikely. Actually, if both C1 and C2 are stars in NGC 1313, a physical association may not be unpalatable (the distance corresponding to the apparent separation on the sky is ~ 10 pc). Therefore, we conclude that the ULX is most probably physically associated to either object C1 or C2. Irrespectively of which of the two objects is the actual counterpart, NGC 1313 X-2 appears to be a high mass X-ray binary with a very massive donor star.

A B0-O9 main sequence star has an initial mass of $\sim 20M_\odot$. In this respect our analysis essentially confirms the original suggestion by Z04, who proposed that the optical counterpart of NGC 1313 X-2 may be an O type main sequence star in NGC 1313. If the colors are affected by the binary interaction, the estimated mass may vary somewhat. A $\sim 20M_\odot$ donor star could easily provide the mass transfer rate required to fuel the accreting black hole through Roche-lobe overflow during the main sequence phase if the orbital separation is ≈ 1 AU. In these conditions, the mass transfer would be stable and the source persistent (Patruno et al. 2005; Patruno & Zampieri, in preparation).

If object C2 is the counterpart, the nature of the system remains unchanged. In this case X-ray irradiation may be significant and give a non-negligible contribution to the optical emission. The mass corresponding to a G4 supergiant is $\sim 10M_{\odot}$. The same caveat discussed for C1 about the possibility that the colors and mass estimate are affected by binary interaction applies also in this case. The mass transfer rate provided by such a donor star through Roche-lobe overflow is certainly adequate also for large orbital separations. Wind accretion may also be a viable alternative.

4.2. M82 X-1

M82 X-1 is at present the only ULX where a QPO has been discovered. An important issue is of course the possible identification of this QPO with one of the QPO types observed in the X-ray light curves of stellar-mass BHCs. In the following we will summarize the main properties of the QPO in M82 X-1, and discuss its similarities and differences with the QPOs observed in BHCs.

- The lowest and highest observed frequencies are 50 ± 5 mHz and 166 ± 6 respectively (Figure 2).
- The frequency distribution over this range is suggestive of a harmonic 1:2:3 ratio between them.
- In the 2004 *XMM* observation the frequency is observed to vary by $\sim 10\%$ in less than one day.
- The QPO peak has a quality value higher than 4 (up to ~ 6 in one case).
- It shows a high fractional rms (up to $\sim 18\%$).
- The underlying band limited noise is strong (fractional rms $\sim 22\%$) and has a characteristic frequency comparable to the QPO frequency.
- The integrated fractional rms of the QPO above 4 keV is higher than below that energy.

Let us compare now all these properties with those of the various types of QPOs observed in BHCs.

Very-low frequency QPOs. An association of the QPO in M82 X-1 with the very low frequency ($\nu \leq 0.02$ Hz) “heart-beat” QPOs observed in GRS 1915+105 is unlikely as their frequency is *lower*. This, assuming an inverse scaling with the black-hole mass, would imply a very low (\sim solar) mass black hole in M82 X-1, which is not in agreement with the spectral evidences (see Mucciarelli et al. 2005b).

High-frequency QPOs. The observed short-time scale variability seems to exclude an association with the high-frequency “hecto-Hertz” QPOs observed in BHCs, since the latter have been detected at rather stable frequencies. Also the presence of a strong underlying band limited

noise, with a characteristic frequency comparable to the QPO frequency, is at variance with the high-frequency “hecto-Hertz” QPOs observed in BHCs. Furthermore, the rms amplitude of the QPO itself in M82 X-1 is roughly an order of magnitude bigger than that of the “hecto-Hertz” QPOs in BHCs, thus making the association very unlikely. For the sake of completeness we stress that the detection of the QPO at ~ 166 mHz reported in this paper lowers the upper limit for the mass of the black hole in M82 X-1 (assuming that this frequency is associated with the Keplerian frequency at the innermost circular orbit around a Schwarzschild black hole) to $\sim 1.2 \times 10^4 M_{\odot}$.

Low-frequency QPOs. In the type-A and type-B QPOs observed in BHCs, the peak appears always at frequencies near 8 and 6 Hz respectively. Moreover, they are both characterized by a weak (a few %) underlying red noise component. These properties make an association with the variable, strong QPO observed in M82 X-1 unlikely. In the case of type-A QPOs, its low coherence and amplitude make the association even less likely.

The properties of the QPO in M82 X-1 are on the contrary reminiscent of those of the third type of BHCs low-frequency QPO, the type C, whose characteristic frequencies vary in the range 0.1-15 Hz. The similarities in fractional rms, variability, quality value, and underlying noise strongly suggest an association between the two features. Furthermore, in the 2004 *XMM* observation there is evidence for a positive correlation of the QPO frequency with the count-rate, and a similar correlation is often observed in type-C QPOs. However, during the 2001 *XMM* observation (when the QPO was detected at a lower frequency) the count rate was higher than during the 2004 observation. Since the count-rate vs. frequency correlation in BHCs is “outburst dependent” (which means that during different outburst a source can show similar frequencies at different count-rates) no conclusion can be derived from the observed phenomenology in M82 X-1. No information on the count-rate variability could be obtained from the *RXTE* observations, given the lack of imaging capabilities of the satellite.

Assuming that the QPO detected in M82 X-1 is a type-C QPO, and scaling the frequency inversely to the BH mass, the observed frequency range (from 50 to 166 mHz) would yield a black hole mass M_{BH} anywhere in the range 10-1000 M_{\odot} . However, type-C QPOs are observed in BHCs throughout the whole Hard-Intermediate State (see Homan & Belloni 2005), and their frequency is known to decrease with the hardness of the energy spectrum. At the lowest observed frequencies, the spectrum is hard and there is often no evidence for the presence of a soft thermal component. As the contribution from a disk appears and increases, the QPO frequency also increases. The *XMM* spectra of both observations in which a QPO has been detected in M82 X-1 show possible evidence for a disk contribution (see Mucciarelli et al. 2005b). To the extent that the two phenomena can be compared, the presence of a soft component would exclude that the type-C QPO in M82 X-1 is in the lowest frequency range, increasing the lower limit for M_{BH} .

5. CONCLUSIONS

We presented an analysis of archive ESO VLT photometric and spectroscopic data of NGC 1313 X-2. The superb quality of the VLT images reveals that two distinct objects, with R magnitudes 23.7 and 23.6, are visible inside the *Chandra* error box. Both are stars in NGC 1313, the first a B0-O9 main sequence star of $\sim 20M_{\odot}$, while the second a G supergiant of $\sim 10M_{\odot}$. Irrespectively of which of the two objects the actual counterpart is, this implies that NGC 1313 X-2 is a high mass X-ray binary with a very massive donor.

We reported also a complete analysis of *XMM-Newton* and *RXTE* observations of M82 X-1. The similarities in fractional rms, variability, quality value, and underlying noise strongly suggest an association between the QPO in M82 X-1 and the low-frequency, type-C QPOs observed in BHCs. This allows us for the first time to put strong constraints to the mass of the central black hole in this source, yielding to a value between a few tens to one thousand solar masses.

ACKNOWLEDGMENTS

Work partially supported by the Italian Ministry for Education, University and Research (MIUR) under grants PRIN-2002-027145, PRIN-2003-027534_004, PRIN-2004-023189 and by INAF-PRIN grant.

REFERENCES

- Belloni, T. et al. 1997, ApJ, 488, L109
- Belloni, T. et al. 2000, A&A, 355, 271
- Belloni, T. et al. 2002, ApJ, 572, 392
- Casella, P., Belloni, T., & Stella, L. 2005, ApJ, 629, 403
- Cox, A.N. 2000, *Allen's Astrophysical Quantities*, Springer
- Bohlin, R.C., Savage, B.D., & Drake, J.F. 1978, ApJ, 224, 132
- Cardelli, J.A., Clayton, G.C. & Mathis, J.S. 1989, ApJ, 345, 245
- Colbert, E.J.M., & Ptak, A.F. 2002, ApJS, 143, 25
- Fiorito, R., Titarchuk, L. 2004, ApJL, 614, L113
- Foschini, L. et al. 2002a, A&A, 392, 817
- Foschini, L., Ho, L.C. & Masetti, N. 2002b, A&A, 396, 787
- Homan, J. et al. 2001, ApJS, 132, 377
- Homan, J., & Belloni, T. 2005, to appear in Proc. of "From X-ray binaries to quasars: Black hole accretion on all mass scales", (Amsterdam, July 2004), eds. T. Maccarone, R. Fender, L. Ho
- Kaaret, P., Corbel, S., Prestwich, A.H., & Zezas, A. 2003, Science, 299, 365
- Kaaret, P., Ward, M.J., & Zezas, A. 2004, MNRAS, 351, 83
- King, A.R. et al. 2001, ApJ, 552, 109
- Leahy, D.A., Darbro, W., Elsner, R.F., Weisskopf, M.C., Kahn, S., Sutherland, P.G. & Grindlay, J.E. 1983, ApJ, 266, 160
- Liu, J., Bregman, J.N., & Seitzer, P. 2002, ApJ, 580, 31
- Liu, J., Bregman, J.N., & Seitzer, P. 2004, ApJ, 602, 249
- Liu, J., & Bregman, J.N. 2005, ApJS, 157, 59
- Liu, J., Bregman, J.N., Seitzer, P. & Irwin, J. 2005, astro-ph/0501310
- Masetti, N. et al. 2003, A&A, 406, L27
- Miller, J.M., Fabbiano, G., Miller, M.C., & Fabian, A.C. 2003, ApJ, 585, 37
- Miller, N.A., Mushotzky, R.F. & Neff, S.G. 2005, ApJ, 623, 109
- Morgan, E.H. et al. 1997, ApJ, 482, 993
- Mucciarelli, P. et al. 2005a, ApJL, 633, 101
- Mucciarelli, P. et al. 2005b, MNRAS, in press (astro-ph/0509796)
- Pakull, M.W., & Mirioni, L. 2002, in Proc. ESA Symp., *New Visions of the X-ray Universe in the XMM-Newton and Chandra Era*, eds. F. Jansen et al. (ESA SP-488) (astro-ph/0202488)
- Patruno, A., Colpi, M., Faulkner, A., & Possenti, A. 2005, MNRAS, in press (astro-ph/0507229)
- Remillard, R.A., et al. 2002, ApJ, 564, 962
- Remillard, R.A., et al. 2002b, ApJ, 580, 1030
- Strohmayer, T.E. 2001a, ApJ, 552, L49
- Strohmayer, T.E. 2001b, ApJ, 554, L169
- Strohmayer, T.E., Mushotzky, R.F. 2003, ApJL, 586, L61
- Swartz, D.A., Ghosh, K.K., Tennant, A.F., & Wu, K. 2004 ApJS, 154, 519
- Tully, R.B. 1988, *Nearby Galaxies Catalog* (Cambridge: Cambridge University Press)
- van der Klis, M. 2005, in "Compact Stellar X-Ray Sources", in press (astro-ph/0410551)
- Zampieri, L. et al. 2004, ApJ, 603, 523 (Z04)

A HIGHLY-IONIZED ABSORBER AS A NEW EXPLANATION FOR THE SPECTRAL CHANGES DURING DIPS FROM X-RAY BINARIES

L. Boirin¹, M. Díaz Trigo², M. Méndez³, A. N. Parmar², and J. S. Kaastra³

¹Observatoire Astronomique de Strasbourg, 11 rue de l'Université, F-67000 Strasbourg, France

²Research and Scientific Support Department of ESA, ESTEC, Postbus 299, NL-2200 AG Noordwijk, The Netherlands

³The SRON, the National Institute for Space Research, Sorbonnelaan 2, 3584 CA Utrecht, The Netherlands

ABSTRACT

Until now, the spectral changes observed from persistent to dipping intervals in dipping low-mass X-ray binaries were explained by invoking progressive and partial covering of an extended emission region. Here, we propose a novel and simpler way to explain these spectral changes, which does not require any partial covering and hence any extended corona, and further has the advantage of explaining self-consistently the spectral changes in both the continuum and the narrow absorption lines that are now revealed by XMM-Newton. In 4U 1323–62, we detect Fe XXV and Fe XXVI absorption lines and model them for the first time by including a complete photo-ionized absorber model rather than individual Gaussian profiles. We demonstrate that the spectral changes both in the continuum and the lines can be simply modeled by variations in the properties of the ionized absorber. From persistent to dipping the photo-ionization parameter decreases while the equivalent hydrogen column density of the ionized absorber increases. In a recent work (see Díaz Trigo et al. in these proceedings), we show that our new approach can be successfully applied to all the other dipping sources that have been observed by XMM-Newton.

Key words: Accretion; accretion disks; X-ray binaries; 4U 1323–62.

1. INTRODUCTION

The lightcurves from dipping low-mass X-ray binaries (LMXBs) such as 4U 1323–62 show dips recurring at the orbital period of the system (Fig. 1 bottom). Dips are due to a structure passing through the line-of-sight at each orbital rotation. This structure is probably a thickened region of the disk related to the impact of the stream from the companion star into the disk. The presence of periodic dips and absence of eclipses from the companion indicate that dipping sources are viewed relatively close to edge-on.

The X-ray spectra of most of the dip sources become harder during dipping (Fig. 1 top). However, simple photo-electric absorption by cool (neutral) material fails to explain the spectral changes from persistent to dipping intervals. Therefore, more complex models have been proposed. In particular, the “complex continuum” approach has been successfully applied to a number of dipping LMXBs including 4U 1323–62 (Bałucińska-Church et al. 1999). It assumes that the X-ray emission originates from two components, and the spectral changes during dips are explained by the partial and progressive covering of one of the components by a cool absorber, while the other component is rapidly and entirely covered by another cool absorber. This approach implies that the latter component comes from a point-like region such as the neutron star surface, whereas the former component comes from a very extended corona.

The improved sensitivity and spectral resolution of *Chandra* and XMM-Newton are allowing narrow absorption features from highly ionized Fe and other metals to be observed in a growing number of X-ray binaries. In particular, Fe XXV (He-like) or Fe XXVI (H-like) 1s-2p resonant absorption lines near 7 keV were reported from the micro-quasars GRO J1655–40, GRS 1915+105 and H 1743–322, and from the neutron star systems Cir X–1, GX 13+1, MXB 1658–298, X 1624–490, X 1254–690, XB 1916–053 and now 4U 1323–62 (references in Boirin et al. 2005). These sources are known to be viewed close to edge-on (many are dippers). This indicates that the highly ionized plasma probably originates in an accretion disk atmosphere or wind, which could then be a common feature of accreting binaries but preferentially detected in systems viewed close from the disk plane.

Here, we report the detection of Fe XXV and Fe XXVI absorption lines from the LMXB 4U 1323–62 and propose a new explanation for the spectral changes between persistent and dipping intervals (details in Boirin et al. 2005). We further show that this new explanation also applies to all the other bright dipping sources observed by XMM-Newton (see Díaz Trigo et al. in these proceedings and details in Díaz Trigo et al. 2005).

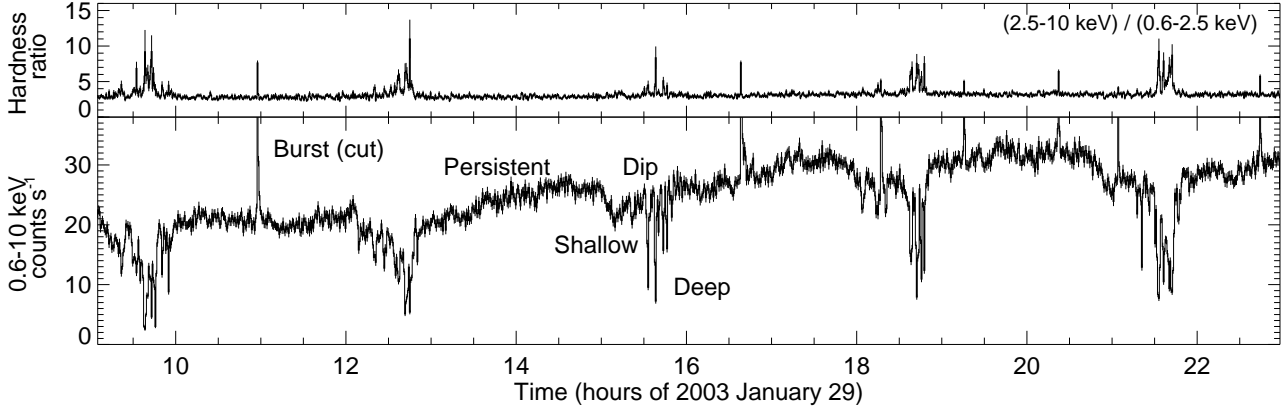


Figure 1. 0.6–10 keV EPIC PN lightcurve of 4U 1323–62 (bottom). The dipping activity is associated with spectral hardening (top). Adapted from Boirin et al. (2005).

2. RESULTS ON 4U 1323–62

We analyzed the 50 ks XMM-Newton observation of 4U 1323–62 performed on 2003 January 29 (Fig. 1). Bursts were excluded and one spectrum was extracted for each category of emission: persistent, shallow dipping and deep dipping. Fe XXV and Fe XXVI 1s-2p resonant absorption lines near 7 keV are clearly detected in the persistent spectrum (Fig. 2 A top), indicating that a highly-ionized disk atmosphere or wind is present in 4U 1323–62. Absorption lines are also present in the dipping spectra (Fig. 2 A middle and bottom) indicating that the structure causing the dips (“bulge” hereafter) is also ionized. However, clear spectral changes in the lines are visible from persistent to deep dipping: the strength of the Fe XXVI line decreases while that of Fe XXV increases, indicating that the bulge is less strongly ionized.

For the first time, to account for the absorption features evident near 7 keV, we include a photo-ionized absorber in the spectral model, rather than individual line profiles. We use the `xabs` model of SPEX, which treats the absorption by a thin slab composed of different ions, located between the ionizing source and the observer. The processes considered are the continuum and the line absorption by the ions and scattering out of the line-of-sight by the free electrons in the slab. The relevant ions are automatically taken into account and their relative column densities are coupled in a physical way via a photo-ionization model.

We find that the persistent and dipping spectra are all well fit by a model consisting of a power-law, a blackbody and a broad Gaussian emission line, modified by absorption from neutral (`abs`) and ionized (`xabs`) material (Fig. 2 B and C). The ionized plasma has a lower ionization parameter and a larger column density during dipping. In all cases, it perfectly accounts for the narrow features near 7 keV. Remarkably, it also produces apparent continuum absorption which becomes substantial and strongly energy-dependent during dipping (compare

panels d in Fig. 2 B and C). Indeed, because the ionization is lower during dipping, there is a wider variety of ions than during persistent emission where most of the species are fully stripped of their electrons. Thus many more absorption lines and edges are expected during dipping (see Fig. 3 A). Furthermore, because the column density is larger, the edges are stronger. This explains the smooth variation of the transmission with energy (outside the sharp changes at the binding energies themselves).

By successfully fitting the dipping spectra using the persistent model, but fixing the parameters of the continuum to the persistent values, and allowing only the parameters of the absorbers (`abs` and `xabs`) to change, we actually demonstrate that the spectral changes from persistent to dipping can be modeled simply by variations in the properties of the neutral and ionized absorbers, with the ionized absorber playing the main role (Table 1). Contrary to the “complex continuum” model, the new proposed approach does not require any partial covering and hence does not require the underlying source of X-ray emission to be particularly extended in 4U 1323–62. The new explanation further presents the advantage of explaining self-consistently the spectral changes both in the continuum *and* the narrow lines.

Table 1. The column density of the neutral ($N_{\text{H}}^{\text{abs}}$) and ionized ($N_{\text{H}}^{\text{xabs}}$) absorbers and the ionization parameter $\log(\xi)$ in 4U 1323–62. During dipping, the ionized absorber has a lower ionization level and a larger column density. There is also more neutral absorber.

	Persistent	Shallow dip	Deep dip
$N_{\text{H}}^{\text{abs}}$	3.50 ± 0.02	3.58 ± 0.03	4.2 ± 0.2
$N_{\text{H}}^{\text{xabs}}$	3.8 ± 0.4	14 ± 1	37 ± 2
$\log(\xi)$	3.9 ± 0.1	3.43 ± 0.08	3.13 ± 0.07

$N_{\text{H}}^{\text{abs}}$ and $N_{\text{H}}^{\text{xabs}}$ are in 10^{22} cm^{-2} and ξ in erg cm s^{-1} .

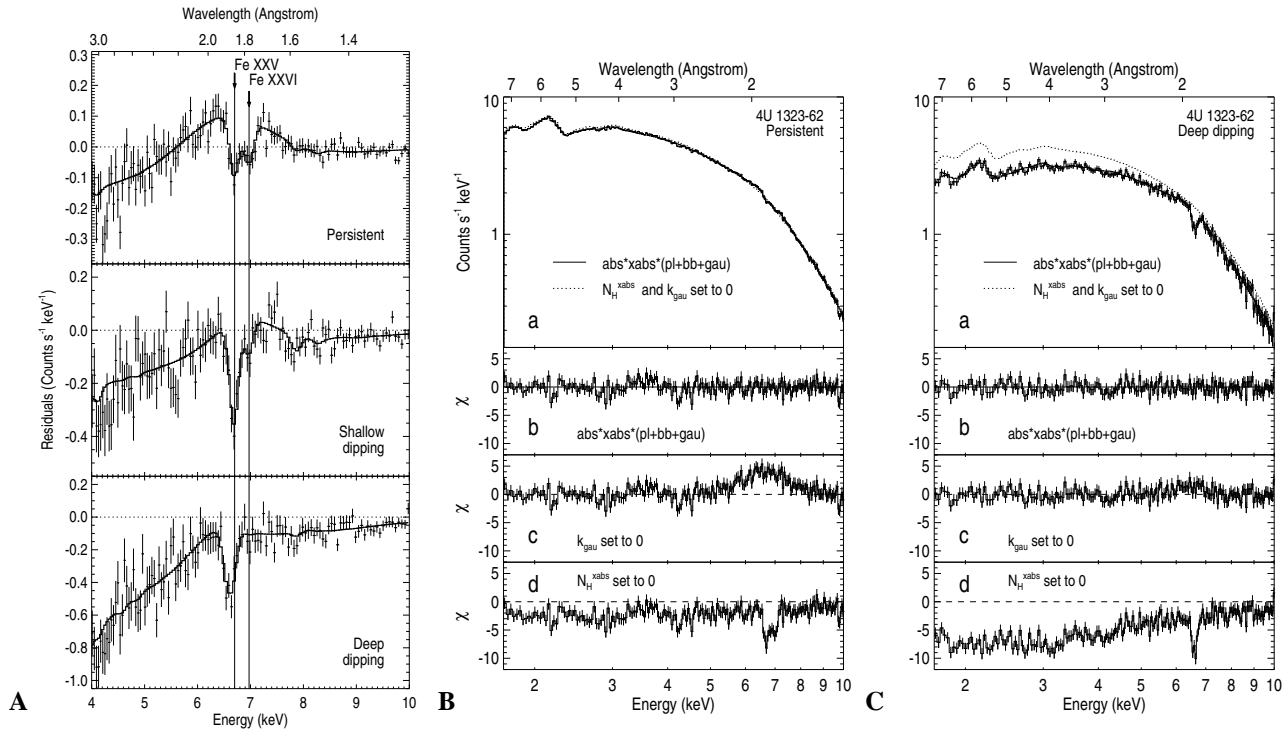


Figure 2. EPIC PN results on 4U 1323–62 from Boirin et al. (2005). **A**) 4–10 keV spectral residuals showing the Fe XXV and Fe XXVI absorption lines during persistent (top) and shallow (middle) emission. During deep dipping (bottom), the Fe XXVI line is not present anymore: the absorber is less strongly ionized. **B**) **a**) Persistent spectrum fit with a model consisting of a power-law (pl), a blackbody (bb) and a broad Gaussian emission line (gau), modified by absorption from neutral (abs) and ionized (xabs) material. **b**) Flat residuals from the above model indicating that the fit is good. **c**) Residuals showing the contribution of the Gaussian emission line at 6.6 keV (by setting its normalization, k_{gau} , to 0). **d**) Residuals showing the contribution of the ionized absorber (by setting $N_{\text{H}}^{\text{xabs}}$ to 0). It perfectly accounts for the narrow Fe XXV and Fe XXVI absorption lines. **C**) Same as **B** but for the deep dipping intervals. The ionized absorber does not only produce the line near 7 keV, but also energy-dependent absorption throughout the spectrum (panel **d**).

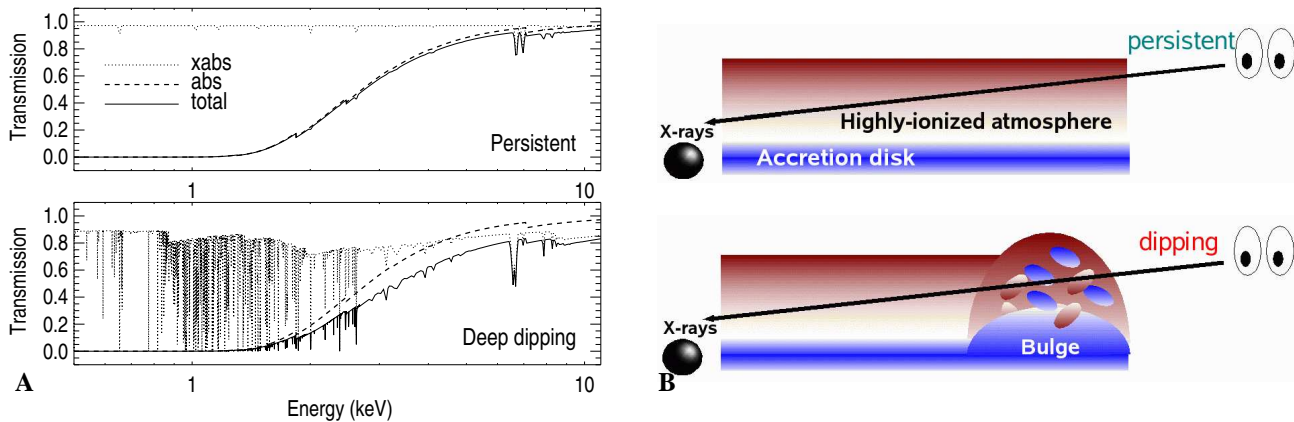


Figure 3. **A**) Transmission of the ionized (dotted line) and neutral absorbers (dashed line), and the total transmission (thick line) during persistent (top) and deep dipping (bottom) intervals of 4U 1323–62 (adapted from Boirin et al. 2005). During persistent segments, the ionized plasma transmits all the photons except those with an energy matching the Fe XXV and Fe XXVI transitions, while during deep dipping, the transmission is affected by lines and edges from many ions and becomes strongly energy-dependent. The neutral absorption is larger during dipping than during persistent states, indicating that part of the neutral absorber is located in the binary rather than in the interstellar medium, at least during dipping. **B**) These results suggest that a highly-ionized atmosphere is present above the accretion disk and seen in absorption during persistent segments (top). During dipping (bottom), the bulge passes through the line-of-sight. It's denser, a bit less ionized and probably contains clumps of neutral material.

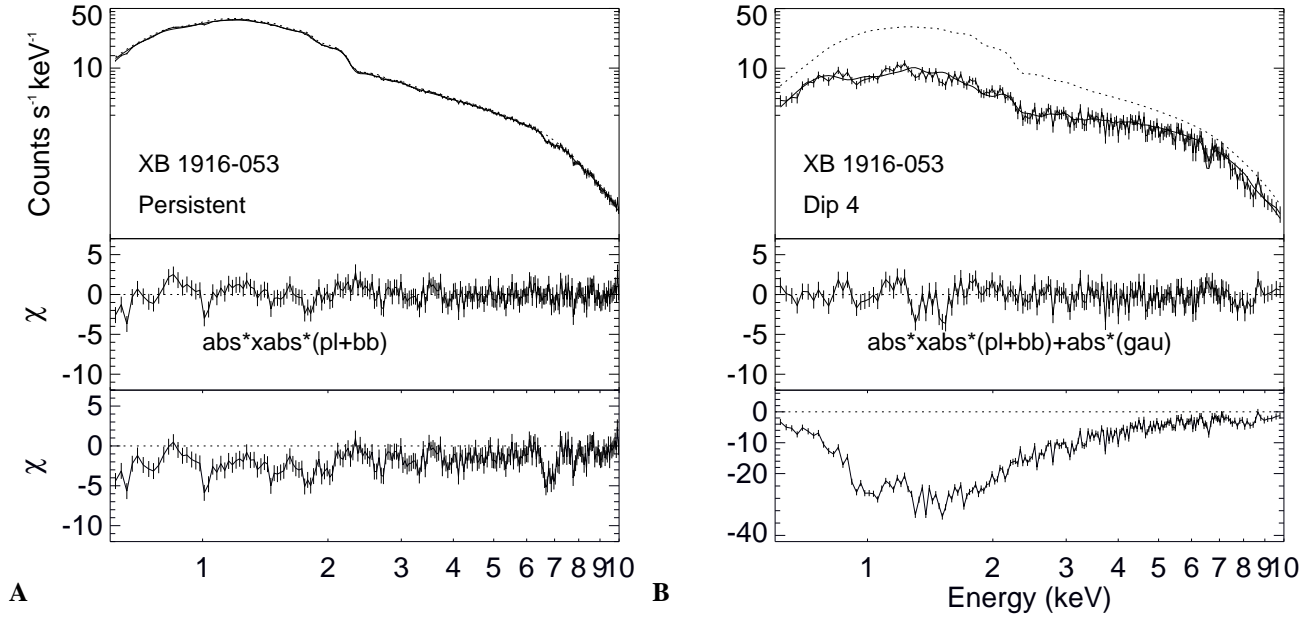


Figure 4. EPIC PN persistent (*left*) and dipping (*right*) spectra of XB 1916–053 fit using a photo-ionized absorber model (from Díaz Trigo et al. 2005). The flat residuals in the *middle* panel indicate that the fits are good. The contribution of the ionized absorber is shown in the *bottom* panel (by setting $N_{\text{H}}^{\text{xabs}}$ to 0). During persistent intervals, it produces mainly the narrow absorption lines near 7 keV, while during dipping, it also produces strong energy-dependent absorption throughout the spectrum.

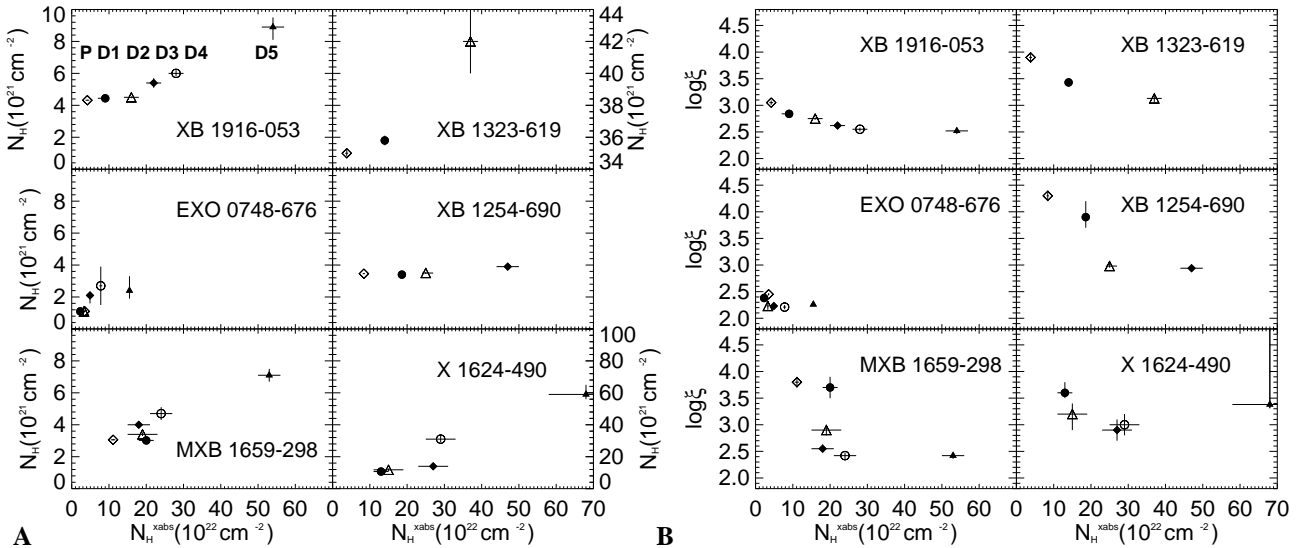


Figure 5. Main properties of the ionized and neutral absorbers in the dipping binaries where the photo-ionization absorber model was tested (from Díaz Trigo et al. 2005). Each symbol represents a different intensity stage of the source, from the persistent level, P, to the deepest dipping level, D5, as indicated in the top left panel. **A)** Column density of the neutral absorber, N_{H} , (including local and interstellar material) versus column density of the local ionized absorber, $N_{\text{H}}^{\text{xabs}}$. In all the sources, the amount of both neutral and ionized material in the line-of-sight increases from persistent to deep dipping stages. **B)** Ionization parameter, ξ , versus column density, $N_{\text{H}}^{\text{xabs}}$, of the ionized absorber. In all the sources, the ionization parameter decreases from persistent to deep dipping while $N_{\text{H}}^{\text{xabs}}$ increases.

3. RESULTS ON OTHER DIPPING SOURCES

To test the new proposed explanation for the spectral changes, Díaz Trigo et al. (2005) analyzed the EPIC PN data of all the bright dipping binaries observed by XMM-Newton: XB 1916–053, EXO 0748–676, X 1254–690, 4U 1746–371, MXB 1658–298 and X 1624–490 (see Díaz Trigo et al. in these proceedings). For each source (except 4U 1746–371 whose dips were too shallow for the analysis to be carried out), the persistent and dipping spectra were fit together with the parameters of the underlying continuum emission tied together, and the parameters of the absorbers (one neutral, abs , and one photo-ionized, $xabs$) left free to vary. Good fits were obtained for each source (see the case of XB 1916–053 in Fig. 4). Thus, the changes in the properties of a neutral and of an ionized absorber in the line-of-sight can account for the spectral changes in the continuum and in the narrow features of all the dipping sources that could be tested so far. From persistent to deep dipping, the amount of neutral absorber increases (Fig. 5 A), corresponding to an increase by a factor ~ 2 in the amount of the local material. At the same time, the column density of the ionized absorber is found to increase by a factor of 4 to 12 (Fig. 5 A) while its ionization parameter decreases (Fig. 5 B). The changes in this ionized material clearly play the main role in explaining the overall energy-dependent spectral changes observed in the dipping sources (see the bottom panel of Fig. 4 A and B showing the contribution of the ionized absorber).

4. CONCLUSIONS AND PROSPECTS

Modeling the spectral changes between persistent and dipping intervals is a powerful means of learning about the bulge and the accretion disk in all the X-ray binaries. Until now, these spectral changes were modeled by invoking absorption of a point-like emission region by a neutral absorber, together with progressive and partial covering of an extended emission region by another neutral absorber. We propose a novel and simpler explanation invoking a neutral absorber and a photo-ionized absorber. It was successfully applied to all the bright dipping sources that could be tested to date: 4U 1323–62, XB 1916–053, EXO 0748–676, X 1254–690, MXB 1658–298 and X 1624–490. No partial covering was needed, indicating that none of the underlying X-ray sources requires to be particularly extended. The new approach has the strong advantage of explaining self-consistently the spectral changes both in the continuum and in the narrow absorption lines that have been revealed by XMM-Newton.

These results suggest a geometry for X-ray binaries such as drawn in Fig. 3 B. A highly-ionized plasma is present above the accretion disk. If the binary is viewed relatively close to edge-on, the ionized plasma lies in our line-of-sight toward the X-rays emitted in the vicinity of the compact object, and signatures of the plasma appear

in the spectrum, such as the Fe XXV and Fe XXVI absorption lines in the persistent spectrum of 4U 1323–62. At the azimuth where the stream of material from the companion star impacts the disk, there is material projected at higher altitudes above the disk. This bulge or thickened part of the disk passes through our line-of-sight during dipping. Contrary to the complex continuum approach, our modeling of the dipping spectra indicates that this material is ionized (but less than the plasma seen during persistent intervals). It probably contains clumps of neutral material.

The precise distribution of the ionized absorber is unknown. Possibly, from the surface of the disk to higher altitudes, the density of the ionized material decreases and hence its ionization parameter increases. If the ionized absorber is present at the radius of the bulge, its layers could be shifted to higher altitudes. This could explain the differences observed between persistent and dipping intervals in a given source, and the differences in the absorbers properties observed from source to source, as a function of inclination. In any case, the geometry inferred from the dipping sources should be valid for all the other accreting binaries which only differ from the dipping ones in being viewed further away from the disk plane. This makes the dipping sources among the best targets to improve our understanding of the disk structure and of the accretion process.

Here are some of the key issues that we would like to address thanks to future detailed X-ray observations of the dipping sources:

- constraints on the distribution of the ionized material: inner and outer radii, height, density gradient, ionization gradient, composition, velocity (static atmosphere versus out-flowing wind);
- response of the ionized material to changes in the underlying source luminosity or spectral energy distribution;
- dependence of the properties of the ionized material on the system parameters such as the disk size or inclination;
- role of the reflection (back-scattering) of X-rays onto the ionized and neutral materials.

REFERENCES

- Bałucińska-Church, M., Church, M. J., Oosterbroek, T., et al. 1999, *A&A*, 349, 495
- Boirin, L., Méndez, M., Díaz Trigo, M., Parmar, A. N., & Kaastra, J. S. 2005, *A&A*, 436, 195
- Díaz Trigo, M., Parmar, A. N., Boirin, L., Méndez, M., & Kaastra, J. S. 2005, *A&A*, in press, astro-ph/0509342

CLOUDS, WINDS, AND JETS IN THE LUMINOUS X-RAY SOURCE CIRCINUS X-1

N. S. Schulz¹, W. N. Brandt², D. K. Galloway³, D. Chakrabarty⁴, and S. Heinz⁵

¹Massachusetts Institute of Technology, Cambridge MA, USA

²The Pennsylvania State University, University Park PA, USA

³The University of Melbourne, Melbourne, Australia

⁴Massachusetts Institute of Technology, Cambridge MA, USA

⁵Massachusetts Institute of Technology, Cambridge MA, USA

ABSTRACT

One of the early highlights of high resolution X-ray spectroscopy was the discovery of P Cygni lines in the highly variable and luminous X-ray source Circinus X-1 during the early days of the Chandra mission. By adapting the preceding paradigm established from ASCA observations that the accretion disk around the neutron star is viewed edge-on, the the complex line structure was interpreted as a combination of accretion disk coronal line emission and absorption from a radiatively driven equatorial disk wind. The detection of ultra-relativistic radio jets at about the same time seemed to support the image of Circinus X-1 as a powerful microquasar, but also casted some doubt on the assumption that the source is viewed edge-on, but instead featured a face-on view. This not only challenges the current model for the observed X-ray emission, it could also force a complex scenario involving jets, winds, and clouds that seems quite unique among accreting compact sources. Furthermore the X-ray emission of Circinus X-1 has undergone radical changes since then as it gradually slipped into a low intensity state which is even at times devoid of the typical outburst pattern with its binary orbit. We observed Circinus X-1 several times with the Chandra HETG spectrometer during this transition. We show some preliminary results from the first of these observations, which provided the unobstructed high resolution X-ray image of this source as well as an X-ray spectrum that is devoid of P Cygni lines but shows line emission as expected from ADC sources. We discuss the results in conjunction with its long-term lightcurve and investigate possible scenarios with respect to its line of sight.

Key words: Binaries; Neutron Stars; Spectroscopy; X-rays.

1. INTRODUCTION

The nature of Cir X-1 in general is still poorly understood and, despite advances in recent years, there remains great uncertainty about even the most basic properties of this system. Since its discovery (Margon et al., 1971), it has appeared bright and variable in X-rays exhibiting a period of 16.6 days (Kaluziński et al., 1976). The compact object in the Cir X-1 system is thought to be a neutron star (Tennant, Fabian, & Shafer, 1986) that can radiate at super-Eddington luminosities. Its heavily reddened optical counterpart (e.g., Moneti (1992)) shows strong, asymmetric H α emission. The system shows two arcminute-scale radio jets (Stewart et al., 1993), and an arcsecond-scale asymmetric jet (Fender et al., 1998) suggesting the presence of relativistic outflow from the source, a claim that was confirmed by the latter authors in early 2004 (Fender et al., 2004). Cir X-1 is now included among the ‘‘Galactic Microquasar’’ X-ray binaries (Mirabel, 2001), although its behavior favors more a Z-source type binary rather than that of a black hole binary (Tennant, Fabian, & Shafer, 1986; Shirey et al., 1999a). The identification by Tennant, Fabian, & Shafer (1986) as an accreting neutron star is based on the detection of several type I X-ray bursts in the field of view with *EXOSAT*, which not only appeared to come from a consistent position but also varied in properties in response to changing source flux. Its identification as a neutron star clearly impacts on the question whether accretion powered X-ray sources containing a neutron star can generate ultra-relativistic jets (Fender et al., 2004).

The existence of the P Cygni lines demonstrated the presence of a high-velocity accretion disk wind with velocities between 400 and 2000 km (Brandt & Schulz, 2000). Unlike in cataclysmic variables, which generally feature polar outflows (Córdova & Horwarth, 1987), the wind is considered to be equatorial. Previous X-ray studies strongly suggested that the spectral variability caused by the observed X-ray absorption is best explained by a model with a nearly edge-on view (Brandt et al., 1996;

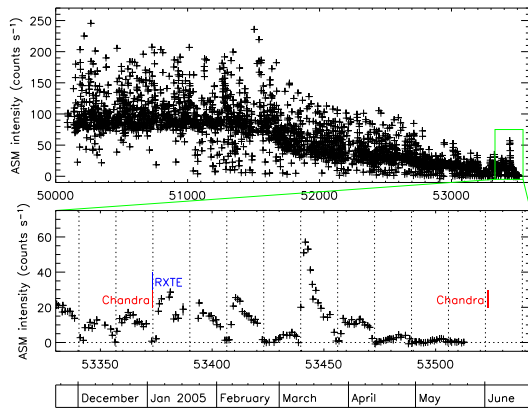


Figure 1. RXTE ASM lightcurve of Cir X-1 from 1996 until the middle of May 2005 (upper panel). A close-up for 2005 (lower panel) still shows the regular flux dips at zero orbital phase and irregular flare events soon after zero phase. Marked are the most recently obtained Chandra observations.

Shirey et al., 1999b; Schulz & Brandt, 2002). Such accretion disk winds have been discussed both theoretically and observationally (e.g. Begelman, McKee, & Shields (1983); Raymond (1993); Chiang (2001); Proga & Kallman (2002)) and quite recently, the existence of such winds was established as a viable explanation of *Chandra* HETGS (Canizares et al., 1995) observations of black hole X-ray binaries which have now revealed variable, blue-shifted absorption lines (Miller, 2005).

The nearly edge-on view of Cir X-1 is currently challenged by the observations of jet emissions in the Radio band (Fender et al., 2004). The suggested energetics of the observed Radio emission not only hinted the existence of an ultra-relativistic jet with $\Gamma \sim 10 - 15$, but also constrained the angle of emission within the line of sight. Under the assumption that the jet is launched perpendicular to the accretion disk and that the X-ray flare at zero phase of the same orbit is providing the energy, an inclination of not more than 5° towards the line of sight is the consequence, suggesting a face-on view of the system. Recent studies of a soft X-ray excess in *BeppoSAX* data seemed to slightly revise the distance towards the source thus relaxing the inclination constraint from the Radio emission slightly, but not dramatically (Iaria et al., 2005).

In the following we present new X-ray spectra obtained recently with the HETGS, which again seem to support a more edge-on interpretation. We also summarize the difficulties as well as advantages of both views, edge-on versus face-on, with respect to the observations so far.

2. THE LONG-TERM LIGHTCURVE

Recently Parkinson et al. (2003) compiled the X-ray lightcurve from archival data of a large variety X-ray

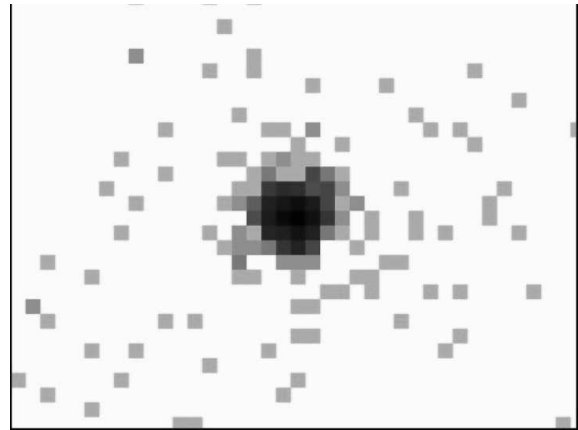


Figure 2. Zero order image of Cir X-1 from obsid 6148. An event filter placed on the zero order point spread function to avoid telemetry overflow allowed to transmit only every 10th photon reducing the effective exposure from 25 ks to 2.5 ks. Each pixel in the image has the size of 0.5 arcsec, the lightest grey is 1 count, the black peak in the middle 83 cts total.

satellites spanning over 30 years between 1968 and 2002. It shows a transient-like behaviour where source activity seemed to quiet down for some period during the early 1980s and its X-ray flux dropped well below 100 mCrab. During this time period Tennant, Fabian, & Shafer (1986) detected the type I X-ray bursts in *EXOSAT* data. Since then the source flux steadily increased to about a flux of 1.5 Crab with intermittent periods of high flaring activity. This high flux was maintained at least throughout the second half of the last decade until the flux started to decline again starting by the year 2000 falling below 100 mCrab in 2005. Whether this long-term behaviour is cyclic needs to be seen, it should be noted, though, that there seems to be a similar decline during the early phases of the archival coverage.

Figure 1 shows the *RXTE* ASM lightcurve that covers the period between 1996 and mid-2005 indicating a steady flux near 100 cts s^{-1} between 1996 and 2000 and the steady decline after that. During the high flux periods the source received massive attention from observers with *ASCA*, *BeppoSAX*, *RXTE*, *Chandra* and *XMM-Newton* (Brandt et al., 1996; Shirey et al., 1999a,b, 2001; Iaria et al., 2001, 2005; Brandt & Schulz, 2000; Schulz & Brandt, 2002). The HETG observation in January 2005 (obsid 6148) was performed during exactly the same orbital phase than the one during June 2000, while it still was at a high flux level. We thus can directly compare spectra of very similar orbital phase between high and low long-term flux levels.

3. THE CHANDRA IMAGE

The observation on January 3rd 2004 showed the source within 0.5 arcsec of the expected position given by (Ar-

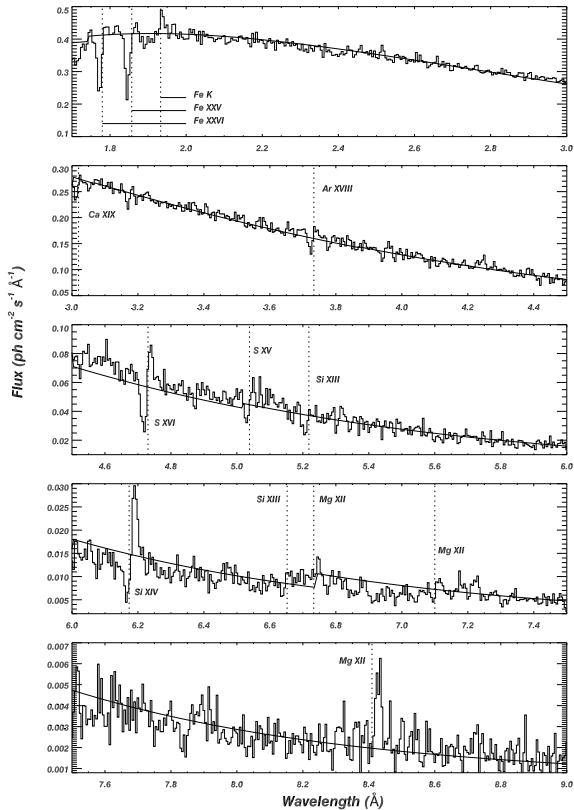


Figure 3. HETG spectrum of Cir X-1 from an observation in 2000 while it still was at its high flux level. The observation was performed during an intensity dip just before the source reached its orbital phase zero (from Schulz & Brandt (2002)).

gue et al., 1984). How well this position confirms the association of Cir X-1 with the faint red counterpart suggested by Moneti (1992) still needs to be seen once a more vigorous analysis of the *Chandra* point spread as well as an *ACIS* subpixel analysis has been performed. The image itself has an effective exposure of 2.5 ks over a period of 25 ks and provides some sensitivity down to $\sim 3 \times 10^{-12}$ erg cm $^{-2}$ s $^{-1}$. Figure 2 shows the image, which is an agreement with a single point source. So far, no significant features within the sensitivity limit are observed.

4. HETGS SPECTRA

The properties of the X-ray lines and their relation with the underlying continuum are rather intriguing and spectra so far have already revealed a great deal of detail (Brandt & Schulz, 2000; Schulz & Brandt, 2002). Figure 3 shows a photon spectrum in the X-ray band between 1.7 Å and 9 Å containing a variety of H- and He-like lines from Mg to Fe. All P Cygni profiles show specific types of variability. The first type is a complex relationship of the equivalent widths of the absorbing as well as the emitting parts of the line profiles with the shape of

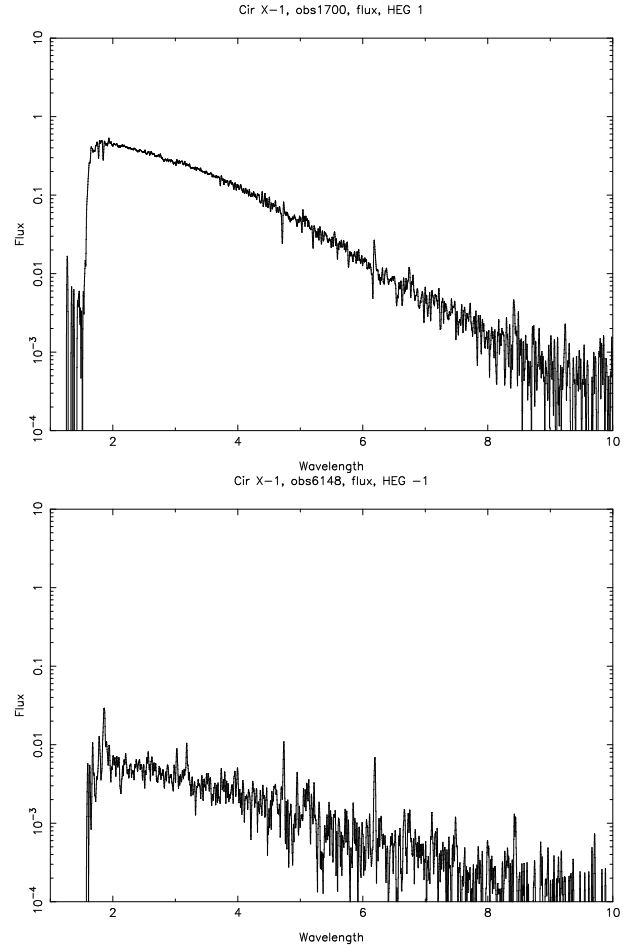


Figure 4. Two HETG spectra taken during the dip just before zero orbital phase. The top spectrum is from the high flux state (obsid 1700), the bottom spectrum from the low flux state (obsid 6148).

the underlying continuum. Schulz & Brandt (2002) interpret this variability as fluctuations in the ionization fraction of the wind triggered by spectral hardness changes of the incident spectrum emitted from the central source on a time scale of ~ 8 hours. A second type of variability is seen around the orbit where the strengths of the profiles diminish with increasing orbital phase. Here very faint lines are seen only during the first half of the orbit, the spectrum is devoid of lines during the rest of the orbit (Galloway, Schulz, & Brandt, 2005).

Figure 4 compares the spectra obtained during the pre-zero orbital phase dip (see Figure 3) at the high flux to the one now obtained during low flux. The source emission between the two observations differs by more than two orders of magnitude. Striking in the low flux case is the absence of P Cygni lines. This, however, only applies to the absorption part. The strengths of the emission lines, on the other hand, is of similar magnitude. In the high flux case, Schulz & Brandt (2002) reported of line strengths for the major H-like ($\text{Ly}\alpha$) lines of Fe, S, and Si values of 3.35 , 6.15 , and 3.14×10^{-4} photons cm $^{-2}$ s $^{-1}$, respectively. Preliminary line fits of the spec-

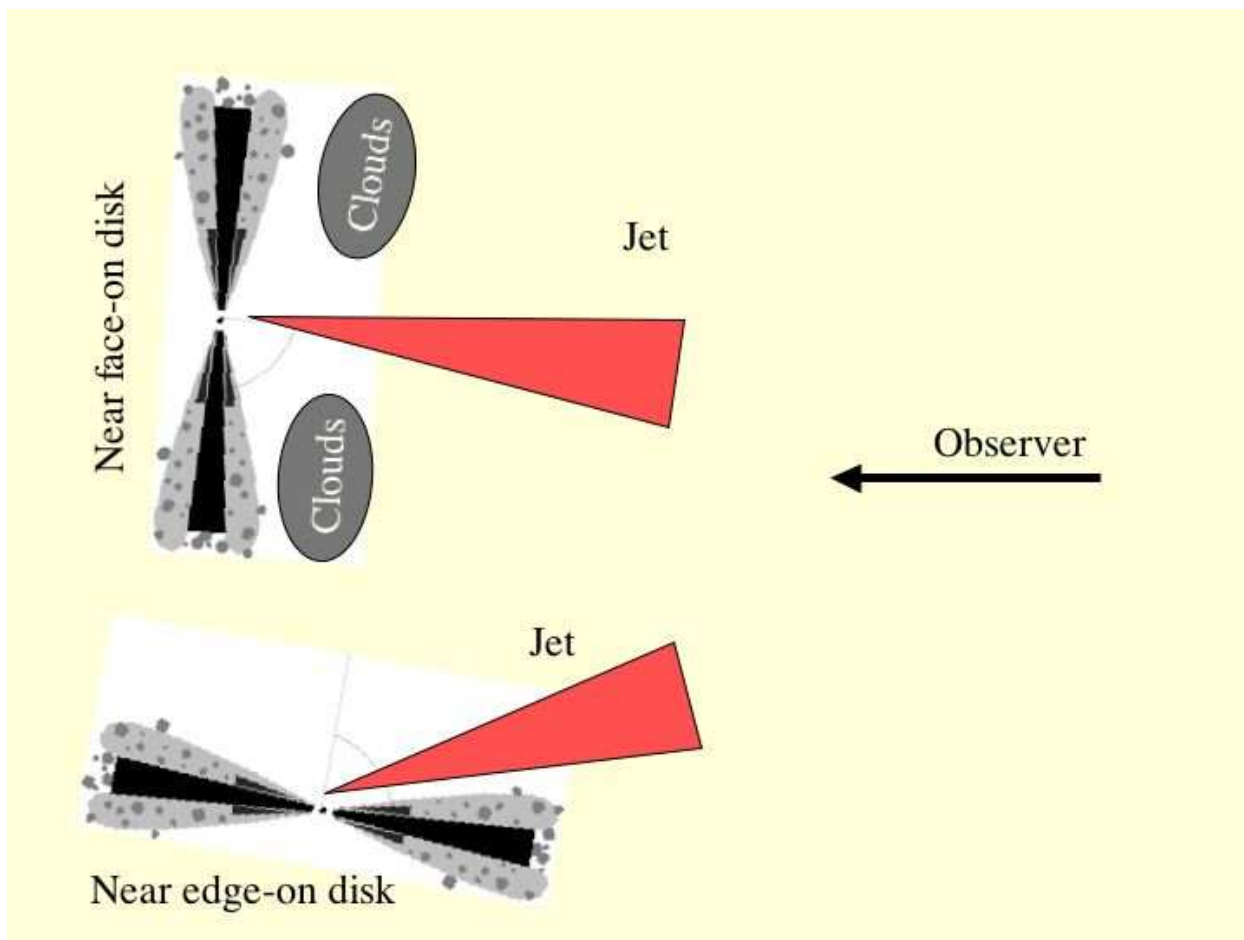


Figure 5. Two possible scenarios involving either a face-on or edge-on view towards the X-ray source in Cir X-1. The face-on view is argued for by the energetics of recent radio jet events. The near edge-on view is favored by X-ray observations.

trum during the low flux produced values of 1.96, 3.59, and 1.91×10^{-4} photons $\text{cm}^{-2} \text{s}^{-1}$ for these lines, respectively. Not only are the flux ratios between these lines remarkably similar, the line fluxes between the two source states are well within a factor of two, whereas the overall source flux changed by two orders of magnitude (see Figure 4). Under the premise that these lines are photoexcited emissions from either the accretion disk itself or some atmospheric layer on top of the accretion disk, this clearly indicates that the illuminating source onto the line emitting region did not change significantly between the two flux states. Consequently, the overall reduction in total luminosity seems more likely a result of absorption or obscuration by material in the line of sight. Brandt et al. (1996) fitted two spectral components to the spectral continuum, both with partial coverage in absorption. One idea for the interpretation of the low flux continuum spectrum is that one or both spectral components exhibit higher absorption or one of the components has vanished entirely. A very preliminary analysis indicates the latter, though more detailed studies of the phenomenon is under way.

5. IMPLICATIONS

The analysis of these new spectra is clearly work in progress and, at this point, we abstain from an in-depth discussion of the nature and detailed physics behind these ionized outflows as much has already been outlined in the introduction. Figure 5 shows cartoons of the two extreme scenarios involving the line of sight towards the X-ray source. Although we do not entirely rule out a solution in between, it is clear that this would render a viable explanation for both, the X-ray emission as well as the energetics of the Radio jets, rather complex.

The near face-on view of the X-ray source (top cartoon in Figure 5) seems favored by the most simplistic solution with respect to the implied jet dynamics observed in the Radio band (Fender et al., 2004). In this case the jet is directly associated with the X-ray flare before the Radio brightening. Viable solutions for the intrinsic jet velocity imply an angle to the line of sight of $< 5^\circ$. In this case the interpretation of the observed X-ray absorption, line emission, and the origin of the P Cygni lines (Brandt & Schulz, 2000) need to be revised. The interpretation of

the blue-shifted ionized line absorption would need to be explained in the context of polar winds as observed in cataclysmic variables. The face-on view also implies a somewhat complex scenario for the observed neutral absorption as well as the line emission as one has to invoke an additional absorber into the line of sight that still provides partial view of the line emitting region. Material ejected from the jet itself seems insufficient as X-ray dips near zero phase are observed even in the case of Radio quietness.

The near edge-on view of the X-ray source (bottom cartoon in Figure 5) provides a rather straight-forward solution for the observed X-ray emissions as here the accretion disk and its atmosphere provide a natural absorber medium. X-ray dips in the lightcurve associated with absorption and broad line emission from accretion disks have mostly been associated with edge-on views of disks, specifically for sources like 4U1822-37 (Cottam et al., 2001) or EXO0748-676 (Jimenez-Garate et al., 2003) to name a few. The spectrum we observed in January 2005 during the source's low flux period clearly falls into this category. Arguments for equatorial winds also emerge from more recent *Chandra* observations of black hole binaries which show similar blue-shifted line absorption as observed Cir X-1 and edge-on views have been established by other means (Miller, 2005). On the other hand, this may leave a fundamental problem with the interpretation that the jet in Cir X-1 is highly relativistic. There are ways around, though they require quite complex solutions. A scenario where the jet itself is not perpendicular to the disk, or may even be strongly bend might come into play as well the realization that the connection between the Radio emergence and the X-ray flares at zero phase is not as straight-forward as being assumed.

Both cases outlined above leave ample room for interpretation and modeling. However, from the X-ray spectra a near edge-on view is clearly preferred. Future analysis should focus on the interplay of absorption in the spectra of various flux states, but also the emission line properties. Throughout these dramatic flux changes, the emission lines near zero phase seem to be the only features that remain relatively unaffected by whatever changes affect the system. Likely originating from the accretion disk they are a valuable diagnostics and are sensitive to geometry such as inclination. Finally, we need to better understand and monitor the X-ray and radio emission, specifically the relation between X-ray flaring and Radio brightness.

ACKNOWLEDGMENTS

Support for this work was provided by the National Aeronautics and Space Administration through the Smithsonian Astrophysical Observatory contract SV3-73016 to MIT for Support of the Chandra X-Ray Center, which is operated by the Smithsonian Astrophysical Observatory for and on behalf of the National Aeronautics Space Administration under contract NAS8-03060.

REFERENCES

- Argue, A. N., Jauncey, D. L., Morabito, D. D. et al. 1984, *MNRAS*, 209, 11
- Begelman, M. C., McKee, C. F., & Shields, G. A. 1983, *ApJ*, 271, 70
- Brandt, W. N., Fabian, A. C., Dotani, et al. 1996, *MNRAS*, 283, 107
- Brandt, W. N. & Schulz, N. S. 2000, *ApJ*, 544, L123
- Canizares, C. R., Davis, J. E., Dewey, D., et al. 2005, *PASP*, 117, 1144
- Chiang, J. 2001, *ApJ*, 549, 537
- Córdova, F. A. & Howarth, I. 1987, in *Exploring the Universe with the IUE Satellite*, ed. Y. Kondo et al. (Dordrecht: Reidel), 395
- Cottam, J., Kahn, S. M., Brinkman, A. C., et al. 2001, *A&A*, 365, 277
- Fender, R., Spencer, R., Tzioumis, T., et al. 1998, *ApJ*, 506, L121
- Fender, R., Wu, K., Johnston, H., et al. 2004, *Nature*, 427, 222
- Galloway, D. K., Schulz, N. S., & Brandt, W. N., *ApJ*, submitted
- Iaria, R., Burderi, L., Di Salvo, T., et al. 2001, *ApJ*, 547, 412
- Iaria, R., Spanò, Di Salvo, T., et al. 2005, *ApJ*, 619, 503
- Jimenez-Garate, M. A., Schulz, N. S., & Marshall, H. L. 2003, *ApJ*, 590, 432
- Kaluziński, L. J., Holt, S. S., Boldt, E. A., & Serlemitsos, P. J. 1976, *ApJ*, 208, L71
- Margon, B., Lampton, M., Bowyer, S., & Cruddace, R. 1971, *ApJ*, 169, L23
- Miller, J. 2005, in *Six Years of Chandra Symposium*, Cambridge, MA, Nov. 2 – 4
- Mirabel, I. F. 2001, *Ap&SS*, 276, 319
- Moneti, A. 1992, *A&A*, 260, L7
- Parkinson, P. M. S., Tournear, D. M., Bloom, E. D., et al. 2003, *ApJ*, 595, 333
- Proga, D. & Kallman, T. R. 2002, *ApJ*, 565, 455
- Raymond, J. C. 1993, *ApJ*, 412, 267
- Shirey, R. E., Bradt, H. V., & Levine, A. M. 1999a, *ApJ*, 517, 472
- Shirey, R. E., Levine, A. M., & Bradt, H. V. 1999b, *ApJ*, 524, 1048

Shirey, R. E. 2001, AAS, 198, 1204S

Stewart, R. T., Caswell, J. L., Haynes R. F., & Nelson,
G. J. 1993, MNRAS, 261, 593

Schulz, N. S. & Brandt, W. N. 2002, ApJ, 572, 971

Tennant, A. F., Fabian, A. C., & Shafer, R. A. 1986,
MNRAS, 221, 27

DISCOVERY AND MODELLING OF DISC PRECESSION IN THE M31 X-RAY BINARY BO 158

R. Barnard¹, S.B. Foulkes¹, C.A. Haswell¹, U. Kolb¹, J.P. Osborne², and J.R. Murray³

¹Department of Physics and Astronomy, The Open University, Walton Hall, Milton Keynes, UK MK7 6AA

²Physics and Astronomy, The University of Leicester, Leicester, UK, LE1 7RH

³Swinburne University of Technology, Australia

ABSTRACT

The low mass X-ray binary (LMXB) associated with the M31 globular cluster Bo 158 is known to exhibit intensity dips on a ~ 2.78 hr period. This is due to obscuration of the X-ray source on the orbital period by material on the outer edge of the accretion disc. However, the depth of dipping varied from $<10\%$ to $\sim 83\%$ in three archival XMM-Newton observations of Bo 158. Previous work suggested that the dip depth was anticorrelated with the X-ray luminosity. However, we present results from three new XMM-Newton observations that suggest that the evolution of dipping is instead due to precession of the accretion disc. Such precession is expected in neutron star LMXBs with mass ratios <0.3 (i.e. with orbital periods <4 hr), such as the Galactic dipping LMXB 4U 1916–053. We simulated the accretion disc of Bo 158 using cutting-edge 3D smoothed particle hydrodynamics (SPH), and using the observed parameters. Our results show disc variability on two time-scales. The disc precesses in a prograde direction on a period of 81 ± 3 hr. Also, a radiatively-driven disc warp is present in the inner disc, which undergoes retrograde precession on a ~ 31 hr period. From the system geometry, we conclude that the dipping evolution is driven by the disc precession. Hence we predict that the dipping behaviour repeats on a ~ 81 hr cycle.

Key words: X-rays: general; X-rays: binaries; Galaxies: individual: M31, Accretion: accretion discs.

1. INTRODUCTION

Bo 158 is source number 158 in the catalogue of globular clusters that were identified in M31 by Battistini et al. (1987). Its X-ray counterpart is located at $\alpha = 00^{\text{h}}43^{\text{m}}14.2^{\text{s}}$, $\delta = 41^{\circ}07'26.3''$ (Di Stefano et al., 2002). Trudolyubov et al. (2002) identified the X-ray source as a likely low mass X-ray binary (LMXB) with a neutron star primary; following their work, we will use the designation “Bo 158” to describe the X-ray source here.

Trudolyubov et al. (2002) report $\sim 83\%$ modulation in the 0.3–10 keV flux of Bo 158 on a 2.78 hour period during the ~ 60 ks 2002 January XMM-Newton observation. The modulation resembles the intensity dips seen in high inclination LMXBs due to photo-electric absorption of X-rays by material that is raised above the body of the accretion disc (White & Swank, 1982). They also report $\sim 30\%$ dips in the 2000, June XMM-Newton lightcurve and $\sim 50\%$ dips in the 0.2–2.0 keV lightcurve of the 1991, June 26 ROSAT/PSPC observation. However, no significant dips were found in the 0.3–10 keV lightcurve of the 2001 June XMM-Newton observation; the authors placed a 2σ upper limit of 10% on the modulation. Trudolyubov et al. (2002) concluded that the depth of the intensity modulation was anti-correlated with the source luminosity.

We present further XMM-Newton observations and modelling results which suggest that the variation in dipping behaviour may instead be due to precession of the accretion disc. Such behaviour is associated with the “superhump” phenomenon that is observed in interacting binaries where the mass ratio of the secondary to the primary is smaller than ~ 0.3 (Whitehurst & King, 1991). Superhumps are briefly reviewed in Sect. 2, followed by details of the observations and data analysis in Sect. 3, and our results in Sect. 4. Numerical modelling of the system is discussed in Sect. 5; the system was simulated by a 3D smoothed particle hydrodynamics (SPH) code. We present our discussion in Sect. 6, and finally our conclusion in Sect. 7.

2. SUPERHUMPS

Superhumps were first identified in the superoutbursts of the SU UMa sub-class of cataclysmic variables. They are manifested as a periodic increase in the optical brightness on a period that is a few percent longer than the orbital period (Vogt, 1974; Warner, 1975). In the model proposed by Osaki (1989), superhumps occur when the outer disc reaches a 3:1 resonance with the secondary. The additional tidal forces exerted on the disc by the secondary

Table 1. Journal of XMM-Newton observations of the M31 core. A1–A3 are available in the public archive, while P4–P6 are proprietary observations. Two observations were made during 2004 July 19; the first observation (a) started at 01:42:12, and the second (b) started at 13:11:22.

Observation	Date	Exp	Filter
A1	2000 Jun 25	34 ks	Medium
A2	2001 Jun 29	56 ks	Medium
A3	2002 Jan 6	61 ks	Thin
P4	2004 Jul 17	18 ks	Medium
P5	2004 Jul 19a	22 ks	Medium
P6	2004 Jul 19b	27 ks	Medium

at this stage cause the disc to elongate and precess, and also greatly enhance the loss of angular momentum, increasing the the mass-transfer rate. The disc precession is prograde in the rest frame, and the secondary repeats its motion with respect to the disc on the beat period between the orbital and precession periods, slightly longer than the orbital period. The secondary modulates the disc’s viscous dissipation on this period, giving rise to maxima in the optical lightcurve, known as superhumps.

The requirement for the 3:1 resonance to fall within the disc’s tidal radius is that the mass ratio of the secondary to the primary be less than ~ 0.33 (Whitehurst & King, 1991). If we assume that the secondary is a main sequence star that fills its Roche lobe, then the relation $m_2 \simeq 0.11 P_{\text{hr}}$ holds, where m_2 is the mass of the secondary in solar units and P_{hr} is the orbital period in hours (e.g. Frank, King, & Raine, 2002). Hence any accreting binary that has a short enough orbital period may exhibit superhumps.

3. OBSERVATIONS AND DATA ANALYSIS

In addition to the three XMM-Newton observations analysed by Trudolyubov et al. (2002), we conducted a programme of four ~ 20 ks observations over 2004, July 16–19. We present results from our analysis of the archival data, along with three of the four 2004 observations; the other observation suffered from flaring in the particle background over 90% of the observation and is not considered further here. A journal of observations is presented in Table 1.

We analysed data from the pn, MOS1 and MOS2 instruments, which share the same $30'' \times 30''$ field of view. For each observation, we selected a circular extraction region with a $40''$ radius, centred on Bo 158, and an equivalent source-free region for the background. The background region was on the same chip as the source, and at a similar angular offset from the optical axis. We extracted lightcurves from the source and background regions in the 0.3–10 keV energy band with 2.6 s binning, and also obtained pn spectra of the source and background regions

along with the associated response files. The spectra were then grouped for a minimum of 50 counts per bin.

4. RESULTS

The 0.3–10 keV EPIC (MOS1 + MOS2 + pn) lightcurves of Observations A1–A3 are presented in Fig. 1, with x- and y- axes set to the same scale, and with 200 s binning. Most striking is Observation A3, with six dipping intervals on a 10017 ± 50 second period (Trudolyubov et al., 2002); the structure of the dipping is seen to vary substantially even over one observation of 60 ks. We emphasise that the 30% dipping reported by Trudolyubov et al. (2002) for observation A1 is an overall average; a deep dip is seen at ~ 28 ks into the observation, but very little evidence of dipping is observed in the intervals of expected dipping at ~ 8 ks and ~ 18 ks into the observation. In this regard, Observation A1 resembles the 1985, October lightcurve of the Galactic superhumping LMXB 4U 1916–053, observed by EXOSAT. In that observation, deep dips are observed only after the first four orbital cycles (Smale et al., 1988). Little evidence of variability is seen in the lightcurve of Observation A2.

In Fig. 2, we present the 0.3–10 keV EPIC lightcurves of Observations P4–P6; the x-axis is scaled to P6, and the y-axis matches that of Fig. 1. The most prominent feature is the dip in P5; it has a depth of $\sim 100\%$ and a total duration of ~ 2500 s. Using the period of Trudolyubov et al. (2002), we identified the expected times of dipping, labelled ‘D’, in P4 and P6, using the deepest part of the dip in P5 as phase zero.

In the P4 lightcurve, there is no evidence for dipping during the first expected dip interval, but some evidence of dipping ~ 4000 s after the second interval, 20 cycles away from the dip in P5. Hence, this possible dip would require a period that is either ~ 200 s shorter or ~ 320 s longer than the 10017 s given by Trudolyubov et al. (2002). However, there is no other evidence for these other periods in the lightcurves of P4, P5 or P6; hence it is clear that the dipping behaviour of Bo 158 evolves on a time scale of a few days.

Several spectral models were fitted to the 0.3–10 keV pn spectrum of P4, each suffering absorption by material in the line of sight. P4 was chosen because it had the longest interval of persistent emission that was not contaminated by background flares; the resulting source spectrum contained ~ 2200 counts. We applied the two models that Trudolyubov et al. (2002) used to model the spectra of A1–A3, namely a power law model and a Comptonisation model (COMP TT in XSPEC). We also applied a two component model. The emission of many Galactic LMXBs has been successfully described by a model consisting of a blackbody and a cut-off power law (e.g. Church & Bałucińska-Church, 1995; Church et al., 1998; Barnard et al., 2003); we approximate this model to a blackbody + power law model, because of the narrow pass-band.

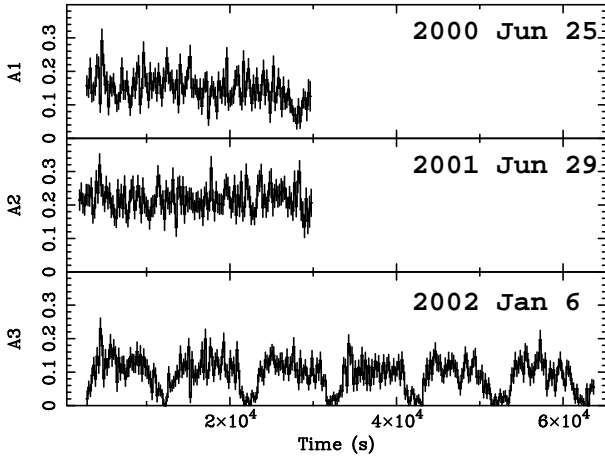


Figure 1. Combined EPIC 0.3–10 keV lightcurves (in count s^{-1}) of Bo 158 from the archival XMM-Newton observations, A1–A3; the dates of each observation are shown.

We find that the best fit parameters for the power law and COMPTT models agree well with the values presented by Trudolyubov et al. (2002); however, the two-component model provided the best fit. We find a 0.3–10 keV flux of $\sim 2 \times 10^{-12}$ erg cm^{-2} s^{-1} for all the fits to the P4 data; this gives a 0.3–10 keV luminosity of $\sim 1.4 \times 10^{38}$ erg s^{-1} , assuming a distance of 760 kpc (van den Bergh, 2000).

The depth of dipping in A1 varies from ~ 0 to $\sim 70\%$ with no significant change in the mean intensity, suggesting that the amplitude of dipping is not simply anticorrelated with the source luminosity. Instead, the variation in dipping behaviour may be caused by disc precession. This hypothesis motivated our simulation of the accretion disc in Bo 158, using three dimensional smoothed partical hydrodynamics, discussed in Sect. 5.

The lightcurves of XMM-Newton observations of Bo 158 show no true eclipses; hence, we know that we are not viewing the system edge on. If the disc were tilted with respect to the binary plane, and precessing, then one might expect to observe dips in some part of the disc precession cycle, but not in others. Dipping is observed throughout observation A3; this suggests that the dipping phase in the disc precession cycle lasts $> \sim 60$ ks. The A1 lightcurve covered three intervals of expected dipping, yet only one dip is seen, toward the end of the observation; we suggest that this dip signals the onset of the dipping phase. Contrariwise, P5 and P6 appear to sample the end of the dipping phase, as a dip is observed in P5, yet no dips are seen in P6.

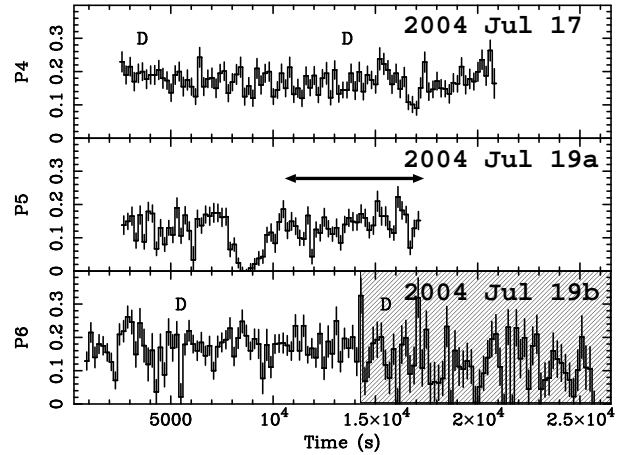


Figure 2. Combined EPIC 0.3–10 keV lightcurves (in count s^{-1}) of Bo 158 from the 2004 XMM-Newton observations, P4–P6; the dates of each observation are shown. The horizontal line in the P5 lightcurve indicated the interval used for spectral fitting. The shaded area of the P6 lightcurve indicates a period of background flaring. Times when dipping is expected are labelled “D”, using the deepest part of the dip in P5 as time zero, and the period of Trudolyubov et al. (2002).

5. SPH SIMULATION OF THE DISC

5.1. Binary Parameters

The accretion disc was modelled using a three-dimensional Smoothed Particle Hydrodynamics (SPH) computer code that has been described in detail in Murray (1996, 1998), Truss et al. (2000), and Foulkes, Haswell, & Murray (2006). We assumed the orbital period to be 10017 s, as obtained by Trudolyubov et al. (2002).

The dipping source Bo 158 is a bright globular cluster X-ray source, with a 2.78 hr binary period. Thirteen Galactic globular clusters contain bright X-ray sources; twelve of these are neutron star LMXBs, while the primary of the other one is unknown (see e.g. in’t Zand et al., 2004). Hence Bo 158 is a likely neutron star LMXB, and we assume the primary mass to be $1.4 M_{\odot}$.

For the secondary, we considered a main sequence star and a white dwarf, since 4U 1916–053 has a likely white dwarf secondary (e.g. Chou et al., 2001). For a Roche lobe-filling main sequence star the approximate relation $m \simeq 0.11 P_{\text{hr}}$ holds (e.g. Frank et al., 2002), giving a mass of $\sim 0.30 M_{\odot}$. If instead the star is a white dwarf, using the mass radius relation of Nauenberg (1972) and Roche geometry gives an implausibly small mass of $0.005 M_{\odot}$. Assuming a main sequence secondary, we found the mass ratio to be 0.2, indicating that superhumps and disc precession were likely.

Finally, the luminosity of the system was taken to be 1.4×10^{38} erg s^{-1} , the 0.3–10 keV luminosity of Bo 158

in Observation P4. Such a high luminosity may be expected to cause warping of the accretion disc, even for a previously flat disc (see e.g. Pringle, 1996); warping is discussed in Sect. 5.3.

The accretion disc had an open inner boundary condition in the form of a hole of radius $r_1 = 0.025a$, where a is the binary separation, centred on the position of the primary object. Particles entering the hole were removed from the simulation. Particles that re-entered the secondary Roche lobe were also removed from the simulation as were particles that were ejected from the disc at a distance $> 0.9a$ from the centre of mass.

We assumed an isothermal equation of state and that the dissipated energy was radiated from the point at which it was generated, as electromagnetic radiation. The Shakura & Sunyaev (1973) viscosity parameters were set to $\alpha_{low} = 0.1$ and $\alpha_{high} = 1.0$, and the viscosity state changed smoothly as described in Truss et al. (2000). The SPH smoothing length, h , was allowed to vary in both space and time and had a maximum value of $0.01a$.

5.1.1. The gas stream

We simulated the mass loss from the secondary by introducing particles at the inner Lagrangian point (L_1). The mass transfer rate and the particle transfer rate were provided as input parameters, and the mass of each particle was derived from these parameters. A particle was inserted with an initial velocity (in the orbital plane) equal to the local sound speed of the donor, c_D , in a direction prograde of the binary axis. The z velocity of the inserted particle was chosen from a Gaussian distribution, with a zero mean and a variance of $0.1c_D$. However, the inflation of the site of collision between the gas stream and outer disc was not modelled.

5.1.2. The initial non-warped accretion disc

The simulation was started with zero mass in the accretion disc and with the central radiation source switched off. A single particle was injected into the simulation every $0.01\Omega_{orb}^{-1}$ at the L_1 point as described above until a quasi-steady mass equilibrium was reached within the disc. This was taken to be when the number of particles inserted at the L_1 point, the mass transfer rate, was approximately equal to number of particles leaving the simulation at the accretor, the accretion rate. The simulations were continued for another 3 orbital periods to ensure mass equilibrium. The number of particles in the simulated accretion disc was approximately 40,000 giving a good spatial resolution; the average number of ‘neighbours’, i.e. the average number of particles used in the SPH update equations, was 8.2 particles. The simulated disc encountered the Lindblad 3:1 resonance and became eccentric. The disc precessed in a prograde direction giving rise to superhumps in the simulated dissipation light-curves (c.f. Foulkes et al., 2004). The radiation source

was then turned on which gave rise to a very small number of particles being ejected from the accretion disc.

5.2. Surface finding algorithm & self-shadowing

Accretion-powered radiation from the inner regions of the disc and the accreting object itself exert a force on the irradiated disc surface. Following Pringle (1996) the radiation source is modelled as a point source at the centre of mass of the accretor. To apply this force, particles on the surface of the accretion disc had to be identified. We used a convex hull algorithm to find the surface particles as described in Murray (1998) and Foulkes et al. (2006). A ray-tracing algorithm was used to determine regions of self-shadow. For each particle found on the disc surface a light-ray was projected from the particle to the position of the radiation source at the centre of the disc. The particle was deemed to be illuminated by the radiation source if this light-ray did not intersect any disc material between the particle surface position and the radiation source (i.e. the particle could see the central radiation source). The radiation force was only applied to particles that were considered to form part of the disc surface and were illuminated by the central radiation source.

5.3. Disc warping and precession measure

For an optically thick disc, a warp can develop as a result of the radiation force (e.g. Pringle, 1996; Ogilvie & Dubus, 2001; Foulkes et al., 2006). This is due to the fact that any radiation absorbed by a specific region on the disc surface will be later re-radiated from the same spot, normal to the disc surface. Hence any anisotropy in the disc structure will cause an uneven distribution of back-reaction forces on the disc surface, further perturbing the disc. A sufficiently high luminosity can induce and sustain a warp even in an originally flat disc (Pringle, 1996, and references therein).

5.4. Numerical modelling results

As a result of the disc precession, viscous stresses in the disc vary significantly with time. The resultant energy dissipation in different regions of the disc, and hence the disc luminosity, varies with time. The disc luminosity was not modelled in detail. We assumed that the luminosity was directly related to the disc regions with significant energy release through viscous dissipation. The viscous dissipation heats the gas in the accretion disc and it is assumed that the heat is radiated away from the point at which it was generated. Superposed on a steady signal there is a repeating series of ‘humps.’ The spacing of the humps corresponds to the superhump period, but are not representative of true optical lightcurves.

In order to determine the superhump period, P_{sh} , we obtained a power density spectrum from ~ 30 superhump

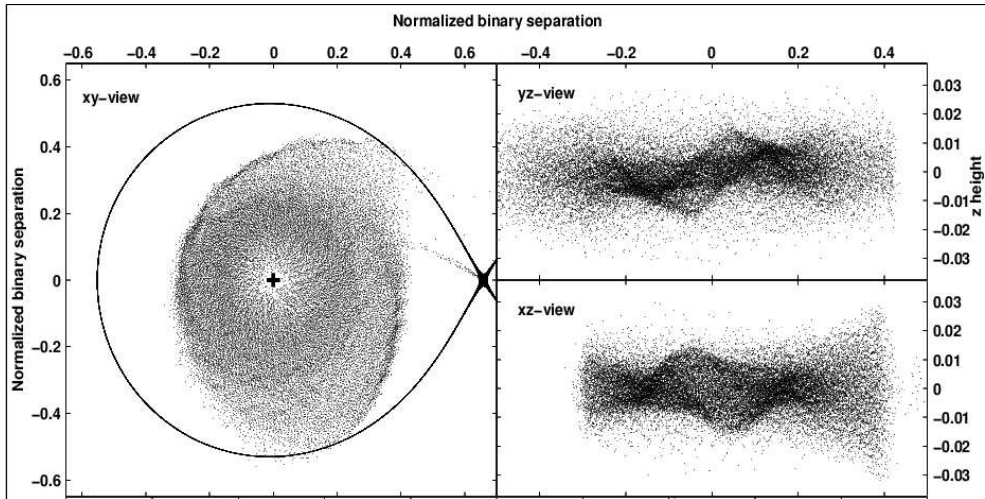


Figure 3. Particle projection plots for the SPH model. The position of each particle is indicated by a small black dot. The left panel is a plan view of the accretion disc as seen from above the disc. The cross at the centre of the plot shows the position of the primary object. The solid dark line is the Roche lobe of the primary and the L_1 point is to the right and middle of the plot. The right panels are particle projection plots on a plane perpendicular to the orbital plane and through the system axis in the xz and yz directions.

cycles of the simulated light curve. We estimated the superhump period to be $(1.035 \pm 0.005)P_{\text{orb}}$. This implies the precession period of the outer regions, $P_{\text{prec}} = (29 \pm 1)P_{\text{orb}}$, or 81 ± 3 hr.

Fig. 3 shows a snapshot from the simulation, from several different angles. The left panel shows an x - y projection of the disc. The disc is clearly asymmetric and elongated, and a spiral density wave is clearly seen. This wave is so intense that it is removing material from the accretion disc and returning it back to the Roche lobe of the secondary; see Foulkes et al. (2004) for a full detailed description of a similar system with a mass ratio of 0.1.

The two upper right-hand plots of Fig. 3, labelled yz -view and xz -view, are side views of the disc in the y - z and x - z directions respectively. The disc warp is clearly apparent in these two plots. The warp is odd symmetrical about the centre of the disc.

The warp amplitude and size precessed as a solid body in a retrograde direction relative to the inertial frame. We found that $P_{\text{warp}} \sim 11 P_{\text{orb}}$. Fig. 4 shows the radial profile of the warp for five consecutive orbital cycles; the maximum extent of the warp is 6 – 11° above the plane of the disc.

6. DISCUSSION

Disc precession is inferred from the 0.3–10 keV lightcurves of Bo 158, as is expected given its extreme mass ratio (short orbital period). As such, it resembles the Galactic superhumping LMXB 4U 1916–053. Since the LMXB Bo 158 is in a globular cluster near the centre of M31, it is unlikely that the optical period will ever be

known. However, our Fourier analysis of the simulated dissipation lightcurves indicates a superhump period that is $3.5 \pm 0.5\%$ longer than the orbital period. Given the association between the dips and superhump period reported by Retter et al. (2002), the 10017 s period may be the superhump period, in which case, the orbital period would be $\sim 4\%$ shorter. Such shortening of the period would not dramatically affect the outcome of our SPH modelling.

Our simulations of the disc show two distinct types of variability in the disc structure. First is the elongation and prograde precession of the disc due to tidal interactions with the secondary at the 3:1 resonance; the disc precesses on period of 81 ± 3 hr. We also see warping of the accretion disc, driven by irradiation of the disc surface by the central X-ray source; the warp is stable exhibits retrograde precession on a ~ 31 -hr period.

It is therefore important to establish which region is responsible for the observed variation in dip morphology. The lightcurves of observations A1–P6 show no eclipses. From Kepler’s law and the ratio of the secondary ratio to the binary separation (Eggleton, 1983), the secondary has an angular radius of $\sim 15^\circ$; hence the inclination $> \sim 75^\circ$. We see from Fig. 6 that the disc warp does not deviate from the plane of the disc by more than 11° in our simulations, suggesting that the observed dips are likely to evolve on the disc precession period.

7. CONCLUSIONS

We have analysed three new XMM-Newton observations of the M31 dipping LMXB Bo 158, in addition to re-analysing the three observations discussed in Tru-

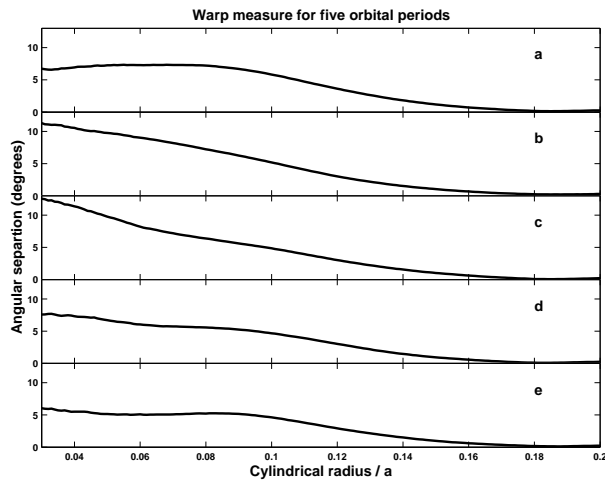


Figure 4. Radial warp profiles. The vertical axis is the warp amplitude. The horizontal axis is distance from the primary object normalized such that the binary separation is 1. Plots (a), (b), (c), (d) and (e) are for five consecutive orbital cycles.

dolyubov et al. (2002). The newer observations spanned ~ 3 days in 2004, July. We find that that the relationship between source intensity and depth of dipping is not so simple as described by Trudolyubov et al. (2002). Instead, we believe that the observed variation in dipping behaviour is caused by precession in the accretion disc; dipping would be confined to a limited phase range in the disc precession cycle.

We modelled the accretion disc with 3D SPH, and found prograde disc precession on a 81 ± 3 hr period, as well as radiatively driven disc warp that precessed on a 31 hr period in a retrograde fashion. We find that the disc precession is most likely to affect the observed dipping behaviour. Hence, we predict that the dipping behaviour of Bo 158 experiences a 81 ± 3 hour cycle; this period is consistent with the observed variation of the dips.

REFERENCES

Barnard, R., Church, M. J., & Bałucińska-Church, M. 2003, *A&A*, 405, 237

Battistini, P., Bonoli, F., Braccesi, A., et al. 1987, *A&AS*, 67, 447

Chou, Y., Grindlay, J. E., & Bloser, P. F. 2001, *ApJ*, 549, 1135

Church, M. J. & Bałucińska-Church, M. 1995, *A&A*, 300, 441

Church, M. J. & Bałucińska-Church, M. 2004, *MNRAS*, 348, 955

Church, M. J., Dotani, T., Balucinska-Church, M., et al. 1997, *Apj*, 491, 388

Church, M. J., Parmar, A. N., Balucinska-Church, M., et al. 1998, *A&A*, 338, 556

Di Stefano, R., Kong, A. K. H., Garcia, M. R., et al. 2002, *ApJ*, 570, 618

Eggleton, P. P. 1983, *ApJ*, 268, 368

Foulkes, S. B., Haswell, C. A., Murray, J. R., & Rolfe, D. J. 2004, *MNRAS*, 349, 1179

Foulkes, S. F., Haswell, C. A., & Murray, J. R. 2006, *MNRAS*, submitted

Frank, J., King, A. R., & Raine, D. 2002, *Accretion Power in Astrophysics*, 3rd Edition (Cambridge University Press)

in't Zand, J., Verbunt, F., Heise, J., et al. 2004, To appear in "The Restless High-Energy Universe" (2nd BeppoSAX Symposium), eds. E.P.J. van den Heuvel, J.J.M. in 't Zand & R.A.M.J. Wijers, *Nucl. Instrum. Meth. B Suppl. Ser.*, astro-ph/0403120

Larwood, J. D. & Papaloizou, J. C. B. 1997, *MNRAS*, 285, 288

Murray, J. R. 1996, *MNRAS*, 279, 402

Murray, J. R. 1998, *MNRAS*, 297, 323

Nauenberg, M. 1972, *Apj*, 175, 417

Ogilvie, G. I. & Dubus, G. 2001, *MNRAS*, 320, 485

Osaki, Y. 1989, *PASJ*, 41, 1005

Press, W. H., Flannery, B. P., & Teukolsky, S. A. 1986, *Numerical recipes. The art of scientific computing* (Cambridge: University Press, 1986)

Pringle, J. E. 1996, *MNRAS*, 281, 357

Retter, A., Chou, Y., Bedding, T. R., & Naylor, T. 2002, *MNRAS*, 330, L37

Shakura, N. I. & Sunyaev, R. A. 1973, *A&A*, 24, 337

Smale, A. P., Mason, K. O., White, N. E., & Gottwald, M. 1988, *MNRAS*, 232, 647

Trudolyubov, S., Borozdin, K. N., Priedhorky, W. C., et al. 2002, *ApJL*, 581, L27

Truss, M. R., Murray, J. R., Wynn, G. A., & Edgar, R. G. 2000, *MNRAS*, 319, 467

van den Bergh, S. 2000, *The galaxies of the Local Group*, Cambridge University Press, Cambridge Astrophysics Series Series, vol no: 35

Vogt, N. 1974, *A&A*, 36, 369

Warner, B. 1975, *MNRAS*, 170, 219

White, N. E. & Swank, J. H. 1982, *ApJL*, 253, L61

Whitehurst, R. & King, A. 1991, *MNRAS*, 249, 25

THE EXTENDED SOFT X-RAY EMISSION REGIONS IN THE LMXB EXO 0748–676 AND AND THE CV UX UMA: GEOMETRIC CONSTRAINTS

K. Mukai

Exploration of the Universe Division, NASA/Goddard Space Flight Center, Greenbelt, MD 20771, USA and Universities Space Research Association

ABSTRACT

XMM-Newton observations have established the simultaneous presence of deeply eclipsed hard X-ray emissions and uneclipsed soft X-rays in the LMXB EXO 0748–676 and in the CV UX UMa. The eclipses in hard X-rays, as well as those in the optical and the UV, constrain the system geometry. This, in turn, can constrain the location and the size of the soft X-ray emitting region. We have explored spherical and cylindrical emission regions and identify two possible solutions for the geometry. In one, the soft X-ray region is larger than the binary, and hence does not suffer a significant eclipse. In the other solution, the emission region is relatively compact. In this solution, a large part of the soft X-ray emission region, the part which would suffer an eclipse, is permanently hidden from our view by the vertically extended structure of the accretion disk. Only the emission from the far side of the disk, which is not subject to an eclipse, reaches the observers above the disk rim.

Key words: Eclipse; Accretion Disk Corona.

1. INTRODUCTION

The study of accretion disks and associated phenomena around protostars, compact stellar objects, and supermassive black holes are a central theme of X-ray astronomy. From a multi-wavelength perspective, accretion disks are most easily observed in nearby binary systems, such as cataclysmic variables (CVs) in which a white dwarf accretes from a late-type companion. The observations of eclipsing CVs can be used to put a tight constraint on the shapes and the temperature distributions of their disks, which often are the main source of the UV/optical light. Detailed optical observations of CVs, combined with innovative techniques such as eclipse mapping and Doppler tomography, were essential in validating the standard model of optically thick, geometrically thin accretion disks. This Shakura-Sunyaev model provides the basic

framework that can be used to explain what happens *in* an accretion disk.

However, much happens *above* an accretion disk. For example, observed power-law X-ray continua of AGN do not come from the surface of their accretion disks, which are too cool to generate X-rays (except, perhaps, some soft excess well below 1 keV). Instead, these soft photons are Compton up-scattered in hot coronae. There are different theories as to where these coronae are located and how exactly they are heated, and existing observations cannot discriminate among them. The geometry of the corona, in turn, is a key ingredient in modeling the relativistic Fe $K\alpha$ line from the AGN disks, the exact parameters of which have been subject of lively debate in recent years. Similar Comptonized continuum are also known in X-ray binaries (both black hole and neutron star systems).

When a binary system displays an eclipsed X-ray component and an uneclipsed X-ray component, the latter must be extended. Although a unique solution of its geometry cannot be obtained from an uneclipsed light curve, a family of solutions may be. One can combine this with consideration of its X-ray spectrum and the energy budget to gain insight into the physics of accretion above the disk plane. In this paper, we report on the possible geometry of soft X-ray emission regions in the LMXB, EXO 0748–676, and the CV, UX UMa.

2. EXO 0748–676: DISCOVERY TO XMM-NEWTON OBSERVATIONS

The low-mass X-ray binary (LMXB) EXO 0748–676 was discovered with *EXOSAT* as a new transient in 1985, and is an eclipsing, dipping, and bursting source (Parmar et al. 1986). The presence of type I X-ray bursts establishes the accreting object as a neutron star. The eclipses recur on the 3.82 hr orbital period; the mass donor (estimated to be a $\sim 0.45 M_{\odot}$ star) must therefore eclipse the neutron star and the inner accretion disk, where the bulk of the X-rays are believed to originate. The dips recur on

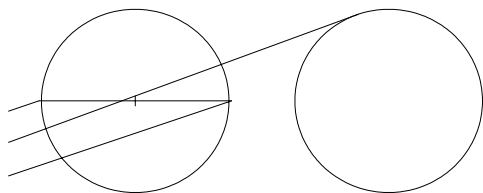


Figure 1. A schematic view of a possible geometry. The circle on the right represents the secondary; the circle on the left represents an X-ray emission region of the same size. The horizontal line through the latter represents the accretion disk; the shadows cast by the secondary, as well as the disk, are represented by the diagonal lines.

the same 3.82 hr period but are variable in details from orbit to orbit, and thought to be caused by azimuthal structures of the accretion disk. The phasing of dips relative to the eclipse implicates the impact of the mass transfer stream on the accretion disk as a likely cause of the structures.

Bonnet-Bidaud et al. (2001) presented their analysis of the early *XMM-Newton* observations of this object. A key discovery is that, while the hard ($E > 2$ keV) X-rays are indeed eclipsed, a significant fraction of the soft ($E < 2$ keV) X-rays remains uneclipsed. Strong, flare-like variability in the soft band is observed well outside the eclipse phases, making a quantitative measurement of the eclipse fraction somewhat subjective. Nevertheless, Bonnet-Bidaud et al. concluded that the emitting region was significantly greater than the companion star.

Homan et al. (2003) present further *XMM-Newton* observations of EXO 0748–676. They find that a clear soft eclipse is seen in some observations, but not in others. They argue, moreover, that the pronounced variability in the soft band should be seen as dips. Dips are deeper and cover wider phase intervals at lower energies, to such an extent that the dip-free intervals are rare and catch the eyes as “soft flares.” If an eclipse happens during a dip-free interval, then soft X-rays are eclipsed. The soft emission that is visible even during deep dips have an extended origin and is not eclipsed by the companion.

3. UX UMA: UV/OPTICAL PHOTOMETRY AND XMM-NEWTON RESULTS

The cataclysmic variable (CV) UX UMa is the brightest eclipsing nova-like system in the optical and in the ultraviolet, with an orbital period of 4.72 hr. The eclipse mapping method has been used on high quality optical and UV data (see, e.g., Baptista et al. 1995) to infer the temperature distribution of the accretion disk in UX UMa, which appears consistent with theoretical expectation for a steady-state, high accretion rate disk. While it is clear

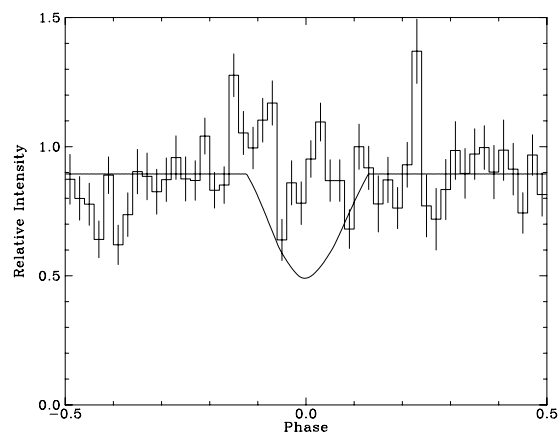


Figure 2. Comparison of observed and simulated light curves. The histogram with error bars is the folded *XMM-Newton* soft-band light curve of UX UMa. The smooth line is the partial eclipse predicted by the geometrical model sketched in Figure 1.

that the eclipse of the inner disk is seen, there are conflicting claims as to whether the eclipse of the white dwarf itself is seen in its UV light curves (Baptista et al. 1995; Froning et al. 2003).

Despite the deep eclipses in the optical and the UV, no eclipse was detected in the *ROSAT* observations (Wood et al. 1995). Pratt et al. (2004) observed UX UMa with *XMM-Newton* in 2002 June, in part to confirm this earlier result. Their spectral and timing analysis show that the X-ray emissions from UX UMa consist of two components. One is a newly discovered hard component that is heavily absorbed. Their spectral analysis suggests that this component contributes little counts below 2 keV. The other is the soft component that is consistent with the *ROSAT* detection, unabsorbed, and contributes only a small fraction of the counts above 3 keV.

Moreover, Pratt et al. have discovered an eclipse of the hard component, while confirming the lack of eclipse of the soft component. The hard component presumably originates from the vicinity of the accreting white dwarf. The soft component must originate in an extended structure to remain uneclipsed. In this respect, the CV UX UMa is strikingly similar to the LMXB EXO 0748–676.

4. GEOMETRICAL CONSTRAINTS

We begin with the schematic shown in Figure 1. In this, the soft X-ray emission region is assumed to be a sphere whose radius is identical to that of the secondary (also approximated by a sphere). It is immediately obvious that such a geometry should result in a significant partial eclipse. The geometry in both EXO 0748–676 and UX UMa is such that the central object (represented by

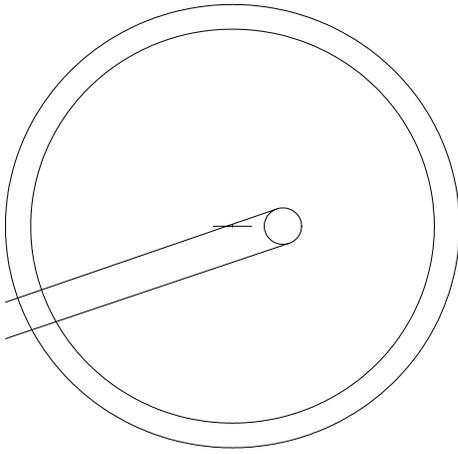


Figure 3. A schematic view of a very extended emission region. The central binary is represented by the small circle (for the secondary) and a flat accretion disk. In this scenario, an extended shell (represented by the large circles) scatters the soft X-ray photons from a central source into our line of site.

a small cross) is eclipsed, which naively would predict a deep, though partial, eclipse of the soft X-ray component as well. Even when we take the shadowing by the accretion disk into account — this would permanently hide a fraction of the lower half of the region from our view — we should still see a partial eclipse. We have simulated the light curve expected for a geometry sketched in Figure 1 (and several like it, changing only the radius of the emission region), and show a comparison with the observed *XMM-Newton* soft-band light curve of UX UMa. Clearly, we do not see the partial eclipse that is predicted by this model.

4.1. A Very Extended Solution

It is possible to create an uneclipsed component by invoking a shell that is larger than the entire binary (Figure 3). In this geometry, a small fraction of the shell is always eclipsed by the secondary; this fraction varies somewhat from phase to phase, because the secondary is off-center (the shell is assumed to be centered on the compact object), but such a variation is small enough to be undetectable. We have explored a range of cylindrical emission regions and reach a similar conclusion: the emission region must be larger than the binary to escape an eclipse.

Such a model is used to explain the uneclipsed EUV component in similar systems. Notably, Mauche & Raymond (2001) have successfully modeled the EUV spectrum of the dwarf nova OY Car in superoutburst as due to scattering of the central source by the accretion disk wind. In this case, the EUV line width (FWHM $\sim 1\text{\AA}$), which is similar to those of the UV (accretion disk wind) lines, is a strong evidence in favor for this model.

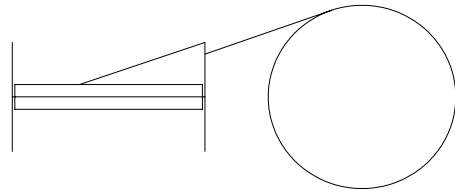


Figure 4. A schematic view of a compact emission region that would nevertheless be uneclipsed. In addition to the secondary, the accretion disk with an outer “wall” restricts our view of the soft X-ray emission region, which is depicted as cylindrical slabs above and below the disk. The outer wall hides a large part of the soft X-ray emitting region, including all the areas that would be eclipsed by the secondary.

In fact, Pratt et al. (2004) also adopted this solution for the soft X-ray component in UX UMa. Further considerations reveal a problem of energetics, however: the soft X-ray emission from the compact object in UX UMa is probably not strong enough for this explanation to work. The extrapolation of the absorption-corrected hard X-ray component is insufficient. The EUV component that powers the wind-scattered component in OY Car is too soft, and is not expected to be bright above 0.5 keV. Further argument against this interpretation for CVs can be found in Wheatley & Mauche (2005; see also Wheatley, this volume).

In the case of EXO 0748–676, the *Chandra* HETG observations show that the lines have modest widths (750 km s^{-1} ; Jimenez-Garate et al. 2003). Such a modest width argues against an accretion disk wind origin. Moreover, the soft X-ray emitting plasma strongly resembles the intrinsic absorber in our line of sight to the central object (Cottam et al. 2001). Thus, the soft X-ray emission region in EXO 0748–676 is probably very close to the accretion disk. How can this be reconciled with the lack of an eclipse?

4.2. A Compact Solution

As it turns out, there is a solution that involves a relatively compact emission region. For this model to work, we only require a structure that hides all regions that are subject to an eclipse by the secondary. In our final sketch (Figure 4), this is represented by a wall at the outer edge of the accretion disk. In fact, we know something like this wall must exist both in EXO 0748–676 and in UX UMa: the hard X-rays suffer strong intrinsic absorption in both systems. This “wall” is thick enough to absorb all soft X-rays ($<2\text{ keV}$) but let through the harder X-rays. We postulate a cylindrical emission region, a large fraction of which remains hidden from our view by this wall.

The remaining, observable part of the emission region is

then never eclipsed. It also represents a small fraction of the total. Assuming a sensible set of symmetries, only the far side of the region above the disk remains visible, so we observe at most 25% of the intrinsic soft X-ray emission.

We have little direct constraint on the detailed shape of the wall or of the emission region. It is probably more natural to think in terms of a strongly flared disk (the flared edge playing the role of the wall) with something like an accretion disk corona. For the moment, we content ourselves with a simple sketch shown in Figure 4.

5. DISCUSSION

The above, more compact, geometry almost certainly applies to EXO 0748–676. The wall, in this case, is the dip-causing structure. During *XMM-Newton* observations, the soft X-ray emission from the central region is dipped out except during certain orbital phases. There is an extended soft X-ray emission region, but interior to the dip-causing structure, that is the origin of the un-dipped, un-eclipsed soft X-ray emission.

This geometry is also consistent with all the available X-ray data on UX UMa. We do not have a conclusive evidence for this interpretation yet, however. A long observation with a *XMM-Newton* or *Chandra* grating instrument can provide the kinematic constraint and will allow us to choose between the very extended and the relatively compact geometries.

If we can prove that the latter is true in UX UMa, that would have important implications. First, CVs — whose accretion disks are generally considered too cold to be X-ray sources — do indeed emit X-rays from the outer accretion disk. This component may also contribute to the observed X-rays from non-eclipsing CVs, so the previous X-ray spectral fits may need to be re-interpreted.

Second, it would imply that an accretion disk around a white dwarf is capable of elevating and heating materials to X-ray emitting temperatures. If so, this is likely to be an intrinsic property of the accretion disk, unrelated to the nature of the compact object. Perhaps all accretion disks generate an accretion disk corona (ADC). In the outer regions of a CV disk, the ADC simply emits soft, thermal X-rays. Deeper in a gravitational potential well, the predominant cooling mechanism of the same ADC might switch to Comptonization of soft, seed photons. In the outer part of a neutron star or a black hole accretion disk, the energetics of the ADC will be dominated by irradiation instead.

However, this remains a speculation at the moment. We believe that further observations of extended soft X-ray emissions in CVs, away from the contaminating influence of neutron stars or black holes, will play an essential role in our understanding of accretion flow well above the disk plane.

ACKNOWLEDGMENTS

I thank Pete Wheatley and Chris Mauche for many stimulating comments regarding the uneclipsed components in deeply eclipsing CVs.

REFERENCES

- Baptista, R., Horne, K., Hilditch, R.W., Mason, K.O. & Drew, J.E. 1995, *ApJ*, 448, 395
- Bonnet-Bidaud, J.-M., Haberl, F., Ferrando, P., Bennie, P.J. & Kendziorra, E. 2001, *A&A*, 365, L282
- Cottam, J., Kahn, S.M., Brinkman, A.C., den Herder, J.W. & Erd, C. 2001, *A&A*, 365, L277
- Froning, C., Long, K.S. & Knigge, C. 2003, *ApJ*, 584, 433
- Homan, J., Wijnands, R. & van den Berg, M. 2003, *A&A*, 412, 799
- Jimenez-Garate, M.A., Schulz, N.S. & Marshall, H.L. 2003, *ApJ*, 590, 432
- Mauche, C.W. & Raymond, J.C. 2001, *ApJ*, 541, 924
- Parmar, A. White, N.E., Giommi, P. & Gottwald, M. 1986, *ApJ*, 308, 199
- Pratt, G.W., Mukai, K., Hassall, B.J.M., Naylor, T. & Wood, J.H. 2004, *MNRAS*, 348, 49
- Wheatley, P.J. & Mauche, C.W. 2005, *ASP Conf. Ser.* 330, 257
- Wood, J.H., Naylor, T. & Marsh, T.R. 1995, *MNRAS*, 274, 31

EPIC-PN OBSERVATIONS OF CYGNUS X-1

J. Wilms¹, E. Kendziorra², M.A. Nowak³, K. Pottschmidt⁴, F.W. Haberl⁵, M. Kirsch⁶, and S. Fritz²

¹Department of Physics, University of Warwick, Coventry, CV4 7AL, United Kingdom

²Institut für Astronomie und Astrophysik, Abt. Astronomie, Universität Tübingen, 72074 Tübingen, Germany

³MIT-CXC, NE80-6077, 77 Massachusetts Ave., Cambridge, MA 02139, USA

⁴Center for Astrophysics and Space Sciences, University of California at San Diego, La Jolla, CA 92093-0424, USA

⁵Max Planck Institut für extraterrestrische Physik, Giessenbachstr., 85748 Garching, Germany

⁶ESA/ESAC, PO Box 50727, 28080 Madrid, Spain

ABSTRACT

In 2004 October and November we observed the black hole candidate four times with *XMM-Newton*'s EPIC-pn camera and simultaneously with the Rossi X-ray Timing Explorer (*RXTE*) and *INTEGRAL*. We present preliminary results on the analysis of the X-ray spectrum and on the source variability, presenting the highest signal to noise ratio data of the Fe $K\alpha$ region of the source ever obtained.

Key words: Black Hole Physics, Cygnus X-1.

1. INTRODUCTION: SCIENCE FROM BRIGHT SOURCES

While a large amount of *XMM-Newton*'s observing time is devoted to the study of faint objects at high z or of X-ray binaries in other galaxies, observations of bright, i.e., high countrate, X-ray sources are nevertheless crucial for our detailed understanding of the physics of many of these objects. It is only with very high signal to noise data from such sources that we can study the physics of accretion to the level needed for understanding the phenomenology of fainter sources.

Many of the questions currently asked in the study of Active Galactic Nuclei (AGN), for example, are very similar to those also asked in the framework of Galactic black hole binaries (BHBs), and often studying both types of systems results in complementary information. For both, AGN and BHBs, the structure of the accretion flow close to the central black hole is still unclear. Current models range from those that explain the broad band spectrum in terms of a patchy Comptonizing electron plasma (the ‘‘accretion disk corona’’) sandwiching a more or less thin accretion disk, perhaps with an inner hot region (e.g., Dove et al., 1997; Petrucci et al., 2001; Zdziarski et al.,

2003; Coppi, 2004), to those suggesting that the X-rays are due to emission from hot spots sitting ‘‘above’’ the black hole (Henri & Petrucci, 1997; Martocchia et al., 2002). It has recently been suggested that these hot spots could be forming the base of the radio jets now observed in these systems, and that possibly the whole X-ray continuum is due to the jets (Markoff et al., 2003, 2005).

In this contribution, we concentrate on two observational tools that could shed more light on the accretion geometry:

1. High signal to noise observations of spectral signatures which depend on the physical processes at work close to the black hole are often sensitive to the accretion geometry. The most promising of these signatures are relativistically broadened Fe $K\alpha$ lines (e.g., Reynolds & Nowak, 2003; Wilms et al., 2001; Fabian et al., 2000). The shape of the lines depends on the observer's viewing angle with respect to the accretion disk, the Fe $K\alpha$ emissivity of the accretion disk, and the angular momentum of the black hole. The different accretion geometries discussed above therefore result in different line profiles (e.g., Dovčiak et al., 2004), which could be detected in data with a high enough signal to noise ratio.
2. Accreting black holes show variability on all time scales, with Galactic sources having strong (30% rms) short term variability out to >100 Hz in their hard state. The nature of the variability can again be used to constrain the geometry of the accretion flow (Churazov et al., 2001; Uttley et al., 2005, and therein). For example, in hard state BHBs a time lag between hard and soft X-rays is observed, which is on the order of $\gtrsim 0.01$ s for light curves centred on ~ 2 keV and ~ 10 keV (Pottschmidt et al., 2000; Nowak et al., 1999b). This X-ray lag is strongly dependent on the source state, with lags in transitional states between the hard state and the (accretion disk dominated) soft state being significantly larger than what is seen in the hard and soft state (Pottschmidt et al., 2000, 2003;

Table 1. EPIC data modes (after Ehle et al. 2005).

	Time res.	Live time [%]	Max. cps	mCrab
MOS				
Full frame (600×600)	2.6 s	100.0	0.70	0.24
Large window (300×300)	900 ms	99.5	1.8	0.6
Small window (100×100)	300 ms	97.5	5	1.7
Timing uncompressed (100×600)	1.5 ms	100.0	100	35
pn				
Full frame (376×384)	73.4 ms	99.9	8	0.9
Ext. full frame (378×384)	200 ms	100.0	3	0.39
Large window (198×384)	48 ms	94.9	12	1.3
Small window (63×64)	6 ms	71.0	130	14
Timing (64×200)	30 μ s	99.5	1500	160
Burst (64×180)	7 μ s	3.0	60000	6300

Kalemci et al., 2003). The magnitude of the time lag and its frequency dependence are such that they can not be explained, e.g., by invoking the diffusion time scale due to Compton scattering in the accretion disk corona (Nowak et al., 1999b), but rather consistent with what one would expect for typical jet sizes (similar lags in AGN, however, seem to be consistent with Comptonization).

All of the (potential) diagnostics discussed above require very high signal to noise data of high time resolution, if possible combined with good energy resolution. These requirements imply observations of bright sources, with an instrument of sufficiently high effective area, and with at least Silicon energy resolution.

Due to the presence of a relativistic Fe $K\alpha$ line (Miller et al., 2002), its strong and energy dependent X-ray variability (Nowak et al., 1999a,b), and its well understood long term variability from the *RXTE* monitoring performed by our group (Wilms et al., 2005), a prime candidate for such studies is the Galactic black hole Cygnus X-1. Using *XMM-Newton*, *RXTE* and *INTEGRAL*, in 2004 Oct/Nov we therefore performed a set of four 10–20 ksec long observations of Cyg X-1, making full use of the high signal to noise provided by the instrument above ~ 3 keV. Until the end of 2004, Cyg X-1 was in *XMM-Newton*'s Earth avoidance zone, such that the observations presented here are amongst the first *XMM-Newton* observations of Cyg X-1. Here, we give first results of the *XMM-Newton* data, results from the other satellites are presented by Fritz et al. (these proceedings).

2. CYG X-1 WITH XMM-NEWTON: PRELIMINARY RESULTS

2.1. High Time Resolution Observations with XMM-Newton

The EPIC instruments on *XMM-Newton* fulfill the requirements discussed in the last section, and especially the EPIC-pn camera provides a variety of data modes with a time resolution of better than a 100 ms. As shown

in Table 1, however, most of these data modes only allow observations of comparably weak sources. The only mode allowing observations of very bright sources is the EPIC-pn Burst mode. This mode, however, has a very low efficiency with a duty cycle of only 3% and shows strong aliasing at high frequencies (Kuster et al., 1999). While studying broad band variability is possible in the Burst Mode, it is not ideal and 97% of all photons are not detected. The most ideal mode providing a high time resolution is therefore the EPIC-pn Timing Mode. In this mode the CCD is read out continuously, resulting in a very high duty cycle. A drawback, however, is the comparably low maximum source brightness of only 160 mCrab, making sources such as Cyg X-1, with typically ~ 300 mCrab, unobservable.

This threshold count rate is not due to a physical limitation of the detector, however, but is rather due to the telemetry limitation of the *XMM-Newton* spacecraft. By increasing the telemetry allotted to the EPIC-pn it is possible to increase the maximum count rate and thus to decrease the danger of the data handling unit of the instrument switching to counting mode, where the transmission of individual events from the EPIC-pn camera is stopped and only the number of events dropped is transmitted. Since all data modes of the EPIC-MOS cameras are limited to sources with < 35 mCrab, such an increase can be obtained by switching off the MOS without the loss of useful scientific information of the source under study. Despite the increase in available telemetry bandwidth for the EPIC-pn to somewhat over 1000 cps, this approach is not sufficient to allow studies of sources with a few 100 mCrab.

For our *XMM-Newton* observations of Cyg X-1, we therefore suggested using a modified version of the EPIC-pn Timing Mode. As outlined in further detail by Kendziorra et al. (2004), in addition to switching off the EPIC-MOS, we increase the EPIC-pn lower energy threshold for events to be transmitted. Since for many studies of black holes the most interesting information for spectral-temporal studies is found in the > 3 keV band, we increase the lower energy threshold of the Timing Mode from its standard value of 200 eV to 2.8 keV. In this band (and depending on the source state) Cyg X-1

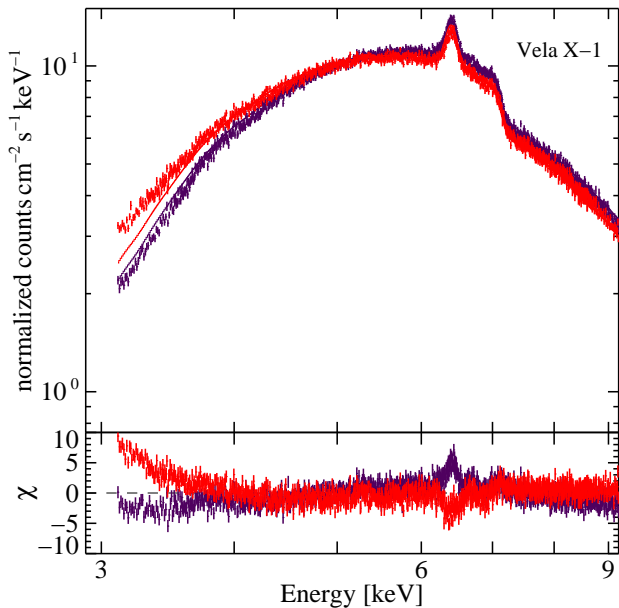


Figure 1. Comparison of a standard EPIC-pn Timing Mode observation of Vela X-1 (dark) with a simulated Modified Timing Mode observation (red/lighter gray), showing the redistribution of events towards lower energies due to the increased lower energy threshold of the Modified Timing Mode.

delivers 500–800 cps. This means that all data measured above the threshold can be transmitted to Earth and that high time resolution, low deadtime measurements can be made in the iron band with Silicon resolution.

2.2. Calibrating the Modified Timing Mode

A problem of increasing the lower energy threshold of the EPIC-pn camera is that a recalibration of the instrument is required. This need arises from the fact that no combination of split events is performed on-board the satellite. Rather, information about the charge deposited by the incoming X-rays in each pixel is transmitted to ground separately and then combined during the first step of the EPIC-pn data analysis. As the lower energy threshold of the EPIC-pn is increased, a larger fraction of the split partners is not transmitted to Earth. Losing these split partners means that the energy reconstruction for double and higher grade events cannot be performed. As a result, the energy resolution of the Modified Timing Mode is slightly reduced and the redistribution of events is changed. Figure 1 shows this effect by comparing the spectrum of Vela X-1 as taken with the standard Timing Mode with a simulated Modified Timing Mode observation, which was obtained by filtering the raw Vela X-1 event data before event recombination and discarding all events with energies below 2.8 keV. Due to the lack of a significant fraction of split partners in the Modified Timing Mode, spectra taken in that mode appear softer since double (and higher grade) events missing their split part-

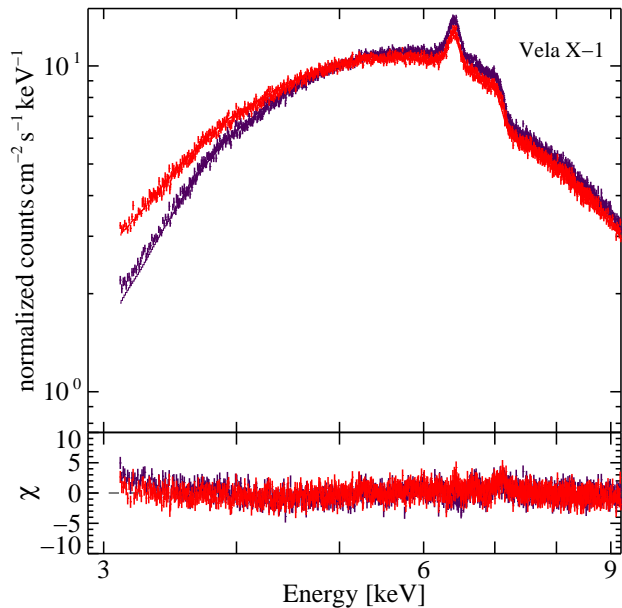


Figure 2. Same data as in Fig. 1, but using a special response matrix for the Modified Timing Mode. The new response matrix accounts for the different sensitivity and the spectral softening introduced by the Modified Timing Mode.

ners now show up as single events with a correspondingly lower energy.

Using the available Timing Mode observations from the *XMM-Newton* archive it is possible to build a new detector response matrix that takes these effects into account. Figure 2 shows the result of fitting the simulated and measured data of Vela X-1 using this new detector response matrix. The matrix accounts for most features introduced by the Modified Timing Mode and the residuals of the Modified and the standard Timing Mode are very similar. Note that no attempt is made in this demonstration to obtain a good fit to the data, e.g., the clear residuals present in the Fe K edge region. The quality of the response matrix is demonstrated, however, by considering that both residuals are very similar (i.e., equally bad).

We conclude that the overall calibration of the Modified Timing Mode is satisfactory, however, there are still some questions remaining. For example, the high count rate in the EPIC-pn leads to an improvement of the charge transfer efficiency (CTE) of the detector compared to dimmer sources, which is not yet taken into account. The absolute energy calibration of the data presented in the following is therefore not yet up to the level of the EPIC-pn standard data modes and all energy values given below could be slightly too high since the standard data reduction pipelines assume a lower CTE and consequently overcompensate during the derivation of pulse height invariant energy values in the case of bright source observations. Furthermore, not all measurements entering the build process of the new response matrix have been completely checked. Due to these reasons, in the following

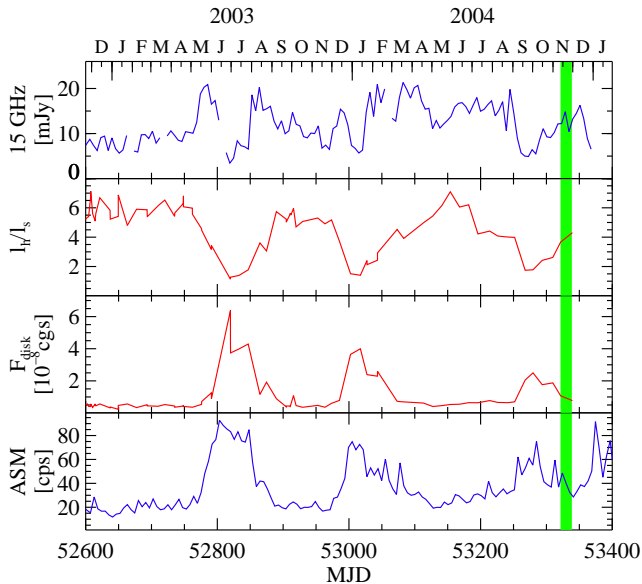


Figure 3. Results from *RXTE* and Ryle radio telescope monitoring of Cyg X-1 in 2003 and 2004, based on Comptonization fits. Shown from top to bottom are the 15 GHz radio flux, the ratio l_h/l_s of the compactness of the accretion disk corona, l_h , and of the accretion disk, l_s , which is a measure for the spectral hardness, the bolometric accretion disk flux, F_{disk} , and the *RXTE*-ASM count rate. The time interval of the *XMM-Newton* observations is shown by the vertical bar.

presentation of first scientific results from Cyg X-1 we will only give very few “hard numbers” and we will refrain from comparing our measurements with the simultaneous *RXTE* and *INTEGRAL* data.

2.3. Cyg X-1: Scientific Results

During our four *XMM-Newton*/*RXTE*/*INTEGRAL* observations, Cyg X-1 was in one of its transitional states between the hard state and the thermally dominated soft state (Fritz, these proceedings). Figure 3 shows the history of the source in the context of the *RXTE* and radio monitoring campaign performed by our group (Wilms et al., 2005; Pottschmidt et al., 2003). This state is very interesting for a further scientific study, since *RXTE* and *Chandra* observations have shown it to be characterized by radio flaring and complex X-ray timing behavior, as well as the presence of a relativistically broadened Fe $K\alpha$ line.

The increased soft X-ray emission during the intermediate state, however, leads to an increased pile-up in the center of the point spread function compared to a pure hard state. In the following analysis we therefore ignored data from the centermost 3 CCD columns. For the case of observation 2 (20/21 Nov. 2004), this means that we ignore 7000000 of the 17000000 events detected above 2.8 keV in this ~ 17 ksec long observation.

As shown in Fig. 4 the signal to noise ratio of the re-

maining data is still sufficient for spectral analysis. Since the raw data clearly show the presence of a narrow line around 6.4 keV, we first model the spectrum outside the 5–8 keV iron band with a power law. Using this continuum, we find that clear residuals remain in the Fe $K\alpha$ region, which can be described by a narrow feature at ~ 6.5 keV plus a further broad feature (Fig. 4). Due to this reason, a power law fit to the whole 4–9 keV spectrum does not result in an acceptable χ^2 .

Modelling the data now with a power law and iron features shows that both, a narrow ($\sigma = 80 \pm 35$ eV) Fe line at 6.52 ± 0.02 keV with equivalent width of 14 eV and a relativistic Kerr line from ionized iron ($E = 6.7 \pm 0.1$ keV) with an emissivity $\propto r^{-4.3 \pm 0.1}$ and an equivalent width of 400 eV are required for a satisfactory description of the data ($\chi_{red}^2 = 1.3$). These parameters are similar to earlier *Chandra* intermediate state observations of a relativistic line in Cyg X-1 (Miller et al., 2002). Differences in the line parameters can be attributed to the dynamic nature of the accretion disk geometry, which is generally taken to be in the process of reconfiguring during the intermediate state. Our *XMM-Newton* observations thus provide independent confirmation for the presence of a relativistic line during the intermediate state.

We stress again, however, that these results are based on a not yet finalized calibration of the Modified Timing Mode. For example, the energy of the line features could be slightly lower than quoted above, due to the overcompensation caused by the improved CTE in bright source. In addition, similarly good fits can also be obtained by adding a strong Fe K-edge, as could be due to strong Compton reflection, to the data, without requiring the presence of a strong and broad line. This result is reminiscent of current discussions about the interpretation of similar strong features in narrow line Seyfert 1 galaxies, which can equally well be described either by reflection dominated spectra or strong relativistic Fe $K\alpha$ lines (Boller et al., 2003; Pounds et al., 2003; Fabian et al., 2004). For the case of Cyg X-1, a final verdict on the nature of the iron features will therefore only be available once the simultaneous *RXTE* and *INTEGRAL* data are added to our spectral analysis.

We finally turn to X-ray time lags as an example for the X-ray timing capabilities of *XMM-Newton*. The left hand side of Fig. 5 shows the X-ray time lag measured in two narrow bands. The X-ray lag is reminiscent of lags determined previously in the intermediate state with *RXTE* in similar bands (Fig. 5, right, see also Pottschmidt et al. 2000), independently confirming the classification of the source state from the spectral data. Compared to proportional counters such as the *RXTE*-PCA, however, the energy resolution possible with Si-based detectors such as the EPIC-pn is much higher. For example, in a preliminary analysis of the energy dependent root-mean-square variability of our data, we find a clear drop in rms in the Fe $K\alpha$ band, akin to similar behavior seen at lower resolution in BHBs and AGN (Markowitz et al., 2003; Życki, 2004, and therein).

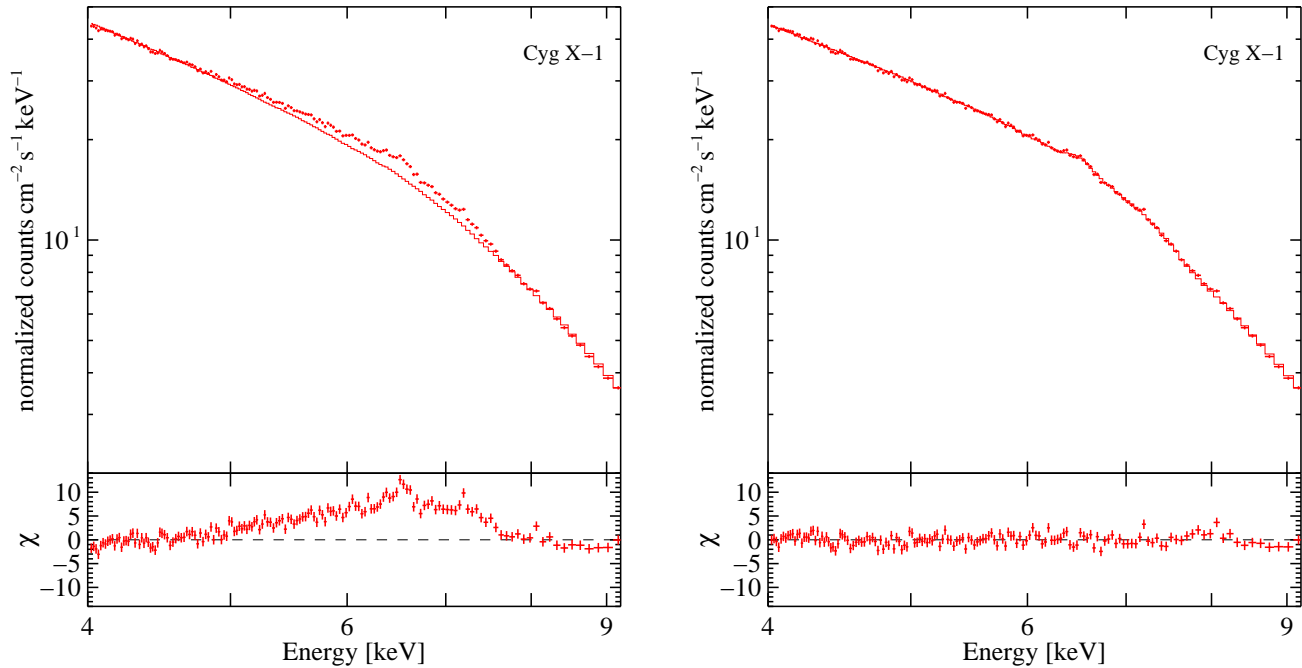


Figure 4. Left: A power-law fit to the EPIC-pn data from obs. 2 measured outside of the 5–8 keV band reveals strong residuals in the Fe $K\alpha$ region, possibly pointing towards the presence of a relativistic line. Right: Same data, but fitting the whole band with a power law and a narrow and a relativistic line.

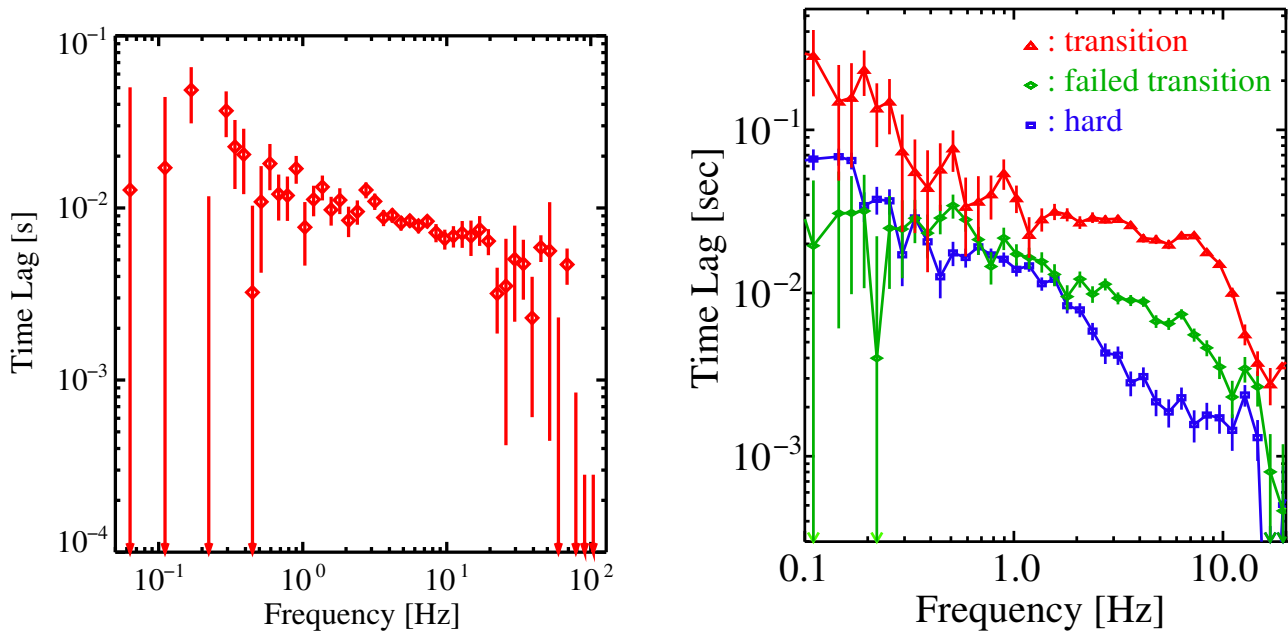


Figure 5. Left: Fourier frequency dependency of the 3.5–5.5 keV vs. 6.0–8.5 keV X-ray time lags obtained for XMM-Newton obs. 2. A positive lag means that the hard X-rays lag the soft ones. Right: 2.5–4 keV vs. 8–13 keV X-ray time lags determined with RXTE for different spectral states of Cyg X-1 (Pottschmidt et al., 2000).

3. SUMMARY AND OUTLOOK

The results presented in the previous sections indicate the significant scientific potential of *XMM-Newton* for studies of the Fe $K\alpha$ band from in bright Galactic sources with the Modified Timing Mode of the EPIC-pn camera. These results include the possible confirmation of the presence of a relativistic Fe $K\alpha$ line during the intermediate state of Cyg X-1. We are optimistic that the remaining issues related to the final calibration of the mode and understanding the pile-up issues, will be solved within the next few months after the submission of this contribution. The final results from the calibration will be made available to the community in the near future.

ACKNOWLEDGMENTS

The observations presented herein were made on behalf of a larger collaboration, which in addition to the authors consists of C. Brocksopp (UCL), P. Coppi (Yale), R.P. Fender (Southampton), M. van der Klis (Univ. Amsterdam), T. Maccarone (Southampton), G.G. Pooley (Univ. Cambridge), N.S. Schulz (MIT), and A.A. Zdziarski (Warsaw). This work is based on observations obtained with *XMM-Newton*, an ESA science mission with instruments and contributions directly funded by ESA member states and NASA. We thank all people who made the observations with the Modified Timing Mode possible. This work has been financed in part by DLR grant 50OR0302.

REFERENCES

Boller, T., Tanaka, Y., Fabian, A., et al. 2003, *MNRAS*, 343, L89

Churazov, E., Gilfanov, M., & Revnivtsev, M. 2001, *MNRAS*, 321, 759

Coppi, P. 2004, in *X-Ray Timing 2003: Rossi and Beyond*, ed. P. Kaaret, F. K. Lamb, & J. Swank, *Am. Inst. Phys., Conf. Ser. 714* (Woodbury: AIP), 79–88

Dove, J. B., Wilms, J., & Begelman, M. C. 1997, *ApJ*, 487, 747

Dovčiak, M., Karas, V., & Yaqoob, T. 2004, *ApJS*, 153, 205

Ehle, M., Breitfellner, M., González Riestra, R., et al. 2005, *XMM-Newton Users' Handbook*, available online at http://xmm.vilspa.esa.es/external/xmm_user_support/documentation/uhb/index.html

Fabian, A. C., Iwasawa, K., Reynolds, C. S., & Young, A. J. 2000, *PASP*, 112, 1145

Fabian, A. C., Miniutti, G., Gallo, L., et al. 2004, *MNRAS*, 353, 1071

Henri, G. & Petrucci, P. O. 1997, *A&A*, 326, 87

Kalemci, E., Tomsick, J. A., Rothschild, R. E., et al. 2003, *ApJ*, 586, 419

Kendziorra, E., Wilms, J., Haberl, F., et al. 2004, in *Proc. SPIE 5488*, 613–622

Kuster, M., Benlloch, S., Kendziorra, E., & Briel, U. G. 1999, in *EUUV, X-ray and Gamma-Ray Instrumentation for Astronomy X*, eds. O. H. Siegmund & K. A. Flanagan, *Proc. SPIE 3765* (Bellingham, WA: SPIE), 673–682

Markoff, S., Nowak, M., Corbel, S., Fender, R., & Falcke, H. 2003, *A&A*, 397, 645

Markoff, S., Nowak, M. A., & Wilms, J. 2005, *ApJ*, in press (astro-ph/0509028)

Markowitz, A., Edelson, R., & Vaughan, S. 2003, *ApJ*, 598, 935

Martocchia, A., Matt, G., & Karas, V. 2002, *A&A*, 383, L23

Miller, J. M., Fabian, A. C., Wijnands, R., et al. 2002, *ApJ*, 578, 348

Nowak, M. A., Vaughan, B. A., Wilms, J., Dove, J. B., & Begelman, M. C. 1999a, *ApJ*, 510, 874

Nowak, M. A., Wilms, J., Vaughan, B. A., Dove, J. B., & Begelman, M. C. 1999b, *ApJ*, 515, 726

Petrucci, P. O., Haardt, F., Maraschi, L., et al. 2001, *ApJ*, 556, 716

Pottschmidt, K., Wilms, J., Nowak, M. A., et al. 2000, *A&A*, 357, L17

Pottschmidt, K., Wilms, J., Nowak, M. A., et al. 2003, *A&A*, 407, 1039

Pounds, K. A., Reeves, J. N., Page, K. L., et al. 2003, *MNRAS*, 341, 953

Reynolds, C. S. & Nowak, M. A. 2003, *Phys. Rep.*, 377, 389

Uttley, P., McHardy, I. M., & Vaughan, S. 2005, *MNRAS*, 359, 345

Wilms, J., Nowak, M. A., Pottschmidt, K., et al. 2005, *A&A*, in press (astro-ph/0510193)

Wilms, J., Reynolds, C. S., Begelman, M. C., et al. 2001, *MNRAS*, 328, L27

Zdziarski, A. A., Lubiński, P., Gilfanov, M., & Revnivtsev, M. 2003, *MNRAS*, 342, 355

Życki, P. T. 2004, *MNRAS*, 351, 1180

SPECTRAL VARIABILITY OF CYGNUS X-1 DURING AN INTERMEDIATE STATE

J. Malzac¹, P.O. Petrucci², E. Jourdain¹, P. Sizon³, M. Cadolle^{3,4}, G. Pooley⁵, C. Cabanac², S. Chaty^{3,6},
T. Belloni⁷, J. Rodriguez^{3,6,8}, J.P. Roques¹, P. Durouchoux³, A. Goldwurm^{3,4}, and P. Laurent^{3,4}

¹Centre d'Etude Spatiale des Rayonnements, (CNRS/OMP/UPS), 31028 Toulouse, France

²Laboratoire d'Astrophysique Observatoire de Grenoble, BP 53 F-38041 GRENOBLE Cédex 9, France

³Service d'Astrophysique, DSM/DAPNIA/SAP, CEA-Saclay, Bat. 709, L'Orme des Merisiers, F-91 191 Gif-sur-Yvette, Cedex, France

⁴APC-UMR 7164, 11 place M. Berthelot, 75231 Paris, France

⁵Cavendish Laboratory, University of Cambridge, Madingley Road, Cambridge CB3 0HE, UK

⁶AIM - Astrophysique Interactions Multi-échelles (Unité Mixte de Recherche 7158 CEA/CNRS/Université Paris 7 Denis Diderot), CEA-Saclay, Bât. 709, L'Orme des Merisiers, F-91 191 Gif-sur-Yvette Cedex, France

⁷INAF - Osservatorio Astronomico di Brera, via E. Bianchi 46, 23807 Merate, Italy

⁸INTEGRAL Science Data Center, Chemin d'Écogia 16, 1290 Versoix, Switzerland

ABSTRACT

We report the results of a simultaneous radio (Ryle telescope) and hard X-ray *INTEGRAL* observation of Cygnus X-1 during an intermediate state. During the 4 day long observation the broad band (3–200 keV) luminosity varied by up to a factor of 2.6 and the source showed an important spectral variability. A principal component analysis demonstrates that most of this variability occurs through 2 independent modes. The first mode consists in changes in the overall luminosity on time scale of hours with almost constant spectra (responsible for 68 % of the variance) We interpret this variability mode as variations of the dissipation rate in the corona, possibly associated with magnetic flares. The second variability mode consists in a pivoting of the spectrum around ~ 10 keV (27 % of the variance). It acts on a longer time-scale: initially soft, the spectrum hardens in the first part of the observation and then softens again. This pivoting pattern is strongly correlated with the radio (15 GHz) emission: radio fluxes are stronger when the *INTEGRAL* spectrum is harder We propose that the pivoting mode represents a 'mini' state transition from a nearly High Soft State to a nearly Low Hard State, and back. This mini-transition would be caused by changes in the soft cooling photons flux in the hot Comptonising plasma associated with an increase of the temperature of the accretion disc. The jet power then appears to be anti-correlated with the disc luminosity and unrelated to the coronal power.

Key words: Gamma-rays: observations – Black hole physics – Radiation mechanisms: non-thermal – X-rays: binaries; radio continuum: stars – X-rays: individual: Cygnus X-1 .

1. INTRODUCTION

Cygnus X-1 is the prototype of black hole candidates. Since its discovery in 1964 (Bowyer et al. 1965), it has been intensively observed by all the high-energy instruments, from soft X-rays to γ -rays. It is a persistent source most often observed in the so-called Low Hard State (hereafter LHS), characterised by a relatively low flux in the soft X-rays (~ 1 keV) and a high flux in the hard X-rays (~ 100 keV). In the LHS, the high-energy spectrum can be roughly described by a power-law with spectral index Γ varying in the range 1.4–2.2, and a nearly exponential cut-off at a characteristic energy E_c of a few hundred keV (see e.g. Gierlinski et al. 1997). Occasionally, the source switches to the High Soft State (HSS). The high-energy power-law is then much softer ($\Gamma > 2.4$) and the bolometric luminosity is dominated by a thermal component peaking at a few keV. Finally, there are also Intermediate States (hereafter IMS) in which the source exhibits a relatively soft hard X-ray spectrum ($\Gamma \sim 2.1 - 2.3$) and a moderately strong soft thermal component (Belloni et al. 1996; Mendez & van der Klis 1997). The IMS often, but not always, appears when the source is about to switch from one state to the other. When it is not associated with a state transition, it is interpreted as a 'failed state transition'. (see Zdziarski et al. 2002, Pottschmidt et al. 2003, Gleissner et al. 2004).

Simultaneous radio/X-ray and high-energy observations of Cygnus X-1 and other sources have shown that the X-ray LHS is correlated with a strong radio emission which is consistent with arising from a jet (Fender 2001). In contrast, during HSS episodes the source appears to be radio weak (Brocksopp et al. 1999). The presence of a compact jet in the LHS was confirmed by Stirling et

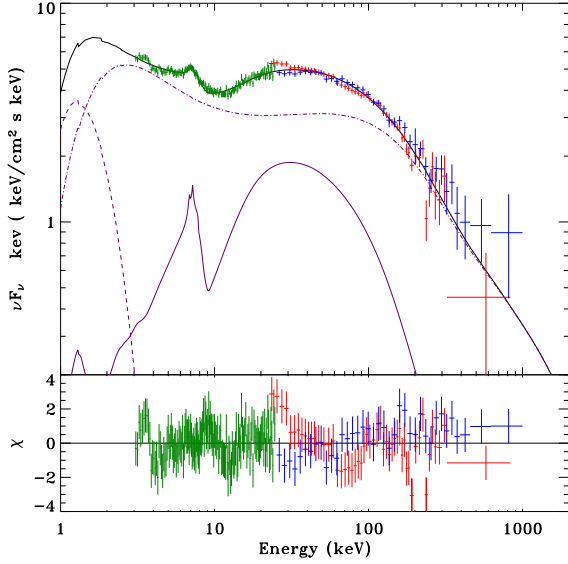


Figure 1. Joint JEM-X/SPI/ISGRI spectrum of Cygnus X-1 averaged over revolutions 79 and 80. The data are fitted with the thermal/non-thermal hybrid Comptonisation model EQPAIR with mono-energetic injection of relativistic electrons with Lorentz factor. The lighter curves show the reflection component (solid), the disc thermal emission (dashed) and the Comptonised emission (dot-dash). The green, red and blue crosses show the JEM-X, IBIS/ISGRI and SPI data respectively. The temperature of the inner disk (DISKPN) was fixed to $kT_{\text{max}}=0.3$ keV in all fits. The soft photon compactness is fixed at $l_s = 10$. The absorbing column density is $N_{\text{h}} = 5 \times 10^{21}$ and the inclination angle 45 degrees. The resulting best fit parameters (see G99) are the following : hard to soft compactness ratio $l_{\text{h}}/l_s=0.85_{-0.03}^{+0.02}$, non-thermal to hard compactness ratio $l_{\text{nth}}/l_{\text{h}}=0.51_{-0.04}^{+0.04}$, electron optical depth $\tau_{\text{p}}=0.55_{-0.06}^{+0.01}$, injection Lorentz factor $\gamma_{\text{inj}}=8.41_{-0.92}^{+0.62}$, reflection amplitude $\Omega/2\pi = 0.71_{-0.03}^{+0.09}$, reflection ionization parameter $\xi=525_{-84}^{+143}$ (erg cm s^{-1}), iron line energy and equivalent width $E_{\text{line}}=7.02_{-0.23}^{+0.32}$ keV, $EW=90_{-24}^{+38}$ eV.

al. (2001) who presented evidence for an extended and collimated radio structure on millisecond scales.

State transitions are generally interpreted as being associated with changes in the geometry of the accretion flow. In the HSS the geometrically thin optically thick disk (Shakura & Sunyaev 1973) extends down to the last stable orbit. The spectrum is dominated by the thermal disc component and peaks at a few keV. The hard X-ray emission is then believed to be produced in a non-thermal corona above and below the disc (Gierliński et al. 1999, hereafter G99). In the LHS the geometrically thin disc is truncated at a few hundred Schwarzschild radii, the innermost part of the accretion flow forms a geometrically thick optically thin and hot disc (Shapiro et al. 1976; Narayan & Yi 1994) where high-energy radiation is pro-

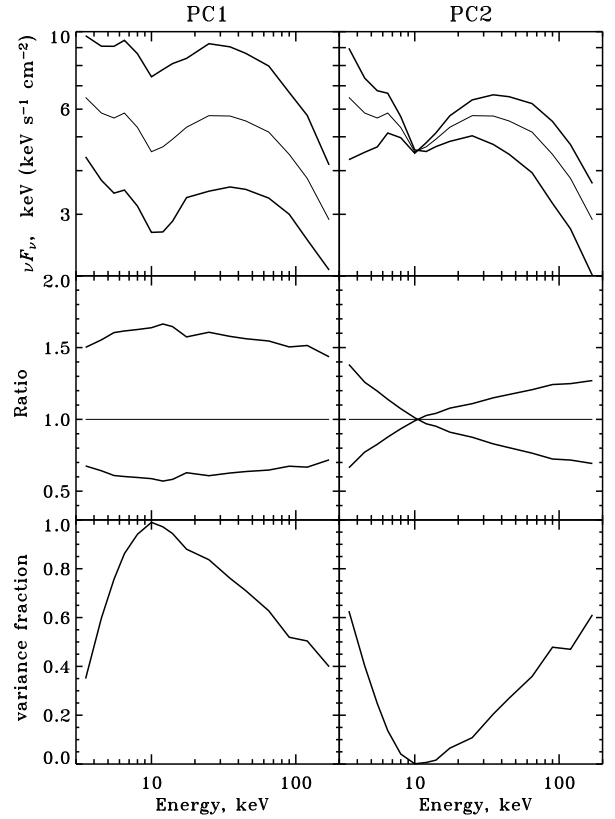


Figure 2. The 2 principal components of variability. The upper panels illustrate the effects of the each component on the shape and normalisation of the spectrum: time average spectrum (light line) and spectra obtained for the maximum and minimum observed values of the normalisation parameter. The middle panels show the ratio of spectra obtained for the maximum and minimum normalisation to the average one. The bottom panels show the contribution of each component to the total variance as a function of energy.

duced through thermal Comptonisation. During spectral transitions to the HSS the inner radius of the cold accretion disk decreases. This reduction of the inner disc radius is associated with either the cold disk penetrating inside the hot inner flow, or the later collapsing into an optically thick accretion disk with small active regions of hot plasma on top of it (Zdziarski et al. 2002). In both cases the enhanced soft photon flux from the disk tends to cool down the hot phase, leading to softer spectra.

Cygnus X-1 represents a prime target for the *INTEGRAL* mission and was extensively observed (Bouchet et al. 2003, Pottschmidt et al. 2003, Bazzano et al. 2003, Cadolle Bel et al., 2005). In this paper we focus on the results of the first observation of Cygnus X-1 in the open time programme. This 300 ks observation was performed on 2003 June 7-11 (rev 79/80) with a 5×5 dithering pattern¹ At this epoch, the *RXTE* All Sky Monitor count rate

¹*INTEGRAL* observations are made of a succession of exposures of about 30 minute duration with varied pointed directions to enable SPI

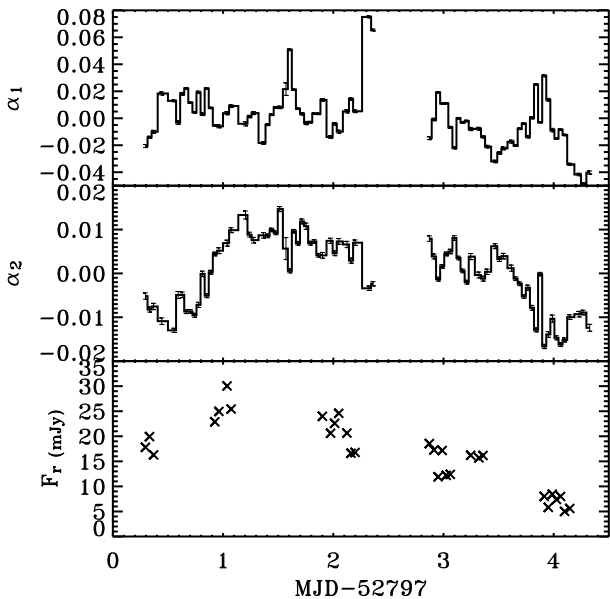


Figure 3. Evolution of the parameters associated to PC 1 (top), PC 2 (middle) and radio light curve (bottom) during the observation

of Cyg X-1 was higher than in typical LHS by up to a factor of 4, and the light curve showed strong X-ray activity characteristic of state (or failed state) transitions. We also combine the *INTEGRAL* data with the results of coordinated radio observations (15 GHz) performed with the Ryle telescope.

2. RESULTS

Fig. 1 shows the the joint *JEM-X/ISGRISPI* spectrum fitted with a thermal/non-thermal hybrid Comptonisation model (EQPAIR model (Coppi 1999; G99; Zdziarski et al. 2002, 2004) with mono energetic injection of non-thermal electrons. The unabsorbed best fit model spectrum is shown on Fig. 5. The appearance of the spectrum confirm that the source was in an IMS. Moreover, the resulting best fit parameters are intermediate between what is found in the LHS and HSS.

In order to study the spectral variability of the source during the observation, we produced light curves in 16 energy bands ranging from 3 to 200 keV with a time resolution of the duration of a science window (i.e. ~ 30 min). The count rate in each band was then renormalised so that its time average matches the energy flux calculated from the best-fit model of the joint average *JEM-X/ISGRISPI* spectrum. Namely, for each energy band we compute the quantity $F(t) = \frac{C(t)}{\bar{C}} \bar{F}$, where $C(t)$ is the mean count rate during pointing t , \bar{C} is the count rate averaged over the whole observation, \bar{F} is the observation average en-

ergy flux in this band given by the best fit model. We use $F(t)$ as a proxy for the instantaneous energy flux, therefore neglecting the effects of the spectral variations on the instrumental response. The time averaged 3–200 keV model flux is $\bar{F}_{3-200} = 2.87 \times 10^{-8}$ ergs cm^{-2} s^{-1} . The energy flux has a rms amplitude of 16 %, and the ratio of the maximum to the minimum luminosity is 2.6.

The light curves exhibit a complex and strong broad band variability of the spectra as well as the overall flux. We use a principal component analysis (PCA see e.g. Kendall, 1980) to seek for variability patterns in our sample. PCA finds n independent components of the variability C_1, C_2, \dots, C_n , so that the flux at energy E_i and time t_j can be written as follow:

$$F(E_i, t_j) = \bar{F}(E_i) + \sum_{k=1}^n \alpha_k(t_j) C_k(E_i), \quad (1)$$

where $\bar{F}(E_i)$ is the time averaged flux at energy E_i . The normalisation coefficients of each PCA component (respectively $\alpha_1, \alpha_2, \dots, \alpha_n$) vary in time. Their fluctuations (including negative values) account for the sample variance. On the other hand the C_k coefficients are constant, they define the variability mode of each PCA component. The PCA components are ordered according to the amount of sample variance they account for (i.e. the observed fluctuations of α_1 cause more variance than those of α_2 which produce more variance than α_3 etc...). The first few Principal Components (those representing most of the variance in the data) should reveal the shape of the relevant spectral components or variability modes. The higher order Principal Components might be expected to be dominated by the statistical and systematic noise in the spectra. To summarise, PCA finds the decomposition that maximises the variability due to lower order components, so that most of the variability can be described using a small number of components.

The results of our PCA analysis of the spectral variability of Cygnus X-1 are illustrated in Fig. 2, which shows how the 2 first principal components affect the flux and spectrum and their respective contribution to the total observed variance as a function of energy. As can be seen on this figure, the first principal component (PC 1) consists in a variability mode dominated by variations in the luminosity (normalisation) with little change in the spectral shape. For this reason, in the following, we will refer to PC 1 as the ‘flaring mode’. This component accounts for 68 % of the sample variance. PC1 correlates very well with the high-energy flux. A least square fit shows that the 3-200 keV flux relates to α_1 through:

$$F_{3-200} = \bar{F}_{3-200}(1 + 7.64\alpha_1), \quad (2)$$

with a linear correlation coefficient of 0.98. So that α_1 can be viewed as a tracer of the hard X-ray luminosity of the source.

As shown in Fig 2, the second PCA component (PC 2) can be described roughly as a pivoting of the spectrum

image deconvolution. Such a 30 minute pointing is called a science window

around 10 keV. The two spectra obtained for the minimum and maximum values of the α_2 parameter controlling the strength of PC 2 are reminiscent of the canonical LHS and HSS spectra. This component is responsible for 27 % of the sample variance, and will be referred as the 'pivoting mode'. α_2 can thus be seen as a tracer of the hardness of the high-energy spectrum.

Considered together the 2 first PCA components account for 95 percent of the observed variance. The remaining residual variability is entirely attributable to both statistical noise and instrumental effects. The intrinsic source variability is largely dominated by PC 1 (flaring mode) and PC 2 (pivoting mode). Fig. 3 shows the time evolution of the PCA parameters α_1 and α_2 . α_1 , which traces the changes in bolometric luminosity at nearly constant spectra shows important variability on time scales of order of a few hours or less, but no clear systematic trend during the 4 days of observation. In contrast, α_2 , which roughly traces the hardness of the spectrum, seems to vary on longer time scales: it jumps during the first 2 days then decreases in the second part of the observation. This suggests that the physical mechanisms responsible for PC 1 and PC 2 are distinct (which is also expected from the fact that, by construction, PC 1 and PC 2 are linearly independent) and apparently acting on different time scales.

In order to study the possible correlations between the radio and hard X-ray emission, we selected the science windows for which we had simultaneous radio pointings. The resulting light curve is shown on the bottom panel of Fig. 3. Fig. 4 shows that the radio emission is strongly correlated to α_2 . The correlation is highly significant. The Spearman rank test correlation coefficient is 0.78 corresponding to a probability that the correlation is by chance of 2×10^{-7} . On the other hand, there is no hint of a correlation with the flaring mode as can be seen in the left panel of Fig. 4. In other terms, the radio emission is strongly correlated with the hardness and apparently unrelated to 2 to 200 keV luminosity.

3. DISCUSSION

We have shown that, during our IMS observation, the variability of Cygnus X-1 can be described by two independent variability modes:

On time-scales of a few hours or less there are important changes in luminosity with little spectral variations (flaring mode). On longer time scales there is a spectral evolution with the the spectrum pivoting around 10 keV.

We further showed that while there is no hint for a correlation between the radio flux and the flaring mode, the radio is strongly correlated with the pivoting of the spectrum, in the sense that the radio flux is stronger when the hard X-ray spectrum is harder.

Actually, the transition from LHS to HSS is known to be

associated with a quenching of the radio emission (Corbel et al. 2000; Gallo, Fender & Pooley 2003). As the transition to the HSS also corresponds to a strong softening of the spectrum, this is consistent with the correlation between hardness and radio flux: when, during the observation, the source gets closer to the HSS the spectrum softens and simultaneously the radio flux decreases. Moreover, compilations of LHS and HSS spectra suggest that the spectral transition between LHS and HSS occurs through a pivoting around 10 keV (see e.g. Fig. 9 of McConnell et al 2002). The evolution of the α_2 parameter shown in Fig. 3 indicates that the source, initially in a 'soft' IMS, switched to a harder state during the first 2 days of observation and then transited back toward a 'soft' state.

It is interesting to speculate on the cause of the two variability modes. We tried to reproduce such variability modes by varying the parameters of the hybrid thermal/non-thermal Comptonisation models shown in Fig. 1. As shown in the left panel of Fig. 5 it is possible to produce variations in luminosity by a factor comparable to what is observed and little spectral changes in the *INTEGRAL* band by varying the coronal compactness l_h by a factor of 2. In this context the flaring mode would correspond to variations of the dissipation rate in the corona possibly due to magnetic reconnection. This variability mode seems to be a characteristic of the HSS (Zdziarski et al. 2002). As we show here, it also provides a major contribution to the variability of the IMS.

Regarding the pivoting mode, it can be produced by changes in the flux of soft cooling photons at constant dissipation in the hot phase. We performed simulations assuming that the accretion disc radiates like a blackbody i.e. its flux $F_{disc} \propto l_s \propto T_{max}^4$ and constant l_h . For an increase of the disc temperature by a factor of 1.7, the disc luminosity grows by a factor of 8. As in this model, the disc flux also corresponds to the soft cooling photon input in the corona and the heating ($\propto l_h$) is kept constant, this leads to a steepening of the spectrum with a pivot around 10 keV of similar amplitude as in PC 2 (see Fig. 5). For the 1996 HSS, G99 found a ratio $l_h/l_s \sim 0.3$ while in the LHS l_h/l_s ranges between 3.5 to 15 (Ibragimov et al. 2005). The range of l_h/l_s (0.4–3.4) required to reproduce the observed amplitude of the pivoting mode matches almost exactly the intermediate range between the HSS and the lower limit of the LHS. The source initially in a (quasi) HSS evolved toward the LHS but as soon as it was reached, it went back toward the HSS.

Since, in the *INTEGRAL* band, the constraints on disc thermal emission are loose we did not attempt to model the data with a varying inner disc radius which is, moreover, difficult to disentangle from fluctuations of the disc temperature. In the fitted models as well as the models shown in Fig. 5, the inner disc radius is fixed at $6 R_g$. Nonetheless our result would also be consistent with the disc moving inward and outward of the hot phase during the state transitions. Indeed, when the inner disc radius is approaching the black hole, its maximum temper-

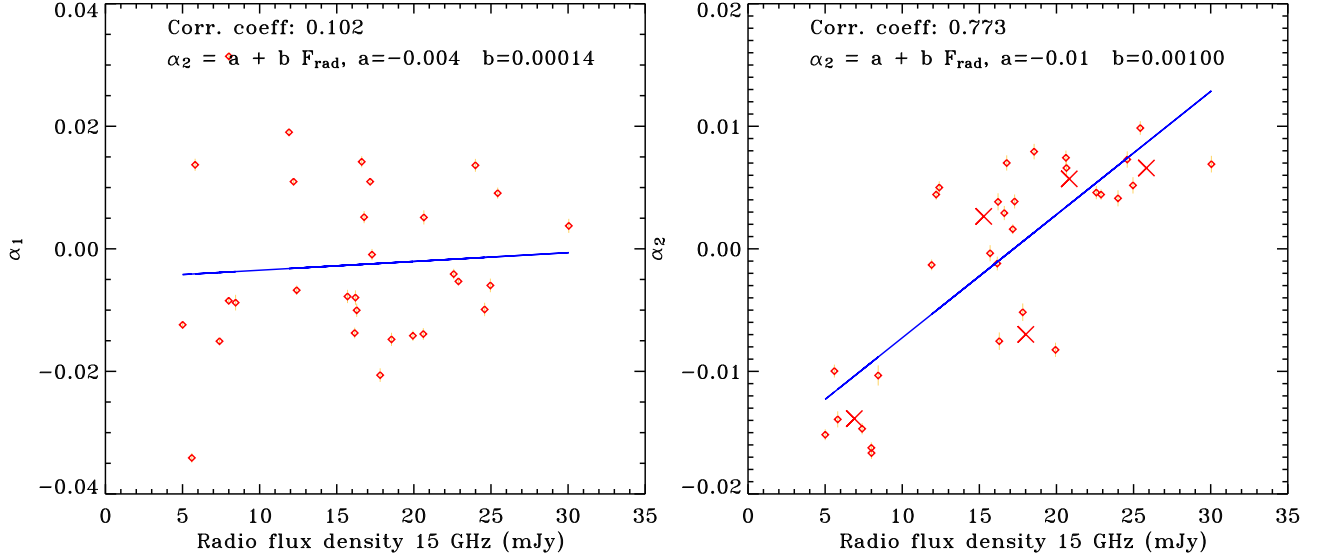


Figure 4. PCA parameters α_1 (left panel) and α_2 (right panel) as a function of the radio flux (diamonds). In both panels, the best linear fits are shown by the solid lines. The crosses indicate the time average over each of the five periods of nearly continuous radio coverage (see Fig 3). While there is no convincing correlation between the radio flux and α_1 , the radio flux is correlated to α_2 at highly significant level.

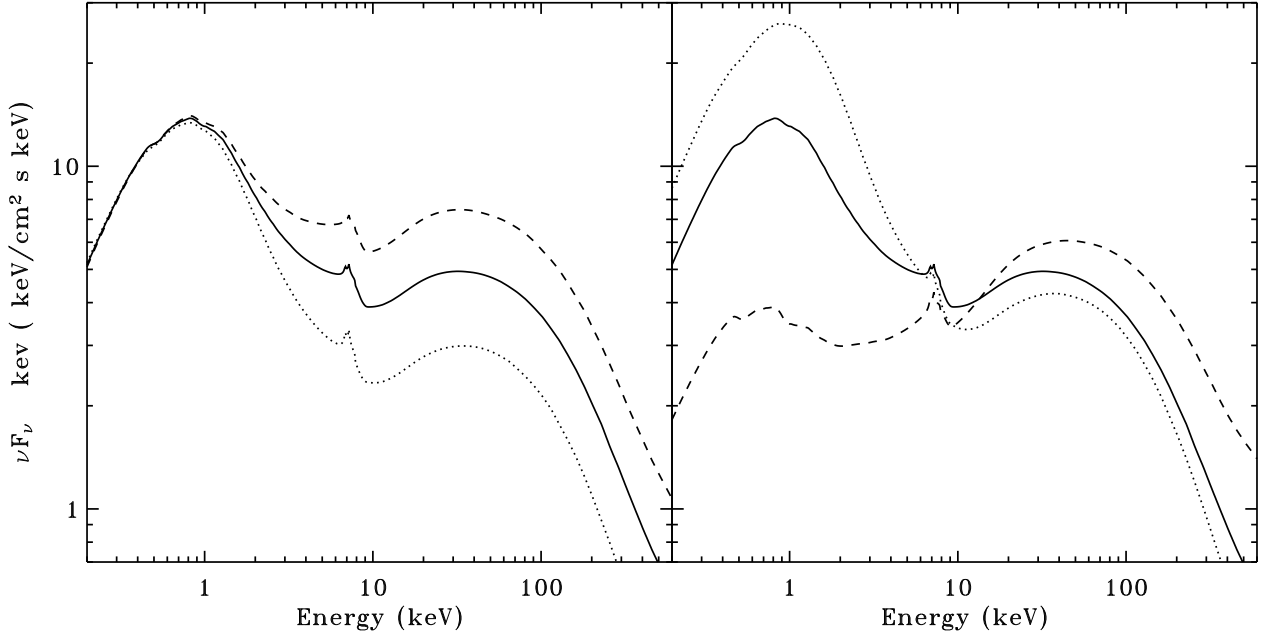


Figure 5. Left panel: effect of varying l_h by a factor of 2 on the EQPAIR model with monoenergetic injection (see Sect. 2). Solid curve: unabsorbed best-fit model ($l_h = 8.5$); Dotted curve $l_h = 5.7$; Dashed curve: $l_h = 11.9$. Right panel: effect of varying the soft photons flux by a factor of 8. Solid curve: unabsorbed best-fit model ($T_{\text{disc}} = 0.3 \text{ keV}$; $l_h/l_s = 0.85$). Dotted curve: $T_{\text{disc}} = 0.357 \text{ keV}$ and $l_h/l_s = 0.42$. Dashed curve: $T_{\text{disc}} = 0.212 \text{ keV}$ and $l_h/l_s = 3.4$.

ature and luminosity increases² leading to a more efficient cooling of the hot flow/corona. The anti-correlation between radio flux and disc luminosity would be due to the jet expanding when the cold accretion disc recedes

²Unless the mass accretion rate is reduced by a larger amount, which seems very unlikely, the evidence being rather that the accretion rate is often (but not always) larger in the soft than in the LHS.

and then shrinking in the second phase of the observation when the disc moves back inward. It is interesting to note that the change in disc flux required (a factor of ~ 8) to explain the spectral evolution is comparable to the amplitude of the variations of the radio flux (a factor of ~ 6). This suggests a direct relation between the disc flux and jet power. The overall change in bolometric

luminosity occurring during the PC2 transition estimated from the fiducial 'hard' and 'soft' state models shown on the left panel of Fig. 5, is about a factor of 2. Because of the relatively short time scale (\sim a day) on which the variation in luminosity occurs, it is unlikely to be driven by changes in the mass accretion rate. Most probably, it is due to a change in the radiative efficiency of the flow. The accretion flow could be less efficient in the LHS, because about half of the accretion power is either swallowed by the black hole or pumped into the jet, while, in the HSS, the cold disc is expected to be radiatively efficient.

The evolution of the hard X-ray corona luminosity during our IMS observation is very puzzling. Indeed, if, as commonly believed for the LHS, the corona constitutes the base of the jet, it is difficult to conceive that changes in the jet power and/or extension is not associated to changes in the energetics of the corona. Similarly, one would expect the corona/hot accretion flow to respond to changes in the disc power and/or distance of the truncation radius. Instead, we infer dramatic changes in the jet and disc power that are anti-correlated with each other, but *completely unrelated* to the fluctuations of the coronal power.

4. CONCLUSION

During our observation, the source presented a strong flux spectral variability occurring through 2 independent variability modes: First, there are changes in the dissipation rate in the corona, due to local instabilities or flares, producing a variability of the hard X-ray luminosity on time-scales of hours and no strong spectral alterations. Strikingly, this coronal activity seems to be unrelated to the evolution of the jet and cold disc luminosity. Second, we observe a slower 4-day evolution starting from a spectrum close to the canonical HSS toward an almost LHS and back. This spectral evolution was characterized by a pivoting of the spectrum around 10 keV. It was correlated with the radio emission which was stronger when the hard X-ray spectrum was harder. It is interpreted in terms of a variable soft cooling photon flux in the corona associated with changes in the thermal disc luminosity and radio-jet power. This interpretation suggests a jump in bolometric luminosity of about a factor of 2 during the transition from LHS to HSS, which might indicate that the LHS accretion flow is radiatively inefficient, half of the accretion power being possibly advected into the black hole and/or the radio jet.

ACKNOWLEDGMENTS

This paper is based on observations with *INTEGRAL*, an ESA project with instruments and science data centre funded by ESA member states (especially the PI countries: Denmark, France, Germany, Italy, Switzerland, Spain), Czech Republic and Poland, and with the participation of Russia and the USA. The Ryle Telescope is supported by PPARC.

REFERENCES

- [1] Bazzano, A., et al. 2003, A&A, 411, L389
- [2] Belloni, T., Mendez, M., van der Klis, M., et al., 1996, ApJ, 472, L107
- [3] Bouchet L., et al. 2003, A&A, 411, L377
- [4] Bowyer, S., Byram, E.T., Chubb, T.A., Friedman, M., 1965, Sci, 147, 394
- [5] Brocksopp, C., Fender, R. P., Larionov, V., Lyuty, V. M., Tarasov, A. E., Pooley, G. G., Paciesas, W. S., & Roche, P. 1999, MNRAS, 309, 1063
- [6] Cadolle Bel, M., Sizun, P., Goldwurm, A., Rodriguez, J., Laurent, P., Zdziarski, A. A., Foschini, L., Goldoni, P., Gouiffes, C., Malzac, J., Roques, J.P.R., 2005, A&A submitted (CB05)
- [7] Corbel, S., et al., 2000, A&A, 359, 251
- [8] Coppi, P. S. 1999, ASP Conf. Ser. 161: High Energy Processes in Accreting Black Holes, 161, 375
- [9] Fender, R. P. 2001, MNRAS, 322, 31
- [10] Gallo, E., Fender, R. P., & Pooley, G. G. 2003, MNRAS, 344, 60
- [11] Gierliński, M., et al., 1997, MNRAS, 288, 958
- [12] Gierliński, M., Zdziarski, A. A., Poutanen, J., Coppi, P. S., Ebisawa, K., & Johnson, W. N. 1999, MNRAS, 309, 496 (G99)
- [Kendall 1980] Kendall, M. G., 1980, "Multivariate Analysis", Second Edition, Charles Griffin and Co. London.
- [13] McConnell, M. L., et al. 2002, ApJ, 572, 984
- [14] Mendez, M. & van der Klis, M. 1997, ApJ, 479, 926
- [15] Narayan, R., & Yi, I. 1994, ApJ, 428, L13
- [16] Pottschmidt, K., et al. 2003, A&A, 411, L383
- [17] Shakura, N. I. , & Sunyaev, R. A., 1973, A&A, 24, 337
- [18] Shapiro, S. L., Lightman, A. P., & Eardley, D. M., 1976, ApJ, 204, 187
- [19] Stirling, A. M., Spencer, R. E., de la Force, C. J., Garrett, M. A., Fender, R. P., & Ogley, R. N. 2001, MNRAS, 327, 1273
- [20] Zdziarski, A. A., Poutanen, J., Paciesas, W. S., & Wen, L. 2002, ApJ, 578, 357
- [21] Zdziarski, A. A., Gierliński, M., Mikołajewska, J., Wardziński, G., Smith, D. M., Alan Harmon, B., & Kitamoto, S. 2004, MNRAS, 351, 791

A MULTI-FLOW MODEL FOR MICROQUASARS

P.O. Petrucci, J. Ferreira, G. Henri, L. Saugé, and G. Pelletier

Laboratoire d'Astrophysique de Grenoble, Grenoble, France

ABSTRACT

We present a new picture for the central regions of Black Hole X-ray Binaries. In our view, these central regions have a multi-flow configuration which consists in (1) an outer standard accretion disc down to a transition radius r_J , (2) an inner magnetized accretion disc below r_J driving (3) a non relativistic self-collimated electron-proton jet surrounding, when adequate conditions for pair creation are met, (4) a ultra relativistic electron-positron beam. This accretion-ejection paradigm provides a simple explanation to the canonical spectral states, from radio to X/ γ -rays, by varying the transition radius r_J and disc accretion rate \dot{m} independently. Some features such as possible hysteresis and the presence of quasi-periodic oscillations could be also described in this paradigm.

Key words: L^{∞} TeX; ESA; X-rays; Microquasars.

1. A NOVEL FRAMEWORK FOR BH XRBS

1.1. General picture

We assume that the central regions of BH XrB are composed of four distinct flows: two discs, one outer "standard" accretion disc (hereafter SAD) and one inner jet emitting disc (hereafter JED), and two jets, a non-relativistic, self-confined electron-proton MHD jet and, when adequate conditions for pair creation are met, a ultra-relativistic electron-positron beam. A sketch of our model is shown in Fig. 1 while the four dynamical components are discussed separately below (see also Ferreira et al. 2005, for more details). This is an extended version of the "two-flow" model early proposed for AGN and quasars (Pelletier et al., 1988; Sol et al., 1989; Pelletier & Roland, 1989; Henri & Pelletier, 1991; Pelletier & Sol, 1992) to explain the highly relativistic phenomena such as superluminal motions observed in these sources. This model provides a promising framework to explain the canonical spectral states of BH XrBs mainly by varying the transition radius r_J between the SAD and the JED. This statement is not new and has already been proposed in the past by different authors (e.g. Esin et al. 1997; Belloni et al. 1997) but our model distinguishes itself from the others by the consistency of its disc-jet structure and by the introduction of a new physical com-

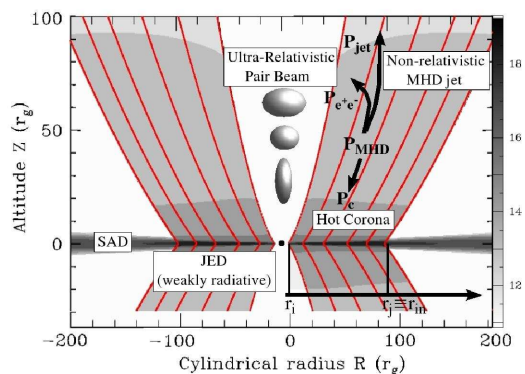


Figure 1. A Standard Accretion Disc (SAD) is established down to a radius r_J which marks the transition towards a low radiative Jet Emitting Disc (JED), settled down to the last stable orbit. The JED is driving a mildly relativistic, self-collimated electron-proton jet which, when suitable conditions are met, is confining an inner ultra-relativistic electron-positron beam. The MHD power P_{MHD} flowing from the JED acts as a reservoir for (1) heating the jet basis (radiating as a moving thermal corona with power P_c), (2) heating the inner pair beam ($P_{e^+e^-}$) and (3) driving the compact jet (P_{jet}). Field lines are drawn in black solid lines and the number density is shown in greyscale ($\log_{10} n/m^{-3}$). This magnetic accretion-ejection structure solution was computed with $\xi = 0.01$, $\varepsilon = 0.01$ and with $m = 10$ and $\dot{m}(r_J) = 0.01$ (see text).

ponent, the ultra-relativistic electron-positron beam, that appears during strong outbursts. We believe that jets from BH XrBs are self-collimated because they follow the same accretion-ejection correlation as in AGN (Corbel et al., 2003; Fender et al., 2003; Merloni et al., 2003). This therefore implies the presence of a large scale vertical field anchored somewhere in the accretion disc (the JED) and we assume that this large scale B_z has the same polarity. The presence of a large scale vertical field threading the disc is however not sufficient to drive super-Alfvénic jets. This field must be close to equipartition as shown by Ferreira & Pelletier (1995) and Ferreira (1997). An important local parameter is therefore the disc mag-

netization $\mu = B_z^2/(\mu_o P_{tot})$ where P_{tot} includes the disc plasma and radiation pressures.

1.2. The outer SAD

We make the conjecture that a SAD no longer exists once μ reaches unity. It can be easily shown that one may reasonably expect μ to increase towards the center (Ferreira et al., 2005). Whenever a BH XrB reaches $\mu \simeq 1$ at a radius $r_J > r_i$, r_i being the last marginally stable orbit, the accretion flow changes its nature to a JED.

1.3. The inner JED

The inner region with $\mu \sim 1$ is fueled by the SAD at a rate $\dot{M}_{a,J} = \dot{M}_a(r_J)$. Since it undergoes mass loss, we parametrize the JED accretion rate following: $\dot{M}_a(r) = \dot{M}_{a,J} \left(\frac{r}{r_J}\right)^\xi$ where ξ measures the local ejection efficiency (Ferreira & Pelletier, 1993).

The dynamical properties of a JED have been extensively studied in a series of papers (see Ferreira 2002 and references therein). The ratio at the disc midplane of the jet torque to the turbulent "viscous" torque is

$$\Lambda \sim \frac{B_\phi^+ B_z / \mu_o h}{\alpha_v P_{tot} / r} \sim \frac{B_\phi^+ B_z}{\mu_o P_{tot}} \frac{r}{\alpha_v h} \quad (1)$$

It is straightforward to see that the necessary condition to drive jets (fields close to equipartition) from Keplerian discs leads to a dominant jet torque. In fact, it has been shown that steady-state ejection requires $\Lambda \sim r/h \gg 1$ (Ferreira, 1997; Casse & Ferreira, 2000). This dynamical property has a tremendous implication on the JED emissivity since it can be shown that the total luminosity of the JED is only a fraction $1/(1 + \Lambda)$ of the accretion disc liberated power (Ferreira et al., 2005). In consequence, the JED is weakly dissipative while powerful jets are being produced regardless of the nature of the central object. As a consequence, the flux emitted by the JED is expected to be unobservable with respect to that of the outer SAD.

1.4. Non-relativistic electron-proton jets from JEDs

Although a large power is provided to the ejected mass (mainly electrons and protons), the mass loss (ξ) is never low enough to allow for speeds significantly relativistic required by superluminal motions: MHD jets from accretion discs are basically non or only mildly relativistic with $u_\infty \sim 0.1 - 0.8 c$ (Ferreira, 1997). This is basically the reason why they can be efficiently self-confined by the magnetic hoop stress. Indeed, in relativistic flows the electric field grows so much that it counteracts the confining effect due to the toroidal field. This dramatically reduces the self-collimation property of jets (Bogovalov & Tsinganos, 2001; Bogovalov, 2001; Pelletier, 2004).

In our framework, jets from magnetic accretion-ejection structure (hereafter MAES) have two distinct spectral components detailed below:

- **A non-thermal extended jet emission:** We expect a small fraction of the jet power P_{jet} to be converted into particles, through first and/or second order Fermi acceleration, populating the MHD jet with supra-thermal particles. These particles are responsible for the bulk emission of the MHD jet. This is similar to models of jet emission already proposed in the literature (Falcke & Biermann, 1995; Vadawale et al., 2001; Markoff et al., 2001, 2003; Markoff, 2004; Falcke et al., 2004). In these models, the jet is assumed to be radiating self-absorbed synchrotron emission in the radio band (producing a flat or even inverted radio spectrum) becoming then optically thin in the IR-Optical bands and providing a contribution up to the X/ γ -rays.
- **A thermal jet basis:** Jet production relies on a large scale magnetic field anchored on the disc as much as on MHD turbulence triggered (and sustained) within it. This implies that small scale magnetic fields are sheared by the disc differential rotation, leading to violent release of magnetic energy at the disc surface and related turbulent heat fluxes (e.g. Galeev et al. 1979; Heyvaerts & Priest 1989; Stone et al. 1996; Merloni & Fabian 2002). The energy released is actually tapping the MHD Poynting flux flowing from the disc surface. We can safely assume that a fraction f of it would be deposited at the jet basis, with a total power $P_c = f P_{MHD}$. The dominant cooling term in this optically thin medium is probably comptonization of soft photons emitted by the outer SAD (with a small contribution from the underlying JED). These are circumstances allowing a thermal plasma to reach a temperature as high as ~ 100 keV, (Pietrini & Krolik, 1995; Mahadevan, 1997; Esin et al., 1997). This plasma being at the base of the jet, it will have a vertical proper motion. Then its spectral behavior is expected to be close to that of a dynamic corona (Malzac et al., 2001).

1.5. The inner ultra-relativistic pair beam

Since the large scale magnetic field driving the self-confined jet is anchored onto the accretion disc which has a non zero inner radius, there is a natural hole on the axis above the central object with no baryonic outflow (this also holds for neutron stars). This hole provides a place for pair production and acceleration with the outer MHD jet acting as a sheath that confines and heats the pair plasma. This is the microquasar version of the "two flow" model that has been successfully applied to the high energy emission of relativistic jets in AGNs (Henri & Pelletier, 1991; Marcowith et al., 1995, 1998; Renaud & Henri, 1998).

The $e^+ - e^-$ plasma is produced by $\gamma - \gamma$ interaction, the γ -ray photons being initially produced by a few relativistic particles by Inverse Compton process, either on synchrotron photons (Synchrotron Self Compton or SSC) or on disc photons (External Inverse Compton or EIC). A key point of the two-flow model is that the MHD jet launched from the disc can carry a fair amount

of turbulent energy, most probably through its MHD turbulent waves spectrum. A fraction of this power can be transferred to the pairs ($P_{e^+e^-} \ll P_{MHD}$). Thus the freshly created pairs can be continuously reheated, triggering an efficient pair runaway process, leading to a dense pair plasma (Henri & Pelletier, 1991). In these conditions, the pair plasma will experience a strong bulk acceleration due to the recoil term of EIC, an effect also known as the "Compton Rocket" effect (O'Dell, 1981; Renaud & Henri, 1998). As shown in previous works, this "rocket" effect is the key process to explain relativistic motion (Marcowith et al., 1995; Renaud & Henri, 1998). For example, values of 5 to 10 can be easily reached in near-Eddington accretion regime around stellar black holes (Renaud & Henri, 1998). Producing this pair plasma requires thus altogether a strong MHD jet, a radiative non-thermal component extending above the MeV range and a minimal $\gamma - \gamma$ optical depth, namely $\tau_{\gamma\gamma} \sim 1$ requiring high luminosity and small size systems (see Ferreira et al. 2005).

2. CANONICAL SPECTRAL STATES OF X-RAY BINARIES

2.1. The crucial roles of r_J and \dot{m}

From Section 1, it is clear that the spectral appearance of a BH XrB critically depends on the size of the JED relative to the SAD, namely r_J . As stated before, r_J is the radius where the disc magnetization $\mu = B_z^2 / (\mu_o P_{tot})$ becomes of order unity. Thus, r_J depends on two quantities $P_{tot}(r, t)$ and $B_z(r, t)$. The total pressure is directly proportional to \dot{m} since $P_{tot} = \rho \Omega_k^2 h^2 \propto \dot{m} m^{-1} r^{-5/2}$. As a consequence, any variation of the accretion rate in the outer SAD implies also a change in the amplitude of the total pressure. But we have to assume something about the time evolution of the large scale magnetic field threading the disc. The processes governing the amplitude and time scales of these adjustments of r_J to a change in \dot{m} are far too complex to be addressed here. They depend on the nature of the magnetic diffusivity within the disc but also on the radial distribution of the vertical magnetic field. We will simply assume in the following that r_J and \dot{m} are two independent parameters. In that respect, our view is very different from that of Esin et al. (1997); Mahadevan (1997) who considered only the dependency of \dot{m} to explain the different spectral states of BH XrBs.

2.2. The Quiescent state

This state is characterized by a very low accretion rate (\dot{m} as low as $\sim 10^{-9}$) with a hard X-ray component. The ADAF model has been successfully applied to some systems with a large transition radius between the ADAF and the outer standard disc, namely $r_{tr} \sim 10^3 - 10^4 r_g$ (e.g. Narayan et al. 1996; Hameury et al. 1997). However, such a model does not account for jets and their radio emission, even though XrBs in quiescence seem also to follow the radio/X-ray correlation (e.g. Fender et al. 2003; Gallo et al. 2004, 2005). Within our framework, a BH XrB in quiescence has a large r_J , so that a large zone in the whole disc is driving jets (Fig. 2a). The low \dot{m} provides a low synchrotron jet luminosity, while the JED is

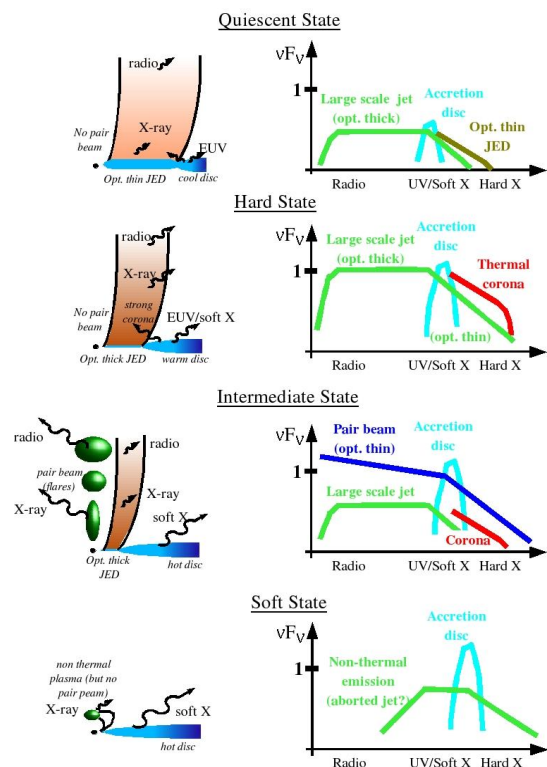


Figure 2. The canonical spectral states of X-ray binaries (cf. Sect. 2 for more details).

optically thin, producing a SED probably very similar to that of an ADAF. We thus expect $r_J \sim r_{tr}$. The weak MHD Poynting flux prevents the ignition of the pair cascade process and no pair beam is produced.

2.3. The Hard state

Within our framework, the JED is now more limited radially than in the Quiescent state, namely $r_J \sim 40 - 100 r_g$ (Fig. 2b). This transition radius corresponds to the inner disc radius r_{in} as obtained within the SAD framework (Zdziarski et al., 2004). The low velocity of the plasma expected at the jet basis is in good agreement with recent studies of XrBs in Hard state (Maccarone, 2003; Gallo et al., 2003). It can also explain the apparent weakness of the Compton reflection (Zdziarski et al., 1999; Gilfanov et al., 1999) as already suggested by Markoff et al. (2003, see also Beloborodov 1999; Malzac et al. 2001) and tested by Markoff & Nowak (2004). In any case, the JED intrinsic emission is weak with respect to that of the outer standard disc: most of the accretion power flows out of the JED as an MHD Poynting flux. Nevertheless, the threshold for pair creation is still not reached and there is no pair beam, hence no superluminal motion. The MHD power is therefore shared between the jet basis, whose temperature increases (the thermal "corona") producing X-rays, and the large-scale jet seen as the persistent (synchrotron) radio emission.

2.4. The Soft state

Our interpretation of the Soft state relies on the disappearance of the JED, i.e. when r_J becomes smaller or equal to r_i (Fig. 2c). Depending on the importance of the magnetic flux in the disc, this may occur at different accretion rates. Thus, the threshold in \dot{m} where there is no region anymore in the disc with equipartition fields may vary. The whole disc adopts therefore a radial structure akin to the standard disc model. Since no MHD jet is produced, all associated spectral signatures disappear. Even if pair production may take place (when \dot{m} is large), the absence of the confining MHD jet forbids the pairs to get warm enough and be accelerated: no superluminal motion should be detected. Note also that the presence of magnetic fields may be the cause of particle acceleration responsible for the weak hard-energy tail (? hereafter McCR03, Zdziarski & Gierlinski 2003 and references therein).

2.5. Intermediate states

These states are generally observed during transitions between Hard and Soft states. Within our framework, they correspond to geometrical situations where r_J is small but remains larger than r_i (Fig. 2d). The flux of the outer standard disc is thus still important while the JED is disappearing. The consequences on the spectral shape are not straightforward since the importance of the different spectral components relative to each other depends on the precise values of r_J and \dot{m} . Such study is out of the scope of the present paper and will be detailed elsewhere.

The crucial point however is that, in our framework, luminous intermediate states (the so-called Very High State or VHS) with high \dot{m} provide the best conditions for the formation of the ultra-relativistic pair beam, as described in details in Sect. 1.5: (1) a high luminosity, (2) a high energy steep power law spectrum extended up to the γ -ray bands and (3) the presence of the MHD jet. The two first characteristics enable a $\gamma - \gamma$ opacity larger than unity, while the MHD jet allows to confine the pair beam and maintain the pairs warm, a necessary condition to trigger a pair runaway process. The total emission would be then dominated by the explosive behavior of the pairs, with the sudden release of blobs. Each blob produced in the beam first radiates in X and γ -ray, explaining the hard tail present in this state, and then, after a rapid expansion, produces the optically thin radio emission. This pair beam would also explain the superluminal ejections observed during this state in different objects (e.g. Sobczak et al. 2000; Hannikainen et al. 2001). We conjecture that the exact moment where this occurs corresponds to the crossing of the "jet line" recently proposed by Fender et al. (2004) (see also Corbel et al. 2004).

3. TIME EVOLUTION OF BH XRBS

The evolution with time of a BH XrB has been reported in Fig. 3 (Ferreira et al. in preparation). This is a synthetic Hardness–Intensity diagram (hereafter HID) as it is generally observed in XrBs in outbursts (e.g. Belloni et al. 2005; Fender et al. 2002, 2004). During such outbursts, the objects follow the A-B-C-D sequence before turning back to A at the end of the outburst. We detailed below

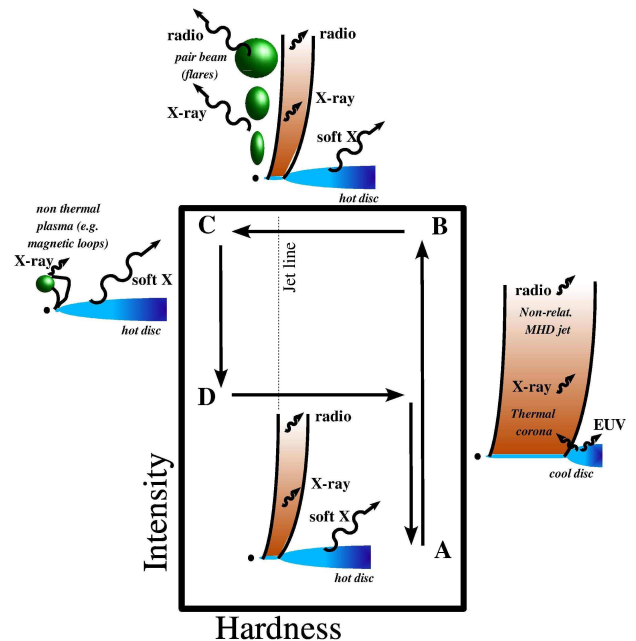


Figure 3. Schematic Hardness–Intensity diagram as it is generally observed in XrBs in outbursts (this figure is clearly inspired by Fig. 7 of Fender et al. 2004). During such outbursts, the objects follow the A-B-C-D sequence before turning back to A at the end of the outburst. The interpretation of this diagram within our framework is detailed in Sect. 3.

the interpretation of this diagram in the framework of our model. We have also overplotted on Fig. 3 the different sketches of our model at different phases (this figure is clearly inspired by Fig. 7 of Fender et al. 2004).

3.1. Ascending the Right Branch:

Let us start at a Low/Hard State located at the bottom of the HID right branch (in A in Fig. 3). In our view, such state would correspond to a JED extending up to typically $r_J \sim 10^2 r_g$. This considerably lowers the emission from the inner radii of the SAD producing a UV/soft X-ray excess. The hard (1-20 keV) power-law component of photon index $\Gamma \sim 1.7$ is attributed to the warm thermal plasma at the base of the jet. The non relativistic MHD jet then produces the persistent IR and radio synchrotron emission.

3.2. The Top Horizontal Branch

Before the jet line: Arriving in B we assume that r_J starts decreasing rapidly. Then, the MAES undergoes an outside-in transition to a SAD. The BH XrBs enter the high intermediate state. The flux of the outer standard disc then increases while the JED is decreasing. Under such circumstances, the MHD Poynting flux released by the JED is still important (through the large \dot{m} that characterizes this part of the HID) but the MHD jet itself fills a smaller volume, a direct consequence being a weaker emission of the thermal "corona" and the non-thermal

MHD jet emission with respect to what it is while in the Hard state.

At the jet line: During its evolution along this top horizontal branch the system can reach a critical phase where the conditions for a strong pair production, inside the MHD jet structure, are fulfilled. In this case, we expect an explosive behaviour of the pairs, with the sudden release of blobs. The emission of these blobs, first in X and γ -ray and then, after a rapid expansion, in IR and radio, will probably dominate the broad band spectrum, producing the hard X-ray tail and the optically thin radio emission present in this state. The production of a series of blobs can even result in an apparently continuous spectrum, from radio to X/ γ -rays. Remarkably, there is no evidence of steady radio jets during this phase but it is generally associated with radio and X-ray flares and/or superluminal sporadic ejections (e.g. Sobczak et al. 2000; Hannikainen et al. 2001). We note that the rapid increase of the pair beam pressure in the inner region of the MHD jet may dramatically perturb the MHD jet production and we expect a suppression of the steady jet emission when a large outburst sets in, in agreement with observations (Fender et al., 2004).

After the jet line: We assume that r_J is still decreasing. We therefore expect the total disappearance of the JED and its MHD jets when $r_J \rightarrow r_i$, thereby also causing the end of the pair beam (if present). The inner regions of the BHXB are a SAD with probably a magnetically active "corona". Indeed, it must be noted that the situation might be slightly more complex than a mere SAD because of the presence of a concentrated magnetic flux. No steady MHD ejection can be produced from the SAD but unsteady events could always be triggered. This is maybe the reason why this region in the HID seems to harbor complex variability phenomena (Belloni et al., 2005; Nespoli et al., 2003).

3.3. Descending the Left Branch

When XrBs reach the left vertical branch (point C in Fig. 3), r_J is smaller than the inner disc radius i.e. the JED and the MHD jet have completely disappeared. The whole disc adopts therefore a radial structure akin to the standard disc model and we enter into the so-called soft state (also called thermal dominant state McCR03) where the spectra are dominated by strong disc emission. The descent from C to D correspond to a decrease in intensity i.e. by a decrease of the accretion rate. This is the beginning of the fading phase of the outburst. In our framework r_J keeps smaller than r_i . We note also that we still expect the presence of magnetic fields that may be the cause of particle acceleration responsible for the weak hard-energy tail generally observed in this state (McCR03, ZG04 and references therein).

3.4. The Low Horizontal Branch

In D r_J begins to increase again. Thus, according to this conjecture, there is an inside-out build up of a JED. Self-collimated electron-proton jets could be produced right away. This means an increase of r_j , the reappearance of the non-thermal MHD jet and the thermal corona at its

basis and a decrease of the SAD emission. But, contrary to the Top Horizontal Branch, the accretion rate is now too low to allow the production of a pair beam. Consequently we do not expect superluminal motions during this phase. When r_J reaches the same value as in the Low/Hard State the system is ready for another duty cycle.

4. SUMMARY AND CONCLUDING REMARKS

We present in this paper a new paradigm for the accretion-ejection properties of Galactic Black Hole X-ray binaries. We assume the existence of a large scale magnetic field of bipolar topology in the innermost disc regions. Such a field allows for several dynamical phenomena to occur whose relative importance determine the observed spectral state of the binary. The dynamical constituents are: (1) an outer standard accretion disc (SAD) for $r > r_J$, (2) an inner Jet Emitting Disc (JED) for $r < r_J$ driving (3) a self-collimated non-relativistic electron-proton surrounding, when adequate conditions are met, (4) a ultra-relativistic electron-positron beam. The dynamical properties of each constituent have been thoroughly analyzed in previous works (e.g. Shakura & Sunyaev 1973; Henri & Pelletier 1991; Ferreira & Pelletier 1995; Marcowith et al. 1997; Renaud & Henri 1998; Saugé & Henri 2003, 2004), but it is the first time where they are invoked altogether as necessary ingredients to reproduce the different spectral states of a same object. We showed that the various canonical states can be qualitatively explained by varying *independently* the transition radius r_J and the disc accretion rate \dot{m} .

REFERENCES

- Belloni, T., Homan, J., P., C., et al. 2005, *astro-ph/0504577*
- Belloni, T., Mendez, M., King, A. R., van der Klis, M., & van Paradijs, J. 1997, *ApJ*, 479, L145+
- Beloborodov, A. M. 1999, in *ASP Conf. Ser. 161: High Energy Processes in Accreting Black Holes*, 295–+
- Bogovalov, S. & Tsinganos, K. 2001, *MNRAS*, 325, 249
- Bogovalov, S. V. 2001, *A&A*, 371, 1155
- Casse, F. & Ferreira, J. 2000, *A&A*, 353, 1115
- Corbel, S., Fender, R. P., Tomsick, J. A., Tzioumis, A. K., & Tingay, S. 2004, *ApJ*, 617, 1272
- Corbel, S., Nowak, M. A., Fender, R. P., Tzioumis, A. K., & Markoff, S. 2003, *A&A*, 400, 1007
- Esin, A. A., McClintock, J. E., & Narayan, R. 1997, *ApJ*, 489, 865
- Falcke, H. & Biermann, P. L. 1995, *A&A*, 293, 665

- Falcke, H., K rding, E., & Markoff, S. 2004, *A&A*, 414, 895
- Fender, R. P., Belloni, T. M., & Gallo, E. 2004, *MNRAS*, 355, 1105
- Fender, R. P., Gallo, E., & Jonker, P. G. 2003, *MNRAS*, 343, L99
- Ferreira, J. 1997, *A&A*, 319, 340
- Ferreira, J. 2002, in "Star Formation and the Physics of Young Stars", J. Bouvier and J.-P. Zahn (Eds), *EAS Publications Series*, astro-ph/0311621, 3, 229
- Ferreira, J. & Pelletier, G. 1993, *A&A*, 276, 625+
- Ferreira, J. & Pelletier, G. 1995, *A&A*, 295, 807+
- Ferreira, J., Petrucci, P. O., Henri, G., Saug , L., & Pelletier, G. 2005, *A&A*
- Galeev, A. A., Rosner, R., & Vaiana, G. S. 1979, *ApJ*, 229, 318
- Gallo, E., Corbel, S., Fender, R. P., Maccarone, T. J., & Tzioumis, A. K. 2004, *MNRAS*, 347, L52
- Gallo, E., Fender, R. P., & Hynes, R. I. 2005, *MNRAS*, 356, 1017
- Gallo, E., Fender, R. P., & Pooley, G. G. 2003, *MNRAS*, 344, 60
- Gilfanov, M., Churazov, E., & Revnivtsev, M. 1999, *A&A*, 352, 182
- Hameury, J.-M., Lasota, J.-P., McClintock, J. E., & Narayan, R. 1997, *ApJ*, 489, 234
- Hannikainen, D., Campbell-Wilson, D., Hunstead, R., et al. 2001, *Astrophysics and Space Science Supplement*, 276, 45
- Henri, G. & Pelletier, G. 1991, *ApJ*, 383, L7
- Heyvaerts, J. F. & Priest, E. R. 1989, *A&A*, 216, 230
- Maccarone, T. J. 2003, *A&A*, 409, 697
- Mahadevan, R. 1997, *ApJ*, 477, 585
- Malzac, J., Beloborodov, A. M., & Poutanen, J. 2001, *MNRAS*, 326, 417
- Marcowith, A., Henri, G., & Pelletier, G. 1995, *MNRAS*, 277, 681
- Marcowith, A., Henri, G., & Renaud, N. 1998, *A&A*, 331, L57
- Marcowith, A., Pelletier, G., & Henri, G. 1997, *A&A*, 323, 271
- Markoff, S. 2004, in *X-ray Binaries to Quasars: Black Hole Accretion on All Mass Scales*, ed. T. J. Maccarone, R. P. Fender, and L. C. Ho
- Markoff, S., Falcke, H., & Fender, R. 2001, *A&A*, 372, L25
- Markoff, S., Nowak, M., Corbel, S., Fender, R., & Falcke, H. 2003, *A&A*, 397, 645
- Markoff, S. & Nowak, M. A. 2004, *ApJ*, 609, 972
- McClintock, J. E. & Remillard, R. A. 2003, *astro-ph/0306213* (McCR03)
- Merloni, A. & Fabian, A. C. 2002, *MNRAS*, 332, 165
- Merloni, A., Heinz, S., & di Matteo, T. 2003, *MNRAS*, 345, 1057
- Narayan, R., McClintock, J. E., & Yi, I. 1996, *ApJ*, 457, 821
- Nespoli, E., Belloni, T., Homan, J., et al. 2003, *A&A*, 412, 235
- O'Dell, S. L. 1981, *ApJ*, 243, L147
- Pelletier, G. 2004, in *Dynamics and dissipation in electromagnetically dominated media*" (Nova Science) edited by M. Lyutikov (astro-ph/0405113)
- Pelletier, G. & Roland, J. 1989, *A&A*, 224, 24
- Pelletier, G. & Sol, H. 1992, *MNRAS*, 254, 635
- Pelletier, G., Sol, H., & Asseo, E. 1988, *Phys. Rev. A*, 38, 2552
- Pietrini, P. & Krolik, J. H. 1995, *ApJ*, 447, 526
- Renaud, N. & Henri, G. 1998, *MNRAS*, 300, 1047
- Saug , L. & Henri, G. 2003, *New Astronomy Review*, 47, 529
- Saug , L. & Henri, G. 2004, *ApJ*, 616, 136
- Shakura, N. I. & Sunyaev, R. A. 1973, *A&A*, 24, 337
- Sobczak, G. J., McClintock, J. E., Remillard, R. A., et al. 2000, *ApJ*, 544, 993
- Sol, H., Pelletier, G., & Asseo, E. 1989, *MNRAS*, 237, 411
- Stone, J. M., Hawley, J. F., Gammie, C. F., & Balbus, S. A. 1996, *ApJ*, 463, 656
- Vadawale, S. V., Rao, A. R., & Chakrabarti, S. K. 2001, *A&A*, 372, 793
- Zdziarski, A. A., Gierliński, M., Mikołajewska, J., et al. 2004, *MNRAS*, 351, 791
- Zdziarski, A. A. & Gierlinski, M. 2003, in *Proceedings of "Stellar-mass, intermediate-mass, and supermassive black holes"*, Kyoto astro-ph/0403683 (ZG04), 99–119
- Zdziarski, A. A., Lubinski, P., & Smith, D. A. 1999, *MNRAS*, 303, L11

A STUDY OF TEMPORAL CHARACTERISTICS OF SELECTED CATAclySMIC VARIABLES : THE BROAD-BAND NOISE STRUCTURE BETWEEN 2-20 KEV

Ş. Balman^{1,2}, B. Külebi², and E. Beklen²

¹ESA-ESTEC, Keplerlaan 1 P.O. Box 299 2200 AG Noordwijk ZH, Netherlands

²Department of Physics, Middle East Technical University, Ankara, 06531, Turkey

ABSTRACT

We present the preliminary analysis of the band-limited noise structure of Cataclysmic Variables (CVs) in the 2-20 keV energy band. We have currently analyzed Rossi X-ray Timing Explorer (RXTE) PCA data and derived time series from 30 CVs using the RXTE archive. In general, CVs of different types all show broad band noise which can be fitted with power laws, using exponential cut-offs, and Lorentzians in a similar way to power spectral (noise) characteristics of X-ray Binaries (XRBs). In general terms the power spectra show a power law index of $(-1.2-2)$. A rather large scale flattening of the power spectra exists in nonmagnetic systems in the low to very low frequency range. We observe that in low and high states/outbursts the noise in the high frequency range and low frequency range is changed. CVs show considerable very low frequency noise. In addition, we have recovered several possible QPOs in the X-ray wavelengths from CVs mainly from Intermediate Polar systems.

Key words: accretion: accretion disks - binaries:close - cataclysmic variables - X-rays: stars: quasi-periodic oscillations.

1. INTRODUCTION

Band limited noise from X-ray binaries (XRBs) have been studied in detail to understand the accretion process in comparison with other sources of colored noise in isolated systems (see van der Klis 2000 for a review). Recently, several QPOs, DNOs (dwarf nova oscillations) and IpDNOs (long period DNOs) have been detected from CVs (mostly in the optical wavelengths, timescales are 3-1000 sec). The favored interpretation is that they are a result of magnetospheric interaction of the accretion flow at the inner disk (DNOs) and magnetically excited traveling waves in the disk for QPOs. (Warner, Woudt & Pretorius 2003; Warner 2004). There are many parallel behaviors with the QPOs seen in X-ray binaries with

high and low frequency X-ray QPOs resembling respectively DNOs and QPOs in CVs. DNOs exhibit frequency drifts, period doubling and 1:2:3 harmonic structure similar to black hole LMXBs (Kluźniak et al. 2005; see also Hameury & Lasota 2005). Our motivation is first, to understand the noise structure in CVs in order to interpret the origin and type of QPOs in CVs.

2. RESULTS

We used the Rossi X-ray Timing Explorer RXTE archive to study the broad band noise structure of CVs. RXTE has observed 55 CVs with more than one pointing on about half the sample. We analyzed the data of 30 CVs obtained with the Proportional Counter Array (PCA). We used archived background subtracted and merged light curves for the analysis in the low frequency range below 0.01 Hz. For the higher frequency range between 0.01-1 Hz, the data were screened and the light curves were created via SEEXTRACT v4.2. The power spectral analyses were carried out by FTOOLS/XRONOS v.5.21. and averaged about/over 30-100 spectra in each case yielding about 1000-2000 sec coherence timescale in the low frequencies (LFN $\nu < 0.01$). A 100-200 sec coherence time scale was used in the high frequency regime (HFN $0.01 < \nu < 1$) while 100-500 spectra were averaged. Figure 1 displays the fitted power spectra of a group of CVs with high states and low states labeled on each panel. The y axis is power normalized such that their integral gives the squared rms fractional variability (therefore the power spectrum is in units of $(\text{rms})^2/\text{Hz}$). The expected (white) noise level is subtracted to obtain the rms fractional variability of the series $((\text{rms})^2 - \text{mean}/\text{Hz})$. The data are fitted successfully (χ^2_ν in a range 1.1-1.9) with a power law plus an exponential cut off model. Occasionally, when necessary, lorentzians were added around wide QPO features to fit the data more properly. The QPOs were largely recovered from Intermediate Polars; only two Polars (AM Her and V834 Cen) and one nonmagnetic CV (SS Cyg) showed QPO like structures in the X-rays (see Table 1).

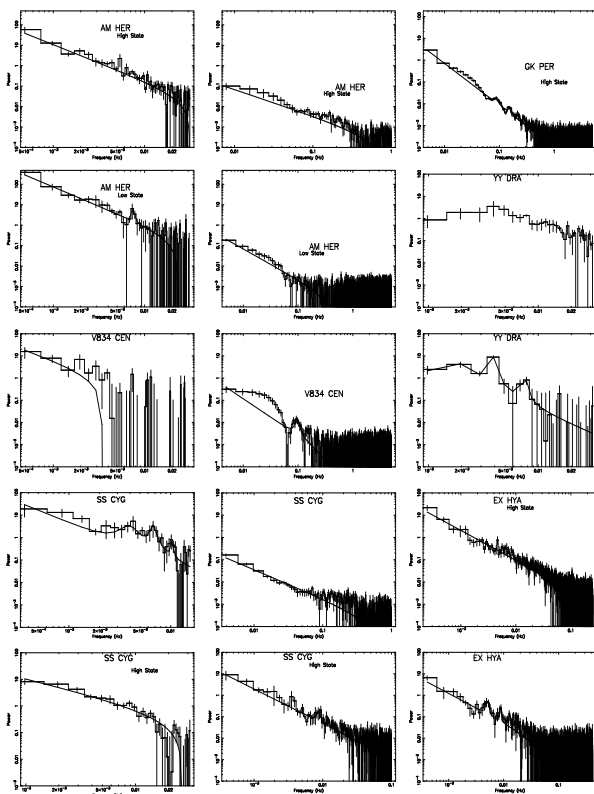


Figure 1. Noise power spectra of selected CVs in 2-20 keV energy band. The objects and their states are labeled on each panel.

3. DISCUSSION

In general CVs show lower broad band noise compared to X-ray binaries (XRBs). Even the highest noise spectrum cuts off below 0.5 Hz during outbursts/high states (like GK Per, Am Her); in quiescence the cut-offs are below 0.1 Hz. The cut-off frequency of nonmagnetic CVs is largely lower than 0.007-0.001 Hz. In general CVs constitute the low end of the Atoll, Z sources and BHCs. The HFN of XRBs do not exist for CVs. The LFN of XRBs is like HFN for CVs and the VLFN for XRBs is LFN for CVs. Then, the very low frequency below 0.0005 Hz that is very abundant in CVs can be considered as ELFN (extremely low frequency noise). The power law indices of the CV power spectra range between $-(1.2-2.0)$ in general with a few exceptions. Intermediate Polars have steep spectra without flattening (except for YY Dra). Some Polars and particularly nonmagnetic CVs show considerable flattening below 0.001 Hz. There seems to be little variability in the LFN range during high states/outbursts. QPOs during high states are in the HFN regime, like in GK Per, V834 Cen and SS Cyg. Coherent QPOs exist only in the LFN range during low or quiescent states (and no significant QPO exists in HFN regime, also) as in EX Hya, SS Cyg, AM Her and YY Dra. These possible LFN QPOs detected in the magnetic CVs should be the equivalent of HBOs in LMXBs. See

Table 1 : The Table of QPOs and Cut-off Frequencies

OBJECT	CUTOFF FR (Hz)	QPO (Hz)	COMMENT
AM Her	0.5		high state
AM Her	0.1	$0.0074^{+0.0008}_{-0.0003}$	low state
V834 Cen	0.26	$0.097^{+0.012}_{-0.007}$	high state
EX Hya	0.015	$0.0051^{+0.0002}_{-0.0001}$	quiescence
		0.0087	quiescence
GK Per	1	$0.089^{+0.003}_{-0.003}$	outburst
		$0.153^{+0.005}_{-0.003}$	outburst
PQ Gem	0.5	$0.086^{+0.003}_{-0.004}$	quiescence
YY Dra		$0.0074^{+0.0008}_{-0.0003}$	quiescence
YY Dra	0.3		outburst
SS Cyg	0.02	$0.0039^{+0.0030}_{-0.0014}$	quiescence
		$0.0067^{+0.0007}_{-0.0007}$	quiescence
		0.011	quiescence
SS Cyg	0.4	$0.0087^{+0.0007}_{-0.0007}$	outburst

Table 1 for QPO details. The CVs in high and low states or in outburst have their LFN and HFN reallocated. During high states and outbursts HFN increases. In quiescence and the low states LFN is dominant and, HFN gets less. The LFN during quiescent/low states is more than in the outburst/high states. This is analogous to XRBs where the broad-band noise is controlled by accretion rate. This scenario strongly supports that the high and low states in CVs are due to changes in the accretion rate.

The nonmagnetic CV T Leo shows extremely high band limited power (4000-6000 rms mean subtracted power) below 0.001 Hz. in the RXTE observation taken during a superoutburst (Howell et al. 1999). The increase in mass accretion rate increases the VLFN (ELFN) range as detected in other Atoll sources. SS Cyg is known to show several QPOs (Mauche 2002; Wheatley et al. 2003). We find similar QPOs in the quiescent state.

REFERENCES

- [1] Hameury, J.-M., Lasota, J.P. 2005, in The Astrophysics of Cataclysmic Variables and Related Objects, ASP Conf. Ser., Vol. 330, J.-M. Hameury, J. P. Lasota (eds), (San Francisco:ASP)
- [2] Howell, S., Ciardi D.R., Szkody, P., van Paradijs, J., Kuulkers, E., Jenifer, C., Sirk, M., Long, K.S. 1999, PASP, 111, 342
- [3] van der Klis, M. 2000, ARA&A, Vol. 38, 717
- [4] Kluzniak, W., Lasota, J.P., Abramowicz, M.A., Warner, B. 2005, A&A, 2005, 440L, 25
- [5] Mauche, C. W. 2002, ApJ, 580, 423
- [6] Warner, B. 2004, PASP, 116, 115
- [7] Warner, B., Woudt, P.A., Preterious, M.I. 2003, MNRAS, 344, 1193
- [8] Wheatley, P.J., Mauche, C.W., Mattei, J.A. 2003, MNRAS, 345, 49

HIDDEN MAGNETIC ACCRETORS: XMM-NEWTON OBSERVATIONS OF LS PEGASI

D.S.Baskill¹ and P.J.Wheatley²

¹Department of Physics & Astronomy, University of Leicester, University Road, Leicester, LE1 7RH, U.K.

²Department of Physics, University of Warwick, Coventry, CV4 7AL, U.K.

ABSTRACT

Cataclysmic variables (CVs) are close binary stars in which a white dwarf accretes material from a Roche-lobe filling late-type companion. If the magnetic field of the white dwarf is strong enough, it can dominate the accretion flow from the inner accretion disk directly onto the magnetic poles of the white dwarf.

A surprising result emerged from our analysis of the entire sample of non-magnetic cataclysmic variables observed with ASCA (Baskill, Wheatley & Osborne, 2005). We found that two extremely hard systems appeared spectrally distinct from the rest of the sample (V426 Oph & LS Peg; see figure 1). These are probably weakly magnetic accretors, but there is no strong evidence of periodic variability - currently the only accepted method of identifying such a system (Patterson, 1994).

Here we report the results of the 45ks XMM-Newton observation of LS Peg. V426 Oph will be observed by XMM-Newton in 2006.

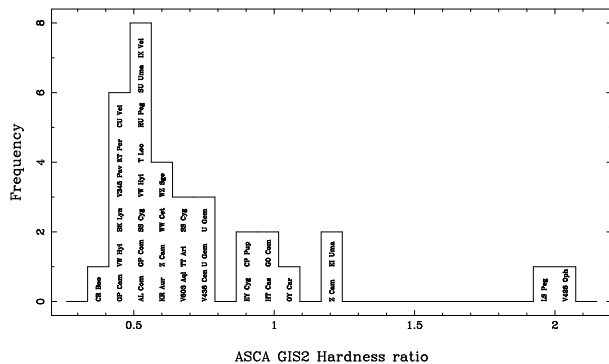


Figure 1. Hardness ratios of all the non-magnetic cataclysmic variables observed with the ASCA GIS2 instrument. Two systems stand out as having an unusually hard spectra: LS Pegasi and V426 Ophiuchi.

Key words: stars, dwarf novae, novae, magnetic, non-magnetic, cataclysmic variables, X-rays.

1. ASCA OBSERVATIONS OF LS PEGASI

Although the ASCA spectra of LS Peg contain few counts (<1000 counts in the combined GIS instruments) it was surprisingly difficult to model, requiring strong X-ray absorption by highly ionised material and a temperature distribution weighted towards high temperatures (Baskill, Wheatley & Osborne, 2005). However, fitting such a complex model is ambiguous at such low signal-to-noise.

A possible 30.9 ± 0.3 minute modulation was detected in the ASCA power spectra (figure 2). Fitting the folded SIS0 light-curve with a sine function yielded an amplitude of 32 ± 5 per cent. Rodríguez *et al.* (2001) independently report a detection of a period at 29.6 ± 1.8 min in the circular polarisation of LS Peg. The coincidence of these detected periods leads us to believe that the modulation detected in the ASCA light-curve may be periodic, and that the modulation in X-rays and circular polarisa-

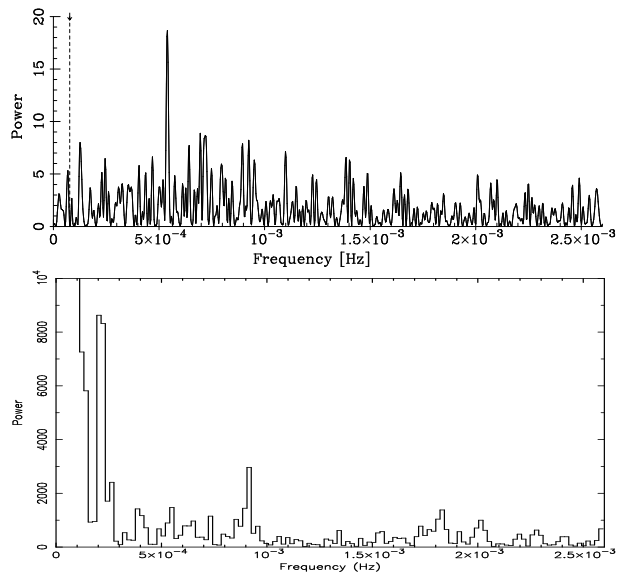


Figure 2. The ASCA SIS0 (top) and XMM-Newton EPIC-MOS1 (bottom) power spectra of LS Pegasi.

tion have a common physical origin. Hence, we proposed an XMM-Newton observation in an attempt to confirm the modulation and so resolve the true nature of LS Peg.

2. XMM-NEWTON OBSERVATIONS OF LS PEG

Our temporal analysis of the XMM-Newton observation of LS Peg has failed to confirm the existence of the modulation detected in the ASCA observation (figure 2).

We began our spectral modelling of the XMM-Newton EPIC-MOS1 data by fitting a hot optically thin gas emission model at a single (7.5keV) temperature (the MEKAL model in *XSPEC*) above 3.5keV, which reveals the need for a significant amount of absorption (see figure 3). Including simple photo-electric absorption (WABS*MEKAL) also cannot reproduce the spectral shape between 1-3keV. Using a partial covering absorbing model instead (PCFABS*MEKAL) results in a much better fit, being able to reproduce the flat low-energy spectrum. This is also consistent with the spectral models expected of intermediate polars e.g. Norton & Watson (1989), Ishida, Mukai & Osborne (1994), Ezuka & Ishida (1999).

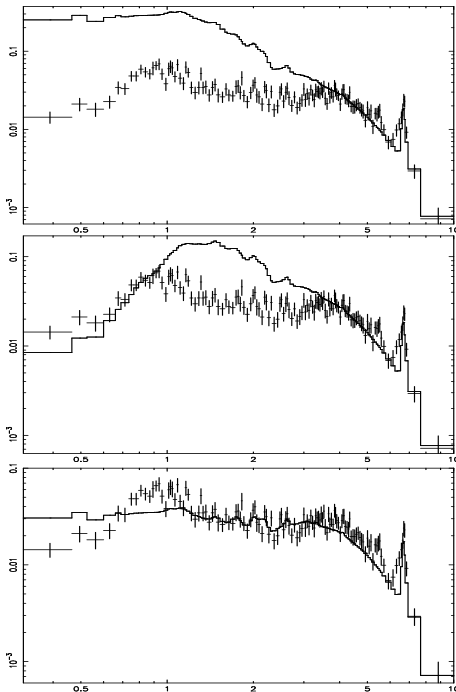


Figure 3. Fitting the XMM-Newton spectrum of LS Peg in *XSPEC*, using a single temperature hot diffuse gas model alone (top), with a simple photo-electric absorption model (middle), and with a partial covering absorbing model (bottom).

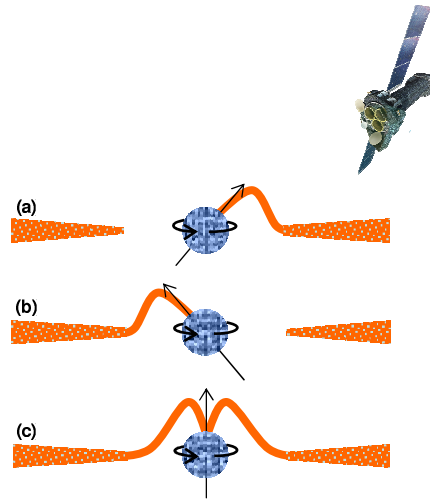


Figure 4. Geometry around the white dwarf in an intermediate polar. If the magnetic field axis of the white dwarf is not perpendicular to the accretion disk, the system (and so X-ray emission) modulates between (a) and (b), as observed by XMM-Newton. However, if the magnetic axis of the white dwarf is aligned perpendicular to the accretion disk (c), no such modulation exists.

3. THE NATURE AND POSSIBLE GEOMETRY OF LS PEGASI

Although no periodic modulation is detected in the XMM-Newton observation of LS Peg, the spectrum indicates that this system is an intermediate polar. Such a result might be expected if the white dwarf's magnetic axis is inclined almost perpendicular to the accretion disk.

When the magnetic axis of the white dwarf is inclined to the accretion disk plane, the accretion flow is modulated at the rotational frequency of the white dwarf (a modulation between geometry a & b in figure 4). However, if the magnetic field axis is aligned close to perpendicular to the accretion disk plane, no such modulation would be observed (figure 4c). In such a case, there would be only a small variation of the accretion stream with viewing angle (which changes as the white dwarf rotates). With such a geometry, even a strongly magnetic system would only be detected via spectroscopy.

REFERENCES

- Baskill D.S., Wheatley P.J. & Osborne J.P. 2005, MNRAS, 357, 626
- Ezuka H. & Ishida M. 1999, ApJS, 120, 277
- Ishida M., Mukai K., & Osborne J.P. 1994, PASJ, 46, 81
- Norton A. & Watson M. 1989, MNRAS, 237, 853
- Patterson J. 1994, PASP, 106, 209
- Rodríguez-Gil P., *et al.* 2001, ApJ, 548, L49

SWIFT, *INTEGRAL*, *RXTE*, AND *SPITZER* REVEAL IGR J16283–4838

Volker Beckmann^{1,2}, J. A. Kennea³, C. Markwardt^{1,4}, A. Paizis^{5,6}, S. Soldi^{5,8}, J. Rodriguez⁷, S. D. Barthelmy¹,
D. N. Burrows³, M. Chester³, N. Gehrels¹, N. Mowlavi^{5,8}, and J. Nousek³

¹NASA Goddard Space Flight Center, Exploration of the Universe Division, Greenbelt, MD 20771, USA

²Joint Center for Astrophysics, Department of Physics, University of Maryland, Baltimore County, MD 21250, USA

³Dept. of Astronomy and Astrophysics, Pennsylvania State Univ., 525 Davey Laboratory, Univ. Park, PA 16802, USA

⁴Department of Astronomy, University of Maryland, College Park, MD 20742, USA

⁵INTEGRAL Science Data Centre, Chemin d'Écogia 16, 1290 Versoix, Switzerland

⁶CNR-IASF, Sezione di Milano, via Bassini 15, 20133 Milano, Italy

⁷Centre d'Etudes de Saclay, DSM/DAPNIA/SaP (CNRS UMR AIM/7158), 91191 Gif-sur-Yvette Cedex, France

⁸Observatoire de Genève, 51 chemin des Maillettes, 1290 Sauverny, Switzerland

ABSTRACT

We present the first combined study of the recently discovered source IGR J16283–4838 with *Swift*, *INTEGRAL*, and *RXTE*. The source, discovered by *INTEGRAL* on April 7, 2005, shows a highly absorbed (variable $N_{\text{H}} = 0.4 - 1.7 \times 10^{23} \text{ cm}^{-2}$) and flat ($\Gamma \sim 1$) spectrum in the *Swift*/XRT and *RXTE*/PCA data. No optical counterpart is detectable ($V > 20$ mag), but a possible infrared counterpart within the *Swift*/XRT error radius is detected in the *2MASS* and *Spitzer*/GLIMPSE survey. The observations suggest that IGR J16283–4838 is a high mass X-ray binary containing a neutron star embedded in Compton thick material. This makes IGR J16283–4838 a member of the class of highly absorbed HMXBs, discovered by *INTEGRAL*.

Key words: gamma rays: observations, X-rays: binaries, X-rays: individual (IGR J16283-4838), stars: neutron.

1. INTRODUCTION

Star formation in our Galaxy takes place mainly in the dense regions of the spiral arms. These regions host massive molecular clouds and also the majority of the single and binary neutron stars ($\sim 10^9$) and black holes ($\sim 10^8$) in the Milky Way. The dense molecular clouds lead to strong star formation activity, which also results in the formation of binary systems, and subsequently to X-ray binary systems. These objects show X-ray flares and outbursts because of accretion processes onto the compact

object. At the same time, the gas and dust of the spiral arms absorb most of the emission in the optical to soft X-ray regime below 10 keV. In addition, dense absorbing atmospheres around the object make the detection of these sources even more difficult. The hard X-ray and soft gamma-ray mission *INTEGRAL* operates at energies above 20 keV. With the large field of view and its observing program focussed on the Galactic plane and center, *INTEGRAL* is a powerful tool to discover highly absorbed sources ($N_{\text{H}} > 10^{23} \text{ cm}^{-2}$). So far a handful of those enigmatic objects has been found by *INTEGRAL*. Most, if not all, of these sources appear to be HMXBs, probably hosting a neutron star as the compact object and show variable absorption. Here we report the discovery and analysis of another highly absorbed source, IGR J16283–4838. This work makes the first use of the combined data of *INTEGRAL*, *Swift*, *RXTE*, and *Spitzer*.

2. OBSERVATIONS

IGR J16283–4838 was discovered (Soldi et al. 2005) during the observation of the Norma arm region by the imager IBIS/ISGRI on-board *INTEGRAL*. The observation lasted from April 7-9, 2005, with an effective ISGRI exposure time of 126 ksec. The source showed a flux of $f_X = (4.8 \pm 0.8) \times 10^{-11} \text{ erg cm}^{-2} \text{ s}^{-1}$ in the 20 - 60 keV band. The analysis of the data prior to the discovery resulted in a 3σ upper limit of $f_{20-60 \text{ keV}} = 1.7 \times 10^{-11} \text{ erg cm}^{-2} \text{ s}^{-1}$. The source showed significant brightening during an *INTEGRAL* observation starting on April 10 (Paizis et al. 2005). After the discovery of IGR J16283–4838 two *Swift* follow-up observations

took place 3 and 5 days after the last *INTEGRAL* observation. The first one started on April 13, 14:02 U.T. with an exposure time of 2.5 ksec, which resulted in an effective *Swift*/XRT exposure of 550 sec. A second observation was performed on April 15 with 2600 sec effective XRT exposure time. Applying a centroid algorithm to the data of April 15 gives a refined position for the source of $R.A. = 16^{\text{h}}28'10.56''$, $DEC = -48^{\circ}38'56.4''$ with an uncertainty of 6'' radius. IGR J16283–4838 was then also observed twice by *RXTE*/PCA, and a counterpart was found in the 2MASS and *Spitzer*/GLIMPSE data bases. Another observation in the K-band was performed with the 6.5m Magellan-Baade telescope on April 21, 2005. This observation indicates that the source seen in the 2MASS is a blend of point sources, with the brightest showing $K = 14.1$ mag (Steeghs et al. 2005). Therefore the identification with the *Spitzer* source is tentative.

3. DISCUSSION

The position within the Galactic plane at only +6.1 arcmin makes a Galactic origin of the source likely, even though some AGN have been seen through the plane by *INTEGRAL*, like the Seyfert 1 galaxy GRS 1734-292. Strong variability as observed in IGR J16283–4838 has been seen in the X-ray spectra of Seyfert galaxies, but the X-ray spectrum is too flat ($\Gamma \simeq 1$) for a Seyfert galaxy. This would still leave the possibility of a blazar as counterpart. But the absorption by the Galaxy in the direction of the source ($N_{\text{H}} = 2.2 \times 10^{22} \text{ cm}^{-2}$) is not high enough to explain the intrinsic absorption of $1.7 \times 10^{23} \text{ cm}^{-2}$, and thus intrinsic strong absorption in the blazar would be required, but this has not been seen so far in blazar spectra.

If we consider IGR J16283–4838 to be a Galactic source, mainly two types of bright and variable hard X-ray emitters are likely to be a counterpart: Low Mass and High Mass X-ray Binaries, LMXBs and HMXBs, respectively. The hard X-ray spectrum with strong absorption indicates the presence of a HMXB in which no pulsation have been detected so far. Also the bright infrared emission, if connected to the X-ray source, would indicate a massive star as the companion of the compact object. The luminosity of the object during the flare can be estimated by taking the brightest stage during the *RXTE* observation and assuming a distance to the object between 1 and 10 kpc. The unabsorbed flux is in this case only 20% larger than the absorbed one, because the significant part of the luminosity is emitted in the hard X-rays. The bolometric luminosity is then in the range $\log L_{\text{burst}} = 34.0 - 36.5$ (where L is in units of erg s^{-1}). The quiescent luminosity of the system is at least a factor of ~ 20 lower with $\log L_{\text{q}} < 33 - 35.2$. This range of values is consistent with measurements from known Be/X-ray binaries with a neutron star as the compact object (Negueruela 1998). In any case the luminosity is far below the Eddington luminosity of a neutron star of $1.4M_{\odot}$ ($L = 1.8 \times 10^{38} \text{ erg s}^{-1}$).

The properties of IGR J16283–4838 are similar to those

of a number of highly absorbed sources ($N_{\text{H}} = 1 - 20 \times 10^{23} \text{ cm}^{-2}$) found in the Galactic plane, especially in the Norma arm region (Walter et al. 2004). Only one of the newly detected highly absorbed sources has been claimed so far not to be a HMXB (IGR J16358–4726; Patel et al. 2004). The fact that most of the absorbed sources so far have shown to be HMXBs (Kuulkers et al. 2005) containing neutron stars does not rule out significant contribution of HMXBs with a black hole as the compact object. It appears that variable absorption is a common feature in highly absorbed HMXBs. This could mean that the absorbing material is linked to the existence of a high mass donor in the binary system. In this case a strong and dense stellar wind (10^{-7} to $10^{-5} M_{\odot} \text{ yr}^{-1}$) from the early-type stellar companion will probably cause the absorption in the system.

4. CONCLUSIONS

The newly discovered hard X-ray source IGR J16283–4838, located in the Norma arm region, is likely to be a HMXB containing a neutron star as the compact object (Beckmann et al. 2005). It is located in the Galactic Plane in the direction of star forming regions in the spiral arms and shows a large flare, which makes an extragalactic origin unlikely. The spectrum is hard ($\Gamma \sim 1$) and strongly absorbed during the flare, which indicates a HMXB rather than a LMXB. The luminosity is comparably low ($L < 10^{37} \text{ erg s}^{-1}$) which is typical for a neutron star HMXB. The strong and variable absorption ($N_{\text{H}} = 0.4 - 1.7 \times 10^{23} \text{ cm}^{-2}$) indicates that IGR J16283–4838 belongs to the class of highly absorbed HMXBs discovered by *INTEGRAL* along the Galactic plane. Bright and absorbed sources like IGR J16283–4838 could contribute significantly to the Galactic hard X-ray background in the 10–200 keV band.

REFERENCES

- Beckmann V., Kennea J. A., Markwardt C., et al. 2005, ApJ accepted, astro-ph/0506170
- Kuulkers E. 2005, Proc. of the Interacting Binaries Meeting of Cefalu, Italy, July 2004, AIP, in press
- Negueruela I. 1998, A&A, 338, 505
- Paizis A., Miller J. M., Soldi S., Mowlavi N. 2005, ATEL, 458
- Patel S.K., Kouveliotou C., Tennant A., et al. 2004, ApJ, 602, L45
- Soldi S., Brandt S., Domingo Garau A., et al. 2005, ATEL, 456
- Steeghs D., Torres M.A.P., Jonker P.G., et al. 2005, ATEL 478
- Walter R., Courvoisier T.J.-L., Foschini L., et al. 2004, Proc. 5th INTEGRAL workshop, ESA-SP 552, 417

SAX J2103.5+4545, THE CLOSEST BE+NEUTRON STAR GALACTIC SYSTEM.

P. Blay¹, A. Camero¹, S. Martínez-Núñez¹, P.Reig², and I. Negueruela³

¹GACE - ICMUV - Universidad de Valencia, PO BOX 22085, 46071 Valencia, Spain

²FORTH, 71110 Heraklion, Crete, Greece

²Physics Department, University of Crete, 71003 Heraklion, Crete, Greece

³Dpto. de Física, Ing. de sistemas y Teoría de la señal, EPSA, Universidad de Alicante, PO BOX 99, 03080 Alicante, Spain

ABSTRACT

In view of the new *INTEGRAL* high energy data and the last two years monitoring of the recently discovered optical counterpart to SAX J2103.5+4545, the properties of this BeX system during the last bright state and the present faint state are reviewed. Our data suggests the applicability of disk truncation theories and disk global oscillation models to this system, and the occurrence of dramatic changes in the structure of the circumstellar matter of the optical counterpart to SAX J2103.5+4545 on time scales of months.

Key words: stars:Be – pulsars: individuals: SAX J2103.5+4545 – X-rays:binaries.

1. INTRODUCTION

SAX J2103.5+4545 is a BeX with a ~ 12.68 d orbital period showing ~ 352 s X-ray pulsations. It was discovered with BeppoSAX data in 1997 during a bright outburst (Hulleman et al. 1998). Its spectral properties and the orbital modulation observed in its flux suggested that the system was a BeX, but the optical counterpart was not identified until recently (Reig et al. 2004). The source shows faint states -with low luminosity (10^{34} erg s⁻¹) and no orbital modulation of the flux- and bright states -with high luminosity (10^{36} erg s⁻¹) and flux modulation with the orbital period of the system- (Baykal et al. 2002). *INTEGRAL* is a high-energy ESA mission with collaborations from Russia and USA. There are 2 main instruments on board *INTEGRAL*, the spectrometer SPI and the imager IBIS (with two detector layers, ISGRI and PICSiT), optimised for fine spectroscopy and imaging, respectively, in γ -ray bands. Two monitors (JEM-X in X-ray bands, and OMC in the optical V band) complement the main instruments. *INTEGRAL* observed the last bright (MJD 52500 to 52900) and faint (MJD 52900 onwards) states underwent by the source (see Blay et al.

2004, Sidoli et al. 2005, and Falanga et al. 2005). We present *INTEGRAL* public data collected during this period together with the first results of the optical monitoring of SAX J2103.5+4545 from the Skinakas Observatory (Crete, Greece).

2. OPTICAL COUNTERPART

The optical counterpart to SAX J2103.5+4545 has been monitored continuously, in the H α region, from the Skinakas Observatory (Crete, Greece) during 2003 and 2004. In Fig. 1 the evolution of the H α (together with the HeI $\lambda 6678$ Å line) is shown. The H α line suffered a major change from August 2003 to September 2003, where a double emission peak feature (a shell spectrum), seen during August 2003, disappeared. From then on, we notice the presence of variable absorption core components, indicative of the presence of some circumstellar emission. It is noticeable that the transition of the H α line from a double peak structure to an absorption profile, filled with some emission, occurs in coincidence with the transition of the system from a bright state to a faint state.

3. HIGH ENERGY (THE ACCRETION PROCESS)

An average *INTEGRAL*/SPI spectra for the bright state, and an average spectra for the faint state are shown in the top panel of Fig. 2.

Light curves were built from *INTEGRAL*/ISGRI lists of events, selected by PIF (Pixel Illumination Fraction) extraction methods. Arrival times were transformed to a heliocentric reference frame and corrected of the orbital motion of the system. The bottom panel of Fig. 2 shows the evolution of the pulse period as derived from *INTEGRAL*/ISGRI data. We notice the complexity of the pulse

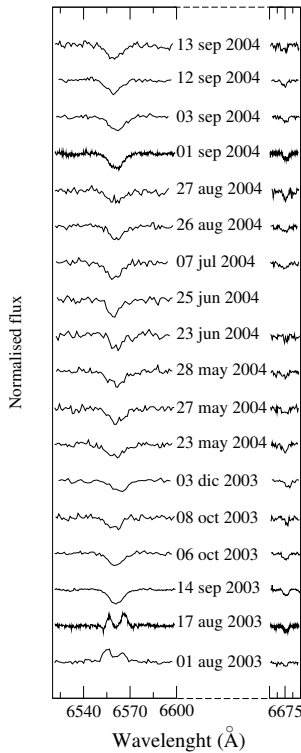


Figure 1. Evolution of the $H\alpha$ and $HeI \lambda 6678 \text{ \AA}$ profiles of the optical counterpart to SAX J2103.5+4545.

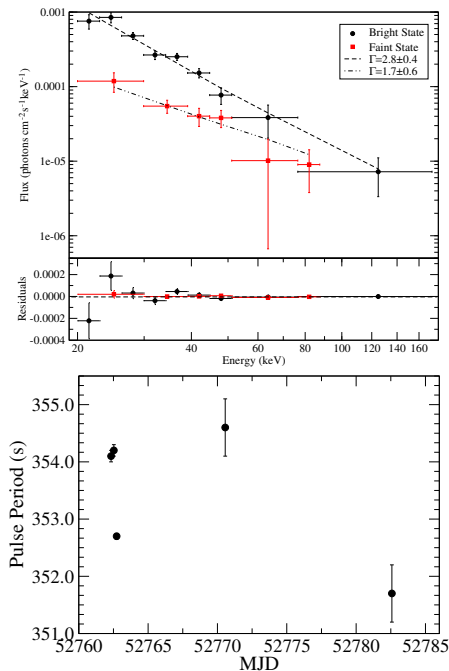


Figure 2. **Top:** Comparison of spectra extracted with *INTEGRAL/SPI* during the bright and the faint states undergone by the system. **Bottom:** Pulse period history of SAX J2103.5+4545 in the 24–45 keV energy range (*INTEGRAL/ISGRI* data) during the last bright state. We notice the complex pulse period evolution of the system.

period evolution, undergoing alternate epochs of spin up and spin down processes.

4. DISCUSSION AND CONCLUSIONS

The complex timing behaviour of the source is evident. SAX J2103.5+4545 is suffering spin up and spin down epochs, which will coincide with changes in the accretion rate. Given the short orbital period of SAX J2103.5+4545 (~ 12.68 days), the NS must exert substantial influence on the circumstellar disk. In the optical band, this influence translates into a highly variable $H\alpha$ line, as seen in Fig. 1. In the framework of the viscous decretion model (Okazaki & Negueruela 2001), the tidal interaction of the NS produces the truncation of the Be star envelope. The truncation radius in SAX J2103.5+4545 would be similar in size to the critical lobe radius at periastron. When the density and/or size of the Be star envelope are large enough, matter fills the critical lobe and is accreted onto the NS. The system is in the bright state. After several orbits the NS exhausts the Be star's disk matter and the system enters a faint state. Once the disk recovers the initial conditions, the cycle starts again. We must keep in mind that global changes in the flux of matter from the donor down to the NS can also produce a similar behaviour. The number of optical observations of SAX J2103.5+4545 is scarce, but the information available indicates a correlation between the long-term optical and X/ γ -ray variability. We expect the enhancement of emission in the $H\alpha$ line as well as larger infrared excesses when next bright state starts. The occurrence of the next bright state is unpredictable. Previous faint states had durations varying between 30 and 300 days.

REFERENCES

- [1] Baykal, A., Stark, M.J., and Swank, J.H. 2002, *ApJ*, 569, 903
- [2] Blay P., Reig P., Martínez-Núñez, S., Camero, A., Connell, P. and Reglero, V. 2004, *A&A*, 427, 293
- [3] Falanga, M., di Salvo, T., Burderi, L., Bonnet-Bidaud, J.M. et al. 2005, *A&A*, 436, 313
- [4] Hulleman, F., in 't Zand, J. J. M. and Heise, J. 1998, *A&A*, 337, L25
- [5] Okazaki A.T. and Negueruela I. 2001, *A&A*, 377, 161
- [6] Reig, P., Negueruela, I., Fabregat, J., Chato, R., Blay, P. and Mavromatakis, F. 2004, *A&A*, 421, 673
- [7] Sidoli, L., Mereghetti, S., Larsson, S., Chernyakova, M., et al. 2005, *A&A*, 440, 1033

THE MIRAX X-RAY TRANSIENT MISSION: RECENT DEVELOPMENTS

João Braga¹, Jorge Mejía¹, Flavio D'Amico¹, Francisco Jablonski¹, Richard Rothschild², John Heise³, Jean in 't Zand³, Rüdiger Staubert⁴, Eckhard Kendziorra⁴, Jörn Wilms⁵, Ron Remillard⁶, Erik Kuulkers⁷, and Eduardo Janot-Pacheco⁸

¹Instituto Nacional de Pesquisas Espaciais (INPE), Av. dos Astronautas 1758, S. J. Campos, SP 12227-010, Brazil

²University of California San Diego (UCSD), 9500 Gilman Dr., La Jolla, CA 92093-0424, USA

³Space Research Organization Netherlands (SRON), Sorbonnelaan 2 3485 CA Utrecht, The Netherlands

⁴Institut für Astronomie und Astrophysik (IAAT), Sand 1, Tbingen 72076, Germany

⁵University of Warwick, Coventry CV4 7AL, United Kingdom

⁶Massachusetts Institute of Technology (MIT), 70 Vassar St., Cambridge, MA 02139, USA

⁷Integral Science Operations Centre (ISOC), European Space Astronomy Centre (ESAC), Apartado 50727, 28080 Madrid (Villafranca del Castillo), Spain

⁸Instituto de Astronomia, Geofísica e Ciências Atmosféricas (IAG), Universidade de São Paulo (USP), Rua do Matão 1226, Cidade Universitária, São Paulo, SP 05508-900, Brazil

ABSTRACT

The Monitor e Imageador de Raios-X (MIRAX) is a small (~ 250 kg) X-ray astronomy satellite mission designed to monitor the central Galactic plane for transient phenomena. With a field-of-view of ~ 1000 square degrees and an angular resolution of ~ 6 arcmin, MIRAX will provide an unprecedented discovery-space coverage to study X-ray variability in detail, from fast X-ray novae to long-term (\sim several months) variable phenomena. MIRAX's instruments will include a soft X-ray (2-18 keV) and two hard X-ray (10-200 keV) coded-aperture imagers, with sensitivities of ~ 5 and ~ 2.6 mCrab/day, respectively. MIRAX is an approved mission of the Brazilian Space Agency (Agência Espacial Brasileira - AEB) and is scheduled to be launched in 2011 in a low-altitude (~ 550 km) circular equatorial orbit. In this paper we present recent developments in the mission planning and design, as well as Monte Carlo simulations of the instrumental background performed using the GEANT-based MGGPOD package.

1. INTRODUCTION

The "Monitor e Imageador de Raios-X" (MIRAX) is a high-energy astrophysics satellite mission which is part of the Scientific Satellite Program at the National Institute for Space Research (INPE) in Brazil. MIRAX has been selected to be the astrophysics mission within this program and has been approved for development by the Brazilian Space Agency (AEB). Since the Brazilian astronomical community is mostly devoted to the fields of

optical and radio astronomy, the development and operation of MIRAX is expected to have a major impact on Brazilian science through the opening of a new observation window for astrophysical research.

The MIRAX project has strong international partnerships. The University of California in San Diego (UCSD) will provide the hard X-ray detectors and participate in the design of the hard X-ray cameras; the Space Research Organization Netherlands (SRON) will provide the soft X-ray imager; the Institut für Astronomie und Astrophysik of the University of Tbingen (IAAT) will provide the on-board computer and participate in software development; and the Massachusetts Institute of Technology (MIT) and the University of Warwick will participate in software development for data acquisition, analysis, storage and distribution.

The main scientific goal of MIRAX is the nearly continuous (9 months per year), broad-band (2 to 200 keV), high-resolution ($\sim 5-7$ arcminutes) monitoring of a specific large region of the sky that is particularly rich of X-ray sources (a $76^\circ \times 44^\circ$ total field centered on the Galactic center and oriented along the Galactic plane). This will not only provide an unprecedented monitoring of the X-ray sky through simultaneous spectral observations of a large number of sources, but will also allow the detection, localization, possible identification, and spectral/temporal study of the entire history of transient phenomena to be carried out in one single mission. With the planned continuous monitoring approach, MIRAX will address key issues in the field of X-ray variability such as black hole state transitions and early evolution, accretion torques on neutron stars (especially through monitoring of X-ray pulsars), relativistic ejections on microquasars

and fast X-ray novae. MIRAX will also be able to contribute to Gamma-Ray Burst (GRB) astronomy, since it is expected that ~ 1 GRB will be detected per month in MIRAX's field-of-view (FOV). MIRAX instruments are expected to be assembled in a dedicated small (~ 250 kg) satellite to be launched in a low altitude, equatorial circular orbit around 2011.

2. MIRAX INSTRUMENTS

2.1. The Hard X-Ray Imagers

The HRIs will be built in collaboration with CASS and will operate from 10 to 200 keV. The detector plane will be a 3×3 array of state-of-the-art CdZnTe crossed-strip detector modules with 0.5 mm spatial resolution developed at CASS, with a total area of 360 cm^2 . Each detector module is a 2×2 array of $32 \text{ mm} \times 32 \text{ mm} \times 2 \text{ mm}$ thick CZT detectors. The detectors will be surrounded by an active plastic scintillator shield and by a passive Pb-Sn-Cu graded shield. A $315 \text{ mm} \times 275 \text{ mm}$ Tungsten coded-mask with 1.3 mm-side square cells (0.5 mm-thick) will be placed 600 mm away from the detector to provide images with $7'30''$ angular resolution. The basic pattern of the mask will be a 139×139 Modified Uniformly Redundant Array (MURA - Gottesman and Fenimore 1989; Braga et al. 2002), which will allow for full shadowgrams to be cast on the position-sensitive detector area and will provide no source ambiguities in the fully-coded field-of-view (FCFOV).

The pointing axes of the two HXIs will be offset by an angle of 29° in order to provide a uniform sensitivity over a 39° FCFOV in one direction; the perpendicular direction will have a $6^\circ 12'$ FCFOV. In such a configuration the FWHM FOV is $58^\circ \times 26^\circ$. During the observations of central Galactic Plane, the wider direction of the FOV will be aligned with the GP.

2.2. The Soft X-Ray Imager

The SXI, provided by SRON, is the spare flight unit of the Wide Field Cameras (WFCs - Jager et al. 1997) of the BeppoSAX mission (Boella et al. 1997), and will operate from 1.8 to 28 keV. The CXM will have a $5'$ angular resolution in a $20^\circ \times 20^\circ$ FWHM FOV. The addition of the WFC to the MIRAX payload will provide soft X-ray spectral coverage which will be extremely important for the study of the several classes of sources in the MIRAX FOV. Furthermore, the excellent performance of the WFCs on BeppoSAX brings to MIRAX an instrument that has already been tested and used very successfully in orbit with very little degradation on a time scale of several years.

3. SIMULATIONS AND HXI SENSITIVITY

Simulations of the hard X-ray imager instrumental background in orbit were carried using the MGGPOD Monte Carlo simulation code (Weidenspointner et al., 2004), a user-friendly suite built around the widely used GEANT package. It provides the results of the interactions of the various radiation fields within the instruments and spacecraft materials. With the knowledge of the instrumental background and the diffuse aperture X-ray flux, we performed detailed image simulations of the central Galactic plane as seen by MIRAX, for several instrument configurations and integration times. Preliminary results indicate that MIRAX will be able to detect a variety of systems, both transient and persistent.

The HXI sensitivity can be estimated based on the expected background level in the low-orbit environment, which is about 20 cts/s for a single imager. The Crab nebula plus pulsar photon count rate will be ~ 108 cts/s. Taken the approximate total contribution of sources in the primary MIRAX FOV (central GP) to be about 1 Crab, the MIRAX sensitivity is expected to be better than $2 \times 10^{-5} \text{ photons cm}^{-2} \text{ s}^{-1} \text{ keV}^{-1}$ at 100 keV (5σ), or ~ 2.6 mCrab/day in the 10-100 keV range (~ 40 times better than the Earth Occultation technique of the Burst and Transient Source Experiment on CGRO). The HXIs will have a one-year "survey" sensitivity, considering a conservative systematics limit of 0.1% of background, of about $10^{-11} \text{ erg cm}^{-2} \text{ s}^{-1}$ in the 10-50 keV band. This is ~ 20 times better than what was achieved by the HEAO 1 A-4 instrument, which carried out the only hard X-ray survey to date (Levine et al., 1984).

In summary, MIRAX will be able to make very unique contributions to the study of energetic transient phenomena in astrophysics by virtue of its observing strategy, which departs significantly from traditional pointed programs and scanning monitors. MIRAX will detect, localize, identify and study unpredictable phenomena which last on the timescales of minutes to days, which would otherwise be missed by traditional observing strategies. In addition, MIRAX will be able to study longer-lived phenomena in exquisite detail from 2-200 keV.

REFERENCES

- Boella, G. et al. 1997, A&AS, 122, 299
- Braga, J. et al. 2002, Rev.Sci.Instr., 73, 3619
- Gottesman, S.R. & E. E. 1989, App.Opt., 28, 4344
- Jager, R. et al. 1997, A&AS, 125, 557
- Levine, A. et al. 1984, ApJS, 54, 581
- Weidenspointner, G. et al., 2004, astro-ph/0406159

THE 2005 OUTBURST OF GRO J1655–40: SPECTRAL EVOLUTION OF THE RISE AS OBSERVED BY SWIFT

C.Brocksopp¹, K.McGowan¹, H.Krimm^{2,3}, O.Godet⁴, P.Roming⁵, K.O.Mason¹, N.Gehrels², M.Still^{2,3}, K.Page⁴, A.Moretti⁶, C.Shrader², S.Campana⁶, and J.Kennea⁵

¹Mullard Space Science Laboratory, University College London, Holmbury St. Mary, Dorking, Surrey RH5 6NT, UK

²NASA/Goddard Space Flight Center, Greenbelt, MD 2077, USA

³Universities Space Research Association, Columbia, MD 20144 USA

⁴Dept. of Physics & Astronomy, University of Leicester, Leicester LE1 7RH, UK

⁵Dept. of Astronomy and Astrophysics, Pennsylvania State University, 525 Davey Laboratory, University Park, PA 16802, USA

⁶INAF-Osservatorio Astronomico di Brera, Via Bianchi 46, I-23807 Merate (LC), Italy

ABSTRACT

After nearly a decade of quiescence, the black hole X-ray transient, GRO J1655–40 became active again in 2005 February. This was perfectly timed for the new *Swift* satellite, which has monitored the outburst using all three instruments on board. Therefore we have obtained X-ray spectroscopy for the energy ranges 0.3–10 keV and 15–150 keV, plus optical and ultraviolet photometry (in *U*, *B*, *V*, *UVW1*, *UVM2* and *UVW2* filters). We use these data to study the broad-band spectral evolution of the outburst. In particular we find that comparison of the lightcurves at different bands reveals different components to the variability. Preliminary, qualitative study suggests that these component are related to the power-law and disc-blackbody, commonly used to model the X-ray spectra, and therefore reflect the behaviour of the jey/corona and accretion disc respectively.

Key words: Multiwavelength; Black Hole Transients.

1. INTRODUCTION

GRO J1655–40 is a well-known black hole X-ray transient which was discovered in 1994 when it entered a series of hard X-ray outbursts lasting until 1995; a number of the peaks were quasi-simultaneous with radio ejections, some of which showed apparent superluminal motion. An additional outburst took place in 1996 and the source has remained in quiescence since then. The spectral evolution of the 1996 outburst showed a suprising lack of correlation between the soft X-ray and optical lightcurves.

A new outburst was entered in 2005 February. Pointed

Swift observations were made on 20 occasions between 2005 March 6 and June 23, using the BAT (Burst Alert Telescope), XRT (X-ray Telescope) and UVOT (Ultraviolet/Optical Telescope), supplemented by additional hard X-ray monitoring with the BAT. The source was observed in three of the “canonical” X-ray spectral states typical of black hole X-ray transients – low/hard (LHS), high/soft (HSS) and very high (VHS). The behaviour accompanying each state was reflected in both the lightcurves and the spectra (see Fig. 1).

We note that full details of the results of this study are presented in Brocksopp et al. 2005.

2. RESULTS - X-RAY SPECTRA

X-ray spectra spanning 0.3–150 keV have been obtained in each of the three spectral states in which GRO J1655–40 was observed. They have been modelled using simple power-laws, plus an additional multicolour disc-blackbody for the HSS and VHS data. An iron emission line was present in the LHS spectrum, improving the fit by 4.6σ , but it was not clear whether this iron line was absent during the softer states or just dominated by the blackbody emission. An iron absorption line was present in some of the later HSS and VHS observations (and may have been present in other HSS/VHS observations but was obscured by calibration artefacts). Sample broad-band spectra, one for each spectral state, are plotted in Fig. 1 (left-hand side).

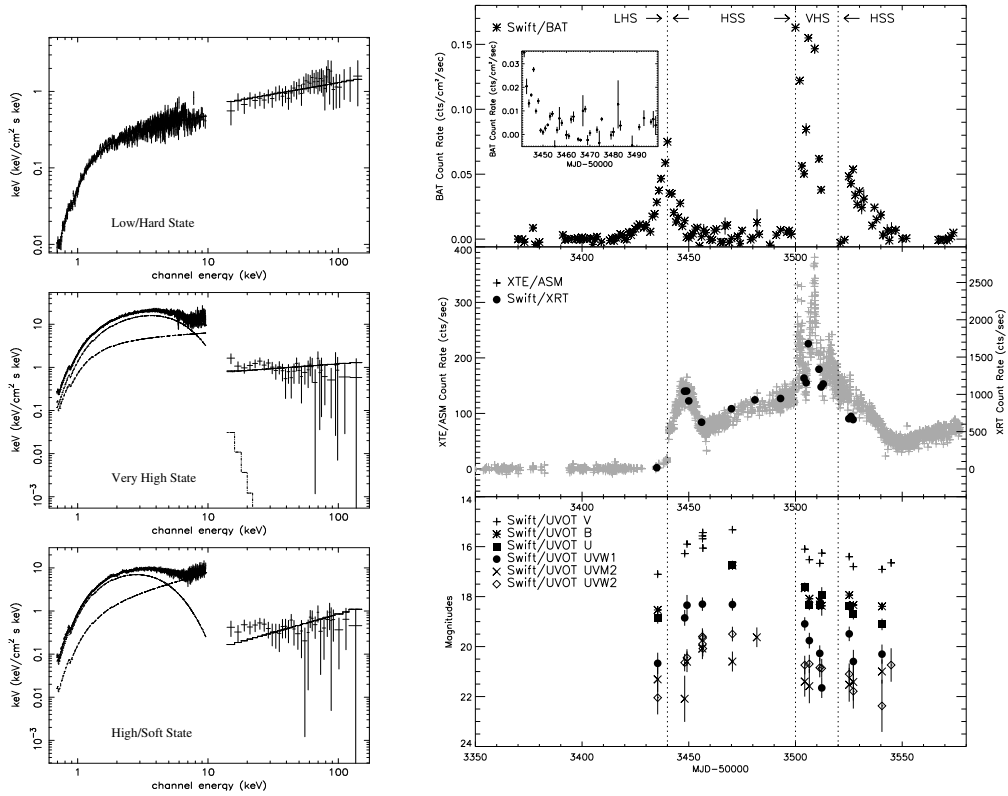


Figure 1. Left: Sample broad-band X-ray spectra plotted in the equivalent of νF_ν -space for each spectral state observed by Swift. We note that the apparent absorption lines around 5–7 keV during the VHS and the apparent excess around 9 keV during the VHS/HSS are calibration artefacts. Right: Plot showing the BAT (top panel), XRT and RXTE/ASM (middle) and UVOT (bottom) lightcurves. The three vertical lines indicate times of LHS–HSS, HSS–VHS and VHS–HSS transitions. The inset plot shows the BAT lightcurve during the HSS – the variability appears to be real.

3. RESULTS - LIGHTCURVES

It is apparent from Fig. 1 (right-hand side) that the three lightcurves are very different from each other. The X-ray plots show a series of peaks, the first of which occurs in the hard X-rays approximately one week before the soft X-rays. Later soft X-ray peaks are delayed only by a day. The period of HSS behaviour is accompanied by a “plateau” phase in the BAT data but a rising phase in the XRT and ASM data. The UVOT data are also increasing in magnitude at this time.

It appears that there are two components to the lightcurves (and such a scenario may also be able to explain the lightcurves of the 1996 outburst; Brocksopp et al. 2005):

- an accretion disc component which brightens smoothly during the rise of the outburst and then drops once the source reached the VHS, providing the UVOT lightcurve and the gradually-rising part of the soft X-ray lightcurve. This is presumably related to the disc blackbody component, typically used when fitting the X-ray spectrum
- a jet and/or corona component which becomes active in soft and hard X-rays at the onset of the outburst; it peaks and decays and then rebrightens

suddenly, resulting in the VHS. Again, this is presumably related to the power-law component (either synchrotron or Comptonisation), typically used when fitting the X-ray spectrum.

REFERENCES

Brocksopp C., McGowan K.E., Krimm H., Godet O., Roming P., Mason K.O., Gehrels N., Still M., Page K., Moretti A., Shrader C.R., Campana S., Kennea J., 2005, MNRAS in press (astro-ph/0510775)

INTEGRAL/OMC: OPTICAL COUNTERPARTS OF ROSAT SOURCES

M.D. Caballero-García¹, A. Domingo¹, D. Rísquez¹, and J.M. Mas-Hesse²

¹Laboratorio de Astrofísica Espacial y Física Fundamental (LAEFF-INTA), POB 50727, E-28080 Madrid, Spain

²Centro de Astrobiología (CSIC-INTA), POB 50727, E-28080 Madrid, Spain

ABSTRACT

Five sources monitored by OMC, located close to five targets from the ROSAT catalogues (RASS BSC and RASS FSC), present a high degree of variability in the optical band, with variations typical of binary systems and active stars. We found periods around half a day for three of them and one day for the two others. The estimated spectral types range from late F to early K. The combined optical and X-ray properties of these objects fit very well with the average properties of binary systems and active stars, respectively, supporting the identification of these OMC stars as the previously unknown optical counterparts of the ROSAT sources.

Key words: binary systems; active stars; variable stars; optical photometry; X-rays.

1. INTRODUCTION

The Optical Monitoring Camera (OMC) is a small telescope with a CCD camera onboard the INTEGRAL satellite (Mas-Hesse et al., 2003). It has been designed to monitor simultaneously, in the optical band (V -Johnson filter), the high-energy sources observed by the main INTEGRAL instruments. The simultaneity of the observations is critical in this case due to the fast and unpredictable variability of the high-energy emitting objects. The field of view (FOV) of the camera is 5×5 degrees, covering the central area of the large FOV of the high energy instruments (SPI and IBIS) and coincident with the Fully Coded FOV of JEM-X.

OMC monitors routinely around 100 stars in each field. The targets of interest are extracted from the *OMC Input Catalog* (Domingo et al., 2003), which contains, among other sources, all those compiled in the ROSAT catalogues: RASS BSC (Voges et al., 1999) and RASS FSC (Voges et al., 2000). Five targets which were selected from the ROSAT catalogues, have been found to show a large degree of variability in the optical. Their

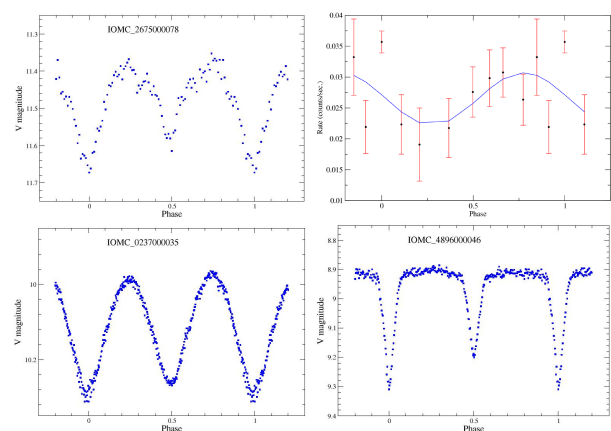


Figure 1. Light curves obtained by OMC (upper-left) and ROSAT (upper-right) of the binary IOMC 2675000078 and light curves obtained by OMC of the binaries IOMC 0237000035 (lower-left) and IOMC 4896000046 (lower-right).

lightcurves are shown in Figs. 1 and 2. Table 1 summarizes their OMC and ROSAT identifications, as well as the optical periods derived from OMC data, and X-ray luminosities derived from the ROSAT fluxes.

Analysis of the ROSAT data with XSAS SW (Zimmermann et al., 2000) shows little absorption in soft X-rays. We have therefore assumed that the optical extinction towards these objects is negligible. We have estimated their distances deriving the corresponding spectral types from their color excesses, as compiled in the Tycho (ESA, 1997) and Tycho-2 (Høg et al., 2000) catalogues, and comparing the apparent with the corresponding absolute magnitudes.

2. ECLIPSING BINARIES

The optical lightcurves of the sources IOMC 2675000078, IOMC 0237000035 and IOMC 4896000046 correspond to contact, contact-WUMA and detached eclipsing binary systems, respectively.

Table 1. Identification, optical periods and ROSAT luminosities of the sample.

Identifier	Period (days)	L_X (erg/s)
IOMC 0237000035	0.46515	2.25×10^{30}
1RXS J095156.0+004722	± 0.00018	
IOMC 1306000026	0.419	1.09×10^{30}
1RXS J054101.8+203624	± 0.002	
IOMC 2674000067	0.967	2.11×10^{30}
1RXS J200219.0+333912	± 0.005	
IOMC 2675000078	0.42233	1.41×10^{31}
1RXS J200912.0+323344	± 0.00003	
IOMC 4896000046	0.9871	1.07×10^{30}
1RXS J095706.3-012019	± 0.0008	

While the variations of their optical emission is due to some type of activity in the photosphere and the geometry of the system during the orbital motion, the X-ray emission observed in all these systems is probably due to emission of the hot corona of (one of) their components (paper in preparation). In the case of the prototype Algol system the precedence of the X-ray emission is clearly coronal but which component causes it is actually not completely understood (Ness et al., 2002; White et al., 1986; Ottmann & Schmitt, 1996).

As listed in Table 1 the rotation periods of these binaries is rather short, between 0.4 and 1 day. The lightcurve of the two systems with the shortest rotation periods shows that they are in contact, which might induce a high degree of activity in their components, giving rise to the observed X-ray flux.

2.1. IOMC 2675000078

1RXS J200912.0+323344 (the likely X-ray counterpart of IOMC 2675000078) was observed as a 34 831 s pointed observation by F. Haberl with HRI instrument onboard ROSAT satellite in 1997 as part of a program to search for cataclysmic variables. We observe a weak modulation with a period of 0.11 ± 0.04 days (i.e., approximately 1/4 of the orbital period). In Fig. 1 we show the ROSAT lightcurve folded with this period. We will discuss in a future paper the possible implications of this shorter X-ray period.

3. ACTIVE STARS

It is known that late type stars of F-M spectral types with high rotation velocities have strong magnetic fields, being active and showing significant brightness variations originated from the photosphere, chromosphere, transition re-

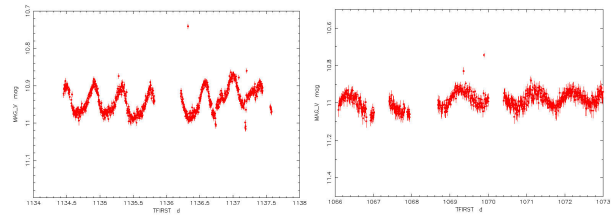


Figure 2. Light curves obtained by OMC of the two active type stars IOMC 1306000026 (left) and IOMC 2674000067 (right).

gion and corona (in the optical, UV and X-ray ranges, respectively). These activity manifestations are correlated with the axial rotational period. Messina et al. (2003) have determined a correlation between L_X/L_{bol} and the amplitude of the optical variations, A_{max} , confirming the dependence of coronal activity on photospheric magnetic fields.

Both IOMC 1306000026 and IOMC 2674000067 fit very well on these correlations, both considering their optical periods, L_X/L_{bol} and A_{max} values. This supports the identification of the OMC targets as the optical counterparts of the ROSAT sources.

REFERENCES

- Domingo, A., Caballero, M. D., Figueras, F., et al., 2003 A&A 411, L281-289
- ESA, 1997, ESA SP-1200
- Høg, E. Fabricius, C., Makarov V. V. et al. 2000, A&A 355, 2
- Mas-Hesse, J. M., Giménez, A., Culhane J. L., et al. 2003 A&A 411, L261-L268
- Messina, S., Pizzolato, N., Guinan, E. F. and Rodonò, M. 2003, A&A 410, 671
- Ness, J.U., Schmitt, J.H.M.M., Burwitz, V., Mewe, R. and Predehl, P., 2002, A&A, 387, 1032
- Ottmann, R. & Schmitt, J.H.M.M., 1996, A&A, 307, 8130
- Voges, W., Aschenbach, B., Boller, Th. et al. 1999, A&A 349, 389
- Voges, W., Aschenbach, B., Boller, Th. et al. 2000, IAU Circ. 7432, 3
- White, N.E., Culhane, J.L., Parmar, A.N., Kellett, B.J., Kahn, S., van den Oord, G.H.J. and Kuijpers, J., 1986, ApJ, 301,262
- Zimmermann, U., Boese, G., Becker, W., Belloni, T., Döbereiner, C., Izzo, C., Kahabka, P. and Schwentker, O., XSAS User's Guide, MPE Report, ROSAT Scientific Data Center, 1998

COMBINING RAYLEIGH TEST AND PIF METHOD FOR TIMING ANALYSIS WITH CODED MASK APERTURE INSTRUMENT. APPLICATION TO QUASI-PERIODIC OSCILLATION DETECTION AND MODELIZATION.

C. Cabanac¹, J. Malzac², J. Odier¹, P-O. Petrucci¹, G. Henri¹, and J. Rodriguez³

¹Laboratoire d'Astrophysique, Observatoire de Grenoble, BP 53X, F-38041 Grenoble, France

¹Centre d'Etude Spatiale des Rayonnements, 31028, Toulouse, France

³Centre d'Etudes de Saclay, DAPNIA/Service d'Astrophysique (CNRS FRE 2591), Bt. 709, Orme des Merisiers, Gif-sur-Yvette Cedex 91191, France

ABSTRACT

Several X-ray binaries exhibits quasi-periodic behavior from low (a few mHz) to high ($\simeq 1$ kHz) frequencies in the whole electromagnetic spectrum (from radio to hard X-ray). Standard way of data processing with coded mask aperture instruments such as IBIS onboard INTEGRAL requires evolved deconvolution algorithm (e.g OSA 5.0 for INTEGRAL data). We propose here a new way of timing analysis using both Rayleigh test and PIF method in order to detect Quasi-periodic Oscillations(QPO) in X-ray binaries and we applied this method to GRS1915+105 INTEGRAL early observations.

In a second part, we have simulated the linear response of soft X-ray photons comptonized by a warm oscillating corona (sausage mode in a disk geometry) using a Monte-Carlo code. The resulting normalized power spectrum obtained is compatible with some of X-ray binaries observations.

Key words: X-ray binaries; QPO; Monte-Carlo code.

1. DETECTING PERIODIC EVENTS IN CODED MASK INSTRUMENTS DATA

1.1. Method used

Coded mask aperture instruments such as those embarked aboard the INTEGRAL spacecraft (JEMX, IBIS or SPI) are used because of their ability to perform spectro-imaging even at high energies.

However, due to the presence of a coded mask, the data collected by the detectors cannot be trivially interpreted : indeed, the signal of each source in the field of view and emitting in the X-rays is then convolved by the pattern of the mask. Thus a simple power spectrum computation on the whole detector would mix the different signals.

Standard analysis (OSA 5.0) requires powerful softwares and high computing abilities to obtain binned light-curve after long time deconvolution. However, it is also possible to use both following methods to obtain an efficient timing analysis :

- **PIF** : Pixel Illumination Factor is more or less the probability that one source illuminates a considered pixel. The more the PIF, the higher the flux coming from the source.

- **Rayleigh test** : A frequency f is chosen arbitrarily. All the $\cos(2\pi.f.t_k)$ are then added (t_k being the different photon arrival time, called *events*). The result of this sum is nil unless the source is emitting at the same frequency f .

- As the flux coming from the source is linearly related to the PIF value, the previous computed sum follows the same law. Thus, our method consists in combining both previous methods by linearly fitting the $\sum_k \cos(2\pi.f.t_k)$ in the PIF plane. Thus, for a given source s that is oscillating at the frequency f , the higher the PIF, the greater the sum and the higher the slope $I_{f,s}$ of this fitted line ($I_{f,s}$ then represents the oscillation amplitude of the source). On the contrary, for a non oscillating source, $I_{f,s}$ will be nil.

1.2. Tests on the Crab and on GRS 1915+105

Following the previous method, a code was written (in Yorick) to detect automatically any periodic component in a given set of data. We applied it first on Crab IBIS/ISGRI observations (spacecraft revolution #102) and then to GRS 1915+105 early IBIS/ISGRI observations (spacecraft revolution #48). The Crab pulse and a low frequency Quasi-periodic Oscillation (hereafter QPO) of 3 mHz in GRS 1915+105 were detected in both observations using our method (see Fig 1).

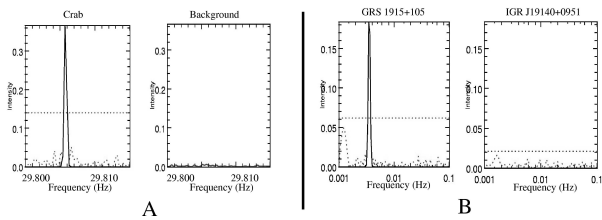


Figure 1. **A** : Intensity I_f plotted vs frequency for the Crab (left) and the background (right) in the 20-25 keV energy band (dashed line). The pulse is well detected by the code (in continuous line) and fitted by a gaussian. **B** : Intensity I_f plotted vs frequency for GRS 1915+105 (left) and the recently discovered X-ray source IGR J19140+0951 (see Rodriguez et al. (2005) for further information on this source) located 1° far from the famous microquasar in the 20-25 keV energy band. Our code detect a rather coherent ($\Delta f = 0.8$ mHz) low frequency QPO at about 3 mHz for GRS 1915+105.

2. SIMULATION OF A PULSATING CORONA

2.1. Code used

As the physical processes underlying the production of QPO is still unclear, we tried to simulate the behavior of an oscillating corona in a simple disk truncated geometry. In this model, the soft thermal photons are emitted randomly : the emission times are just following a poissonian distribution. Then they are comptonized on a high energy plasma (considered as a perfect gas) where the temperature (and thus the electron density) is partially oscillating at a given frequency f (propagation terms of this wave among the disk are taken into account). The code we used was a modified version of a simple linear Monte-Carlo simulation of a comptonizing corona developed by J. Malzac (see Malzac (1999)).

2.2. Early results

We performed a simulation with the following physical parameters : the number of soft seed photons emitted by the thermal component ($T_{\text{soft}} = 0.2$ keV) has been set to 10^7 and the average temperature of the warm plasma T_{CORONA} has been set to 153 keV. In addition, we took a value of 2.5 Hz concerning the frequency of the warm plasma oscillations and a perturbation level (compared to the mean temperature) ϵ of 0.2. Results can be seen in Fig 2.

We observe the same dependency in energy between the simulated QPO spectra and the observed ones. As it is already suggested in Rodriguez et al. (2004), the fact that the cut-off in the QPO spectra seems strongly related to the energy of the electron gas could be easily interpreted : in that case, the modulation of the X-ray flux would be contained in the comptonized photons and not in the other emission processes (e.g, synchrotron).

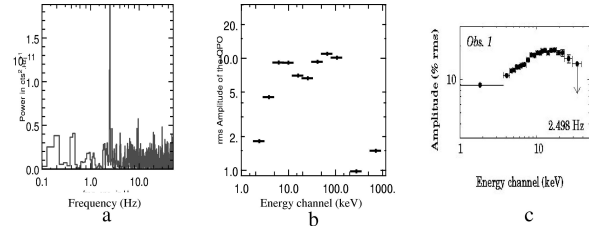


Figure 2. **a** : Power spectrum of the simulated oscillating corona showing the 2.5 Hz QPO in the 45-100 keV energy band. **b** Spectra (compared to the rms) of the simulated 2.5 Hz QPO clearly showing a cut-off at an energy similar to the value of the temperature T_{CORONA} of the warm plasma. **c**: Spectra of the observed 2.5 Hz QPO in GRS 1915+105 (RXTE PCA/HEXTE data). A cut-off also seems to be required and the energy cut-off value is thus similar to the temperature of a comptonizing corona obtained by spectral fits (see Rodriguez et al. (2004) for further informations).

3. CONCLUSION AND PERSPECTIVES

Early results using our new timing analysis combining Rayleigh test and PIF method have shown that it is possible to detect efficiently some QPO in INTEGRAL IBIS/ISGRI data and the same method could be extended to other coded mask instruments. Next challenge will be to apply this method to several X-ray sources in order to detect any QPO at higher energy than described before (RXTE/PCA cross-section drops down beyond 40 keV) and to better understand which physical processes are at the origin of the QPO.

In any case, the simulation of a hot oscillating comptonizing corona shows that it can be sufficient to generate QPO, and the fact that the QPO spectra is similar to the observation is also in agreement with the hypothesis that the QPO occurs in the comptonizing corona. New simulations with other parameters (different temperature of the plasma, dependency on the QPO frequency) and their comparison with observations will give us other useful constrains.

REFERENCES

- Malzac, J. 1999, pH-D Thesis Université Paul Sabatier-Toulouse III
- Rodriguez, J., Corbel, S., Hannikainen, D. C., Belloni, T., Paizis, A., Vilhu, O. 2004, ApJ, 615, 416
- Rodriguez, J., Cabanac, C., Hannikainen, D. C., Beckmann, V., Shaw, S. E., Schultz, 2005. A&A, 432, 235

***XMM-NEWTON* OBSERVATIONS OF PSR B1259–63 NEAR THE 2004 PERIASTRON PASSAGE.**

M. Chernyakova^{1,2}, A. Lutovinov³, J. Rodriguez⁴, and S. Johnston⁵

¹*INTEGRAL* Science Data Center, 16 Ch. d'Ecogia, CH-1290 Versoix, Switzerland

²Observatoire de Genève, 51 chemin des Maillettes, 1290 Sauverny, Switzerland

³Space Research Institute, 81/32 Profsoyuznaya, 117997 Moscow, Russia

⁴CEA Saclay, DSM/DAPNIA/Service d'Astrophysique (CNRS UMR 7158 AIM), 91191 Gif-Sur-Yvette Cedex, France

⁵Australia Telescope National Facility, CSIRO, P.O. Box 76, Epping, NSW 1710, Australia.

ABSTRACT

PSR B1259–63 is in a highly eccentric 3.4 year orbit with a Be star and crosses the Be star disc twice per orbit, just prior to and just after periastron. We present here the results of new *XMM-Newton* observations of the PSR B1259–63 system during the beginning of 2004, as the pulsar approaches the disc of the Be star. We combine these results with earlier X-ray data from *BeppoSAX*, *XMM-Newton* and *ASCA*. The X-ray light curve looks similar to the radio light curve with a rapid increase in the flux around the time of the disc crossing. This supports a model in which the X-ray emission from the system is due to inverse Compton scattering of the pulsar wind relativistic particles with $\gamma \sim 10 - 100$ on the Be star soft photons.

Key words: pulsars : individual: PSR B1259–63 – X-rays: binaries – X-rays: individual: PSR B1259–63 .

1. INTRODUCTION

PSR B1259–63 is a ~ 48 ms radio pulsar in a highly eccentric ($e \sim 0.87$), 3.4 year orbit with a Be star SS 2883. Be stars are well-known to be sources of strong highly anisotropic matter outflow. Both a dilute polar wind and a denser equatorial disc have been invoked to reconcile models for infra-red, ultra-violet and optical observations. Timing analysis of the PSR B1259–63 system show that the disc of Be star is highly tilted with respect to the orbital plane and that the line of intersection of the disc plane and the orbital plane is at almost 90° to the orbital major axis. Thus the pulsar crosses the disc twice per orbit.

The properties of the radio emission from this system are very different before and after the periastron passage. Radio observations show that when the pulsar is far from

periastron the observed radio emission is comprised entirely of pulsed emission from the pulsar itself. Due to the misalignment of the Be star disc with the orbital plane, pulsed radio emission disappears entirely as the pulsar enters the disc and is hidden behind it (relative to the observer). Shortly before the disc crossing **unpulsed** radio emission appears and within several days rises to a peak value several times higher than the intensity of the pulsed emission far from the periastron. Afterwards the unpulsed flux slightly decreases, as the pulsar passes through periastron before reaching a second peak just after the pulsar crosses the disc for the second time. This unpulsed radio emission is still detected until at least 100 days after the periastron passage (Johnston et al. 2005 and references there in).

Since its discovery system PSR B1259-63 was observed several times with different X-ray instruments. The most recent published observations of the system in X-rays were carried out with the *ASCA* satellite in 1994 and 1995 (Hirayama et al. 1999, and references therein). These observations showed that X-ray emission is approximately twice as high at the time of the disc crossing than at periastron.

2. OBSERVATIONS AND DATA ANALYSIS

Thus X-ray and radio data have similar two-peak structure around the periastron. However X-ray data are much more sparse than radio ones, and it was not clear whether similar to radio data X-ray emission rapidly grows around the moment of the first disk crossing, or its behavior is much smoother. To answer this question we have organized a set of *XMM-Newton* observations of the system, as the pulsar approaches the disk.

A simple power law with a photoelectrical absorption describes the data well, with no evidence for line features. The results are given in Figure 1 in comparison with the results obtained by *ASCA*.

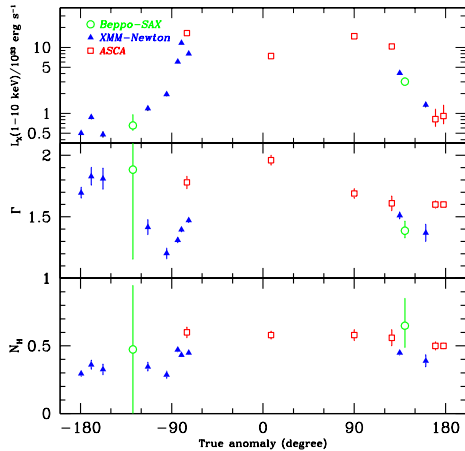


Figure 1. Summary of XMM-Newton BeppoSAX and ASCA observations of the PSR B1259-63. The figure shows the time variation of the X-ray luminosity, spectral slope and column density as a function of orbital phase.

3. DISCUSSION

In all models explaining the unpulsed emission from PSR B1259-63 the collision of the relativistic pulsar wind with the (non-relativistic) wind of the Be star plays a crucial role. Due to the interaction of the winds a system of two shock waves arises between the stars. In the beginning both the relativistic and non-relativistic winds are radial but after passing the shocks particles turn and start to flow along the contact surface, losing their energy in form of synchrotron and inverse Compton (with the seed photons being the Be star soft photons) emission. The big difference in the velocities of the winds at different sides of the contact surface can lead to the growth of instability and two winds could be macroscopically mixed between the shocks. In this case the massive non-relativistic wind will slow down the drift velocity of the relativistic particles. The frequency of the emission depends on the Lorentz factor of the relativistic electrons. Up to now there is no unified self-consistent theory of the pulsar magnetosphere allowing us to predict the value of the Lorentz factor γ of the particles in the relativistic pulsar wind. The range of the predicted values is quite wide, from $\gamma \sim 10^7$ (e.g. Muslimov & Harding 2004), to $\gamma \sim 100$ (e.g. Kirk et al. 2002), and as low as $\gamma \sim 10$ (Malov 2003).

Models with assumptions of low and high Lorentz factors have been applied to the PSR B1259-63 system. Tavani & Arons (1997) assumed a high Lorentz factor of $\gamma = 10^6$. Under this assumption, synchrotron emission of the relativistic electrons leads to the X-ray emission. While as shown in Figure 2 this model was in a good agreement with ASCA observations (marked with squares), new XMM-Newton data (marked with triangles) show a much more rapid growth than it was predicted. In the model with moderate Lorentz factor, $\gamma = 10 - 100$,

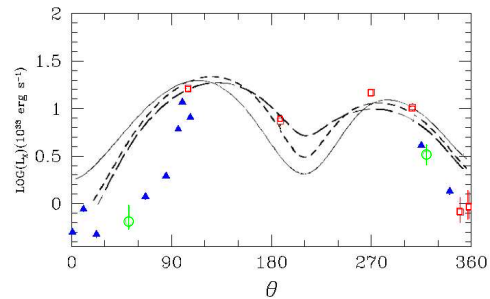


Figure 2. Comparison of the X-ray data with the prediction of the Tavani & Arons model

discussed by Chernyakova & Illarionov (1999, 2000), the observed X-ray emission is due to inverse Compton scattering of the pulsar wind relativistic particles on the Be star soft photons. The observed radio emission within this model is due to the synchrotron emission of the electrons of the pulsar wind. In this case the intensity of the observed unpulsed X-ray and radio emission strongly depends on the outflow velocity of the relativistic particles after the shock wave. The lower the drift velocity, the higher is the X-ray and radio luminosity. The interaction with the pulsar leads to the partial destruction of the Be star disc (Ivanov et al. 1998). The matter starts to be ejected from the disc shortly before and lasts for a while after the pulsar passage through it, perturbing the outflow beyond the shock. This leads to a mix of relativistic and non-relativistic winds, and hence to an increase of the unpulsed radio and X-ray emission. XMM-Newton data presented here supports this model, showing an increase of the absorption column relative to the apastron value during the period the unpulsed radio emission is detected.

Thus in the model of Chernyakova & Illarionov the X-ray and radio emission is generating by the same population of particles, and the lightcurves should be similar. Unfortunately in the 2004 observations, there are no simultaneous X-ray and radio observations for the quantitative comparison, but the observed rapid increase of the X-ray flux strongly supports the model.

REFERENCES

- Chernyakova M., Illarionov A., 1999 MNRAS, 304, 359
- Chernyakova M., Illarionov A., 2000 ApSS, 274, 177
- Hirayama M. et al., 1999 ApJ 521, 718
- Ivanov P. et al., 1998 ApJ, 507, 131
- Johnston S. et al., 1992 ApJ, 387, L37
- Kirk, J. G. et al., 2002 A&A, 388, L29
- Malov I., 2003 AstL, 29, 502
- Muslimov A., Harding A., 2004 ApJ, 617, 471
- Tavani M., Arons J., 1997 ApJ, 477, 439

COMPLETE HISTORY OF THE NEWLY DISCOVERED ACCRETING PULSAR 2RXP J130159.6-635806.

M. Chernyakova^{1,2}, A. Lutovinov³, J. Rodriguez⁴, and M. Revnivtsev^{5,3}

¹*INTEGRAL* Science Data Center, 16 Ch. d'Ecogia, CH-1290 Versoix, Switzerland

²Observatoire de Genève, 51 chemin des Maillettes, 1290 Sauverny, Switzerland

³Space Research Institute, 81/32 Profsoyuznaya, 117997 Moscow, Russia

⁴CEA Saclay, DSM/DAPNIA/Service d'Astrophysique (CNRS UMR 7158 AIM), 91191 Gif-Sur-Yvette Cedex, France

⁵Max-Planck-Institute für Astrophysik, Germany

ABSTRACT

We report on analysis of the poorly studied source 2RXP J130159.6-635806 at different epochs with *ASCA*, *BeppoSAX*, *XMM-Newton* and *INTEGRAL*. The source shows coherent X-ray pulsations at a period ~ 700 s with an average spin up rate of about $\dot{\nu} \sim 2 \times 10^{-13}$ Hz s⁻¹. A broad band (1-60 keV) spectral analysis of 2RXP J130159.6-635806 based on almost simultaneous *XMM-Newton* and *INTEGRAL* data demonstrates that the source has a spectrum typical of an accretion powered X-ray pulsar, i.e. an absorbed power law ($\Gamma \sim 0.5 - 1.0$) with a high energy (at ~ 25 keV) cut-off. The long term behaviour of the source, its spectral and timing properties, tend to indicate a high mass X-ray binary with Be companion. We also report on the identification of the likely infrared counterpart to 2RXP J130159.6-635806.

Key words: X-rays, pulsars: individual: 2RXP J130159.6-635806.

1. INTRODUCTION

On February 7, 2004, during a routine Galactic plane scan, the *INTEGRAL* observatory detected a source which was not in the *INTEGRAL* reference catalog. Search in the archive led to the identification of several *ROSAT* sources in the *INTEGRAL* error box. Among them 2RXP J130159.6-635806 is the closest one to the best estimate of the source position obtained with *INTEGRAL* (Chernyakova et al., 2004). The only mention of this source in the literature before the observations reported here and in Chernyakova et al. (2005) can be found in Kaspi et al. (1995).

Here we present the analysis of all available X-ray data from *ASCA*, *BeppoSAX*, *INTEGRAL*, and *XMM-Newton* in order to understand the nature of this variable source and investigate its properties.

2. RESULTS OF THE ANALYSIS

During the *XMM-Newton* monitoring programme of PSR B1259-63, two sources were clearly detected. The best coordinates we derive for 2RXP J130159.6-635806 are RA_{J2000}=13^h01^m58^s.8, DEC_{J2000}=-63°58'10" (the conservative error estimation is 3"). This position is about 6" from the best *ROSAT* position of 2RXP J130159.6-635806. The uncertainty of the localisation of 2RXP J130159.6-635806 with *ROSAT* is 5", therefore we conclude that most likely *XMM-Newton* source and the *ROSAT* one are the same.

The 1993–2004 time history of the 2 – 10 keV flux from 2RXP J130159.6-635806 as observed by *ASCA* and *XMM-Newton* is shown in the upper panel of Figure 1. While during the *ASCA* (1994 – 1995) and the first half of the *XMM-Newton* observations (2001 – 2003) the flux of the source was practically constant, an outburst occurred between the end of January and the beginning of February 2004. During this period the source flux increased by a factor of more than 5. This outburst was also detected by *INTEGRAL* in the 20 – 60 keV energy range.

The *XMM-Newton* and *ASCA* data show that the spectrum of the source in 2 – 10 keV energy range is well described by a simple power law modified by absorption. For all observations, the value of the photo-absorption is practically constant with an average value of $N_{\text{H}} = (2.48 \pm 0.07) \times 10^{22}$ cm⁻², which is higher than it follows from the measurements of the interstellar hydrogen in the Galaxy at this place. This indicates that part of the absorption might be intrinsic to the source. *INTEGRAL* data show a presence of a high-energy cut-off at about ~ 25 keV, typical for accreting X-ray pulsars

Analyzing the light curve of 2RXP J130159.6-635806 we found that it demonstrates near coherent strong variations with a characteristic time about 700 s. The values of the pulse period obtained between 1994 and 2004 are shown in Figure 2. An average spin up rate changes from $\dot{P} \simeq$

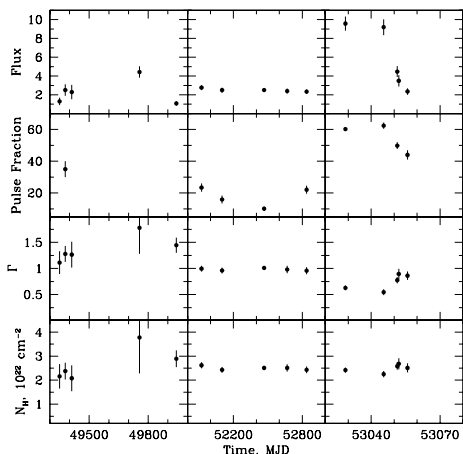


Figure 1. Time evolution of the spectral parameters of 2RXP J130159.6-635806 and 2 – 10 keV pulse fraction (in %). Flux is given in units of 10^{-11} erg/s/cm². labelfig:allspec

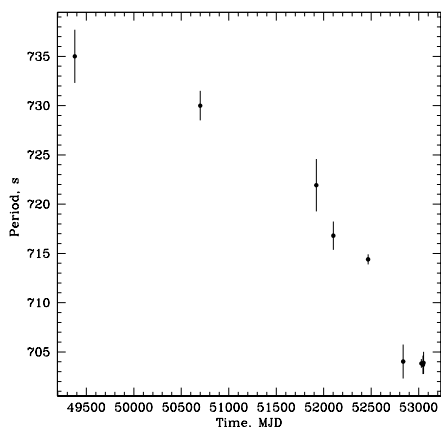


Figure 2. Time evolution of 2RXP J130159.6-635806 pulse period.

-6×10^{-8} s s⁻¹ in 1994 – 2001, to approximately $\dot{P} \simeq -2 \times 10^{-7}$ s s⁻¹ in 2001 – 2004.

3. OPTICAL COUNTERPART

The accretion powered X-ray pulsars are usually found within high-mass X-ray binaries (HMXB). The HMXB may be divided mainly into those with main-sequence Be star companions, and those with evolved OB supergiants companions.

Most of Be/X-rays binaries are transients, displaying X-ray outburst and long period of quiescence, when no X-ray flux is detected. A smaller group of Be/X-rays binaries are persistent sources with rather low X-ray luminos-

ity ($< 10^{35}$ erg/s), relatively long (> 200 s) pulse periods and very weak iron line at 6.4 keV. (e.g. Negueruela 2004 and references therein).

The supergiant binaries may be further subdivided into two classes, depending on whether the mass transfer is due to the Roche lobe overflow, or a capture from the stellar wind. As the typical spin period for the pulsars with the companions filling its Roche lobe is less than 20 seconds (e.g. Corbet 1986) such a companion seems to be unlikely for 2RXP J130159.6-635806. The wind-fed supergiant binaries has long (of several hundreds seconds) spin period, and are persistent sources with short, irregular outbursts (e.g. Corbet 1986). All the known systems display approximately the same X-ray luminosity $\sim 10^{36}$ erg/s. Variable X-ray activity of 2RXP J130159.6-635806 indicates that this binary system unlikely contains an OB supergiant.

In any of the cases mentioned above we should expect that the optical companion of the X-ray source should be bright in the optical and infrared spectral bands. In order to check this we used the results of 2MASS surveys and found a source with coordinates (equinox 2000) RA=13^h01^m58^s.7, DEC=-63°58′09″ (at $\sim 1.1''$ from the best *XMM-Newton* position) and magnitudes $J = 12.96 \pm 1.33$, $H = 12.05 \pm 0.03$, $K_s = 11.35 \pm 0.09$. The good agreement between both positions would tend to suggest that this source is the likely counterpart to 2RXP J130159.6-635806. Using the value of Galactic absorption $N_H = 1.7 \times 10^{22}$ cm⁻² we estimate the dereddened magnitudes $J_{der} = 10.73 \pm 1.33$, $H_{der} = 10.72 \pm 0.03$, $K_{s,der} = 10.51 \pm 0.09$ (only statistical uncertainties are quoted). If the companion star is a Be main sequence star with surface temperature around 10000 K and the radius around 6-10 R_\odot we can expect to see its infrared brightness $J, H, K \sim 10 - 11$ if the binary system is at the distance $\sim 4 - 7$ kpc. An additional tentative argument in favour of such source distance is the source location in the direction to the Crux spiral arm tangent, as HMXBs are concentrated towards galactic spiral arms. At such a distance unabsorbed intrinsic luminosity of 2RXP J130159.6-635806 is about $\sim 5 \times 10^{34} - 10^{35}$ erg/s, i.e. compatible with the typical luminosities of the persistent Be/X-rays binaries.

REFERENCES

- Chernyakova M. et al., 2004, ATel, 251, 1
- Chernyakova M. et al., 2005, MNRAS in press (astro-ph/0508515)
- Corbet R., MNRAS 1986 220, 1047
- Kaspi et al., 1995, ApJ 453, 424
- Negueruela et al. 2004, astro-ph/0411335
- Shaw et al., A&A, 426, L33

IRRADIATION MODELS FOR ULTRA-LUMINOUS X-RAY SOURCES AND FITS TO HST DATA

Chris Copperwheat¹, Mark Cropper¹, Roberto Soria^{1,2}, and Kinwah Wu¹

¹Mullard Space Science Laboratory, University College London, Holmbury St. Mary, Dorking, Surrey, RH5 6NT, UK

²Harvard-Smithsonian Center for Astrophysics, 60 Garden Street, Cambridge, MA 02138, USA

ABSTRACT

We have created a model to describe the optical emission from ULXs in terms of an irradiated companion star and disk. Here we detail our model, and present the initial results of its application to HST observations of three ULX optical counterparts. We list stellar parameters for the companion stars in these systems, and provide constraints on the black hole masses.

Key words: accretion, accretion discs; black hole physics; X-rays: galaxies; X-rays: stars.

1. INTRODUCTION

Ultra-luminous X-ray sources (ULXs) are point-like, non-nuclear sources with apparent isotropic luminosities greater than 10^{39} ergs s^{-1} . The brightest sources have X-ray luminosities in excess of 10^{40} ergs s^{-1} , implying bolometric luminosities of order 10^{41} ergs s^{-1} . This is significantly larger than the Eddington luminosity limit for an accreting stellar-mass black hole (BH). The nature of these objects are still unclear. The accreting object may be an intermediate mass black hole (IMBH) with mass $50 - 1000M_{\odot}$, or it may be an ordinary stellar-mass BH with its emission beamed towards us. We seek to understand ULXs through observations of their optical counterparts. We find that optical/IR observations are powerful tools which complement X-ray observations in determine the properties and hence the nature of ULXs.

2. MODEL

We consider a binary model, with the compact object accreting material from a companion star. We assume the X-ray emission is isotropic, and hence take the IMBH interpretation as a starting point. The brightest ULXs require an accretion rate greater than that which could be supplied by a stellar wind, so we assume the matter is

transferred onto the compact object through Roche lobe overflow. We constrain the geometry of the system so that the companion star is filling its Roche lobe. This constraint necessitates a small binary separation and a large companion star. A large amount of X-ray flux will be incident on the surface of this star, and the optical/IR characteristics of this star will be modified. The irradiation will induce intensity and colour shifts compared to normal stars, which we use as a diagnostic. We assume the system is in a quasi-steady state, and the irradiated surfaces are in thermal, radiative and hydrostatic equilibrium. We consider the effects of radiative transport and radiative equilibrium in the irradiated surface of the star and an irradiated accretion disk. We consider a plane-parallel model and adopt the radiative transport formulation of Milne (1926) and Wu et al. (2001) to describe the heated surface. We determine the total emergent radiation from a distorted, Roche lobe filling star numerically. We do the same for the disk, using a thin disk geometry.

The model is described more completely in Copperwheat et al. (2005). We extend this to use the isochrones produced by the Geneva stellar evolution models of Lejeune & Schaerer (2001) to provide stellar parameters which we use to produce new isochrones, with colours and magnitudes appropriate for an irradiated star and disk. We repeat this process as we vary the other important parameters, such as BH mass, and the inclination and orientation of the binary system.

3. APPLICATION TO ULX X-7 IN NGC 4559

HST observations have revealed eight candidates for the optical counterpart of ULX X-7 in NGC 4559; a ULX with $L_x \simeq 10^{40}$ ergs s^{-1} (Soria et al. , 2005). We find that three of the candidates (2, 3 and 4) are consistent with our model irradiated star and disk only when we use a very low inclination and a very high BH mass. If the inclination is such that the optical emission contains an appreciable disk component, these candidates do not fit with any BH and star combination. For most reasonable inclinations and binary phases, candidates 1, 5, 6 and 8 remain viable (Figure 1).

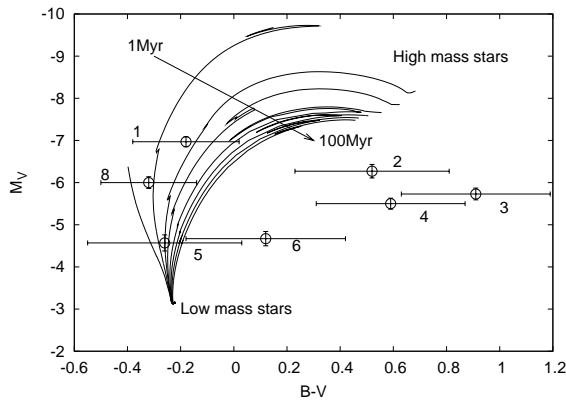


Figure 1. A colour – magnitude diagram showing our theoretical isochrones plotted with the candidates for the counterpart of ULX X-7 in NGC 4559. We use here an inclination of $\cos i = 0.5$ and a BH mass of $100M_{\odot}$. For these parameters, candidates 2, 3 and 4 are inconsistent with being the optical counterpart.

Soria et al. (2005) concluded that candidate 1 was the most likely counterpart to the ULX. The other candidates were found to be consistent with the unperturbed isochrones for stars with masses $10 - 15M_{\odot}$ and ages of approximately 20Myr. If we assume the companion star is also this age and that candidate 1 is indeed the counterpart, then by comparing the 20Myr isochrone with the observed magnitudes we find the mass of the companion star to be $11 - 12M_{\odot}$ and the radius to be $40 - 50R_{\odot}$. We find also that when we use a BH mass of greater than a few hundred solar masses in our model, the 20Myr isochrone we produce is inconsistent with the optical observations.

4. APPLICATION TO ULX-1 IN M101

Kuntz et al. (2005) examined HST observations of a unique counterpart to ULX-1 in M101 and suggested they were consistent with a B-type supergiant. Again, by applying our irradiation model we find it to be of an earlier spectral type, consistent with an F0-A0 supergiant, depending on the BH mass. In this case we cannot constrain the BH mass, but the lack of orbital variation observed by Kuntz et al. (2005) suggests a disk-dominated system, which may imply a more massive BH.

5. APPLICATION TO ULX X-6 IN M81

Liu et al. (2002) detailed HST observations of ULX X-6 in M81, and suggested it is an O8/O9 MS star with a mass of $26 - 50M_{\odot}$ and an age of < 5 Myr. When we apply our irradiation model, we find the optical observation to be consistent with a B-type MS star with a significantly lower mass ($5 - 8M_{\odot}$) and an age that is up to an order of magnitude greater than that found by Liu

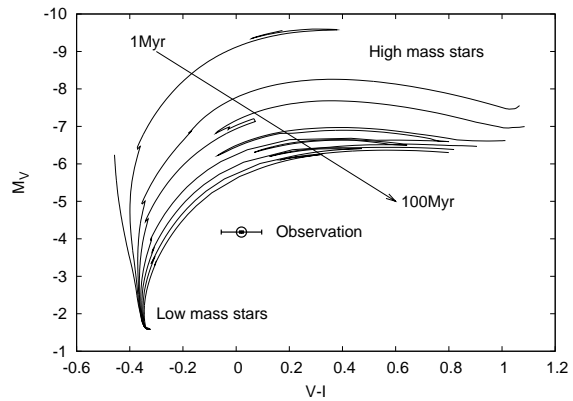


Figure 2. A colour – magnitude diagram showing our theoretical isochrones plotted with the counterpart of ULX X-11 in NGC 3031. We use here an inclination of $\cos i = 0.5$ and a BH mass of $10M_{\odot}$. The observation is inconsistent with the isochrones produced by our model for this BH mass.

et al. (2002), depending on the BH mass we use in our model. Additionally, we find that we can provide a lower limit on the BH mass. The field stars in the vicinity of the ULX have an age range of $1 - 100$ Myr. We find the (V-I) colour of the observation is inconsistent with our theoretical isochrones in this range when we use a BH mass of less than $\simeq 100M_{\odot}$ (Figure 2).

6. CONCLUSIONS

We find that by applying our irradiation model to the optical counterparts of ULXs, we can determine the parameters of the companion stars, and in some cases provide constraints on the mass of the black hole. We find the companion stars to be older, less massive and of a later spectral type than currently reported.

REFERENCES

- Copperwheat C.M., Cropper M., Soria R., Wu K., 2005, MNRAS, 362, 79
- Kuntz K.D., Gruendl R.A., Chu Y.-H., Rosie Chen C.-H., Still, M., Muka K., Mushotzky R.F., 2005, ApJ, 620, L31
- Lejeune T. & Schaerer D., 2001, A&A, 366, 538
- Liu J.-F., Bregman J.N. & Seitzer P., 2002, ApJ, 580, L31
- Milne E.A., 1926, MNRAS, 87, 43
- Soria R., Cropper M., Pakull M., Mushotzky R., Wu K., 2005, MNRAS, 356, 12
- Wu K., Soria R., Hunstead R.W., Johnston H.M., 2001, MNRAS, 320, 177

INTEGRAL OBSERVATION OF THE X-RAY BURSTER KS 1741-293

G. De Cesare^{1,2,3}, A. Bazzano³, G. Stratta⁴, M. Del Santo³, A. Tarana³, and P. Ubertini³

¹Dipartimento di Astronomia, Università degli Studi di Bologna, Via Ranzani 1, I40127 Bologna, Italy

²Centre d'Etude Spatiale des Rayonnements, CNRS/UPS, B.P. 4346, 31028 Toulouse Cedex 4, France

³IASF-INAF, via Fosso del Cavaliere 100, I00133 Roma, Italy

⁴OMP/LATT 14 Avenue E. Belin 31400 Toulouse, France

ABSTRACT

KS 1741-293 was firstly detected in 1989 with the X-ray wide field camera TTM (3-10 keV) on board of the Rontgen-Kvant-Mir observatory. During these observations this source exhibited two X-ray bursts allowing to identify it as a neutron star in a Low mass X-ray Binary. During the BeppoSAX/WFC monitoring of the Galactic Centre Region, KS 1741-293 was also reported at a flux level of 6 mCrab in the 2-9 keV and 25 mCrab in the 9-25 keV energy range. Thanks to the deep and regular INTEGRAL observation of the Galactic Centre region, KS 1741-293 has been observed by the X-ray monitor JEM-X and the imager IBIS in a wide energy range, giving for the first time relevant information on its high energy behaviour. Furthermore, two X-ray bursts have been detected by JEM-X. We report on IBIS and JEM-X data analysis in terms of flux monitoring, spectral properties and bursts detection. The data reduction has been done with the most recent release of the standard analysis software (OSA 5.0).

Key words: X-rays binaries, INTEGRAL.

1. INTRODUCTION

The first bursting sources were discovered already in 1975 with SAS 3 and OSO-8. All X-ray sources showing type I burst are low mass X-ray binaries (LMXBs). Woosley and Taam (1976) and Maraschi and Cavaliere (1976) independently discussed the origin of the phenomenon: X-ray bursts are explained by thermonuclear flashes of the material accreting from the companion star on the surface of the neutron star.

The X-ray burster KS 1741-293 was firstly reported by in't Zand et al. (1991) as one of the 2 new transient sources near the galactic centre during observation with the X-ray wide-field camera TTM on board the Rontgen-Kvant-Mir observatory, in 1989. The source was de-

tected on 3 consecutive days and two type I X-ray burst were detected in the energy range 5.7–27.2 keV. The source was inside the error box of MXB1743-29, a bursting source detected in 1976 with SAS-3. More recently, in the BeppoSAX era (1996-2002), this source was detected, together to a large sample of galactic sources, during the WFC monitoring of the Galactic Center Region (in't Zand et al., 2004) at a peak flux of the order of 30 mCrab in the WFC energy band. KS 1741-293 was also detected by ASCA during the 107 pointing observation on a 5x5 deg region around the Galactic Center showing an apparent variability by a factor of 50 while no burst have been reported by Sakano et al. (2002). No hard X-ray detection has been reported by the first gamma-ray imager, SIGMA, and indeed the source is not in the hard X-Ray SIGMA survey, covering the 40-100 keV range (Revnivstev et al., 2004). KS1741-293 is listed in the BATSE/CGRO instrument deep sample as one of the 179 sources monitored along the CGRO operative life (Harmon et al., 2004) even though it is not a firm detection.

We show here for the first time the high energy spectrum of KS 1741-293 obtained with INTEGRAL. In section §2 we report the INTEGRAL observations and data analysis, in section §3 we briefly discuss the main results of this analysis.

2. OBSERVATION AND DATA ANALYSIS

The hard X- and gamma-ray observatory INTEGRAL was launched on October 17, 2002 by the a Russian PROTON launcher. The satellite makes revolution around the Earth in three days, along a highly eccentric orbit and the observing time is optimized by this choice. The wide-field Gamma-ray imaging and wide-band spectral capabilities of INTEGRAL coupled with the Core program strategy, are a powerful tool to further investigate the high energy behavior of X-ray bursters as firstly reported by Bazzano et al. (2004). The scientific instruments on board are the hard X- and gamma-ray imager IBIS (Ubertini et al., 2003) covering the energy band 20 keV–10

Table 1. KS1741-293 IBIS data set. The visibility periods 1, 2, 3 include all the public data and the core program data. The last periods 4 and 5 include the core program data only.

Period	Rev.	Start (MJD)	End (MJD)	exp. (ks)
1	46-63	52698	52792	306
2	103-120	52871	52921	1333
3	164-185	53052	53115	921
4	229-249	53246	53306	159
5	291-307	53431	53479	43

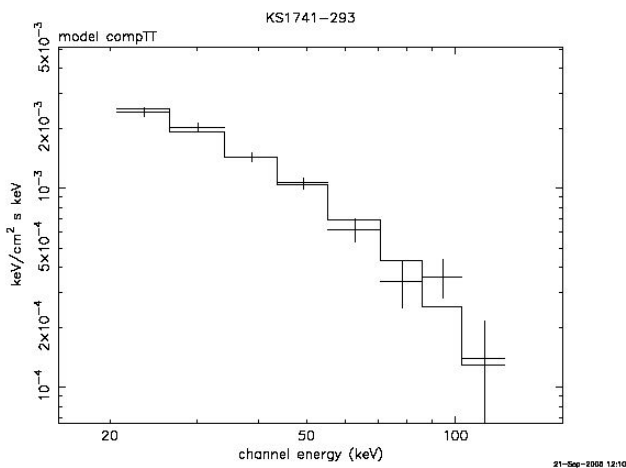


Figure 1. IBIS/ISGRI KS 1741-293 spectrum obtained in the 3th visibility period

MeV, the gamma-ray spectrometer SPI (Vedrenne et al., 2003) in the same energy band but devoted to fine spectroscopy, the X-ray monitor JEM-X (3–35 keV) (Lund et al., 2003) and the optical camera OMC (Mas-Hesse et al., 2003). We report here on the IBIS and JEM-X data analysis, performed with the last Off-line Science Analysis (OSA) software (release 5.0). Since IBIS is a coded mask telescope, the maximum of sensitivity corresponds to the fully coded field of view (FCFV) and for this analysis, we have selected the IBIS pointing in which KS 1741-293 is in the FCFV, including all the public data from revolution 46 (2003-02-28) to revolution 185 (2004-04-19), and the Core Program data (Winkler et al., 2003) from the revolution 46 to the revolution 307 (2005-05-19). The details of the observations are listed in table 1.

3. RESULTS

We have monitored KS 1741-293 during a period of more than two year, from the end of February 2003 to end of May 2005, including in our analysis all the public and

core program data until April 2004 (periods 1, 2, 3). The source has been clearly detected in the periods 1 and 3. The signal in the period 2 is of order of 10 sigma, but, a more refined analysis of the image has shown that this effect could be due to the 1A 1742-294 tail (21 arcmin far from KS 1741-293). The one second resolved light curves obtained from JEM-X data in the revolution 53 (science window 58) and 63 (science window 92) exhibit two X-ray burst in the energy range 315 keV. The burst morphology confirms previous observations with no double peaked time profile unlike to the profile reported for MXB1743-29 as discussed by in't Zand et al. (1991).

The spectra of LMXB bursters show, on average, similarities with the ones from Black Hole binary systems and consist of a soft, disk component with temperatures of the order of a few keV and a low energy gamma-ray tail. Sometimes a cut-off at around 50 keV is present in the spectra and 2 different states have been detected for some of them (for a comprehensive review see Barret (2001)). The KS 1741-293 spectrum (fig. 1) has been extracted from the period 3 data. It is well fitted with a comptonized model (comptt) with an estimated plasma temperature of about 20 keV.

REFERENCES

- Barett D., Adv. Space Res.43, 28, 307, 2001
- Bazzano A., et al, SP-552,309, 2004, Proceedings of the 5th INTEGRAL Workshop
- Harmon, B.A. et al., ApJSS, 154, 585 (2004)
- Lund, N. et al., Astronomy & Astrophysics, Vol. 411,L231, 2003
- Maraschi, L. and Cavaliere A., Highlight in Astronomy, Vol. 4, part I, 127,1977
- Mas-Hesse J.M., et al, Astronomy & Astrophysics, Vol. 411,L261, 2003
- Revnivstev, M.G. et al., Astronomy Letter, Vol. 30, 527, 2004
- Sakano, M. et al. ApJSS 138,19 (2002)
- Ubertini, P., et al. Astronomy & Astrophysics, Vol. 411,L131, 2003
- Vedrenne, G. et al., Astronomy & Astrophysics, Vol. 411,L63, 2003
- Winkler C., et al., Astronomy & Astrophysics, Vol. 411,L1, 2003
- Woosley ,S.E. and Taam, r.E. , Nature, 263,101, 1976
- in't Zand, J. et al. Adv. Space Res. 11, 8187,1991
- in't Zand, J. et al. Nuclear Physics B Proceedings Supplements, Volume 132, p. 486-495 , 2004

UNVEILING X-RAY PROPERTIES OF NEW INTERMEDIATE POLARS

D. de Martino¹, G. Matt², K. Mukai³, J.-M. Bonnet-Bidaud⁴, V. Burwitz⁵, F. Haberl⁵, L. Chiappetti⁶, B.T. Gänsicke⁷, C. Motch⁸, and M. Mouchet⁹

¹INAF, Astronomical Observatory of Capodimonte, 80131 Naples, Italy

²Department of Physics, University of Roma III, 00146 Rome, Italy

³Exploration of the Universe Division, NASA/GSFC, Greenbelt MD 20771, USA

⁴Service d'Astrophysique, Saclay, 91191 Gif-sur-Yvette, France

⁵MPE, 85741 Garching, Germany

⁶INAF, IASF Milano, 20133 Milan, Italy

⁷Department of Physics, University of Warwick, CV4 7AL Coventry, United Kingdom

⁸Observatory of Strasbourg, UMR 7550 CNRS, 67000 Strasbourg, France

⁹APC UMR 7164, University Denis Diderot, 75005 Paris, France

ABSTRACT

We present first X-ray observations with the *XMM-Newton* satellite of the new magnetic Cataclysmic Variables HT Cam, UU Col and RX J2133+51. Strong rapid X-ray pulses reveal the rotational period of the accreting white dwarf thus unambiguously confirming these systems as true members of the Intermediate Polar class. These systems also reveal complex properties which make Intermediate Polars an intriguing class still to be fully explored.

Key words: Cataclysmic Variables; X-rays; Accretion.

1. INTRODUCTION

New optically identified Cataclysmic Variables (CVs) have recently increased the Intermediate Polar class (IPs) by at least a 30% (Gansicke et al., 2005), rejuvenating the issue on the evolution and link between the two subclasses of magnetic CVs (Polars and IPs). A wide range of spin-to-orbit period ratios has also stimulated new theoretical works on the evolution of white dwarf (WD) spin equilibria (Norton et al., 2004), where the WD magnetic moment, the mass accretion rate play an essential role. Differently from optical strongly affected by X-ray reprocessing, X-ray observations are essential to identify the true WD spin period and the accretion mode. Also, a soft X-ray component similar to that observed in the synchronous and highly magnetized Polar is now being detected in an increasing number of IPs [Haberl et al. (2002); Staude et al. (2003); de Martino et al. (2004)], reinforcing the debated question on the progeny of Polars, i.e. whether IPs will synchronize during their evo-

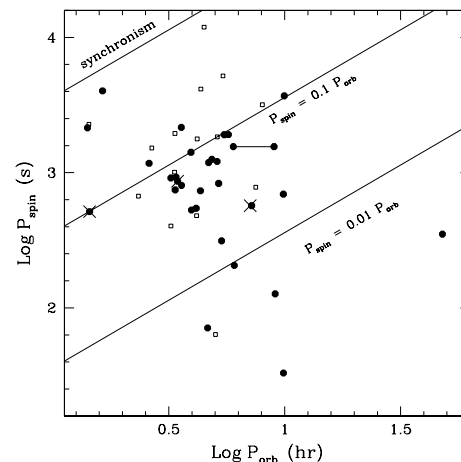


Figure 1. The spin-orbit period plane of IPs. Diagonal lines from top to bottom indicate $P_{\text{spin}}/P_{\text{orb}}=1$, 0.1 and 0.01. Dots: X-ray confirmed IPs; squares: optical candidates and crosses: HT Cam ($P_{\text{spin}}=515$ s; $P_{\text{orb}}=86$ min), UU Col ($P_{\text{spin}}=864$ s; $P_{\text{orb}}=3.5$ hr) and RX J2133+51 ($P_{\text{spin}}=571$ s; $P_{\text{orb}}=7.2$ hr).

lution towards short orbital periods. In the framework of our programme with *XMM-Newton* aiming at determining unambiguously the IP nature of new optical candidates, we present here part of the results obtained from X-ray observations of three new systems (see Fig. 1).

2. HT CAM: A LOW MASS TRANSFER RATE IP

A 39 ks (EPIC) observation in March 2003 confirms the 515 s optical (Tovmassian et al., 1998) period as the true WD spin period. Discrete Fourier Transforms (DFT) in

the 0.2-15 keV range (Fig. 2) as well as in selected energy bands show the dominance of the spin frequency (ω). No signal is detected at either the beat ($\omega - \Omega$) or the orbital (Ω) frequencies, indicating that accretion occurs via a disc. Spin pulse fraction is $\sim 40\%$ with no energy dependence in the whole EPIC range. The EPIC spectra are well represented by a multi-temperature plasma with $kT_{\max}=20$ keV and power law index $\alpha=0.7$ and metal abundance $A_Z=0.6$ plus a gaussian centred at the neutral 6.4 keV iron line (EW=50 eV) plus a low ($N_{\text{H}} = 5.7 \times 10^{20} \text{ cm}^{-2}$) total absorber. Hence HT Cam is not affected by strong absorption and the spin pulses are due to changes in the observable emitting volume. The low accretion rate of $2.4 \times 10^{-11} d_{100\text{pc}}^2 M_{\odot}/\text{yr}$ is consistent with that predicted by gravitational radiation for its short orbital period. A detailed analysis of the RGS spectra as well as of the optical/UV behaviour can be found in de Martino et al. (2005).

3. UU COL: A FAINT SOFT X-RAY IP

The faint high galactic latitude UU Col was observed for 28 ks (EPIC) in September 2004. The DFT in the whole EPIC range (Fig. 2) and in selected energy bands shows the dominance of the 864 s period detected by Burwitz et al. (1996) except in the 0.3-0.5 keV range where the second harmonic is stronger than the fundamental. This implies that the main accreting pole dominates in the hard X-rays whilst both poles, probably offset, contribute in the soft X-rays. While no orbital periodicity is observed, the signal at the beat ($\omega - \Omega$) is also detected, indicating that material accretes via a disc as well as flows above it (hybrid accretion mode). The spin folded light curves have a complex energy dependence indicating the presence of multiple components. The EPIC spectra indeed reveal a complex spectrum which does not require a temperature stratification but two MEKAL models at 11 keV and 0.18 keV with very low abundance $A_Z=0.4$ plus a black-body at 50 eV partially absorbed (50%) by a dense column with $N_{\text{H}} = 1.0 \times 10^{23} \text{ cm}^{-2}$. The RGS spectra are also well fitted by these components. The soft-to-hard X-ray bolometric flux ratio is 0.2. A mass accretion rate of $1.5 \times 10^{-12} d_{100\text{pc}}^2 M_{\odot}/\text{yr}$ for $d > 740$ pc is consistent with the secular value for its orbital period. A detailed analysis of the RGS, EPIC and OM data will be reported elsewhere.

4. RX J2133+51: A NEW SOFT X-RAY IP

The first 16 ks (EPIC) observation of this recently discovered IP (Bonnet-Bidaud et al., 2005) was carried out in May 2005. The DFT in the whole EPIC range (Fig. 2) reveals equal power at the fundamental and first harmonic of the optically identified 571 s period. The beat period cannot be detected and a low frequency variability is suspected and needs to be confirmed by the second observation. The power spectra in selected energy ranges reveal complex behaviour in the soft (below 0.5 keV) and

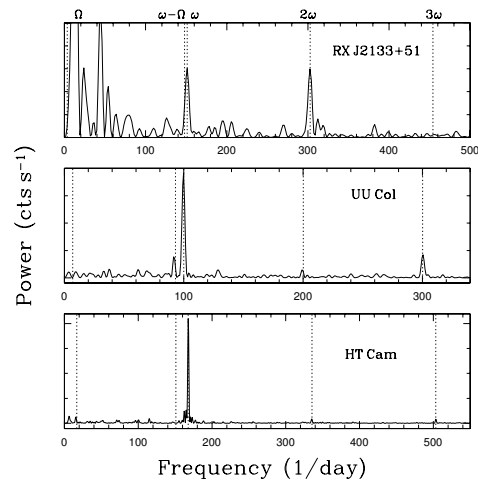


Figure 2. The EPIC-pn DFTs of HT Cam (bottom), UU Col (middle) and RX J2133+51 (top). The spin (ω), the beat ($\omega - \Omega$) and the orbital (Ω) frequencies are marked with dotted vertical lines.

hard ranges. The EPIC spectra indeed require a complex composite model consisting of a multi-temperature plasma with $kT_{\max}=67$ keV, $\alpha=1.0$ and metal abundance $A_Z=0.8$, plus a gaussian at the 6.4 keV iron line (EW=50 eV) plus a black-body at 96 eV and a total absorber ($N_{\text{H}}^1 = 1.7 \times 10^{21} \text{ cm}^{-2}$) and a second partial (48%) dense absorber ($N_{\text{H}}^2 = 1.2 \times 10^{23} \text{ cm}^{-2}$). The RGS spectra are also well represented by the same model. RX J2133+51 hence is similar to RX J1548-45 (Haberl et al., 2002) showing a strong highly absorbed hot black-body component. The bolometric soft-to-hard flux ratios is high (0.83). This preliminary analysis hence reveals that the number of soft X-ray IPs might increase in the near future.

REFERENCES

- Burwitz, V., Reinsch, K., Beuermann, K. et al. 1996, A&A 310, L25
 Bonnet-Bidaud, J.-M., Mouchet, M., de Martino, D., et al. 2005, A&A in press (astro-ph 0509347).
 de Martino, D., Matt, G., Belloni, T., et al. 2004, A&A 415, 1009
 de Martino, D., Matt, G., Mukai, K., et al. 2005, A&A 437, 935
 Gänsicke, B.T., Marsh, T.R., Edge, A., et al. 2005, MNRAS 361, 141
 Haberl, F., Motch, C., Zickgraf, F.-J. 2002, A&A 387, 201
 Norton, A., Wynn, G.A., Sommerscales, R.V. 2004, ApJ 614, 349
 Staude, A., Schwobe, A., Krumpe, M., et al. 2003, A&A 406, 253
 Tovmassian, G., Greiner, J., Kroll, P., et al. 1998, A&A 335, 227

X-RAY AND SOFT GAMMA-RAY BEHAVIOUR OF THE GALACTIC SOURCE 1E 1743.1–2843

M. Del Santo¹, L. Sidoli², A. Bazzano¹, M. Cocchi¹, G. De Cesare¹, A. Paizis³, and P. Ubertini¹

¹Istituto di Astrofisica Spaziale e Fisica cosmica di Roma – INAF, via del Fosso del Cavaliere 100, 00133 Roma, Italy

²Istituto di Astrofisica Spaziale e Fisica cosmica di Milano – INAF, via E. Bassini 15, 20133 Milano, Italy

³ISDC, Chemin d'Écogia 16, 1290 Versoix, Switzerland

ABSTRACT

The X-ray persistent source 1E 1743.1–2843, located in the Galactic Centre region, has been detected by all X-ray telescope above 2 keV, whereas it is not visible in the soft X-rays (i. e. *Rosat*) because of the high column density along the line-of-sight. Moreover, the nature of this source remains still unknown. The gamma-ray satellite *INTEGRAL* has long observed the Galactic Centre region in the framework of the Core Programme. We report on results of two years of *INTEGRAL* observations of 1E 1743.1–2843 detected for the first time in the soft gamma-ray band. Since the source does not show any evidence for strong variability, we present the broad-band spectral analysis using not simultaneous *XMM-Newton* observations.

Key words: X-ray and gamma-ray: observations; X-rays: binaries; stars: individual: 1E 1743.1–2843.

1. INTRODUCTION

1E 1743.1–2843 is one of the most absorbed ($N_H > 10^{23}$) X-ray sources of the Galactic Centre (GC) region, suggesting a distance close or even greater than the GC. In the last years the source has been observed by numerous X-ray telescopes up to 20 keV, but it has never been detected in the hard X-rays, because of the lack of combined high spatial resolution and good sensitivity instruments at high energies. *BeppoSAX* has long observed the Galactic Centre region, but it has never detected any bursting activity (in't Zand 2000), nor periodic pulsation from this source (Cremonesi et al. 1999). Also *XMM-Newton* observations reported by Porquet et al. (2003), limited to the range below 10 keV, did not solved the mystery of the source nature; they underlined that high energy observations could help in the determination of the compact object nature. We report here on the first detection in the soft gamma-ray domain (up to 70 keV) obtained during a two years monitoring with the gamma-ray imager IBIS, on-board the *INTEGRAL* satellite. A broad band spectral analysis has been also performed using re-analysed *XMM-Newton* data.

2. OBSERVATIONS AND DATA ANALYSIS

We have analysed public IBIS/ISGRI observations of the Galactic Centre region performed in 2003 and the 2004 observations of Core Programme. The 2003 effective exposure time is ~ 2 Ms; ~ 1 Ms in 2004. Data were reduced using OSA 5.0. The 20–40 keV temporal behaviour has been extracted from the whole data set while spectral analysis concern only the 2003 pointings. Searching the source field in the *XMM-Newton* public archive we found 2 *XMM-Newton* observations performed on 2000 September 19th (obs. 401) and 21th (obs. 501). Among these, only one of the *XMM-Newton* observations (obs. 401) has been reported in literature (Porquet et al. 2003). Here we present a re-analysis of this observation, now non-affected by pile-up problems. *XMM-Newton* data have been analysed by SAS 6.5. In order to exclude pile-up effects, we selected an annular region with inner radius of 10" and outer radius of 40". Background spectra were obtained from source-free regions of the same observations.

3. RESULTS AND DISCUSSION

The Galactic Centre is pointed by *INTEGRAL* during two visibility windows per year. The temporal behaviour of 1E 1743.1–2843 over 2 years of IBIS observations for a total of about 3 Ms is shown (Fig. 1). The source shows marginal variability over few months times scale,

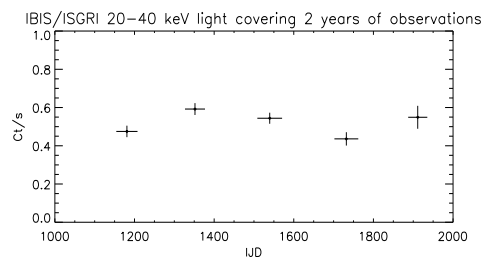


Figure 1. 20–40 keV temporal behaviour of 1E 1743.1–2843 with *INTEGRAL* starting from February 2003 till April 2005.

Table 1. Model parameters obtained by the broad-band spectral fit using XMM-Newton (two observations) and ISGRI (2003 mean spectrum). The meaning of the symbols is the following: pow=power-law, bb=blackbody, dbb=disk-blackbody in XSPEC; α is the power-law photon index, kT is the blackbody temperature or the inner disk temperature, depending on the adopted model.

Model	N_{H} (10^{22} cm^{-2})	kT (keV)	α	$F_{(2-10)}^a$	$F_{(1-100)}^b$	χ^2/dof
Obs. 401						
bb+po	$19.5^{+1.1}_{-0.9}$	$1.8^{+0.1}_{-0.1}$	$3.1^{+0.1}_{-0.1}$	3.9	7.3	468/375
diskbb+po	$18.6^{+0.8}_{-0.7}$	$3.1^{+0.1}_{-0.1}$	$2.5^{+0.1}_{-0.2}$	3.5		475/375
Obs. 501						
bb+po	$18.0^{+1.3}_{-1.0}$	$1.6^{+0.1}_{-0.1}$	$3.3^{+0.1}_{-0.1}$	3.2	5.9	392/323
diskbb+po	$19.8^{+0.9}_{-0.9}$	$2.6^{+0.2}_{-0.2}$	$2.9^{+0.1}_{-0.1}$	3.3		401/323

^a The 2–10 keV flux of the unabsorbed fit model in units of $10^{-10} \text{ erg cm}^{-2} \text{ s}^{-1}$.

^b The broad-band flux (1–100 keV) of the unabsorbed best-fit model in units of $10^{-10} \text{ erg cm}^{-2} \text{ s}^{-1}$.

in agreement with results reported by Belanger et al. (2005). Because of its rather constant high energy behaviour, we fitted the average IBIS/ISGRI spectrum of 2003 with non-simultaneous PN, MOS1 and MOS2 data (Fig. 2). We used two models: a black body plus a power law and a multi-temperature disc plus a power law. Spectral parameters are presented in Tab. 1. The two observations show parameters consistent within the errors. The steepness of the power law component indicates a soft hard-X-ray spectrum for this source. We confirm the further indication by Cremonesi et al. (1999) which rules out the HMXB nature. So far, the observational scenario seems to be in favour of a LMXB system. Starting from this hypothesis, the nature of the compact object needs to be discussed. We have estimated luminosities and related fractions in Eddington luminosity both for Neutron Star (NS) and Black Hole (BH), considering three possible distances for 1E 1743.1–2843. We assumed $M_{\text{NS}} = 1.4 M_{\odot}$ and $M_{\text{BH}} = 10 M_{\odot}$.

Let's suppose that the accreting object is a NS.

During more than 20 years of observations, the lack of type-I X-ray bursts is noteworthy. Nevertheless it is in agreement with the estimated luminosities in Eddington luminosity fractions (Tab. 2). Type-I X-ray bursts become rare going up a few percent of Eddington luminos-

Table 2. Luminosities of 1E 1743.1–2843 at different distances calculated both for a NS and BH.

Distance	$L_{1-100\text{keV}}$ (erg/s)	L/L_{Edd} (BH)	L/L_{Edd} (NS)
8.5 kpc	5.2×10^{36}	0.3%	3%
12 kpc	1.0×10^{37}	0.8%	5%
20 kpc	2.9×10^{37}	2.0%	11%

ity (Lewin et al. 1995). So, in this first case we have 2 possibilities: the NS is a rare burster from which we did not detect any thermonuclear flash or the system is a bright LMXRB located behind the Galactic Centre at a distance at least >15 kpc.

Let's suppose that the accreting object is a BH.

By our spectral parameters, 1E 1743.1–2843 should be a BH binary in the canonical high/soft state, contrary to the low/hard state proposed by Porquet et al. (2003). BH binaries in the soft state show luminosities as at least a few percent of L_{Edd} (Maccarone 2003). In this case the source distance cannot be less than 20 kpc. Considering that nearly all LMXRBs with persistent X-ray emission contain a NS (van der Klis 2004) and the strong variability usually associated to BH binary systems, this assumption seems to be less strong than the NS one.

Persistency, BB temperatures and faint and steep power law component support the NS nature for this source.

REFERENCES

- [1] Belanger, G. et al., 2005, ApJ, in pub. (astro-ph/0508128)
- [2] Cremonesi, D. et al., 1999, A&A, 345, 826
- [3] in't Zand, J., 2000, ESA SP-459, 4th INTEGRAL Workshop
- [4] Lewin, W. H. G. et al., 1995, in “X-ray binaries”, eds. Cambridge Astroph. Ser.
- [5] Maccarone, T. 2003, A&A, 409, 697
- [6] Porquet, D. et al., A&A, 406, 299
- [7] van der Klis, M. 2004, in “Compact stellar X-ray sources”, eds. Cambridge University Press

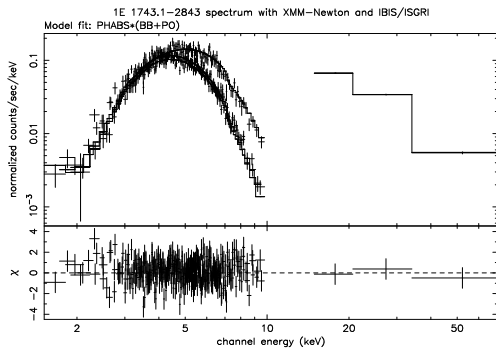


Figure 2. Count rate absorbed spectrum, BB+PO model fit and residuals of MOS1, MOS2, PN (obs. 501) and ISGRI data.

THE NATURE OF HIGHLY-IONIZED ABSORBERS IN DIPPING LOW-MASS X-RAY BINARIES

M. Díaz Trigo¹, A. Parmar¹, L. Boirin², M. Méndez³, and J. S. Kaastra³

¹Research and Scientific Support Department of ESA, ESTEC, Postbus 299, 2200 AG Noordwijk, The Netherlands

²Observatoire Astronomique de Strasbourg, 11 rue de l'Université, F-67000 Strasbourg, France

³SRON, National Institute for Space Research, Sorbonnelaan 2, 3584 CA Utrecht, The Netherlands

ABSTRACT

X-ray observations have revealed that many low-mass X-ray binaries (LMXBs) exhibit narrow absorption features identified with Fe XXV and Fe XXVI. The changes in both the X-ray continuum and the Fe absorption features during dips from the LMXB XB 1323–619 have been modeled as resulting primarily from an increase in column density and a decrease in the ionization state of a highly-ionized absorber (see Boirin et al. in these proceedings). We successfully fit the same ionized absorber model to the persistent and dipping emission from all the other bright dipping LMXBs observed by XMM-Newton (EXO 0748–676, XB 1254–690, X 1624–490, MXB 1659–298, 4U 1746–371 and XB 1916–053) and demonstrate that complex spectral changes in the X-ray continua observed from the dip sources as a class can be most simply explained primarily by changes in the highly ionized absorbers present in these systems. We observe also small changes in the equivalent hydrogen column of neutral material, which may be related to the inclination of the system. Since the ionized plasma has a cylindrical geometry with a maximum column density close to the plane of the accretion disk and dipping sources are simply normal LMXBs viewed from close to the orbital plane this implies that ionized plasmas are a common feature of LMXBs.

Key words: X-ray binaries – Accretion, accretion disks – X-rays: EXO 0748–676, XB 1254–690, X 1624–490, MXB 1659–298, 4U 1746–371, XB 1916–053.

1. INTRODUCTION

Around 10 galactic low-mass X-ray binaries (LMXBs) show periodic dips in their X-ray light curves (Fig. 1). The dips recur at the orbital period of the system and are believed to be caused by periodic obscuration by material located in a thickened outer region of the accretion disk due to its interaction with the inflowing gas stream from the companion. The presence of periodic dips and

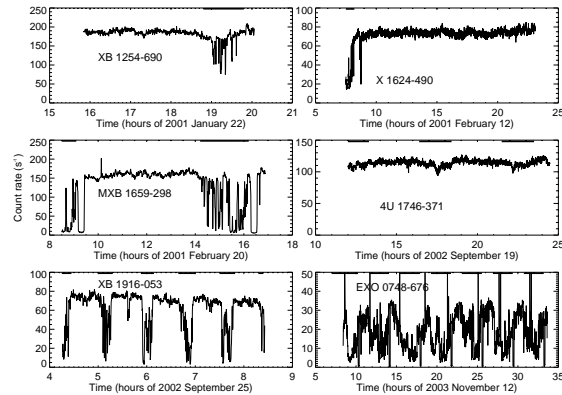


Figure 1. EPIC pn 0.6–10 keV lightcurves of the LMXBs analyzed in this work. The thick horizontal lines mark the intervals used to extract dip spectra.

absence of eclipses from the companion indicate that dipping sources are viewed relatively close to edge-on.

The improved sensitivity and spectral resolution of *Chandra* and XMM-Newton is allowing narrow absorption features from highly-ionized Fe and other metals to be observed from a growing number of X-ray binaries. In particular, Fe XXV or Fe XXVI 1s-2p resonant absorption lines near 7 keV were reported from the micro-quasars GRO J1655–40, GRS 1915+105 and H 1743–322, and from the neutron star systems Cir X–1, GX 13+1, MXB 1659–298, X 1624–490, XB 1254–690, XB 1916–053 and XB 1323–619 (see references in Díaz Trigo et al. (2005)). Most of the sources are known to be viewed close to edge-on (many are dippers). This indicates that the highly ionized plasma probably originates in an accretion disk atmosphere or wind, which could be a common feature of accreting binaries but preferentially detected in systems viewed close to edge-on. Boirin et al. (2005) demonstrated that the changes between persistent and dipping intervals *both* in the X-ray continuum and the Fe absorption features from XB 1323–619 can be modeled as resulting primarily from an increase in column density and a decrease in

Table 1. The persistent (Dip 1 for X1624–490) values of N_{H} (col. 2), $N_{\text{H}}^{\text{xabs}}$ (col. 6) and $\log(\xi)$ (col. 8) and the changes in N_{H} (col. 3) and $N_{\text{H}}^{\text{xabs}}$ (col. 7) from persistent to the deepest dip intervals observed for each source. N_{Hgal} is the averaged interstellar value for the $0^\circ.5$ region in the sky containing the source. $\Delta N_{\text{H}}/(N_{\text{Hpers}}-N_{\text{Hgal}})$ is the relative change in N_{H} local to the source from persistent to the deepest dip interval. Col. 9 shows the value of $\log(\xi)$ during the deepest dip for each source. N_{H} for EXO 0748–676 is constrained to be $\geq 1.1 \times 10^{21}$ atom cm^{-2} . All values of N_{H} , $N_{\text{H}}^{\text{xabs}}$ and their changes are expressed in units of 10^{22} atom cm^{-2} .

LMXB	N_{Hpers}	ΔN_{H}	N_{Hgal}	$\Delta N_{\text{H}}/$ ($N_{\text{Hpers}}-N_{\text{Hgal}}$)	$N_{\text{H}}^{\text{xabs}}_{\text{pers}}$	$\Delta N_{\text{H}}^{\text{xabs}}$	$\log(\xi)_{\text{pers}}$	$\log(\xi)_{\text{dip}}$	Dip depth
XB 1916–053	0.432 ± 0.002	0.46 ± 0.07	0.27	2.8 ± 0.4	4.2 ± 0.5	50 ± 3	3.05 ± 0.04	$2.52^{+0.02}_{-0.06}$	80%
XB 1323–619 ^a	3.50 ± 0.02	0.7 ± 0.2	1.57	0.4 ± 0.1	3.8 ± 0.4	33 ± 2	3.9 ± 0.1	3.13 ± 0.07	75%
EXO 0748–676	0.11	$0.13^{+0.09}_{-0.05}$	0.11	∞	3.5 ± 0.2	12.0 ± 0.5	2.45 ± 0.02	2.26 ± 0.03	>85%
XB 1254–690	0.346 ± 0.002	0.04 ± 0.01	0.31	1.0 ± 0.3	8.4 ± 0.3	39 ± 3	4.3 ± 0.1	2.94 ± 0.05	50%
MXB 1659–298	0.306 ± 0.003	0.40 ± 0.04	0.19	3.5 ± 0.4	11.1 ± 0.6	42 ± 3	3.8 ± 0.1	$2.42^{+0.02}_{-0.06}$	>85%
X 1624–490 ^b	10.7 ± 0.5	48^{+6}_{-3}	2.22	$5.7^{+0.7}_{-0.4}$	13 ± 2	55 ± 9	3.6 ± 0.2	≥ 3.3	80%

^aValues for XB 1323–619 are derived from the spectral fits in Boirin et al. (2005).

^bThe changes for X 1624–490 are calculated between the Dip 1 and Dip 5 stages.

the ionization state of a highly-ionized absorber. At the lower ionization levels seen during dips, lower-Z abundant ions such as H-like Ne, Si, and S and intermediate ionization states of Fe are present and their absorption features blend together at CCD energy resolution. This and the appearance of strong edges from the same ions result in an apparent change in the continuum, which is consistent with that actually observed during dips.

Here we demonstrate that the model applied by Boirin et al. (2005) to XB 1323–619 explains the spectral changes, both in the continuum and in the narrow absorption features, between persistent and dipping intervals of all the bright dipping LMXBs observed by XMM-Newton. Details may be found in Díaz Trigo et al. (2005).

2. DATA ANALYSIS AND RESULTS

We re-analysed all the XMM-Newton observations of bright dipping LMXBs in a similar way as it was done for XB 1323–619. Their EPIC pn 0.6–10 keV lightcurves are shown in Fig. 1. We fit the spectra of all the sources with a continuum consisting of a power-law, and a blackbody modified by absorption from neutral material (the `abs*(bb+p1)` model in SPEX). For each source we fit simultaneously all the EPIC pn spectra of the persistent and dipping intervals with the continuum parameters tied together, while we allowed to vary all the other parameters. We included Gaussian emission profiles when emission features were evident near 1 keV and/or 6 keV. To account for the absorption features around 7 keV we included absorption from a photo-ionized plasma (`xabs`) in the spectral model. The `xabs` model treats the absorption by a thin slab composed of different ions, located between the ionizing source and the observer. The processes considered are the continuum and the line absorp-

tion by the ions and scattering out of the line-of-sight by the free electrons in the slab. All relevant ions are automatically taken into account. We are able to account for the complex changes in the 0.6–10 keV continuum and absorption lines during dips from the LMXBs studied here (with the exception of 4U 1746–371 where the dips are very shallow) by large increases in the column density, $N_{\text{H}}^{\text{xabs}}$, and decreases in the amount of ionization, ξ , of a highly-ionized absorber (see Table 1), together with much smaller increases in the N_{H} of a neutral absorber (for X 1624–490 the increase in the column densities of the neutral and ionized absorbers are comparable). The eclipsing binaries EXO 0748–676 and MXB 1659–298 (together with the non-eclipsing system X 1624–490) show the largest change in N_{H} . This suggests that the size of the change in N_{H} may be related to the inclination angle. Thus we would be seeing X 1624–490 and XB 1254–690 very close to, and relatively far from, the planes of the accretion disks. The spectral changes during dips from LMXBs are often modeled using the “complex continuum” approach. There the X-ray emission originates from a point-like blackbody or disk-blackbody component, together with an extended power-law component. The spectral changes during dips are explained by the partial and progressive covering of the extended component by an opaque absorber. We have self-consistently demonstrated that changes in the properties of an ionized absorber provide an alternative explanation for the overall spectral changes during dips from all the dipping LMXBs studied by XMM-Newton.

REFERENCES

- Boirin L., Méndez M., Díaz Trigo M., Parmar A. N. and Kaastra J. S. 2005, A&A, 436, 195
- Díaz Trigo M., Parmar A. N., Boirin L., Méndez M. and Kaastra J. S. 2005, A&A, in press, astro-ph/0509342

THE BROAD BAND SPECTRUM OF CYG X-1

S. Fritz¹, J. Wilms², K. Pottschmidt³, M. A. Nowak⁴, I. Kreykenbohm^{1,5}, and A. Santangelo¹

¹Institut für Astronomie und Astrophysik, Sand 1, 72076 Tübingen, Germany

²Department of Physics, University of Warwick, Coventry, CV7 1AL, UK

³Center for Astrophysics and Space Sciences, University of California, San Diego, La Jolla, CA 92093-0424, USA

⁴MIT-CXC, NE80-6077, 77 Massachusetts Ave., Cambridge, MA 02139, USA

⁵INTEGRAL Science Data Centre, 16 Ch. d'Ecogia, 1290 Versoix, Switzerland

ABSTRACT

We present first results on *INTEGRAL* and *RXTE* from our multi-mission observing campaign on Cygnus X-1. The black hole binary Cyg X-1 has been observed simultaneously by *INTEGRAL*, *RXTE*, and *XMM-Newton* for four times in 2004 November and December, when Cyg X-1 became first observable with *XMM-Newton* (see contribution by Wilms et al., these proceedings). One of the scientific aims of this campaign was the measurement of a high signal to noise spectrum of Cyg X-1 from 2.5 keV to >600 keV in order to constrain models for the hard spectral component. We show here first results of our ongoing analysis obtained by modeling the broad band spectrum with simple empirical models as well as with Comptonization models.

Key words: Interacting Binaries; Cyg X-1.

1. INTRODUCTION

Cyg X-1 has been observed by *INTEGRAL*, *RXTE*, and *XMM-Newton* simultaneously on 2004 November 14/15 (hereafter called obs1), 20/21 (obs2), 26/27 (obs3), and on December 2/3 (obs4). The total observation time was ~ 320 ksec for the *INTEGRAL* observation and ~ 152 ksec for *RXTE*. As Cyg X-1 is highly variable we decided to study the four observations independently. Our observation took place during one of the transitional states of Cyg X-1 between the hard and the soft state.

Here, we present first results of our ongoing analysis obtained with *INTEGRAL* and *RXTE*. For *RXTE* we used data from the *PCA* and *HEXTE*, covering an energy range from 3 keV to 120 keV. The *INTEGRAL* data comprises information of the three instruments *JEM-X*, *IBIS (ISGR)* and *SPI*, including energies up to 1 MeV. The data extraction was done using HEASOFT 5.3.1 and *INTEGRAL* OSA 5.

2. FITTING THE BROAD BAND SPECTRUM

In order to compare our results of this long observation with results obtained during the *RXTE* monitoring campaign, we decided to fit our data with the same models used by Wilms et al. (2005, all correlations mentioned below refer to the data within this paper). In addition to the different continuum models we always included a Fe line at 6.4 keV and interstellar photo electric absorption. The aim of this first analysis was to check if the parameters found to fit the 3–120 keV energy range could also fit the data up to 1 MeV.

2.1. Broken Power Law Fits

The spectra of black hole candidates can be empirically described by an absorbed broken power law with an exponential cutoff (Nowak et al., 2005). The χ_{red}^2 values obtained with this model range from 1.13 (obs1) to 0.94 (obs4). Broken power law fits can reproduce the spectrum equally well as the more complex *eqpair* model. The best fit parameters are $\Gamma_1 \approx 2.0$, $E_{\text{break}} \approx 10$ keV, $\Gamma_2 \approx 1.6$ and a folding energy ranging from 126 keV (obs1) to 149 keV (obs3). The values found for Γ_1 and Γ_2 agree very well with the strong linear correlation of this two parameters found in the *RXTE* monitoring campaign.

2.2. Fits using *compTT*

compTT (Titarchuk, 1994; Titarchuk & Lyubarskij, 1995; Titarchuk & Hua, 1995) is the first Comptonization model we used. The soft emission is modeled by adding a *diskbb* component which provides the seed photons for the Comptonization (therefore we set the temperature of the seed photons equal to kT_{in} , the temperature at the inner edge of the disk). This continuum is partly reflected off the accretion disk (*XSPEC*

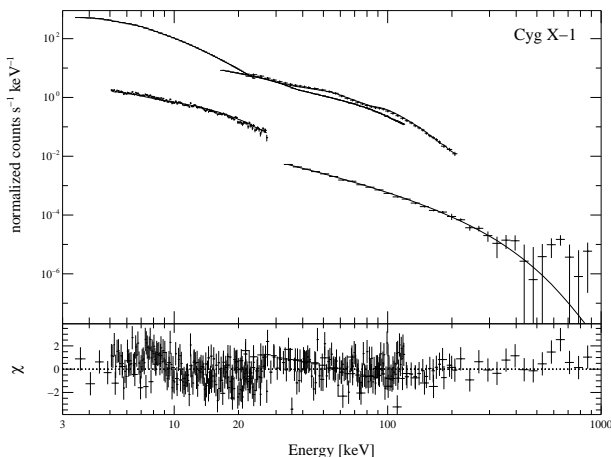


Figure 1. Best fit to the observation of 2004 November 20/21 (obs2) using the *eqpair* model. There are slight indications for a hard tail, but this could also be due to instrumental uncertainties.

model reflect). The parameters from this fit are in principle consistent with former results although the values for the electron temperature ($kT_e \sim 69$ keV) and optical depth ($\tau \sim 0.7$) give a Compton- y parameter $y = 4kT_e/m_e c^2 \max(\tau, \tau^2) \sim 0.35$ which differs from the value 0.5 found in the *RXTE* monitoring data for the hard state observations and is indicative for the transitional states. Consistent with this conclusion, the values for the reflection covering factor are slightly higher than in previous hard state results. The χ_{red}^2 values of the *compTT* fits are very similar to those we get using the simple model, they range from 1.22 (obs3) to 0.96 (obs1).

2.3. Fits using *eqpair*

The third model we used is the hybrid thermal/non-thermal Comptonization code *eqpair* by Coppi (1992) in which the temperature of the Comptonizing medium is computed self-consistently. The distribution of the seed photons is defined by a disk blackbody. An example of an *eqpair* fit can be seen in Fig. 1 which shows the best fit to obs2. Table 1 summarizes the best fit parameters for all our observations. The compactness ratio, ℓ_h/ℓ_s , and the optical depth, τ , which describe the hard spectral component, are in good agreement with the previous results. Our values for the compactness ratio also go very well with the correlations found between this parameter and the parameters of the broken power law fits in the *RXTE* monitoring.

3. SUMMARY

We modeled the broad band spectrum of Cyg X-1 with a simple power law model as well as with more physically motivated Comptonization models. All fits are in

Table 1. Best fit parameters for the *eqpair* model.

	obs1	obs2	obs3	obs4
N_{H} [10^{22} cm^{-2}]	$0_{-0}^{+0.12}$	$0_{-0}^{+0.12}$	$0_{-0}^{+0.20}$	$0_{-0}^{+0.11}$
T_{in} [keV]	$1.08_{-0.02}^{+0.03}$	$1.09_{-0.08}^{+0.05}$	$1.18_{-0.03}^{+0.01}$	$1.12_{-0.10}^{+0.05}$
norm	62_{-4}^{+6}	43_{-4}^{+8}	46_{-2}^{+4}	41_{-2}^{+2}
$E_{\text{K}\alpha}$ [keV]	$6.41_{-0.13}^{+0.03}$	$6.27_{-0.13}^{+0.05}$	$6.34_{-0.13}^{+0.05}$	$6.25_{-0.12}^{+0.05}$
$\sigma_{\text{K}\alpha}$ [keV]	$0.79_{-0.04}^{+0.13}$	$0.82_{-0.07}^{+0.14}$	$0.62_{-0.06}^{+0.13}$	$0.75_{-0.05}^{+0.14}$
ℓ_h/ℓ_s	$2.76_{-0.01}^{+0.02}$	$3.15_{-0.03}^{+0.03}$	$3.69_{-0.02}^{+0.04}$	$3.96_{-0.03}^{+0.03}$
τ	$1.19_{-0.03}^{+0.01}$	$1.19_{-0.03}^{+0.03}$	$1.45_{-0.01}^{+0.02}$	$1.44_{-0.07}^{+0.01}$
$\Omega/2\pi$	$0.33_{-0.01}^{+0.01}$	$0.30_{-0.01}^{+0.01}$	$0.27_{-0.01}^{+0.01}$	$0.27_{-0.01}^{+0.01}$
ξ	0_{-0}^{+13}	1_{-1}^{+10}	3_{-3}^{+10}	1_{-1}^{+13}
$\chi_{\text{red}}^2 / \text{dof}$	1.18/343	1.27/342	1.73/341	1.19/338

good agreement with former results of the *RXTE* monitoring campaign, the parameters describe the extended energy range equally well. Our data show indications of a spectral hardening above ≈ 300 keV, which could possibly be a hard tail, but could also be due to instrumental uncertainties. The next step will be fitting the broad band spectrum with models taking the existence of the jet into account.

REFERENCES

- Coppi, P. S. 1992, Mon. Not. R. Astron. Soc., 258, 657
- Nowak, M. A., Wilms, J., Heinz, S., et al. 2005, *Astrophys. J.*, 626, 1006
- Titarchuk, L. 1994, *Astrophys. J.*, 434, 570
- Titarchuk, L. & Hua, X.-M. 1995, *Astrophys. J.*, 452, 226
- Titarchuk, L. & Lyubarskij, Y. 1995, *Astrophys. J.*, 450, 876
- Wilms, J., Nowak, M. A., Pottschmidt, K., Pooley, G. G., & Fritz, S. 2005, *A&A* in press

ELUCIDATING THE NATURE OF NEW SLOAN DIGITAL SKY SURVEY "CVS" WITH XMM-NEWTON

Lee Homer¹, Paula Szkody¹, Bing Chen², Arne Henden³, Gary D. Schmidt⁴, Scott. F. Anderson⁵, Nicole M. Silvestri⁵, and J. Brinkmann⁶

¹Department of Astronomy, University of Washington, Box 351580, Seattle, WA 98195, USA

²XMM-Newton Science Operations Centre, ESA/Vilspa, 28080, Madrid, Spain; VEGA IT GmbH, c/o European Space Operations Centre, Darmstadt, Germany

³Universities Space Research Association; US Naval Observatory, Flagstaff Station, P.O. Box 1149, Flagstaff, AZ 86002-1149, USA; American Association of Variable Star Observers, 25 Birch Street, Cambridge, MA 02138, USA

⁴The University of Arizona, Steward Observatory, Tucson, AZ 85721, USA

⁵Department of Astronomy, University of Washington, Box 351580, Seattle, WA 98195, USA

⁶Apache Point Observatory, 2001 Apache Point Road, P.O. Box 59, Sunspot, NM 88349-0059, USA

ABSTRACT

We report follow-up XMM-Newton and optical observations of the two stars identified as candidate intermediate polars from their Sloan Digital Sky Survey spectra: SDSS J102347.67+003841.2 = FIRST J102347.6+003841 and SDSS J093249.57+472523.0. We also include a brief summary of the overall results from our on-going XMM-Newton follow-up programme of candidate magnetic cataclysmic variables (mCVs) found in SDSS.

Key words: individual: (SDSS J093249.57+472523.0, SDSS J102347.67+003841.2) — novae, cataclysmic variables — stars: magnetic — X-rays: stars.

1. INTRODUCTION

The Sloan Digital Sky Survey (SDSS) has proven highly effective in the identification of new accretion-powered binaries; its five colour photometry plus high quality follow-up spectra have revealed > 100 cataclysmic variables (CVs) and related objects (Szkody et al 2002-2005). This large sample facilitates the optical selection of candidate magnetic (m)CVs, thus potentially probing to lower accretion rates than available with earlier X-ray identification/selection methods. In an on-going programme of XMM-Newton observations we are obtaining X-ray measures, such as basic spectral parameters and fluxes to further improve our understanding of these systems, and confirm their magnetic classifications (or not).

2. OBSERVATIONS AND DATA REDUCTIONS

For each target we have obtained low-resolution spectra from the EPIC cameras, with count rates (pn) ranging from 0.08 to 0.4 cps. Our spectral and lightcurve extractions followed the standard procedures from the ABC guide and Vilspa help pages; however we always reextracted event lists from the ODF files to incorporate the

latest calibration products. In the optical we obtained spectroscopy, spectro-polarimetry and time-series photometry, often simultaneous or contemporaneous with the X-ray observations. In most cases, we also obtained B -band imaging from the OM and performed custom extractions from the ODFs to produce binned lightcurves with time-resolutions comparable to our ground based data.

3. MOST RECENT RESULTS

Here we provide brief details on our results for SDSS J0932 and J1023; full details including figures appear in Homer et al 2006a.

3.1. SDSS J093249.57+472523.0

Two epochs of photometry show 7 deep and narrow eclipses; the $O - C$ analysis yields a best fit ephemeris: $HJD(TT) = 2453122.2324(1) + E * 0.0661618(4)d$. In addition, during May there was evidence for a periodic, non-eclipse modulation with $P=1.04 * P_{orb}$: perhaps a superhump?

A blue, high-excitation emission line spectrum, indicative of a magnetic CV, was seen in both the SDSS survey, and contemporaneously with our X-ray observations. Given our low S/N, the X-ray spectral fits allow for either a hard bremsstrahlung or power law emission model, but in each case a partial covering model with low Galactic column + high local $N_H = 1 \times 10^{23} \text{cm}^{-2}$ and fraction 0.9 was needed; this suggests either an accretion curtain or (time-averaging over) X-ray dipping. Overall, observations suggest an intermediate polar nature: the X-ray/optical spectra are consistent with mCV or high- i active LMXB, but an F_X/F_{opt} comparable to other intermediate polars (IPs), and more than $100\times$ too low for an LMXB. However, the absence of additional photometric periodicities leaves its IP candidacy in doubt; more optical photometric monitoring needed.

Table 1. Summary of results from our XMM-Newton and optical follow-up programme on SDSS “CVs”

SDSS J	Class	P^a (h)	V_{avg}	f_X^b ($\text{erg s}^{-1} \text{cm}^{-2}$)	Description
072910.68+365838.3	Polar	2.5	20.6	4×10^{-13}	Single-pole accretor, unusual 0.57 keV line during “flare” ¹
075240.45+362823.2	Polar	2.74	18.3	4×10^{-12}	Single-pole accretor, $L_{\text{BB}}/L_{\text{br}} = 0.35 - 0.5$ ¹
170053.30+400357.6	Polar	1.94	18.7	1×10^{-12}	Anti-phased X-ray and optical orb. modn.– 2-pole accretor? ¹
015543.40+002807.2	Polar	1.45	16.5-18.5	3×10^{-12}	Shortest P_{orb} eclipsing polar, exhibits low/high states ²
132411.57+032050.5	LARP ^c	2.6	17.6	$< 6 \times 10^{-15}$	X-rays only from M dwarf secondary ³
155331.12+551614.1	LARP	4.39	18.8	7×10^{-14}	As for 1324, long-term avg. $\dot{M} < 3 \times 10^{-12} M_{\odot}/\text{yr}$ ³
144659.95+025330.3	IP	3.8/.8	18.0	2×10^{-12}	Large amp. spin modn. in opt./X-ray. P_{orb} from radial vels. ⁴
093249.57+472523.0	IP?	1.59/?	18.8	2×10^{-13}	X-ray/opt. spectra suggest IP, but no spin modulation seen ⁵
102347.67+003841.2	LMXB	1.94	16-17.5	6×10^{-13}	Only one (small) outburst to date, variable ⁵ X-ray emission dominated by non-thermal component

Notes: ^aFor IPs both orbital and spin periods given, others P_{orb} , ^bUnabsorbed X-ray flux in 0.01-10 keV band, ^cLARP=Low accretion rate polar. References: ¹Homer et al 2005, ²Schmidt et al 2005, ³Szkody et al 2004b, ⁴Homer et al 2006b, ⁵Homer et al 2006a

3.2. SDSS J102347.67+003841.2

First observed in a rare high state, when it exhibited: (i) radio emission (detected in FIRST survey, Bond et al 2002); (ii) a high excitation emission line spectrum (Szkody et al. 2003); (iii) a blue continuum with $V \approx 16$. Hence, a highly magnetic CV was suggested. In its more usual low state (as for our observations), one sees: (i) a red mid-G V stellar spectrum, with $V \approx 17.5$; (ii) a smooth optical modulation on the $P=4.75$ h orbit. Moreover, lightcurve modelling, and radial velocities imply $M_{\text{acc}} > 1.4 M_{\odot}$ (Thorstensen & Armstrong 2005 - TA05), making SDSS J1023 an LMXB (usually observed in quiescence)

Our optical minimum phases well with TA05, giving a refined ephemeris: $\text{HJD}(\text{TT}) = 2453081.8546(3) + E * 0.198094(1)\text{d}$. The X-ray lightcurve shows 60% (peak-peak) variation, possibly periodic on 1.66 h. If this were the white dwarf spin in an IP, it would require a unique P_{spin} to P_{orb} ratio.

Approximating the X-ray emission of a CV as a thermal plasma, we find an acceptable fit for a 40 keV MEKAL, with (fixed) low column $N_H = 1 \times 10^{19} \text{cm}^{-2}$. Or for LMXB in quiescence, fitting a power law (+ optional neutron star atmosphere), we find good fits for the PL alone with $\Gamma = 1.3$, and $N_H = 9 \times 10^{19} \text{cm}^{-2}$; the NSA contribution is negligible.

In summary, our observations support the LMXB hypothesis of TA05: (i) for $d=2$ kpc, $L_X = 10^{32.4} \text{erg/s}$ – typical for LMXBs in quiescence; (ii) X-ray emission dominated by power law (>97%) – fits with anti-correlation for low L_X systems (see Jonker et al 2004); (iii) X-ray variability akin to that of both Cen X-4 and EXO 1745-248, but origin of hard X-rays still a mystery; (iv) only one outburst known to date – implies large quiescent intervals, consistent with faint, low temperature NSA component. In contrast, many characteristics do not fit with a magnetic CV interpretation: (i) activity behaviour unlike any CV subclass – infrequent and low amplitude outburst(s);

(ii) MEKAL spectrum fine for active CV, but what of its origin in absence of substantial mass transfer, it cannot be the chromospheric emission of the donor star, being both too hard and bright.

4. CONCLUSIONS

The XMM-Newton and optical follow-up of candidate magnetic CVs from SDSS has proven highly successful. Out of the 9 systems studied to date, only one has not turned out to be an mCV, and this a probable transient LMXB! We have added 1 or 2 IPs to their small numbers, as well as 2 polars with extremely low accretion rates, possibly pre-polars. The new eclipsing system SDSS J0155 has already yielded detailed constraints on the nature of its accretion flow, along with full binary parameters; it is ripe for further phase-resolved spectroscopy on 10m-class telescopes. Together with the other 3 polars, we find no evidence for the so-called soft X-ray excess; in agreement with the results of the latest XMM-Newton survey of the brighter polars by Ramsay, Cropper and co-workers.

REFERENCES

- Bond, H. E., White, R. L., Becker, R. H., & O’Brien, M. S. 2002, *PASP*, 114, 1359
Homer, L., Szkody, P., Chen, B. et al. 2005, *ApJ*, 620, 929
— . 2006a, *AJ*, in press
Homer, L., et al. 2006b in preparation.
Jonker, P. G., Galloway, D. K., McClintock, J. E. et al. 2004, *MNRAS*, 354, 666
Schmidt, G.D., Szkody, P., Homer, L. et al. 2005, *ApJ*, 620, 422
Szkody, P. et al. 2003, *AJ*, 126, 1499
— . 2004, *AJ*, 128, 1882
— . 2005, *AJ*, 129, 2386
Szkody, P., Homer, L., Chen, B. et al. 2004, *AJ*, 128, 2443
Thorstensen, J. R. & Armstrong, E. 2005, *AJ*, 130, 759

COMPARISON BETWEEN TWO OUTBURSTING GALACTIC BLACK HOLES

A. Joinet, E. Jourdain, J. Malzac, and J.P. Roques

CESR, CNRS/UPS, 9 Avenue du Colonel Roche, BP4346, 31028 Toulouse cedex 4, France

ABSTRACT

The accreting Galactic Black Holes (BHs) H1743-322 and GX339-4 have been observed during their 2003 and 2004 outburst respectively with PCA/RXTE and SPI/INTEGRAL observatories. We studied the spectro-temporal evolution of H1743-322 during its transition state combined with a strong X and γ -ray flaring activity. We will compare this source with GX339-4 as a key source in the elaboration of alternative jet models.

Key words: Transient; BHC; hard X-ray emission.

1. INTRODUCTION

Outbursting Galactic BHs are known to go through a complex multistate which can be followed by studying its spectral and timing evolution. In the X/ γ energy domain, their energy spectra consists of two main components which allow to characterise the state of the sources.

- In the high/soft state, the soft X-ray emission (below 10 keV) dominates the spectrum in the form of a blackbody component
- In the low/hard state, the hard X-ray emission (above 10 keV) dominates the spectrum in the form of a X-ray powerlaw component with an exponential cutoff around 100 keV

We refer to McClintock & Remillard (2003) for the complete spectro-temporal criteria used to define each state of a source. The main goal here, is to do a phenomenological study of the outbursting Galactic BHs H1743-322 and GX339-4 by comparing their spectro-temporal characteristics along the transition state. We used data extracted from PCA/RXTE and SPI/INTEGRAL observations. A large part of this study are based on the results from the reference Joinet et al. (2005) where details about the data analysis as well as the discussion about the spectral modulation of H1743-322 can be found.

2. TEMPORAL VARIABILITY AND STATE TRANSITION (LONG TERM VARIABILITY)

After a long period in quiescence (upper than 7 years for H1743-322 and almost 3 years for GX 339-4 from ASM/RXTE observations), these sources was found to exhibit a gradual increase of the X-ray luminosity. As seen from Figure 1, the light curves of both sources exhibit a complex temporal variability and multistate during the rise phase. The low/hard to high/soft state transition observed during their outburst can be interpreted in terms of a geometry evolution.

Particularly, we extracted several spectra of H1743-322 along this transition state (see Figure 2) and modelised them using a multicomponent model described in Joinet et al. (2005). Up to the beginning of the flaring activity (revolution 60), the blackbody emission grows progressively as it is expected when the accretion disk surface increases. In the same time, we note the decrease of the hard X-ray emission coming from the soft photons componentised by a hot electron plasma (or corona) (see Joinet et al. (2005)). The decrease of the optical depth of the hot corona could be explained either by material ejection during the major radio ejection event (revolution 58) or by its condensation into an optically thick disk. The same relative hard to soft component evolution related to state transition was observed for GX339-4 (Figure 2).

3. THE FLARING ACTIVITY IN THE CASE OF H1743-322 (SHORT TERM VARIABILITY)

As shown in Figure 1, H1743-322 exhibited around the maximum of luminosity, correlated X and γ flare events within a timescale of about one day. From revolution 60, we separate periods for which the flux of the source is higher than 300 mCrab in the 20-36 keV energy range (flare events) from the other ones (no flare events). We can notice from extracted spectra (see Figure 3) and the associated fit parameters (see Table 5 in Joinet et al. (2005)) that the spectral shape remained unchanged (so the overall geometry of the source) while the luminosity of the source is multiplied by a factor of two during the

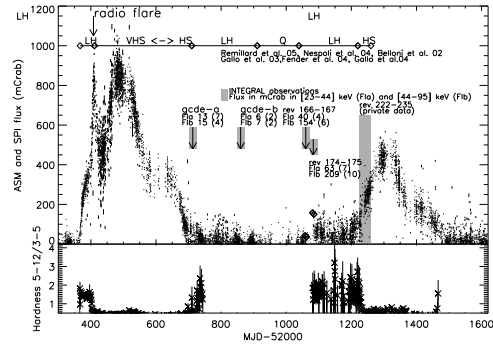
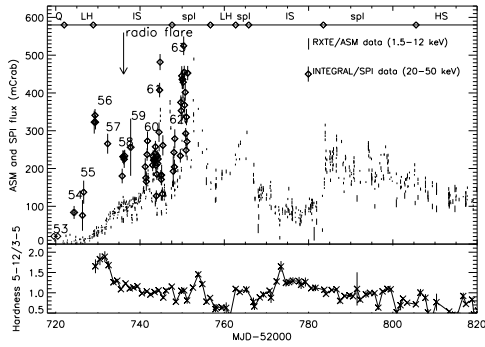


Figure 1. Left panel : Light curve of H1743-322 during its 2003-2004 outburst. We also give the revolution numbers corresponding to SPI data. The different states harboured by the source are summarized on the graph (using the classification of McClintock & Remillard (2003)): Q=quiescent, LH=Low Hard, IS= Intermediate, spl=Steep powerlaw or Very high, HS=High Soft. Right panel : Light curve of GX339-4 during its 2002-2004 outburst.

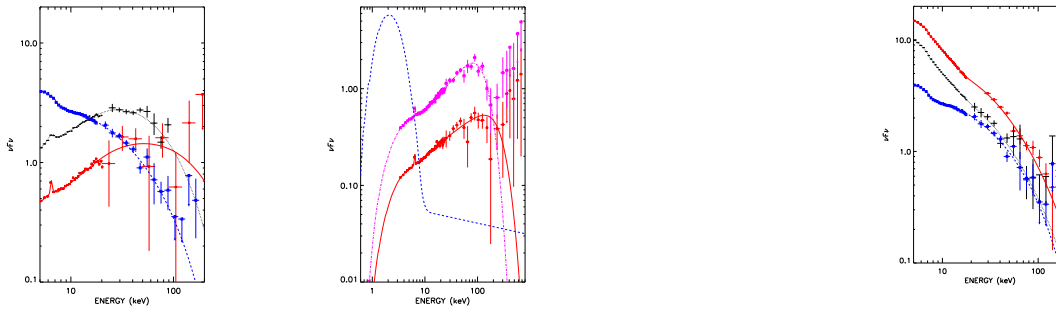


Figure 2. Spectra from simultaneous PCA and SPI observations. Left panel : H1743-322 during INTEGRAL's rev. 55, 56 and 58 (classified below 10 keV as the lower, middle and higher curve respectively). Right panel : GX339-4 in low/hard state during rev. 166 (red points) and 175 (pink circles) (Joinet et al., 2005b). The best model (blue dashed line) fitting the source data of 1998 outburst (Belloni et al., 1999) is drawn to indicate the spectral shape evolution during a low/hard to high/soft state transition which is similarly observed for H1743-322.

flaring period.

4. RELATIVISTIC RADIO JET AND STATE TRANSITION

A relativistic radio jet emission was observed in GX339-4 and H1743-322 during the rise phase of the outburst. In both cases, it is noticed from the ASM hardness in the 3-12 keV energy range (Figure 1), that just after this radio event, there is a clear softening of the source. Secondly, this occurs during the low/hard to soft/state transition. Then, an extended radio jet emission was observed following the radio flare event for both sources: it could be explained by an interaction of the plasma ejected during the outbursting phase with the interstellar medium (Corbel et al., 2005)

To conclude, we have pointed out some spectro-temporal

Figure 3. Spectra from simultaneous PCA and SPI observations of H1743-322 during rev. 58, 60-63 (no flare events) and 61-63 (flare events) (lower, middle and higher curve respectively).

similarities between both outbursting Galactic BHs H1743-322 and GX339-4. The goal of such a study is the elaboration of a scheme to explain the radio flare event and its links with the state transition together with the observed chaotic events in X and γ -ray energy range (flaring activity) as the source reaches the maximum of luminosity. The modelisation of the radio jet contribution in the X and γ -ray energy range should be investigated.

REFERENCES

- Belloni T., et al. 1999, ApJ 519, L159
- Capitanio F., et al. 2005, ApJ 622, 503
- Corbel S., et al. 2005, ApJ 632, 504
- Fender R.P. & Kuulkers E. 2001, MNRAS 324, 923
- Joinet A., et al. 2005, ApJ 629, 1008
- Joinet A., et al. 2005b, in preparation
- McClintock, J.E. & Remillard, R.A. 2003, in "Compact Stellar X-ray Sources" eds. W.H.G. Lewin and M. van der Klis, Cambridge University Press., astro/0306213

3A 0535+262 IN OUTBURST

P. Kretschmar¹, K. Pottschmidt², C. Ferrigno³, I. Kreykenbohm^{4,5}, A. Domingo⁶, J. Wilms⁷, R. Rothschild², W. Coburn⁸, E. Kendziorra⁴, R. Staubert⁴, G. Schönherr⁴, A. Santangelo⁴, and A. Segreto³

¹ESA – European Space Astronomy Center, 28080 Madrid, Spain

²Center for Astrophysics and Space Science, UCSD, La Jolla, CA, USA

³Istituto di Astrofisica Spaziale (IASF-INAF), Palermo, Italy

⁴Institut für Astronomie und Astrophysik – Astronomie, Univ. of Tübingen, 72076 Tübingen, Germany

⁵INTEGRAL Science Data Centre, 1290 Versoix, Switzerland

⁶Laboratorio de Astrofísica Espacial y Física Fundamental, LAEFF-INTA, 28080 Madrid, Spain

⁷Department of Physics, University of Warwick, CV4 7AL Warwick, United Kingdom

⁸Space Sciences Laboratory, University of California, CA 94720-7450 Berkeley, USA

ABSTRACT

The Be/X-ray binary 3A 0535+262 has the highest magnetic field determined by cyclotron line studies of all accreting X-ray pulsars, despite an open debate if the fundamental line was rather at 50 or above 100 keV as observed by different instruments in past outbursts. The source went into quiescence for more than ten years since its last outbursts in 1994. Observing during a ‘normal’ outburst August/September 2005 with *Integral* and *RXTE* we find a strong cyclotron line feature at ~ 45 keV and have for the first time since 1975 determined the low energy pulse profile.

Key words: X-rays: binaries; stars: magnetic fields.

1. INTRODUCTION

The Be/X-ray binary and accreting pulsar 3A 0535+262 was first detected by Ariel V (Rosenberg et al., 1975) and has been studied intensively since. For an exhaustive review see Giovannelli & Graziati (1992). The X-ray intensity of 3A 0535+262 varies by almost three orders of magnitude with three basic intensity states: quiescence with flux levels below ~ 10 mCrab, normal outbursts (10 mCrab–1 Crab), and very large (“giant”) outbursts.

Since the last giant outburst in 1994 and two subsequent weaker outbursts spaced at the orbital period (Finger et al., 1996), the source had gone into quiescence. It reappeared in a giant outburst in May/June 2005 (Tueller et al., 2005; Smith et al., 2005) but so close to the Sun that it could only be observed by a few instruments. Another outburst at the ‘normal’ level was detected by Finger M.H. (2005a,b) and led to our *Integral* and *RXTE* TOO observations. During the *Integral* observations the average flux in the 5–100 keV range was 300 mCrab

2. DATA REDUCTION

All *Integral* data have been reduced using the Offline Scientific Analysis software v. 5 (OSA5). To generate phase resolved spectra and lightcurves from ISGRI data, alternative software provided by the IASF Palermo (<http://www.pa.iasf.cnr.it/~ferrigno/INTEGRALsoftware.html>) has been used in addition to the OSA5 software. *RXTE* data have been reduced using HEASOFT v5.3.1.

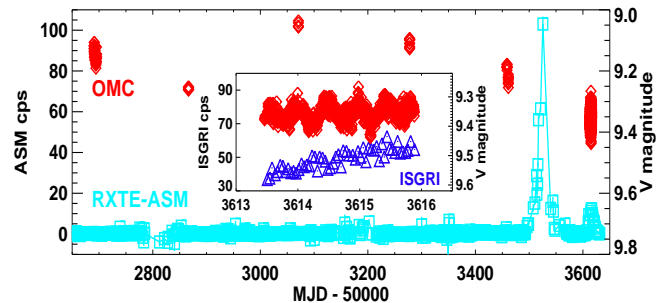


Figure 1. Long term lightcurves of the binary system 3A 0535+262/HD 245770 obtained with the *RXTE* ASM (left Y axis) and the *Integral* OMC (right Y axis). The inset shows the OMC and ISGRI lightcurves during the *Integral* TOO observations.

3. OPTICAL & ALL-SKY MONITOR DATA

3A 0535+262 has been monitored serendipitously by the Optical Monitoring Camera (OMC) onboard *Integral*, e.g., during Crab observations. The long term lightcurve shows a marked decline of the optical brightness in the time leading up to the outburst. During the outburst, small variability, typical for Be systems is observed.

4. PULSATIONS

A quick-look analysis of the *Integral* data without correcting for orbital motion finds a pulse period of 103.3765 ± 0.0014 s for the reference time MJD 53613.46176 (2005-08-30, 11:04:56). For the generation of lightcurves and pulse profiles, the uncorrected motion was taken into account as a pulse drift of $-(8.5 \pm 0.8) \times 10^{-8}$ s/s.

The broad-band pulse profile is shown in Fig. 2. This is the first determination of the low energy pulse profile since Bradt et al. (1976). Similar to other accreting pulsars, the source displays a complex pattern in the soft X-ray range and a simple two-peaked profile, with very different spectral shape of the pulses, at higher energies. The pulse profile is similar to that seen in previous outbursts but differs significantly in various details, hinting at a variable accretion geometry.

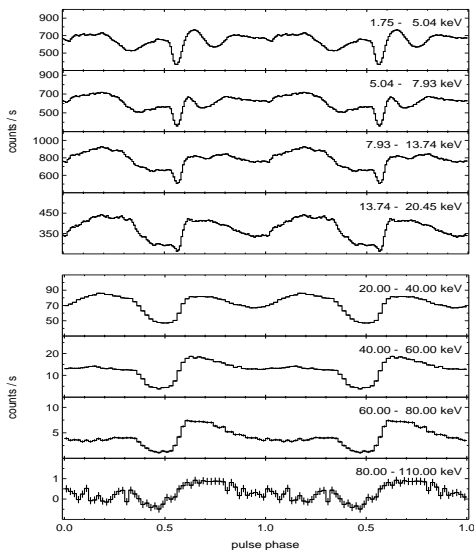


Figure 2. Broad-band pulse profile of 3A 0535+262 combining data from *RXTE*-PCA and *Integral*-ISGRI observations during this outburst.

5. SPECTROSCOPY

Pulse phase averaged spectra were generated from all *Integral* data of the TOO observation and from the available *RXTE* data. While the data are not strictly contemporaneous, the spectra agree well in all important characteristics. Fig. 3 shows results of preliminary fits to the near real time data using a model based on a power law continuum with a ‘‘Fermi-Dirac cutoff’’, modified by one or two lines with a gaussian optical depth profile (Kreykenbohm et al., 2004). The best fit values for important parameters are given in Table 1, the main parameters agree very well. The strong broad line feature at ~ 45 keV proves that the pulsar’s B field is $\sim 4 \times 10^{12}$ G instead of almost 10^{13} G as often claimed in the literature. In contrast to previous outbursts, a feature above 100 keV is only weakly visible.

Table 1. Comparison of salient model parameters.

Parameter	<i>Integral</i>	<i>RossiXTE</i>
Energy ₁ [keV]	45.4 ± 0.4	45.6 ± 0.4
Depth ₁	0.45 ± 0.01	0.62 ± 0.03
Width ₁ [keV]	10.3 ± 0.5	12.7 ± 0.8
Energy ₂ [keV]	99 ± 4	102 ± 3
Depth ₂	0.5 ± 0.1	0.7 ± 0.2
Width ₂ [keV]	8 ± 3	8 ± 3
folding Energy	17.7 ± 0.6	17.0 ± 0.3

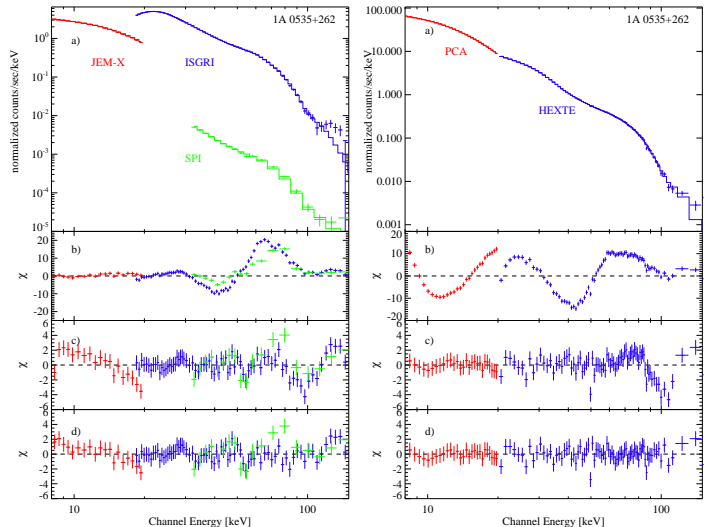


Figure 3. Preliminary fits to the near real time data for *Integral* (left) and *RXTE* (right). On both sides, panel a) shows the folded best fit model, panels b), c) and d) show fit residuals if the data is modeled with no cyclotron line, a single broad line at ~ 45 keV or two line features at ~ 45 and ~ 100 keV, respectively.

REFERENCES

- Bradt, H., Mayer, W., Buff, J., et al. 1976, *ApJ*, 204, L67
- Finger, M. H., Wilson, R. B., & Harmon, B. A. 1996, *ApJ*, 459, 288
- Finger M.H. 2005a, *The Astronomer’s Telegram*, 595
- Finger M.H. 2005b, *The Astronomer’s Telegram*, 597
- Giovannelli, F. & Graziati, L. S. 1992, *Space Sci. Rev.*, 59, 1
- Kreykenbohm, I., Wilms, J., Coburn, W., et al. 2004, *A&A*, 427, 975
- Rosenberg, F. D., Eyles, C. J., Skinner, G. K., & Willmore, A. P. 1975, *Nature*, 256, 628
- Smith, D. M., Hazelton, B., Coburn, W., et al. 2005, *The Astronomer’s Telegram*, 557
- Tueller, J., Ajello, M., Barthelmy, S., et al. 2005, *The Astronomer’s Telegram*, 504

OBSERVATION OF V 0332+53 OVER THE 2004/2005 OUTBURST WITH *INTEGRAL*

I. Kreykenbohm^{1,2}, N. Mowlavi², K. Pottschmidt³, J. Wilms⁴, S. E. Shaw^{2,5}, R. E. Rothschild³, N. Produit²,
W. Coburn⁶, P. Kretschmar⁷, A. Santangelo¹, and R. Staubert¹

¹Institut für Astronomie und Astrophysik – Astronomie, University of Tübingen, 72076 Tübingen, Germany

²*INTEGRAL* Science Data Centre (ISDC), 1290 Versoix, Switzerland

³CASS, University of California, San Diego, La Jolla, CA 92093, U.S.A.

⁴Department of Physics, University of Warwick, Coventry, CV4 7AL, UK

⁵School of Physics and Astronomy, University of Southampton, SO17 1BJ, UK

⁶Space Sciences Laboratory, University of California, Berkeley, Berkeley, CA, 94702-7450, U.S.A.

⁷European Space Astronomy Centre (ESAC), European Space Agency, 28080 Madrid, Spain

ABSTRACT

We present the spectral and temporal analysis of the 2004/2005 outburst of the transient X-ray pulsar V 0332+53 as observed with *INTEGRAL*. After the discovery of the third cyclotron line in phase averaged spectra (Kreykenbohm et al., 2005; Pottschmidt et al., 2005), detailed pulse phase spectroscopy revealed remarkably little variability of the cyclotron lines through the 4.4 s X-ray pulse (Pottschmidt et al., 2005). During the decline of the outburst, the flux was observed to decay exponentially until 2005 Feb 10 and linearly thereafter. The spectrum was found to become harder with time, while the folding energy remained constant. The energy of the fundamental cyclotron line increased with time from 26.5 keV in the *RXTE* observation up to 29.5 keV in the last *INTEGRAL* one indicating that the emission region is moving closer to the surface of the neutron star.

Key words: Pulsars: V0332+53 - stars: magnetic fields.

1. INTRODUCTION: V 0332+53

The recurring transient X-ray pulsar V 0332+53 was discovered in 1983 in *Tenma* data (Tanaka, 1983). Subsequently, a larger outburst was found to have occurred in the summer of 1973 when analyzing *Vela 5B* data (Terrell & Priedhorsky, 1984). The analysis revealed a 4.4 s pulse period and an indication for a 34.25 d orbital period (Stella et al., 1985). The optical counterpart is the O8–9 star BQ Cam (Negueruela et al., 1999).

Analysis of the *Tenma* data revealed a spectral shape similar to that seen in other accreting X-ray pulsars with a flat power law, an exponential cutoff, and a cyclotron resonant scattering feature (CRSF) at an energy of ~ 28 keV.

In 1989 September the source experienced another outburst, this time observed by *Ginga* (Makino, 1989). With the energy range of the Large Area Counters adjusted to cover the 2–60 keV range, CRSFs were detected at 28.5 and 53 keV.

Most recently, V 0332+53 went into outburst in 2004 November and was seen by the *RXTE*/All Sky Monitor (ASM) to reach an intensity of ~ 1 Crab in the 1.5–12 keV band (Remillard, 2004). A long series of observations with *RXTE* and *INTEGRAL* were made throughout the outburst.

2. FLUX EVOLUTION

During the decline phase, the observed fluxes first decay exponentially up to MJD 53412, followed by a linear decrease (see Fig. 1). The decay timescales are different at lower and higher energies: while a decay time of 30 d is observed above 20 keV, it is only 20 d below 15 keV. Such behavior is typically observed in systems where an irradiated disk is present which, however, is not the case for V 0332+53. Since $L_X \propto \dot{M}$, this picture suggests that $\dot{M} \propto M_{\text{disk}}$. The transition to the linear phase would then be triggered by a yet unknown change in the disk.

3. SPECTRAL EVOLUTION

To study the evolution of the spectrum over the outburst, we used the simple *cutoffpl* model, modified by two Gaussian absorption lines to model the CRSFs at ~ 27 keV and ~ 51 keV for all observations. While the folding energy remains constant at ~ 7.5 keV, the power law index Γ decreases from -0.18 in the first observation to -0.4 in the last observations – the spectrum of

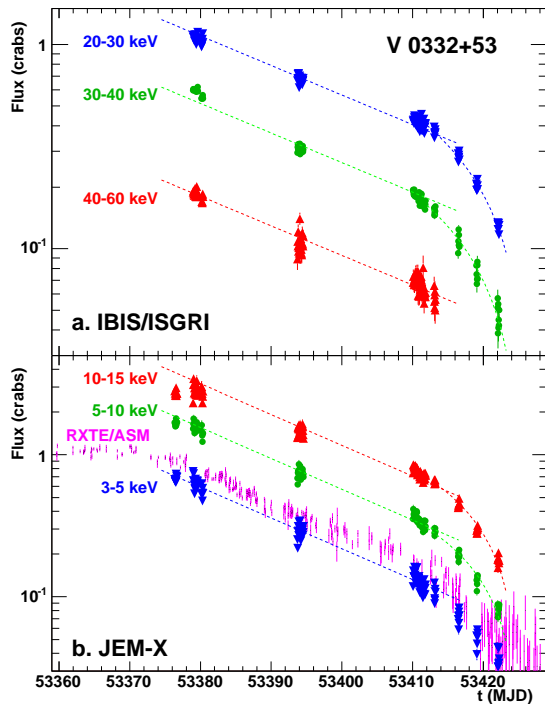


Figure 1. Flux evolution for V0332+53 as observed by the *INTEGRAL* instruments ISGRI and JEM-X (Mowlavi et al., 2005).

V0332+53 hardens over the outburst. The fundamental cyclotron line also changes over the outburst: the energy increases from 27.5 keV in the first *INTEGRAL* observation to 29.5 keV in the last observations. Moreover, during the previous *RXTE* observation, the fundamental CRSF was observed at 26.3 keV (Pottschmidt et al., 2005) resulting in a total increase of more than 3 keV. This change is highly significant: fitting the last *INTEGRAL* observations with a CRSF energy fixed to 27.5 keV results in strong residuals and a completely unacceptable fit. The same holds true for the continuum: fixing the other continuum parameters also results in unacceptable fits. The determination of the parameters of the second CRSF, however, is problematic for the second half of the observations as with decreasing flux, statistics become poor.

4. DISCUSSION

The exponential decay of the flux and the transition to a linear phase later is frequently observed in SXTs and dwarf novae (King & Ritter, 1998). While the emission mechanism is entirely different for V0332+53, the similarity is striking and a yet unidentified change in the disk can be assumed to trigger the transition to the linear phase. The luminosity dependence of the energy of CRSFs had already been observed previously (Mihara, 1995) and was assumed to be due a change in height of the CRSF formation region in the accretion column. Based on our data, we derive a change in height of

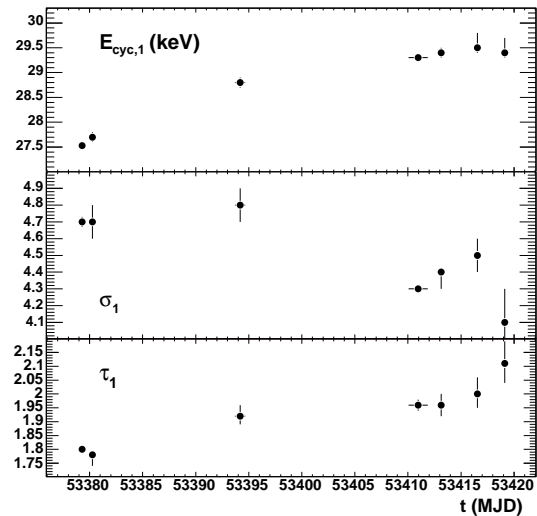


Figure 2. Evolution of the spectral parameters of the fundamental CRSF during the decay of the outburst (Mowlavi et al., 2005).

~ 300 m; however, a slightly different picture is also possible: the CRSF emission region can be assumed to be extended along the accretion column. The observed broad CRSFs would then be superposition of many narrower lines, each from a different height in the column. As the accretion rate drops, the extend of the emission region and its height both decrease and hence the energy of the CRSF increases while it gets narrower as is observed for V0332+53 (see Fig. 2).

REFERENCES

- King A.R., Ritter H., 1998, Mon. Not. R. Astron. Soc. 293, L42
- Kreykenbohm I., Mowlavi N., Produit N., et al., 2005, Astron. Astrophys. 433, L45
- Makino F., 1989, IAU Circ. 4858, 1
- Mihara T., 1995, Ph.D. thesis, RIKEN, Tokio
- Mowlavi N., Kreykenbohm I., Shaw S.E., et al., 2005, Astron. Astrophys. submitted
- Negueruela I., Roche P., Fabregat J., Coe M.J., 1999, Mon. Not. R. Astron. Soc. 307, 695
- Pottschmidt K., Kreykenbohm I., Wilms J., et al., 2005, Astrophys. J. in press
- Remillard R., 2004, ATel 371, 1
- Stella L., White N.E., Davelaar J., et al., 1985, Astrophys. J. 288, L45
- Tanaka Y., 1983, IAU Circ. 3891, 2
- Terrell J., Priedhorsky W.C., 1984, Astrophys. J. 285, L15

THE XMM-NEWTON VIEW OF GRS 1915+105 DURING A PLATEAU

A. Martocchia^{* 1}, G. Matt², T. Belloni³, M. Feroci⁴, V. Karas⁵, and G. Ponti⁶

¹CNRS / Observatoire Astronomique de Strasbourg, 11 Rue de l'Université, F-67000 Strasbourg, France

²Dipartimento di Fisica, Università degli Studi "Roma Tre", Via della Vasca Navale 84, I-00146 Roma, Italy

³INAF / Osservatorio Astronomico di Brera, via E. Bianchi 46, I-23807 Merate, Italy

⁴INAF / IASF, Area di Ricerca di Tor Vergata, Via Fosso del Cavaliere 100, I-00133 Roma, Italy

⁵Astronomical Institute, Academy of Sciences, Boční II, CZ-140 31 Prague, Czech Republic

⁶Institute of Astronomy, Madingley Road, Cambridge CB3 0HA, United Kingdom

⁶Dipartimento di Astronomia, Università di Bologna, via Ranzani 1, I-40127 Bologna, Italy

ABSTRACT

Two XMM-Newton observations of the black-hole binary GRS1915+105 were triggered in 2004 (April 17 and 21), during a long "plateau" state of the source. We analyzed the data collected with EPIC-pn in Timing and Burst modes, respectively. No thermal disc emission is required by the data; the spectrum is well fitted by four components: a primary component (either a simple power law or thermal Comptonization models) absorbed by cold matter with abundances different than those of standard ISM; reprocessing from an ionized disc; emission and absorption lines; and a soft X-ray excess around 1 keV. The latter is not confirmed by RGS (which were used in the second observation only); if real, the excess could be due to reflection from optically thin photoionized plasma, in which case it may provide a way to disentangle intrinsic from interstellar absorption.

Key words: Black hole physics – Accretion, accretion disks – X-rays: binaries – X-rays: individuals: GRS 1915+105 .

GRS 1915+105 is a well-known black-hole (BH) binary, also classified as a *superluminal microquasar*, with very peculiar variability properties (for a recent review on this source see Fender & Belloni, 2004). Due to very large obscuration, the spectral type of GRS 1915+105's companion (a K-M III star) was discovered lately, via infrared observations, which also helped to finally determine the mass of the central compact object, which has been constrained to $M_c = 14 \pm 4 M_\odot$ (Greiner et al., 2001).

A XMM-Newton ToO observation of GRS 1915+105 was proposed in AO2. The observation was intended to be

^{*}Present address: UPS / Centre d'Etude Spatiale des Rayonnements, 9 Av. du Colonel Roche, F-31028 Toulouse, France

triggered by the occurrence of a "plateau" state of the source similar to that observed during the *BeppoSAX* 1998 observation, when relativistic Fe lines were observed (Martocchia et al. 2002, 2004); this was necessary also in order to have the source in a less dramatic variability state, and at a lower flux level to minimize technical problems due to instrumental pile-up and telemetry. The observation was triggered in April 2004, divided into two parts: OBS1 (April 17) and OBS2 (April 21; see Martocchia et al. 2005 for details).

We succeeded at both a) observing the source in a well-defined, stable physical/spectral state and b) collecting EPIC-pn useful data, only marginally corrupted by telemetry problems. In both observations the source has been caught in the conventional "C" spectral state / χ variability mode as defined by Belloni et al. (2000; see also Fender & Belloni, 2004). It shows a QPO at ~ 0.6 Hz – i.e. what is expected in "plateau" intervals when the frequency vs. spectral hardness correlation is taken into account – with a possible harmonic signal at 1.2 Hz.

We adopted a power law continuum model, which mimics emission by a hot corona or Comptonized thermal emission e.g. from the jet basis; however, an optically thick reflector is required to account for the smeared edge at ~ 7 keV. The latter component yields evidence of an accretion disk being present, or just optically thick, only at quite large distance from the central compact object, at least in the first observation ($r_i/r_g > 300$ in OBS1, ~ 20 in OBS2). That the disk is truncated, i.e. not present in the innermost part, is suggested also by the non-detection of thermal disk emission.

Several line residuals are superimposed on the modeled continuum (see Fig. 1). Part of these may be due to calibration uncertainties, especially at the energies where changes in the EPIC effective area take place (e.g. 1–3 keV). However, we found clear evidence of ionized iron emission around ~ 7 keV: data are well fitted with two

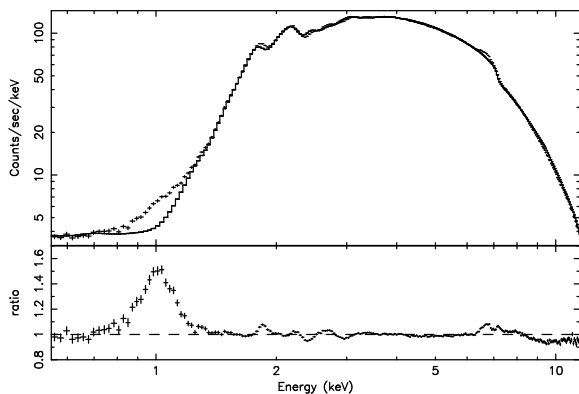


Figure 1. The OBS1 spectrum and data/model ratio, after fitting to a simple power law plus cold absorption model, clearly show the most significant residuals. From: Martocchia et al. (2005).

ionized Fe $K\alpha$ lines, possibly affected by mild relativistic broadening (being produced far away from the BH event horizon), plus a narrow absorption feature at ~ 6.95 keV.

Finally, we register the puzzling presence of an intense, broad excess around 1 keV in EPIC-pn data; the RGS spectrum does not confirm this, showing instead a fast decline, and no apparent features. Several alternative hypotheses, which can be invoked to explain the RGS–pn discrepancy, are discussed in Martocchia et al. (2005). Assuming (as a still unsubstantiated working hypothesis) that the 1 keV excess is real, it could be satisfactorily explained in terms of reflection by an optically thin wind. The excess is indeed well fitted with a power law plus a line, unobscured by material intrinsic to the system. The centroid energy of the gaussian line (~ 0.97 keV), its width (90 eV), and its EW against the reflected continuum (5.6 keV), point to a blend of Ne K and Fe L lines. The value of the equivalent H column density (as given by the OBS1 best fit, and frozen while fitting OBS2 data) results to be interestingly similar to the value of the obscuration by low Z elements (H, He, C, N, O) at the source core – $N_{\text{H}} \sim 1.6 \times 10^{22} \text{ cm}^{-2}$: in the disk wind hypothesis, this may therefore be taken as an upper limit to the *interstellar* matter column density. This value matches well with the expected galactic absorption in that direction (Dickey & Lockman 1990).

On the other hand, a significant fraction of the absorber must be *local* to the source. We adopted a variable absorption model (VARABS in XSPEC), assuming neutral matter and grouping the elements on the base of both physical and practical considerations: elements which have probably a common origin, but also elements which are not very abundant (and therefore cannot be easily measured independently one from the other) with very abundant ones (e.g. Co and Ni with Fe). A significant overabundance of the heavier elements with respect to the lighter ones is apparent, which suggests that a significant fraction of the absorber, traced by heavier species, is local to the source. Clearly, the intrinsic absorption may be subject to substantial changes on longer timescales, as

already observed with *Rossi-XTE* in correspondence of similar “plateaux” (Belloni et al. 2000).

Line features are less apparent in OBS2 than in OBS1; a 6.4 keV iron emission line is instead marginally found, with an EW of 6 ± 4 eV. The results of OBS2 are consistent with a picture in which the disk is more extended downwards, and more ionized. However, the estimates of the disk radii must be taken with caution, since they are now determined only via the reflection component. Moreover, the OBS2 spectrum at the higher energies can be at least partly affected by Burst-mode calibration problems.

A priori, some of the features in both spectra may be affected by dust halo scattering, too. We cannot check this hypothesis with our data, given the lack of imaging capabilities of timing modes; however, while spectral modelling of such effects is not easy, they would not help explaining the 1 keV excess. In order to try disentangle the different spectral components we used the *rms* vs. *E* method by Ponti et al. (2004). The resulting *rms* is lower than 0.1 all over the energy band, i.e. all spectral components are compatible with being constant, on timescales bigger than ~ 100 s, during the observation.

REFERENCES

- [1] Belloni, T., Klein-Wolt, M., Mendez, M., van der Klis, M., & van Paradijs, J. 2000, A&A 355, 271
- [2] Dickey, J.M., & Lockman, F.J. 1990, ARA&A 28, 215
- [3] Fender, R., & Belloni, T. 2004, ARA&A 42, 317
- [4] Greiner, J., Cuby, J.G., & McCaughrean, M.J., 2001, Nature 414, 522
- [5] Martocchia, A., Matt, G., Karas, V., Belloni, T., Feroci, M. 2002, A&A 387, 215
- [6] Martocchia, A., Matt, G., Karas, V., Belloni, T., Feroci, M. 2004, in: Proc. II *BeppoSAX* Symposium, *The restless high-energy universe*, Amsterdam (The Netherlands), 5-8/5/2003. Eds. E.P.J. Van den Heuvel, J.J.M. In’t Zand and R.A.M.J. Wijers, Elsevier, Nucl. Physics B (Proc. Suppl.) 132, 404
- [7] Martocchia, A., Matt, G., Belloni, T., Feroci, M., Karas, V., Ponti, G. 2005, A&A – in press: astro-ph/0510651
- [8] Ponti, G., Cappi, M., Dadina, M., Malaguti, G. 2004, A&A 417, 451

AN OBSERVATION OF THE QUIESCENT CLASSICAL NOVA CP PUP

M. Orio¹, K. Mukai², E. Sion³, M. Still⁴, and S. Zharikov⁵

¹INAF- Turin Observatory, Strada Osservatorio 20, I-10025 Pino Torinese (TO) , Italy, and Dept. of Astronomy, University of Wisconsin, 475 N. Charter Str., Madison, WI 53706, USA

²Goddard Space Flight Center, Code 662, LHEA, Greenbelt, MD 20771, USA

³Dept. of Astronomy & Astrophysics, Villanova, PA 19085, USA

⁴South African large telescope, PO Box 9, Observatory 7935, South Africa

⁵Observatorio Astronomico Nacional, Instituto de Astronomia, UNAM,, PO Box 439027, San Diego, CA 92143-9027, USA

ABSTRACT

We present preliminary results of a very recent observation of the quiescent nova CP Pup at quiescence. The X-ray spectrum is best fit with a cooling flow model and shows lines of high ionization stages. The light curve is modulated with the orbital period.

Key words: binaries: close–novae, cataclysmic variables – X-rays: stars.

1. INTRODUCTION

Cataclysmic Variables (CV) in general, and classical novae in particular, are relatively faint but interesting X-ray sources at quiescence, because the X-rays originate from the accretion region. Important details still have to be investigated to understand how accretion occurs in the secular evolution of these systems. *XMM Newton*, thanks to its large effective area, is the ideal instrument to study accreting systems. Non magnetic cataclysmic variables, like all dwarf novae and probably most classical novae, have quiescent X-ray luminosities in the range $10^{30} - 10^{32}$ erg s⁻¹. Only very few quiescent classical novae reach 10^{33} erg s⁻¹ (see Orio et al. 2001a). Mukai et al. (2003) showed that *Chandra* grating spectra of non-magnetic CV, including V603 Aql, can be modelled as cooling flows. The parameters that fit the spectrum are the mass accretion rate \dot{m} , the width of the emission lines (assuming a constant velocity broadening for all lines) and the maximum plasma temperature. If a line spectrum is detected, we can derive a reliable range for the most crucial parameter in CV secular evolution, the mass accretion rate \dot{m} . Only one classical nova and few dwarf novae are accessible for high S/N spectra obtained with X-ray gratings (see also Orio et al. 2001). A handful of other objects are in the luminosity range in which a few

lines can be detected with the RGS, and the continuum level and the iron line complexes close to 7 keV are detected with EPIC-pn (e.g. Ramsay et al. 2001). Unlike other CV, most classical novae are more than 1 kpc away from us, so they are always faint X-ray sources at quiescence, and seldom observed. CP Pup is the third brightest classical nova in X-rays at quiescence.

CP Pup had an outburst in 1942, and it was very fast and luminous. It is thought to be a non-magnetic, disk accretor system with a inclination of $30 \pm 5^\circ$ (Szkody & Feinswog 1988). CP Pup is quite closer than most classical novae, at ≈ 700 pc. The only quiescent nova which is bright enough for a high S/N X-ray grating spectrum is V603 Aql (Mukai & Orio 2005). CP Pup was observed with ROSAT (Balman et al. 1995). In that observation, its X-ray spectrum appeared harder than other accreting novae, with a possible modulation of the flux of the orbital period, which for CP Pup is unusually short, only 88.4 minutes.

2. THE XMM-NEWTON OBSERVATION: THE SPECTRUM

CP Pup was observed for 14 consecutive hours with XMM-Newton in June of 2005. The results illustrate how even observations of low luminosity cataclysmic variables with XMM-Newton yield very useful results of good quality (the X-ray luminosity of CP Pup is only about 10^{33} erg s⁻¹). Very little is known about accretion in novae, so these data are very new and very valuable. The EPIC-pn spectrum (Fig. 1) is best fit with cooling flow model, typical for disk accreting CV (see Mukai et al. 2003), as opposed to a photoionization model, which is appropriate for several magnetic CV. The iron K- α complex is observed in the pn spectrum (see Fig. 2). The He-like line is the most prominent, and the fluorescence line is higher than the H-like complex. This complex ap-

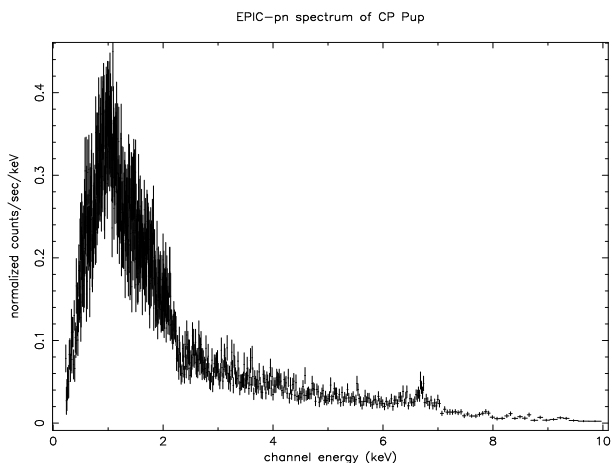


Figure 1. The EPIC-pn spectrum, fit with a cooling flow model with $N(H)=1.5 \times 10^{21} \text{ cm}^{-2}$, and a maximum temperature of 80 keV.

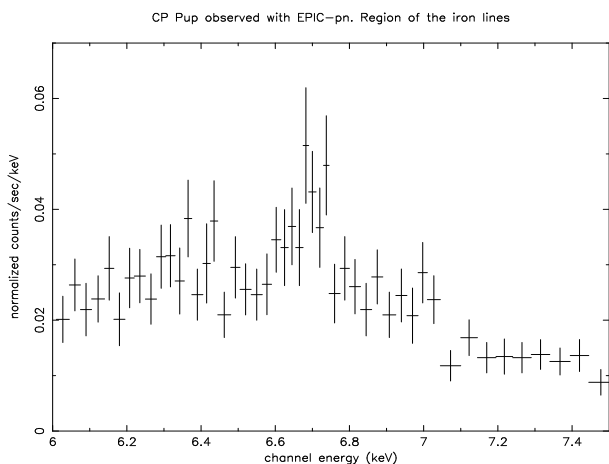


Figure 2. Close up of the iron lines region.

pears to have a strong satellite component, an indication of temperature below 3 million K.

There is evidence of emission lines in the low S/N RGS grating spectra: H-like emission lines of Ne, Si and O are prominent enough to be detected, and they are all lines that were observed in the grating spectrum of V603 Aql (see Fig.3). Overall we notice a striking similarity with V603 Aql, the brightest old nova at quiescence, (see Mukai and Orio 2005). Especially prominent neon lines are detected like in V603 Aql, suggesting high neon abundance also in CP Pup.

3. THE X-RAY LIGHT CURVE

The X-ray light curve is a puzzle: There is a clear modulation ($\approx 40\%$) of X-ray flux with the orbital period (see Fig. 4). This would be much more easily understood if the system were magnetic, yet there is additional evidence at other wavelengths that it is not. However, if

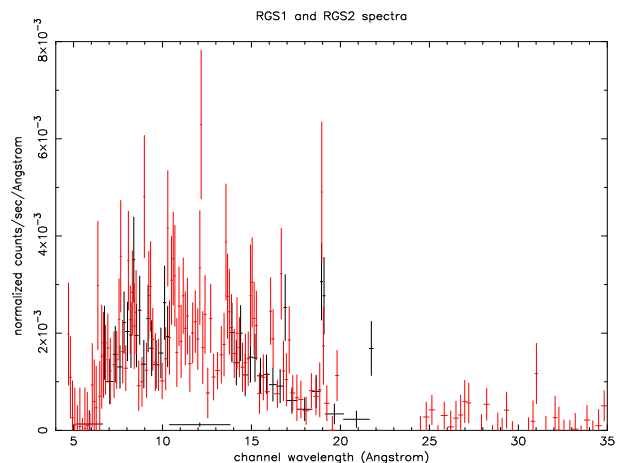


Figure 3. RGS1 (in black) and RGS2 (in red) spectra.

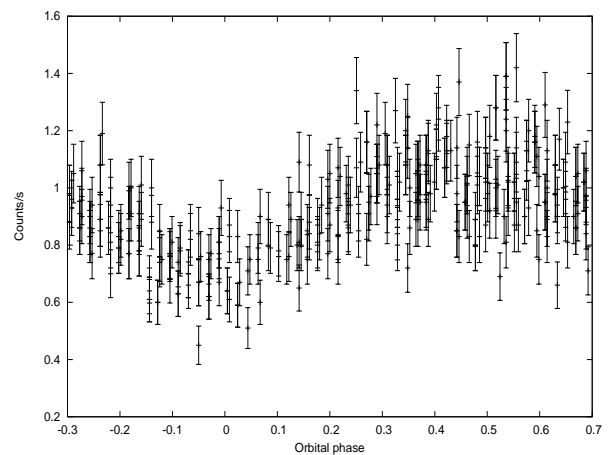


Figure 4. The EPIC-pn light curve of CP Pup, binned every 10 seconds and folded with the orbital period.

CP Pup is indeed a low inclination system, this modulation is not well understood in a standard boundary layer model. New optical observations with large telescopes may be very useful to clarify the issues concerning the inclination, which needs to be confirmed in order to try and build a physical model.

REFERENCES

- Balman, S., Orio, M. & Ögelman, H. 1995, 449, L47
- Mukai, K., Kinkhabwala, A., Peterson, J. R., Kahn, S. M., & Paerels, F. 2003, ApJ, 586, L77
- Mukai, K., & Orio M., 2005, ApJ, 622, 602
- Orio, M., Covington, J. & Ögelman, H. 2001, A&A, 373, 552
- Ramsay, G., et al., 2001, A&A, 365, L294
- Szkody, P., & Feinswog, L. 1988, ApJ, 334, 422

DISCOVERY OF X-RAY ECLIPSES FROM THE TRANSIENT SOURCE LOCATED AT ONLY 0.1PC FROM SGR A*

D. Porquet¹, N. Grosso², G. Bélanger³, A. Goldwurm³, F. Yusef-Zadeh⁴, R.S. Warwick⁵, and P. Predehl¹

¹Max-Planck-Institut für extraterrestrische Physik, Garching, Germany

²Laboratoire d'Astrophysique de Grenoble, Université Joseph-Fourier, BP53, 38041 Grenoble Cedex 9, France

³CEA Saclay, DSM/DAPNIA/SAP, 91191 Gif-sur-Yvette Cedex, France

⁴Department of Physics and Astronomy, Northwestern University, Evanston, IL 60208, USA

⁵Department of Physics and Astronomy, University of Leicester, Leicester LE1 7RH, UK

ABSTRACT

We present the discovery of X-ray eclipses with XMM-Newton from the transient source CXOGC J174540.0-290031 located at the Galactic Center at only 2.9'' (0.1 pc) South of the position of Sgr A*. In summer 2004, sharp and deep eclipses have been observed with a period of $27,961 \pm 5$ s and a duration of $1,100 \pm 100$ s, while no eclipses were present in Spring 2004. In the framework of semi-detached binary systems, we estimate the mass of secondary star to less than $1.0 M_{\odot}$ and the mass of the compact object to less than $60 M_{\odot}$.

Key words: X-rays; Galactic Center; Eclipses.

1. INTRODUCTION

The Galactic Center region is a very rich area of the sky that contains various astrophysical sources including many X-ray binaries. The current generation of X-ray satellites, Chandra and XMM-Newton, allow the discovery and the timing and spectral study of objects with X-ray luminosities between 10^{32} and 10^{35} erg/s.

2. CXOGC J174540.0-290031

During the large XMM-Newton multi-wavelength project to monitor Sgr A*, in Spring and Summer 2004 (4 XMM-Newton revolutions), a brightening in the 2-10 keV energy band of a factor 2 within a radius of $10''$ around Sgr A* was detected (Bélanger et al., 2005). This X-ray excess was coincident with CXOGC J174540.0-290031, a moderately bright transient, discovered by Chandra in July 2004 (Muno et al., 2005). Figure 1 displays the EPIC light curves of this object (within a radius of $10''$)

during each XMM-Newton revolution (Porquet et al., 2005). Five sharp and deep X-ray periodic features are clearly detected during the revolution 866 with a period of $27,961 \pm 5$ s, a duration of $1,100 \pm 100$ s, a depth of about 79%, and an eclipse fraction of about 3.9% compared to the orbital period (Fig.2). Similar values were found for the next observation (rev. 867), while there was no detection of X-ray eclipses with depth larger than 19% in Spring 2004 (rev. 788 and 789). However the 2–10 keV luminosity was almost constant with about $2 \times 10^{34} (d_{8\text{kpc}})^2$ erg/s over the four observations.

In the framework of eclipsing semidetached binary, we have constrained: the mass of the secondary star to be less than $1 M_{\odot}$ (i.e. this binary is a low-mass X-ray binary); and the mass of the compact object to be less than $60 M_{\odot}$ (Porquet et al., 2005).

We propose to explain the absence of the X-ray eclipse in Spring 2004 by the shift of the X-ray emitting region above the compact object (Porquet et al., 2005), possibly coincident with the base of the jet detected in radio at the same epoch (Bower et al., 2005).

REFERENCES

- Bélanger G., Goldwurm A., Melia F. et al. 2005, ApJ, in press [astro-ph/0508412]
- Bower G. C., Roberts D. A., Yusef-Zadeh F. et al. 2005, ApJ, in press [astro-ph/0507221]
- Muno M., Lu J. R., Baganoff F. K. et al. 2005, ApJ, in press [astro-ph/0503572]
- Porquet D., Grosso N., Bélanger G. et al. 2005, A&A, in press [astro-ph/0507283]

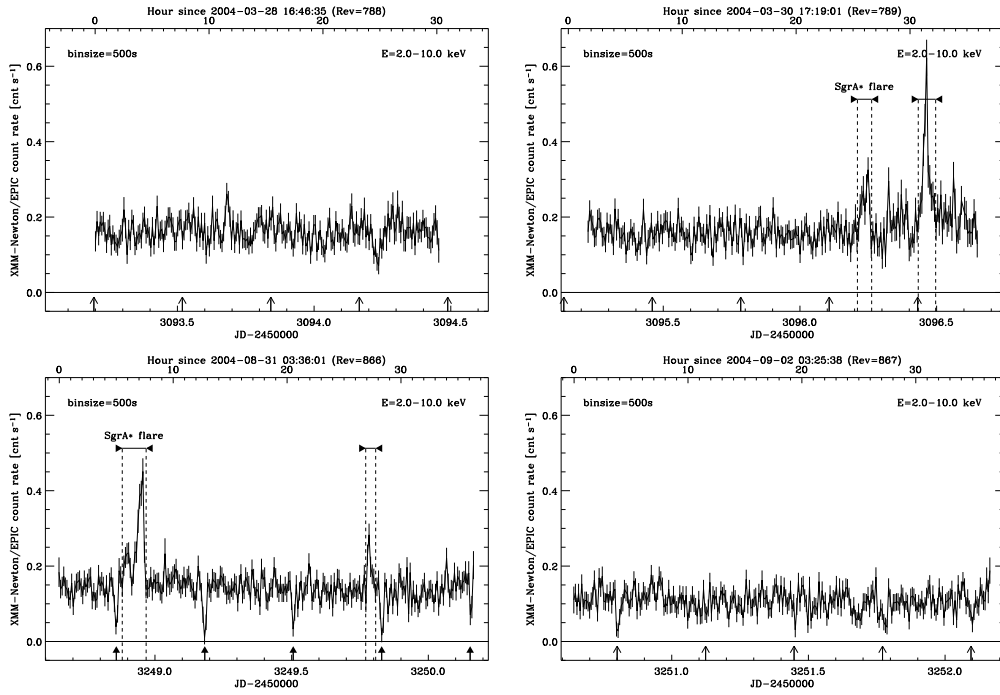


Figure 1. The 2-10keV EPIC light curve. The horizontal arrows indicate time intervals affected by X-ray flares from Sgr A*. The quiescent X-ray emission of Sgr A* and the diffuse X-ray emission have been removed. Vertical arrows point to the five X-ray eclipses observed during the revolution 866 which were used to determined the eclipse ephemeris. Vertical thin arrows mark the predicted X-ray eclipses for the other revolutions (788, 789, and 867). While several X-ray eclipses are observed at the position of the eclipse ephemeris during the revolution 867, no obvious deep eclipses are observed during the revolutions 788 and 789 (Spring 2004 observations).

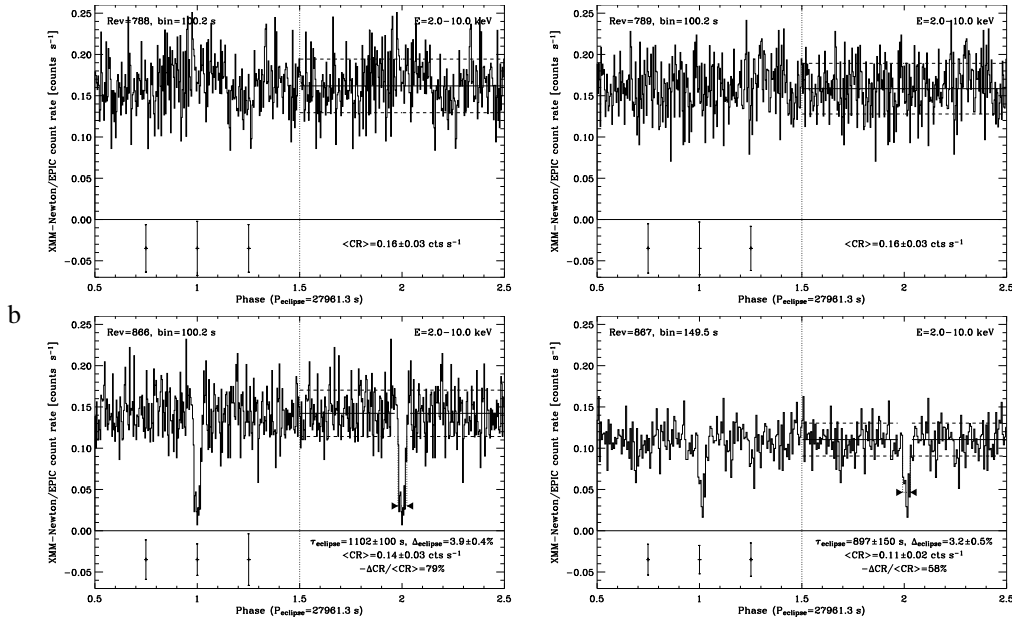


Figure 2. EPIC folded light curves for revolutions 788, 789, 866, and 867 in the 2-10 keV energy range. Two consecutive periods are plotted. The horizontal continuous and dashed lines in the second period indicate the average count rate level, $\langle CR \rangle$, and one sigma dispersion, respectively. The duration of the eclipse τ_{eclipse} is marked by arrows. The eclipse fraction Δ_{eclipse} is defined as the ratio of the eclipse duration to the orbital period. The depth of the eclipse is defined by the relative count rate variation at the observed eclipse maximum. For clarity, only three 1σ error bars are indicated.

GRS 1758–258 WITH *INTEGRAL* AND *RXTE*: ANOTHER DIM SOFT STATE

K. Pottschmidt¹, M. Chernyakova², A. A. Zdziarski³, P. Lubiński^{3,2}, D. M. Smith⁴, and N. Bezyiff⁴

¹CASS, University of California, San Diego, La Jolla, CA 92093-0424, USA

²*INTEGRAL* Science Data Centre, 1290 Versoix, Switzerland

³Nicolaus Copernicus Astronomical Center, 00-716 Warszawa, Poland

⁴Department of Physics, University of California, Santa Cruz, Santa Cruz, CA 95064, USA

ABSTRACT

The Galactic Center black hole candidate (BHC) GRS 1758–258 has been observed extensively within *INTEGRAL*'s Galactic Center Deep Exposure program in 2003 and 2004, while also being monitored with *RXTE*. We present quasi-simultaneous PCA, ISGRI, and SPI spectra from four GCDE observation epochs. During the first epoch GRS 1758–258 displayed another of its rare dim soft states like the one observed in 2001. In the recently emerging picture of the hardness-intensity evolution of black hole transient outbursts in which hard and soft states are observed to occur in a large overlapping range of luminosities (hysteresis), the dim soft state is not peculiar.

Key words: black hole physics; stars: individual: GRS 1758–258; gamma rays: observations; X-rays: binaries; X-rays: general.

1. INTRODUCTION

Most of the time GRS 1758–258 displays X-ray properties typical for the canonical hard state of black hole binaries, i.e., a power law spectrum with indices of $\Gamma=1.4$ – 1.9 and an exponential cutoff above 100 keV. A weak soft excess is also sometimes seen. However, a sudden drop of the power law component within a few days occurred in 2001 February, leading to a much softer and dimmer source state (Smith et al., 2001a, and Fig 1). As predicted by Smith et al. (2001b) based on the two-flow accretion model (Chakrabarti & Titarchuk, 1995), the soft spectral component decayed more slowly than the hard one, on a timescale of ~ 28 days. Here, we report results of monitoring observations of GRS 1758–258 with *INTEGRAL* and *RXTE* in 2003 and 2004. While the source was in its usual variable hard state during most of the time, the data obtained in spring 2003 clearly correspond to another dim soft state.

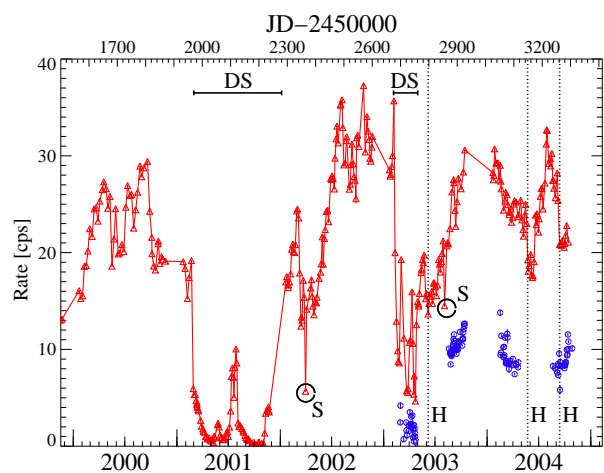


Figure 1. 2.5–25 keV *RXTE*/PCA (red triangles) and 20–60 keV *INTEGRAL*/ISGRI (blue circles) monitoring lightcurves of GRS 1758–258. The dim soft states (“DS”) as well as times of softening (“S”) and hardening (“H”) are indicated, see text for details.

2. LIGHTCURVES & SPECTRA IN 2003/2004

Version 4.2 of the Offline Scientific Analysis package was used to extract *INTEGRAL* spectra and lightcurves (Fig 1, blue circles) obtained during four Galactic Center viewing epochs (JEM-X did not yield any useful epoch-summed data; single-pointing ISGRI spectra were extracted from energy resolved images and then epoch-summed). HEASOFT v5.3.1 was used for the extraction of long term PCA lightcurves (Fig 1, red triangles) as well as spectra summed over those monitoring observations coinciding with the *INTEGRAL* epochs. Our basic phenomenological model for the simultaneous fits to the summed *INTEGRAL*/*RXTE* spectra of each epoch consists of an absorbed cutoff power law (no cutoff is required for epoch 1) plus a Gaussian Fe $K\alpha$ line and a multicolor disk blackbody component, if required. We

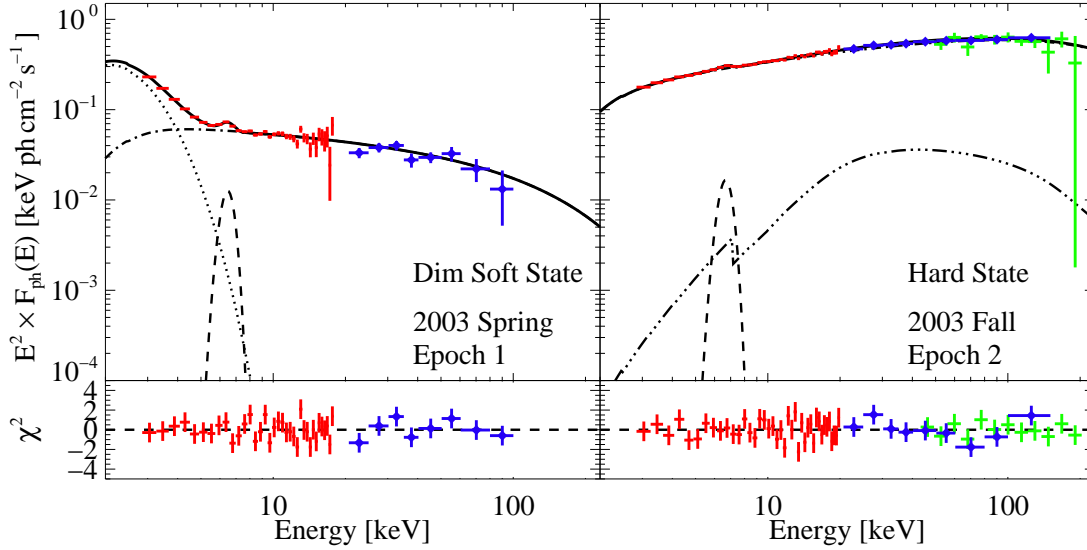


Figure 2. Unfolded spectra and residuals for the *compTT* fits to epochs 1 and 2 (red: PCA, blue: ISGRI, green: SPI).

Table 1. Best fit parameters for the *compTT* fits to the summed INTEGRAL/RXTE spectra of the four epochs.

	Epoch 1	Epoch 2	Epoch 3	Epoch 4
$N_{\text{H}}/10^{22}$ [cm $^{-2}$]	$1.50^{+0.21}_{-0.26}$	$1.37^{+0.20}_{-0.15}$	1.50	1.50
kT_{in} [eV]	482^{+14}_{-16}	379^{+116}_{-378}	441^{+86}_{-55}	501^{+71}_{-90}
$A_{\text{disk}}/10^3$	$2.5^{+0.4}_{-0.3}$	$-0.38^{+0.54}_{-0.04}$	$0.28^{+0.72}_{-0.07}$	
τ	$0.29^{+0.43}_{-0.13}$	$0.71^{+0.16}_{-0.07}$	$1.00^{+0.21}_{-0.21}$	$0.37^{+0.24}_{-0.12}$
kT_{e} [keV]	64^{+4}_{-15}	78^{+34}_{-15}	49^{+29}_{-9}	114^{+32}_{-35}
E_{Fe} [keV]	$6.41^{+0.13}_{-0.24}$	$6.62^{+0.21}_{-0.30}$	$6.74^{+0.15}_{-0.26}$	$6.47^{+0.32}_{-0.25}$
EW_{Fe} [eV]	208.0	61.0	42.6	64.3
c_{ISGRI}	$0.76^{+0.08}_{-0.08}$	$0.83^{+0.03}_{-0.02}$	$0.82^{+0.01}_{-0.02}$	$0.87^{+0.02}_{-0.02}$
c_{SPI}		$-0.96^{+0.05}_{-0.04}$	$0.97^{+0.10}_{-0.09}$	$0.97^{+0.12}_{-0.11}$
$10^2 \Omega/2\pi$		$-10.0^{+5.6}_{-5.6}$	$13.8^{+5.0}_{-5.5}$	–
χ^2/dof	37.2/34	52.5/63	57.3/51	49.8/52
χ^2_{red}	1.09	0.83	1.12	0.96

also applied a thermal Comptonization model (*compTT*; Titarchuk, 1994) to all four epochs, allowing for reflection. Both modeling approaches resulted in equally good descriptions of the data. Systematic errors of 0.5% and 2% were added to the PCA and ISGRI spectra, respectively. Fig. 2 shows the *compTT* fits for epochs 1 and 2. In epoch 1 the source was too soft for SPI.

3. THE DIM SOFT STATE IN CONTEXT

The 2003 dim soft state is 0–20% less luminous than the hard state, depending on the epoch and spectral model.

While this is different from the soft state in persistent HMXBs, like Cyg X-1, where softening is associated with higher bolometric luminosities, it is well within the range of hysteretic behavior displayed by LMXB transients, like GX 339–4, where a large range of soft state intensities is observed (Zdziarski et al., 2004). The dim soft state would thus correspond to the outburst decay of a transient. This can be understood since GRS 1758–258 most likely has a low mass companion and is accreting via Roche lobe overflow (Rothstein et al., 2002). In addition to the clear dim soft states (indicated by “DS” in Fig. 1), the PCA lightcurve shows short soft episodes as well as instances of sudden hardening (“S” and “H”, respectively, see also Pottschmidt et al., 2005). These are additional examples of quasi-independent changes of the hard and soft components, further supporting the interpretation in terms of two independent accretion flows.

REFERENCES

- Chakrabarti, S. & Titarchuk, L. G. 1995, *ApJ*, 455, 623
- Pottschmidt, K., Chernyakova, M., Zdziarski, A. A., et al. 2005, *A&A*, submitted (astro-ph/0509006)
- Rothstein, D. M., Eikenberry, S. S., Chatterjee, S., et al. 2002, *ApJ*, 580, L61
- Smith, D. M., Heindl, W. A., Markwardt, C. B., & Swank, J. H. 2001a, *ApJ*, 554, L41
- Smith, D. M., Heindl, W. A., Swank, J. H., & Markwardt, C. B. 2001b, *ATEL*, 66
- Titarchuk, L. 1994, *ApJ*, 434, 570
- Zdziarski, A. A., Gierliński, M., Mikołajewska, J., et al. 2004, *MNRAS*, 351, 791

XMM-NEWTON AND CHANDRA LETGS X-RAY SPECTROSCOPY OF SUPERSOFT X-RAY BINARIES

K. Reinsch¹, V. Burwitz², and R. Schwarz³

¹Georg-August-Universität Göttingen, Institut für Astrophysik, Friedrich-Hund-Platz 1, D-37077 Göttingen, Germany

²Max-Planck-Institut für extraterrestrische Physik, P.O. Box 1312, D-85741 Garching, Germany

³Astrophysikalisches Institut Potsdam, An der Sternwarte 16, D-14482 Potsdam, Germany

ABSTRACT

With current generation X-ray observatories, detailed diagnostics of the high-temperature environment of white dwarf binaries accreting close to the Eddington limit (supersoft X-ray binaries, SSXBs) and of the nuclear burning region on their photospheres have become possible. High-resolution X-ray spectroscopy of SSXBs with the Chandra LETGS and the XMM-Newton RGS has revealed complex absorption and emission line spectra which probably reflect a combination of high-gravity stellar atmospheres, dynamical processes in the atmosphere, patchy absorption structures, X-ray scattering, and coronal-like emission from the wind.

Key words: stars: novae, cataclysmic variables; X-rays: spectroscopy; X-rays: stars.

1. INTRODUCTION

Luminous supersoft stellar X-ray sources (SSXBs) have been established as a population of accreting binaries by the discovery of several systems during the ROSAT All-Sky Survey (Trümper et al., 1991) and follow-up multi-wavelength studies. They are observationally distinguished by their very soft X-ray spectra with blackbody temperatures from 10 to 80 eV and luminosities of $10^{36} - 10^{38}$ erg/s (Kahabka & van den Heuvel, 1997).

Several SSXBs have been identified as accreting close binaries with orbital periods of ~ 1 day or less. They are interpreted as white dwarfs which accrete matter from a more massive main-sequence secondary at a rate \dot{M}_{acc} just sufficient to permit (quasi-) stable nuclear burning near its surface (van den Heuvel et al., 1992). This implies that the luminosity must be close to the Eddington limit of a solar mass object. Stable burning stops below $\sim 10^{-7} M_{\odot}/\text{yr}$, giving place to shell flashes. The conventional model predicts that at $\dot{M}_{\text{acc}} > 4 \times 10^{-7} M_{\odot}/\text{yr}$, a red-giant envelope develops and X-ray emission is temporarily quenched. Hachisu et al. (1996), however, have

shown that no static envelope solution on the white dwarf exists for $\dot{M}_{\text{acc}} > 10^{-6} M_{\odot}/\text{yr}$. Instead, excess matter should be expelled by a strong wind providing a potential channel to grow the white dwarf mass to near the Chandrasekhar limit.

With high-resolution X-ray spectroscopy detailed diagnostics of the high-temperature environment of white dwarf binaries accreting close to the Eddington limit and of the nuclear burning region on their photospheres have become possible. Here, we summarize the first results of our recent X-ray observations of selected SSXBs.

2. ANALYSIS OF INDIVIDUAL SYSTEMS

2.1. QR And (RX J0019.8+2156)

The brightest galactic SSXB, QR And, has been observed at persistent X-ray luminosity since its discovery during the ROSAT All-Sky Survey. The XMM-Newton EPIC pn spectrum can be reasonably well fitted with a blackbody with $kT_{\text{bb}} = 20$ eV and $nH = 6.9 \cdot 10^{20} \text{ cm}^{-2}$ (reduced $\chi^2 = 3.8$ for 57 degrees of freedom) (Fig. 1). This temperature is quite low compared to other SSXBs. The lack of dips in the orbital soft X-ray light curve suggests that either the orbital inclination of QR And is lower than 75° previously anticipated, or the X-ray emission is not confined to the surface of the white dwarf, but comes from an extended structure, e. g. a corona or a wind.

2.2. RX J0439.8-6809

During a 40ks observation with the Chandra LETGS source photons of RX J0439.8-6809 have been detected in the narrow 40–70 Å wavelength interval, only (Fig. 2). A white-dwarf LTE atmosphere fit to the data yields an effective temperature of $T_{\text{eff}} = (3.15 \pm 0.10) 10^5$ K and a neutral hydrogen column density $n_{\text{H}} = (3.2 \pm 0.4) 10^{20} \text{ cm}^{-2}$. The latter is compatible with $n_{\text{H}} = (4.0 \pm$

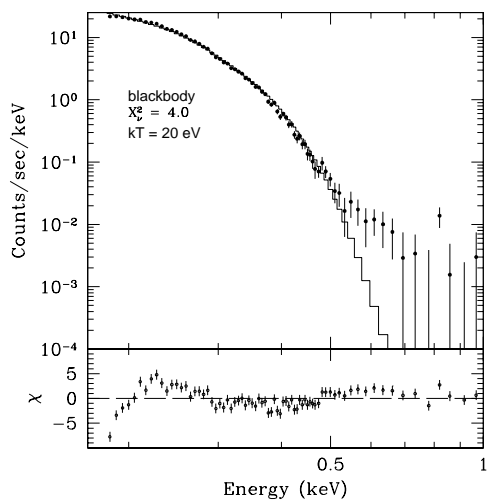


Figure 1. XMM-Newton EPIC pn spectrum of QR And.

1.0) 10^{20} cm^{-2} obtained with the HST Imaging Spectrograph (van Teeseling et al., 1999). The significant residuals indicate that the X-ray spectrum of RX J0439.8-6809 is far more complex than this simple model.

2.3. RX J0513.9-6951

High-resolution X-ray spectra of the transient SSXB RX J0513.9-6951 obtained during two target of opportunity campaigns with the Chandra LETGS show a very complex structure and deviate strongly from simple Planckian distributions (Fig. 2). Probably, the spectra are a combination of absorption features of a hot white dwarf atmosphere and of emission line features, most likely originating in a corona or wind above the accretion disk. A more detailed discussion of this data is presented in an accompanying paper (Burwitz et al., 2005).

3. CONCLUSIONS

With the advent of high-resolution X-ray spectroscopy using the Chandra LETGS and the XMM-Newton RGS a detailed study of the physical conditions in white dwarf binaries accreting close to the Eddington limit has become possible. Their soft X-ray spectra reflect the complex emission and absorption processes involved by the hot high-gravity stellar atmosphere, its structure and dynamics, and the interaction of the emitted photons with the expected strong wind emerging from the system. Currently, we are still at the beginning to fully explore the diagnostic information available from the wealth of absorption and emission features seen in the spectra. Their interpretation requires the extension of NLTE-modeling to soft X-ray wavelengths (see e.g. Lanz et al. (2005); Petz et al. (2005); Rauch et al. (2005)) as well as further exploration of the underlying atomic data.

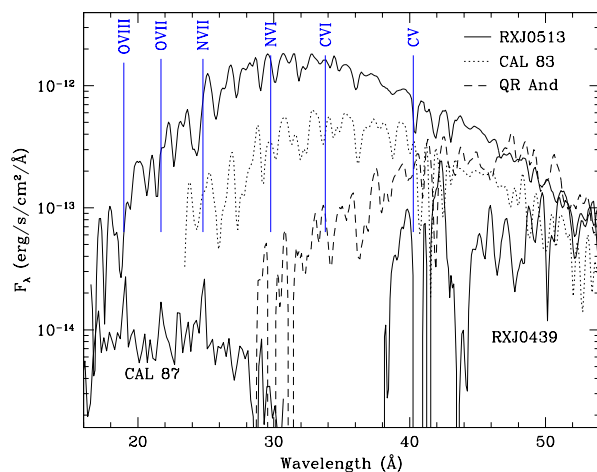


Figure 2. Chandra LETGS spectra of bright SSXBs. From top to bottom: RX J0513.9-6951 (Burwitz et al., 2005), CAL 83 (Paerels et al., 2001; Lanz et al., 2005), QR And, RX J0439.8-6809 (Reinsch et al., 2001), CAL 87 (shifted down by own decade, Greiner et al. (2004)).

ACKNOWLEDGMENTS

This work has been supported in part by the DLR/BMBF under project no. 50 OR 0206.

REFERENCES

- Burwitz V., Reinsch K., Greiner J., et al., this volume
- Greiner J., Iyudin A., Jimenez-Garate M., Burwitz V., Schwarz R., et al., 2004, Rev. Mex. AA, 20, 18
- Hachisu I., Kato M., Nomoto K., 1996, ApJ, 470, L97
- Kahabka P., van den Heuvel E.P.J., 1997, ARAA, 35, 69
- Lanz T., Telis G. A., Audard M., Paerels F., Rasmussen A. P., Hubeny I., 2005, ApJ, 619, 517
- Paerels F., Rasmussen A.P., Hartmann H.W., Heise J., Brinkman A.C., de Vries, C. P., den Herder, J. W., 2001, A&A, 365, L308
- Petz A., Hauschildt, P.H., Ness J.-U., Starrfield S., 2005, A&A, 431, 321
- Rauch T., Werner K., Orio M., 2005, AIP Conf. Proc. 774, 361
- Reinsch K., Beuermann K., Gänsicke B.T., van Teeseling A., 2001, ASP Conf. Ser., 234, 245
- Trümper J., Hasinger G., Aschenbach B., 1991, Nature, 349, 579
- van den Heuvel E.P.J., Bhattacharya B., Nomoto N., Rappaport S., 1992, A&A, 262, 97
- van Teeseling, A., Gänsicke, B.T., Beuermann, K., Dreizler, S., Rauch, T., & Reinsch, K., 1999, A&A, 351, L27

IRON LINE ANALYSIS OF THE X-RAY SYSTEM 4U 1538-52

José J. Rodes, José M. Torrejón, and J. Guillermo Bernabéu

University of Alicante, Campus Sant Vicent del Raspeig, 03080 Alicante, Spain

ABSTRACT

The X-ray binary pulsar 4U 1538-52 has been observed by the Rossi X-Ray Timing Explorer (RXTE) satellite. We have analysed the X-ray spectra of the high mass binary X-ray pulsar 4U 1538-52 over the energy range from 3 keV to 100 keV using all the available data from the RXTE archives. In this work, we investigate: a) the description of the continuum by physical models and b) the geometry of the emitting plasma from the iron line analysis.

Key words: X-rays: binaries.

1. INTRODUCTION

4U 1538-52 is a high mass X-ray binary system formed by a compact object (neutron star) and a high mass B0 I star ($\sim 17 M_{\odot}$). Uhuru was the first satellite X-ray observatory that detected this system (Giacconi et al. 1974). The neutron star has a spin period ~ 529 s (Davison 1977; Becker et al. 1977). The orbital period is ~ 3.73 days (Clark 2000) and, assuming a distance of 5.5 kpc, the X-ray luminosity is $\sim 4 \cdot 10^{36}$ erg \cdot s $^{-1}$ (Becker et al. 1977; Parkes et al. 1978). The continuum of this system has usually been described either by an absorbed power law modified by a high energy cutoff, a power law modified by a Fermi-Dirac cutoff or two power laws with indices of opposite sign multiplied by an exponential cutoff. However, the direct physical interpretation of the parameters of these continuum models is difficult and we used them to search for cyclotron resonant scattering features or other type of spectral lines. We have found that a blackbody component or an accretion disk consisting of multiple blackbody components plus a comptonization of soft photons in a hot plasma describe all the spectra properly (bb+compTT and diskbb+compTT, respectively). In this work we present the spectrum of 4U 1538-52 in the energy band 3-100 keV and discuss the parameter values from the previous models. These models require an iron emission line at ~ 6.4 keV and a cyclotron absorption feature at ~ 20 keV are added in the model. On the other

hand, we investigate the geometry of the system studying the iron line variation.

2. DATA

Spectra were obtained from the High Energy Astrophysics Science Archive Research Center (HEASARC), provided by NASA's Goddard Space Flight Center. RXTE observed this source in three different runs, carried out during 1996, 1997 and 2001. Two of them have spectra for a complete orbital period. We have selected the energy bands 3-20 keV from the Proportional Counter Array (PCA; Jahoda et al. 1996) and 17-100 keV from the High Energy X-ray Timing Experiment (HEXTE; Rothschild et al. 1998) to fit the models. In order to improve the statistical significance of the data, we added the data of both HEXTE clusters. We also binned several channels together of the HEXTE data at higher energies and chose the binning as a compromise between increased statistical significance while retaining a reasonable energy resolution.

3. DISCUSSION AND CONCLUSIONS

3.1. Phase resolved spectroscopy

We performed spectral analysis on the energy spectrum of 4U 1538-52 in the energy range 3-100 keV and obtained the phase resolved spectra using the orbital ephemeris from Makishima et al. (1987). Using previous models, we obtain a reduced chi-squared between 0.50 and 1.19 describing all the spectra very well.

First we have analyzed the parameters deduced from the blackbody plus thermal comptonization model. Assuming a distance of 5.5 kpc, we obtained the luminosity of the source giving values from $2.3 \cdot 10^{36}$ to $7.3 \cdot 10^{36}$ erg/s (RXTE 1997 observation of an orbital cycle) and from $2.9 \cdot 10^{36}$ to $6.7 \cdot 10^{36}$ erg/s (RXTE 2001 observation of an orbital cycle). Under this description, the temperature of the injected soft photons (kT_0) is very high, 0.27-1.50

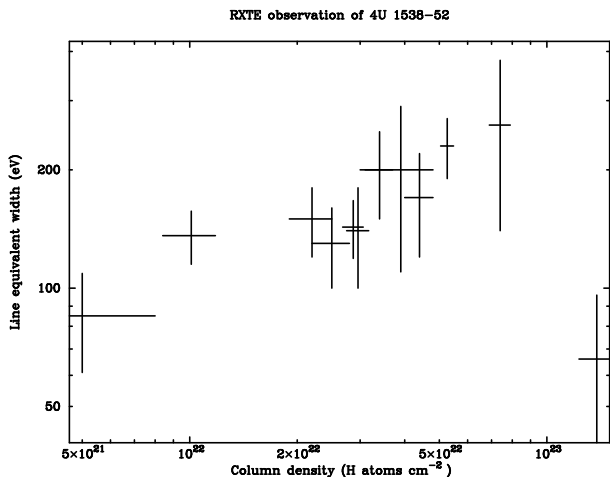


Figure 1. Iron line equivalent width versus column density of hydrogen. The values derived from the spectral fits to the RXTE 2001 spectra is plotted.

keV in 1997 data and 0.96-1.20 keV in 2001 data, while the temperature of the plasma (kTe) is very low, 3.2-8.0 keV and 2.1-5.3 keV, respectively. We compute the radius of the Wien soft photon source by equating the bolometric luminosity of the soft photon source with that of a black body of area $\pi \cdot R_w^2$ (Torrejón et al 2004). For RXTE 1997 data, the radius varies from 0.5 to 10 km in the extreme case indicating an emission from the entire surface or boundary layer instead of a hot spot. While for RXTE 2001 the radius is compatible (~ 0.5 km) for a polar cap in a neutron star. Although this model describe continuum spectra properly, the parameters are not expected.

On the other hand, the second model gives radius of the Wien soft photon without physical sense (ranging from 0.01 km to 910 km). Although the spectra of this source can be well described by thin comptonization model, the previous values of R_w are unacceptable. Therefore, we conclude that there is no evidence of a disk in this system.

3.2. The fluorescence iron line

We plot the iron line equivalent width versus column density of hydrogen. As we can see in figure 1, there is a good degree correlation of EW on N_H (uncertainties are at 90% confidence level for a single parameter). This is what can be expected if emission comes from a neutral absorbing gas with cosmic abundances which is distributed spherically around the X-ray source. We note that emission line during eclipse was also observed around 6.4 keV, thus indicating the fluorescent emission reprocessed by an extended region of cool matter.

We also show the variation in equivalent width of the iron emission line with the source flux in 3-20 keV energy range (see figure 2). Our results suggest that the EW is high at low luminosity and low at high luminosity. Inoue (1985) and Makishima (1986) estimated the equiv-

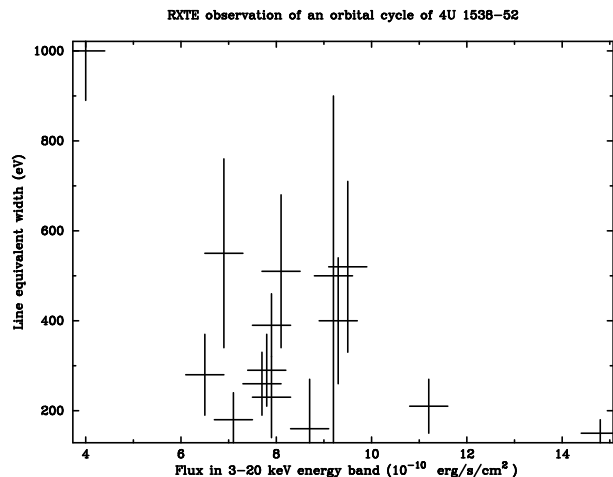


Figure 2. The variation in equivalent width (EW) of the iron emission line with the source flux in 3-20 keV is shown. The EW is high when the source flux is low and it is low when the source flux is high.

alent widths of the fluorescence iron line emission from neutral matter in a sphere surrounding the X-ray source using a power law type incident spectrum. In accretion powered X-ray pulsars, the iron line equivalent width can be higher if the compact object is hidden from direct view and only X-rays scattered into the line of sight by an accretion disk corona or wind are visible. This may explain the higher value of iron equivalent width during low luminosity of 4U 1538-52 and is consistent with the X-ray coming from a spherical plasma surrounding the neutron star rather than from an accretion disk.

REFERENCES

- Coburn, W. 2001, Ph. D. thesis, University of California, San Diego.
- Haberl, F. & White, N.H. 1989, ApJ, 343, 409.
- Kreykenbohm I., Coburn W., Wilms J., et al. 2002, A&A, 395, 129.
- Inoue H. 1985, Space Sci. Rev., 40,317.
- Makishima K. 1986, in *The Physics of Accretion onto Compact Objects*, eds. K. O. Mason, M. G. Watson & N. E. White, p. 249.
- Makishima K., Koyama K., Hayakawa S. & Nagase F. 1987, ApJ, 314, 619.
- Naik S. & Paul, B. 2002, JApA, 23, 27.
- Rodes J.J., Torrejón J.M. & Bernabéu G. 2004, in *Joint European and National Astronomical Meeting*, Granada.
- Torrejón J.M., Kreykenbohm I., Orr A., Titarchuk & Noguera I. 2004, A&A, 423, 301.

FAINT X-RAY SOURCES IN THE GALACTIC CENTRE

A. J. Ruiter¹, K. Belczynski^{1,2}, and T. E. Harrison¹

¹New Mexico State University, Department of Astronomy, 1320 Frenger Mall, Las Cruces, NM 88003

²Tombaugh Fellow

ABSTRACT

We study the population of X-ray binaries in the Galactic Centre (GC). The observed population (Muno et al. 2003) consists of ~ 2000 faint sources. Wind-fed NS binaries (Pfahl et al. 2002) and quiescent RLOF NS/BH transients (Belczynski & Taam 2004) have been studied via population synthesis methods as possible candidates for this XRB population, though these systems are not numerous enough in order to account for the observations. Muno et al. (2004) proposed that intermediate polars may be able to explain the GC population of faint X-ray point sources. We extend the population synthesis studies previously undertaken for NS and BH XRBs to include the population of intermediate polars, and calculate the GC XRB population. Our calculations produce about 2000 intermediate polars with X-ray luminosities between $10^{31} - 10^{33}$ erg/s. It is found that the faint, hard X-ray point sources in the GC can be explained by intermediate polars.

Key words: Galactic Centre; X-ray binaries; white dwarfs.

1. INTRODUCTION

An X-ray survey of the Galactic Centre (GC) with the ACIS-I on Chandra (Wang et al. 2002) first revealed the presence of ~ 1000 spectrally hard X-ray sources (2–8 keV). A deeper Chandra survey (see Muno et al. 2003) revealed 2357 X-ray point sources, ~ 1800 of which are detected within the hard Chandra band. It has been hypothesized that wind-fed neutron star accretors with high- and intermediate-mass companions (Pfahl et al. 2002) or RLOF NS/BH binaries (Belczynski & Taam 2004) may be responsible for the GC population. However, population synthesis studies have shown that these systems are not abundant enough to be responsible for the entire observed GC population. Muno et al. (2004) suggested that the observed faint sources are likely accreting white dwarf (WD) binaries. Intermediate Polars (IPs), which involve a magnetic accreting white dwarf, and usually a

main sequence (MS) or evolved companion, are the most luminous subclass of Cataclysmic Variables in the X-ray band. In our study we model the number of IPs and their X-ray luminosities in the GC. All different types of IPs are considered: WD-WD, WD-MS and WD-evolved companions, but we select only systems which are bright enough to make the Muno (2 – 8 keV) X-ray luminosity threshold of 10^{31} erg/s.

2. MODEL DESCRIPTION

Our study has been carried out using the population synthesis code *StarTrack* (Belczynski et al. 2002; Belczynski et al. 2005, in prep). Stars are evolved with the metallicity and wind-mass-loss dependent stellar models as described in Belczynski et al. (2002) which incorporate physical processes important for binary evolution, such as magnetic braking, tidal interactions, detailed mass transfer calculations and gravitational radiation. All single and binary stars are evolved from the ZAMS and pass through the following phase sequence: Main Sequence, Hertzsprung Gap, Red Giant Branch, core He Burning, Asymptotic Giant Branch. Also, evolution of Helium stars is followed in detail. We assume that the IP X-ray luminosity is a function of the accretion rate, accreting WD physical properties, and the efficiency with which the accretion luminosity is converted to hard X-ray luminosity in the Chandra band. We also take into account non-symmetric X-ray emission from IPs. For further details on the IP X-ray luminosity model, see Ruiter et al. 2005 (in prep). We then assign a fraction of CV systems (any RLOF system with a WD accretor) that are intermediate polars (subclass of magnetic WD accretors); our standard model uses an IP fraction of 5% (Kube et al. 2003). The stellar population of the GC is evolved through 10 Gyr and all IP systems are extracted and their luminosities and numbers are compared to those of the Muno survey.

Table 1. Galactic Centre numbers of synthetic intermediate polar systems. Observed number of sources in GC is ~ 2000 (Muno et al. 2003)

IP type in GC	IP frac. 1%	IP frac. 5%	IP frac. 20%
WD-MS	361	1804	7220
WD-Evolved	3	14	58
WD-WD	28	140	563
Total	392	1958	7841

3. RESULTS/CONCLUSIONS

We find that the number of synthetic IP systems predicted by our model for the Galactic Centre depends strongly on the IP fraction. The number of systems with X-ray luminosities within the Muno survey ($> 10^{31}$ erg/s) is found within the range 400 – 8000 (see Table 1). However, for our standard model IP fraction of 5% we find ~ 2000 IPs. In Table 1 we also show the types of different IPs formed in our simulations. The most frequent type is a magnetic WD accreting from a low mass MS star ($< 1M_{\odot}$). Such systems are too faint to be detected in the ongoing infrared search for counterparts of GC faint X-ray sources (Bandyopadhyay et al. 2005). In Figure 1 we show the luminosity distribution of synthetic IPs (left panel), and a corresponding X-ray luminosity function for the population (right panel). It is noted that only 40% of IPs are bright enough to make the Muno survey X-ray luminosity threshold: we show these systems with the solid line. For comparison we also show the entire synthetic IP population with a dotted line. It is noted that the power-law slope of the X-ray luminosity function for IPs corresponding to the Muno survey is ~ 0.9 . We have studied the physical properties of the IP population, most of which are magnetic WDs accreting from low-mass MS stars. Based on the full population synthesis calculation for the GC we conclude that the faint X-ray sources found in the Muno et al. survey may be explained by the model population of IPs.

ACKNOWLEDGMENTS

AJR and KB would like to acknowledge the support of KBN Grant 1 P03D 022 28.

REFERENCES

[1] Bandyopadhyay, R. M., Miller-Jones, J. C. A., Blundell, K. M., Bauer, F. E., Podsiadlowski, Ph., Gosling, A. J., Wang, Q. D., Pfahl, E., & Rappaport, S., astro-ph 0509346

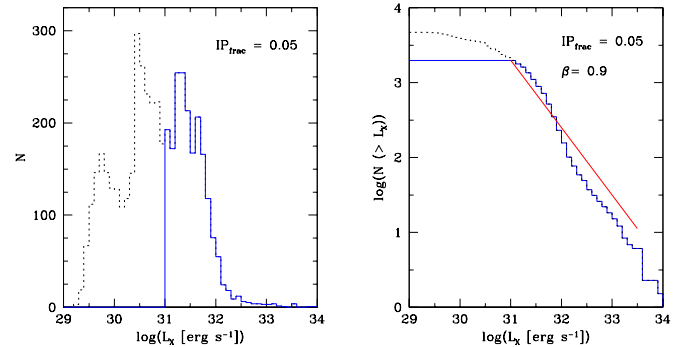


Figure 1. Left: luminosity distribution of synthetic IP systems in the Galactic Centre for the model with an IP fraction of 0.05. Right: corresponding X-ray luminosity function (XLF). The entire IP population is shown with a dotted line, while a subset of these, the IPs corresponding to the Muno et al. survey, are shown with an overlaid solid line (for this we also show the power law slope of the XLF with a solid line).

- [2] Belczynski, K., Kalogera, V., & Bulik, T., 2002b, ApJ, 572, 407
- [3] Belczynski, K., & Taam, R., 2003 ApJ, 616, 1159
- [4] Kube, J., Gansicke, B. T., Euchner, F., & Hoffmann, B., 2003, A&A, 404, 1159
- [5] Pfahl, E., Rappaport, S., & Podsiadlowski, P., 2002, ApJ, 571, L37
- [6] Muno, M. P., Baganoff, F. K., Bautz, M. W., Brandt, W. N., Broos, P. S., Feigelson, E. D., Garmire, G. P., Morris, M. R., Ricker, G. R., & Townsley, L. K., 2003, ApJ, 589, 225
- [7] Muno, M. P., Arabadjis, J. S., Baganoff, F. K., Bautz, M. W., Brandt, W. N., Broos, P. S., Feigelson, E. D., Garmire, G. P., Morris, M. R., & Ricker, G. R., 2004, ApJ, 613, 1179
- [8] Norton, A. J., & Watson, M. G., 1989, MNRAS, 237, 715
- [9] Wang, Q. D., Gotthelp, E. V., & Lang, C. C., 2002, Nature, 415, 148

XMM-NEWTON OBSERVATIONS OF THE MICROQUASARS GRO J1655-40 AND GRS 1915+105

G. Sala¹, J. Greiner¹, F. Haberl¹, E. Kendziorra², K. Dennerl¹, M. Freyberg¹, and G. Hasinger¹

¹Max-Planck-Institut für extraterrestrische Physik, Postfach 1312, D-85741 Garching, Germany

²Institut für Astronomie und Astrophysik Tübingen, Sand 1, D-72076 Tübingen, Germany

ABSTRACT

We present results of a sequence of XMM-Newton observations of the two microquasars GRO J1655-40 and GRS 1915+105. The observations were performed using the EPIC pn camera in the Burst mode. The observations of GRO J1655-40 in a bright state have made possible a substantial improvement in the calibration of the Burst mode, with determination of the rate dependence of the Charge Transfer Efficiency (CTE). We detect He-like Fe K-shell absorption features in the EPIC-pn spectrum of GRO J1655-40, indicating the presence of a highly ionized absorber, and clear absorption features at 0.71 and 0.72 keV in the RGS spectrum, most probably identified as blueshifted Fe XVIII.

Key words: binaries: close - stars: individual (GRO J1655-40, GRS 1915+105)- X-rays: stars.

1. INTRODUCTION

Microquasars are accreting binary systems in our Galaxy ejecting jets at relativistic velocities. The microquasars GRO J1655-40 and GRS 1915+105 were the two first superluminal sources discovered in our Galaxy. The dynamical mass of the central object, determined to be $7 M_{\odot}$ for GRO J1655-40 (Orosz & Bailyn, 1997) and $14 M_{\odot}$ for GRS 1915+105 (Greiner et al., 2001), indicates that it is a black hole in both cases. GRO J1655-40 and GRS 1915+105 also share the peculiarity of being thought to contain a maximally spinning black hole (Zhang et al., 1997). ASCA observations of GRO J1655-40 in August 1994 and August 1995 provided the first detection of absorption lines in an accretion powered source (Ueda et al., 1998). The energy of the lines was found to depend on the X-ray intensity, being 6.95 keV (Fe XXVI $K\alpha$) at 2.2 Crab, and 6.63 and 7.66 keV (Fe XXV $K\alpha$ and $K\beta$) at 0.27-0.57 Crab, revealing the presence of a highly ionized absorber. Similar absorption features were also detected for GRS 1915+105 (Kotani et al., 2000).

After 7 years of quiescence, GRO J1655-40 started a period of activity in February 2005, with RXTE/ASM showing a first outburst between March 10 and April 1,

reaching ~ 2 Crab, followed by a month and a half of increasing X-ray flux and a strong outburst on May 20, when the source reached more than 4 Crab. Here we present the results of four XMM-Newton observations of GRO J1655-40 performed on 27 February (40 ks, TOO), and on 14, 15 and 16 March 2005 (GT, 15 ks each).

2. EPIC-PN CTE CORRECTION

The bright state of GRO J1655-40 at the time of our XMM-Newton observations (almost twice brighter than the Crab, the source used for Burst mode calibration) has shown that the Charge Transfer Efficiency (CTE) in the Burst mode has a stronger rate-dependence than previously modeled. An inaccurate calibration of the EPIC-pn CTE leads to a bad energy determination, which becomes evident in the large residuals around the instrumental Si and Au edges. From our GRO J1655-40 observations, the offset in energy has been found to be rate dependent, being stronger at the center of the PSF, which implies that it can not be directly corrected in the extracted spectrum. We have determined the CTE gain for different rates, selecting and evaluating the energy gain linear factor for spectra extracted from different regions of the

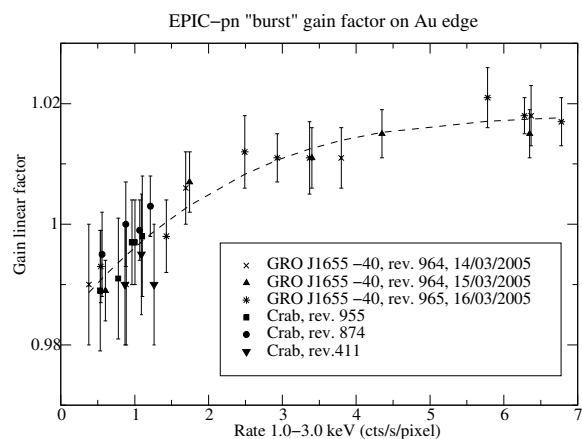


Figure 1. Calibration of the gain linear factor f as a function of rate per pixel r .

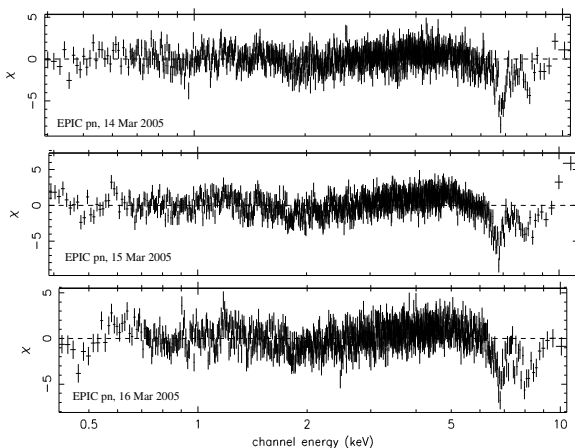


Figure 2. EPIC pn residuals of GRO J1655-40 spectra of our three March 2005 observations, after fitting an absorbed multi-temperature disk model.

detector (Fig. 1). We have also included the Crab calibration observations to improve the determination of the dependence of the gain linear factor f with the rate per pixel r (cts/s/pixel), which we find can be approximated by $f = 0.98 + 0.015r - 2.2 \times 10^{-3}r^2 + 1.1 \times 10^{-4}r^3$. After correcting the event tables with this linear gain, no more residuals appear around the Au and Si edges.

3. GRO J1655-40 AND GRS 1915+105

For our first XMM-Newton observation of GRO J1655-40, performed on 27 February 2005, some days before the start of the first outburst, a simultaneous RXTE observation is available, which has allowed to determine the X-ray spectrum up to 60 keV. The simultaneous fit to XMM-Newton and RXTE/PCA data shows that the spectrum can be modeled by a multi-temperature accretion disk, plus a power law with index ~ 1.5 . During our March observations (with exposures of ~ 15 ks), performed close to the maximum of the first outburst, the spectra of the EPIC pn camera, which was used in the Burst mode, show that the emission is dominated by the multi-temperature accretion disk component, with $kT_{in} = 1.2-1.3$ keV, hotter than the typical temperature observed during the 1996-1997 outburst (Sobczak et al., 1999). We detect two absorption features at 6.8 and 8.0 keV, corresponding to Fe XXV $K\alpha$ and K absorption lines (Fig. 2). The simultaneous RGS data provide the first high resolution spectra of GRO J1655-40, showing clear absorption lines at 0.71 and 0.72 keV (Fig. 3), which could be identified either as OVII at zero velocity, or as a blueshifted Fe XVIII L-shell doublet. The blueshift would indicate in this case an outflowing absorber at 3000 km/s.

The absence of other absorption features in the RGS spectrum is puzzling: if the lines at ~ 0.7 keV correspond to OVII K-shell at zero velocity, we would expect to see an even stronger absorption of OVII $K\alpha$ at ~ 0.57 keV that is not present; and if they are Fe XVIII absorption,

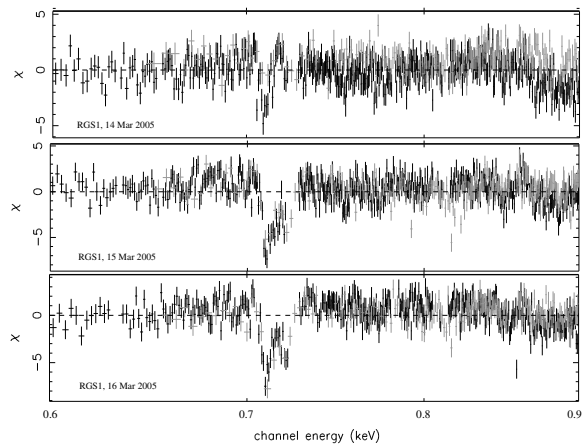


Figure 3. RGS 1 order 1 (black) and 2 (grey) residuals for our March 2005 observations of GRO J1655-40.

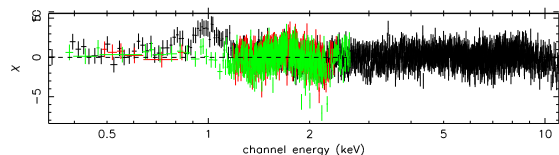


Figure 4. EPIC pn and RGS residuals of the GRS 1915+105 spectrum.

Fe XVII should be also present. In addition, the lack of observable OVIII and the presence of Fe XXV can only be explained by a highly ionized gas, with temperatures higher than $kT \sim 1.7$ keV. But at higher temperatures, Fe XVIII would not be expected to be present, constraining the possible temperature of the absorber to a narrow range, higher than the disk temperature derived from its thermal emission ($kT \sim 1.2 - 1.3$ keV).

XMM-Newton observed GRS 1915+105 on 3 May 2004, with 20 ks exposure time, and the EPIC-pn camera in the Burst mode. The EPIC and RGS spectra can be fitted with an absorbed power law, and no evident absorption features are observed. Since the source was not so bright as GRO J1655-40, no CTE problems are found and no residuals appear around the Si and Au edges. Nevertheless, the best-fit leaves an excess in the EPIC-pn spectrum around 1 keV not observed in the two RGS spectra, which could indicate some calibration problem.

ACKNOWLEDGEMENTS We thank J. Vink, J. Kaastra and Y. Ueda for useful discussions in El Escorial. GS acknowledges a MEC postdoctoral fellowship.

REFERENCES

- Greiner, Cuby & McCaughrean 2001, Nature, 414, 522
- Kotani et al. 2000, ApJ, 539, 413
- Orosz & Bailyn 1997, ApJ, 477, 876
- Sobczak et al. 1999, ApJ, 520, 776
- Ueda et al. 1998, ApJ, 492, 782
- Zhang, Cui & Chen 1997, ApJ, 482, L155

CYCLOTRON LINE STUDIES IN MAGNETIZED X-RAY PULSARS

G. Schönherr^{1,2,3}, J. Wilms², P. Kretschmar³, I. Kreykenbohm^{1,4}, W. Coburn⁵, R. E. Rothschild⁶, and A. Santangelo¹

¹Institut für Astronomie und Astrophysik, Universität Tübingen, Sand 1, 72076 Tübingen, Germany

²Department of Physics, University of Warwick, Coventry CV4 7AL, UK

³European Space Astronomy Centre, ESA, Apartado 50727, 28080 Madrid, Spain

⁴INTEGRAL Science Data Centre, 16 Chemin d’Ecogia, 1290 Versoix, Switzerland

⁵Space Science Laboratory, University of California, Berkeley, CA 94720-7450, USA

⁶Center for Astrophysics & Space Sciences, University of California, San Diego, CA 92093-0111, USA

ABSTRACT

Cyclotron resonance scattering features (CRSFs), also referred to simply as “cyclotron lines”, are detected as absorption lines in high-energy spectra of magnetized accreting neutron stars. They form in the presence of a strong magnetic field due to resonant scattering processes with electrons which are quantized in discrete Landau energy levels perpendicular to the B -field. Providing the only direct estimate of the magnetic field strength of an accreting neutron star, cyclotron lines are of fundamental importance to understanding the physics of magnetized X-ray pulsars. Their line profiles reflect the geometrical and physical properties of the accretion column near the magnetic poles of the neutron star, and therefore constitute a diagnostic tool for accessing the physics of accretion. Today’s high-energy telescopes allow for a resolution of those line shapes. Continuing an earlier approach by P. Kretschmar (Kretschmar et al., 2004), and making a renewed effort of simulating cyclotron lines with a revised Monte Carlo code based on the work of R. Araya (Araya & Harding, 1999), we fit our theoretical models to recent observational data.

Key words: CRSFs; neutron stars; γ -rays; X-rays.

1. INTRODUCTION

Considerable progress has been achieved in the field of instrumental high energy astronomy since the first detection of a cyclotron line in a Her X-1 spectrum with Balloon-HEXE in 1979. Spectra with a remarkable energy resolution of the cyclotron line shapes are obtained by instruments from e.g. the *INTEGRAL* and *RXTE* satellites. However, a theoretically established XSPEC model for analysis of these data is lacking. Instead it is

still common procedure to fit CRSFs with simple but unsatisfactory Lorentzian or Gaussian shapes. In the following, we discuss new results leading towards more realistic modeling of cyclotron lines and better future exploitation of their diagnostic potential.

2. LINE FORMATION

Cyclotron lines have been observed in spectra of many magnetized accreting neutron stars as absorption features in the 10 to 100 keV energy regime. Due to the high magnetic field, the kinetic energies of the plasma electrons in the accretion region are quantized perpendicular to the B -field in discrete so-called Landau levels. Photons with energies of $\sim n$ times the fundamental Landau energy undergo resonant scattering with the Landau electrons. They are trapped in the dense plasma of the accretion mound, being absorbed, quasi instantly re-emitted or spawned and absorbed again by the Landau electrons. Those photons may escape once their energy has changed sufficiently from the resonant Landau energies. Thus, they produce absorption features in the observed spectrum at the Landau line energies:

$$E_n = m_e c^2 \frac{\sqrt{1 + 2nB/B_{crit} \sin^2 \theta} - 1}{\sin^2 \theta} \frac{1}{1 + z}$$

where ($n = 0, 1, 2, \dots$), B/B_{crit} is the magnetic field strength in units of the QM critical field $B_{crit} = 4.4 \cdot 10^{13}$ G, θ is the angle between the photon and the magnetic field, $m_e c^2$ is the electron rest energy and z denotes the gravitational redshift.

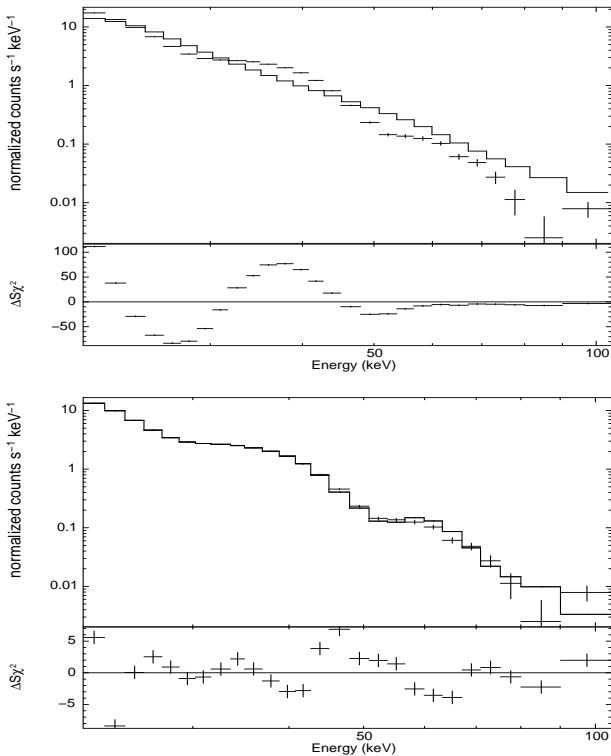


Figure 1. *V0332+53* outburst spectrum fitted with a *cutoffpl* model (top) and the same continuum model multiplied by our new XSPEC table model for cyclotron line features (bottom).

3. MODELS

We model CRSFs using a revised version of a Monte Carlo code developed by Araya et al. (Araya & Harding, 1999, 2000) including relativistic scattering cross sections and photon spawning. Two extreme cases of plasma geometries in the accretion mound are considered: a slab of infinite extension corresponding to the so-called “pencil beam” scenario of strongly beamed radiation, and a cylinder of infinite length representing the “fan beam” picture of a wide radiation cone. Physical conditions are furthermore adjusted by the choice of electron parallel temperature T_e , Maxwellian e^- momentum distribution and the energetic and angular distribution of the injected Monte Carlo photons. ($f(E) \sim$ high energy cutoff powerlaw, isotropic photon injection). Calculations are valid for the low-density / high-field ($B < B_{\text{crit}}$) regime of internally irradiated plasmas.

4. RESULTS

A recent *INTEGRAL* observation of the outburst of *V0332+53* in Januar 2005 was chosen for a comparison of preliminary models to real source data. Multiplicative

XSPEC table models have been constructed for both geometrical extremes from simulations on a parameter grid of varying B and $\cos\theta$. The continuum input spectrum parameters have been estimated from standard continuum and line fits of the observational data. Fig. 1 shows at the top the time-averaged *V0332+53* spectrum (Kreykenbohm et al., 2005) fitted with the *XSPEC cutoffpl* model. In the bottom plot the data is fitted with a *cutoffpl* multiplied by our cyclotron line model. The best fit is obtained for cylinder geometry, $B/(1+z) = 0.53$ and $\cos\theta = 0.6$ producing a reduced χ^2 of $\chi^2_{\text{red}} = 12$. The fit quality is not yet satisfactory, however, this had to be expected due to the narrowness of model parameter space. The magnetic field strength obtained agrees nicely with the one from standard fits.

5. CONCLUSIONS AND OUTLOOK

Our revised Monte Carlo cyclotron models indicate that we can qualitatively explain CRSFs in real observed source data. Our approach differs from common fitting procedures in the following key points:

- All lines are fitted simultaneously with one model, ensuring consistence of for instance line energy ratios with theory.
- A non-trivial line shape is modelled.
- Fits allow for the determination of physical parameters in addition to the magnetic field strength, such as plasma geometry and electron parallel temperature, giving insight into the physical conditions in the accretion column.

These points are not only desirable but have also become a necessity when considering high-quality data with complex line shapes as seen e.g. in the fundamental line of *V0332+53*, which could so far only be fitted by artificially overlaying several Gaussians in standard procedures (Kreykenbohm et al., 2005; Pottschmidt et al., 2005). This work is ongoing, aiming at a systematic testing of theoretical models on observed cyclotron line spectra and a dynamic fine-tuning of simulations and models in the near future. It serves as a proof of concept that modeling X-ray pulsar spectra with more realistic CRSFs will be possible once the computation of our Monte Carlo grids has finished.

REFERENCES

- Araya, R. & Harding, A., 1999, *ApJ* 517, 334–354
- Araya, R. & Harding, A., 2000, *ApJ* 544, 1076–1080
- Kretschmar, P., et al., 2004, *Proc. 4th INTEGRAL Workshop*
- Kreykenbohm, I., et al., 2005, *A&A* 433, L45–L48
- Pottschmidt, K., et al., 2005, *ApJL*, in press

XMM MONITORING OF THE ECLIPSING POLAR HU AQUARI

Robert Schwarz¹, Axel D. Schwope¹, Vikram S. Dhillon², and Thomas R. Marsh³

¹Astrophysikalisches Institut Potsdam, An der Sternwarte 16, D-14482, Germany

²Department of Physics, University of Warwick, Coventry, CV4 7AL, UK

³Department of Physics & Astronomy, University of Sheffield, Sheffield, S3 7RH, UK

ABSTRACT

We present results of an ongoing XMM monitoring campaign of the bright eclipsing polar HU Aqr. During four pointings performed between 2002 and 2005 the system was found in different accretion states ranging from intermediate to very low mass-transfer rates. On the long run these data uniquely constrain the distribution of the different radiation components in the accretion zone (cyclotron, bremsstrahlung, reprocessed soft X-ray emission) as a function of the instantaneous, specific accretion rate. An interesting, first result is the equilibrium of the primary hard X-ray flux and the soft, blackbody-like component during the intermediate state (Fig. 5). The last XMM pointing was accompanied by 4 hours of truly simultaneous ULTRACAM high-speed photometry at the VLT providing additional sub-second variability information in three optical bands (Fig 1). These data resolve the eclipse ingress/egress with an unprecedented high S/N and directly determine the location of the accretion spot on the white dwarf (Fig. 2). During all states the atmosphere of the white dwarf and the heated cap surrounding the accretion spot is directly discernable from XMM-OM UV light curves and optical photometry. From our new eclipse timings we find a third case (after DP Leo and NN Ser; Schwope et al. 2002 (A&A 392, 541); Brinkworth et al. 2005, astro-ph0510331) for a strong negative period derivative in a CV (Fig. 3) of $\dot{P} = -8.1 \times 10^{-12}$, which indicates either a true decrease of the binary orbit or is mimicked by a third body.

Key words: Accretion – AM Herculis binaries – stars: binaries: eclipsing – stars: individual: HU Aqr – X-rays: stars.

ACKNOWLEDGMENTS

This work was supported by the DLR-Verbundforschung under grant 50 OR 0404.

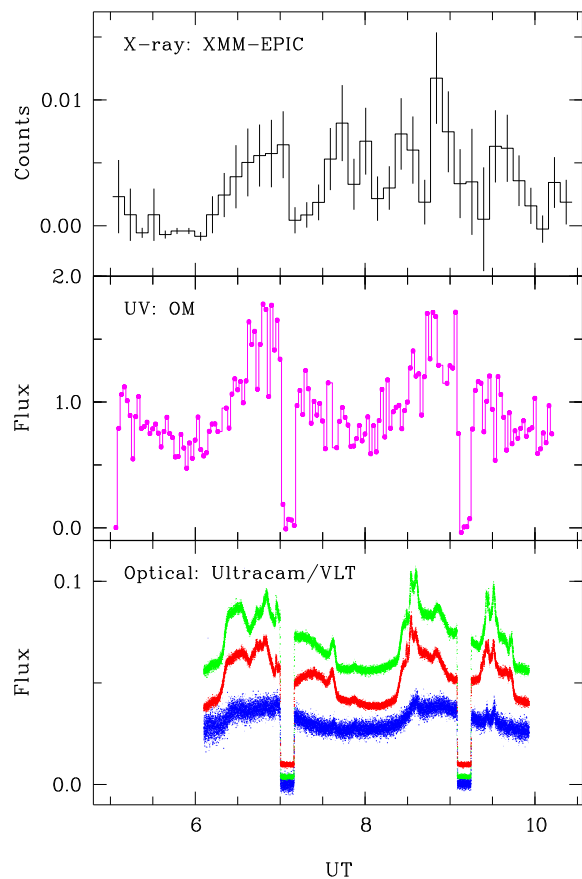


Figure 1. Simultaneous XMM and Ultracam high-speed photometry at the VLT taken in May 2005 during an episode of very low accretion activity. The top panel shows residual X-ray emission from the accretion plasma, while the UV light curve displayed in the middle panel is dominated from the heated photosphere below the accretion shock. In the lowest panel ULTRACAM ugr high-speed data at 0.5 sec resolution are shown, which is sensitive to photospheric radiation (u-band) and additional cyclotron emission (g- and r- band).

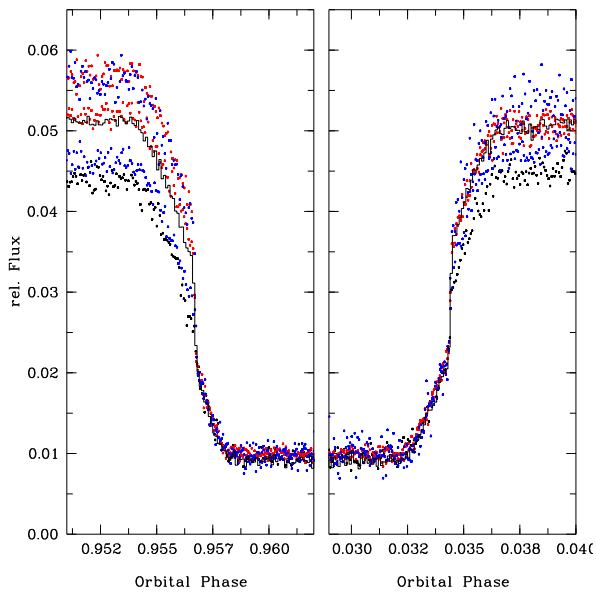


Figure 2. A blow up of the ULTRACAM r-band light curves around eclipse phase. This data resolves the egress and ingress of the white dwarf (28 sec) and the accretion spot (1.2 sec) with unrivaled high signal-to-noise and will allow to discern the linear dimensions of the emission components directly. The dots represent data from four individual runs, while the line is the resulting phase-average light curve.

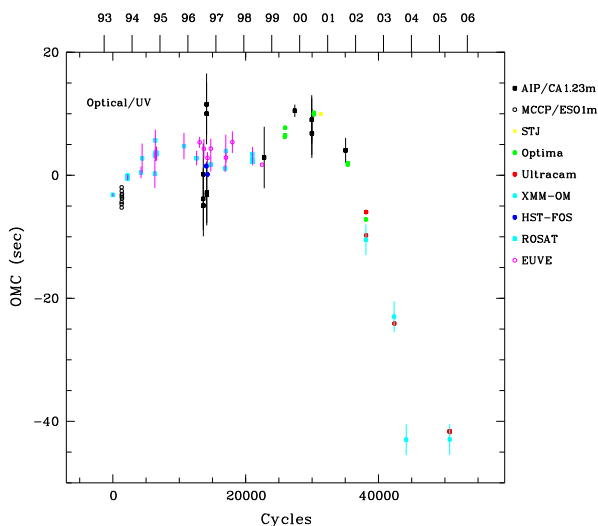


Figure 3. Monitoring of the eclipse egress of HU Aqr over a 12-years baseline using various space and ground based facilities. The new optical and X-ray timings suggest a large period derivative with respect to a linear ephemeris. This unexpected behaviour does either indicate the presence of a third body or a true period decrease of the binary. For the latter case the angular momentum loss would be a factor of 100 higher than the value expected for a short period CV where angular momentum-loss is thought to be only driven by gravitational radiation.

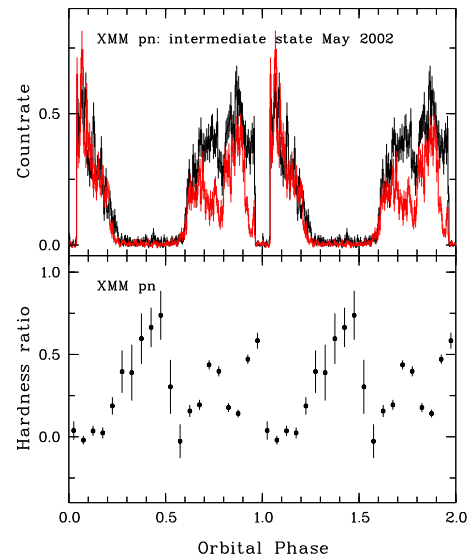


Figure 4. XMM EPIC light curve of HU Aqr taken during the intermediate state in May 2002. Count rates in the soft ($< 300\text{eV}$, red) and hard ($> 0.5\text{keV}$) bands are shown separately. Around $\phi \sim 0.65$ and $\phi \sim 0.9$ broad and narrow absorption features are evident, which also have an impact on the hardness ratio (lower panel).

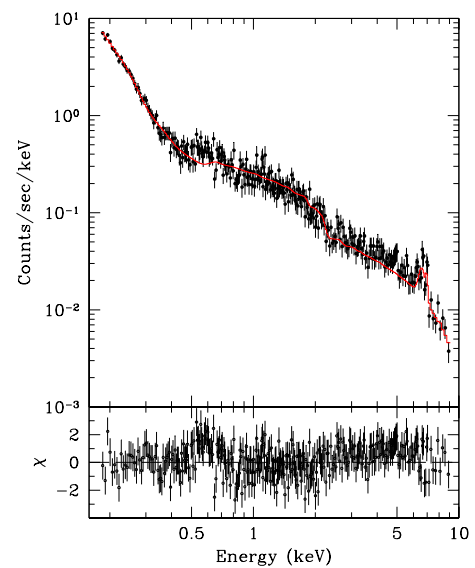


Figure 5. X-ray spectrum of HU Aqr taken during the intermediate accretion state in May 2002. Two-component blackbody and thermal plasma model with $T_{\text{bb}} = 34\text{eV}$ and $T_{\text{mek}} = 39\text{keV}$ is required to roughly fit the data. The fit residuals show hints of line emission around 0.6 and 6.4 keV, which correspond to OVII and the fluorescence iron line. Both lines indicate presence of additional low temperature plasma and a harder reflection components. The ratio between the soft and hard bolometric fluxes is only 2, and therefore strongly reduced when compared to a ROSAT high state observation.

AM HER – CAUGHT IN THE ACT WITH XMM-NEWTON!

A. Schwope¹, R. Schwarz¹, B. Gänsicke², V. Burwitz³, and K. Reinsch⁴

¹Astrophysikalisches Institut Potsdam, An der Sternwarte 16, 14482 Potsdam, Germany

²Department of Physics, University of Warwick, Coventry, CV4 7AL, UK

³Max-Planck Institut für Extraterrestrische Physik, Giessenbachstrasse, 85748 Garching, Germany

⁴Georg-August-Universität Institut für Astrophysik, Friedrich-Hund-Platz 1, 37077 Göttingen, Germany

ABSTRACT

AM Herculis, the prototype of the strongly magnetic cataclysmic variables, escaped observations with XMM-Newton so far due to visibility constraints. We report on a very preliminary analysis of the first XMM-Newton observations of this classical polar performed in July 2005. AM Herculis recovered shortly for a two-weeks period from an extended low state lasting 1.8 years and was found in an intermediate (close to high) accretion state. It was accreting in its normal or regular one-pole mode. This observation yielded spectra and light curves with extraordinary high quality. We discuss briefly the X-ray and UV light curves as well as X-ray spectra obtained with EPIC-pn and the RGS.

Key words: AM Herculis.

1. XMM-NEWTON OBSERVATIONS

AM Herculis as the key object for magnetically controlled accretion has been observed with every high-energy observatory so far. It was foreseen for a long RGS-prime observation in the GTO program but never observed since it was situated in the XMM-Newton blind spot. The visibility changed over the years and we could conduct a first unconstrained observation with XMM-Newton in AO4 (July 2005). Due to severe visibility constraints the whole observation which was planned to cover at least three binary cycles ($P_{\text{orb}} = 186$ min) was broken in a total of 5 visits of length 9 ksec each.

XMM-Newton observations were performed in the period July 19–27, 2005 (revs. 1027–1031). Two observations were affected by high background resulting in the complete loss of X-ray data of one visit. EPIC-MOS was defined as detector for a possible low state and used in large window mode. These are strongly affected by pile-up and not considered here further. The detector for the high state was EPIC-pn and used in timing mode with

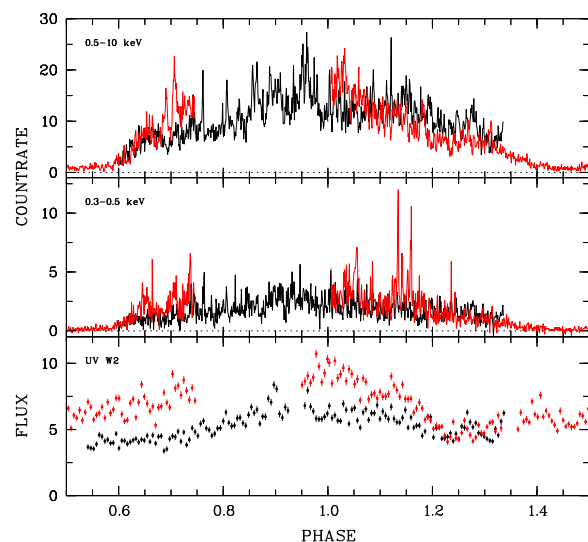


Figure 1. EPIC-pn light curves in soft and hard bands and OM-UVW2 ultraviolet light curve of AM Her obtained during two visits of the source in July 2005. Bin size is 60 s for the OM, 10 s for EPIC. Phase zero corresponds to inferior conjunction of the secondary. OM flux is given in units of 10^{-14} erg cm^{-2} s^{-1} .

the thick filter. The OM was used in timing mode with filter UVW2. This is the filter operating at the shortest wavelengths ($\lambda_c \sim 2200$ Å) and has the smallest effective area. The OM is in particular sensitive for reprocessed radiation from the accretion process proper and contains line emission from the accretion stream and continuum emission from the white dwarf’s photosphere (accretion-heated and undisturbed).

The EPIC-pn and OM-UVW2 timing mode photons were extracted from the raw data with SAS 6.1. Phase-folded EPIC-pn X-ray and OM-UVW2 ultraviolet light curves are displayed in Fig. 1. The X-ray band was subdivided in soft and hard bands comprising the two main spectral components, a black-body like heated photosphere and

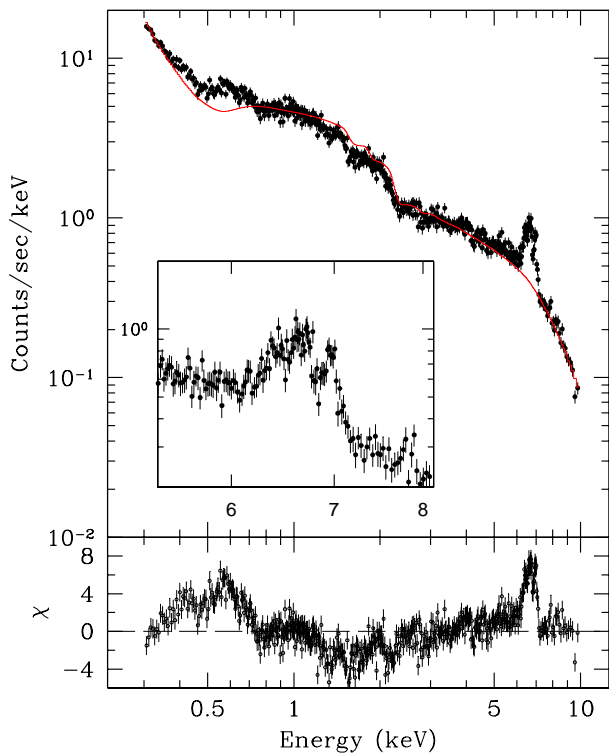


Figure 2. Mean EPIC-pn spectrum of AM Her. The red line is the result of a simple fit invoking only bremsstrahlung and blackbody components. The inset shows a zoom focusing on the Fe-line complex between 6 and 7 keV.

a bremsstrahlung-like cooling plasma, respectively. The source reached a mean-bright phase count rate with the EPIC-pn camera of about 15 s^{-1} . Individual soft flares without hard X-ray counterpart are reflecting the impact of dense blobs of matter on the accretion region. They reached about 15 s^{-1} just in the soft band, i.e. they contain several hundred photons, sufficient for a spectral analysis, the determination of the temperature and an estimate of the mass of individual blobs of matter. The whole EPIC-pn observation yielded more than 250000 photons which will allow phase-dependent spectral studies of all the components.

The mean EPIC-pn spectrum is displayed in Fig. 2 together with a model fit representing the broad continuum slope. It includes a cold absorbed superposition of a 29 eV blackbody and a 15 keV thermal bremsstrahlung component and has been chosen to highlight the main line emission features which appear as strong residuals around 0.6 and 6.7 keV, respectively. They indicate a more complex spectrum from a stratified cooling plasma, a reflection component from the surface of the white dwarf, and a possible warm or partial absorber (see e.g. Beardmore et al. 1994, Done & Magdziarz 1998, Ishida et al. 1997). These spectral components are currently investigated by phase-dependent X-ray modeling. The soft X-ray excess seems to be mild with $F_{\text{bb,bol}}/F_{\text{tb,bol}} \simeq 6$. The faint phase is dominated by

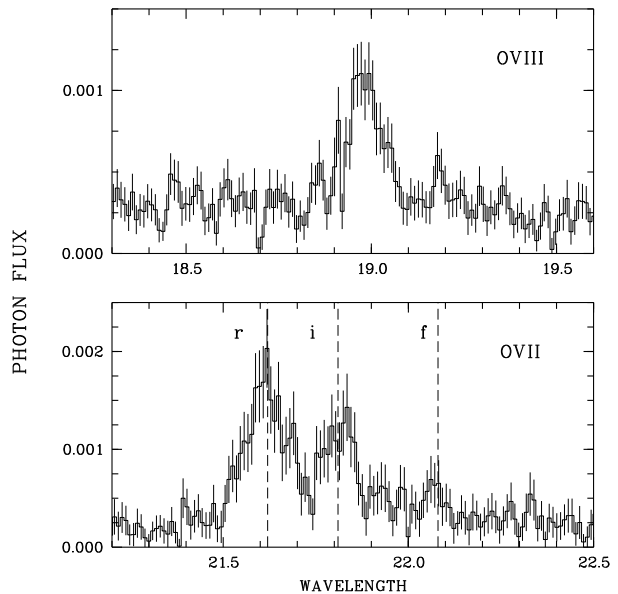


Figure 3. Cutout of the mean RGS-spectrum of AM Her centering on the He- and H-like oxygen lines.

hard emission. The measured ultraviolet flux indicates that the source was encountered in an intermediate state of accretion (see IUE-spectroscopy in different accretion states by Gänsicke et al. 1995).

The Fe-line complex between 6 and 7 keV consists of an Fe fluorescence line at 6.4 keV and He- and H-like species at 6.7 and 7.0 keV. The H/He line ratio hints to a temperature of about 10 keV. The phase-dependent line flux and flux ratios (He/H) of the Fe-lines will be combined with those of other species to make an attempt to constrain the temperature stratification of the cooling plasma directly from observations. The RGS-spectrum contains a weak continuum and several emission lines, most prominent are Oxygen lines from H- and He-like ions (Fig. 3). The lines in the average spectrum appear to be resolved, the H-like line has a width of 0.07 \AA (corrected for the instrumental profile) indicating a Doppler width of about 1200 km s^{-1} . This number represents an upper limit due to velocity smearing. The low f/i-ratio of the He-like triplet is typical of a plasma in the high-density limit. However, the strong underlying radiation field might mimic line ratios of a high-density plasma (cf. Mauche 2002 and references therein).

Acknowledgements This work was supported by the DLR under grant 50 OR 0404.

REFERENCES

- Beardmore A.P., et al. 1995, MNRAS 272, 749
- Done C., Magdziarz P. 1998, MNRAS 298, 737
- Ishida M., et al. 1997, MNRAS 287, 651
- Gänsicke B., et al. 1995, A&A 303, 127
- Mauche C. 2002, ASPC 261, 113

ACTIVITY OF V1223 SGR OBSERVED WITH INTEGRAL

Vojtěch Šimon, René Hudec, Filip Munz, and Jan Štrobl

Astronomical Institute, Academy of Sciences of the Czech Republic, 251 65 Ondřejov, Czech Republic

ABSTRACT

We report on the observations of the intermediate polar V1223 Sgr by IBIS and OMC onboard *INTEGRAL* in a state of brightness which we call a shallow low state. We have a unique opportunity to investigate the relation between the activity in the optical and far X-ray region on long time scales; we present far X-ray spectra (E up to 60 keV) and the relation between far X-ray and optical flux. We demonstrate their stability during this state over an interval of 400 days. Even in this state, both the profile of the optical modulation with the orbital period and the phase of the minimum light in the OMC data are in good agreement with those determined by Jablonski & Steiner (1987) for the high state. The beat period is still dominant, which suggests that the stream-disk overflow still operates in this state of activity.

Key words: accretion, accretion discs; binaries: close; circumstellar matter; stars: individual: V1223 Sgr; X-rays: binaries.

1. INTRODUCTION

V1223 Sgr is an intermediate polar (IP) with the magnetic field of the white dwarf (WD) weak enough to allow a formation of the disk (e.g. Beuermann et al. (2004)). The orbital period is $P_{\text{orb}} = 0.1402440$ days (Warner & Cropper, 1984) and the rotational period of the WD is $P_{\text{rot}} = 746$ sec (Osborne et al., 1985). P_{rot} is observed in X-rays while the beat period $P_{\text{beat}} \approx 794$ sec (Steiner et al., 1981) is seen in the optical. This system displays a strong long-term activity, dominated by episodes of low states (Garnavich & Szkody, 1988). Also a brief outburst from a high state, with the duration of ~ 6 hours and an amplitude of ~ 1.5 mag, was reported by van Amerongen & van Paradijs (1989). X-ray observations of IPs often concentrate on isolated series with the aim at study of the rotational modulation and/or the spectrum. The relation between the X-ray and optical activity, especially on long time scales, remains to be established.

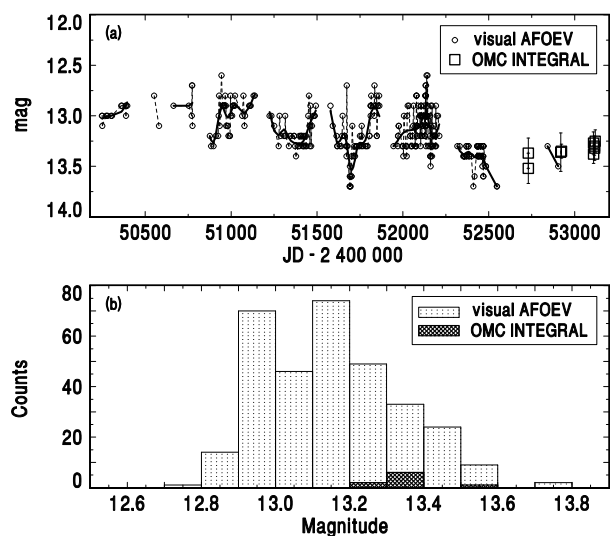


Figure 1. (a) Recent activity of V1223 Sgr in the optical passband. The smoothed curve represents the fit by the code HEC13 (written by Dr. P. Harmanec, the method of Vondrák (1969, 1977)). (b) The statistical distribution of the brightness for the fit by HEC13 and the OMC data.

2. DATA SOURCES AND ANALYSIS

The *INTEGRAL* data used here were obtained in the framework of the Galactic Plane Scans and the deep observations of the Galactic center. These observations can be grouped into three intervals of time. The IBIS IS-GRI data were reduced by OSA software ver. 4.2 and the fluxes were extracted by 2-D Gaussian fit using `mosaic_spec` (part of the new OSA release). The optical data were obtained from the OMC images (100 sec exposure times only).

3. RESULTS

We report on the observations of the intermediate polar V1223 Sgr by IBIS and OMC onboard *INTEGRAL* in a state of brightness which we call a shallow low state

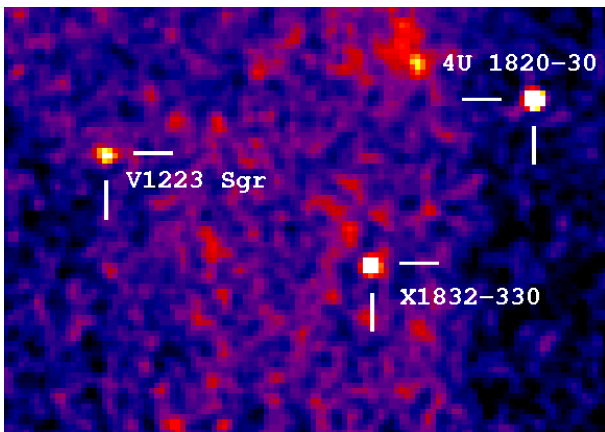


Figure 2. Mosaic of the field of V1223 Sgr obtained by IBIS in the 25–40 keV passband, with the starting exposure time in JD 2452730.2 and the integration time of 66700 sec. Size of the field is $9.5^\circ \times 6.8^\circ$. North is up, East to the left.

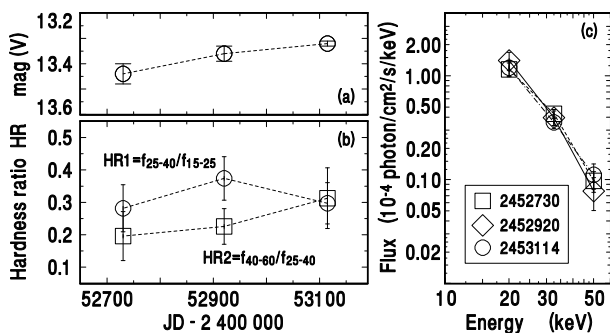


Figure 3. Time variations of the V band magnitude (a) and hardness ratios of far X-ray intensities (b) of V1223 Sgr. The points in each panel are connected by the line only for convenience. (c) The corresponding far X-ray spectra from IBIS. The Julian Date of each spectrum is listed.

($V \approx 13.5$; Fig. 1ab), while the magnitude in the high state is about $V \approx 12.8 - 13.0$ (e.g. Garnavich & Szkody (1988)). A trend of a slow decay of the optical brightness of V1223 Sgr with several short episodes of a shallow low state was apparent for several years before this event (Fig. 1a).

V1223 Sgr is clearly detected in the softer passband of IBIS (Fig. 2). We establish the relation between the activity in the optical and far X-ray spectral region on long time scales in a shallow low state (Fig. 3ab). We show the stability of this relation, and of the profile of the X-ray spectra (E up to 60 keV (Fig. 3c)) during this state over an interval of 400 days. The spectral profile remains largely unchanged during this time interval, which suggests that the extreme tail of the bremsstrahlung X-ray spectrum displays a remarkable stability.

Our observations imply the luminosity in the 15–25 keV

passband to be $\sim 1.2 \times 10^{33}$ erg/s and still a relatively bright disk (i.e. by several magnitudes brighter than the deep low states observed by Garnavich & Szkody (1988)). The irradiation of the disk by X-rays thus appears to play a role since the disk should be already in the region of thermal instability during our observations – outbursts and a large decrease of the optical flux are thus expected, which is not observed.

Even in the shallow low state, both the profile of the optical modulation with the orbital period and the phase of the minimum light in the OMC data are in good agreement with those determined by Jablonski & Steiner (1987) for the high state. Using the method of Scargle (1982) contained in the code AVE, we find that the beat modulation still dominates over the rotational modulation, which suggests that stream-disk overflow still operates in the shallow low state. This overflow thus persists even when the mass transfer rate decreases ~ 3 times with respect to the high state.

ACKNOWLEDGMENTS

This research is based on observations with *INTEGRAL*, an ESA project with instruments and science data centre funded by ESA member states (especially the PI countries: Denmark, France, Germany, Italy, Switzerland, Spain), Czech Republic and Poland, and with the participation of Russia and the USA. This study was supported by the project ESA PRODEX INTEGRAL 90108 and by ESA PECS project 98023, and partly by the grant 205/05/2167 of the Grant Agency of the Czech Republic. We thank Dr. Harmanec for providing us with the code HEC13. The code AVE developed by the GEA society is available at URL: www.astrogea.org/soft/ave/aveint.htm.

REFERENCES

- Beuermann K., et al. 2004, A&A, 419, 291
- Garnavich P. & Szkody P. 1988, PASP, 100, 1522
- Jablonski F. & Steiner J.E. 1987, ApJ, 323, 672
- Osborne J., et al. 1985, Sp.Sc.Rev., 40, 143
- Scargle J.D. 1982, ApJ, 263, 835
- Steiner J.E., et al. 1981, ApJ, 249, L21
- van Amerongen S. & van Paradijs J. 1989, A&A, 219, 195
- Vondrák J. 1969, BAIC, 20, 349
- Vondrák J. 1977, BAIC, 28, 84
- Warner B. & Cropper M. 1984, MNRAS, 206, 261
- Winkler C., et al. 2003, A&A, 411, L1

CONSTRAINTS ON THE SYSTEM PARAMETERS OF THE RAPID BURSTER

Vojtěch Šimon

Astronomical Institute, Academy of Sciences of the Czech Republic, 251 65 Ondřejov, Czech Republic

ABSTRACT

We constrain the length of the orbital period P_{orb} of the remarkable low-mass X-ray binary, the Rapid Burster (MXB 1730–335), to lie between 3.5 and 5.5 hours, and the radius of the disk $R_{\text{disk}} = 0.9 R_{\text{lobe}} = 3.7 \times 10^{10}$ cm – 5.0×10^{10} cm. All this emerged from the analysis of the parameters of a group of outbursts observed by *ASM/RXTE*, and making use of the model of King & Ritter (1998). This helps us in linking the properties of this object to the group of X-ray binaries. P_{orb} of the Rapid Burster thus lies above the period gap of LMXBs and its donor is an M4–K5 main-sequence star.

Key words: Stars: neutron; accretion, accretion discs; binaries: close; circumstellar matter; X-rays: binaries; Stars: individual: Rapid Burster.

1. INTRODUCTION

MXB 1730–335 (Rapid Burster, RB) is a remarkable system (Lewin et al., 1976) lying in the globular cluster Liller 1 at the distance of $d \approx 8$ kpc (Liller, 1977; Ortolani et al., 1996). RB displays two types of X-ray bursts during the outbursts: Type I – thermonuclear runaway of the accreted matter on the neutron star (NS), and Type II – spasmodic accretion (e.g. Lewin et al. (1995)). The outbursts of RB are similar to those in soft X-ray transients (SXTs) (see e.g. Chen et al. (1997) for a review on SXTs). The outbursts of SXTs are interpreted in terms of the thermal instability of the accretion disk (e.g. Dubus et al. (2001); King & Ritter (1998)). The orbital period P_{orb} of RB has been unknown since its discovery in 1976. Since P_{orb} of X-ray binaries lie in a very wide range (11 min – several days) (e.g. Ritter & Kolb (2003)), even an estimate of P_{orb} of RB makes sense.

2. DATA SOURCE AND ANALYSIS

Daily means of the *ASM/RXTE* sum band 1.5–12 keV observations (Levine et al., 1996)

(<http://xte.mit.edu>) were used. This analysis considers the outbursts of Group A with Phase 1 (intense persistent emission) (Fig. 1a) (see Guerriero et al. (1999) for details). The outbursts were matched to a representative outburst, taken as a template. The rising branch was used for folding the individual events. From the physical point of view, the rising branch represents the phase of the propagation of the heating front through the disk (Fig. 1abc), using the model of Dubus et al. (2001).

3. DISCUSSION

The initial part of the decaying branch of the outbursts of Group A is roughly exponential with the e -folding time $\tau = 8$ days while the final decay can be regarded as approximately linear (Fig. 1abc). The scatter of the decaying branches can be attributed to the rapid variability on the time scale of a few days rather than the systematic changes of the decay rate. Arrivals of the spiral arms into the inner disk region are a possible cause (see the models by Truss et al. (2002)). The physical interpretation of the exponential decay can be offered in terms of irradiation of the disk by X-rays strong enough to ionize all of the disk out to its outer edge according to the model by King & Ritter (1998).

Here we present an approach which enables us to constrain the length of P_{orb} of RB from the parameters of outbursts of Group A, using the model of King & Ritter (1998) and Shahbaz et al. (1998). Conversion of the X-ray flux of RB can be carried out in the following way: 3×10^{-12} erg/cm²/s per 1 PCA ct/s (2–20 keV) (Guerriero et al., 1999). The intensity of RB at the peak of outburst (from the fitted profile in Fig. 1) is then $I_{\text{max}} = 19$ ct/s = 0.253 Crab = 3290 PCA ct/s, which yields the peak flux $F = 9.9 \times 10^{-9}$ erg/cm²/s. Correction for the extinction $N_{\text{H}} = 1 \times 10^{22}$ cm⁻², using the spectra of the persistent emission by Masetti et al. (2000) and the cross sections by Morrison & McCammon (1983), increases the flux in the 0.7–12 keV passband by a factor of ~ 1.25 with respect to that observed in the 1.5–12 keV passband. The luminosity of RB at the outburst peak is thus $L_{\text{max}} \approx 9.5 \times 10^{37}$ erg/s (0.7–12 keV).

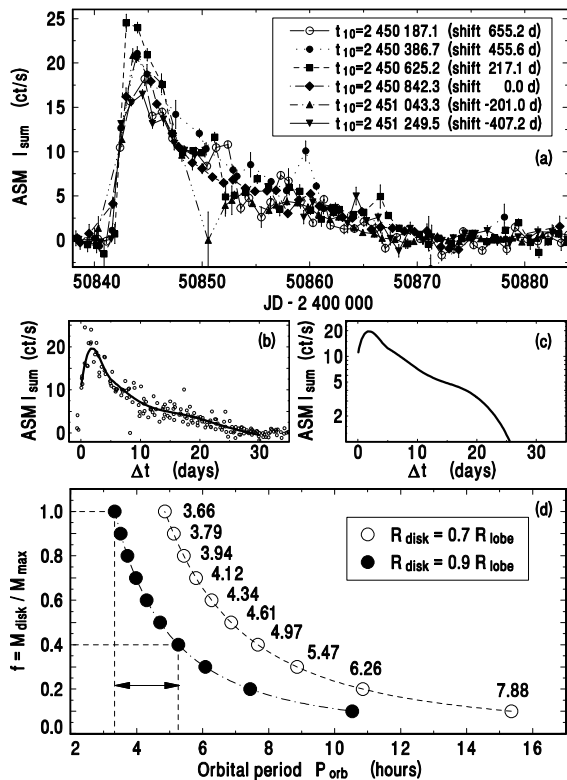


Figure 1. (a) Superposition of 6 outbursts of Group A, shifted along the time axis to match the rising branch of the template at $I_{\text{sum}} = 10$ ct/s (the moment t_{10} in JD is listed). (b) Merged ASM/RXTE light curves from Fig. 1a. Δt gives the time interval with respect to crossing $I_{\text{sum}} = 10$ ct/s on the rising branch. The folded light curves were smoothed by the code HEC13 (author Dr. P. Harmanec, method of Vondrák (1969, 1977)). (c) The fit displayed in the logarithmic scale of the ordinate. (d) P_{orb} of RB versus the factor f . The numbers at the points denote R_{disk} in units of 10^{10} cm. The most likely range of P_{orb} of RB is marked by the horizontal arrow.

The disk mass at the outburst peak is $M_{h(0)} = (L_{\text{max}} \tau) / (\eta c^2) \approx 4.9 \times 10^{23}$ grams. $\eta = 0.15$ (King & Ritter, 1998) and c is the speed of light. The radius of the disk at the outburst peak is $R_{h(0)} = [(3 M_{h(0)}) / (3 \cdot 10^{-8} f)]^{1/3}$ cm. f is the ratio of the mass of the hot disk at L_{max} with respect to its maximum possible mass. The $P_{\text{orb}} - R_{\text{disk}}$ relation for various values of f is shown in Fig. 1d. P_{orb} can be determined if we assume a reasonable value of $R_F = R_{h(0)} / R_{\text{lobe}}$, giving $R_{h(0)}$ as a fraction of the radius of the lobe of the NS, R_{lobe} . Here we use $R_F = 0.9$ and 0.7 .

$$P_{\text{orb}} = \left(\frac{R_{\text{lobe}}}{1.63 \times 10^{10}} \right)^{3/2} \left(\frac{M_{\odot}}{M_{\text{NS}}} \right)^{1/2} \text{ [hr]} \quad (1)$$

P_{orb} is longer than ~ 3.5 hours (Fig. 1d). We argue that the plausible values of f lie in the range $0.4 - 1.0$ (since the

Table 1. Constraints on the system parameters of the Rapid Burster.

Mass of the neutron star: $M_{\text{NS}} = 1.4 M_{\odot}$ (def.)
Disk radius in outburst: $R_{\text{disk}} = 0.9 R_{\text{lobe}} = 3.7 \times 10^{10} \text{ cm} - 5.0 \times 10^{10} \text{ cm}$
Orbital period: $P_{\text{orb}} = 3.5 - 5.5$ hours
Spectral type of the donor *: M4V–K5V
Radius of the donor *: $0.3 - 0.6 R_{\odot}$
Mass of the donor *: $0.3 - 0.6 M_{\odot}$
* Using the relations of Smith & Dhillon (1998).

largest part of the decaying branch is exponential), which enables us to constrain P_{orb} even better. The resulting constraints on the system parameters are in Table 1.

ACKNOWLEDGMENTS

This research has made use of the observations provided by the ASM/RXTE team and was supported by the grant 205/05/2167 of the Grant Agency of the Czech Republic, the project ESA PRODEX INTEGRAL 90108 and ESA PECS project 98023. I am indebted to Dr. Harmanec for providing me with the code HEC13.

REFERENCES

- Chen W., et al. 1997, ApJ, 491, 312
 Dubus G., et al. 2001, A&A, 373, 251
 Guerriero R., et al. 1999, MNRAS, 307, 179
 King A.R. & Ritter H. 1998, MNRAS, 293, L42
 Levine A.M., et al. 1996, ApJ, 469, L33
 Lewin W.H.G., et al. 1976, ApJ, 207, L95
 Lewin W.H.G., et al. 1995, in X-ray Binaries, Cambridge Univ. Press, p.175
 Liller W. 1977, ApJ, 213, L21
 Masetti N., et al. 2000, A&A, 363, 188
 Morrison R. & McCammon D. 1983, ApJ, 270, 119
 Ortolani S., et al. 1996, A&A, 306, 134
 Ritter H. & Kolb U. 2003, A&A, 404, 301
 Shahbaz T., et al., 1998, MNRAS, 301, 382
 Smith D.A. & Dhillon V.S. 1998, MNRAS, 301, 767
 Truss M.R., et al. 2002, MNRAS, 337, 1329
 Vondrák J. 1969, BAIC, 20, 349
 Vondrák J. 1977, BAIC, 28, 84

OPTICAL AND X-RAY OUTBURSTS IN THE INTERMEDIATE POLAR GK PER

Vojtěch Šimon

Astronomical Institute, Academy of Sciences of the Czech Republic, 251 65 Ondřejov, Czech Republic

ABSTRACT

We present the properties of the complicated long-term evolution of the dwarf nova-like outbursts of the intermediate polar GK Per. We show how the maximum brightness of the outbursts has stabilized during the interval following the abrupt increase of the recurrence time in the early 1970's. We show and discuss the complicated relation between the profiles of the light curves of outbursts, observed in X-ray (*ASM/RXTE* data; 1.5–12 keV) and optical regions – the largest discrepancies between the light curve in these regions occur near the maximum of the optical light. *ASM/RXTE* observations show the onset and end of the recent outbursts to be simultaneous with those of the optical event (when covered by the observations) – the large delay of the optical outburst seen in 1978 (King et al., 1979) does not repeat at present. We discuss the implications of our observations on the physical processes in the system.

Key words: Stars: white dwarfs; accretion, accretion discs; binaries: close; circumstellar matter; X-rays: binaries; Stars: individual: GK Per.

1. INTRODUCTION

GK Per (Nova Per 1901), an optical counterpart of A 0327+43, is an intermediate polar with $P_{\text{orb}} = 1.99$ days (Crampton et al., 1986) and $P_{\text{spin}} = 351$ sec (Watson et al., 1985). The optical outbursts of GK Per are accompanied by brightenings in X-rays (e.g. King et al. (1979); Šimon (2002)). The basic features of three similar outbursts were modeled by Kim et al. (1992) in the framework of the thermal instability disk model.

2. DATA SOURCE AND ANALYSIS

The optical data come from the AFOEV database (CDS, Strasbourg, France). The individual observations were grouped into the night bins. The X-ray

data are the daily means of the *ASM/RXTE* sum band 1.5–12 keV observations (Levine et al., 1996) (<http://xte.mit.edu>), shifted to achieve the zero intensity in quiescence.

3. RESULTS

We show that the variations of the outburst recurrence time T_C in GK Per are large but generally not chaotic (Fig. 1a). A long-term trend of an increase of T_C can be resolved in the $O - C$ curve beyond any doubt and is accompanied by a brightening of the peak magnitude and increase of the relative energy RE of outburst (Fig. 1bc). RE is obtained by the transformation of the light curve from magnitudes into intensities and its integration over the outburst. It appears that both the peak magnitude and RE stabilized within a few epochs (Fig. 1abc) and remained at the values significantly different from those before the jump of T_C (see Šimon (2002)). A possible solution of the recent behaviour is as follows. T_C in quiescent dwarf novae is inversely proportional to the quiescent viscosity parameter α_{cool} (e.g. Warner (1995)). If α_{cool} is allowed to have a lower value after the jump of T_C than before it then a larger amount of matter can accumulate in the disk during a longer quiescent interval. This can then power a brighter outburst.

We find that each of the four optical outbursts which occurred during the operation of *ASM/RXTE* is accompanied by an X-ray brightening in the 1.5–12 keV passband. The onsets of outburst and the initial rises of the flux in the optical and X-ray passband can be regarded as simultaneous, taking the rounding of the profile of the X-ray light curve by the moving averages into account. However, the profiles of the light curve in the optical and X-ray regions are largely discordant. While the optical light curves display a sharp top, the X-ray curves possess clearly flat-topped maxima, even with a depression coincident with the moment of the optical maximum in outburst at the epoch $E = 6$ (Fig. 1g, see also Šimon (2002)). The X-ray flux largely rises only during the rapid initial rise of the optical outburst in the events at $E = 5, 6, 7$, and remains roughly constant or even decreases even when the optical flux continues to rise (Fig. 1fgh). The

duration of the X-ray outburst is about as long as that of the optical event when a good coverage is available (e.g. Fig. 1de).

The previous X-ray observations of GK Per were interpreted in terms of a lower absorption in quiescence than in outburst (Norton et al., 1988). We thus offer the following interpretation of the relation of the X-ray and optical behaviour. During phase 1, the heating front propagates both outside-in and inside-out. This is the phase of the steep rise of the flux in both the X-ray and optical passband. The accretion curtain is not fully formed yet and the X-ray flux can therefore rise because of a low absorption. During the subsequent phase 2, the heating front propagates only inside-out – this is the phase of a slow rise of the optical brightness to the optical maximum. The accretion curtain is already developed and the X-ray flux remains roughly constant or even decreases because of a large absorption. The models by Kim et al. (1992) predict that a brightening in the X ray and UV passbands can precede the optical outbursts in GK Per by 80–120 days. Such a precursor is absent at least from the outbursts at $E = 5, 6, 7$. The case of the outburst at $E = 8$ is uncertain but due to the noise the onset of the X-ray outburst can be consistent with the optical one. Nevertheless, the long precursor did occur in the much fainter and shorter 1978 outburst (King et al., 1979).

ACKNOWLEDGMENTS

This research has made use of the observations provided by the *ASM/RXTE* team and the AFOEV database, operated at CDS, France. My thanks also to numerous amateur observers worldwide whose observations made this analysis possible. This study was supported by the grant 205/05/2167 of the Grant Agency of the Czech Republic, the project ESA PRODEX INTEGRAL 90108 and ESA PECS project 98023. I thank Dr. P. Harmanec for providing me with the code HEC13.

REFERENCES

- Crampton D., et al. 1986, *ApJ*, 300, 788
 Kim S.-W., et al. 1992, *ApJ*, 384, 269
 King A.R., et al. 1979, *MNRAS*, 187, 77
 Levine A.M., et al. 1996, *ApJ*, 469, L33
 Norton A.J., et al. 1988, *MNRAS*, 231, 783
 Šimon V. 2002, *A&A*, 382, 910
 Vondrák J. 1969, *BAIC*, 20, 349
 Vondrák J. 1977, *BAIC*, 28, 84
 Warner B. 1995, *Cataclysmic Variables*, Cambridge Univ. Press
 Watson M.G., et al. 1985, *MNRAS*, 212, 917

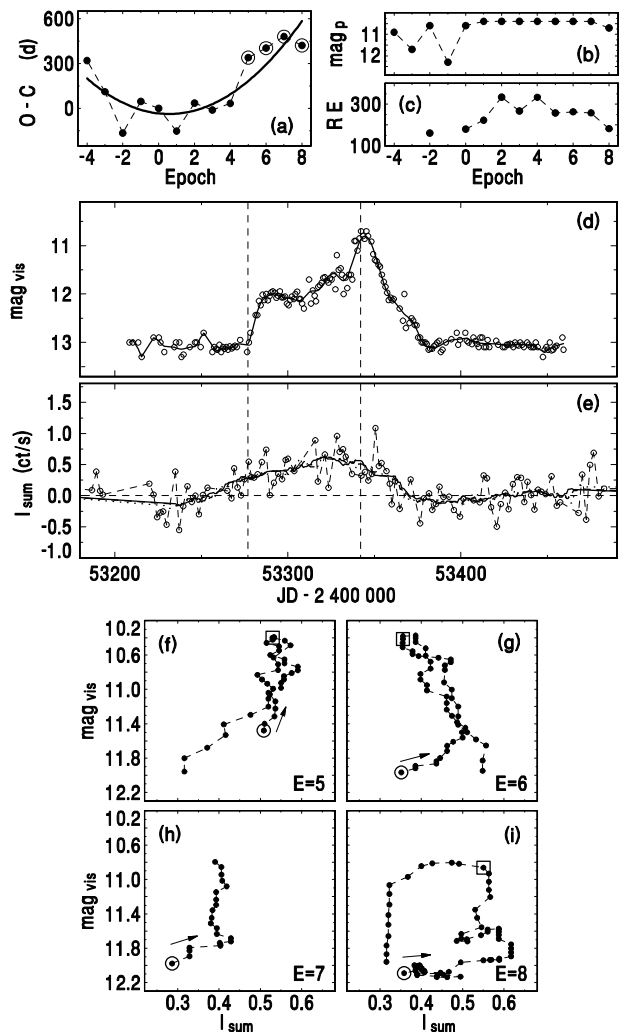


Figure 1. (a) $O-C$ diagram for the moments of the outburst maxima in the years 1970–2005. The ephemeris $T_{\max} = 2444681 + 1030 E$ was used. Four outbursts for which *ASM/RXTE* data exist are marked by the open circles. Variations of the peak magnitude (b) and the relative energy RE (c). An example of the relation between the outburst light curves in the optical (d) and X-ray (e) passbands. The optical data are fitted by the code *HEC13* (author: Dr. P. Harmanec, method: Vondrák (1969, 1977)). The X-ray data are two-day means, formed from the daily means that had the quoted uncertainty $\sigma_q < 0.4$ ct/s, and are fitted by the moving averages for various filter half-widths ($Q = 10 - 15$ days). The moments of the onset and the maximum light of the optical outbursts are marked by the vertical dashed lines. (fghi) The relation between the optical magnitude and X-ray intensity during outburst. The individual outbursts are abbreviated by their epochs. Only the parts of the optical light curve brighter than $12 \text{ mag}_{\text{vis}}$ are used to avoid artifacts caused by the moving averages of the steep initial rise in X-rays. The initial point (open circle) and the moment of the maximum of the optical light of the outburst (open box) are marked if covered by observations.

ACTIVITY OF THE UNIQUE X-RAY TRANSIENT CI CAM (XTE J0421+560)

V. Šimon¹, C. Bartolini², A. Piccioni², A. Guarnieri², and D. Hanžl³

¹Astronomical Institute, Academy of Sciences of the Czech Republic, 251 65 Ondřejov, Czech Republic

²Dipartimento di Astronomia, Università di Bologna, via Ranzani 1, 40127 Bologna, Italy

³Nicholas Copernicus Observatory and Planetarium, Kraví hora 2, 61600 Brno, Czech Republic

ABSTRACT

We emphasize the large difference between the optical color behaviour during the 1998 outburst and during the consequent quiescent interval of CI Cam. The variations of the optical/IR continuum on the time scale of weeks and months play a significant role after the outburst and cannot be explained by the changes of the extinction intrinsic to CI Cam. We find that the variations of the source of the optical light appear to be related to those of the X-ray source. We argue that the 1998 outburst can be explained by the thermal instability of the accretion disk, analogous to the outbursts of soft X-ray transients, if the disk in CI Cam heats up an extended envelope and/or a strong jet is formed.

Key words: accretion, accretion discs; binaries: close; circumstellar matter; stars: individual: CI Cam (XTE J0421+560); X-rays: binaries.

1. INTRODUCTION

CI Cam MWC 84 is an optical counterpart of the unique X-ray transient XTE J0421+560 (e.g. Frontera et al. (1998)), interpreted as a periastron passage of the compact object (Hynes et al., 2002) or a disk instability (Robinson et al., 2002). The outburst changed the appearance of the system (e.g. Clark et al. (2000); Hynes et al. (2002)). A possible orbital period $P_{\text{orb}} = 19$ days was reported by Barsukova et al. (2005a). The distance is about 3–5 kpc (Miroshnichenko et al., 2002; Robinson et al., 2002).

2. DATA SOURCES AND ANALYSIS

The optical data were obtained by Maksutov 180/1000 mm, SBIG ST-6 (Ondřejov) and 400/1700 mm tel., SBIG ST-7 (Brno), and were supplemented by

those of Barsukova et al. (2002, 2005b); Henden (2002); Henden & Sumner (2004). The 1.5–12 keV observations from *ASM/RXTE* (Levine et al., 1996) (<http://xte.mit.edu>), *BeppoSAX* (Parmar et al., 2000) and *XMM* (Boirin et al., 2002) served as the X-ray data. The resulting curves are shown in Fig. 1.

3. RESULTS

The form of the optical and near-IR activity of CI Cam changed from rapid variations prior to the 1998 outburst (Bergner et al., 1995) to smooth gradual variations occurring on the time scale of weeks and months (Fig. 1a). The most prominent variations are observed in the *I* band, with the amplitude decreasing toward the *V* (and *U*) pass-band. The brightness variations are accompanied by complicated shifts in the color diagrams (Fig. 1bcd) – they cannot be explained by the changes of the extinction intrinsic to CI Cam. There are large differences between the color variations during the 1998 outburst and after it. We argue that the variations of the optical/IR continuum must significantly contribute to the color changes, since the variations in the individual filters are not independent on each other. There appears to be a relation of the source of the optical light and the X-ray source in quiescence (Fig. 1ef). Even if the donor star and its wind are the dominant sources of the optical luminosity in quiescence, they still appear to affect both the intensity and absorption of X-rays which are likely to come from the accretion onto the compact object. We offer an interpretation in terms of a density enhancement in the transferring matter.

We can constrain the emission mechanism in outburst (Fig. 1g). Since M_V of SXTs in outburst tends to brighten with the increasing P_{orb} (and hence with a larger disk radius), CI Cam would have to possess a very large disk if this disk were the site of the luminosity during the outburst, in contradiction with the very short duration and rapid decay in the X-ray (e.g. *ASM/RXTE*, Robinson et al. (2002)) and optical region. We argue that most of the luminosity observed during the 1998 outburst comes

from a site different from the disk – this is also supported by the reddening of $B - V$ and $V - R$ during the outburst (Fig. 1c) (a bluer color at maximum is expected in the case of the brightening of the disk of a roughly unchanged radius). We offer an interpretation in terms of the thermal instability of the disk + heating of the extended envelope by the brightened small disk and/or a formation of a strong jet. We note that CI Cam is not the only SXT that reddened during outburst (e.g. 4U 1543–47 (Buxton & Bailyn, 2004)). The periastron passage is an unlikely explanation, since no other outbursts have been observed by *ASM/RXTE* since 1998 in spite of $P_{\text{orb}} = 19$ days proposed by Barsukova et al. (2005a).

ACKNOWLEDGMENTS

This research has made use of the observations provided by the *ASM/RXTE* team. This study was supported by the grant 205/05/2167 of the Grant Agency of the Czech Republic, the project ESA PRODEX INTEGRAL 90108 and ESA PECS project 98023. We thank Dr. Harmanec for providing us with the code HEC13.

REFERENCES

- Barsukova E.A., et al. 2002, *AZh*, 79, 309
 Barsukova E.A., et al. 2005a, *ATel*, No.416
 Barsukova E.A., et al. 2005b, conf. VAC-2004, Moscow, June 3–10, 2004 (attached to *ATel* 416)
 Belloni T., et al. 1999, *ApJ*, 527, 345
 Bergner Y.K., et al. 1995, *A&AS*, 112, 221
 Boirin L., et al. 2002, *A&A*, 394, 205
 Buxton M.M. & Bailyn C.D. 2004, *ApJ*, 615, 880
 Clark J.S., et al. 2000, *A&A*, 356, 50
 Frontera F., et al. 1998, *A&A*, 339, L69
 Henden A. 2002, <ftp://ftp.nofs.navy.mil/pub/outgoing/aah/sequence/cicam.dat>
 Henden A. & Sumner B. 2004, *AJ*, submitted
 Hynes R.I., et al. 2002, *A&A*, 392, 991
 Levine A.M., et al. 1996, *ApJ*, 469, L33
 Miroschnichenko A.S., et al. 2002, *A&A*, 390, 627
 Orlandini M., et al. 2000, *A&A*, 356, 163
 Parmar A.N., et al. 2000, *A&A*, 360, L31
 Robinson E.L., et al. 2002, *ApJ*, 565, 1169
 Shahbaz T. & Kuulkers E. 1998, *MNRAS*, 295, L1
 Vondrák J. 1969, *BAIC*, 20, 349
 Vondrák J. 1977, *BAIC*, 28, 84

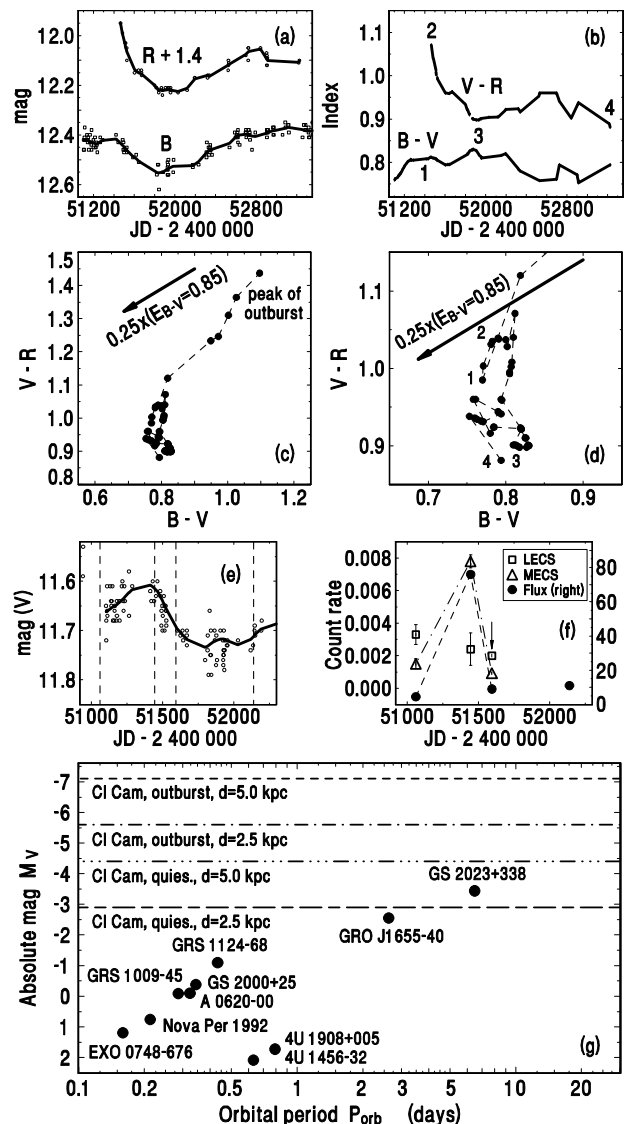


Figure 1. (a) Examples of the post-outburst light curves of CI Cam (daily means). The smooth lines represent the fits by the code HEC13 (author: Dr. P. Harmanec, method: Vondrák (1969, 1977)). (b) Examples of the time evolution of the color indices, determined from the fits in (a). The short vertical lines denote the positions of the observations for which the fits were made. (cd) Color-color diagrams. The lines connecting the points denote the time evolution. The vectors mark the reddening of CI Cam $E(B - V) = 0.85$ according to Robinson et al. (2002). The relation between the optical (e) and X-ray activity (f). The dashed vertical lines in (e) represent the moments of the X-ray observations. The points in (f) are connected by the line only for convenience. The data in JD 2451595 are the upper limits, as marked by the arrow. (g) Absolute magnitude M_V of soft X-ray transients (SXTs) (filled circles) at the outburst maximum versus P_{orb} . The parameters of 10 SXTs, except for CI Cam, come from Shahbaz & Kuulkers (1998). M_V of CI Cam in quiescence and outburst are marked by the horizontal lines.

XMM-NEWTON OBSERVATIONS OF THE SOFT INTERMEDIATE POLAR RXJ062518.2+733433

A. Staude, A. Schwope, R. Schwarz, J. Vogel, and M. Krumpe

Astrophysikalisches Institut Potsdam, An der Sternwarte 16, 14482 Potsdam, Germany

ABSTRACT

We report on observations of the soft intermediate polar 1RXSJ062518.2+733433 in the X-rays, UV, and the optical. Synchronously to a 30 ksec exposure with XMM-Newton's EPIC, the OM observed in filter UVM2, and ground-based observations were performed in the R-band. The X-ray observation covers 1.75 binary orbits and 25 white dwarf spin cycles, in which the EPIC-PN collected ~ 37000 source counts. A timing-analysis was performed on the data of various energy bands to determine the origin of the variability. The hard X-rays are varying mainly on the white dwarf's spin period, whereas the soft X-rays and the UV/optical data show strong variability on side-band periods. The average X-ray spectrum can be fitted by a black-body with $kT=60$ eV and two MEKALs with different amounts of absorption.

1. RESULTS

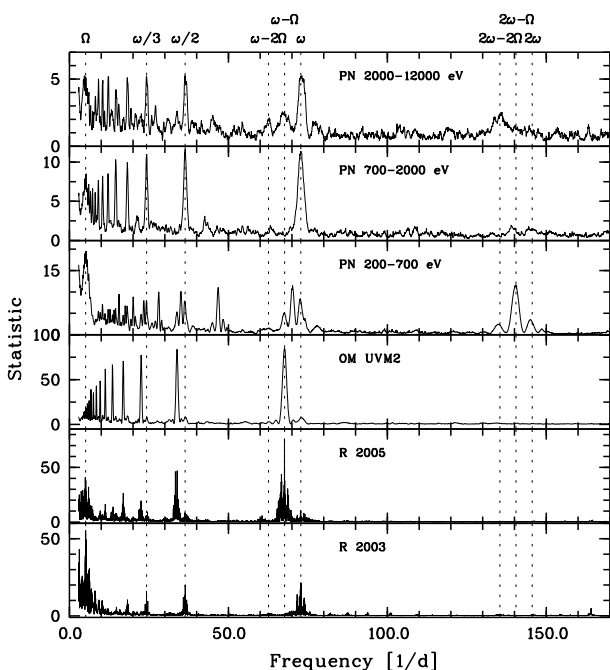


Figure 1. Periodograms of the light-curves from Fig. 3, and, for comparison, of the R-band data from 2003.

Fig. 3 shows the light curves obtained simultaneously on

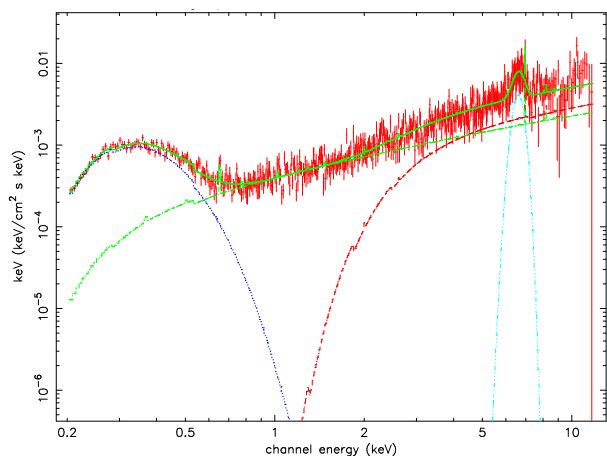


Figure 2. The EPIC-PN spectrum with overplotted fit and its components. (Parameters in Tab. 1)

March 31, 2005. In all wavelength ranges a variability near 20 min is seen. In the soft X-rays (200-700 eV) and in the R-band data there is a strong dependence of the amplitude of variability on the orbital phase. The analysis is supported by additional optical photometry obtained in three nights in March and April 2005.

In Fig. 1 the results of a period analysis with AOV in the different energy bands are shown. The dominating period in the harder X-ray bands is identical to the value for the spin period tentatively derived by Staude et al. (2003), $P_{spin} = 1187.246(4)$ s ($P_{orb} = 16987(23)$ s). At longer wavelengths, the variability on this period becomes weaker. In the soft X-rays, $2\omega - \Omega$ and $\omega - \Omega$ are also significant, while the latter is the dominant signal in the UV and the optical. The basic frequencies ω and Ω are marked in the figure, as well as (sub)harmonics of the spin frequency and side-band frequencies. AOV (Schwarzenberg-Czerny, 1989) tends to create sub-harmonics (contrary to the Fourier-transform, which creates harmonics).

The EPIC-PN spectrum is shown in Fig. 2. The data were fitted with Xspec using a multi-component model, $wabs_1(mekal_1) + wabs_2(mekal_2 + bbody + gaussian)$.

2. DISCUSSION

Compared to the R-band data from Staude et al. (2003), the object was nearly one magnitude fainter in 2005. In

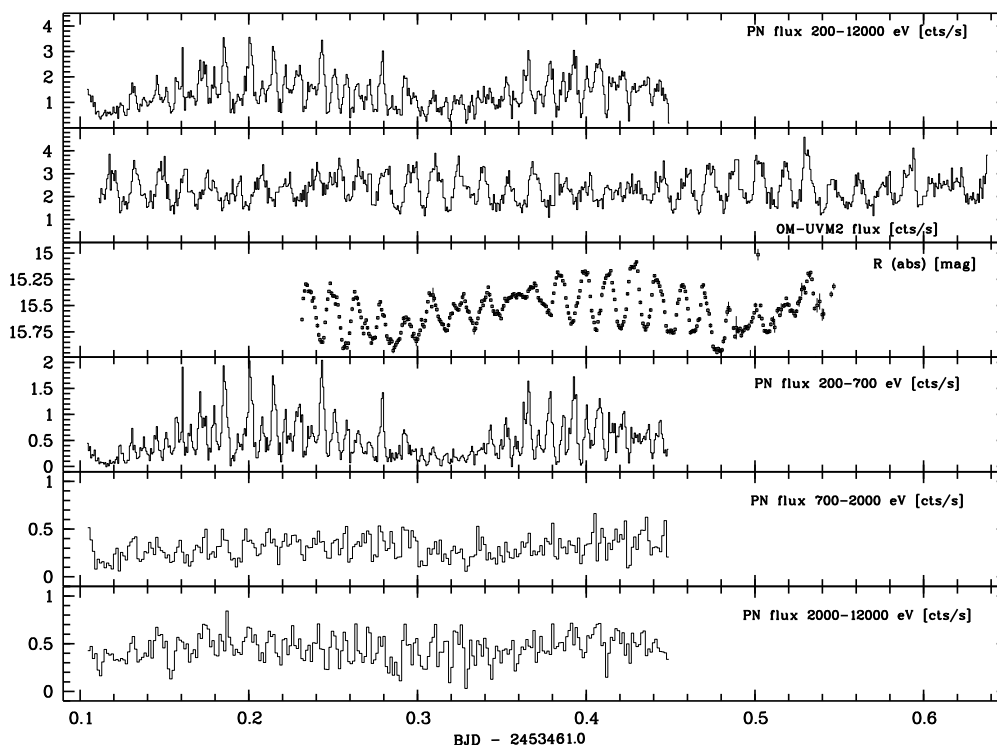


Figure 3. The light-curves of RXJ0625, simultaneously obtained on March 31, 2005, by XMM (PN and OM) and with the AIP 70cm-telescope (R). The data shown here are binned in time, 60s for the top four panels, 120s for the lower two.

Table 1. The main parameters of the spectral model.

wabs ₁	nH	$5.4 (1.3) 10^{22} \text{ cm}^{-2}$
mekal ₁	kT	not restricted
wabs ₂	nH	$2.7 (0.5) 10^{20} \text{ cm}^{-2}$
mekal ₂	kT	not restricted
bbody	kT	60 (1) eV
gaussian	LineE	6.6 (0.04) keV
	Sigma	0.28 (0.04) keV

2003, the optical short-term variability occurred on the period which we could now identify with the true white dwarf spin (Fig. 1, lowest panel), whereas in 2005 it occurred on $\omega - \Omega$.

The optical data from 2003 can be interpreted such, that a higher mass-loss rate of the secondary star led to the formation of an accretion disk, so that the short-term variation in the optical data is tracing the reprocessing sites of the radiation from the accreting pole on its radially symmetric inner rim.

The beat-period ($\omega - \Omega$), as the dominant period in the optical and UV light from 2005, shows that their emission or the visibility of their origin was strongly dependent on the orientation of the white dwarf's magnetic field with respect to the secondary star. As indicated by the lower brightness of the system, the mass-loss rate was lower, and it is likely that the matter was captured earlier by the magnetic field, preventing the formation of a highly symmetric accretion disk.

In the fit to the PN spectrum, the plasma temperature for the MEKAL components was not restricted. A successful fit was achieved only after inclusion of a second highly absorbed MEKAL component. In a phase-averaged spec-

trum this can be understood as being the result of either two accreting poles with different accretion conditions, or as one (visible) accreting pole with a changing amount of absorption due to occultation by an accretion curtain. The hard X-ray component is thought to be originating in a shock in the accretion column above the magnetic pole. Since there is nearly no variability of the count-rate of the hard photons on the beat frequency, the accretion rate does not seem to be dependent on the stars' orientation. Thus the accretion leading to the emission of hard photons is likely to happen via an accretion disk, although this statement seems to contradict the conclusions drawn from the other energy bands.

The soft X-ray photons (200 - 700 eV) are fitted well by a black-body, and seem to be arising on the white dwarf (because of the strong signal at ω). The strength of $\omega - \Omega$ shows that the orientation of the stars has influence on the emission. Stream-fed accretion, penetrating the white dwarf's surface and heating it, is thus likely to be the origin of the soft X-ray component. The frequency $2\omega - \Omega$ is a hint to a second accreting pole, opposite to the main one, since it denotes the existence of a similar accretion geometry after just half a spin-cycle (Wynn & King, 1992).

We could not yet identify the peak at $\sim 47 \text{ d}^{-1}$ and its sub-harmonics with any side-band frequency of the main periodicities.

REFERENCES

- Schwarzenberg-Czerny, A. 1989, MNRAS, 241, 153
 Staude, A., Schwobe, A. D., Krumpke, M., Hambaryan, V., Schwarz, R. 2003, A&A, 406, 253
 Wynn, G. A. & King, A. R. 1992, MNRAS, 255, 83

X-RAY STUDY OF MASS-ACCRETION FLOWS ONTO WEAKLY-MAGNETIZED NEUTRON STARS

Hiromitsu Takahashi and Kazuo Makishima

Department of Physics, University of Tokyo, 7-3-1 Hongo Bunkyo-ku Tokyo 113-0033 Japan

ABSTRACT

To investigate the physics of mass accretion onto weakly-magnetized neutron stars (NSs), which are often called low-mass X-ray binaries (LMXBs), energy spectra of 18 LMXBs observed by the RXTE satellite were analyzed. While the X-ray luminosity is sufficiently lower than the Eddington limit for a $1.4 M_{\odot}$ NS, the energy spectra of the sample objects were represented successfully with a combination of two optically-thick components, one from a standard accretion disk and the other from the NS surface. As the accretion rate increases, the disk luminosity increased but that of the NS surface saturated or even decreased. When the mass accretion rate (hence the luminosity) becomes comparable to or even higher than the Eddington limit, the LMXB spectra were discovered to consist of three optically-thick components; the softest one from a retreated disk, the hardest one from the NS surface, and an additional intermediate component presumably from outflows caused by the increased radiation pressure.

Key words: stars: binaries: general — stars: individual(4U 1608-522, GX 5-1, GX 17+2) — stars: neutron — X-ray: stars .

1. INTRODUCTION

Physics of accretion flows (e.g., accretion disks), especially in black hole binaries, has been relatively well understood when the mass accretion rate \dot{M} is moderate and hence the gravitational force dominates others. However, much less is known when the mass accrete is so high that the radiation pressure becomes comparable to the gravitation. In particular, observational confirmation of “outflows” of a portion of the accreting matter, which is expected under a high radiation pressure, has been very scarce.

To study the accretion flow under such a high accretion rate, LMXBs are one of the best targets. Since the mass of NSs, typically $\sim 1.4M_{\odot}$, is about an order of magnitude lower than those of black holes, the radiation pressure of an LMXB becomes significant even at relatively low accretion rates. Moreover, unlike black holes which could swallow the matter before it fully radiates, a NS has

a solid surface with a radius ~ 10 km; therefore, the matter cannot settle down to the bottom of the gravitational potential (i.e., the NS surface) without radiating away the acquired energy.

Employing the Eastern model (Mitsuda et al., 1984, 1989; Makishima et al., 1989), we analyzed a huge amount of publicly available data of 18 luminous LMXBs obtained by RXTE (Takahashi, 2005). When the X-ray luminosity of each LMXB is lower than the Eddington limit (2.1×10^{38} ergs $^{-1}$), all the spectra averaged per observation (typical exposures of \sim ks) are well reproduced by the Eastern model, as exemplified in § 2. In § 3, we study two “Z-sources”, GX 5-1 and GX 17+2, of which the luminosities are comparable to or even higher than the Eddington limit. Their properties are consistently explained by a modified Eastern model which incorporates significant matter outflows.

2. 4U 1608-522 IN UPPER BANANA BRANCH

Energy spectra of 4U 1608-522 in so called Upper Banana branch (UB) are well represented by the Eastern model with a combination of a soft multi-color disk (MCD) model and a hard blackbody (BB) emission, of which the temperatures are ~ 1.5 and ~ 2.5 keV, respectively. The former component represents emission from the optically-thick accretion disk, and the latter from the central NS. Figure 1 shows the 3–30 keV MCD luminosity L_{disk} , the BB luminosity L_{BB} in the same band, and their sum L_{tot} , as a function of \dot{M} which is estimated from parameters of the MCD model (Mitsuda et al., 1984). It is clear that L_{disk} is well proportion to \dot{M} . Since $L_{\text{disk}} \propto r_{\text{in}}^2 T_{\text{in}}^4$ and $\dot{M} \propto r_{\text{in}}^3 T_{\text{in}}^4$, where r_{in} and T_{in} are the innermost disk radius and temperature, respectively, this result implies that r_{in} is constant, namely the accretion disk exists stably. On the other hand, L_{BB} is seen to depend less steeply on \dot{M} . According to the virial theorem, a half of the released gravitational energy of the accreting matter should be radiated from the accretion disk as L_{disk} , and the other half becomes the Keplerian energy of the matter which should be eventually radiated as L_{BB} if all the matter accretes onto the NS surface. In that case, L_{BB} should be proportion to L_{disk} . Therefore, Figure 1 indicates that only a fraction of the mass flow through the disk reaches the NS surface, while the rest

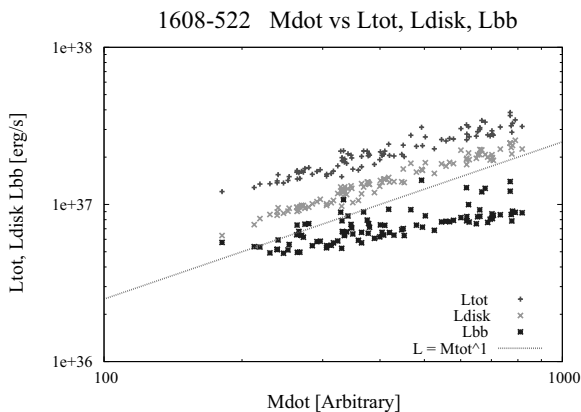


Figure 1. The dependences of L_{disk} , L_{BB} and L_{tot} on \dot{M} , calculated over the 95 datasets of 4U 1608-522 in UB.

presumably forms outflows. Since the total luminosity $L_{\text{tot}} \sim 4 \times 10^{37} \text{ erg s}^{-1}$ is close to the Eddington limit, we suppose that the outflow is driven by radiation pressure. As the total luminosity increases, the ratio of L_{BB} to L_{disk} decreases from 0.6 to 0.4. Then, the fraction of the matter outflow is estimated to be $\sim 30\%$ of \dot{M} .

3. GX 5-1 AND GX 17+2 IN FLARING BRANCH

To study the physical state under higher radiation pressure than that of 4U 1608-522, we analyzed ‘‘Flaring branch’’ (FB) data of two Z sources, GX 5-1 and GX 17+2, of which the luminosities (several times $10^{38} \text{ erg s}^{-1}$) reach the Eddington limit. They represent two subclasses of Z-sources; one class of the objects including GX 5-1 shows a decrease in the hard X-ray (10–40 keV) counts as they evolve deeper into FB, while the other class including GX 17+2 behaves in the opposite way. This difference between the two subclasses may be caused by inclination angles; namely the former is observed with higher inclinations, and the latter with lower ones (Kuulkers et al., 1994, 1996).

Figure 2 shows energy spectra of GX 5-1 and GX 17+2 in FB. Indeed, the spectrum of GX 5-1 is detected only up to $\sim 20 \text{ keV}$, while that of GX 17+2 reaches $\sim 30 \text{ keV}$. The GX 5-1 spectrum cannot be reproduced by a single MCD model ($\chi^2/\text{d.o.f.} \sim 3$), and needs the MCD and BB components ($\chi^2/\text{d.o.f.} \sim 1.2$). The temperatures and radii are obtained as $\sim 0.9 \text{ keV}$ and $\sim 60 \text{ km}$ for the MCD component, and $\sim 1.5 \text{ keV}$ and $\sim 20 \text{ km}$ for the BB. In contrast, we discovered that the GX 17+2 spectrum is well represented by the MCD and two BB (BB1 and BB2) models, of which the temperatures are $\sim 0.6 \text{ keV}$, $\sim 1.3 \text{ keV}$ and $\sim 2.5 \text{ keV}$, respectively. The temperatures and radii of the softer two emission (MCD and BB1) are comparable with those of GX 5-1, whereas the hard BB2 component is not observed from GX 5-1.

In addition to the BB2 temperature $\sim 2.5 \text{ keV}$, of which the value is similar to those observed from 4U 1608-522, the radius of the BB2 emission region $\sim 4 \text{ km}$ is also close to the NS radius. Therefore, the BB2 emission is considered to be emitted from the NS surface. The tem-

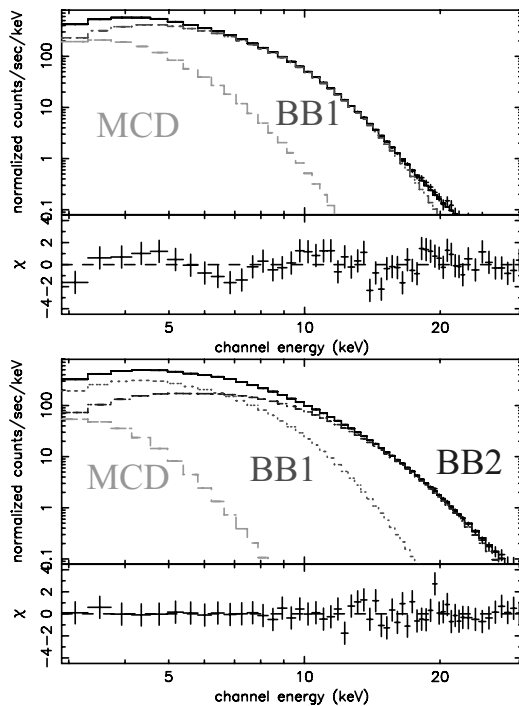


Figure 2. Energy spectra of GX 5-1 and GX 17+2 in FB, fitted with the MCD, BB1, and BB2 components.

perature and radius of the BB1 component are just in between those of the MCD (e.g. the accretion disk) and BB2 (NS surface) components. Since these Z sources should exhibit more enhanced outflows than 4U 1608-522 with the lower luminosity, we interpret that BB1 is emitted from the outflow which becomes optically thick.

These facts have led us to propose the following picture. (1) The innermost portion of the accretion disk becomes inflated due to its own radiation pressure, causing the optically-thick inner disk edge to retreat back and hence the temperature there to decrease. (2) Through the inflated inner disk, the matter partially accretes onto the NS surface, as a quasi-spherical flow, thus producing the BB2 component from the NS surface. (3) The rest of the matter keeps escaping as the outflow, and the increased optical depth of the outflow causes it to emit the BB1 component. (4) The BB1 emitter is not totally spherical, and obscures the BB2 region when viewed from a relatively edge-on inclination as in GX 5-1.

REFERENCES

- Kuulkers, E. et al. 1994, A&A, 289, 795
- Kuulkers, E. et al. 1996, A&A, 311, 197
- Makishima, K. et al. 1989, PASJ, 41, 531
- Mitsuda K. et al. 1984, PASJ, 36, 741
- Mitsuda, K. et al. 1989, PASJ, 41, 97
- Takahashi, H. 2005, PhD. thesis, Univ. of Tokyo,

MAGNETIC ACCRETION IN AN EXTREME ENVIRONMENT: THE CASE OF THE LOW-ACCRETION RATE POLAR WX LMI

J. Vogel, A. Schwope, R. Schwarz, and A. Staude

Astrophysikalisches Institut Potsdam, An der Sternwarte 16, 14482 Potsdam, Germany

ABSTRACT

The class of low-accretion rate polars was uncovered recently in optical spectroscopic surveys (HQS, SDSS). Contrary to their high-accretion rate cousins which were discovered numerously in the RASS, they did not show up as prominent X-ray emitters. They were identified on the basis of highly peculiar optical spectra with broad cyclotron harmonics in emission mimicing quasar emission lines. They could form an important part of the population of close interacting binaries, being either normal CVs in extended low states of accretion or pre-CVs on their track towards Roche-lobe overflow. Here we present preliminary results of a multiwavelength study of the prototypical system WX LMi (HS 1023+3900) involving X-ray spectroscopy, ultraviolet, optical and IR-photometry, and optical low-resolution spectroscopy.

1. INTRODUCTION

Polars are magnetic cataclysmic binaries consisting of a late-type main-sequence star and a strongly magnetic white dwarf locked in synchronous rotation. In normal polars accretion happens via Roche-lobe overflow and accretion streams towards the magnetic poles where the accretion energy is released mainly as X-ray thermal radiation, optical cyclotron radiation and a prominent soft X-ray component. The energy balance between those components is of debate since the days of discovery of the very first systems. The soft component makes them prominent sources in the soft X-ray sky and they were found numerously in the ROSAT all-sky survey. The detection bias is large and the true space density highly uncertain. Recently a few systems with very low accretion rate (a factor 100 – 1000 below the canonical values for Roche-lobe overflow) were uncovered in optical spectroscopic surveys (HQS, SDSS). They offer the opportunity to study the physics of accretion in an environment of extreme low-accretion rate/high magnetic field. They might serve as tracers to uncover the unbiased sample of magnetic CVs. Establishing their detailed properties is the first important step in understanding their role in close

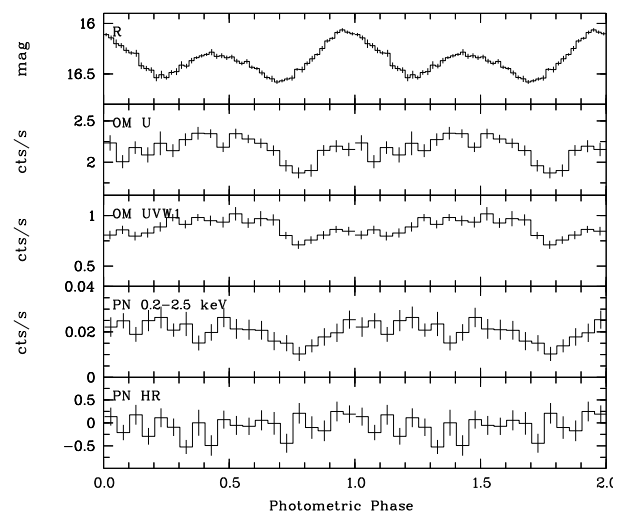


Figure 1. The phase-folded light-curves of WX LMi, obtained with XMM (PN and OM) and with the AIP 70cm-telescope (R). The data shown here are binned in phase, 200s for the top panel, 500s for the lower four. The hardness ratio is for the energy bands 200 - 700 eV and 700 - 2500 eV. The R band lighcurve clarifies the two accretion spots, which are visible alternatively.

binary evolution. To this end we initiated an in-depth study of WX LMi, the brightest of the currently known 6 systems. XMM-Newton observations were performed to test the bombardment accretion scenario, to measure the white dwarf's temperature and to constrain the magnetic activity of the secondary star.

2. THE DATA

WX LMi was discovered during follow-up of quasar candidates from the Hamburg Quasar Survey (HQS, Reimers et al. 1999). Phase-resolved low-resolution spectroscopy of WX LMi (Reimers et al. 1999, Schwope et al. 2002)

clearly reveals the presence of two accretion spots on the southern hemisphere emitting strongly beamed optical cyclotron radiation. Detailed modeling allowed the magnetic field strength and the plasma temperature to be determined (61 and 69 MG, 1 – 2 keV, respectively). At such high field strengths and low temperatures probably no accretion shock forms. Accretion heating rather happens via particle bombardment of the atmosphere (Fischer & Beuermann 2001), just as the plasma cooling happens mainly via cyclotron radiation instead of bremsstrahlung in the hard X-ray regime. In order to test the predictions of the bombardment model XMM-Newton observations with a full phase coverage of three orbits (30 ksec) were performed in March 2004.

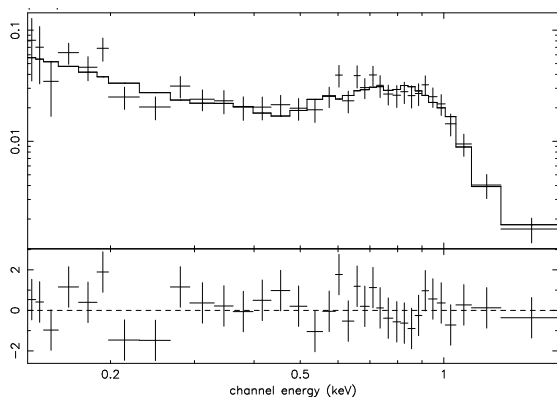


Figure 2. The EPIC-PN spectrum and the fit with an absorbed multi-temperature plasma emission model, yielding a plasma temperature T_{max} of $1.09(\pm 0.24)$ keV and a hydrogen column density $N_H = 8 \cdot 10^{19} \text{ cm}^{-2}$. The energy channels are binned with a minimum of 20 counts in each bin. Above 2 keV no significant X-ray emission was detected.

Figure 2 shows the EPIC-PN spectrum. There is no significant X-ray detection in the energy range above 2 keV. The spectrum can be fitted well with an absorbed $T_{max} = 1.23(\pm 0.28)$ keV multi-temperature MEKAL model. This plasma temperature lies within the regime for a coronal source as well as in the domain one expects for the plasma being accreted. The comparison of the phase-folded PN lightcurve (Figure 1) with the R-band lightcurve suggests a correlation of the X-ray emission with the visibility of the two spots. At optical flux minimum around phase 0.75 when both spots are self-eclipsed there is 50% residual X-ray flux. This can be attributed to the active secondary ($L_{x,M2} \sim 1 \times 10^{29}$ ergs/s). The luminosities in the cyclotron ($L_{1/2,cyc} \sim 7.0/3.6 \times 10^{28}$ ergs/s) and X-ray spectra are comparable, which supports the bombardment scenario by Fischer & Beuermann. The OM lightcurves (see Figure 1) are likewise affected by the visibility of the two accretion spots due to the emission from the heated white dwarf atmosphere. Those regions are not seen in the soft X-ray spectrum, which sets certain constraints on the maximum temperature and size of the heated atmosphere.

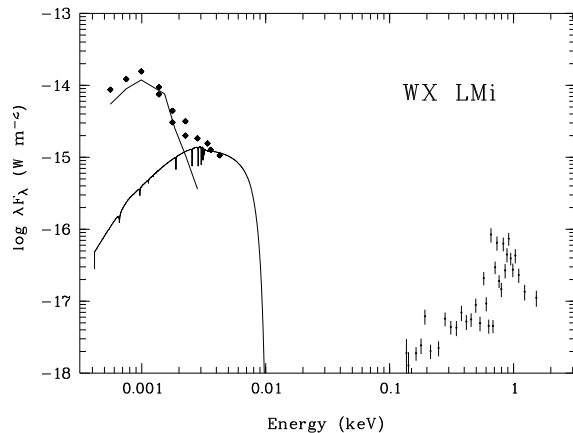


Figure 3. Broad-band spectral energy distribution of WX LMi (two points at the same energy mark minimum and maximum measurements): JHK from 2MASS catalog, UBVR obtained with the AIP 70 cm telescope, OM U, OM UVW1 and EPIC PN spectrum. Overplotted are the spectrum of a M4.5 star and a model spectrum for a nonmagnetic white dwarf with a temperature of 8000 Kelvin.

The OM flux in the U and UVW1 filter around phase 0.75 shows a very cold white dwarf. With model spectra for nonmagnetic white dwarfs no satisfying fit can be achieved. But assuming a white dwarf radius of $R_{WD} = 8.7 \cdot 10^8$ cm and a distance of 100 pc (Schwarz 2001) a white dwarf temperature of 8000 Kelvin is most likely. This gives a lower limit for the white dwarf age of ~ 1 Gyr and possibly means that WX LMi has never been accreting at a rate normally expected for CVs and is a pre-CV at the onset of accretion.

ACKNOWLEDGMENTS

J.V. and R.S. are supported by the Deutsches Zentrum für Luft- und Raumfahrt (DLR) GmbH under contract No. FKZ 50 OR 0404. A.St. is supported by the DFG under contract No. SCHW 536/20-1.

REFERENCES

- Fischer A. & Beuermann K. 2001 A&A 373 211
- Reimers D., Hagen H.-J. and Hopp U. 1999 A&A 343 157
- Schwarz R., Schwöpe A.D. & Staude A. 2001 A&A 374 189
- Schwöpe A.D. et al. 2002 ASPC 261 102

XMM-NEWTON OBSERVATIONS OF THE TWO ANOMALOUS X-RAY PULSARS 1RXS J170849.0-400910 AND 1E 1048.1-5937

S. Zane¹, N. Rea^{2,3}, G.L. Israel³, A. Tiengo⁴, S. Mereghetti⁴, L. Stella³, M. Mendez², R. Turolla⁵, T. Oosterbroek⁶, and F. Haberl⁷

¹Mullard Space Science Laboratory, University College London, Holmbury St. Mary, Dorking Surrey, RH5 6NT, UK

²SRON - National Institute for Space Research, Sorbonnelaan 2, 3584 CA, Utrecht, The Netherlands

³INAF–Astronomical Observatory of Rome, Via Frascati 33, I-00040, Monteporzio Catone (Rome), Italy

⁴INAF-Istituto di Astrofisica Spaziale e Fisica Cosmica G. Occhialini, Via Bassini 15, I-20133 Milano, Italy

⁵University of Padua, Physics Department, via Marzolo 8, I-35131, Padova, Italy

⁶Science Payload and Advanced Concepts Office, ESA-ESTEC, Postbus 299, NL-2200 AG, Noordwijk, The Netherlands

⁷Max-Planck-Institut für extraterrestrische Physik, 85741 Garching, Germany

ABSTRACT

We report the results of *XMM-Newton* observations of the two Anomalous X-ray pulsars 1RXS J170849.0-400910 and 1E 1048.1-5937. We discuss their long term evolution and the existence of correlations between X-ray flux, spectral hardness and pulsed fraction.

Key words: X-rays; Neutron Stars; magnetars.

1. 1RXS J170849.0-400910

The Anomalous X-ray pulsar (AXP) 1RXS J170849.0-400910 is a particularly interesting source, for at least two reasons. First, although early data suggested it was a fairly stable rotator (Israel et al., 1999), in the last four years it experienced at least two glitches (Kaspi et al. 2000, Kaspi et al. 2003, Dall’Osso et al. 2003) with different post-glitch recoveries. Second, an absorption line at ~ 8 keV has been detected at 4σ confidence level (CL; Rea et al. 2003), in the phase-resolved spectrum taken with BeppoSax in 2001. This was the longest observation ever performed for this AXP, and it was taken when the source was not totally recovered from its second glitch.

We observed the source with *XMM-Newton* during the post-glitch epoch, for 50ks on 28-29 Aug 2003 (see Rea et al. 2005 for more details). By comparing these data with those collected over the past five years, we found a clear correlation between the spectral index Γ and the luminosity L : the spectrum became harder as the flux rose in correspondence of the two glitches and then softened as the luminosity dropped, following the glitch recovery (see Fig.1). However, we found no evidence for absorption features in the *XMM-Newton*. In particular, for a line

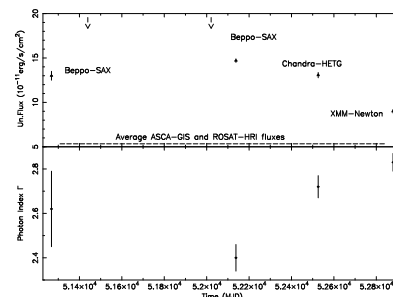


Figure 1. Flux and spectral hardening evolution of 1RXS J170849.0-400910. The dashed line is the average flux measured with *Asca* and *Rosat*. The two arrows mark the time of the two glitches. During the second *BeppoSax* observations, taken shortly after the second glitch, an absorption line at ~ 8 keV has been detected (Rea et al., 2003). Taken from (Rea et al., 2005).

at ~ 8 keV we derived a 95% upper limit for the depth of 0.15. For comparison, the depth of the line observed with *BeppoSax* at this energy was 0.8 ± 0.4 at 90% CL.

Quite interestingly all the observed phenomenological features including the glitching activity, the observed $\Gamma - L$ correlation, and, possibly, the transient appearance of a cyclotron line may be explained by the onset of a twist in the external magnetosphere. As suggested by Thompson et al. (2002), “magnetars” (AXPs and SGRs) may differ from radio pulsars in the fact that their internal magnetic field is highly twisted, up to 10 times the external dipole. At intervals, it can twist up the external field, leading to the build up of stresses in the star crust, crustal fractures and possibly glitches. Twisted magnetospheres can also support current flows. In turn, the pres-

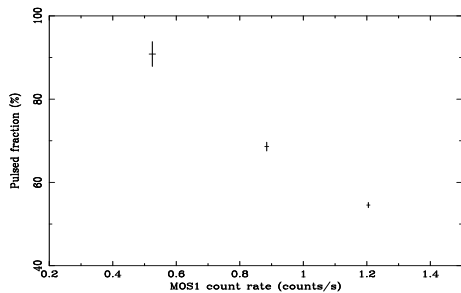


Figure 2. Correlation between PF and count rate, as measured by XMM-Newton. From Tiengo et al. (2005).

ence of charged particles (e^- and ions) produces both a large resonant scattering depth and an extra heating of the star surface (by returning currents). However, since i) the e^- distribution is spatially extended and ii) the resonant frequency for e^- -cyclotron depends on the local value of the magnetic field, repeated scatterings onto e^- could lead to the formation of a high energy tail instead of a narrow line. Both e^- scattering depth and released luminosity increase with the twist angle, and, since the spectral hardness increases with depth, this implies a positive $\Gamma-L$ correlation (as observed). Finally, this scenario may explain the transient appearance of a cyclotron line during the epoch in which the twist was substantial. In fact, magnetospheric charges also provide a substantial depth to the resonant proton scattering. When the X-ray luminosity at the resonant frequency exceeds the luminosity produced by the returning currents, ions are effectively confined in a thin layer close to the surface leading to the appearance of a spectral line instead of a power law tail.

2. 1E1048.1-5937

Among other AXPs, 1E1048.1-5937 is particularly important for understanding the connection between AXPs and SGRs. It is the first AXP for which X-ray bursts have been discovered and it is one of those with hardest spectrum and most variable period evolution (both characteristics are typical of SGRs). Long term variations in its X-ray flux have been reported in the past using data from different satellites (Oosterbroek et al., 1998) and have recently more firmly established by Mereghetti et al. (2004), and by the RXTE monitoring programme (Gavriil & Kaspi, 2004). Here we present results based on 3 XMM-Newton observations taken in 2000, 2003 and 2004, which allow a systematic study of long terms changes based on a homogeneous dataset (see Tiengo et al. 2005 for a more detailed discussion).

We find that the canonical AXPs model, consisting of an absorbed blackbody plus a power law component, can reproduce all spectra, while a two blackbodies model is rejected by the high quality spectrum taken with a 50ks observation in 2003. In the attempt to establish a

more physical link between the thermal and the power law components, we also fitted the 3 spectra with a simple Comptonization model (CBB = Comptonized Black Body). The basic idea is that soft thermal photons (emitted, e.g., at the star surface) are upscattered by a population of relativistic e^- with small optical depth and mean Lorentz factor $\langle\gamma\rangle$. If the soft photon input is a blackbody at T_{BB} , the emerging photon spectrum is given by $CE^{-\alpha} \int_0^E dE' E'^{1+\alpha} / [\exp(E'/kT_{BB}) - 1]$, where $\alpha = 1 - \ln \tau_{es}^B / \ln A$, τ_{es}^B is the scattering depth in a magnetized medium, $A \sim 4\langle\gamma^2\rangle/3$ is the mean energy amplification factor per scattering, and C is a normalization factor. We have found that a two component model made of a CBB and a colder blackbody successfully reproduces all observations. In this case the radius of the colder blackbody is consistent with the star radius, while a smaller area is associated with the hotter thermal component. This may suggest that a magnetically active hot region is present at the star surface: accelerated high energies particle heat the region and upscatter soft photons, producing the comptonized spectrum.

XMM-Newton data clearly revealed a spectral difference between the three observations, with spectral changes not monotonically related with the X-ray luminosity (when the flux is at the highest level, in 2003, the spectral hardness is intermediate). However, we find a coherent pattern between flux and pulsed fraction (PF) (shown in Fig.2). The reality of this correlation is quite robust, since in Fig.2 we are comparing PFs and fluxes measured with the same detector operating in the same mode in the three observations (0.6-10 keV, MOS1). Accounting for the existence of an empirical anti-correlation between flux and PF is crucial when the source energetics is inferred by measurements of the pulsed flux. For instance, we estimated that the total energy release of the RXTE flares peaking in Nov. 2000 and June 2001 can be at least double (2 and 20×10^{40} ergs) the value derived assuming a constant PF = 0.94 (Gavriil & Kaspi, 2004).

REFERENCES

- Dall’Osso S., et al. 2003, ApJ, 499, 485
 Gavriil F.P., & Kaspi V.M. 2004, 609, L67
 Israel, G.L., et al. 1999, ApJ, 518, L107
 Kaspi, V.M., Lackey, J.R., Chakrabarty, D. 2000, ApJ, 537, L31
 Kaspi, V.M., et al. 2003, ApJ, 588, L93
 Mereghetti, S., et al. 2004, ApJ, 608, 427
 Oosterbroek T., et al. 1998, A&A 334, 925
 Rea et al. 2003, ApJ, 586, L65
 Rea et al. 2005, MNRAS, 371, 710
 Thompson, C., Lyutikov, M., Kulkarni, S.R., 2002, ApJ, 574, 332
 Tiengo, A., et al. 2005, A&A, 437, 997

IGR J17252–3616: AN ECLIPSING PULSAR OBSERVED BY *INTEGRAL* AND *XMM-NEWTON*

J.A. Zurita Heras^{1,2}, G. De Cesare³, R. Walter^{1,2}, A. Bodaghee^{1,2}, G. Bélanger⁴, T.J.-L. Courvoisier^{1,2}, S.E. Shaw^{5,1}, and J.B. Stephen⁶

¹INTEGRAL Science Data Centre, Versoix, Switzerland

²Observatoire de Genève, Sauverny, Switzerland

³IASF-INAF, Via Fosso del Cavaliere 100, 00133 Roma, Italy

⁴Service d'Astrophysique, DAPNIA/DSM/CEA, 91191 Gif-sur-Yvette, France

⁵School of Physics and Astronomy, University of Southampton, Highfield, SO171BJ, UK

⁶IASF/CNR, Via Piero Gobetti 101, 40129 Bologna, Italy

ABSTRACT

We report here the analysis of the *INTEGRAL* and *XMM-Newton* observations on IGR J17252–3616. The source is located at R.A. (2000.0) = $17^{\text{h}}25^{\text{m}}11.4^{\text{s}}$ and Dec. = $-36^{\circ}16'58.6''$ ($4''$). We found one infrared counterpart, 2MASS J17251139–3616575, located $1''$ away. The source is a binary X-ray pulsar with a spin period of 413.7 ± 0.3 s and an orbital period of 9.72 ± 0.09 d. IGR J17252–3616 is a persistent source with an average 20–60 keV flux of ~ 6.4 mCrab. The spectrum can be fitted with a flat power law plus an energy cutoff, typical of accreting pulsars. A large hydrogen column density ($N_{\text{H}} \sim 15 \cdot 10^{22}$ atoms cm^{-2}), suggesting an intrinsic absorption, and the Fe $K\alpha$ line at 6.4 keV are clearly detected. Phase-resolved spectroscopy does not show any variation in the continuum except the total emitted flux. The absorption is constant along the pulse phase. This source is the hard X-ray counterpart of EXO 1722–363 as they both show common timing and spectral features. The observations suggest that the source is a wind-fed accreting pulsar accompanied by a supergiant star.

Key words: X-rays: binaries, X-rays: individual: IGR J17252–3616=EXO 1722–363.

1. INTRODUCTION

The imager IBIS/ISGRI on board the X-ray and γ -ray observatory *INTEGRAL* allowed the (re)discovery of several hard X-ray sources due to its unique sensitivity in the 20–200 keV energy range. Many of those objects show common features in their spectra, such as a high intrinsic low-energy absorption, and they are believed to be high mass X-ray binaries (HMXB) (Walter et al., 2005).

The discovery of IGR J17252–3616 was reported on

February 9, 2004 (Walter et al., 2004). A follow-up with *XMM-Newton* was performed in order to investigate its nature in a wide high energy band.

2. OBSERVATIONS

IGR J17252–3616 is located close to the galactic centre which has been regularly observed with *INTEGRAL* as part of the core programme (CP). The CP strategy consists of pointings lasting ~ 30 minutes and distributed in various grids around the galactic centre and plane. A total exposure of 6.5 Ms was accumulated with public and CP data (MJD 52671–53294). The source was observed by *XMM-Newton* on March 21, 2004, from 13:02:45 to 16:04:45 UTC for a total exposure of 11 ks.

3. IMAGING, TIMING AND SPECTRAL ANALYSIS

A single X-ray source corresponds to the *INTEGRAL* position in the EPIC/MOS1 image (see Fig. 1). Its position is R.A. (2000.0) = $17^{\text{h}}25^{\text{m}}11.4^{\text{s}}$ and Dec. = $-36^{\circ}16'58.6''$ ($4''$). There is one infrared counterpart, 2MASS J17251139–3616575, located $1''$ away with a magnitude in the Ks-band of 10.7.

The source is persistent and variable in the 20–60 keV energy range with an average flux of ~ 6.4 mCrab. A significant peak at 9.72 ± 0.09 d is visible in a Lamb-Scargle periodogram and the folded light curve is shown in Fig. 2. A minimum flux consistent with an eclipse is visible at phase 0.

Moreover, a pulsation has been detected in EPIC/pn and confirmed in IBIS/ISGRI data ($P_{\text{s}} = 413.7 \pm 0.3$ s, see

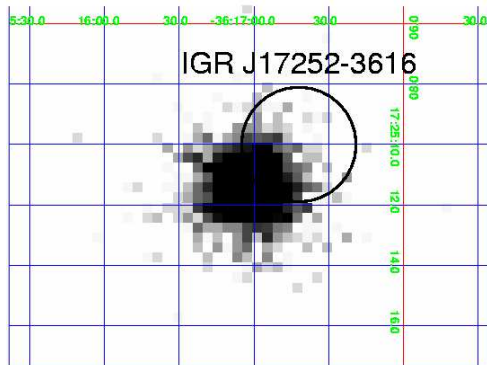


Figure 1. EPIC/MOS1, 0.8–10 keV extracted image. ISGRI position and uncertainty are reported.

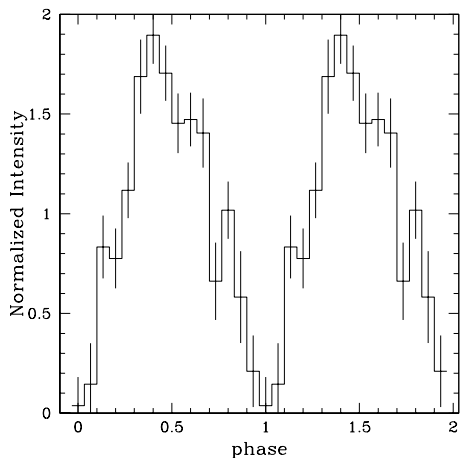


Figure 2. Orbital folded light curve with the best period of 9.72 ± 0.09 d

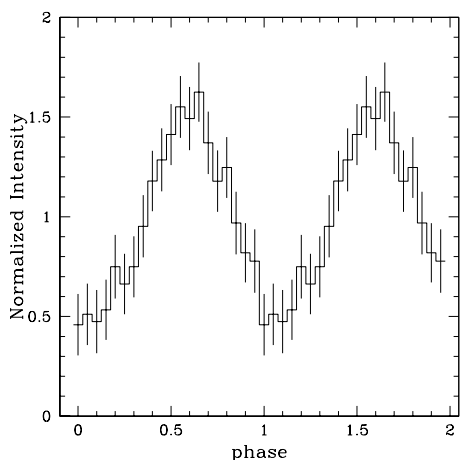


Figure 3. 20–40 keV folded light curve with the pulse period of $P_s = 413.7 \pm 0.3$ s

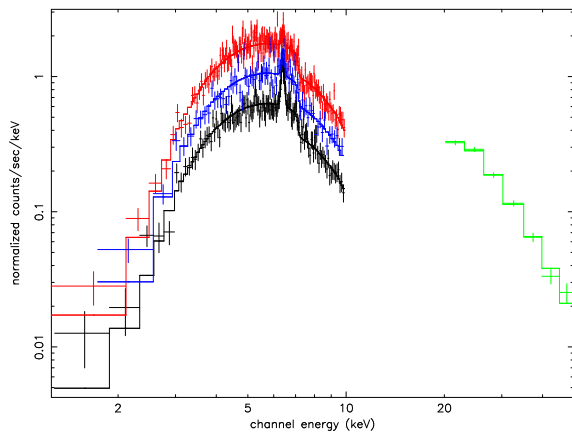


Figure 4. Combined spectral analysis. X-ray band: EPIC/pn phase-resolved spectra. Hard X-ray band: ISGRI average spectrum.

Fig. 3). There is no evidence of spin period variation in ISGRI data.

The EPIC and ISGRI spectra were fitted together. A cutoff powerlaw model gives typical values of an accreting pulsar ($\Gamma = 0.0 \pm 0.1$, $E_{\text{cut}} = 8.2 \pm 0.4$ keV, $\chi^2/\text{d.o.f.} = 401/376$). The Fe $K\alpha$ line at 6.4 keV and a large hydrogen column density ($N_{\text{H}} \sim 15 \cdot 10^{22}$ atoms cm^{-2}) are also observed. Phase-resolved spectroscopy did not show any significant variation of the spectral shape with the phase excepting the change in the normalisation (see Fig. 4).

IGR J17252–3616 can be associated with EXO 1722–363. From Ginga observations in 1987 and 1988, Tawara et al. (1989) and Takeuchi et al. (1990) detected a pulsation of 413.9 s, important variations of the intensity in X-rays, a hard spectrum with important low-energy absorption and an emission line at 6.2 keV. Using RXTE data, Corbet et al. (2005) resolved the orbital period of 9.741 days and detected a varying high column density. These investigations conclude that the system is a wind-fed accreting pulsar.

REFERENCES

- Corbet, R. H. D., Markwardt, C. B., & Swank, J. H. 2005, ApJ, in press
- Takeuchi, Y., Koyama, K., & Warwick, R. S. 1990, PASJ, 42, 287
- Tawara, Y., Yamauchi, S., Awaki, H., et al. 1989, PASJ, 41, 473
- Walter, R., Bodaghee, A., Barlow, E. J., et al. 2004, The Astronomer’s Telegram, 229, 1
- Walter, R., Zurita Heras, J. A., Bassani, L., et al. 2005, submitted to A&A